

UNIVERSITÀ
DEGLI STUDI
DI PADOVA

Università degli Studi di Padova
Dipartimento di Scienze Chimiche

PhD course in Molecular Sciences

Curriculum: Chemistry

Cycle: XXXIV

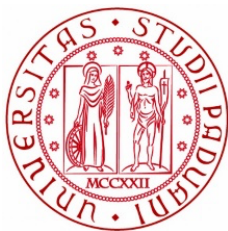
Unlocking the Synthetic Potential of Light Excited Aryl Ketones

Coordinator: Prof. Leonard Jan Prins

Supervisor: Dr. Luca Dell'Amico

PhD student: Javier Mateos López

ACADEMIC YEAR 2020-2021



Dr. Luca Dell'Amico, RTD-B at the department of Chemical Sciences:

I state that the present study, entitled “*Unlocking the Synthetic Potential of Light Excited Aryl Ketones*”, presented by Javier Mateos López to receive the degree of Doctor, has been carried out under my supervision at the Università degli Studi di Padova from September 2017 to September 2021.

Padova, September the 27th 2021

Doctoral Thesis Supervisor

Dr Luca Dell'Amico

Abstract

The carbonyl system is one of the most prevalent functional groups in Nature. It is present in several classes of organic compounds that are essential for our daily life. Specifically, aryl ketones are a paradigmatic case of study in terms of photophysical and photochemical applications. Their use in synthetic photochemistry has been studied in detail during the 20th century. This thesis deals with the development of previously unexplored synthetic methods enabled by using new technologies. In particular, the utilization of microfluidic photoreactors enhanced the synthetic performance and scalability of several photochemical methods, *e.g.*, Paternò–Büchi and photoenolization/Diels–Alder processes, while opening the way to unprecedented reactivity. Additionally, the careful mechanistic analysis of the occurring processes has been of pivotal importance during my PhD studies. Thus, the diastereoselectivity prediction for dearomative Paternò–Büchi reactions, the development of versatile organic photocatalysts and the investigation of challenging trifluoromethoxylation reactions have been studied on a rationale basis.

Acknowledgments

“El hombre sabio querrá estar siempre con quien sea mejor que él.”

Platón, ca. 380 aC

Alegoría de la caverna, libro VII de la República

I always try to learn as much as I can from everyone who is around me. For this reason, I would like to acknowledge to all the people I had the pleasure to know during these four years. However, some of them had a special influence in my personal and scientific development.

I must start thanking my supervisor, Luca Dell’Amico, for all the assistance and advice he gave me during these years. The experience I gained during this period is unvaluable. You achieved the main goal that every PhD thesis supervisor should envisage: I feel prepared for the next steps of my scientific career.

I thank my PhD visiting period supervisor, Tobias Ritter. It was impressive the incredible amount of knowledge he transmitted me in only six months.

I would also like to acknowledge Andrea Sartorel for the fruitful scientific discussions we had along these years.

També li he d’agrair, d’una manera molt especial, a qui considero un dels millors mentors (i amics) que et pots trobar en un món tan caòtic com el de la ciència, el Xavi. Guardo molt curiosament tots els consells que m’has regalat, sigui a la terrassa del Mandrilo, en una taula del “Pippo” o mirant qualsevol partit del Barça. Moltes gràcies per ajudar-me a construir el que sóc ara. Tinc molt clar en quin tipus de *geni* em vull convertir. Espero poder transmetre aquesta idea a tanta gent com fas tu.

Aunque la transferencia de conocimiento no es tan fácil como muchos quisieran, todo el tiempo que pasé trabajando con Fabio fue uno de los momentos de mi doctorado que más aprendí. Muchas gracias por enseñarme tanto, por todos los momentos discutiendo en la pizarra y por haber hecho que el tándem funcionase a buen ritmo. De Mülheim, no solo me llevo química, sino haber conocido a un gran científico y amigo. Mucha suerte en tus nuevas etapas, eres un gran ejemplo a seguir.

Gracias por todas las chelas Alberto, contigo ha sido con quien más experiencias he compartido estos años, aquí no hay espacio para todas. Recuerdo muy especialmente todas y cada una de ellas, aunque en algunas no nos pudiéramos levantar al día siguiente. Aún así, si alguien está leyendo esto y quiere aprender algo de química “*útil de verdad*”, permíteme que te recomiende como profesor.

Muchísimas gracias Sara, has sido un apoyo increíble este último año. Jamás imaginé poder aprender tanto en el tramo final del doctorado.

Grazie mille Pedrito, sei il migliore amico e compagno d'avventure che si possa desiderare. Mi mancherai tantissimo (e anche le tue torte salate). Non sono stato in grado di imparare tanto quanto avrei voluto imparare da te, tre anni sono stati pochissimi. Ma sono sicuro che troveremo qualche momento per tornare a riunire a i “tres mosqueteros”.

Grazie Francesco, sei il genio più in forma che abbia mai conosciuto (e che mai conoscerò di sicuro). Ho sempre trovato incredibile la tua capacità di finire progetti senza lamentarti mentre mi facevi a pezzi salendo i colli Euganei.

I would also like thank to all the amazing friends I did in the lab for such amazing experiences: Suva, Alessio C, Alessio CC, Michi, Tommi, Edo, Philipp, Tim, Samira and Johannes. And also to all the people that I had the pleasure to meet during the period they stayed in the lab: Nicholas, Philip, Davide, Lorenzo M, Lorenzo R, Giorgia, Gian Luca, Federica and Angelo.

“[...] el Amor no sólo es el más antiguo de los dioses y el de mayor dignidad sino también el más eficaz para que los hombres, tanto vivos como muertos, consigan virtud y felicidad.”

*Platón, ca. 380 aC
Symposium*

Agradezco enormemente todo el cariño que he recibido de parte de mi familia durante estos años. Gracias a mis abuelos: Andrés y Marina, me hubiese gustado que vieseis esta aventura acabar; y Emilio y Catalina, por preocuparos por mi en todo momento. Muchas gracias a mis tíos y primos, en especial a mi tía Amparo y mi prima Beatrice. Fuisteis mis hadas madrinas en uno de los momentos más extraños que he vivido. Gracias por hacer que diez días de cuarentena en Alemania pareciesen horas.

Muchísimas gracias a mis padres. Nada de esto hubiese sido posible sin vosotros. Este es el fruto de 24 años de escolarización, pero también de 27 años de amor y esfuerzo. Gracias por enseñarme tantas cosas, sois el claro ejemplo de trabajo duro. Gracias Borja, por todos los consejos que me has dado desde pequeño y por haber sido siempre el espejo donde mirarme. ¡Os quiero mucho!

Finalment, tot això tampoc hagués estat possible sense qui considero el vuitè far de Menorca i la veritable llum d'aquesta tesi. Gràcies Maria per aguantar tots els meus mals moments, ajudar a aixecar-me i il·luminar les noves aventures. És molt fàcil continuar pel bon camí quan ets tu qui el guia. T'estimo.

List of Publications

Publications covered in this thesis – reversed chronological order:

11. Duhail, T.; Bortolato, T.; Mateos, J.; Anselmi, E.; Jelier, B.; Togni, A.; Magnier, E.; Dagousset, G.; Dell'Amico, L.
Radical α -Trifluoromethoxylation of Ketones under Batch and Flow Conditions by Means of Organic Photoredox Catalysis.
Org. Lett. **2021**, *23*, 7088-7093
(Chapter IV – Section 2)
10. Mateos, J.; Cuadros, S.; Vega-Peñaloza, A.; Dell'Amico, L.
Unlocking the Synthetic Potential of Light-Excited Aryl Ketones: Applications in Direct Photochemistry and Photoredox Catalysis.
Synlett **2021**. DOI: 10.1055/a-1403-4613.
(Chapter I)
9. Franceschi, P.; Mateos, J.; Vega-Peñaloza, A.; Dell'Amico, L.
Microfluidic Visible-Light Paternò-Büchi Reaction of Oxindole Enol Ethers.
Eur. J. Org. Chem. **2020**, 2020, 6718–6722.
(Chapter II – Section 2)
8. Vega-Peñaloza, A.; Mateos, J.; Companyó, X.; Escudero-Casao, M.; Dell'Amico, L.
A Rational Approach to Organo-Photocatalysis: Novel Designs and Structure-Property Relationships.
Angew. Chem. Int. Ed. **2021**, *60*, 1082–1097.
(Chapter IV – Introduction)
7. Mateos, J.; Vega-Peñaloza, A.; Franceschi, P.; Rigodanza, F.; Andreetta, P.; Companyó, X.; Pelosi, G.; Bonchio, M.; Dell'Amico, L.
A Visible-Light Paternò-Büchi Dearomatisation Process towards the Construction of Oxeto-Indolinic Polycycles. *Chem. Sci.* **2020**, *11*, 6532–6538.
(Chapter II – Section 1)
6. Mateos, J.; Rigodanza, F.; Vega-Peñaloza, A.; Sartorel, A.; Natali, M.; Bortolato, T.; Pelosi, G.; Companyó, X.; Bonchio, M.; Dell'Amico, L.
Naphthochromenones: Organic Bimodal Photocatalysts Engaging in Both Oxidative and Reductive Quenching Processes.
Angew. Chem. Int. Ed. **2020**, *59*, 1302–1312.
(Chapter IV – Section a)
5. Mateos, J.; Meneghini, N.; Bonchio, M.; Marino, N.; Carofiglio, T.; Companyó, X.; Dell'Amico, L.
Microfluidic Light-Driven Synthesis of Tetracyclic Molecular Architectures.
Beilstein J. Org. Chem. **2018**, *14*, 2418–2424.
(Chapter III – Section 2)

4. Mateos, J.; Cherubini-Celli, A.; Carofiglio, T.; Bonchio, M.; Marino, N.; Companyó, X.; Dell'Amico, L.
A Microfluidic Photoreactor Enables 2-Methylbenzophenone Light-Driven Reactions with Superior Performance.
Chem. Commun. **2018**, 54, 6820–6823.
(Chapter II – Section 1)

Publications published during the doctoral period not covered in this thesis – reversed chronological order:

3. Juliá, F.; Shao, Q.; Duan, M.; Plutschack, M. B.; Berger, F.; Mateos, J.; Lu, C.; Xue, X-S.; Houk, K.N.; Ritter, T.
High Site Selectivity in Electrophilic Aromatic Substitutions: Mechanism of C–H Thianthrenation.
J. Am. Chem. Soc., **2021**, DOI: 10.1021/jacs.1c06281
2. Cherubini-Celli, A.; Mateos, J.; Bonchio, M.; Dell'Amico, L.; Companyó, X.
Transition Metal-Free CO₂ Fixation into New Carbon-Carbon Bonds.
ChemSusChem **2018**, 11, 3056–3070.

Publications published prior to Padova not covered in this thesis:

1. Gavara, R.; Mateos, J.; Sabaté, F.; Belda, R.; Llinares, J. M.; García-España, E.; Rodríguez, L.
Luminescent Supramolecular Heterometallic Macrocycles and Their Encapsulation on Cholate Gels: Luminescent Supramolecular Heterometallic Macrocycles and Their Encapsulation on Cholate Gels.
Eur. J. Inorg. Chem. **2018**, 2018, 4550–4555.

Abbreviations

In the following pages, a list of abbreviations and acronyms used along the thesis is summarized.

2-MBP:	2-Methylbenzophenone
3D:	three dimension
A:	Absorption
Ac:	Acetyl
Ace:	Acetone
Ar:	Aryl substituent
ASAP:	Atmospheric solids analysis probe
BC:	Before Christ
BDE:	Bond dissociation energy
Bn:	Benzyl
Boc:	tert-butoxycarbonyl
BP:	Benzophenone
Cbz:	benzyloxycarbonyl group
CFL:	Compact fluorescent lamp
CV:	Cyclic voltammetry
Cy:	Cyclohexyl
Cz:	Carbazole
de:	Diastereomeric excess
DFT:	Density functional theory
dr:	Diastereomeric ratio
DMAP:	4-Dimethylaminopyridine
DMF:	Dimethylformamide
DMSO:	Dimethylsulfoxide
E:	Energy
E_T:	Triplet energy
EDA:	Electron-donor acceptor
EDG:	Electron-donating group
EnT:	Energy transfer
equiv.:	equivalents
ESI:	Electrospray ionization
Et:	Ethyl
EtOAc:	Ethyl acetate
EtOH:	Ethanol
EWG:	Electron-withdrawing group
F:	Fluorescence
Fc:	Ferrocene
GC:	Gas chromatography
HAT:	Hydrogen atom transfer

HOMO:	Highest occupied molecular orbital
HRMS:	High-resolution mass spectrometry
IC:	Internal conversion
ID	Internal diameter
<i>i</i>Pr:	Isopropyl substituent
IR:	Infrared
ISC:	Intersystem crossing
IUPAC:	International Union of Pure and Applied Chemistry
LED:	Light-emitting diode
LFER:	Linear free energy relationship
LFP:	Laser flash photolysis
LUMO:	Lowest unoccupied molecular orbital
Me:	Methyl
MeCN:	Acetonitrile
MFP:	Microfluidic photoreactor
MO:	Molecular orbital
NBO:	Natural bond orbital
NMR:	Nuclear magnetic resonance
NTC:	Naphthochromenone
Nu:	Nucleophile
OD:	Optical density
Ox:	Oxidation
P:	Phosphorescence
PB:	Paternò-Büchi
PC:	Photocatalyst
PES:	Potential energy surface
PET:	Photo-induced electron transfer
PG:	Protecting group
Ph:	Phenyl
PhMe:	Toluene
r-c:	radical-chain
Red:	Reduction
rt:	Room temperature
S:	Singlet
SCE:	Standard calomel electrode
SEE:	Silyl enol ether
STY:	Space-time yield
T:	Temperature
T₁:	First triplet excited state
TBAF:	Tetra <i>n</i> -butylammoniumfluoride
TBS:	<i>tert</i> -butyldimethylsilyl
TD-DFT:	Time-dependent density functional theory
TFA:	Trifluoroacetic acid
THF:	Tetrahydrofuran
TIPS:	Triisopropylsilyl
TLC:	Thin layer chromatography

TMS:	Trimethylsilyl
TOF:	Time of flight
UV:	Ultraviolet
TBS:	tert-butyl dimethyl silyl group
Tf:	Trifluoromethanesulfonyl
VB:	Valence bond
Vis:	Visible
VR:	Vibrational relaxation

Table of Contents

Chapter I

<i>Introduction and Objectives – From Excited Aryl Ketone Chemistry to Flow Photochemistry</i>	- 1 -
1. The “nature of light”	- 2 -
Goals of this PhD thesis	- 3 -

Chapter I – Section 1

<i>Introduction – Photochemistry of Aryl Ketones</i>	- 5 -
1.1.1 Structure of aryl ketones	- 6 -
1.1.2 Photophysics of aryl ketones	- 7 -
1.1.3 Reactivity of aryl ketones in the ground state – a brief overview	- 10 -
1.1.4 Reactivity of aryl ketones in the excited state	- 12 -

Chapter I – Section 2

<i>Introduction – Flow Photochemistry</i>	- 27 -
1.2.1 Importance of the experimental set-up in photochemical reactions	- 28 -
1.2.2 Fundamentals of flow set-ups	- 28 -
1.2.3 Main advantages of flow over batch setups in photochemical processes	- 30 -

Chapter II

<i>Synthetic Transformations Driven by Triplet State Benzophenones</i>	- 35 -
2. The Paternò-Büchi reaction	- 36 -

Chapter II – Section 1

<i>Dearomative Paternò-Büchi Reaction – Towards the construction of Oxeto-Indolinic Polycycles</i>	- 39 -
2.1.1 Introduction	- 40 -
2.1.2 Challenges of the project	- 41 -
2.1.3 Section overview	- 42 -

2.1.4 Results and discussion	- 43 -
2.1.5 Conclusions	- 55 -
2.1.6 Experimental Section	- 56 -

Chapter II – Section 2

<i>Dearomative Paternò-Büchi Reaction – Microfluidic Visible-Light Dearomatization of Oxindole Enol Ethers</i>	- 85 -
2.2.1 Introduction	- 86 -
2.2.2 Challenges of the project	- 87 -
2.2.3 Section overview	- 88 -
2.2.4 Results and discussion	- 89 -
2.2.5 Conclusions	- 95 -
2.2.6 Experimental Section	- 96 -

Chapter II – Section 3

<i>Dearomative Paternò-Büchi Reaction – The Effect of Visible-Light Irradiation on the Reaction Manifold</i>	- 121 -
2.3.1 Introduction	- 122 -
2.3.2 Challenges of the project	- 125 -
2.3.3 Section overview	- 125 -
2.3.4 Results and discussion	- 125 -
2.3.5 Conclusions	- 139 -
2.3.6 Experimental Section	- 140 -

Chapter III

<i>Synthetic Transformations Driven by Triplet State o-Alkyl Substituted Benzophenones</i>	- 147 -
3. The photoenolization process	- 148 -

Chapter III – Section 1

<i>Microfluidic Photoreactors – Unveiling the Superior Performances of 2-Methylbenzophenone Light-Driven Reactions</i>	- 151 -
3.1.1 Introduction	- 152 -
3.1.2 Challenges of the project	- 153 -

3.1.3 Section overview	- 153 -
3.1.4 Results and discussion	- 153 -
3.1.5 Conclusions	- 163 -
3.1.6 Experimental Section	- 164 -

Chapter III – Section 2

<i>Microfluidic Photoreactors – Light-Driven Synthesis of Tetracyclic Molecular Architectures</i>	- 175 -
3.2.1 Introduction	- 176 -
3.2.2 Challenges of the project	- 177 -
3.2.3 Section overview	- 177 -
3.2.4 Results and discussion	- 178 -
3.2.5 Conclusions	- 182 -
3.2.6 Experimental Section	- 183 -

Chapter III – Section 3

<i>Microfluidic Photoreactors – Light-Driven Construction of Naphthochromenones as a New Potential Class of Photocatalysts</i>	- 195 -
3.3.1 Introduction	- 196 -
3.3.2 Challenges of the project	- 196 -
3.3.3 Section overview	- 196 -
3.3.4 Results and discussion	- 197 -
3.3.5 Conclusions	- 202 -
3.3.6 Experimental Section	- 203 -

Chapter IV

<i>The Evolution of Aryl Ketone-Derived Products – Applications in Organophotoredox Catalysis</i>	- 219 -
4. Introduction to photocatalysis	- 220 -

Chapter IV – Section 1

<i>Organophotoredox Catalysis – Structure-Activity Relationships in Organic Photoredox Catalysis</i>	- 227 -
4.1.1 Introduction	- 228 -

4.1.2 Challenges of the project	- 228 -
4.1.3 Section overview	- 229 -
4.1.4 Results and discussion	- 230 -
4.1.5 Conclusions	- 251 -
4.1.6 Experimental Section	- 252 -

Chapter IV – Section 2

<i>Photoredox Catalysis – Radical α-Trifluoromethoxylation of Ketones.....</i>	- 273 -
4.2.1 Introduction	- 274 -
4.2.2 Challenges of the introduction of OCF ₃ moieties	- 275 -
4.2.3 Section overview	- 277 -
4.2.4 Results and discussion	- 278 -
4.2.5 Conclusions	- 286 -
4.2.6 Experimental Section	- 287 -

General Conclusions and Future Perspectives.....	- 311 -
---	---------

A mis padres

Chapter I

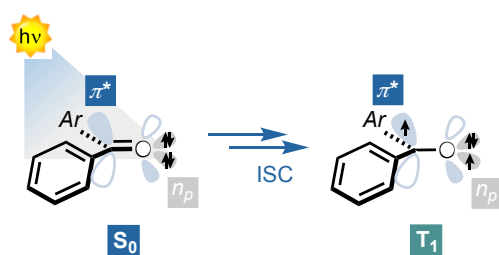
Introduction and Objectives–

From Excited Aryl Ketone Chemistry to Flow Photochemistry

— **Chapter I - General Overview – Introduction to Excited Aryl Ketone Chemistry and Flow Photochemistry** —

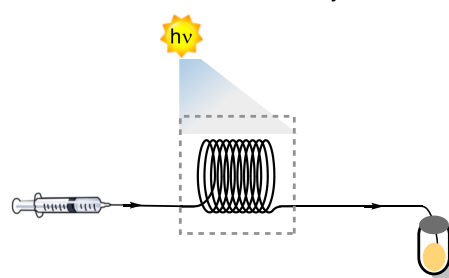
Section 1.

Introduction to Aryl Ketone Photochemistry



Section 2.

Introduction to Flow Photochemistry



Publications:

Section 1: Mateos, J.; Cuadros, S.; Vega-Peñaloza, A.; Dell'Amico, L. *Unlocking the Synthetic Potential of Light-Excited Aryl Ketones: Applications in Direct Photochemistry and Photoredox Catalysis.*, *Synlett*, **2021**. DOI: 10.1055/a-1403-4613.

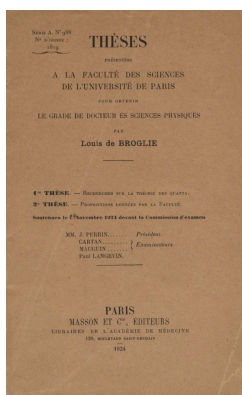
1. The “nature of light”

Humanity has been enlightened by the properties of light since the very beginning of civilizations. Two of the most notable Mediterranean civilizations in classical antiquity were the Phoenicians and the Greek city states.¹ The prefix *photo-* (which, nowadays, refers to light-related topics and has been adopted from greek) perfectly defines the interest of this culture on “*the nature of light*”. In fact, one of the most famous contemporary scientific debates derives from their society.

The logic behind “*the nature of light*” was initially formulated by Plato in his “*emission theory*” ca. 400 years BC.² Then, his student Aristotle updated the theory considering a “*state of actual transparency in a potentially transparent medium*”.³ Nevertheless, our modern understanding of light derives from the scientific revolution of the 17th century, when Sir Isaac Newton (1643-1747) and Christiaan Huygens (1629-1695) clashed on the nature of light. On the one hand, the first proposed that light behaved as “*a shower of particles*” in his corpuscular theory. On the other hand, the second centered his arguments towards the wave-like nature of light.⁴

— The nature of light —

A. de Broglie PhD thesis - wave-particle theory of matter



B. 5th Solvay conference picture taken by Irving Langmuir in 1927

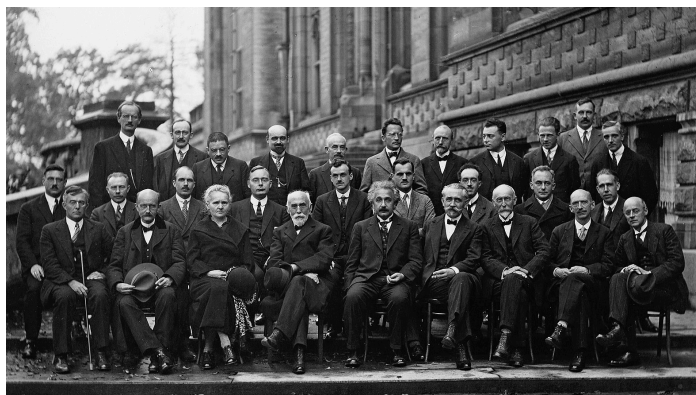


Figure 1.1. - Moments that defined the modern conception of “*light*”. a) PhD thesis of Louis-Victor de Broglie (1924). b) Attendants of the 5th Solvay Congress “*Electrons and Photons*” (1927).

¹ Malkin, I. *Mediterranean Paradigms and Classical Antiquity*; Taylor and Francis: Hoboken, **2013**.

² Winer, G. A., Cottrell, J. E., Gregg, V., Fournier, J. S., Bica, L. A. *Fundamentally misunderstanding visual perception: Adults' beliefs in visual emissions*. *American Psychologist*, **2002**, 57, 417-424.

³ Lewis, N. "Robert Grosseteste", *The Stanford Encyclopedia of Philosophy*; Edward N. Zalta, **2021**.

⁴ Aspect, A. From Huygens' Waves to Einstein's Photons: Weird Light. *Comptes Rendus Physique* **2017**, 18, 498–503.

The understanding of the “*nature of light*” was pushed forward by the works of Max Planck and Alfred Einstein at the beginning of the 20th century. Remarkably, the pinnacle of this debate was reached in 1924 with the publication of the PhD thesis of Louis-Victor de Broglie entitled “*Recherches sur la théorie des quanta*” (Figure 1.1a). In his dissertation, de Broglie included the wave-particle duality theory of matter for the first time.⁵ This research topic was selected as the general theme of the 5th Solvay congress in 1927 entitled “*Electrons and Photons*”.⁶ Indeed, one of the most famous pictures of modern science was taken during this congress by the Nobel prize Irving Langmuir (Figure 1.1b). Arising from these intense debates, Gilbert N. Lewis popularized the term “*photons*” in 1926.⁷ Despite there are numerous scientific studies using light prior to the 5th Solvay congress,⁸ the understanding of “*photon*” as an elemental particle with an associated energy, expanded the horizons of several research fields. In fact, photochemistry, which is described by the IUPAC as “*the branch of chemistry concerned with the chemical effects of light (far UV to IR)*” seized this knowledge to develop and understand novel light-triggered processes.⁹

Goals of this PhD thesis

The general definition of photochemistry allows me to introduce the focus and objectives of this PhD thesis. The light-excitation of molecules triggers the development of novel transformations. In line with this idea, the main goal of the research I conducted over my doctoral studies is to enlarge the synthetic organic chemist toolbox by providing new avenues to the chemistry of light-excited molecules, and in particular aryl ketones. To do so, all the photochemical reactions reported in this work have a mechanistic rationale behind, providing valuable information about the reported transformations, while paving the way to further developments.

This PhD thesis is divided in four main chapters:

- **Chapter I:** The goal of this chapter is to introduce the main concepts and processes happening in synthetic organic photochemistry. This introductory part is mainly focused on: *i*) the use of aryl ketones such as benzophenone, and *ii*) the importance of microfluidic photoreactors in modern synthetic chemistry mediated by light.

⁵ de Broglie, L. *Recherches sur la Théorie des Quanta*, PhD Thesis, Masson, Paris, 1924.

⁶ VI. General Discussion At The Fifth Solvay Conference. In *Niels Bohr Collected Works*; Elsevier, 1985; 6, 99–106.

⁷ Lewis, G. N. *The Conservation of Photons*. *Nature* 1926, 118, 874–875.

⁸ Ciamician, G. *The Photochemistry of the Future*. *Science* 1912, 36, 385–394.

⁹ *The IUPAC Compendium of Chemical Terminology: The Gold Book*, 4th ed.; Gold, V., Ed.; International Union of Pure and Applied Chemistry (IUPAC): Research Triangle Park, NC, 2019. p. 2259

- **Chapter II:** This chapter focuses on the utilization of aryl ketones for the development of novel visible-light indole-dearomatization processes. The goal of this section is to define general and selective transformations by combining diverse techniques for the elucidation of the operative reaction manifold.
- **Chapter III:** In this part of the dissertation, novel microfluidic photoreactors have been reported to exploit the photochemistry of 2-alkylbenzophenones and explore undeveloped manifolds with coumarins. The objective of Chapter III is to define the importance of flow photochemistry in the reactivity of light-excited aryl ketones to produce scaffolds with interesting relevant properties as photoredox catalysts.
- **Chapter IV:** In this chapter, organic photocatalysis is introduced. By presenting this topic, structure-property relationships of novel photocatalysts can be defined. Hence, the goal is to develop general and redox-balanced sensitizers capable to engage in both oxidative and reductive processes with a high synthetic potential for the development of new transformations such as the trifluoromethoxylation of ketones.

Chapter I – Section 1

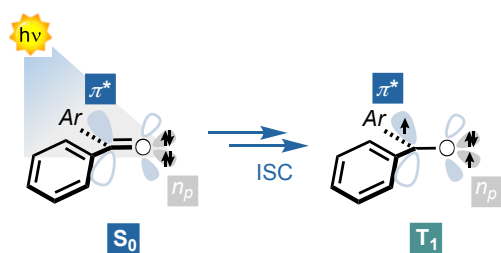
Introduction –

Photochemistry of Aryl Ketones

– Chapter I - General Overview – Introduction to Excited Aryl Ketone Chemistry and Flow Photochemistry

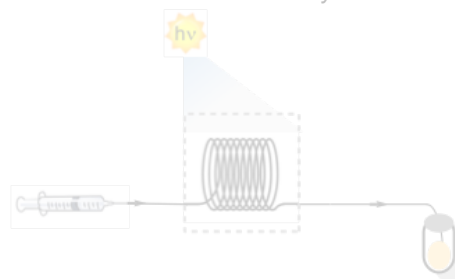
Section 1.

Introduction to Aryl Ketone Photochemistry



Section 2.

Introduction to Flow Photochemistry



- Here I define the main photophysical properties of aryl ketones and summarize the modern techniques used for its characterization.
- I summarize the diverse type of reactions triggered by excited-aryl ketones.

1.1.1 Structure of aryl ketones

An aryl ketone can be defined as “an aromatic ring with a carbonyl substituent” where the simplest molecular formula is C_7H_5O (Figure 1.2).¹⁰ This type of carbonyl compounds differ from aliphatic ketones (substituted with alkylic chains) on the characteristic aryl ring pending from the sp^2 -hybridized carbon of the carbonyl moiety. Depending on the nature of the second carbonyl substituent such type of compounds can be divided as benzaldehyde derivatives **1** ($R^1=H$), acetophenone derivatives **2** ($R^1=Alk$) or benzophenone (BP) derivatives ($R^1=Ar$) **3**. Additionally, diverse functional groups can be attached to the R^1 position, (e.g. carbonyls or unsaturated chains). Nevertheless, due to the diverse photochemical properties of these compounds, they are not discussed in this introduction.

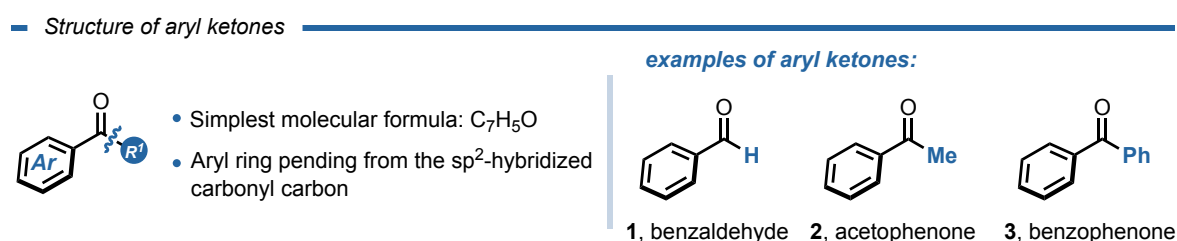


Figure 1.2. - Molecular structure of aryl ketones.

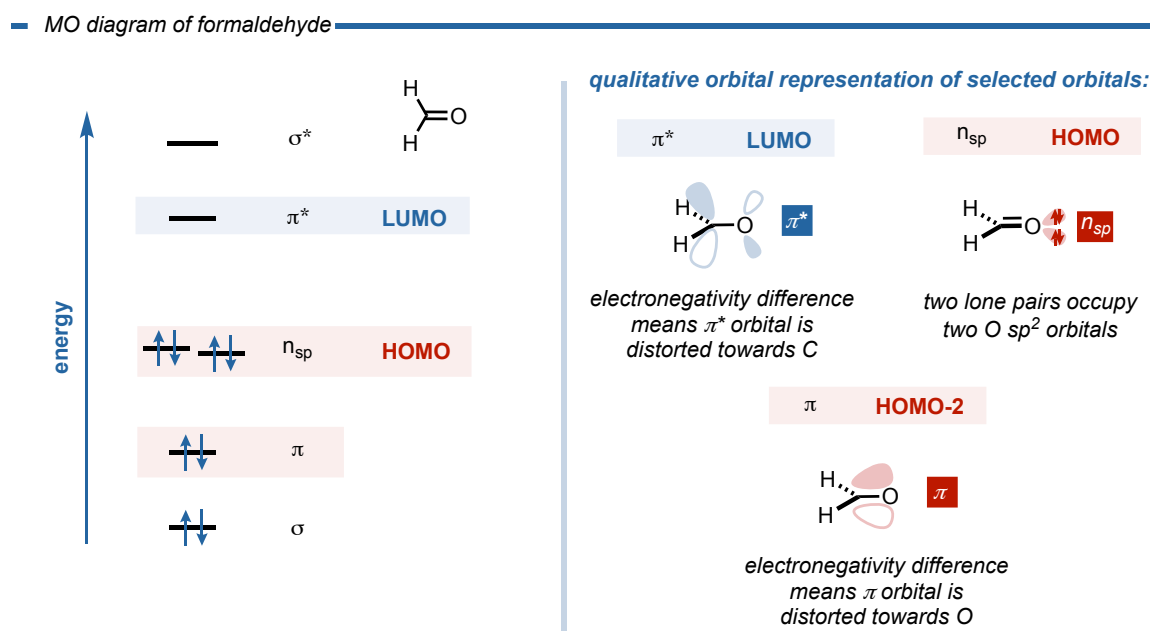


Figure 1.3. - Orbital energy diagram of formaldehyde and qualitative representation of the key orbitals.

¹⁰ Pretsch, E.; Bühlmann, P.; Badertscher, M. *Structure Determination of Organic Compounds: Tables of Spectral Data*, 4th, rev.enl. ed ed.; Springer: Berlin, 2009, p. 36.

Apart from the molecular composition of aryl ketones, the molecular orbital (MO) energy diagram of carbonyls are crucial to understand their reactivity and photophysics (Figure 1.3).¹¹ Indeed, the key orbitals to understand both the excited- and ground- state reactivities of carbonyl compounds are the n_{sp} and the π^* orbitals.¹² The first, is located at the unbound electrons of the carbonyl oxygen (HOMO). The second is located at the Csp^2 and the O atoms of the carbonyl, and distorted towards the carbon atom (LUMO). However, also the π orbital (HOMO-2) makes the difference in terms of photochemical properties when comparing with aliphatic ketones (*vide infra*).¹³

1.1.2 Photophysics of aryl ketones

Light absorption

Light absorption is the essential phenomena of photochemistry. Indeed, it is the initial interaction between a molecule and a photon. It occurs when light is absorbed from a molecular structure, accepting the energy from the electromagnetic field stimulating diverse processes. The energy (E) of such photons is defined by equation 1 in Figure 1.4, where h is the Planck constant and ν is the wavenumber, defined by equation 2.¹³ This energy can change the initial state of a molecule (S_0) to a more energetic state (*i.e* S_1 when the absorption A is equal to E_1 energy or S_2 when using E_2 energy) as depicted in the simplified Jablonski diagram of Figure 1.4.¹⁴

From a synthetic perspective, the absorption of the reaction mixture is crucial to determine the energy needed to trigger a photochemical reaction. For instance, the use of highly energetic light-sources, emitting in the UV region (<400 nm, $E > 71.5$ kcal·mol⁻¹), can decompose both products and starting materials. On the other hand, the use of poorly energetic sources, emitting in the IR region (>700 nm, $E < 40.9$ kcal·mol⁻¹), can lead to unsubstantial changes in the transformation. For this reason, the common technique for the determination of the absorption is the absorption spectroscopy. This method is based on the Lambert-Beer law (equation 3 in Figure 1.4) where the absorbance of a sample at a given wavelength depends

¹¹ Klessinger, M.; Michl, J. *Excited States and Photochemistry of Organic Molecules*; VCH: New York, **1995**. p. 1 – 62.

¹² Clayden, J.; Greeves, N.; Warren, S. G. *Organic Chemistry*, 2nd ed.; Oxford University Press: Oxford ; New York, **2012**. p. 81 – 106.

¹³ Turro, N. J.; Ramamurthy, V.; Scaiano, J. C. *Modern Molecular Photochemistry of Organic Molecules*; University Science Books: Sausalito, California, **2010**.

¹⁴ The description of this process is behind the scope of this thesis and has been widely studied in literature. For a more detailed discussion on this process see: Klessinger, M.; Michl, J. *Excited States and Photochemistry of Organic Molecules*; VCH: New York, **1995**. p. 243 – 308.

on the concentration of the absorbing compound. Thus, the distance (*l*) and the concentration (*c*) defines the absorbance of the sample.

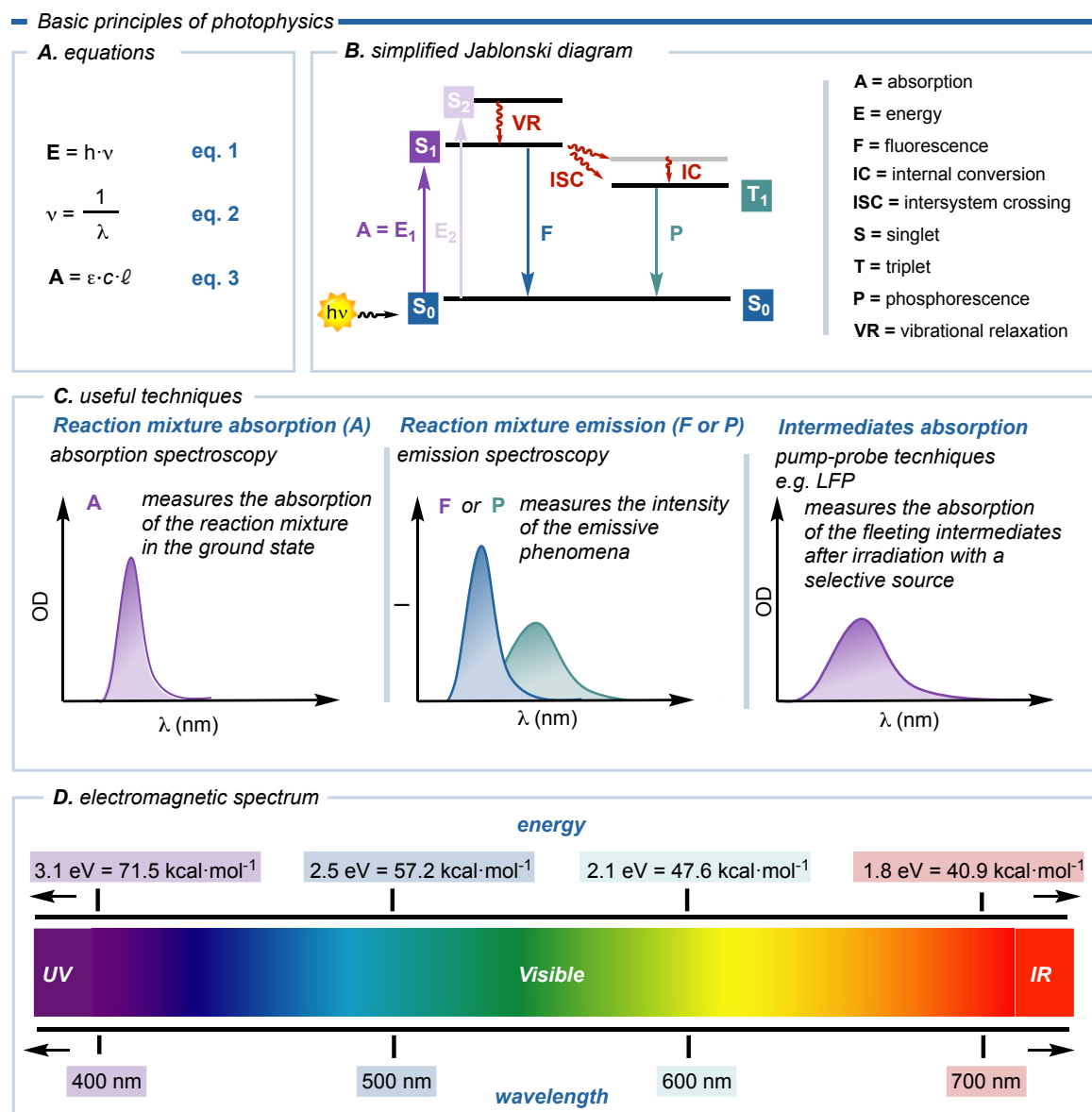


Figure 1.4. - Basic principles of photophysics. a) basic equations, b) simplified Jablonski diagram and compendium of the processes and states, c) useful techniques used in synthetic photochemistry and d) electromagnetic spectrum.

Light emission

After excitation from the ground state to a higher electronic excited state, the molecule can suffer different unimolecular deactivation processes to dissipate the absorbed energy. Such processes can be depicted in a simplified Jablonski diagram (Figure 1.4).¹⁵ In this case, the diagram schematically displays the singlet S₀, S₁ and S₂, and the triplet T₁ configurations.

¹⁵ Lakowicz, J. R., In *Principles of Fluorescence Spectroscopy*; Ed.; Springer US: Boston, MA, 2006; p. 1–26.

- On one hand, from the S_1 state, the molecule can return to the ground state by fluorescence (F). This type of energetic decay is known as radiative decay, since the “loss” of energy is transferred by emitting photons. The energy of the emitted photons can be determined by using a fluorimeter.¹⁵
- On the other hand, the S_1 state can reach the T_1 state by intersystem crossing (ISC), and after losing the excess of vibrational energy it can decay to the ground state by emitting photons by phosphorescence (P). The energy of the emitted photons can be determined by emission spectroscopy or, if required, by more advanced techniques such as laser flash photolysis (LFP).¹⁶
- Additionally, diverse radiationless transitions as for example internal conversion (IC), can occur. In this case, the excited molecule loses energy by vibrational relaxation (VR).

Case of study – benzophenone

Light excited states do not have to be considered only as more energetic forms of molecules.¹⁷ They must be considered as new chemical entities due to their new electronic distribution (from fully occupied or unoccupied to singly occupied orbitals). In fact, the one-electron molecular orbital representation is an exceptional tool to assess these new features (Figure 1.5a).¹¹ One of the main examples, where the excited-state has unique photochemical features and is considered as one of the main paradigms of photochemistry is found in BP.¹⁸

When a photon is absorbed by BP ($\lambda > 350$ nm, Jablonski diagram in Figure 1.5b), an electron from the nonbonding oxygen n_p orbital is promoted onto the carbonyl π^* orbital reaching the first singlet excited state ($S_0 \rightarrow S_1$, Figure 1.5c). It can also be excited with more energetic wavelengths ($\lambda > 260$ nm) promoting the π to π^* transition S_2 . Nevertheless, after IC of S_2 , it will quickly decay to S_1 (ca. 1 ps). Additionally, since the promotion from the ground state (S_0) to the first triplet excited state (T_1) is spin forbidden by El-Sayed rules,¹⁹ the latter can only be generated when passing by S_1 . Hence, after a rapid isoenergetic ISC,²⁰ an $S_1 \rightarrow T_2$ transition occurs (ca. 10-25 ps). This new vibrational level (T_2) has a triplet π - π^* character

¹⁶ Henriksen, N. E.; Engel, V. *Femtosecond Pump-Probe Spectroscopy: A Theoretical Analysis of Transient Signals and Their Relation to Nuclear Wave-Packet Motion*. *International Reviews in Physical Chemistry* **2001**, *20*, 93–126.

¹⁷ Balzani, V.; Ceroni, P.; Juris, A. *Photochemistry and Photophysics: Concepts, Research, Applications*; Wiley-VCH: Weinheim, **2014**. p. 103

¹⁸ Hoffmann, R.; Swenson, J. R. *Ground- and Excited-State Geometries of Benzophenone*. *J. Phys. Chem.* **1970**, *74*, 415–420.

¹⁹ El-Sayed, M. A. *Spin—Orbit Coupling and the Radiationless Processes in Nitrogen Heterocyclics*. *The Journal of Chemical Physics* **1963**, *38*, 2834–2838.

²⁰ Klessinger, M.; Michl, J. *Excited States and Photochemistry of Organic Molecules*; VCH: New York, **1995**. p. 251–252.

that quickly decays to a lower energy $n-\pi^*$ transition known as the T_1 state ($T_2 \rightarrow T_1$, Figure 1.5c).¹³ When compared with aliphatic ketones, the lack of aromatic ring substituents, makes the T_2 state more energetic. Hence, the described pathway is not available for such compounds, having slower ISC rates to reach T_1 directly from S_1 . Indeed, the T_1 excited state makes the difference in terms of reactivity.²¹

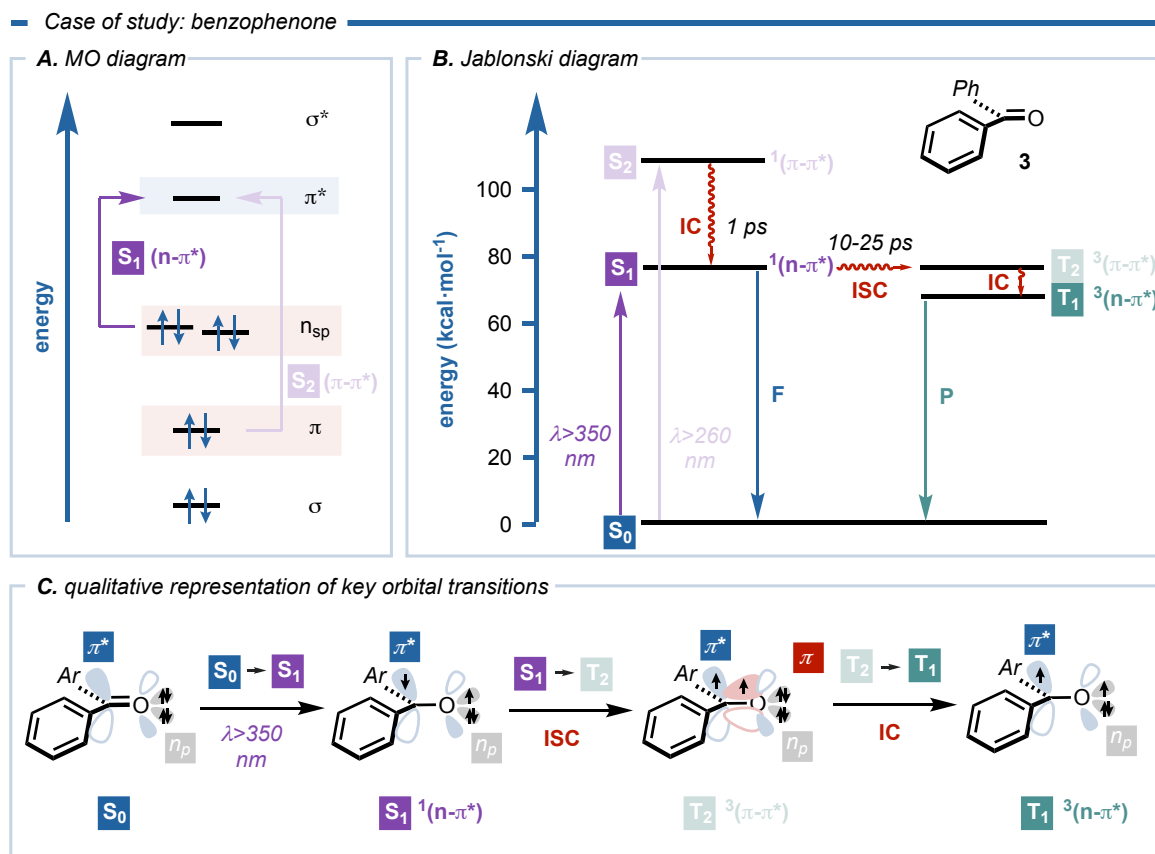


Figure 1.5. - Basic principles of benzophenone photochemistry. a) One-electron molecular orbital representation. b) Simplified Jablonski diagram. c) Qualitative representation of the key orbitals involved in the transitions.

1.1.3 Reactivity of aryl ketones in the ground state – a brief overview

The carbonyl system is one of the most prevalent functional groups in Nature. It is present in several classes of organic compounds and macromolecules that are essential in biological processes.²² The abundance of this group can be also related with the myriad of reactions where the motif is present.

²¹ Dormán, G.; Nakamura, H.; Pulsipher, A.; Prestwich, G. D. *The Life of Pi Star: Exploring the Exciting and Forbidden Worlds of the Benzophenone Photophore*. *Chem. Rev.* **2016**, *116*, 15284–15398.

²² Martin, T. W.; Derewenda, Z. S. *The Name Is Bond — H Bond*. *Nat. Struct. Biol.* **1999**, *6*, 403–406.

Reactivity explained by the molecular orbital theory

Under classical thermal reactivity, aryl ketones are prone to undergo nucleophilic addition, reduction, or reductive amination reactions (furnishing tertiary alcohols **4**, secondary alcohols **5** or tertiary amines **6**, respectively) at the carbonyl C-atom, among other remarkable transformations (Figure 1.6a).²³ Also, they can act both as a pronucleophiles (when α -enolizable positions are present, such as in the case of acetophenone **2**) or electrophiles in aldol-based chemistry (such is the case of benzaldehyde **1**).²⁴ This broad reactivity is routinely exploited for the formation of new C-C and C-heteroatom bonds within small building blocks and more complex organic molecules, and it can be easily explained by the use of molecular orbital theory.

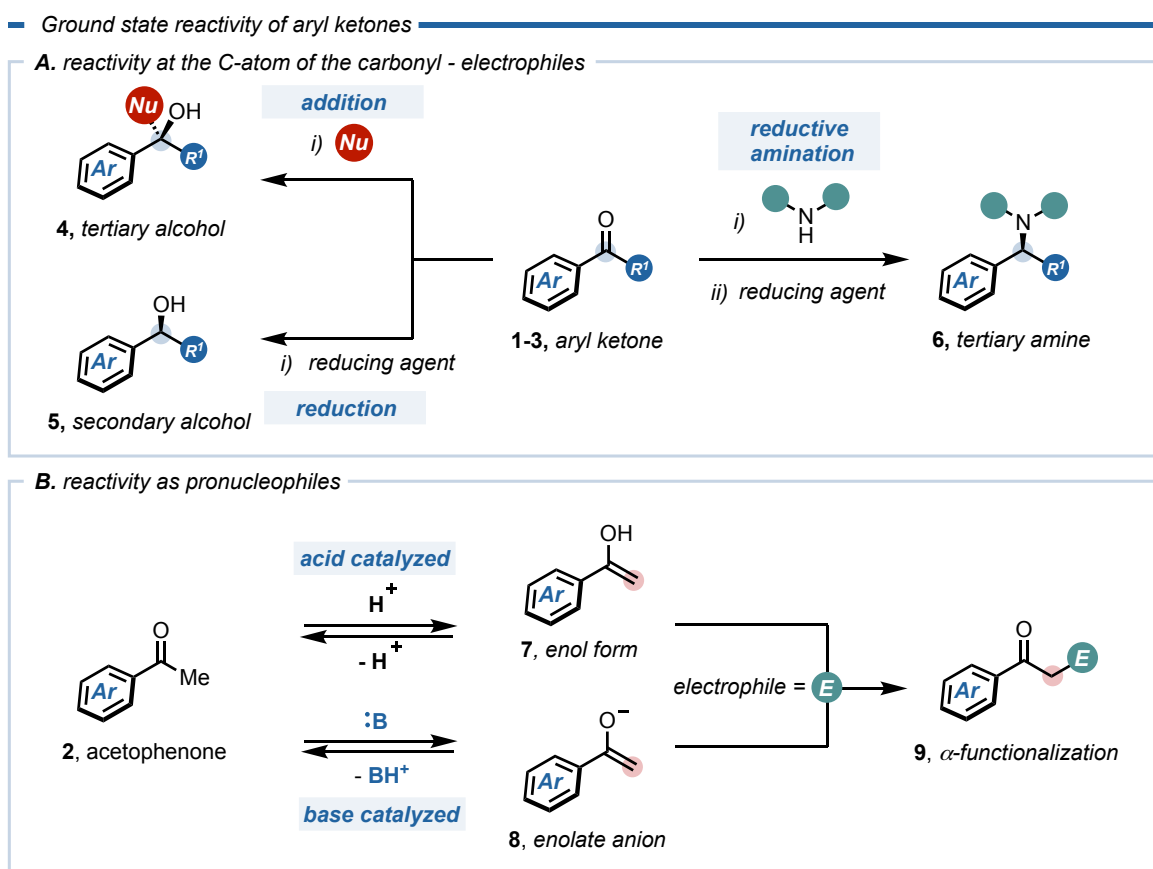


Figure 1.6. - Reactivity of aryl ketones in the ground state a) acting as electrophile or b) acting as pronucleophile.

²³ Dickens, T. K.; Warren, S. G. *Chemistry of the Carbonyl Group: A Step-by-Step Approach to Understanding Organic Reaction Mechanisms*, Second edition.; John Wiley & Sons: Hoboken, New Jersey, **2018**.

²⁴ Palomo, C.; Oiarbide, M. *The Aldol Addition Reaction: An Old Transformation at Constant Rebirth*. *Chem. Eur. J.*, **8**, **2002**, 36 – 44.

Regarding to the use of aryl ketones as electrophiles, its ground state reactivity is explained by means of the polarity difference between the carbon and oxygen atom in the C=O bond. (Figure 1.7) The C-atom, where a positive charge density is located, is prone to react with nucleophilic species. In particular, the addition of a nucleophile (Nu) to the C=O bond occurs through the overlap between the most energetic electron pair (HOMO) of the Nu and the empty π^* orbital of the carbonyl compound (LUMO) (Figure 1.7 right). This addition occurs in a given angle (107°), known as Bürgi-Dunitz trajectory.²⁵ In such event, the initial planar geometry is lost forming a tetrahedral intermediate. The structural relative arrangements of the reagents determine the final reaction outcome. Several synthetic strategies point to increase the HOMO-LUMO interaction by moving the orbitals energetically closer. In line with this assumption, carbonyl compounds can be activated by lowering the LUMO energy by means of its coordination with Lewis acids or protonation with Brønsted acids to ensure the overlap with less energetic HOMO orbitals of nucleophiles.²⁶

— Reactivity explained by the molecular orbital theory

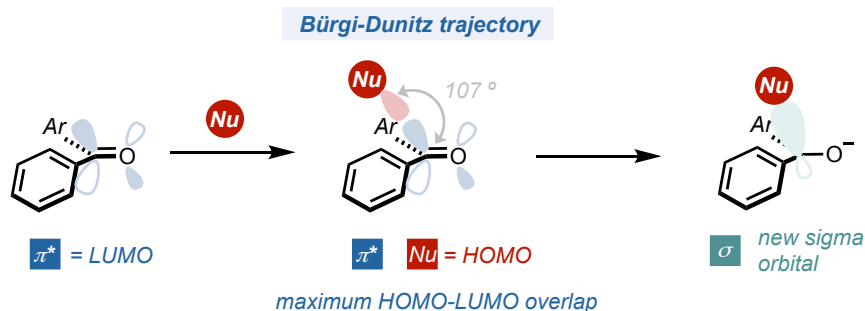


Figure 1.7. - Qualitative representation of the reactivity of aryl ketones as electrophiles using the molecular orbital theory.

1.1.4 Reactivity of aryl ketones in the excited state

The versatility the T_1 state of aryl ketones

The reactivity of the T_1 state of aryl ketones has been widely explored in the last century.²¹ The interest of the synthetic community on light-excited aryl ketones relies on the numerous applications of such reagents both as catalysts and reagents. In fact, the long lifetime (up to 3 μs in benzene) and the amphoteric character of this T_1 biradical allows its use in mechanistically diverse manifolds. These reactivity patterns can be divided in four groups (Figure 1.8):

²⁵ Bürgi, H. B.; Dunitz, J. D.; Lehn, J. M.; Wipff, G. *Stereochemistry of Reaction Paths at Carbonyl Centres*. *Tetrahedron* **1974**, *30*, 1563–1572.

²⁶ Melchiorre, P.; Marigo, M.; Carlone, A.; Bartoli, G. *Asymmetric Aminocatalysis-Gold Rush in Organic Chemistry*. *Angew. Chem. Int. Ed.* **2008**, *47*, 6138–6171.

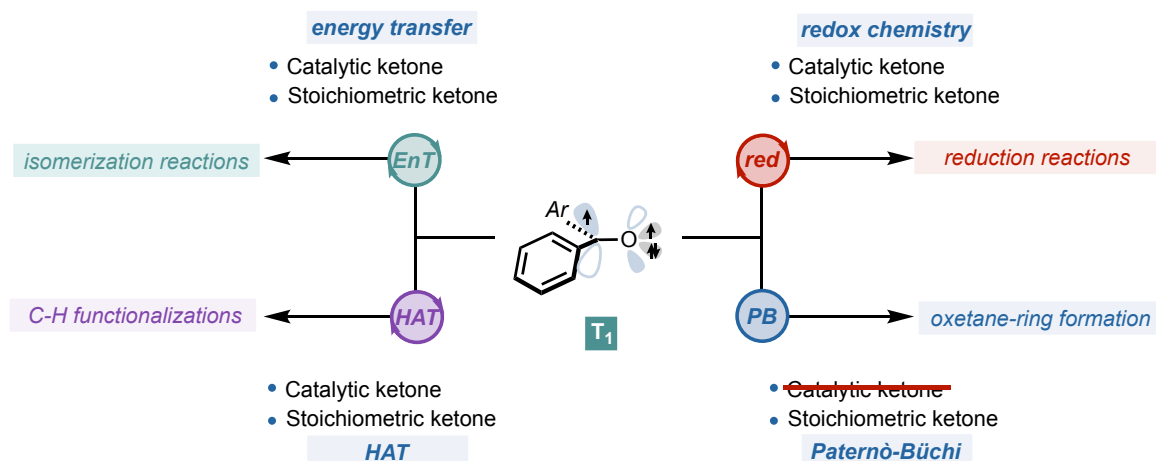


Figure 1.8. - Reactivity of the triplet state of aryl ketones.

- i) *energy transfer (EnT) mechanism*, where the aryl ketone triplet energy (E_T) sensitizes the triplet state of an additional molecule. In this type of reactions, the carbonyl compound can be used both in catalytic loadings and stoichiometric amounts, although the first case is commonly preferred. One of the main examples of its use as triplet sensitizers is in alkene isomerization reactions.²⁷ Nevertheless, sensitized homolysis²⁸ and cycloaddition²⁹ reactions have been also reported.
- ii) *hydrogen atom transfer (HAT) manifold*, where the half-filled n_p -orbital abstracts a hydrogen from a Csp^3 or an heteroatom. This reactivity has been known since 1900³⁰ and it has been an important field of study that continues to date.³¹ One of the main reasons for this interest, is the applicability of this path in the functionalization of inert aliphatic C-H bonds for the construction of complex scaffolds.³²

²⁷ Neveselý, T.; Wienhold, M.; Molloy, J. J.; Gilmour, R. *Advances in the E → Z Isomerization of Alkenes Using Small Molecule Photocatalysts*. *Chem. Rev.* **2021**, DOI: acs.chemrev.1c00324.

²⁸ Teders, M.; Henkel, C.; Anhäuser, L.; Strieth-Kalthoff, F.; Gómez-Suárez, A.; Kleinmans, R.; Kahnt, A.; Rentmeister, A.; Guldi, D.; Glorius, F. The Energy-Transfer-Enabled Biocompatible Disulfide–Ene Reaction. *Nature Chem* **2018**, *10*, 981–988.

²⁹ Blum, T. R.; Miller, Z. D.; Bates, D. M.; Guzei, I. A.; Yoon, T. P. *Enantioselective Photochemistry through Lewis Acid–Catalyzed Triplet Energy Transfer*. *Science* **2016**, *354*, 1391–1395.

³⁰ Ciamician, G.; Silber, P. *Chemische Lichtwirkungen*. *Ber. Dtsch. Chem. Ges.* **1900**, *33*, 2911–2913.

³¹ Capaldo, L.; Ravelli, D. Hydrogen Atom Transfer (HAT): A Versatile Strategy for Substrate Activation in Photocatalyzed Organic Synthesis. *Eur. J. Org. Chem.* **2017**, *2017*, 2056–2071.

³² Parsaee, F.; Senarathna, M.C.; Kannangara, P.B., Alexander, S.N., Archen, P.D.E., Weline, E.R., *Radical philicity and its role in selective organic transformations*. *Nat Rev Chem*, **2021**, *5*, 486–499.

- iii) *redox chemistry*, where a charge transfer (CT) process occurs in the excited state producing the highly reducing ketyl radical intermediate. This manifold attracted the attention of different groups to study the properties of the occurring photoinduced electron transfer (PET) process. However, its application for synthetic purposes is still limited and has been recently explored in combination with different catalytic systems.³³
- iv) *Paternò-Büchi (PB) reaction*, where the ketone is used as a reagent with alkenes, allowing the construction of oxetane rings in a single step.³⁴ Such manifold is one of the most studied photoreactions of the last century due to the difficulty to obtain oxetanes in thermal conditions as well as for the complex mechanistic scenarios governing the selectivity of the transformation.³⁵

Energy transfer

The use of deep UV-light sources (emitting at $\lambda < 254$ nm) is a common strategy to directly access triplet states of common organic molecules. However, highly energetic light sources are detrimental for the reaction outcome, favoring decomposition pathways. For this reason, diverse sensitizers have been developed over the years to circumvent this issue. The purpose of these sensitizers is to transfer the energy of its triplet state (reached after ISC from its singlet state), to the triplet state of a different molecule that does not absorb the incident light.³⁶ After such event, the sensitizer is deactivated to its ground state and the sensitized molecule reaches a highly electronic excited state unreachable by direct excitation with the used light source. These sensitizers are also called *energy transfer catalysts* and trigger numerous photoreactions.³⁷ Indeed, aryl ketones have been commonly used for this purpose.

As depicted previously in this section, the excitation of aryl ketones leads to a long-lived T_1 state without significant energetic loss after ISC. This excited state has an $n-\pi^*$ character with a half-filled n_{sp} orbital and a half-filled π^* orbital (Figure 1.9a). Remarkably, the energy of this biradical species can be easily tuned by placing different aryl ring substituents as well

³³ Masuda, Y.; Ishida, N.; Murakami, M. *Aryl Ketones as Single-Electron-Transfer Photoredox Catalysts in the Nickel-Catalyzed Homocoupling of Aryl Halides*. *Eur. J. Org. Chem.* **2016**, 2016, 5822–5825.

³⁴ D'Auria, M. *The Paternò-Büchi Reaction – a Comprehensive Review*. *Photochem. Photobiol. Sci.* **2019**, 18, 2297–2362.

³⁵ Fréneau, M.; Hoffmann, N. *The Paternò-Büchi Reaction—Mechanisms and Application to Organic Synthesis*. *J. Photochem. Photobiol. C.* **2017**, 33, 83–108

³⁶ Generally, the direct irradiation of the sensitized molecule requires high energies to reach its singlet state and the the decays to the triplet by an unefficient ISC. In this way, EnT catalysts are able to absorb light at less energetic wavelengths, reaching its triplet state without a significant energy loss.

³⁷ Strieth-Kalthoff, F.; James, M. J.; Teders, M.; Pitzer, L.; Glorius, F. *Energy Transfer Catalysis Mediated by Visible Light: Principles, Applications, Directions*. *Chem. Soc. Rev.* **2018**, 47, 7190–7202.

as changing the second carbonyl substituent. An excellent example of the latter case is observable between acetophenone **2** and benzophenone **3**, ($E_T = 74.0$ and 69.1 kcal·mol⁻¹, respectively).³⁸ Indeed, the energy value is highly important to predict the reactivity of the sensitizer (Figure 1.9b). While electron-rich heterocycles like indole **11** have high triplet energies ($E_T = 70.8$ kcal·mol⁻¹), unreachable using the triplet state of benzophenone, stilbene **10** has a reduced triplet energy ($E_T = 49.3$ kcal·mol⁻¹), thus enabling the energy transfer. For this reason, a predictive solution to assess the synthetic feasibility an EnT is calculating the E_T difference (ΔE_T).²⁷ When $\Delta E_T < 0$, the process can occur with the selected sensitizer. Contrarily, if $\Delta E_T > 0$, the process is unfeasible and further sensitizer optimization or acceptor activation is needed.³⁷

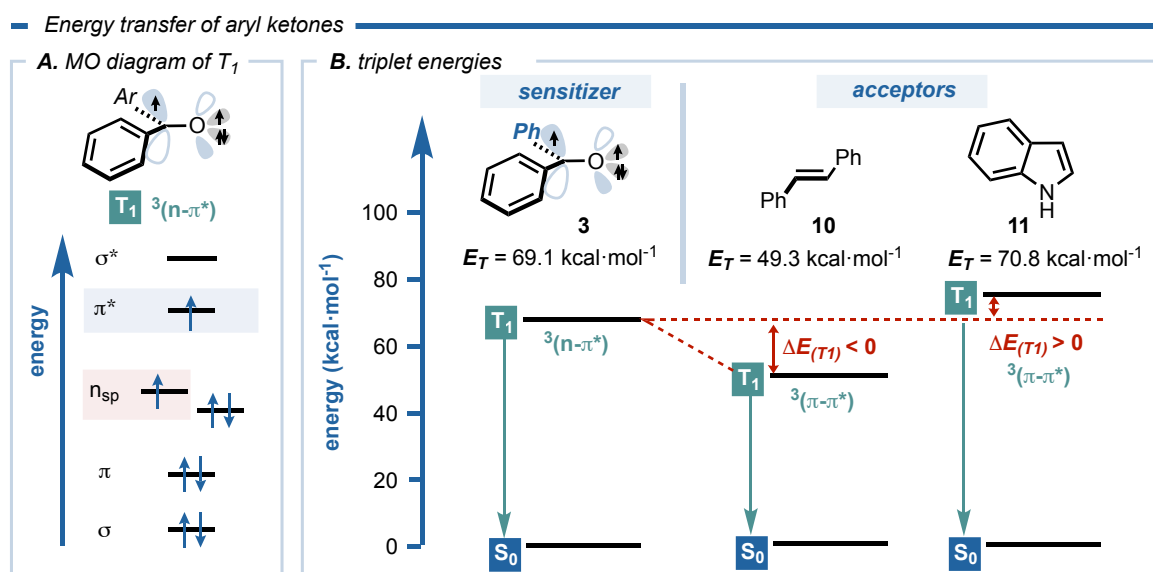


Figure 1.9. - Energy transfer of aryl ketones. a) MO diagram of the T_1 of aryl ketones. b) Comparison of the triplet energy of benzophenone with diverse acceptors.

Case of study – Aryl ketone-mediated isomerization of alkenes

The $E \rightarrow Z$ isomerization of alkenes is one of the most prominent applications of EnT catalysis.³⁹ Hammond and co-workers already applied this strategy to isomerize diversely functionalized alkenes more than 60 years ago.⁴⁰ Hence, with the renaissance of

³⁸ Lamola, A. A.; Hammond, G. S. *Mechanisms of Photochemical Reactions in Solution*. XXVIII.1 Values of Triplet Excitation-Energies of Selected Sensitizers. *J. Am. Chem. Soc.*, **1964**, *86*, 4537 – 4540.

³⁹ Siau, W.-Y.; Zhang, Y.; Zhao, Y. *Stereoselective Synthesis of Z-Alkenes*. In *Stereoselective Alkene Synthesis*, Top. Curr. Chem., **2012**, *327*, 33–58.

⁴⁰ Hammond, G. S.; Saltiel, Jack.; Lamola, A. A.; Turro, N. J.; Bradshaw, J. S.; Cowan, D. O.; Counsell, R. C.; Vogt, Volker.; Dalton, Christopher. *Mechanisms of Photochemical Reactions in Solution*. XXII. 1 Photochemical Cis-Trans Isomerization. *J. Am. Chem. Soc.* **1964**, *86*, 3197–3217.

photocatalysis in recent years, the attention in such reactions has also reemerged. In this regard, the Gilmour group has devoted many efforts towards the development of the field.²⁷

Selected example of EnT catalysis with aryl ketones

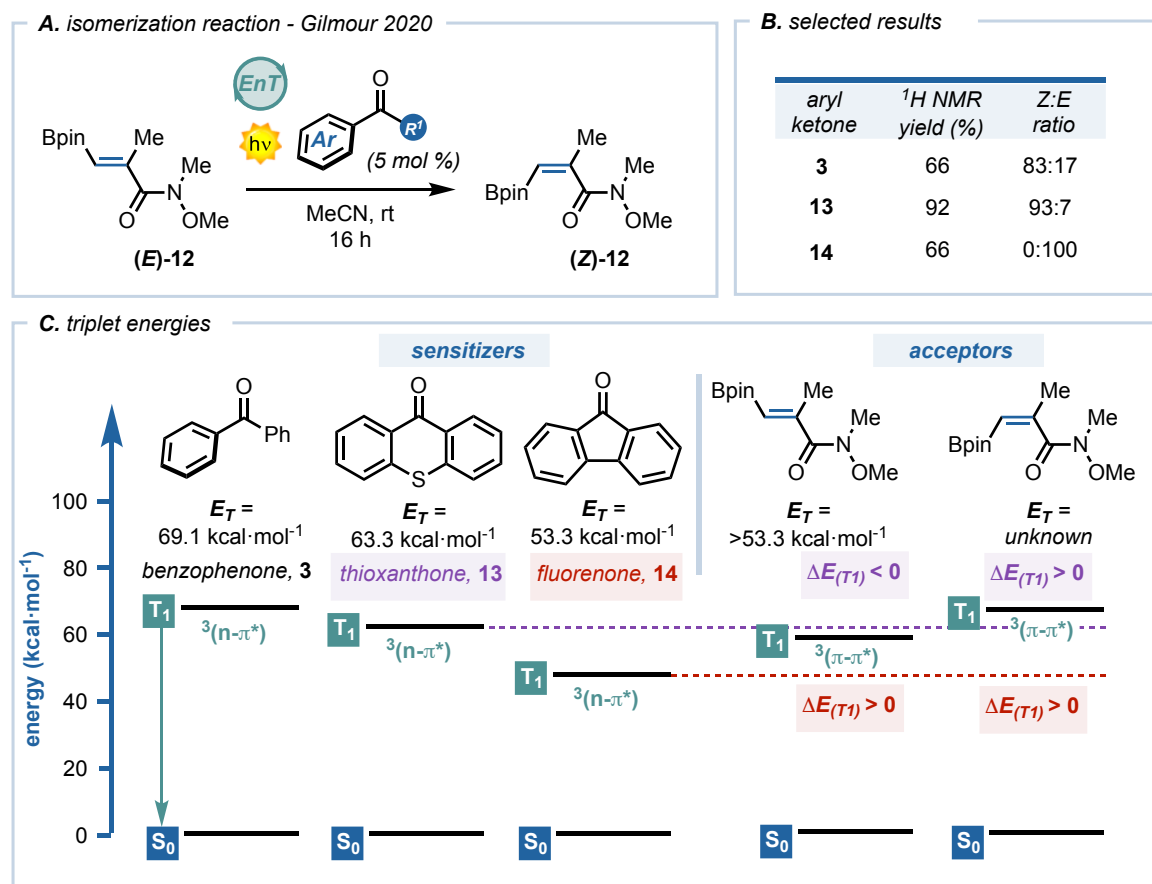


Figure 1.10. - a) $E \rightarrow Z$ isomerization strategy boron-containing E -alkenes reported by Gilmour in 2020.⁴¹ b) Selected results of the reaction optimization. c) Comparison of the triplet energy of the acceptors with diverse aryl ketone sensitizers.

One of the recent applications of alkene isomerization is reported in Figure 1.10a. In this work, Gilmour and co-workers used catalytic amounts of aryl ketones to enable the isomerization of boron-containing E -alkenes **12**, important motifs in the development of novel strategies for the pharmaceutical industry.⁴¹ Interestingly, the use of different carbonyl sensitizers resulted in different $Z:E$ isomerization ratios (Figure 1.10b). This is ascribable to the difference of E_T of the different sensitizers and isomers. For instance, when using BP **3** ($E_T = 69.1 \text{ kcal}\cdot\text{mol}^{-1}$), the $Z:E$ isomer ratio was observed in a modest 83:17. This fact, is mainly due to the high triplet energy of **3** which is able to sensitize both isomers (Figure

⁴¹ Molloy, J. J.; Schäfer, M.; Wienhold, M.; Morack, T.; Daniliuc, C. G.; Gilmour, R. Boron-Enabled Geometric Isomerization of Alkenes via Selective Energy-Transfer Catalysis. *Science* **2020**, *369*, 302–306.

1.10c). On the other hand, thioxanthone **13** with a decreased E_T ($E_T = 63.3 \text{ kcal}\cdot\text{mol}^{-1}$) resulted the optimal catalyst for the process. Thus, seizing the different E_T of the isomers to preferentially transfer the energy to the (*E*)-alkene. Finally, when the triplet energy of the aryl ketone was further decreased ($E_T = 53.3 \text{ kcal}\cdot\text{mol}^{-1}$ for fluorenone **14**) no isomerization was observed and the initial alkene was recovered in 66% ^1H NMR yield.

Hydrogen abstraction

The activation of inert $\text{Csp}^3\text{-H}$ bonds pursuing the construction of complex molecules is an intense field of research.⁴² Diverse strategies, spanning from the use of transition-metal complexes⁴³ to reactive radical species,³¹ have been applied. Simultaneously, several research groups have studied the mechanism of hydrogen abstraction protocols by means of the Marcus theory to predict such transformations.⁴⁴ Nevertheless, valence bond (VB) diagrams are able to predict hydrogen abstraction barriers as well as general reactivity trends.⁴⁵ Interestingly, light-excited aryl ketones have always been an important reagent for the activation of C-H bonds (Figure 1.11). For this reason, the utilization of the VB theory gives a clear picture of the process between the triplet state of aryl ketones and aliphatic C-H bonds (Figure 1.11a). The half-filled n_p orbital possesses both a high energy and a radical character able to abstract an hydrogen from an inactivated C-H bond. Additionally, the n_p orbital is localized and well-oriented, allowing a perpendicular access to the orbital overlap with the C-H σ orbital (Figure 1.11b top). This process generates the ketyl radical **19-H** and the carbon centered radical **20**. For this reason, the Evans-Polanyi relationship⁴⁶ in HAT processes is an invaluable tool to predict the reactivity trend with diverse C-H bonds. In fact, it correlates the activation energy parameters (k_{HAT}) with the bond dissociation enthalpies (BDE).⁴⁷ Thus, by comparing the BDEs of the broken C-H ($\text{BDE}_{\text{Csp}^3\text{-H}} = 105.0\text{-}89.7 \text{ kcal}\cdot\text{mol}^{-1}$) with the formed O-H bond of the ketyl radical ($\text{BDE}_{\text{O-H}} = 105 \text{ kcal}\cdot\text{mol}^{-1}$) a general trend has been proposed. As observable in Figure 1.11b, methane **15** is the less reactive alkane towards HAT activation due to its high C-H BDE ($\text{BDE}_{\text{Csp}^3\text{-H}} = 105.0 \text{ kcal}\cdot\text{mol}^{-1}$) while the C-H bonds in the α -position to an

⁴² Rogge, T.; Kaplaneris, N.; Chatani, N.; Kim, J.; Chang, S.; Punji, B.; Schafer, L. L.; Musaev, D. G.; Wencel-Delord, J.; Roberts, C. A.; Sarpong, R.; Wilson, Z. E.; Brimble, M. A.; Johansson, M. J.; Ackermann, L. C-H Activation. *Nat Rev Methods Primers* **2021**, *1*, 1 – 43.

⁴³ Crabtree, R. H.; Lei, A. Introduction: CH Activation. *Chem. Rev.* **2017**, *117*, 8481–8482.

⁴⁴ Mayer, J. M. Understanding Hydrogen Atom Transfer: From Bond Strengths to Marcus Theory. *Acc. Chem. Res.* **2011**, *44*, 36–46.

⁴⁵ Lai, W.; Li, C.; Chen, H.; Shaik, S. Hydrogen-Abstraction Reactivity Patterns from A to Y: The Valence Bond Way. *Angew. Chem. Int. Ed.* **2012**, *51*, 5556–5578.

⁴⁶ Salamone, M.; Galeotti, M.; Romero-Montalvo, E.; van Santen, J. A.; Groff, B. D.; Mayer, J. M.; DiLabio, G. A.; Bietti, M. Bimodal Evans–Polanyi Relationships in Hydrogen Atom Transfer from $\text{C}(\text{sp}^3)\text{-H}$ Bonds to the Cumyloxyl Radical. A Combined Time-Resolved Kinetic and Computational Study. *J. Am. Chem. Soc.* **2021**, *143*, 11759–11776.

⁴⁷ Evans, M. G.; Polanyi, M. Inertia and Driving Force of Chemical Reactions. *Trans. Faraday Soc.* **1938**, *34*, 11 – 24.

heteroatom **17** or in the benzylic positions **18** are the fastest ($BDE_{Csp^3-H} = 92.1$ and 89.7 kcal·mol⁻¹ respectively).

Hydrogen abstraction of aryl ketones

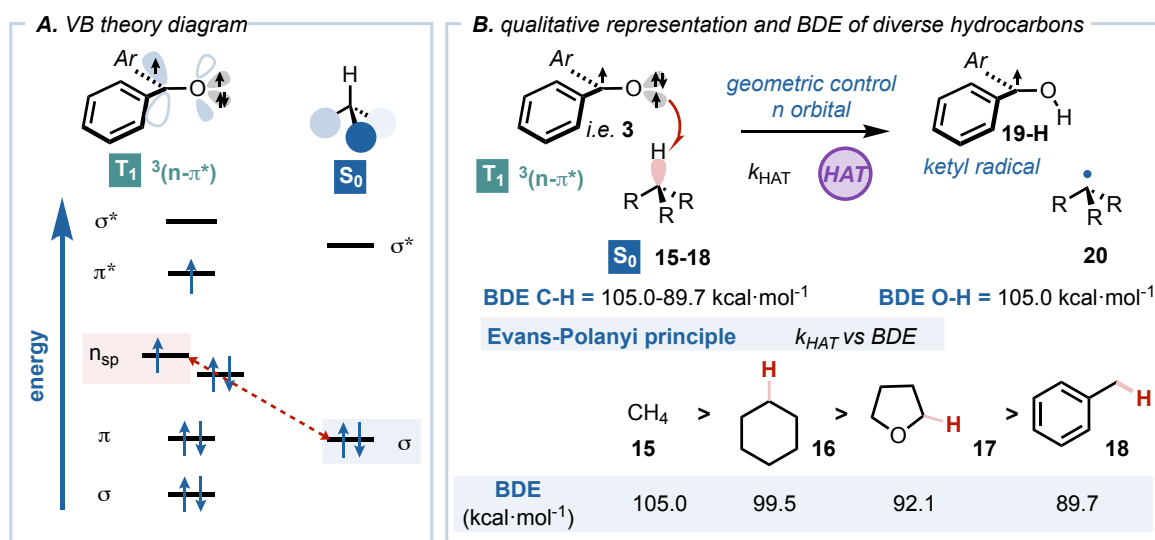


Figure 1.11. - Hydrogen abstraction of aryl ketones with aliphatic Csp³-H bonds. a) VB theory diagram. b) Geometric control and Evans-Polanyi principle to predict the abstraction trend.

Case of study – Aryl ketone-mediated catalytic activation of THF

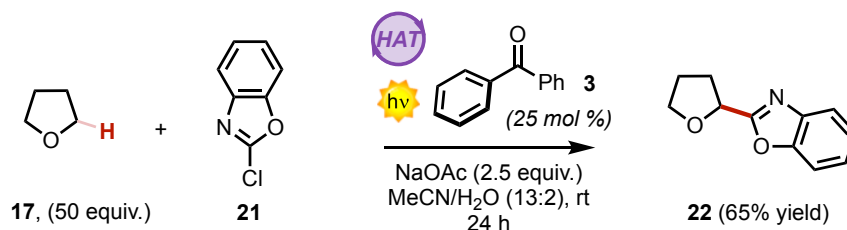
The C-H activation of aliphatic bonds using aryl ketones in catalytic amounts has experienced a tremendous growth in the last decade. On one hand, the groups of Martin and Molander pioneered the development of novel transformations using benzophenone derivatives in combination with earth-abundant metal catalysts.^{48,49} On the other hand, diverse catalytic metal-free systems have been developed.³¹ Such reactions seize the reactivity of the formed C-centered radicals towards the formation of novel C-C bonds. One of these examples is depicted in Figure 1.12. In his work, Opatz and co-workers used 2-chlorobenzoxazole derivatives **21** for the trapping of the generated radicals after HAT between THF **17** and benzophenone **3**.⁵⁰ The generated product **22** was formed in good yields (65% yield) in the presence of catalytic amounts of the sensitizer (25 mol%) after 24 hours of continuous irradiation. Interestingly, the authors proposed a mechanistic scenario where two consecutive HAT processes take place. After excitation of the aryl ketone and the consequent formation

⁴⁸ Shen, Y.; Gu, Y.; Martin, R. *Sp³ C-H Arylation and Alkylation Enabled by the Synergy of Triplet Excited Ketones and Nickel Catalysts*. *J. Am. Chem. Soc.* **2018**, *140*, 12200–12209.

⁴⁹ Campbell, M. W.; Yuan, M.; Polites, V. C.; Gutierrez, O.; Molander, G. A. *Photochemical C-H Activation Enables Nickel-Catalyzed Olefin Dicarbofunctionalization*. *J. Am. Chem. Soc.* **2021**, *143*, 3901–3910.

⁵⁰ Lipp, A.; Lahm, G.; Opatz, T. *Light Induced C-C Coupling of 2-Chlorobenzazoles with Carbamates, Alcohols, and Ethers*. *J. Org. Chem.* **2016**, *81*, 4890–4897.

of its T_1 state, it is quenched by THF **17**. This step generates the C-centered radical **23** and the ketyl radical **19-H** through a favorable activation energy ($BDE_{C_{sp^3-H} \text{ 17}} = 92.1 \text{ kcal}\cdot\text{mol}^{-1}$ vs $BDE_{O-H \text{ 19-H}} = 105.0 \text{ kcal}\cdot\text{mol}^{-1}$). Then, the C-centered radical **23**, attacks **21** generating the N-centered radical **24**. This intermediate close the catalytic cycle by abstracting the H of the ketyl radical. Finally, intramolecular elimination of the chlorine atom generated HCl furnishing product **22**.



— Selected example of HAT catalysis with aryl ketones —

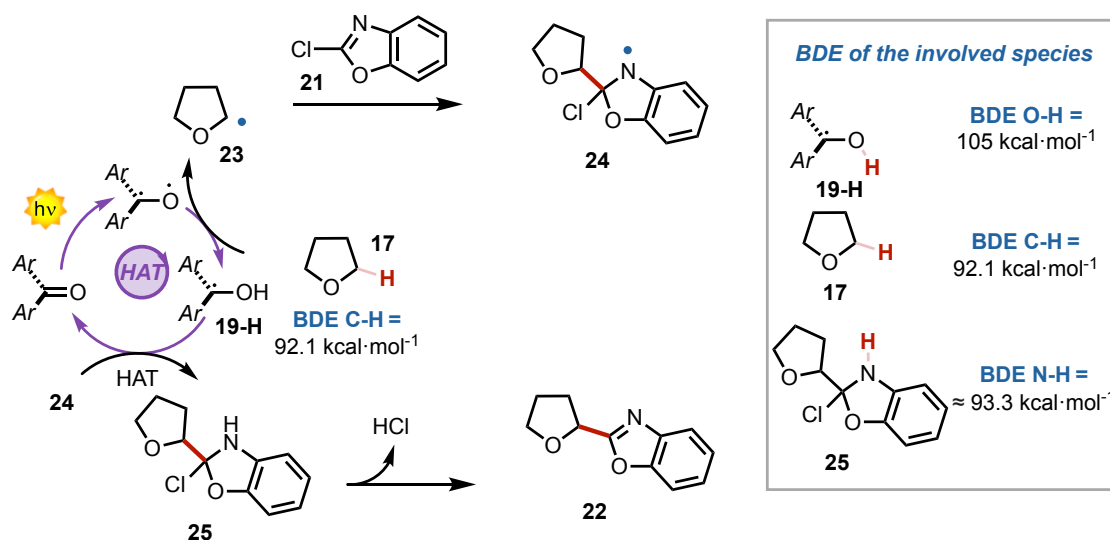


Figure 1.12. - Aryl ketone-mediated catalytic activation of THF reported by Opatz and co-workers.⁵⁰

Electron transfer reactions

As Lennart Ebersson stated in 1982 “*the simplest elementary act in homogeneous solution chemistry is the exchange of an electron between two chemical entities.*”⁵¹ In this process, no bonds are formed or broken, while there is an electron exchange. From this key step, it derived the name of the transformation. The process is called *electron transfer* and the predominant rationale behind it has been explained by means of the Weller and Marcus

⁵¹ Ebersson, L. *Electron Transfer Reactions in Organic Chemistry*; Hafner; Springer, Berlin, Heidelberg, 1987; Vol. 25.

theories.^{52,53} Additionally to the electron exchange, the newly formed species have different chemical properties impacting in the final reaction outcome. Nevertheless, many electron-transfer processes require additional energy to occur. For this reason, photons energy and hence photochemistry is an excellent partner to trigger such events. By harnessing photons energy, *photoinduced electron transfer* takes place between a donor molecule (which gets oxidized) and an acceptor molecule (which gets reduced).⁵⁴ As for the prior reactivities discussed in this section, the VB theory exceptionally depicts the orbitals involved in the PET processes between the T₁ state of aryl ketones (acting as acceptors) and diverse donor molecules ($E_{\text{HOMO}} > E_{\text{nsp}}$ of benzophenone, Figure 1.13).

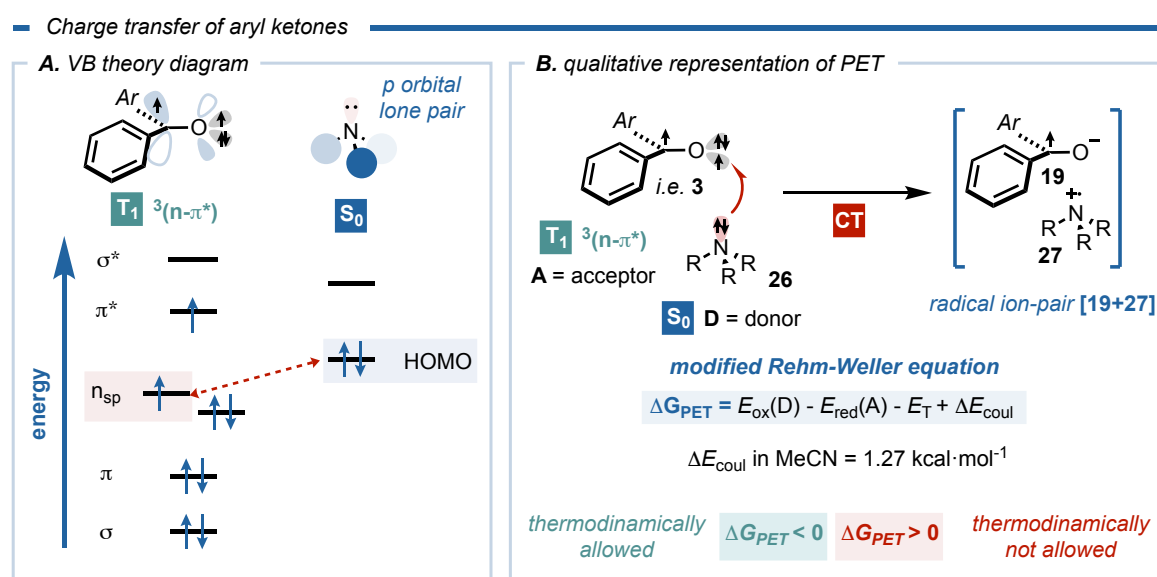


Figure 1.13. - Photoinduced electron transfer processes between light-excited aryl ketones and amines. a) VB theory diagram. b) Radical ion-pair formation and utilization of the modified Rehm-Weller equation to predict PET processes.

In the case of PET processes between light-excited aryl ketones and amines, the half-filled n_{p} orbital, interacts with the HOMO orbital of the amine (lone pair located at the p orbital, Figure 1.13a). This interaction promotes an electron from the donor to the acceptor. To rationalize the viability to form the photochemically induced radical ion-pair [19+27], chemists possess an exceptional tool. By using the modified Rehm-Weller equation (Figure 1.13b down), it is possible to estimate whether an electron-transfer process is

⁵² Weller, A. *Exciplex and Radical Pairs in Photochemical Electron Transfer*. *Pure and Applied Chemistry* **1982**, 54, 1885–1888.

⁵³ Marcus, R. A. *Chemical and Electrochemical Electron-Transfer Theory*. *Annu. Rev. Phys. Chem.* **1964**, 15, 155–196.

⁵⁴ Mattay, J. *Charge Transfer and Radical Ions in Photochemistry*. *Angew. Chem. Int. Ed.* **1987**, 26, 825–845.

thermodynamically allowed ($\Delta G_{\text{PET}} < 0$, exergonic process) or not ($\Delta G_{\text{PET}} > 0$, endergonic process).⁵⁴ To apply this equation, some experimental values are required: *i*) the oxidation and reduction potentials in solution of the donor and the acceptor, respectively ($E_{\text{ox}}(D)$ and $E_{\text{red}}(A)$); and *ii*) in combination with the triplet energy of the aryl ketone (E_T). Additionally, the difference of coulomb interaction energy of the two radical ions formed in the used solvent has to be adjusted (ΔE_{coul}).

Definition of EDA complex and examples with aryl ketones

— An exceptional case: charge transfer complexes of aryl ketones in the ground state —

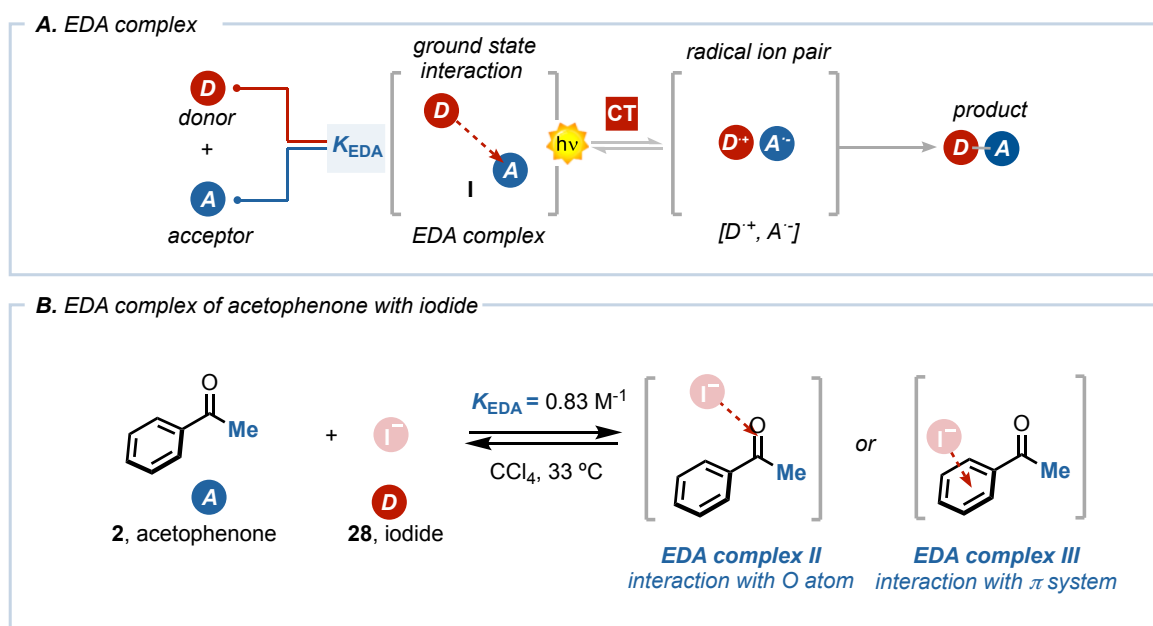


Figure 1.14. - Charge transfer processes enabled by ground-state aggregations. a) EDA complex. b) EDA complex between acetophenone and iodide.

The ground-state association of an electron-rich substrate (donor, **D**) with an electron-acceptor molecule (acceptor, **A**) furnishes an EDA complex **I** (Figure 1.14a).⁵⁵ This type of aggregates, are characterized by having different physical properties than the two separated components. As it is an aggregate formed in solution, it possesses an association constant (K_{EDA}) which determines the equilibria between the two separated species and the complex formation. However, its main peculiarity is the formation of a new absorption band, called *charge-transfer band*.⁵⁶ The irradiation of such band promotes the PET between both reaction partners by using less energetic photons. Interestingly, EDA complexes have been known

⁵⁵ Crisenza, G. E. M.; Mazzarella, D.; Melchiorre, P. *Synthetic Methods Driven by the Photoactivity of Electron Donor–Acceptor Complexes*. *J. Am. Chem. Soc.* **2020**, *142*, 5461–5476.

⁵⁶ Foster, R. *Electron Donor-Acceptor Complexes*. *J. Phys. Chem.* **1980**, *84*, 2135–2141.

since the 1950's but the strategy has attracted the synthetic chemistry community recently.⁵⁷ Nevertheless, no synthetic applications of EDA complexes between aryl ketones and donor molecules are known to date to the best of my knowledge.

Despite the lack of synthetic applications of EDA complexes between aryl ketone systems with donor species, diverse works confirming their existence have been published (Figure 1.14b).⁵⁸ Foster and Goldstein reported in 1967 the ground-state formation of a 1:1 complex between acetophenone **2** and iodide **28**. In their work, the authors assessed the association constants of diversely substituted acetophenones and iodide in CCl₄ at 33 °C ($K_{EDA} = 0.83 \text{ M}^{-1}$ for [**2**+**28**]). Interestingly, they proposed two different EDA complexes depending on the orbital interaction between the iodide electrons and the carbonyl compound (EDA complex II vs EDA complex III).

Case of study – Aryl ketone-mediated CT processes in the excited state

The utilization of organic molecules to trigger PET processes in photoredox catalysis has been an important part of my PhD studies (*see Chapter IV*). Therefore, I herein want to highlight the importance of aryl ketones under this type of catalysis. As previously mentioned, aryl ketones experience PET processes when *e.g.*, tertiary amines are present in the media in hyperstoichiometric amounts. Different studies have been used to evidence the importance of amines in CT quenching processes with carbonyls.⁵⁹ Nevertheless, few photoredox catalytic cycles have been proposed evidencing this step with such aromatic compounds. Many of the works with aryl ketones propose an initial HAT mechanism to form the ketyl radical intermediate **19** in the presence of tertiary amines.⁶⁰ In 2016, Murakami and coworkers proposed a PET activation for the homocoupling of aryl halides by using catalytic amounts of thioxanthone **13** and a Ni catalyst (Figure 1.15).³³ The authors proposed a mechanism consisting in three cooperative redox cycles. Initially, the T₁ excited state of **13** gets reduced by a tertiary amine ($E_{ox} = 0.65 \text{ V vs SCE}$).⁶¹ Thus, forming ketyl radical **19** and the amine radical cation. Remarkably, this process is thermodynamically allowed by applying the

⁵⁷ Mulliken, R. S.; Person, W. B. *Donor-Acceptor Complexes*. *Annu. Rev. Phys. Chem.* **1962**, *13*, 107–126.

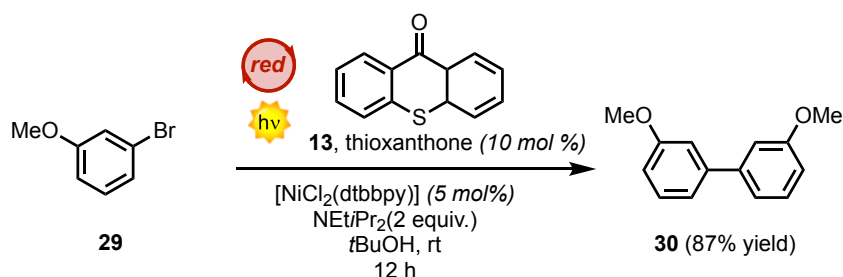
⁵⁸ Foster, J.; Goldstein, M. *Spectroscopic Studies of Some Aryl Ketone—Iodine Complexes*. *Spectrochimica Acta Part A: Molecular Spectroscopy* **1968**, *24*, 807–812.

⁵⁹ a) Yip, R. W.; Loutfy, R. O.; Chow, Y. L.; Magdzinski, L. K. *The Triplet State of Ketones in Solution: Quenching of Triplet Acetone by Amines*. *Can. J. Chem.* **1972**, *50*, 3426–3431. b) Turro, N. J.; Engel, R. *Quenching of Biacetyl Fluorescence and Phosphorescence*. *J. Am. Chem. Soc.* **1969**, *91*, 7113–7121. c) Peters, K. S.; Lee, J. *Picosecond Dynamics of the Photoreduction of Benzophenone by DABCO*. *J. Phys. Chem.* **1993**, *97*, 3761–3764.

⁶⁰ Grimm, M. L.; Allen, W. J.; Finn, M.; Castagnoli, N.; Tanko, J. M. *Reaction of Benzophenone Triplet with Aliphatic Amines. What a Potent Neurotoxin Can Tell Us about the Reaction Mechanism*. *Bioorganic & Medicinal Chemistry* **2011**, *19*, 1458–1463.

⁶¹ Masui, M.; Sayo, H.; Tsuda, Y. *Anodic Oxidation of Amines. Part I. Cyclic Voltammetry of Aliphatic Amines at a Stationary Glassy-Carbon Electrode*. *J. Chem. Soc., B*: **1968**, 973–976.

modified Rehm-Weller equation ($\Delta G_{\text{PET}} = -9.7 \text{ kcal}\cdot\text{mol}^{-1}$). Then, the ketyl radical ($E_{\text{red}} = -1.62 \text{ V vs SCE}$) reduces 0.5 equiv. of the Ni^{II} species **31** ($E_{\text{red}} = -1.20 \text{ V vs SCE}$) to form Ni^0 species and regenerating the ground state thioxanthone catalyst **13**. Subsequently, the Ni^0 species is oxidatively added to the arylhalide **29** to form the arylnickel(II) complex **33**. **33** is then dichotomized in two ways: *i*) forming NiBr_2 and the diarylnickel **34**. Finally, the latter Ni^{II} intermediate reductively forms the product arising with Ni^0 **32**, starting again the catalytic cycle.



Selected example of SET catalysis with aryl ketones

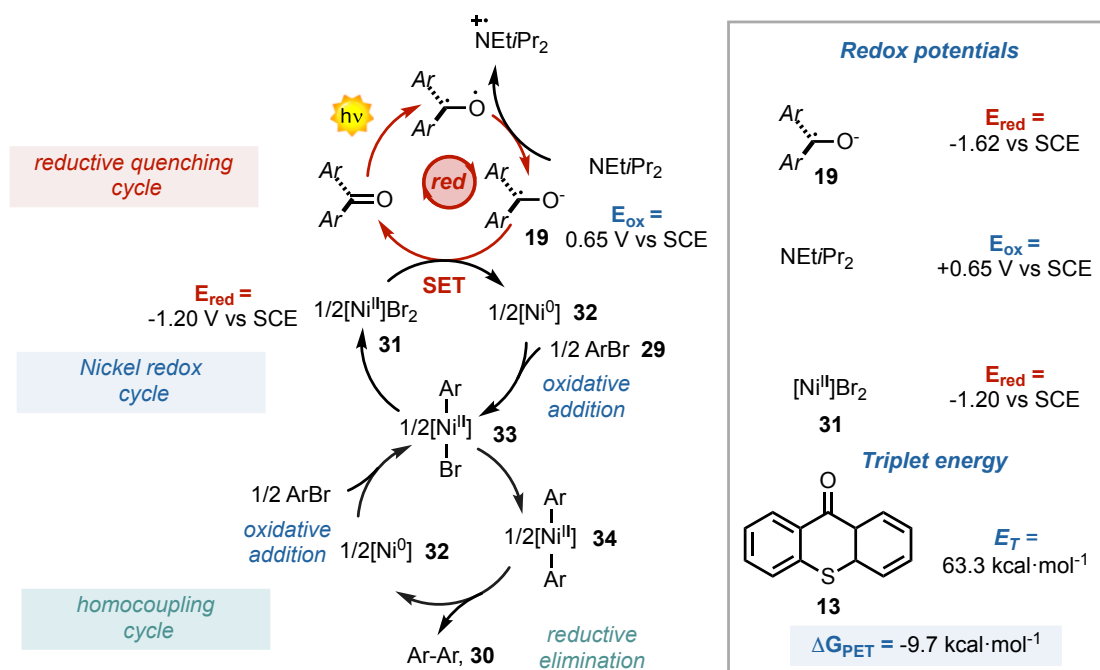


Figure 1.15. - Aryl ketone-mediated photoredox catalysis reported by Murakami and co-workers.³³

Paternò-Büchi reaction

Additionally to the previously described processes where the excited state of aryl ketones is used as a mediator to trigger EnT, HAT or CT manifolds, light-excited carbonyls can be used as a reagent for the formation of covalent bonds. This is the case of the Paternò-Büchi reaction, where the T_1 biradical is covalently linked to an alkene moiety **35** to form

oxetanes **37** (Figure 1.16).³⁴ In conventional PB reactions, the T₁ state of aryl ketones react with alkenes to form the 1,4 biradical intermediate **36a-b**. Remarkably, the nature of the alkene dictates the initial orbital interaction of the reaction.⁶² When using electron-rich alkenes, the n_p half-filled orbital of the aryl ketones reacts with the π orbital of the alkene (red arrow). On the other hand, when using electron-poor alkenes it is the half-filled π* orbital of the carbonyl orbital (green arrow). Interestingly, PB reaction involving CT process can also occur. For this reason, depending on the initial interaction, the selectivity of the transformation can be predicted. Indeed, the study of this reaction is one of the main topics of this dissertation and it will be discussed in more detail in *Chapter II*.

— Utilization of excited-aryl ketones as reagents: the Paternò-Büchi reaction

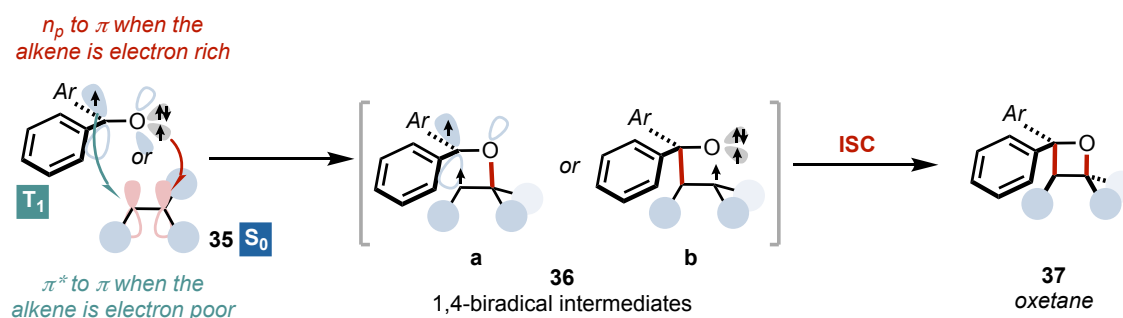


Figure 1.16. - Orbital interactions in the Paternò-Büchi reaction.

Case of study – PB reaction vs EnT

An interesting comparison for the Paternò-Büchi reaction is done between the PB manifold and the EnT manifold. Since both reactions occur when using alkenes in combination with excited aryl ketones both mechanisms can occur simultaneously. Nevertheless, diverse parameters can be used to predict the reactivity. In fact, Arnold and coworkers studied the implications of diverse carbonyl systems in the presence of norbornene **38** (Figure 1.17).^{63,64}

One of the key parameters to predict which will be the active path is accounting the difference of triplet energies (ΔE_T). Taking into account that norbornene is a strained disubstituted alkene, it presents a high E_T unreachable for many sensitizers ($E_T = 72.0$

⁶² Turro, N. J.; Dalton, J. C.; Dawes, K.; Farrington, G.; Hautala, R.; Morton, D.; Niemczyk, M.; Schore, N. *Molecular Photochemistry. L. Molecular Photochemistry of Alkanones in Solution. α-Cleavage, Hydrogen Abstraction, Cycloaddition, and Sensitization Reactions*. *Acc. Chem. Res.* **1972**, *5*, 92–101

⁶³ Arnold, D. R.; Hinman, R. L.; Glick, A. H. *Chemical Properties of the Carbonyl n, π State*. *The Photochemical Preparation of Oxetanes*. *Tetrahedron Letters* **1964**, *5*, 1425–1430.

⁶⁴ Arnold, D. R.; Trecker, D. J.; Whipple, E. B. *The Stereochemistry of the Pentacyclo[8.2.1.1.0.0]Tetradecanes and -Dienes. Norbornene and Norbornadiene Dimers*. *J. Am. Chem. Soc.* **1965**, *87*, 2596–2602.

kcal·mol⁻¹).⁶⁵ Hence, by using stoichiometric amounts of benzophenone **3** as the aryl ketone reagent, EnT cannot occur since its E_T is lower than the one of the alkene ($\Delta E_T > 0$, Figure 1.17 left).⁶³ For this reason, the oxetane product **39** is obtained as a single product. Contrarily, the utilization of catalytic amounts (10 mol%) of light-excited acetophenone allows the triplet sensitization of the alkene to favor the [2+2]-cycloaddition reaction of norbornene ($\Delta E_T < 0$, Figure 1.17 right).⁶⁴ Thus, product **40** formed as a mixture of cyclobutane isomers. Despite the EnT is the active path in this case, PB manifolds cannot be excluded when isomerization is not possible due to ring strain. In these special cases, a transposed PB reactions can take place.⁶⁶

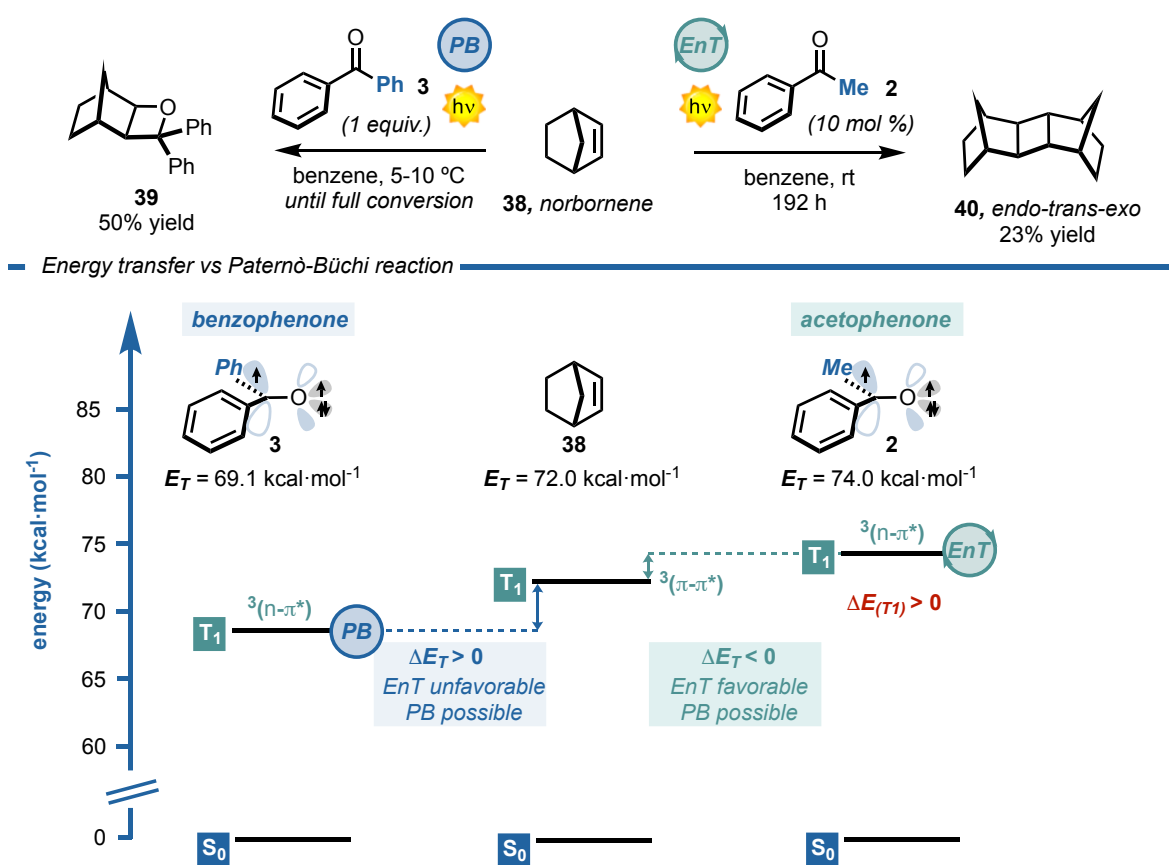


Figure 1.17. - Differences between the PB and EnT reported by Arnold and co-workers.^{63, 64}

⁶⁵ Unett, D. J.; Caldwell, R. A. *The Triplet State of Alkenes: Structure, Dynamics, Energetics and Chemistry*. Res. Chem. Intermed. **1995**, 21, 665–709.

⁶⁶ Kumarasamy, E.; Raghunathan, R.; Kandappa, S. K.; Sreenithya, A.; Jockusch, S.; Sunoj, R. B.; Sivaguru, J. *Transposed Paternò-Büchi Reaction*. J. Am. Chem. Soc. **2017**, 139, 655–662.



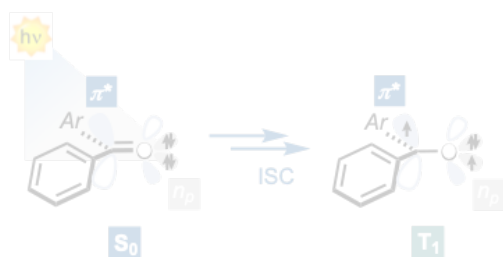
Chapter I – Section 2

Introduction – Flow Photochemistry

— **Chapter I - General Overview – Introduction to Excited Aryl Ketone Chemistry and Flow Photochemistry** —

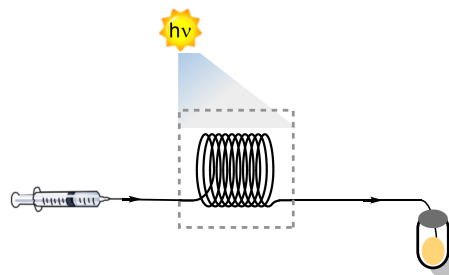
Section 1.

Introduction to Aryl Ketone Photochemistry



Section 2.

Introduction to Flow Photochemistry



- I introduce the different type of setups used in synthetic photochemistry.
- I define the advantages of using flow photoreactors in synthesis.

1.2.1 Importance of the experimental set-up in photochemical reactions

When pursuing a photochemical reaction, chemists deal with a special reagent: light. Generally, the user initially mix all the reagents and solvents in a reaction vessel. Then, an external energy source (normally in form of heating) fosters the transformation. This batch strategy is the common technique taught in undergraduate courses and nowadays is the most extended set-up for the preparation of pharmaceuticals and agrochemicals in lab- and large-scale manufacture.⁶⁷ However, when photons are the reaction promoters, batch set-ups have some limitations leading to reproducibility issues.⁶⁸ This is mainly caused by: *i*) the used wavelength, *ii*) the intensity of the light source, *iii*) the geometry of the reactor, *iv*) the distance between the light source and the reactor, and *v*) the temperature control. Additionally, even if the optimal conditions are achieved, the scalability of the process becomes the next hindrance. Compared with thermal chemistry, where passing from *milligrams* to *grams* of product is generally associated with the utilization of bigger vessels,⁶⁹ the utilization of bigger flasks in synthetic photochemistry is not an adequate scale-up strategy.⁶⁸ Indeed, light cannot penetrate into the interior of the vessel and only the walls are irradiated. In this case, to maintain the same reaction efficiency, an increased irradiance is needed. For all these reasons, in-flow processes, where reagents and products are continuously flowing along the set up became a powerful tool to overcome all these limitations.

1.2.2 Fundamentals of flow set-ups

When developing reactions in flow conditions generally require more planning compared with standard batch protocols.⁷⁰ The main initial question when approaching to flow techniques is whether its use is for the development of new chemical methodologies or for process purposes. Indeed, for the development of new synthetic methodologies the utilization of flow photochemistry is an excellent starting point. For this reason, simple homogeneous conditions are commonly selected, avoiding the use of connections of expensive modules to achieve multi-step processes that require wider experience on the field. Nevertheless, it is

⁶⁷ Cole, K. P.; Johnson, M. D. *Continuous Flow Technology vs. the Batch-by-Batch Approach to Produce Pharmaceutical Compounds*. *Expert Review of Clinical Pharmacology* **2018**, *11*, 5–13.

⁶⁸ Buzzetti, L.; Crisenza, G. E. M.; Melchiorre, P. *Mechanistic Studies in Photocatalysis*. *Angew. Chem. Int. Ed.* **2019**, *58*, 3730–3747.

⁶⁹ Rossetti, I.; Compagnoni, M. *Chemical Reaction Engineering, Process Design and Scale-up Issues at the Frontier of Synthesis: Flow Chemistry*. *Chemical Engineering Journal* **2016**, *296*, 56–70.

⁷⁰ Guidi, M.; Seeberger, P. H.; Gilmore, K. *How to Approach Flow Chemistry*. *Chem. Soc. Rev.* **2020**, *49*, 8910–8932.

important to know the anatomy of a photoflow set-up to realize about the key-enabling features of this technology (Figure 1.18).⁷¹

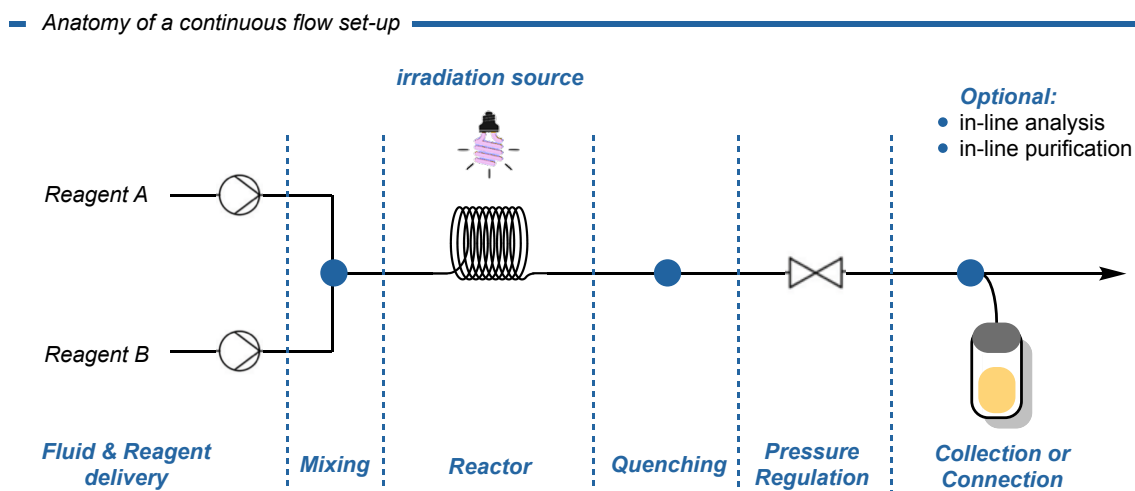


Figure 1.18. - Anatomy of a continuous flow photochemical set-up.

Flow systems coupled with photochemical conditions are commonly composed by:

- i) a fluid and reagent delivery system, driven by hydrodynamic pumps⁷² that control the precise movement of the fluids. This part is responsible of controlling the residence time of the reaction crude as well as the stoichiometry of the reagents. Remarkably, the majority of flow reactors incorporate at least one liquid delivery unit.⁷³
- ii) a mixer, that ensures the correct and fast mixing of the pumped reagents. Thus, depending on the type of phase needed for the reaction (liquid-liquid, solid-liquid or gas-liquid), different mixers can be used to allow an optimal conditions.⁷⁴
- iii) a reactor unit, which is the core of every flow system.⁷⁵ It is the section where the chemical reaction occurs and they can be divided as chip, coil (which are the ones used in this dissertation), and packed bed reactors.

⁷¹ For more extensive descriptions on the assembly of flow set-ups see: Britton, J.; Jamison, T. F. *The Assembly and Use of Continuous Flow Systems for Chemical Synthesis*. *Nat Protoc* **2017**, *12*, 2423–2446.

⁷² Murray, P. R. D.; Browne, D. L.; Pastre, J. C.; Butters, C.; Guthrie, D.; Ley, S. V. *Continuous Flow-Processing of Organometallic Reagents Using an Advanced Peristaltic Pumping System and the Telescoped Flow Synthesis of (E/Z)-Tamoxifen*. *Org. Process Res. Dev.* **2013**, *17*, 1192–1208.

⁷³ Plutschack, M. B.; Pieber, B.; Gilmore, K.; Seeberger, P. H. *The Hitchhiker's Guide to Flow Chemistry*. *Chem. Rev.* **2017**, *117*, 11796–11893.

⁷⁴ Yoshida, J.; Nagaki, A.; Iwasaki, T.; Suga, S. *Enhancement of Chemical Selectivity by Microreactors*. *Chem. Eng. Technol.* **2005**, *28*, 259–266.

⁷⁵ a) Ley, S. V.; Fitzpatrick, D. E.; Myers, R. M.; Battilocchio, C.; Ingham, Richard. J. *Machine-Assisted Organic Synthesis*. *Angew. Chem. Int. Ed.* **2015**, *54*, 10122–10136. b) Rehm, T. H. *Reactor Technology Concepts for Flow Photochemistry*. *ChemPhotoChem* **2020**, *4*, 235–254.

- iv) an irradiation source that enables the correct light-irradiation of the reactor. The recent advancements in this field allowed to substitute the previously used Hg lamps, by cheap CFL bulbs, selective LEDs and lasers.⁷⁶
- v) a quenching unit, that ensures that any side-reaction does not occur in the collection vessel. It is commonly used to avoid unnecessary safety problems when highly reactive intermediates are used. Nevertheless, when high product and by-product stability is observed its use is optional.
- vi) a pressure regulating unit, used to ensure a constant pressure in the reactor during a continuous-flow process. This section is key when working with solid-liquid and gas-liquid mixtures. However, in liquid monophasic reactions where solids or gases are not formed its use is optional.
- vii) a collection unit, where the final mixture is collected.
- viii) in-line analysis and in-line purification units, which are also optional modules that enable the characterization and elimination of impurities to couple the reactor with a following reaction step.

Remarkably these modules and connections are standardized, making the different sections interchangeable, allowing the implementation of multi-step processes. In addition to the versatility of such section, the common tubing used for photochemical applications is generally made of transparent and inert perfluorinated materials (*i.e.* PTFE, PEEK, PFA and FEP), thus, ensuring the stability of the reaction as well as the correct light penetration.

1.2.3 Main advantages of flow over batch setups in photochemical processes

The use of continuous flow photoreactors has demonstrated its potential to overcome the issues generally associated with photochemical batch protocols. In fact, the use of flow technologies ensures an optimal irradiation of the reaction mixture, enhancing the reactivity of photoreactions by improving their irradiation, selectivity and mixing. Additionally, photochemical reactions are generally accelerated (from hours in batch to minutes, or even seconds, in flow) and scaled-up, obtaining higher productivities. For these reasons, herein I highlight the advantages of using the flow setup as a key enabling technology in synthetic photochemistry.⁷⁶

⁷⁶ Cambié, D.; Bottecchia, C.; Straathof, N. J. W.; Hessel, V.; Noël, T. *Applications of Continuous-Flow Photochemistry in Organic Synthesis, Material Science, and Water Treatment*. *Chem. Rev.* **2016**, *116*, 10276–10341.

Improved irradiation

As explained in the previous section, the absorption of the reaction mixture is crucial to foster a photochemical process. This effect is well-demonstrated using the Lambert-Beer law, that considers the transmittance of the absorbing reaction (Figure 1.19).⁷⁷

Higher distance decreases reaction transmittance

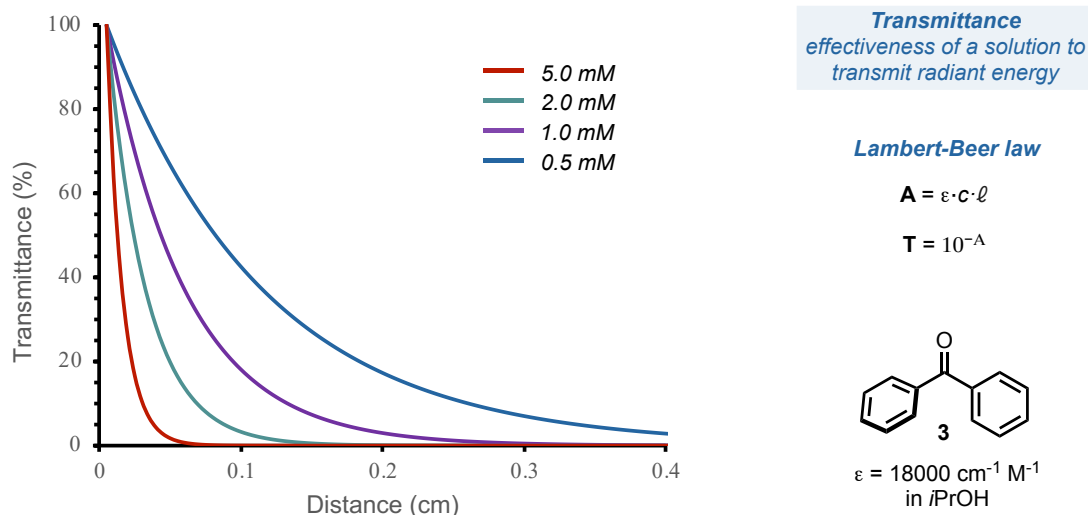


Figure 1.19. - Effect on the transmittance of the reaction sample at different distances when changing the reaction concentration (benzophenone **3** $\epsilon_{(253 \text{ nm})}$ in *i*PrOH = $18000 \text{ cm}^{-1} \cdot \text{M}^{-1}$).

The transmittance⁷⁸ of a reaction solution measures the effectiveness of a solution to transmit radiant energy. In fact, the distance has a high importance. Considering four different solutions of benzophenone at different concentrations (Figure 1.19), the amount of radiant power that reaches the interior (distance > 0.1 cm) is strongly diminished in comparison with the surface (distance < 0.1 cm). Hence, the walls of the vessel absorb a larger number of photons than the inner part. Contrarily, when a coil or a chip (with an inner diameter < 0.1 cm)⁷⁶ the reactor has a constant length with a high transmittance overtime. Thus, making flow photoreactors more efficient for light absorption purposes.

Easy to scale-up

One of the general parameters used to evaluate a chemical reaction performance is by measuring the chemical yield of the transformation. This is a powerful method to numerically compare the reaction outcome. Nevertheless, yields only consider the amount of starting

⁷⁷ Noël, T. A Personal Perspective on the Future of Flow Photochemistry. *Journal of Flow Chemistry* **2017**, 7, 87–93.

⁷⁸ As described by the IUPAC: The ratio of the transmitted radiant power to that incident on the sample.

material that has reacted to produce the desired product. For this reason, chemists (specially for process purposes) developed other parameters to compare the reaction performances. A more specific analysis of the reaction outcome involves the productivity by using space-time yield metrics (STY, Figure 1.20). This parameter considers the amount of produced product as a function of time. Hence, it implicitly contemplates the reaction concentration and the overall reaction time (taking into account quenching and purification processes).⁷⁹

— Numbering-up strategy, batch vs flow

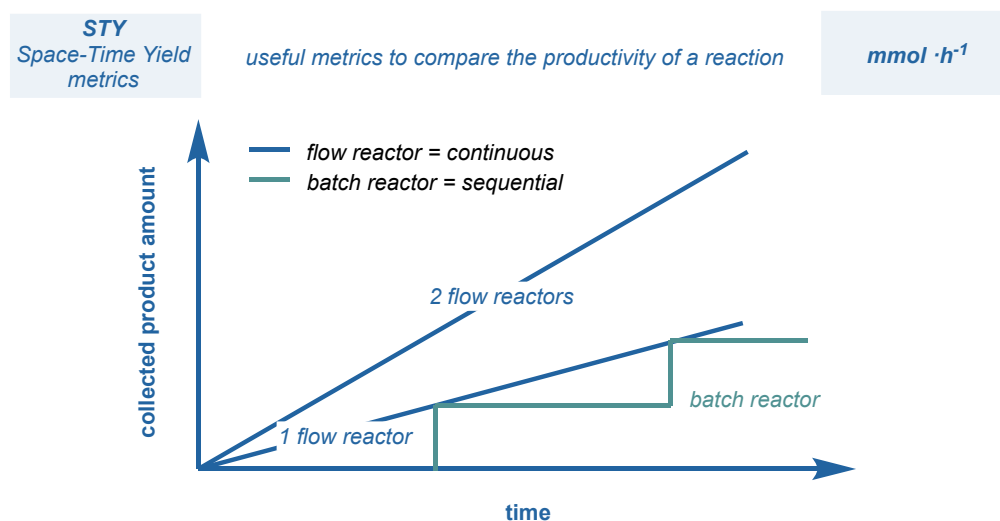


Figure 1.20. - Generalized graphical comparison of STY metrics of batch vs flow manufacturing.

When comparing STY metrics between batch and flow protocols, the latter clearly outcompetes traditional methods. In fact, one of the most common strategy to scale-up reactions in flow is the “numbering-up”.⁶⁹ Thus, by placing reactors in parallel, the productivity of the reaction is dramatically increased (linear trend, Figure 1.20). Hence, by placing a greater number of reactors the productivity is linearly increased. The higher productivity of this strategy allowed the implementation of photochemical transformations in pharmaceutical and fine-chemical industry, previously hampered by the batch scale-up that has a sequential trend (Figure 1.20).⁶⁷

Increased selectivity

The utilization of microchannels enhances the mass-, heat- and photon- transport.⁶⁹ This phenomenon impacts on the selectivity of the reaction. When considering a batch set-up, the reaction time of a photochemical process is defined by how many time the reaction vessel is

⁷⁹ Meyer, S.; Tietze, D.; Rau, S.; Schäfer, B.; Kreisel, G. *Photosensitized Oxidation of Citronellol in Microreactors. Journal of Photochemistry and Photobiology A: Chemistry* **2007**, 186, 248–253.

irradiated. Analogously, in flow reactors, the reaction time is defined by the average time that the reactants *reside* in the irradiated reactor. Thus, it is also called *residence time*. For this reason, side-reactions promoted by the overheating or overirradiation of the reactor are avoided.

Fast mixing

An optimal mixing is key to suppress the formation of side-products, that can originate from local concentration gradients.⁷⁴ In fact, synthetic chemists normally neglect the mixing effect in the reaction outcome. When homogeneity is achieved immediately after adding one reagent to another, we can consider that the mixing time between two reaction components is much shorter than the reaction time.⁸⁰ In such scenario, no mixing effects are generally observed. However, in some cases the reaction occurs before the solution is fully mixed.⁸¹ Thus, proceeding before having an homogeneous media. In fact, selectivity and degradation issues are commonly observed. For this reason, the common strategy used in batch protocols to slow down the initial fast reaction kinetics is by decreasing the reaction temperature. Nevertheless, in microreactors the mixing efficiency is substantially increased due to the reduced dimensions of the device. In some cases, this substantial advantage allows to carry out the reaction without taking special care on the initial mixing temperature.

Multiphasic synthesis

Gas-liquid and solid-liquid reactions are very common in chemical industry. The preparation of peptides and in some cases proteins is generally accomplished using a solid support.⁸² Additionally, gases (such as ethylene) are used for the preparation of useful reagents.⁸³ However, in these cases the mass transfer from one phase to another is commonly the rate-determining step. In batch, the interphase area is low and undefined. Thus, long reaction times are usually required to access the desired reactivity. Contrarily, microreactors increase the interphase area and consequently the mass transfer between the two phases is larger. This fact, leads to faster reactions, making flow chemistry an important alternative for such transformations.

⁸⁰ Tabeling, P. *A Brief Introduction to Slippage, Droplets and Mixing in Microfluidic Systems*. *Lab Chip* **2009**, *9*, 2428.

⁸¹ Yoshida, J.; Takahashi, Y.; Nagaki, A. *Flash Chemistry: Flow Chemistry That Cannot Be Done in Batch*. *Chem. Commun.* **2013**, *49*, 9896–9904.

⁸² Hartrampf, N.; Saebi, A.; Poskus, M.; Gates, Z. P.; Callahan, A. J.; Cowfer, A. E.; Hanna, S.; Antilla, S.; Schissel, C. K.; Quartararo, A. J.; Ye, X.; Mijalis, A. J.; Simon, M. D.; Loas, A.; Liu, S.; Jessen, C.; Nielsen, T. E.; Pentelute, B. L. *Synthesis of Proteins by Automated Flow Chemistry*. *Science* **2020**, *368*, 980–987.

⁸³ Juliá, F.; Yan, J.; Paulus, F.; Ritter, T. *Vinyl Thianthrenium Tetrafluoroborate: A Practical and Versatile Vinylating Reagent Made from Ethylene*. *J. Am. Chem. Soc.* **2021**, *143*, 12992–12998.

Case of study – Enhanced efficiency of the photochemistry of aryl ketones in flow

The exploitation of aryl ketones photochemistry is one of the main topics of this dissertation. For this reason, it is crucial to understand the importance of flow setups benefits over batch protocols when comparing the synthetic applications of carbonyl compounds. As previously explained in this chapter, benzophenone derivatives are an important class of triplet sensitizers. Different groups have exploited such molecules for the construction of complex scaffolds.

In 2016, Lefebvre, Hoffmann and Rueping, investigated the use of microfluidic photoreactors (MFP) for the trifluoromethylation of olefins using benzophenones as organic photocatalysts (Figure 1.21).⁸⁴ Regardless the operative mechanism, the irradiation of a reaction mixture containing 10 mol% of benzophenone **42** in the presence of one equivalent of the Langlois reagent and *N*-Ph maleimide **41**, furnished the trifluoromethylated product **43** both in flow and batch conditions. Remarkably, when comparing both strategies, reduced reaction times were observed (30 min in flow vs 6 hours in batch) with similar reaction yields (54% in flow vs 61% in batch). Nevertheless, the productivity by means of STY was exceptionally increased in flow (54 times higher in flow). Thus, highlighting the importance of such protocols in aryl ketone photochemical transformations.

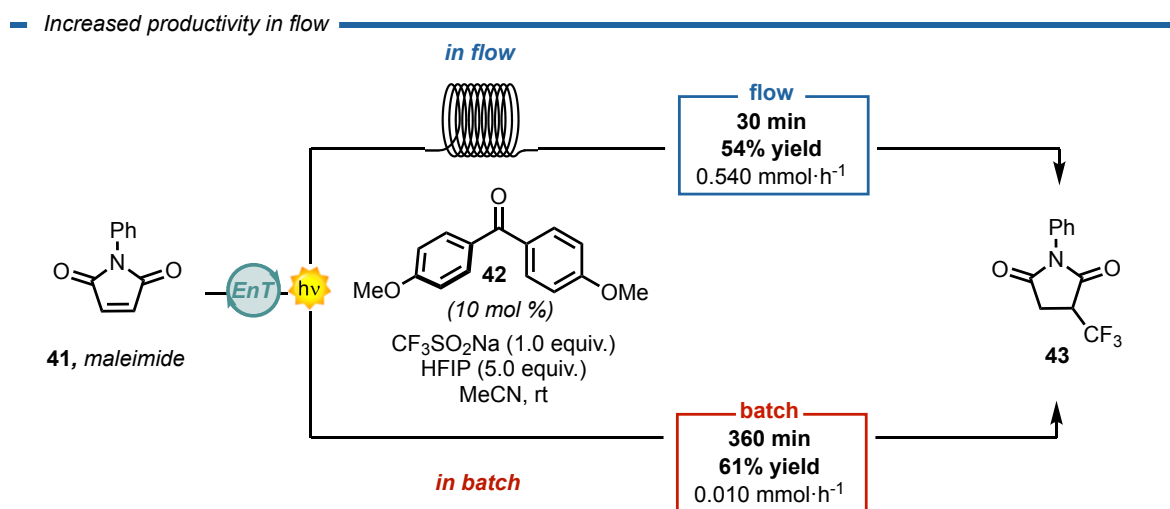


Figure 1.21. - Flow chemistry-enhanced productivity of light-excited aryl ketone chemistry reported by Lefebvre, Hoffmann and Rueping.⁸⁴

⁸⁴ Lefebvre, Q.; Hoffmann, N.; Rueping, M. Photoorganocatalysed and Visible Light Photoredox Catalysed Trifluoromethylation of Olefins and (Hetero)Aromatics in Batch and Continuous Flow. *Chem. Commun.* **2016**, 52, 2493–2496.

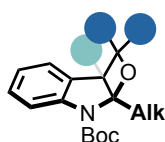
Chapter II

Synthetic Transformations Driven by Triplet State Benzophenones

— Chapter II - Synthetic Transformations Driven by Triplet State Benzophenones

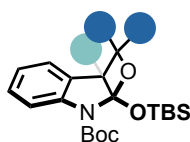
Section 1.

Towards the construction of Oxeto-Indolinic Polycycles



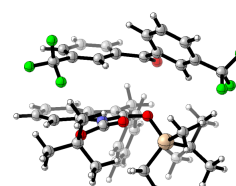
Section 2.

Microfluidic Visible-Light Dearomatization of Oxindole Enol Ethers



Section 3.

A Mechanistic Interrogation of the Process. The Effect of Visible-Light Irradiation



Goals:

- To develop new efficient visible-light Paternò-Büchi reactions.
- To exploit the utilization of previously overlooked biorelevant heterocyclic partners in Paternò-Büchi reactions (such as indoles and oxindole derivatives).
- Propose new models for the diastereoselectivity prediction in visible-light Paternò-Büchi reactions with indoles and oxindole derivatives.

Publications:

Section 1: Mateos, J.; Vega-Peñaloza, A.; Franceschi, P.; Rigodanza, F.; Andreetta, P.; Companyó, X.; Pelosi, G.; Bonchio, M.; Dell'Amico, L. *A Visible-Light Paternò-Büchi Dearomatisation Process towards the Construction of Oxeto-Indolinic Polycycles*. *Chem. Sci.* **2020**, *11*, 6532–6538

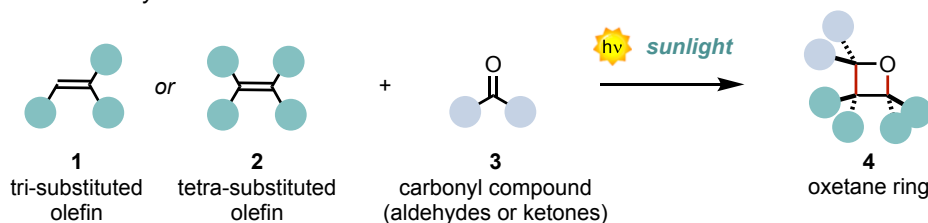
Section 2: Franceschi, P.; Mateos, J.; Vega-Peñaloza, A.; Dell'Amico, L. *Microfluidic Visible-Light Paternò-Büchi Reaction of Oxindole Enol Ethers*. *Eur. J. Org. Chem.* **2020**, *2020*, 6718–6722.

Section 3: Submitted manuscript

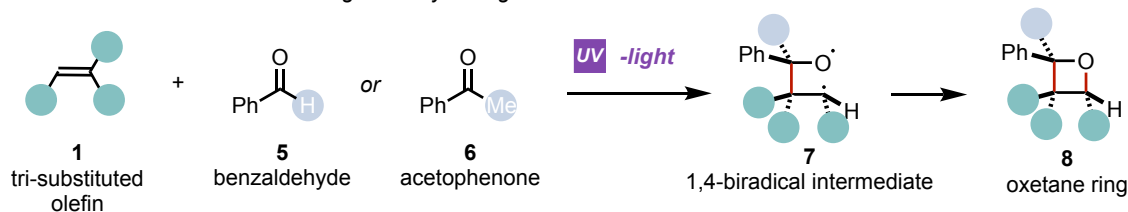
2. The Paternò-Büchi reaction

The photochemical [2+2]-cycloaddition between an olefin and an excited-state carbonyl compound is known as the Paternò-Büchi (PB) reaction. This transformation owes his name to the pioneers Prof. Emmanuele Paternò and Prof. George Hermann Büchi. The first, initially reported the reaction. In fact, in 1909, Paternò described how a mixture of tri- or tetra-substituted olefins (**1** or **2**) and carbonyl compounds (**3**) irradiated with sunlight furnished the oxetane product **4** in synthetically useful yields (Scheme 2.1A).¹ In 1954, Büchi studied in-depth the reaction mechanism of the process (Scheme 2.1B).² In this last case, Büchi and co-workers identified for the first time the 1,4-biradical intermediate **7** when using **1** with benzaldehyde **5** or acetophenone **6**.

A. the initial discovery of Emanuele Paternò



B. the initial mechanistic investigations by George Hermann Büchi



Scheme 2.1. - Pioneering reports on the Paternò-Büchi reaction.

Importantly, oxetanes are key motifs in drug discovery, insecticide development as well as in polymer chemistry (*e.g.* Oxetanocin A **9**, EDO **10** and EHMO **11** respectively in Figure 2.1).³ For this reason, the PB reaction is a useful strategy to construct oxetanes in high yields in a single-step.⁴ In fact, when compared to the classical polar strategies, the formation of these heterocycles foresees the use of tedious procedures in multi-step conditions.⁵

¹ Paternò, E.; Chieffi, G. *Sintesi in Chimica Organica per Mezzo Della Luce. Nota II. Composti Degli Idrocarburi Non Saturi Con Aldeidi e Chetoni.* Gazz. Chim. Ital **1909**, 39, 341

² Büchi, G.; Inman, C. G.; Lipinsky, E. S. *Light-Catalyzed Organic Reactions. I. The Reaction of Carbonyl Compounds with 2-Methyl-2-Butene in the Presence of Ultraviolet Light.* J. Am. Chem. Soc. **1954**, 76, 4327–4331

³ Bull, J. A.; Croft, R. A.; Davis, O. A.; Doran, R.; Morgan, K. F. *Oxetanes: Recent Advances in Synthesis, Reactivity, and Medicinal Chemistry.* Chem. Rev. **2016**, 116, 12150–12233.

⁴ D'Auria, M. *The Paternò-Büchi Reaction – a Comprehensive Review.* Photochem. Photobiol. Sci. **2019**, 18, 2297–2362.

⁵ Burkhard, J. A.; Wuitschik, G.; Plancher, J.-M.; Rogers-Evans, M.; Carreira, E. M. *Synthesis and Stability of Oxetane Analogs of Thalidomide and Lenalidomide.* Org. Lett. **2013**, 15, 4312–4315.

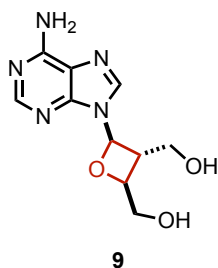
Altogether, the advantages of this light-triggered transformation pushed the boundaries of the reaction. Thus, the broadening of the reaction knowledge was driven by two parallel but synergistic avenues. On the one hand, the synthetic community developed different methods with a myriad of reaction partners.⁴ On the other hand, the physical organic chemistry community proposed different prediction models for the regio- and diastereoselectivity of the reaction.⁶

— oxetanes in drug discovery, insecticide development and polymer chemistry

Drug discovery

Oxetanocin A

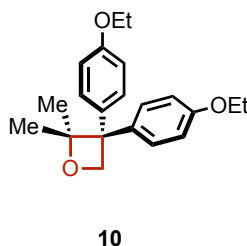
inhibits the reverse transcriptase of HIV by mimicking adenosine



Insecticide development

EDO

25-times more potent than DDT and active against DDT-resistant strains



Polymerization

EHMO

key intermediate for the synthesis of a wide variety of monomers

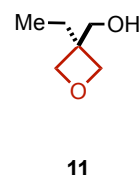


Figure 2.1. - Oxetanes in drug discovery, insecticide development and polymer chemistry.

In the following pages, I will describe our efforts towards the construction of novel polycycles with promising applications in medicinal chemistry as well as the mechanistic study of such novel transformations.

⁶ Fréneau, M.; Hoffmann, N. *The Paternò-Büchi Reaction—Mechanisms and Application to Organic Synthesis*. *J. Photochem. Photobiol. C* **2017**, *33*, 83–108



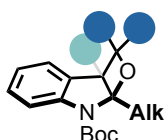
Chapter II – Section 1

Dearomative Paternò-Büchi Reaction – Towards the construction of Oxeto-Indolinic Polycycles

Chapter II - Synthetic Transformations Driven by Triplet State Benzophenones

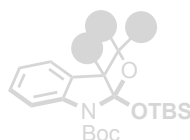
Section 1.

Towards the construction of Oxeto-Indolinic Polycycles



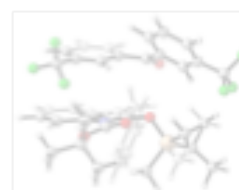
Section 2.

Microfluidic Visible-Light Dearomatization of Oxindole Enol Ethers



Section 3.

A Mechanistic Interrogation of the Process, the Effect of Visible-Light Irradiation



- To develop a visible-light mediated Paternò-Büchi reaction.
- To use indoles as reaction partners for the application of dearomative processes.⁷

⁷ The project discussed in this chapter has been conducted in collaboration with Dr. Alberto Vega Peñaloza, Pietro Franceschi, Philip Andreetta (involved in the synthesis and characterization of the starting indole derivatives as well as in the final oxeto-indolinic products) and Dr. Francesco Rigodanza (involved in the photochemical and electrochemical characterization of the reaction). I individually found the reactivity with indoles and optimized the reaction conditions as well as prepared several entries of the reaction scope.

This work has been published: Mateos, J.; Vega-Peñaloza, A.; Franceschi, P.; Rigodanza, F.; Andreetta, P.; Companyó, X.; Pelosi, G.; Bonchio, M.; Dell'Amico, L. *A Visible-Light Paternò-Büchi Dearomatisation Process towards the Construction of Oxeto-Indolinic Polycycles*. *Chem. Sci.* **2020**, *11*, 6532–6538

2.1.1 Introduction

The generation of new chemical architectures starting from abundant, inexpensive materials is one of the main goals of the synthetic chemical community.⁸ The evolution of 3-D molecular arrangements starting from planar π -systems is of particular interest due to the possibility of assembling complex polycyclic structures from readily available aromatic feedstocks.⁸ In this context, the polycycles originating from indoles are one of the most relevant class of pharmacophores,⁹ since their wide occurrence in natural alkaloids and drugs.^{8,9} The development of effective methods towards the dearomatization of indoles is an attractive strategy to access complex polycyclic indoline scaffolds. Light-driven dearomatization methods are recently emerging as a complementary sustainable approach to accessing strained polycyclic systems, difficult or impossible to obtain under polar reactivity (Figure 2.2).¹⁰ In fact, the common strategy for the photochemical construction of this polycycles rely on the use of energy transfer (EnT) photocatalysts capable of sensitize indole moieties.¹¹ On the other hand, the formation of heterocyclic polycycles such as oxetanes is of wide interest.³ Oxetanes are present in a variety of biologically active molecules, being promising structural modules in drug discovery.¹² Regrettably, the construction of oxetane-based polycyclic scaffolds is a challenging synthetic task owing to the high ring strain of this heterocycle when compares to the *all-carbon* analogue.

⁸ **a)** Wertjes, W. C.; Southgate, E. H.; Sarlah, D. Recent Advances in Chemical Dearomatization of Nonactivated Arenes. *Chem. Soc. Rev.*, **2018**, 47, 7996–8017. **b)** Zheng, C.; You, S.-L. *Catalytic Asymmetric Dearomatization by Transition-Metal Catalysis: A Method for Transformations of Aromatic Compounds*. *Chem*, **2016**, 1, 830–857. **c)** Humphrey, G. R.; Kuethe, J. T. *Practical Methodologies for the Synthesis of Indoles*. *Chem. Rev.* **2006**, 106, 2875–2911.

⁹ Kaushik, N.; Kaushik, N.; Attri, P.; Kumar, N.; Kim, C.; Verma, A.; Choi, E. *Biomedical Importance of Indoles*. *Molecules* **2013**, 18 (6), 6620–6662.

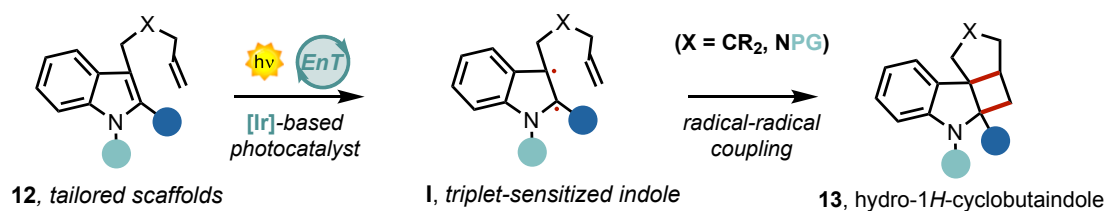
¹⁰ Okumura, M.; Sarlah, D. Visible-Light-Induced Dearomatizations. *Eur. J. Org. Chem.* **2020**, 2020, 1259–1273.

¹¹ **a)** Zhu, M.; Zheng, C.; Zhang, X.; You, S.-L. Synthesis of Cyclobutane-Fused Angular Tetracyclic Spiroindolines via Visible-Light-Promoted Intramolecular Dearomatization of Indole Derivatives. *J. Am. Chem. Soc.* **2019**, 141 (6), 2636–2644. **b)** Oderinde, M. S.; Mao, E.; Ramirez, A.; Pawluczyk, J.; Jorge, C.; Cornelius, L. A. M.; Kempson, J.; Vetrichelvan, M.; Pitchai, M.; Gupta, A.; Gupta, A. K.; Meanwell, N. A.; Mathur, A.; Dhar, T. G. M. Synthesis of Cyclobutane-Fused Tetracyclic Scaffolds via Visible-Light Photocatalysis for Building Molecular Complexity. *J. Am. Chem. Soc.* **2020**, 142, 3094–3103.

¹² Carreira, E. M.; Fessard, T. C. Four-Membered Ring-Containing Spirocycles: Synthetic Strategies and Opportunities. *Chem. Rev.* **2014**, 114, 8257–8322.

— common photochemical strategy for indole dearomatization

Selected example: *J. Am. Chem. Soc.*, **2019**, *141*, 2636—2644



Formation of strained polycycles — from planar to 3D structures

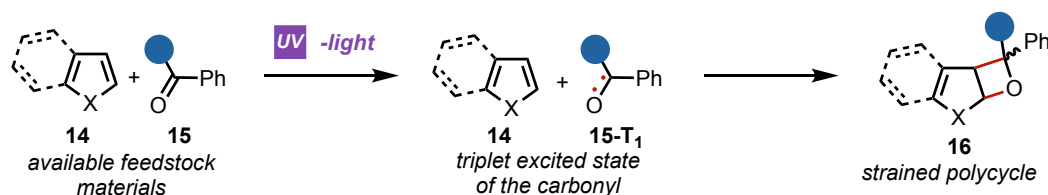
Figure 2.2. - Common photosensitized strategy for the dearomatization of indoles.

2.1.2 Challenges of the project

We envisaged that the PB reaction, where the direct excitation of a carbonyl compound triggers a [2+2]-heterocycloaddition with an olefin, could yield strained polycycles in a single step avoiding the use of EnT photocatalysts (Figure 2.3).^{1,2}

— direct excitation of carbonyls yielding strained polycycles

Classical Paternò-Büchi reaction: Intermolecular cycloaddition



main issues UV light irradiation - Hg-lamp apparatus - low regiocontrol - low diastereocontrol - substrate dependent

Figure 2.3. - Main issues in the classical Paternò-Büchi reaction yielding strained polycycles.

Due to the high relevance of oxetanes, both in natural products and synthetic molecules, this reaction has an immense synthetic potential.⁴ Capitalizing on this, a number of total synthesis have found the PB reaction as the key step for the assembly of complex biorelevant compounds.⁶ However, its progress towards large-scale synthesis have been largely hampered by the need of UV-light sources (Hg or Xe lamps) together with the corresponding specific reaction setups (e.g. quartz vessels). Further limitations of the reported PB methodologies are posed by the lack of generality and selectivity, leading to high substrate-dependency and poor

regio- and diastereocontrol.^{4,6} These drawbacks have precluded the development of general and scalable PB methods for the dearomatization of heterocycles,¹³ including indoles.¹⁴

The successful development of a PB reaction with indoles would open the way to the construction of biorelevant indolinic scaffolds with up to three contiguous stereocenters in one step from readily available aromatic feedstocks. However, the realization of such a general method is complicated by additional synthetic issues, including: *i*) the polar aldol-type addition between the reagents; *ii*) the electronic nature of the indole's alkene moiety, which has to match with the amphoteric nature of the excited carbonyl species; and not less important *iii*) the presence of light-driven side reactions, such as the dimerization of the carbonyl compound.¹⁵ From a broader perspective, a general and scalable light-driven indole dearomatization process should also involve the use of visible-light (>400 nm), thus avoiding side reactions, potential product decomposition as well as the need of sophisticated reaction setups.¹⁶

2.1.3 Section overview

In this section, I report a scalable and photocatalyst-free visible-light PB process for the dearomatization of indoles (Figure 2.4). The method is based on the use of available aromatic ketones (such as benzophenone), inexpensive illumination sources (*e.g.*, visible-light LEDs) and simple reaction setups. Structurally strained oxeto-indolinic polycycles are accessed with excellent regio- and diastereocontrol. Importantly, the unprecedented use of visible light (405 or 465 nm) in a PB reaction is key to suppress the undesired side reactions, while guaranteeing a clean, safe and efficient process. The generality of the method is proved for a large variety

¹³ **a)** Schreiber, S. L.; Satake, K. Application of the Furan Carbonyl Photocycloaddition Reaction to the Synthesis of the Bis(Tetrahydrofuran) Moiety of Asteltxin. *J. Am. Chem. Soc.* **1983**, 105, 6723–6724. **b)** D'Auria, M.; Racioppi, R.; Rofrano, F.; Stoa, S.; Viggiani, L. Investigation of the Hydroxyl Directing Effect on the Paternò-Büchi Reaction on 5-(2-Triisopropylsilyloxazolyl)Methanol Derivatives. *Tetrahedron* **2016**, 72, 5142–5148. **c)** Abe, M.; Torii, E.; Nojima, M. Paternò-Büchi Photocyclization of 2-Siloxyfurans and Carbonyl Compounds. Notable Substituent and Carbonyl (Aldehyde vs Ketone and Singlet- vs Triplet-Excited State) Effects on the Regioselectivity (Double-Bond Selection) in the Formation of Bicyclic Oxetanes. *J. Org. Chem.* **2000**, 65, 3426–3431. **d)** Rivas, C.; Bolivar, R. A. Synthesis of Oxetanes by Photoaddition of Carbonyl Compounds to 2,5-Dimethylthiophene. *Journal of Heterocyclic Chemistry* **1973**, 10, 967–971. **e)** D'Auria, M.; Emanuele, L.; Racioppi, R. Stereoselectivity in the Paternò-Büchi Reaction on Chiral Allylic Alcohols, for A Discussion of the Hydroxy Directing Effect. *LOC* **2005**, 2, 132–135. **f)** D'Auria, M.; Emanuele, L.; Racioppi, R.; Valente, A. Paternò-Büchi Reaction between Aromatic Carbonyl Compounds and 1-(3-Furyl)Alkanols. *Photochem. Photobiol. Sci.* **2008**, 7, 98–103.

¹⁴ **a)** Machida, M.; Takechi, H.; Kanaoka, Y. Photoreaction of N-(ω -Indol-3-Ylalkyl)Phthalamides: *Intramolecular Oxetane Formation of the Aromatic Imide System*. *Tetrahedron Letters* **1982**, 23, 4981–4982. **b)** Julian, D. R.; Tringham, G. D. *Photoaddition of Ketones to Indoles: Synthesis of Oxeto[2,3-*b*]Indoles*. *J. Chem. Soc., Chem. Commun.* **1973**, 1, 13b-14.

¹⁵ Cohen, S. Gerald.; Baumgarten, R. J. Photoreduction of Benzophenone by Amines, Alcohols, and Hydrocarbons. Medium Effects. *Photochemical Oxidative Deamination*. *J. Am. Chem. Soc.* **1967**, 89, 3471–3475

¹⁶ Schultz, D. M.; Yoon, T. P. Solar Synthesis: Prospects in Visible Light Photocatalysis. *Science* **2014**, 343, 1239176–1239176

of indoles and aromatic ketones, delivering oxeto-indolinic polycycles (35 examples) with up to three all-substituted stereocenters in high yields (up to >98%) and complete regio- and diastereocontrol. Remarkably, the present method is suitable for the construction of biorelevant pharmacophoric cores as well as for the functionalization of indole-based drugs. Implementation under a microfluidic setup allows the gram scale synthesis (up to 1.20 g) of the oxeto-indolinic products with improved synthetic performances.

— intermolecular visible-light Paternò-Büchi dearomatization process —

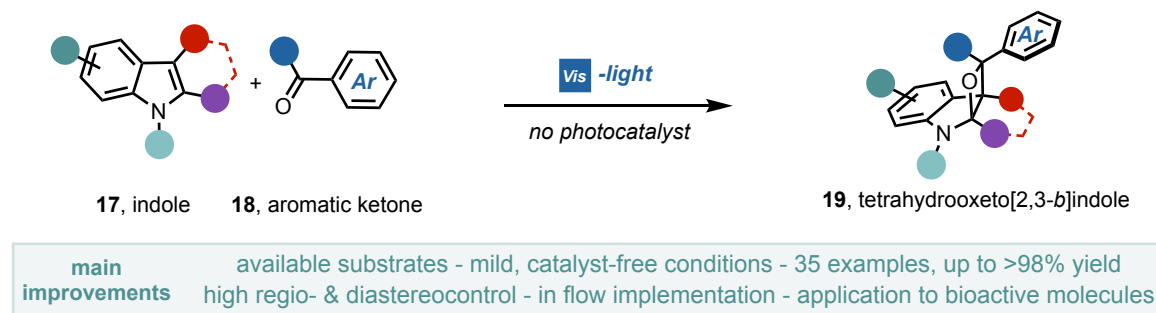
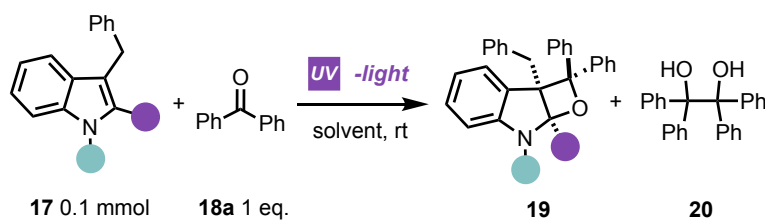


Figure 2.4. - Developed visible-light Paternò-Büchi reaction with indoles.

2.1.4 Results and discussion

Reaction optimization

We initiated our study testing different indoles **17a-d** in the presence of benzophenone **18a**. 3-Benzyl indoles were selected with the aim of generating a valuable *all-carbon* quaternary stereocenter within product **19** (Table 2.1). Irradiation at 365 nm of an equimolar mixture of unprotected 3-benzyl indole **17a** and benzophenone **18a** in toluene resulted in the complete recovery of unreacted starting materials (Table 2.1, entry 1). A similar fate accompanied *N*-methyl indole **17b** substrate, although with formation of **20** in trace amounts. We reasoned that reducing the electron density on the indole double bond would facilitate its reactivity with the triplet (T_1) biradical excited state of **18a**. Indeed, subjecting the *N*-Boc indole **17c** to the reaction conditions furnished the strained fused oxetane **19c**, albeit in modest yield (17%). In fact, extensive UV-light irradiation led to increasing amounts of the dimer **20** along with product decomposition. To further modulate the electronics of the reactive double bond, we placed a methyl group at C2-position of the indole (**17d**). In this case, prolonged reaction times (5h, Table 2.1, entry 4) result in improved reaction performances (55% yield). Nevertheless, marginal amounts of **20** were still detected. Thus, hindering the isolation of **19d**. At this juncture, an extensive screening of the reaction conditions was performed by testing different solvents (Table 2.1, entries 5 and 6). Unfortunately, none of these parameters shown beneficial effects on the suppression of the formation of **20**.



entry			17	reaction time	solvent	light source	(19) yield %	dr
1	H	H	17a	3 h	PhMe	365 nm	- 19a	-
2	Me	H	17b	3 h	PhMe	365 nm	- 19b	-
3	Boc	H	17c	3 h	PhMe	365 nm	17 19c	>20:1
4	Boc	Me	17d	5 h	PhMe	365 nm	55 19d	>20:1
5	Boc	Me	17d	5 h	MeCN	365 nm	35 19d	>20:1
6	Boc	Me	17d	5 h	CH ₂ Cl ₂	365 nm	nr 19d	-

Table 2.1. - Initial optimization of the reaction conditions between indoles and diaryl ketones.

Suppressing the undesired pinacol reaction

At this point, reasoning on the possible competitive photoreactions taking place, we assumed that an inferior amounts of T_1 ketone excited state as well as the use of a solvent with lower C-H bond dissociation could preferentially channel the system towards the intended PB reactivity. This is consistent with the operation of two alternative side-reaction manifold *i* and *ii* (Figure 2.5).¹⁷

- i*) On the one hand, the use of electron-rich amines, such as electron-rich nitrogen heterocycles **17b**, leads to a CT pathway (Figure 2.5a). In this case, one molecule of **21** reduces the T_1 state of **18a** in favour of the corresponding ketyl radical **22**. Then, **22** deprotonates the acidic α -position of **23** triggering the formation of the pinacol product **20**. This is in line with the observed experimental trend when passing from **17a** to **17d**. For this reason, the indole protecting group plays an important role in the reaction outcome.
- ii*) On the other hand, the solvent also plays an important role in this PB reaction. When using solvents with a low C-H BDE (such as toluene $\Delta H_{\text{BDE}} = 89.6 \text{ kcal}\cdot\text{mol}^{-1}$)¹⁸ the protonated ketyl radical **22-H** is directly formed after HAT. Thus, favouring the homodimerization towards **20**. In this case, this side-reaction can be avoided using different solvents (like acetone) and decreasing the amount of T_1 of **18a**.

¹⁷ Dormán, G.; Nakamura, H.; Pulsipher, A.; Prestwich, G. D. The Life of Pi Star: Exploring the Exciting and Forbidden Worlds of the Benzophenone Photophore. *Chem. Rev.* **2016**, *116*, 15284–15398.

¹⁸ Blanksby, S. J.; Ellison, G. B. Bond Dissociation Energies of Organic Molecules. *Acc. Chem. Res.* **2003**, *36*, 255–263.

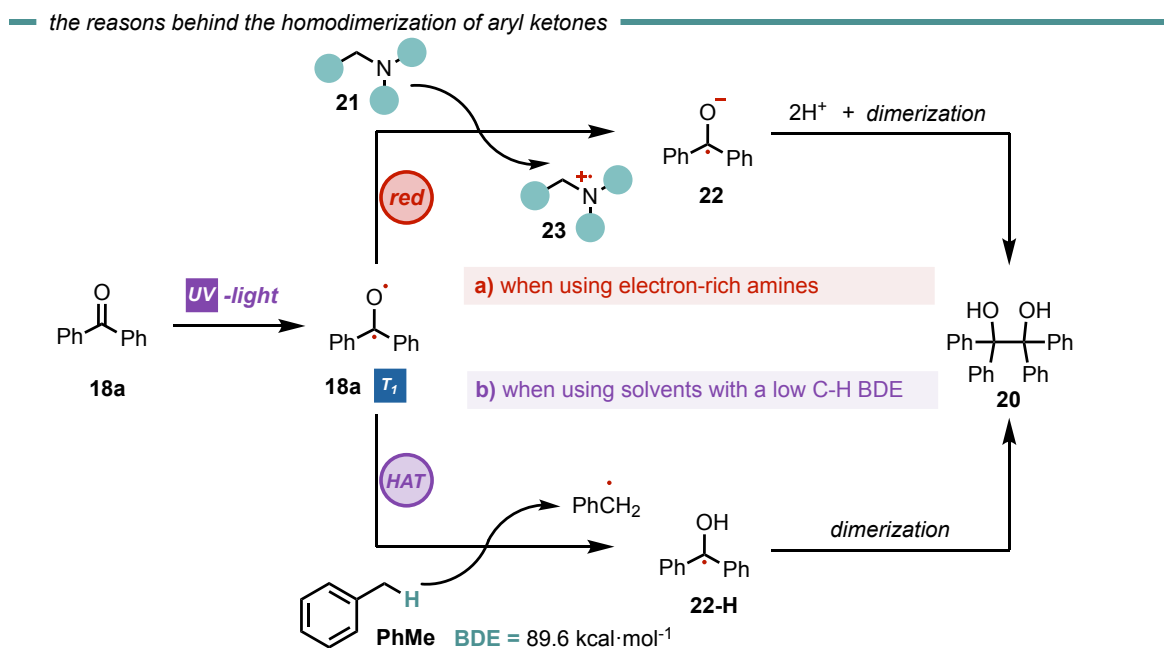
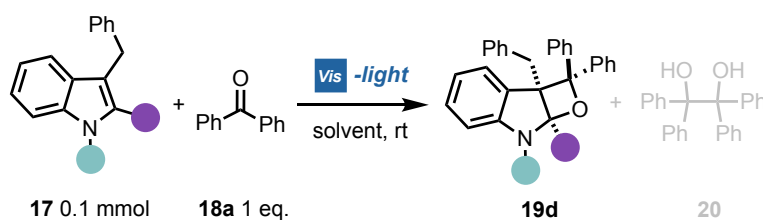


Figure 2.5. - The two possible pathways behind the homodimerization of diaryl ketones. a) CT pathway. b) HAT pathway.

Given the two possible reaction manifolds, we decided to investigate the role of the light source and the solvent to suppress the formation of the pinacol by-product. So far, to reduce the amount of T₁ excited state, we employed a light source with a maximum emission set at 400 nm (vs 365 nm), close to the limit of absorption of benzophenone **18a**. Interestingly, despite the reaction was slower (9 hours to reach full conversion), **20** was only detected in trace amounts along with a promising 67% isolated yield of **19d** (Table 2.2, entry 1). A slightly red-shifted light source, resulted in the optimal balance between reactivity and reaction time, delivering **3** in quantitative yield and complete diastereocontrol after 12 h (Table 2.2, entry 2). Importantly, neither homodimer **20** nor product **19d** decomposition were detected. The use of higher C-H BDE solvents revealed acetone to be the best solvent for the present system, with quantitative formation of **19d** (>98% yield) in reduced reaction time (7 h in entry 3 vs 12 h in entry 2). Under these conditions product **19d** was obtained by simple solvent evaporation.



entry			17	reaction time	solvent	light source	(19) yield %	dr
1	Boc	Me	17d	9 h	PhMe	400 nm	67 19d	>20:1
2	Boc	Me	17d	12 h	PhMe	405 nm	>98 19d	>20:1
3	Boc	Me	17d	7 h	Acetone	405 nm	>98 19d	>20:1

Table 2.2. - Rational optimization of the reaction conditions.

The role of the light source

Before evaluating the generality and limits of the present PB process, we investigated the photochemical bases of the observed reactivity. Overimposing the absorption spectrum of benzophenone **18a** (under the optimized conditions) with the 405 nm LED emission spectrum, revealed a region (390-400 nm) of possible absorption (Figure 2.6).

— absorption of **18a** vs Emission of the 405 nm LED

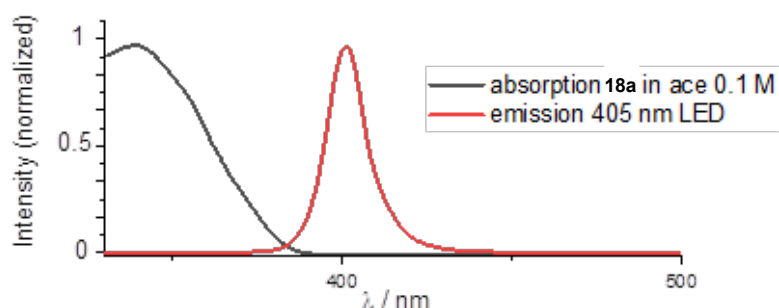


Figure 2.6. - Normalized absorption of **18a** vs normalized emission of the 405 nm LEDs used in this study.

A more accurate 3D analysis of the excitation/emission spectra of **18a**, clearly demonstrates that excitation at 405 nm (Figure 2.7, pink line) results in the generation of the corresponding T₁ excited state (green region). As expected, excitation at 365 nm (Figure 2.7, black line) resulted in the generation of a more intense emission signal (red region). These analyses confirm that the direct excitation of **18a** can take place also under visible light illumination.

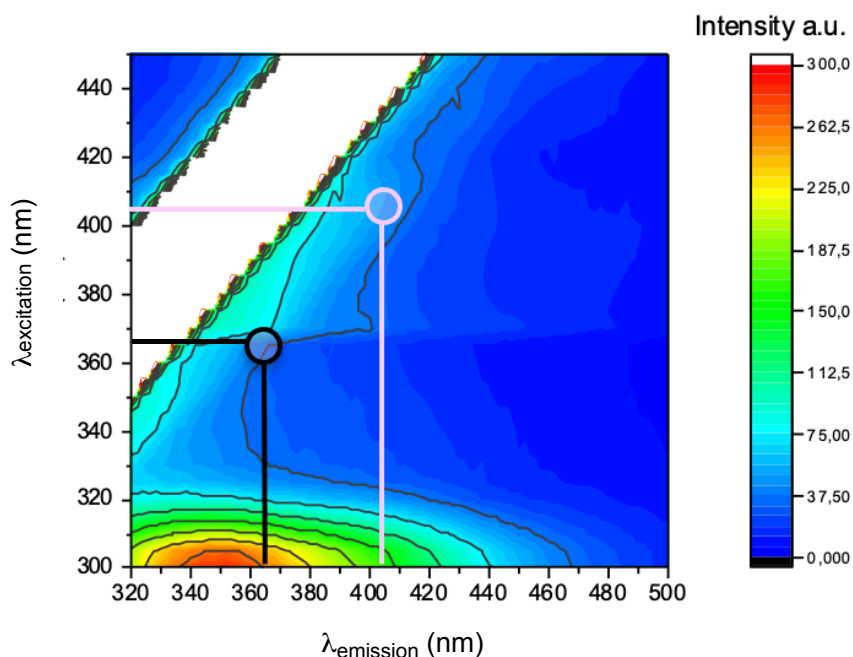


Figure 2.7. - 3D analysis of the excitation source and the emission of **18a**.

We then evaluated any possible ground- or excited-state association of the reagents.¹⁹ The absorption spectra of the isolated species (**17d** and **18a**) and the reaction mixture (**17d** + **18a**) did not present any significant spectral variations. Instead, Stern-Volmer analysis of **18a** excited state revealed an efficient quenching of the T_1 by **17d** (Figure 2.8), with no detection of excimer emission spectra. Taken together, these observations point to a direct excitation of **18a** under visible light towards the formation of its T_1 state, followed by the indole trapping.

¹⁹ Spectroscopical analysis ruled out the hypothesis of direct indole **17d** excitation that could lead to a transposed Paternò-Büchi reaction:
Kumarasamy, E.; Raghunathan, R.; Kandappa, S. K.; Sreenithya, A.; Jockusch, S.; Sunoj, R. B.; Sivaguru, J. *Transposed Paternò-Büchi Reaction*. *J. Am. Chem. Soc.* **2017**, *139*, 655–662.

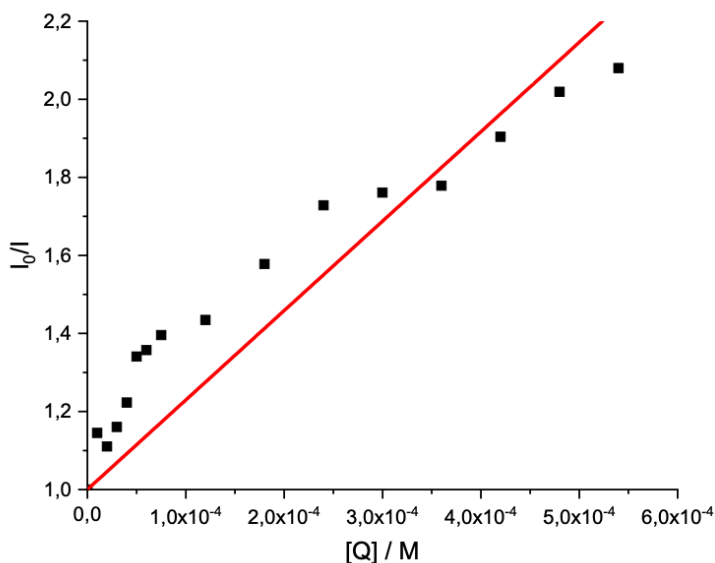
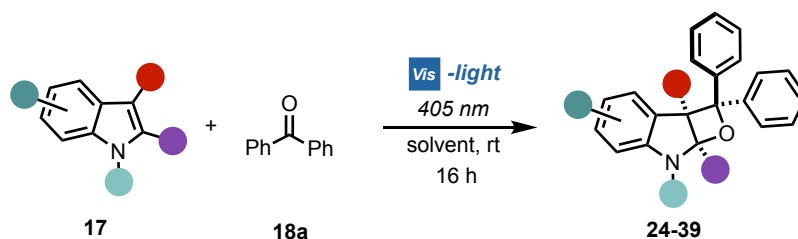


Figure 2.8. - Stern-Volmer of **18a** in the presence of **17d** in MeCN. ($\lambda_{\text{ex}}=365$ nm)

Generality of the reaction

Having revealed the reason of the observed reactivity, we next explored the generality of this visible-light PB reaction. Since toluene (PhMe) and acetone (ace) gave quantitative yields in the optimized conditions, we selected both as the best solvents for this reaction. For this reason, all the reactions were performed under both conditions, providing a general evaluation of the synthetic protocol.

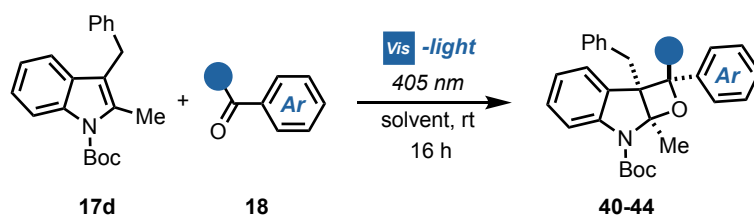
When looking at the effects in the indole moiety (Table 2.3), 3-benzylindoles with substituents at the *ortho*, *meta* and *para* positions furnished the corresponding tricyclic products **24-28** in high yields spanning from 72% to >98% and complete diastereocontrol. 3-Methyl and 3-hydroxymethyl indoles formed products **29** and **30** as single diastereoisomers in excellent yields (up to 85%). Remarkably, the reaction of 3-allylindole produced the product **31** in up to 67% yield with exquisite site-, regio- and diastereoselectivity. Indole derivatives bearing different substituents on the aromatic ring (**32-35**), diverse *N*-protecting groups (**36** and **37**) as well as various C2-substituents (**38** and **39**) efficiently participated in the visible-light PB reaction, furnishing diversified strained tetrahydrooxeto[2,3-*b*]indole scaffolds in yields up to 92% and >20:1 dr.



indole scope					
<p>24 PhMe: >98% yield Ace: >98% yield >20:1 dr</p>	<p>25 PhMe: >98% yield Ace: 40% yield >20:1 dr</p>	<p>26 PhMe: 78% yield Ace: 44% yield >20:1 dr</p>	<p>27 PhMe: 72% yield Ace: 67% yield >20:1 dr</p>	<p>28 PhMe: >98% yield Ace: 92% yield >20:1 dr</p>	
<p>29 PhMe: 82% yield Ace: 78% yield >20:1 dr</p>	<p>30 PhMe: 80% yield Ace: 85% yield >20:1 dr</p>	<p>31 PhMe: 67% yield Ace: 62% yield >20:1 dr</p>	<p>32 PhMe: 72% yield Ace: 72% yield >20:1 dr</p>	<p>33 PhMe: 50% yield Ace: 52% yield >20:1 dr</p>	
<p>34 PhMe: 83% yield Ace: 60% yield >20:1 dr</p>	<p>35 PhMe: 47% yield Ace: 49% yield >20:1 dr</p>	<p>36 PhMe: 71% yield Ace: 71% yield >20:1 dr</p>	<p>37 PhMe: 92% yield Ace: 96% yield >20:1 dr</p>	<p>38 Ace: 50% yield PhMe: 48% yield >20:1 dr</p>	<p>39 PhMe: 22% yield Ace: 7% yield >20:1 dr</p>

Table 2.3. - Substrate table when using different indole derivatives.

When moving to different substituted benzophenones, the reaction performed smoothly (Table 2.4) forming the corresponding product **40-44** in high yields (up to 86%) and excellent diastereocontrol (>20:1).



— benzophenone scope

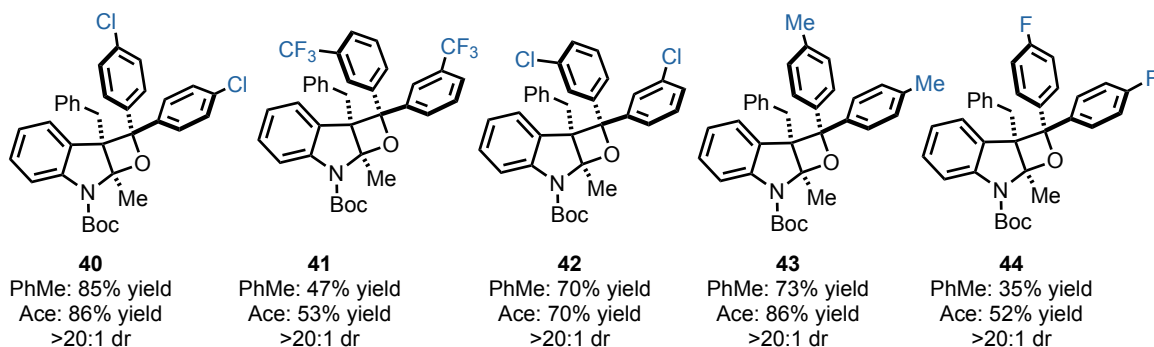
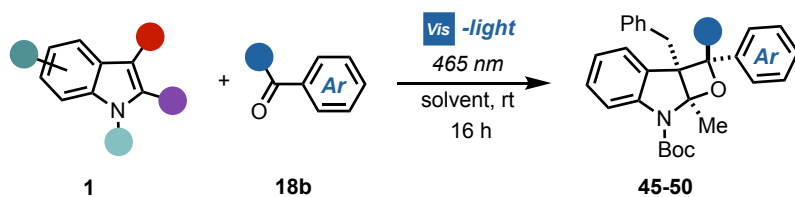


Table 2.4. - Substrate table when using different benzophenone derivatives.

Remarkably, also the prochiral benzil **18b** successfully engaged in the [2+2] heterocycloaddition process, delivering up to 0.50 g of dearomatized product **45** in batch conditions (>98% yield) with complete stereocontrol over the three generated stereocenters (Table 2.5). Its relative stereochemistry was inferred by X-ray analysis on single crystal. Diverse benzil derivatives formed quantitatively with complete diastereocontrol (**46-48**). Also, differently substituted indoles performed well, delivering the products **49** and **50** in up to 85% yield. All the benzil derivatives, with a more red-shifted absorption, successfully reacted under 465 nm illumination with no traces of side products.



benzil scope

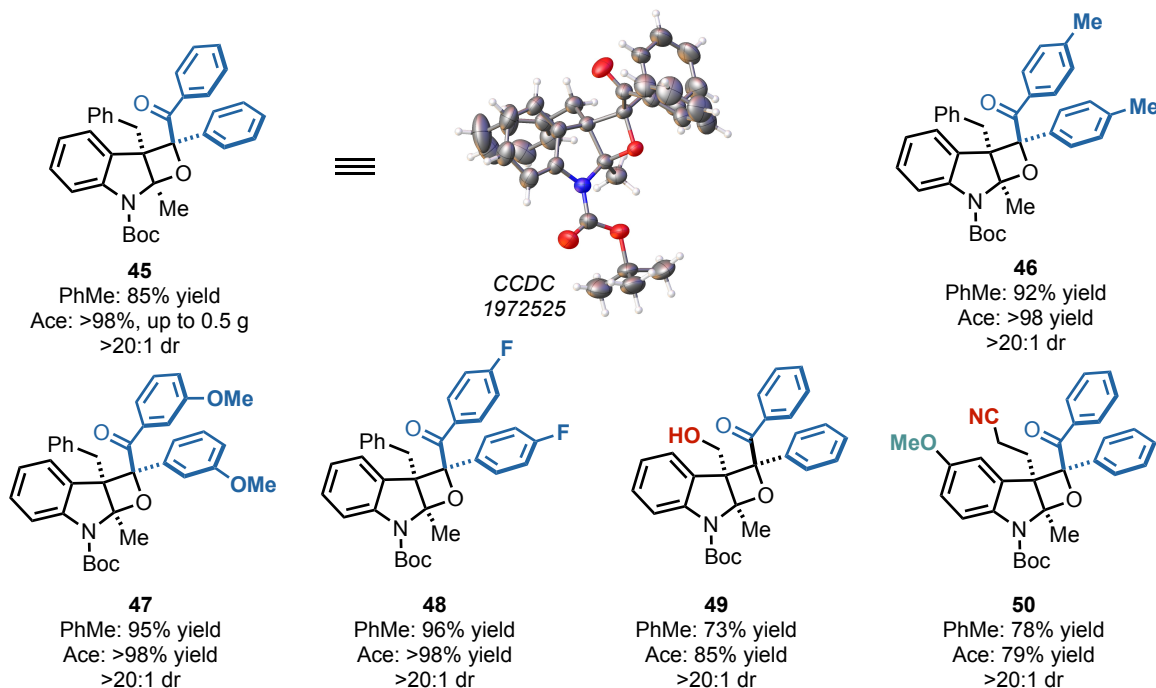
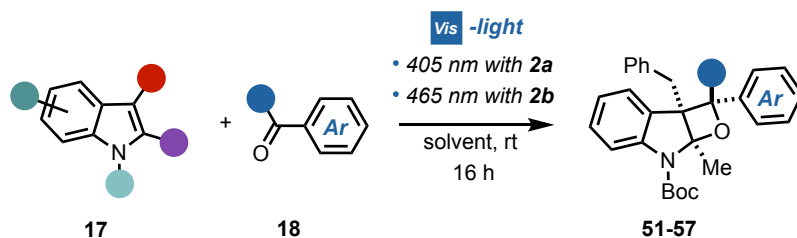


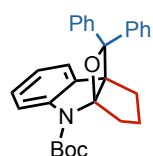
Table 2.5. - Substrate table when using different benzil derivatives.

We next sought to apply the developed dearomatization protocol to accessing relevant bioactive pharmacophoric cores (Table 2.6). A series of oxeto-indolinic derivatives **51-54**, bearing up to three contiguous stereocenters, were synthesised in high yields (48%-82%) and complete diastereocontrol. Further, marketed drugs such as Melatonin proved a useful substrate for the present method, affording the corresponding product **55** in 42% yield. Thus, demonstrating the synthetic potential of the developed method towards structural modifications of bioactive ingredients. Interestingly, enantiopure *N*-protected Tryptophan took part in the developed method both with **18a** and benzil **18b**, delivering attractive chiral tetrahydrooxeto[2,3-*b*]indole **56** and **57** in high yields and 2.5:1 to 5:1 dr, respectively.



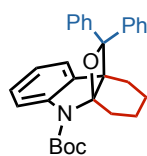
pharmacophores scope

tryptoline derivatives



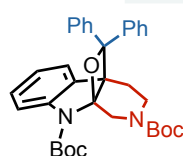
51

PhMe: 48% yield
Ace: 65% yield
>20:1 dr



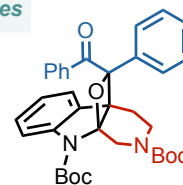
52

PhMe: 69% yield
Ace: 59% yield
>20:1 dr



53

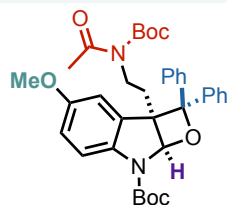
PhMe: 82% yield
Ace: 68% yield
>20:1 dr



54

PhMe: 67% yield
Ace: 67% yield
>20:1 dr

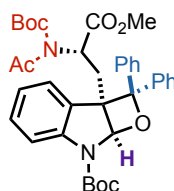
melatonin derivative



55

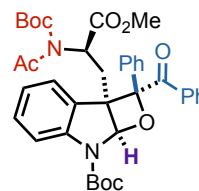
PhMe: 26% yield
Ace: 42% yield
>20:1 dr

tryptophan derivatives



56

Ace: 73% yield
2.5:1 dr



57

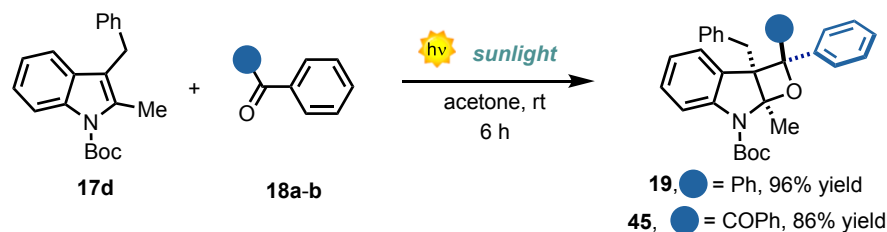
Ace: 79% yield
5:1 dr

Table 2.6. - Substrate table when using different pharmacophore derivatives.

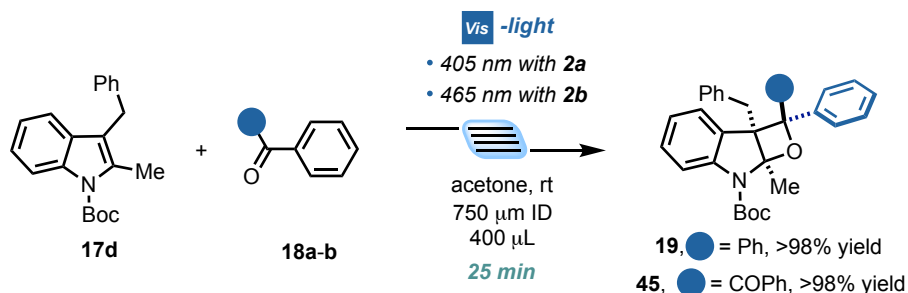
Large-scale synthesis and product manipulation

At this point, we wanted to further demonstrate the generality and the operational simplicity of the developed method. For this reason, the benchmark reactions of indole **17d** with ketones **18a** and **18b** were performed under natural sunlight irradiation (as Emmanuele Paternò set-up the reaction more than in 1909).¹ Both reactions performed smoothly delivering the corresponding products **19** and **45** in 96% and 86%, within 6 h reaction time (Scheme 2.1a).

A. natural sunlight irradiation



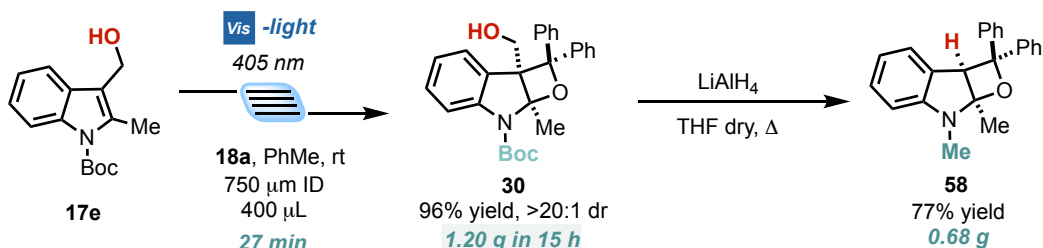
B. microfluidic synthesis



Scheme 2.2. - 3D analysis of the excitation source and the emission of **2a**.

Additionally, the synthetic method was implemented under a microfluidic photoreactor²⁰ (Scheme 2.1b). The oxeto-indolinic products **19** and **45** formed rapidly, within 25 min residence time, in quantitative yields. Encouraged by these results, we set up a large-scale microfluidic synthesis of **30**, which was obtained with improved synthetic performances and productivity with respect to the batch setup (96% yield and $0.176 \text{ mmol}\cdot\text{h}^{-1}$ in flow vs 80% yield and $0.080 \text{ mmol}\cdot\text{h}^{-1}$ in batch). The microfluidic setup allowed the isolation of **30** in up to 1.20 g within 15 h (Scheme 2.2).

large scale synthesis and product manipulation



Scheme 2.3. - Microfluidic large scale synthesis of **30** and manipulation.

²⁰ Cambié, D.; Bottecchia, C.; Straathof, N. J. W.; Hessel, V.; Noël, T. Applications of Continuous-Flow Photochemistry in Organic Synthesis, Material Science, and Water Treatment. *Chem. Rev.* **2016**, *116*, 10276–10341.

Thanks to the large-scale synthesis of compound **30**, we were able to study the manipulation of it (Scheme 2.2). The use of LiAlH_4 delivered the *N*-methyl protected tetrahydrooxeto[2,3-*b*]indole **58** in 77% yield (0.68 g) with the unexpected formal removal of the hydroxymethyl group. It should be noted that *N*-methyl indoline-alkaloids possess widespread biological activities,⁸ and the oxeto-scaffold **58** is an unprecedented representative of this class of molecules.

Limitations

Despite the broad generality of the method, we found some limitations. These restrictions are due to two main reasons: *i*) the use of visible-light instead of UV-light; and *ii*) the instability of the oxeto-indolinic products, preventing the isolation of different compounds and limiting the manipulation of this scaffold.

In the first case, the use of visible-light sources, hindered the use of benzaldehyde and acetophenone derivatives (Figure 2.9). This class of molecules represent an important category of prochiral carbonyl compounds. Nevertheless, the marked UV absorption of these two families prevented the application of the developed method.

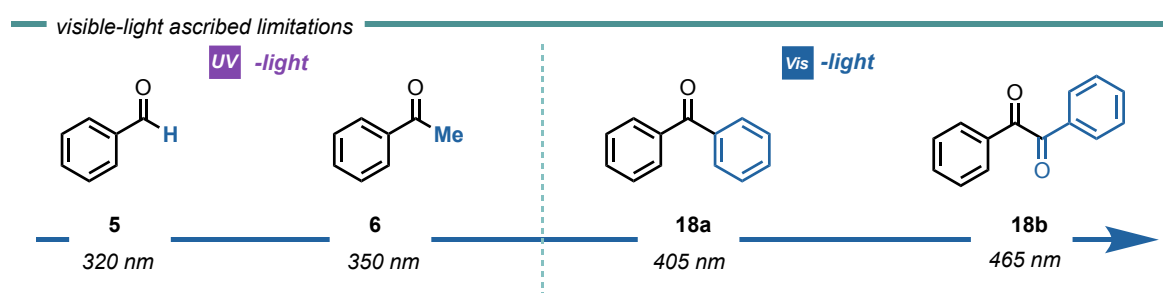


Figure 2.9. - Limitations ascribed to the use of visible-light sources.

In the second case, the method presents an important limitation in terms of possible manipulation of the oxeto-indolinic products (Figure 2.10). When **19** was treated with acids, spanning from strong acids such as TFA ($\text{pK}_a = -0.25$ in water and 3.45 in DMSO)²¹ to acetic acid ($\text{pK}_a = 4.76$ in water) no deprotection of the Boc group was observed. Instead, the two initial starting materials **17d** and **18a** were isolated in quantitative yields. This fact can be ascribed to the instability of this polycyclic scaffolds towards a retrocyclic reaction.

²¹ Bordwell, F. G. *Equilibrium Acidities in Dimethyl Sulfoxide Solution*. *Acc. Chem. Res.* **1988**, 21, 456–463.

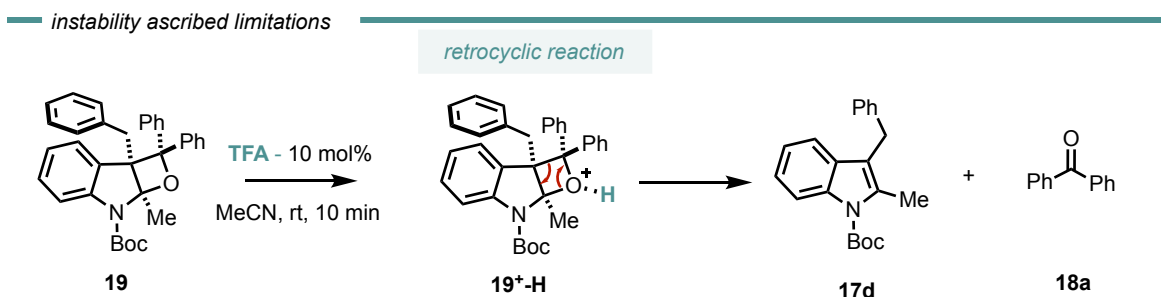


Figure 2.10. - Limitations ascribed to the instability of the oxeto-indolinic products in acidic conditions.

2.1.5 Conclusions

In summary, in this section I report an extremely mild visible-light PB process able to access strained oxeto[2,3-*b*]indole scaffolds starting from readily available substrates. This has been accomplished by the careful selection of the visible light source (405 or 465 nm), which enabled the complete shutting down of the ketone dimerization side reaction. The generality of the PB process has been demonstrated for a large variety of indoles and aromatic ketones with excellent results (up to >98% yield and complete dr). Importantly, the reaction is applicable to the assembly of diverse pharmacophoric cores and for the installation of oxetanes into diverse indole-based marketed drugs. Further, the reaction can be easily performed under natural sunlight as well as into a microfluidic photoreactor with definite advantages in terms of scalability (g scale), generality and productivity (up to 0.176 mmol·h⁻¹). Finally, oxeto-indolinic products can be easily converted into biorelevant *N*-methylated counterparts (up to 0.68 g).

2.1.6 Experimental Section

The NMR spectra were recorded on Bruker 400 Avance III HD equipped with a BBI-z grad probe head 5mm and Bruker 500 Avance III equipped with a BBI-ATM-z grad probehead 5mm. The chemical shifts (δ) for ^1H and ^{13}C are given in ppm relative to residual signals of the solvents (CHCl_3 @ 7.26 ppm ^1H NMR, 77.16 ppm ^{13}C NMR, Acetone @ 2.09 ppm ^1H NMR, 30.60 ppm ^{13}C NMR). Coupling constants are given in Hz. The following abbreviations are used to indicate the multiplicity: s, singlet; d, doublet; t, triplet; q, quartet; m, multiplet; br, broad signal.

The ^1H , ^{13}C and ^{19}F NMR spectra are available in literature free of charge.²²

High-Resolution Mass Spectra (HRMS) were obtained using Waters GCT gas chromatograph coupled with a time-of-flight mass spectrometer (GC/MS-TOF) with electron ionization (EI).

Chromatographic purification of products was accomplished using flash chromatography on silica gel (SiO_2 , 0.04-0.063 mm) purchased from Machery-Nagel, with the indicated solvent system according to the standard techniques. Thin-layer chromatography (TLC) analysis was performed on pre-coated Merck TLC plates (silica gel 60 GF254, 0.25 mm). Visualization of the developed chromatography was performed by checking UV absorbance (254nm) as well as with aqueous ceric ammonium molybdate and potassium permanganate solutions. Organic solutions were concentrated under reduced pressure on a Büchi rotary evaporator.

Materials: Commercial grade reagents and solvents were purchased at the highest commercial quality from Sigma Aldrich or FluoroChem and used as received, unless otherwise stated.

The diverse reaction set up images are available free of charge in literature.²²

Light sources emission spectra

The following spectra were recorded using an AvaSpec ULS3648 high-resolution fiber-optic spectrometer which was placed at a fixed distance of 0.5 cm from the light source.

(more info at: <https://www.avantes.com/products/spectrometers/starline/item/209-avaspec-uls3648-high-resolution-spectrometer>).

²² Mateos, J.; Vega-Peñaloza, A.; Franceschi, P.; Rigodanza, F.; Andreetta, P.; Companyó, X.; Pelosi, G.; Bonchio, M.; Dell'Amico, L. A Visible-Light Paternò-Büchi Dearomatisation Process towards the Construction of Oxeto-Indolinic Polycycles. *Chem. Sci.* **2020**, *11*, 6532–6538

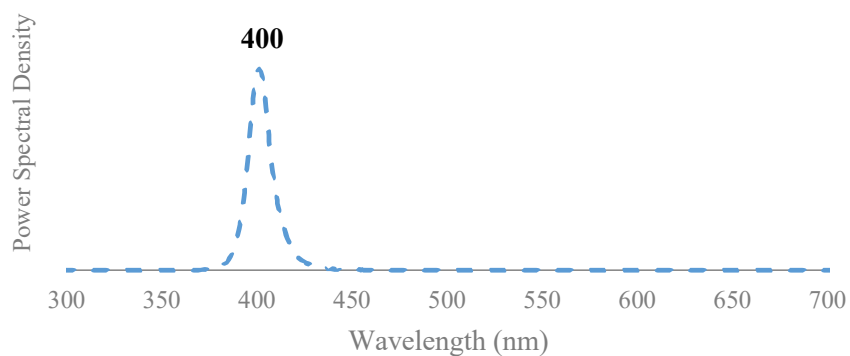


Figure 2.11. - Emission spectra of the 400 nm LEDs used in this section.

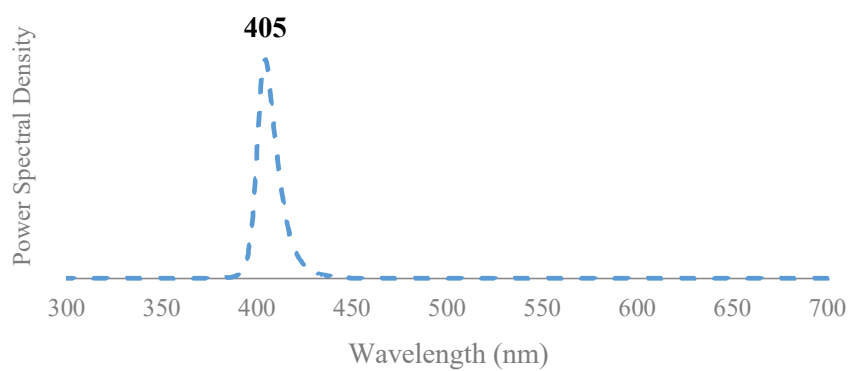


Figure 2.12. - Emission spectra of the 405 nm LEDs used in this section.

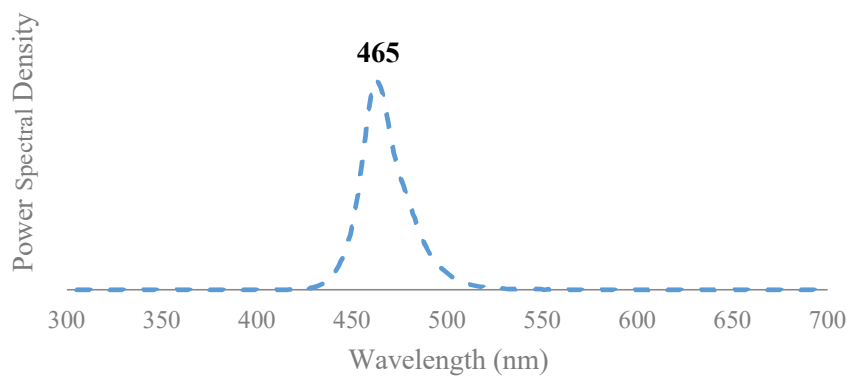
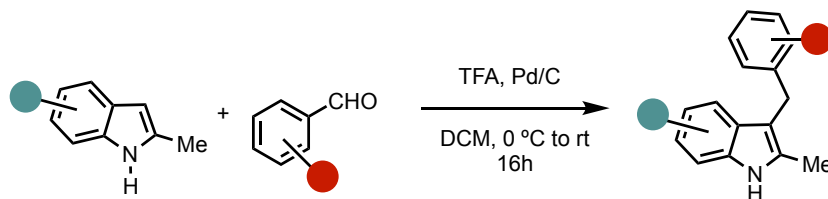


Figure 2.13. - Emission spectra of the blue LEDs used in this section.

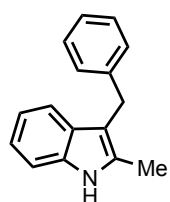
Synthesis and characterization of the used indole derivatives

— Preparation of 3-benzyl-sustituted indoles as synthetic precursors



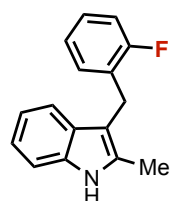
In a two-necked round bottom flask, a solution of 2-methylindole (0.66 g, 5 mmol) and benzaldehyde (765 μ L, 7.5 mmol) in dichloromethane (25 mL, 0.2 M) was added to a stirring ice-cold mixture of trifluoroacetic acid (38 μ L, 0.5 mmol, 10 mol%) and Pd/C (5 wt%) in DCM. This flask was filled with hydrogen and the mixture was stirred at 0 °C. After full consumption of the starting material, monitored by TLC (2% acetone in hexane), the palladium on carbon was filtered and the solvent was concentrated under reduced pressure. The crude product was purified by chromatography (9:1, hexane:EtOAc), giving 2-methyl-3-benzyl indole as a white solid that turned red overtime (1.04 g, 94% yield).

3-benzyl-2-methyl-1H-indole (17b).



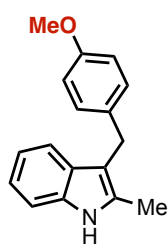
$^1\text{H-NMR}$ (400 MHz, CDCl_3): δ : 7.73 (*br s*, 1H, NH), 7.38 (d, $J = 8.0$ Hz, 1H, Ar), 7.27 — 7.20 (m, 5H, Ar), 7.16 — 7.07 (m, 2H, Ar), 7.03 — 7.00 (m, 1H, Ar), 4.06 (s, 2H, CH_2), 2.37 (s, 3H, CH_3) ppm. **$^{13}\text{C-NMR}$ (101 MHz, CDCl_3):** δ 141.6, 135.3, 131.6, 128.9, 128.2, 125.6, 121.0, 119.2, 118.4, 110.6, 110.1, 30.1, 11.8. ppm.

3-(2-fluorobenzyl)-2-methyl-1H-indole.



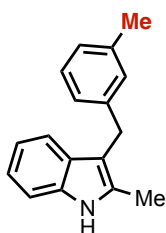
$^1\text{H-NMR}$ (400 MHz, CDCl_3): δ 7.81 (*br s*, 1H, NH), 7.46 (d, $J = 8.0$ Hz, 1H, Ar), 7.31 (d, $J = 8.0$ Hz, 1H, Ar), 7.16 — 6.96 (m, 6H, Ar), 4.10 (s, 2H, CH_2), 2.43 (s, 3H, CH_3) ppm. **$^{13}\text{C-NMR}$ (101 MHz, CDCl_3):** δ 162.2, 159.7, 150.8, 135.3, 131.9, 130.4 (d, $J = 4.5$ Hz), 128.8, 128.4 (d, $J = 8.0$ Hz), 127.4 (d, $J = 16.4$ Hz), 123.9 (d, $J = 3.6$ Hz), 121.1, 119.3, 118.3, 115.1 (d, $J = 22.9$ Hz), 110.2, 109.1, 22.8 (d, $J = 4.1$ Hz), 11.8 ppm. **$^{19}\text{F-NMR}$ (376 MHz, CDCl_3):** δ -118.56 (q, $J = 6.8$ Hz, 1F, C-F Ar) ppm. **HRMS(ESI-MS)** calculated for $\text{C}_{16}\text{H}_{15}\text{FN}^+$ [$\text{M}+\text{H}^+$] 140.1110, found 240.1109.

3-(4-methoxybenzyl)-2-methyl-1H-indole.



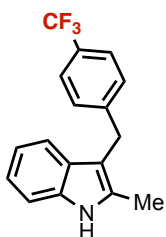
¹H-NMR (400 MHz, CDCl₃): δ 7.61 (*br s*, 1H, NH), 7.44 (d, *J* = 8.0 Hz, 1H, Ar), 7.29 — 7.24 (m, 5H, Ar), 7.17 — 7.14 (m, 1H, Ar), 7.10 — 7.07 (m, 1H, Ar), 4.11 (s, 2H, CH₂), 2.34 (s, 3H, CH₃) ppm. **¹³C-NMR (101 MHz, CDCl₃):** δ 141.8, 135.4, 131.8, 129.0, 128.4 (x2), 128.4 (x2), 125.8, 121.1, 119.3, 118.5, 110.7, 110.4, 30.2, 11.8 ppm.

3-(3-methylbenzyl)-2-methyl-1H-indole.



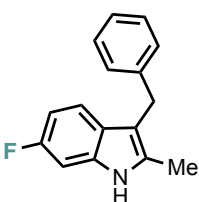
¹H-NMR (400 MHz, CDCl₃): δ 7.77 (*br s*, 1H, NH), 7.31 (d, *J* = 8.0 Hz, 1H, Ar), 7.20 — 7.01 (m, 6H, Ar), 7.17 — 7.14 (m, 1H, Ar), 7.10 — 7.07 (m, 1H, Ar), 4.09 (s, 2H, CH₂), 2.43 (s, 3H, CH₃), 2.33 (s, 3H, CH₃) ppm. **¹³C-NMR (101 MHz, CDCl₃):** δ 141.6, 137.8, 135.3, 131.6, 129.1, 129.0, 128.2, 126.5, 125.4, 121.0, 119.3, 118.5, 110.7, 110.2, 30.1, 21.5, 11.9 ppm. **HRMS(ESI-MS)** calculated for C₁₇H₁₈N⁺ [M+H⁺] 236.1361, found 236.1370.

3-(4-trifluoromethylbenzyl)-2-methyl-1H-indole.

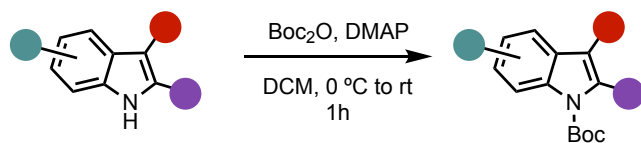


¹H-NMR (400 MHz, CDCl₃): δ 7.87 (*br s*, 1H, NH), 7.48 (d, *J* = 8.0 Hz, 2H, Ar), 7.38 — 7.31 (m, 4H, Ar), 7.38 — 7.31 (m, 4H, Ar), 7.12 (t, *J* = 6.4 Hz), 7.06 (t, *J* = 6.4 Hz, Ar), 4.14 (s, 2H, CH₂), 2.42 (s, 3H, CH₃) ppm. **¹³C-NMR (101 MHz, CDCl₃):** δ 145.8, 135.3, 131.9, 128.6, 128.5 (x2), 125.2 (q, *J* = 3.8 Hz), 121.3, 119.5, 118.1, 110.3, 109.6, 30.0, 11.8 ppm. **¹⁹F-NMR (376 MHz, CDCl₃):** δ -62.66 (s, 3F, CF₃) ppm. **HRMS(ESI-MS)** calculated for C₁₇H₁₅F₃N⁺ [M+H⁺] 290.1078, found 290.1081.

6-fluoro-2-methyl-1H-indole.

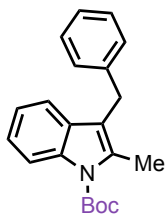


¹H-NMR (400 MHz, CDCl₃): δ 7.75 (*br s*, 1H, NH), 7.30 — 7.24 (m, 6H, Ar), 6.98 (dd, *J* = 9.6, 2.3 Hz, 1H, Ar), 6.81 (ddd, *J* = 9.8, 8.6, 2.3 Hz, 1H, Ar), 4.07 (s, 2H, CH₂), 2.40 (s, 3H, CH₃) ppm. **¹³C-NMR (101 MHz, CDCl₃):** δ 159.5 (d, *J* = 236.1 Hz), 141.4, 135.1 (d, *J* = 12.4 Hz), 131.8 (d, *J* = 3.7 Hz), 128.4 (x2), 128.2 (x2), 125.8, 125.4, 118.9 (d, *J* = 24.0 Hz), 110.6, 107.8 (d, *J* = 26.0 Hz), 96.7 (d, *J* = 26.0 Hz), 30.1, 11.8 ppm. **¹⁹F-NMR (376 MHz, CDCl₃):** δ -123.08 — -123.15 (m, 1F, C-F Ar) ppm. **HRMS(ESI-MS)** calculated for C₁₆H₁₅FN⁺ [M+H⁺] 240.1110, found 240.1093.



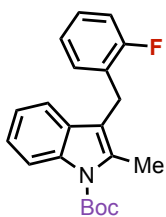
3-benzyl-2-methylindole (221.3 mg, 1 mmol, 1.0 equiv.) and DMAP (12.2 mg, 0.1 mmol, 0.1 equiv.) were dissolved in dichloromethane (5 mL, 0.2 M). Subsequently, di-*tert*-butyl dicarbonate (334 μ L, 1.5 mmol, 1.5 equiv.) were added dropwise at 0 °C. After full consumption of the starting material, monitored by TLC (5% ethyl acetate in hexane), the reaction was quenched with 10 mL of HCl 4M. The organic layer was washed with 1x10 mL of HCl 4M, 1x10 mL of a saturated NaHCO₃ solution and 1x10 mL brine solution. The organic layer was dried over MgSO₄, filtered and concentrated under reduced pressure. The crude product was purified by chromatography (95:5, hexane:EtOAc), giving *N*-Boc-3-benzyl-2-methylindole as a white solid (306 mg, 95% yield).

***tert*-butyl 3-benzyl-2-methyl-1*H*-indole-1-carboxylate (17d).**



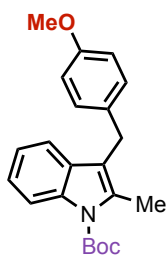
¹H-NMR (400 MHz, CDCl₃): δ 8.14 (d, J = 8.5 Hz, 1H, Ar), 7.37 (d, J = 8.0 Hz, 1H, Ar), 7.27—7.14 (m, 7H, Ar), 4.05 (s, 2H, CH₂), 2.60 (s, 3H, CH₃), 1.70 (s, 9H, C(CH₃)₃) ppm. ¹³C-NMR (101 MHz, CDCl₃): δ 150.8, 140.3, 135.8, 134.0, 130.1, 128.4 (\times 2), 128.1 (\times 2), 125.9, 123.3, 122.4, 118.2, 116.8, 115.3, 83.5, 29.8, 28.3 (\times 3), 14.1 ppm.

***tert*-butyl 3-(2-fluorobenzyl)-2-methyl-1*H*-indole-1-carboxylate (17f).**



¹H-NMR (400 MHz, CDCl₃): δ 8.14 (d, J = 8.5 Hz, 1H, Ar), 7.39 (d, J = 8.1 Hz, 1H, Ar), 7.26—7.16 (m, 3H, Ar), 7.08—6.97 (m, 3H, Ar), 4.07 (s, 2H, CH₂), 2.61 (s, 3H, CH₃), 1.72 (s, 9H, C(CH₃)₃) ppm. ¹³C-NMR (101 MHz, CDCl₃): δ 162.1, 159.7, 150.8, 135.8, 134.5, 130.0 (d, J = 4.5 Hz), 130.0, 127.6 (d, J = 8.0 Hz), 127.0 (d, J = 16.4 Hz), 124.0 (d, J = 3.6 Hz), 123.4, 122.5, 118.1, 115.5, 115.4, 115.2, 115.0, 83.6, 28.3 (\times 3), 27.4, 22.5 (d, J = 4.1 Hz), 14.1 ppm. ¹⁹F-NMR (376 MHz, CDCl₃): δ -118.21 (q, J = 7.1 Hz, 1F, C-F Ar) ppm. HRMS(ESI-MS) calculated for C₂₁H₂₃FN₂O₂⁺ [M+H⁺] 340.1635, found 340.1632.

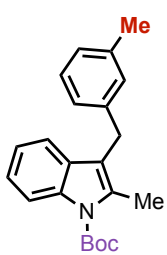
tert-butyl 3-(4-methoxybenzyl)-2-methyl-1H-indole-1-carboxylate (17g).



¹H-NMR (400 MHz, CDCl₃): δ 8.10 (d, *J* = 8.5 Hz, 1H, Ar), 7.33 (d, *J* = 8.1 Hz, 1H, Ar), 7.20—7.09 (m, 4H, Ar), 6.78 (d, *J* = 8.2 Hz, 2H, Ar), 3.98 (s, 2H, CH₂), 3.75 (s, 3H, OCH₃), 2.58 (s, 3H, CH₃), 1.69 (s, 9H, C(CH₃)₃) ppm. **¹³C-NMR (101 MHz, CDCl₃):** δ 157.9, 150.9, 135.8, 133.9, 132.4, 130.1, 129.0 (× 2), 123.3, 122.4, 118.3, 117.3, 115.4, 113.8 (x2), 83.5, 29.0, 28.3 (× 3), 14.1 ppm. **HRMS(ESI-MS)** calculated for C₂₂H₂₆NO₃⁺ [M+H⁺] 351.1934,

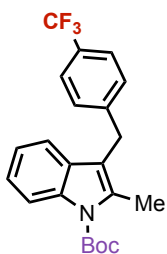
found 351.1930.

tert-butyl 3-(3-methylbenzyl)-2-methyl-1H-indole-1-carboxylate (17h).



¹H-NMR (400 MHz, CDCl₃): δ 8.15 (d, *J* = 8.5 Hz, 1H, Ar), 7.39 (d, *J* = 8.1 Hz, 1H, Ar), 7.27—7.23 (m, 1H, Ar), 7.20—7.15 (m, 2H, Ar), 7.04—7.00 (m, 3H, Ar), 4.04 (s, 2H, CH₂), 2.62 (s, 3H, CH₃), 2.32 (s, 3H, CH₃), 1.73 (s, 9H, C(CH₃)₃) ppm. **¹³C-NMR (101 MHz, CDCl₃):** δ 150.9, 140.3, 138.0, 135.8, 134.1, 130.2, 128.9, 128.3, 126.8, 125.2, 123.3, 122.5, 118.3, 117.0, 115.4, 83.5, 29.8, 28.4 (×3), 21.5, 14.2 ppm. **HRMS(ESI-MS)** calculated for C₂₂H₂₆NO₂⁺ [M+H⁺] 336.1885, found 336.1880.

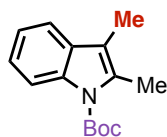
tert-butyl 3-(4-trifluoromethylbenzyl)-2-methyl-1H-indole-1-carboxylate (17i).



¹H-NMR (400 MHz, CDCl₃): δ 8.14 (d, *J* = 8.5 Hz, 1H, Ar), 7.51 (d, *J* = 8.1 Hz, 2H, Ar), 7.34—7.15 (m, 5H, Ar), 7.20—7.15 (m, 2H, Ar), 7.04—7.00 (m, 3H, Ar), 4.12 (s, 2H, CH₂), 2.60 (s, 3H, CH₃), 1.72 (s, 9H, C(CH₃)₃) ppm. **¹³C-NMR (101 MHz, CDCl₃):** δ 150.8, 144.5, 135.8, 134.4, 129.8, 128.4 (x2), 125.3 (q, *J* = 3.8 Hz), 123.6, 122.6, 118.0, 115.9, 115.5, 83.8, 29.8, 28.3 (× 3), 14.2 ppm. **¹⁹F-NMR (376 MHz, CDCl₃):** δ -62.75 (s, 3F, CF₃) ppm.

HRMS(ESI-MS) calculated for C₂₂H₂₃F₃NO₂⁺ [M+H⁺] 390.1603, found 390.1605.

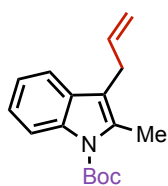
tert-butyl 2,3-dimethyl-1H-indole-1-carboxylate (17j).



¹H-NMR (400 MHz, CDCl₃): δ 8.11 — 8.03 (m, 1H, Ar), 7.43 — 7.34 (m, 1H, Ar), 7.23 — 7.15 (m, 2H, Ar), 2.51 (s, 3H, CH₃), 2.17 (s, 3H, CH₃), 1.66 (s, 9H, C(CH₃)₃) ppm. **¹³C-NMR (101 MHz, CDCl₃):** δ 150.8, 135.6, 132.8,

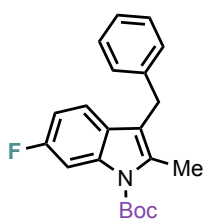
130.8, 123.2, 122.3, 117.7, 115.3, 113.7, 83.2, 28.3, 13.9, 8.7 ppm.

tert-butyl 3-allyl-2-methyl-1H-indole-1-carboxylate (17k).



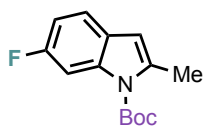
¹H-NMR (400 MHz, CDCl₃) δ 8.12 (d, *J* = 8.0 Hz, 1H, Ar), 7.46 (d, *J* = 8.2 Hz, 1H, Ar), 7.28 — 7.21 (m, 2H, Ar), 5.96 (ddt, *J* = 17.0, 10.0, 5.9 Hz, 1H, Csp²-H), 5.09 — 5.03 (m, 2H, Csp²-H₂), 3.45 (d, *J* = 6.0 Hz, 2H, CH₂), 2.56 (s, 3H, CH₃), 1.71 (s, 9H, C(CH₃)₃) ppm. **¹³C-NMR (101 MHz, CDCl₃)**: δ 150.8, 136.0, 135.8, 133.7, 130.0, 123.3, 122.3, 118.0, 115.7, 115.4, 115.1, 83.4, 28.3 (x3), 28.3, 13.9 ppm. **HRMS(ESI-MS)** calculated for C₁₇H₂₂NO₂⁺ [M+H⁺] 272.1572, found 272.1569.

tert-butyl 3-benzyl-6-fluoro-2-methyl-1H-indole-1-carboxylate (17l).



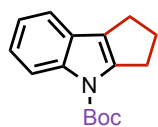
¹H-NMR (400 MHz, CDCl₃): δ 7.96 (d, *J* = 8.0 Hz, 1H, Ar), 7.34 — 7.24 (m, 6H, Ar), 5.96 (dt, *J* = 8.8, 2.3 Hz, 1H, Ar), 4.08 (s, 2H, CH₂), 2.66 (s, 3H, CH₃), 1.77 (s, 9H, C(CH₃)₃) ppm. **¹³C-NMR (101 MHz, CDCl₃)**: δ 160.5 (d, *J* = 236.1 Hz), 150.6, 140.2, 136.1 (d, *J* = 12.4 Hz), 134.2 (d, *J* = 3.7 Hz), 128.5 (x2), 128.2 (x2), 126.4, 126.2, 118.7 (d, *J* = 24.0 Hz), 116.7, 110.5 (d, *J* = 26.0 Hz), 103.1 (d, *J* = 26.0 Hz), 84.0, 29.9, 28.3 (x3), 14.3 ppm. **¹⁹F-NMR (376 MHz, CDCl₃)**: δ -119.51 — -119.58 (m, 1F, C-F Ar) ppm. **HRMS(ESI-MS)** calculated for C₂₁H₂₂FNO₂⁺ [M+H⁺] 340.1635, found 340.1633.

tert-butyl 6-fluoro-2-methyl-1H-indole-1-carboxylate (17m).



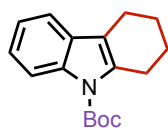
¹H-NMR (400 MHz, CDCl₃): δ 7.84 (dd, *J* = 8.0, 2.3 Hz, 1H, Ar), 7.36 — 7.26 (m, 1H, Ar), 6.93 (dt, *J* = 8.2, 2.3 Hz, 1H, Ar), 6.27 (s, 1H, CH), 2.57 (s, 3H, CH₃), 1.68 (s, 9H, C(CH₃)₃) ppm. **¹³C-NMR (101 MHz, CDCl₃)**: δ 162.2, 157.4, 146.3, 137.7 (d, *J* = 3.9 Hz), 125.1 (d, *J* = 1.6 Hz), 150.6, 140.2, 136.1 (d, *J* = 12.4 Hz), 134.2 (d, *J* = 3.7 Hz), 119.3 (d, *J* = 9.8 Hz), 110.2 (d, *J* = 24.0 Hz), 107.1 (d, *J* = 1.1 Hz), 102.6 (d, *J* = 29.0 Hz), 84.8, 27.0 (x3), 16.7 ppm. **¹⁹F-NMR (376 MHz, CDCl₃)**: δ -119.65 — -119.72 (m, 1F, C-F Ar) ppm. **HRMS(ESI-MS)** calculated for C₁₄H₁₇FNO₂⁺ [M+H⁺] 250.1238, found 250.1244.

tert-butyl 2,3-dihydrocyclopenta[b]indole-4-carboxylate (17n).



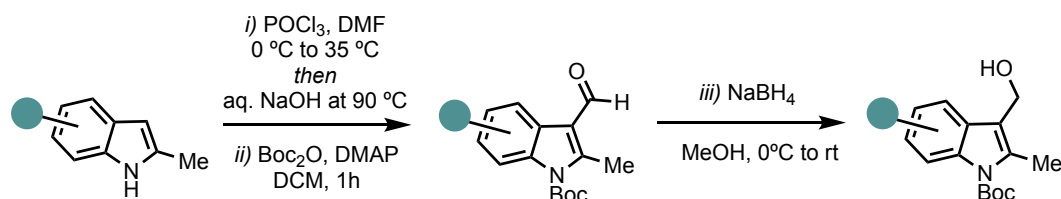
¹H-NMR (400 MHz, CDCl₃): δ 8.15 (s, 1H, Ar), 7.34 (d, *J* = 7.2 Hz, 1H, Ar), 7.17 — 7.22 (m, 2H, Ar), 3.06 (t, *J* = 7.6 Hz, 2H, CH₂), 2.73 — 2.76 (m, 2H, CH₂), 2.44 — 2.49 (m, 2H, CH₂), 1.63 (s, 9H, C(CH₃)₃) ppm. **¹³C-NMR (101 MHz, CDCl₃)**: δ 149.9, 143.9, 140.1, 126.7, 124.4, 122.8, 122.5, 118.4, 115.7, 82.9, 29.1, 28.2, 27.3 (x3), 24.0 ppm.

tert-butyl 1,2,3,4-tetrahydro-9H-carbazole-9-carboxylate (17o).



¹H-NMR (400 MHz, CDCl₃): δ 8.12 (m, 1H, Ar), 7.37 (m, 1H, Ar), 7.20 (m, 2H, Ar), 2.98 (m, 2H, CH₃), 2.63 (m, 2H, CH₂), 1.85 (m, 4H, 2xCH₂), 1.65 (s, 9H, C(CH₃)₃) ppm. **¹³C-NMR (101 MHz, CDCl₃):** δ 150.7, 135.8, 135.6, 129.9, 123.3, 122.3, 117.4, 116.7, 115.4, 83.1, 28.3 (x3), 25.6 (x2), 22.3, 21.1 ppm.

— Preparation of 3-hydroxymethyl-substituted indoles

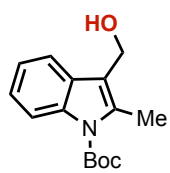


POCl₃ (1.73 mL, 18.6 mmol) was added dropwise to DMF (5 mL) at 0 °C. The reaction mixture was stirred at this temperature for 30 min. Then, a solution of 2-methylindole (2.03 g, 15.5 mmol) in 5 mL of DMF (3.1 M) was added slowly. The resulting reaction mixture was allowed to warm up to 35 °C and kept at this temperature for 40 min. The reaction was allowed to cool down to room temperature and 10 g of ice were added followed by 30 mL of a 5M NaOH solution. The reaction mixture was heated at 90 °C for 30 min and allowed to cool down to room temperature again. An additional 10 g of ice were added and stirred for 30 min. The precipitate was filtered and washed with water the crude products was used without further purification steps.

ii) The crude product was protected following the procedure previously described and used without further purification steps.

*iii) Intermediate II (1.16 g, 4.5 mmol) was dissolved in 20 mL of MeOH (0.23M). Then, 1.5 equivalents of NaBH₄ (253 mg, 6.75 mmol) were added portionwise at 0 °C. After full consumption of the starting material, monitored by TLC, the reaction was quenched with 20 mL of water. The reaction mixture was extracted with 3x15 mL of EtOAc. The combined organic layers were dried over MgSO₄, filtered and concentrated under reduced pressure. The crude product was purified by chromatography (8:2, hexane:EtOAc), furnishing **17e** as a yellowish solid in 91% overall yield (1.05 g, 4.1 mmol) after three consecutive steps.*

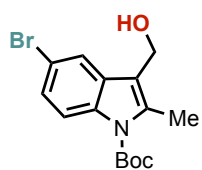
tert-butyl 3-(3-hydroxymethyl)-2-methyl-1H-indole-1-carboxylate (17e).



¹H-NMR (400 MHz, CDCl₃): δ 8.13—8.12 (m, 1H, Ar), 7.65—7.62 (m, 1H, Ar), 7.29—7.24 (m, 2H, Ar), 4.83 (s, 2H, CH₂), 2.65 (s, 3H, CH₃), 1.71 (s, 9H, C(CH₃)₃) ppm. **¹³C-NMR (101 MHz, CDCl₃):** δ 150.7, 135.8, 135.7, 128.9, 123.7, 122.8, 118.0, 117.6, 115.5, 83.9, 55.5, 28.3 (×3), 14.0 ppm.

HRMS(ESI-MS) calculated for C₁₅H₁₉NO₃⁺ [M+H⁺] 262.1365, found 262.1367.

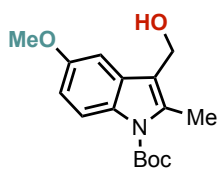
tert-butyl 3-(3-hydroxymethyl)-5-bromo-2-methyl-1H-indole-1-carboxylate (17o).



¹H-NMR (400 MHz, Acetone-d₆): δ 8.04 (d, *J* = 8.2 Hz, 1H, Ar), 7.79 (s, 1H, Ar), 7.36 (dd, *J* = 8.9, 2.5 Hz, 1H, Ar), 4.71 (d, *J* = 6.2 Hz, 2H, CH₂), 3.93 (t, *J* = 4.9 Hz, 1H, OH), 2.59 (s, 3H, CH₃), 1.69 (s, 9H, C(CH₃)₃) ppm. **¹³C-NMR (101 MHz, Acetone-d₆):** δ 150.2, 136.1, 134.6, 131.6, 125.7,

121.3, 118.0, 116.8, 115.2, 84.1, 54.0, 27.4 (×3), 13.2 ppm. **HRMS(ESI-MS)** calculated for C₁₅H₁₉BrNO₃⁺ [M+H⁺] 340.0470, found 340.0472.

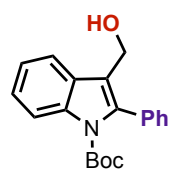
tert-butyl 3-(3-hydroxymethyl)-5-methoxy-2-methyl-1H-indole-1-carboxylate (17p).



¹H-NMR (400 MHz, CDCl₃): δ 7.97 (d, *J* = 8.2 Hz, 1H, Ar), 7.06 (d, *J* = 2.6 Hz, 1H, Ar), 6.85 (dd, *J* = 8.9, 2.5 Hz, 1H, Ar), 4.76 (s, 2H, CH₂), 3.85 (s, 3H, OCH₃), 2.58 (s, 3H, CH₃), 1.67 (s, 9H, C(CH₃)₃) ppm. **¹³C-NMR (101 MHz, CDCl₃):** δ 156.0, 150.6, 136.3, 130.4, 117.5, 116.3, 112.2,

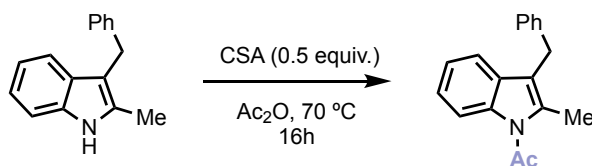
100.9, 83.8, 55.7, 55.5, 28.3 (×3), 14.0 ppm. **HRMS(ESI-MS)** calculated for C₁₆H₂₂NO₄⁺ [M+H⁺] 292.1471, found 292.1472.

tert-butyl 3-(3-hydroxymethyl)-2-phenyl-1H-indole-1-carboxylate (17q).



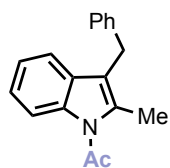
¹H-NMR (400 MHz, CDCl₃): δ 8.29 (d, *J* = 8.2 Hz, 1H, Ar), 7.77 (d, *J* = 8.1 Hz, 1H, Ar), 7.46—7.33 (m, 7H, Ar), 7.20—7.15 (m, 2H, Ar), 7.04—7.00 (m, 3H, Ar), 4.65 (s, 2H, CH₂), 1.27 (s, 9H, C(CH₃)₃) ppm. **¹³C-NMR (101 MHz, CDCl₃):** δ 150.1, 137.7, 136.7, 133.4, 129.8 (×2), 128.7, 128.0, 128.0 (×2),

124.9, 123.1, 119.6, 119.1, 115.3, 83.4, 55.9, 27.5 (×3) ppm. **HRMS(ESI-MS)** calculated for C₂₀H₂₂NO₃⁺ [M+H⁺] 324.1521, found 324.1521.

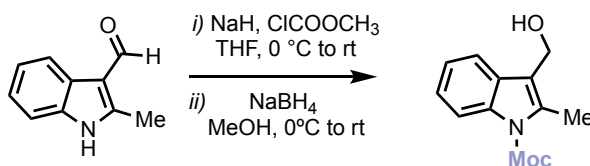


3-benzyl-2-methylindole (0.68 mmol, 150 mg) and 10-camphorsulfonic acid (0.34 mmol, 8.0 mg) were dissolved in acetic anhydride (1.5 mL, 0.45 M) at 0 °C. The reaction was heated at 70 °C and stirred vigorously for 16h. After full consumption of the starting material, monitored by TLC, the reaction was quenched with 5 mL of brine. 10 mL of EtOAc were added and the organic layer was washed with 3x10 mL of a saturated NaHCO₃ solution. The organic layer was dried over MgSO₄, filtered and concentrated under reduced pressure. The crude product was purified by chromatography (95:5, hexane:EtOAc), giving *N*-Ac-3-benzyl-2-methylindole as a yellowish solid in 30% yield (90 mg, 0.2 mmol).

1-(3-benzyl-2-methyl-1*H*-indol-1-yl)ethan-1-one (17r).



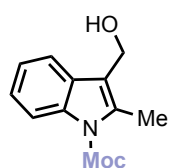
¹H-NMR (400 MHz, CDCl₃): δ 7.98 (d, *J* = 8.5 Hz, 1H, Ar), 7.40 (d, *J* = 8.0 Hz, 1H, Ar), 7.27—7.19 (m, 7H, Ar), 4.08 (s, 2H, CH₂), 2.79 (s, 3H, COCH₃), 2.64 (s, 3H, CH₃) ppm. ¹³C-NMR (101 MHz, CDCl₃): δ 170.3, 139.9, 135.8, 133.9, 130.6, 128.5 (x2), 128.2 (x2), 126.1, 123.8, 123.0, 118.7, 118.4, 115.0, 29.9, 27.7, 14.6 ppm. HRMS(ESI-MS) calculated for C₁₈H₁₈NO⁺ [M+H⁺] 264.1310, found 264.1318.



i) 2-methylindole-3-carboxaldehyde (715 mg, 4.5 mmol) were dissolved in 10 mL of anhydrous THF. Subsequently, 2.5 equivalents of NaH 60% in mineral oil (410 mg, 10.3 mmol) were added portionwise at 0 °C. After 10 min, methyl chloroformate (420 μL, 1.2 equivalents) were added at 0°C dropwise. After full consumption of the starting material, monitored by TLC, the reaction was quenched with 20 mL of brine and extracted with 3x15 mL of EtOAc. The combined organic layers were dried over MgSO₄, filtered and concentrated under reduced pressure. The crude product was used without further purification steps.

ii) The crude product was dissolved in 20 mL of MeOH (0.23M). Then, 1.5 equivalents of NaBH₄ (253 mg, 6.75 mmol) were added portionwise at 0 °C. After full consumption of the starting material, monitored by TLC, the reaction was quenched with 20 mL of water. The reaction mixture was extracted with 3x15 mL of EtOAc. The combined organic layers were dried over MgSO₄, filtered and concentrated under reduced pressure. The crude product was purified by chromatography (7:3, hexane:EtOAc), furnishing **17t** as a yellowish solid in 45% overall yield (438 mg, 2.0 mmol) after two steps.

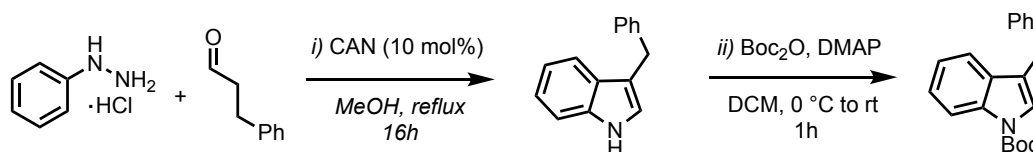
methyl 3-(hydroxymethyl)-2-methyl-1*H*-indole-1-carboxylate (**17t**).



¹H-NMR (500 MHz, CDCl₃): δ 8.09—8.07 (m, 1H, Ar), 7.63—7.61 (m, 1H, Ar), 7.31—7.25 (m, 2H, Ar), 4.80 (s, 2H, CH₂), 4.05 (s, 3H, COCH₃), 2.61 (s, 3H, CH₃) ppm. ¹³C-NMR (125 MHz, CDCl₃): δ 152.9, 135.7, 135.7, 129.3, 124.1, 123.3, 118.3, 118.3, 115.6, 55.5, 53.7, 13.7 ppm. HRMS(ESI-MS)

calculated for C₁₂H₁₄NO₃⁺ [M+H⁺] 220.0968, found 220.0972.

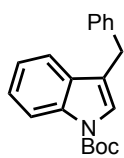
Preparation of C2 unsubstituted indoles



Phenyl hydrazine hydrochloride (1.44 g, 10 mmol, 1.0 equivalent) and cerium ammonium nitrate (1.1 g, 2 mmol, 0.2 equivalents) were dissolved in 20 mL of MeOH (0.5 M). Subsequently, hydrocinnamaldehyde (1.3 mL, 10 mmol, 1.0 equivalents) were added dropwise and the mixture was heated to reflux and stirred for 16 h. The reaction was cooled to room temperature and quenched with 20 mL of water. Then, extracted with 3x20 mL of EtOAc. The combined organic layers were washed 3x15 mL of brine and the organic layer was dried over MgSO₄, filtered and concentrated under reduced pressure. The crude product was purified by chromatography (9:1, hexane:EtOAc), furnishing **17a** as a yellow solid in 60% overall yield (1.2 g, 6.0 mmol).

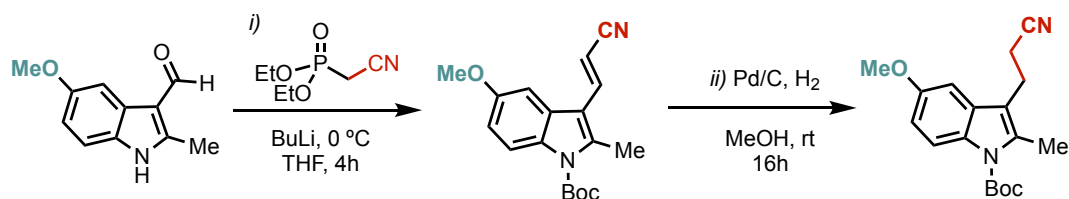
ii) The crude product was *N*-Boc protected following the previously described procedure and purified by column chromatography (95:5, hexane:EtOAc) furnishing **17c** in 92% yield.

tert-butyl 3-benzyl-1*H*-indole-1-carboxylate (**17c**).



¹H-NMR (500 MHz, CDCl₃): δ 8.18 (br, 1H, Ar), 7.48 (d, *J* = 7.4 Hz, 1H, Ar), 7.41 (br, 1H, Ar), 7.36 – 7.32 (m, 5H, Ar), 7.26 – 7.21 (m, 2H, Ar), 4.08 (s, 2H, CH₂), 1.70 (s, 9H, C(CH₃)₃) ppm. **¹³C-NMR (125 MHz, CDCl₃):** δ 149.8, 139.6, 135.6, 130.5, 128.6 (x2), 128.4 (x2), 126.2, 124.3, 123.5, 123.3, 120.0, 119.3, 115.2, 83.4, 31.3, 28.1 (x3) ppm

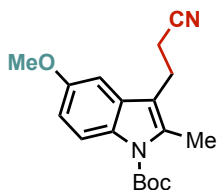
— Preparation of C2-cyanoethyl substituted indoles



i) To a solution of diethylcyanomethyl phosphonate (842 μL, 5.2 mmol, 1.3 equiv.) in anhydrous THF (10 mL) at 0°C, BuLi (192 μL, 4.8 mmol, 2.5M in hexanes, 1.2 equiv.) was added dropwise and the mixture was stirred for 1h at the same temperature. A solution of 5-methoxyindole-3-carboxaldehyde (1.15 g, 4.0 mmol, 1 equiv.) in anhydrous THF (7 mL) was prepared, the solution of the Wittig reagent was added dropwise via cannula. After the addition, the reaction mixture was stirred at 0°C for 4h. The reaction was then concentrated, and the product was used without further purification.

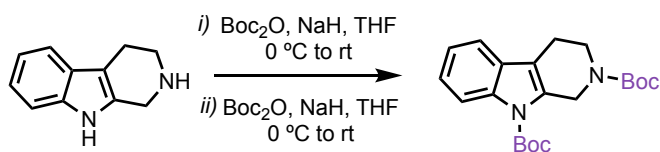
ii) The crude was dissolved in 20 mL of MeOH (0.2 M). Then, the round-bottom flask was back-filled three times with H₂. After 16h, the reaction was filtered through a pad of celite and concentrated under reduced pressure. The crude product was purified by chromatography (9:1, hexane:EtOAc), furnishing **17u** as a yellow solid in 45% overall yield (254.3 g, 1.8 mmol) after two steps.

tert-butyl 3-(2-cyanoethyl)-5-methoxy-2-methyl-1*H*-indole-1-carboxylate (**17u**).



¹H-NMR (400 MHz, Acetone-*d*₆): δ 8.03 (d, *J* = 8.2 Hz, 1H, Ar), 7.13 (d, *J* = 2.6 Hz, 1H, Ar), 6.88 (dd, *J* = 8.9, 2.5 Hz, 1H, Ar), 3.85 (s, 3H, OCH₃), 3.08 (t, *J* = 7.2 Hz, 2H, CH₂), 2.74 (t, *J* = 7.2 Hz, 2H, CH₂), 2.60 (s, 3H, CH₃), 1.70 (s, 9H, C(CH₃)₃) ppm. **¹³C-NMR (101 MHz, Acetone-*d*₆):** δ 156.1, 150.3, 135.0, 130.3, 130.0, 119.5, 116.1, 115.2, 111.8, 100.7, 83.4, 55.0, 27.5 (x3), 19.9, 17.2, 13.5 ppm. **HRMS(ESI-MS)** calculated for C₁₈H₂₃N₂O₃⁺ [M+H⁺] 315.1630, found 315.1632.

— N-Boc diprotection of tetrahydro-β-carboline



Two identical steps were performed in order to obtain **17v**.

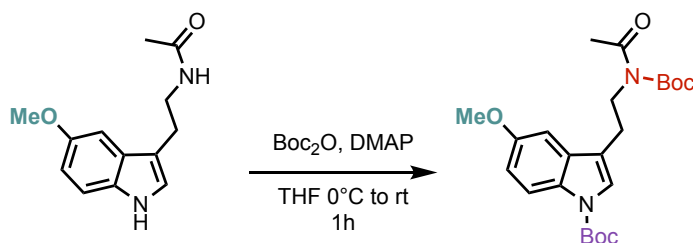
Tetrahydro-β-carboline (861 mg, 5.0 mmol, 1.0 equiv.) was dissolved in THF. Then, NaH (240 mg, 60 wt % mineral oil suspension, 6 mmol, 1.2 equiv.), was added portionwise at 0 °C. The mixture was warmed to room temperature, and di-*tert*-butyl dicarbonate (1.7 mL, 7.5 mmol, 1.5 equiv.) was added and stirred overnight at room temperature. After full consumption of the starting material, monitored by TLC, water was added, and the mixture was extracted with Et₂O. The combined organic layers were washed with brine, dried over MgSO₄ and concentrated under reduced pressure. The crude product was used without further purification and subjected to the same procedure.

The crude product was purified by chromatography (9:1, hexane:EtOAc), furnishing **17v** as a yellow solid in 73% overall yield (1.35 g, 3.7 mmol) after two consecutive steps.

di-*tert*-butyl 2,3,4,9-tetrahydrol-1*H*-β-carboline-2,9-dicarboxylate (17v).

¹H-NMR (400 MHz, CDCl₃): δ 8.21 (d, *J* = 8.1 Hz, 1H, Ar), 7.43 (d, *J* = 8.0 Hz, 1H, Ar), 7.35 — 7.22 (m, 2H, Ar), 4.84 (br, 2H, CH₂), 3.76 (br, 2H, CH₂), 2.76 (br, 2H, CH₂), 1.70 (s, 9H, C(CH₃)₃), 1.53 (s, 9H, C(CH₃)₃) ppm. ¹³C-NMR (101 MHz, CDCl₃): δ 155.0, 150.0, 135.9, 128.9, 124.0, 122.7, 117.7, 115.4, 83.9, 80.0, 44.4, 40.2, 28.5 (x3), 28.3 (x3), 21.2 ppm.

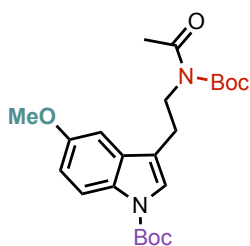
— N-Boc diprotection of melatonin



Melatonin (500 mg, 2.1 mmol, 1.0 equiv.) was dissolved in anhydrous THF (21.5 mL, 0.1 M) and DMAP (14.0 mg, 0.1 mmol, 0.05 equiv.) was added. Subsequently, di-*tert*-butyl dicarbonate (1.12 mL, 5.0 mmol, 2.4 equiv.) were added dropwise at 0 °C. After full consumption of the starting material, monitored by TLC (5% ethyl acetate in hexane), the

reaction was quenched with 15 mL of HCl 4M. The organic layer was washed with 1x10 mL of HCl 4M, 1x10 mL of a saturated NaHCO₃ solution and 1x10 mL brine solution. The organic layer was dried over MgSO₄, filtered and concentrated under reduced pressure. The crude product was purified by chromatography (95:5, hexane:EtOAc), giving **17w** as a transparent oil (729.3 mg, 83% yield).

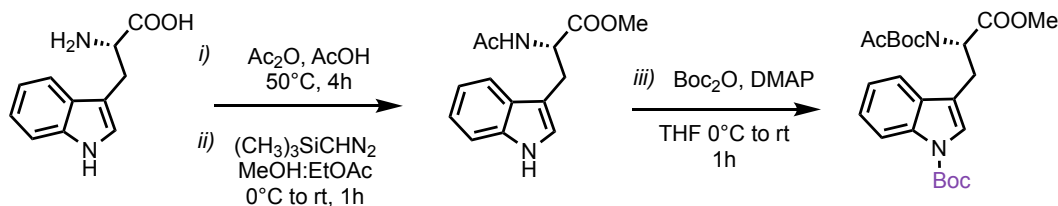
***tert*-butyl-3-(2-(*N*-(*tert*-butoxycarbonyl)acetamido)ethyl)-5-methoxy-1*H*-indole-1-carboxylate (**17w**).**



¹H-NMR (400 MHz, CDCl₃): δ 8.01 (br, 1H, Ar), 7.38 (s, 1H, Ar), 7.15 (s, 1H, Ar), 6.94 (dd, *J* = 8.9, 2.5 Hz, 1H, Ar), 3.98 (t, *J* = 8.6 Hz, 1H, CH₂), 3.90 (s, 3H, OCH₃), 2.90 (t, *J* = 8.6 Hz, 1H, CH₂), 2.53 (s, 3H, COCH₃), 1.67 (s, 9H, C(CH₃)₃), 1.47 (s, 9H, C(CH₃)₃) ppm. **¹³C-NMR (101 MHz, CDCl₃):** δ 173.0, 155.9, 153.1, 123.8, 116.0, 113.1, 101.9, 83.2, 83.1, 55.8, 44.3, 28.2 (x3), 27.9 (x3), 27.1, 24.3 ppm.

HRMS(ESI-MS) calculated for C₂₃H₃₃N₂O₆⁺ [M+H⁺] 433.2260, found 433.2254.

— Protection of the tryptophan derivative

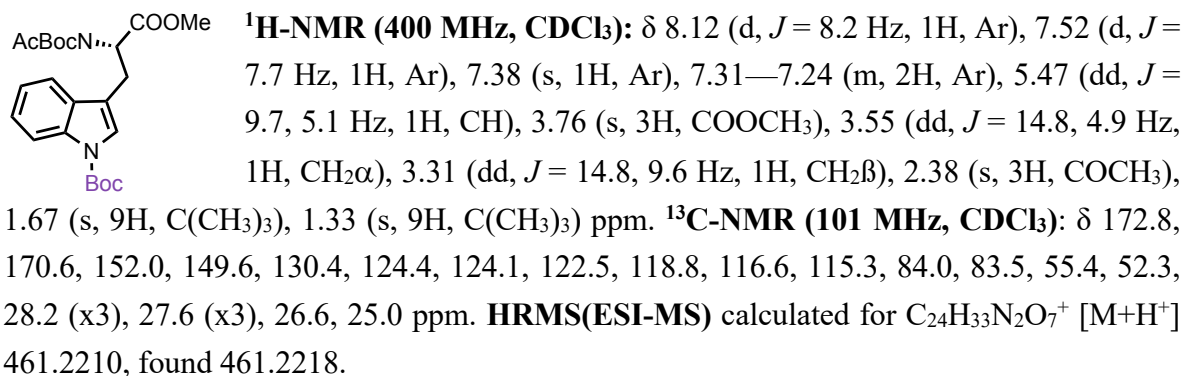


i) (*L*)-Tryptophan (1.02 g, 5.0 mmol, 1.0 equiv.) was added portion wise to acetic acid (2 mL, 2M). Subsequently, acetic anhydride (4.5 mL, 47.5 mmol, 9.5 equiv.) was added. The mixture was stirred for 4h at 50 °C. The reaction mixture was poured into 10 g of ice. Then, extracted with 2x20 mL of EtOAc, the combined organic layers were washed with 10 mL of a 2M NaOH solution and 10 mL of brine. The organic layer was dried over MgSO₄, filtered and concentrated under reduced pressure. The crude product was used without further purification steps.

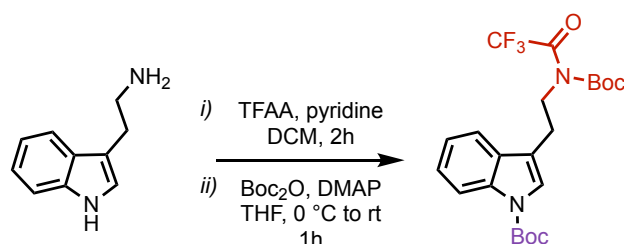
ii) The crude was dissolved in MeOH:EtOAc, (3:7, 45 mL, 0.1 M). Subsequently, trimethylsilyldiazomethane (6.5 mL, 13 mmol, 2.0 M in Et₂O, 2.6 equiv.) was added dropwise at 0 °C. The mixture was stirred for 1h at room temperature. Then, acetic acid (1.14 mL, 20 mmol, 4.0 equiv.) was added dropwise and stirred for additional 5 min. The reaction was extracted with 3x10 mL of EtOAc. The combined organic layers were dried over MgSO₄, filtered, and concentrated under reduced pressure. The reaction crude product was used without further purification steps.

iii) The crude was dissolved in anhydrous THF (10 mL, 0.5 M) and DMAP (610.8 mg, 5.0 mmol, 1.0 equiv.) was added. Subsequently, di-*tert*-butyl dicarbonate (5.6 mL, 25.0 mmol, 5.0 equiv.) were added dropwise at 0 °C. After full consumption of the starting material, monitored by TLC (5% ethyl acetate in hexane), the reaction was quenched with 15 mL of HCl 4M. The organic layer was washed with 1x10 mL of HCl 4M, 1x10 mL of a saturated NaHCO₃ solution and 1x10 mL brine solution. The organic layer was dried over MgSO₄, filtered and concentrated under reduced pressure. The crude product was purified by chromatography (95:5, hexane:EtOAc), giving **17x** as a yellowish oil (874.9 mg, 38% yield) after three consecutive steps.

***tert*-butyl (R)-3-(2-(*N*-(*tert*-butoxycarbonyl)acetamido)-3-methoxy-3-oxopropyl)-1*H*-indole-1-carboxylate (**17x**).**



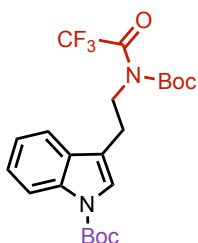
— Protection of tryptamine



i) Tryptamine (3.2 g, 20 mmol, 1.0 equiv.) was dissolved in anhydrous DCM (150 mL). Subsequently, pyridine (18 mL) was added. The solution was cooled at 0 °C and trifluoroacetic anhydride (3.1 mL, 22 mmol, 1.1 equiv.) was added dropwise, the mixture was stirred at this temperature for 5 min. The ice bath was removed, and the mixture was stirred for another 2h at room temperature. After addition of 150 mL saturated NaHCO₃, the phases were separated, and the organic layer washed with 50 mL of a saturated NH₄Cl solution and 50 mL of water. The organic phase was dried over MgSO₄ and concentrated under reduced pressure. The crude product was used without further purification.

ii) As previously described., the crude product was purified by chromatography (95:5, hexane:EtOAc), giving **17y** as a transparent oil (6.9 g, 76% yield).

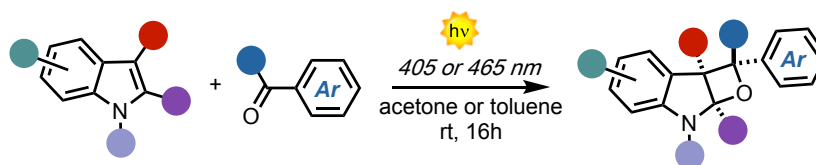
tert-butyl-3-(2-(N-(tert-butoxycarbonyl)-2,2,2-trifluoroacetamido)ethyl)-1H-indole-1-carboxylate (17y).



¹H-NMR (400 MHz, CDCl₃): δ 8.15 (br, 1H, Ar), 7.65 (d, *J* = 8.5 Hz, 1H, Ar), 7.45 (s, 1H, Ar), 7.38—7.28 (m, 2H, Ar), 4.03 (t, *J* = 8.6 Hz, 1H, CH₂), 3.05 (t, *J* = 8.6 Hz, 1H, CH₂), 1.69 (s, 9H, C(CH₃)₃), 1.47 (s, 9H, C(CH₃)₃) ppm. **¹³C-NMR (101 MHz, CDCl₃):** δ 159.7 (q, *J* = 40.5 Hz), 150.8, 149.6, 135.6, 130.2, 124.6, 123.7, 122.7, 118.9, 116.3 (q, *J* = 110.9 Hz), 115.5, 85.9, 83.6, 46.7, 28.3 (x3), 27.4 (x3), 23.8 ppm. **¹⁹F-NMR (376 MHz, CDCl₃):** δ -69.63 (s, 3F, COCF₃) ppm. **HRMS(ESI-MS)** calculated for C₂₂H₂₈F₃N₂O₅⁺ [M+H⁺] 457.1872, found 457.1865.

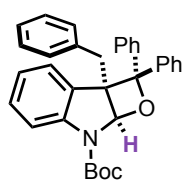
Synthesis and characterization of the PB products

Preparation of oxeto-indolinic polycycles



In a 4 mL vial, indole (0.1 mmol, 1.0 equiv.) and the benzophenone derivative (0.1 mmol, 1.0 equiv.) were added. The two reagents were dissolved in acetone or toluene (1 mL, 0.1 M) and the reaction mixture was bubbled with N₂ for one minute. Then, the vial was placed in front of the selected light source and irradiated for 16 h. The crude product was purified by chromatography (95:5, hexane:EtOAc) if needed or directly evaporated, giving the oxetane products in the stated yields and diastereomeric ratios.

tert-butyl-2a-benzyl-2,2-diphenyl-2a,7a-dihydrooxeto[2,3-*b*]indole-7(2*H*)-carboxylate (19c).

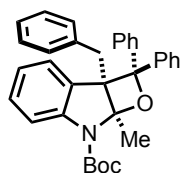


50% yield

¹H-NMR (200 MHz, Acetone-*d*₆): δ 7.96 (dd, *J* = 8.4, 2.2 Hz, 2H, Ar), 7.58 – 7.54 (m, 3H, Ar), 7.53 – 7.50 (m, 3H, Ar), 7.38 – 7.34 (m, 1H, Ar), 7.15 (t, *J* = 7.8 Hz, 2H, Ar), 7.04 – 6.95 (m, 5H, Ar), 6.86 – 6.82 (m, 3H, Ar), 6.67 (br, 1H, CH), 3.53 (d, *J* = 16.7 Hz, 1H, CH_α), 3.15 (d, *J* = 16.7 Hz, 1H, CH_β), 1.54 (s, 9H, C(CH₃)₃) ppm. **¹³C-NMR (50 MHz, Acetone-*d*₆):** δ 143.5, 143.4, 136.5, 129.4 (x2), 128.3 (x2), 127.9, 127.8 (x2), 127.3, 127.2

(x2), 126.4, 126.2 (x2), 126.2, 125.5 (x2), 121.9, 114.9, 94.6, 91.9, 39.0, 27.5 (x3). ppm. **HRMS(ESI-MS)** calculated for $C_{33}H_{32}NO_3^+$ [$M+H^+$] 490.6225, found 490.6230

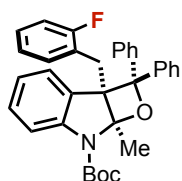
***tert*-butyl-2a-benzyl-7a-methyl-2,2-diphenyl-2a,7a-dihydrooxeto[2,3-*b*]indole-7(2*H*)-carboxylate (19d).**



>98% yield

1H -NMR (400 MHz, Acetone- d_6): δ 7.91 (d, J = 8.3 Hz, 2H, Ar), 7.57 (d, J = 8.2 Hz, 1H, Ar), 7.52 (d, J = 8.5 Hz, 2H, Ar), 7.45 (q, J = 6.9 Hz, 3H, Ar), 7.32—7.13 (m, 1H, Ar), 7.05—6.90 (m, 7H, Ar), 6.81—6.78 (m, 3H, Ar), 3.87 (d, J = 15.7 Hz, 1H, $CH_2\alpha$), 3.21 (d, J = 15.7 Hz, 1H, $CH_2\beta$), 1.88 (s, 3H, CH_3), 1.62 (s, 9H, $C(CH_3)_3$) ppm. **^{13}C -NMR (101 MHz, Acetone- d_6):** δ 151.5, 145.2, 144.0, 143.3, 137.2, 130.5, 129.7 (x3), 128.1, 128.0 (x3), 127.8 (x3), 127.1 (x3), 126.9, 126.1 (x3), 126.0, 125.7, 121.8, 115.2, 81.0, 62.8, 36.9, 27.7 (x3), 23.4 ppm. **HRMS(ESI-MS)** calculated for $C_{34}H_{34}NO_3^+$ [$M+H^+$] 504.2460, found 504.2453.

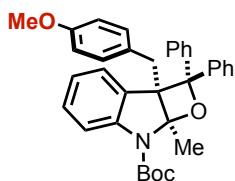
***tert*-butyl-2a-(2-fluorobenzyl)-7a-methyl-2,2-diphenyl-2a,7a-dihydrooxeto[2,3-*b*]indole-7(2*H*)-carboxylate (25).**



>98% yield

1H -NMR (400 MHz, Acetone- d_6): δ 7.91 (d, J = 7.9 Hz, 2H, Ar), 7.59 (d, J = 8.2 Hz, 1H, Ar), 7.53 (d, J = 7.9 Hz, 2H, Ar), 7.45 (q, J = 7.3 Hz, 3H, Ar), 7.32 (t, J = 7.3 Hz, 1H, Ar), 7.11—6.92 (m, 6H, Ar), 6.81 (t, J = 7.5 Hz, 1H, Ar), 6.72 (t, J = 7.6 Hz, 1H, Ar), 6.46 (t, J = 7.8 Hz, 1H, Ar), 3.70 (d, J = 17.0 Hz, 1H, $CH_2\alpha$), 3.34 (d, J = 17.0 Hz, 1H, $CH_2\beta$), 1.87 (s, 3H, CH_3), 1.63 (s, 9H, $C(CH_3)_3$) ppm. **^{13}C -NMR (101 MHz, Acetone- d_6):** δ 162.01 (d, J = 243.3 Hz), 152.4, 146.2, 144.7, 144.0, 131.2, 130.7 (d, J = 3.5 Hz), 129.2, 129.0 (x2), 128.7 (d, J = 8.7 Hz), 128.0, 127.9 (x2), 127.2 (d, J = 22.1 Hz), 126.9 (x2), 126.6 (x2), 125.3 (d, J = 13.8 Hz), 124.5, 124.4, 122.9, 116.1, 115.7 (d, J = 23.3 Hz), 101.7, 93.0, 82.0, 63.1, 30.6, 28.6 (x3), 23.3 ppm. **^{19}F -NMR (376 MHz, Acetone- d_6):** δ -117.10 (q, J = 7.4 Hz, 1F, C-F Ar) ppm. **HRMS(ESI-MS)** calculated for $C_{34}H_{33}FNO_3^+$ [$M+H^+$] 522.2439, found 522.2440.

***tert*-butyl-2a-(4-methoxybenzyl)-7a-methyl-2,2-diphenyl-2a,7a-dihydrooxeto[2,3-*b*]indole-7(2*H*)-carboxylate (26).**

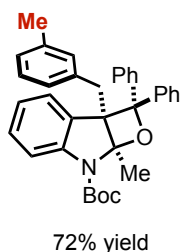


78% yield

1H -NMR (400 MHz, Acetone- d_6): δ 7.90 (d, J = 8.3 Hz, 2H, Ar), 7.58 (d, J = 8.3 Hz, 1H, Ar), 7.52 (d, J = 8.4 Hz, 2H, Ar), 7.45 (t, J = 7.9 Hz, 3H, Ar), 7.31 (t, J = 7.3 Hz, 1H, Ar), 7.06—6.91 (m, 4H, Ar), 6.81 (t, J = 8.1 Hz, 1H, Ar), 6.69 (d, J = 8.2 Hz, 2H, Ar), 6.56 (d, J = 8.1 Hz, 2H, Ar), 3.78 (d, J = 15.7 Hz, 1H, $CH_2\alpha$), 3.63 (s, 3H, OCH_3), 3.14 (d, J = 15.7 Hz, 1H, $CH_2\beta$), 1.88 (s, 3H, CH_3), 1.62 (s, 9H, $C(CH_3)_3$) ppm. **^{13}C -NMR (101 MHz, Acetone- d_6):** δ 158.9, 152.4, 146.1, 144.9, 144.3, 131.6 (x2), 131.5, 129.6,

129.0, 128.9 (x2), 127.9 (x2), 127.8, 127.0 (x2), 126.9, 126.6 (x2), 122.6, 116.0, 114.0, 101.9, 93.0, 81.9, 63.8, 55.2, 36.9, 30.6, 28.6 (x3), 24.1 ppm. **HRMS(ESI-MS)** calculated for $C_{35}H_{36}NO_4^+$ $[M+H^+]$ 534.2566, found 534.2571.

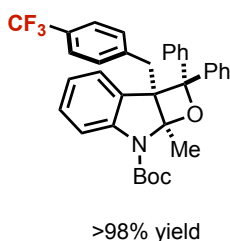
***tert*-butyl-2a-(3-methylbenzyl)-7a-methyl-2,2-diphenyl-2a,7a-dihydrooxeto[2,3-*b*]indole-7(2*H*)-carboxylate (27).**



1H -NMR (400 MHz, Acetone- d_6): δ 7.91 (d, J = 8.3 Hz, 2H, Ar), 7.60—7.41 (m, 6H, Ar), 7.32 (t, J = 7.8 Hz, 1H, Ar), 7.07—6.92 (m, 4H, Ar), 6.88—6.78 (m, 3H, Ar), 6.65 (s, 1H, Ar), 6.51 (d, J = 7.9 Hz, 1H, Ar), 3.84 (d, J = 15.7 Hz, 1H, $CH_2\alpha$), 3.18 (d, J = 15.7 Hz, 1H, $CH_2\beta$), 2.07 (s, 3H, CH_3), 1.88 (s, 3H, CH_3), 1.62 (s, 9H, $C(CH_3)_3$) ppm. **^{13}C -NMR (101 MHz, Acetone- d_6):** δ 152.4, 146.1, 144.8, 144.2, 137.9, 137.9, 133.3, 131.6, 131.5,

130.6, 129.3, 128.9 (x2), 128.5, 127.9 (x2), 127.8, 127.4, 127.3, 127.0 (x2), 126.6 (x2), 122.6, 116.0, 101.9, 93.0, 81.9, 63.7, 37.7, 28.6 (x3), 24.1, 21.3 ppm. **HRMS(ESI-MS)** calculated for $C_{35}H_{36}NO_3^+$ $[M+H^+]$ 518.2617, found 518.2622.

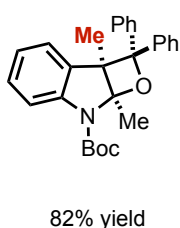
***tert*-butyl 2a-(4-trifluoromethylbenzyl)-7a-methyl-2,2-diphenyl-2a,7a-dihydrooxeto[2,3-*b*]indole-7(2*H*)-carboxylate (28).**



1H -NMR (400 MHz, Acetone- d_6): δ 7.93 (d, J = 8.3 Hz, 2H, Ar), 7.59 (d, J = 8.3 Hz, 1H, Ar), 7.53 (d, J = 8.4 Hz, 2H, Ar), 7.48—7.44 (m, 3H, Ar), 7.38—7.31 (m, 3H, Ar), 7.07—6.93 (m, 6H, Ar), 6.80 (t, J = 8.1 Hz, 1H, Ar), 3.98 (d, J = 15.7 Hz, 1H, $CH_2\alpha$), 3.34 (d, J = 15.7 Hz, 1H, $CH_2\beta$), 1.93 (s, 3H, CH_3), 1.63 (s, 9H, $C(CH_3)_3$) ppm. **^{13}C -NMR (101 MHz, Acetone- d_6):** δ 152.4, 146.1, 144.6, 144.0, 143.0, 131.2 (x2),

130.8, 129.2, 129.3 (q, J = 137.0 Hz, CF_3), 129.0 (x2), 128.0, 128.0 (x2), 127.6, 127.1, 127.0 (x2), 126.6 (x2), 125.4 (q, J = 3.7 Hz), 122.8, 116.2, 101.8, 92.9, 82.1, 63.5, 37.5, 28.6 (x3), 24.2 ppm. **^{19}F -NMR (376 MHz, Acetone- d_6):** δ -63.37 (s, 3F, CF_3) ppm. **HRMS(ESI-MS)** calculated for $C_{35}H_{33}F_3NO_3^+$ $[M+H^+]$ 572.2334, found 572.2340.

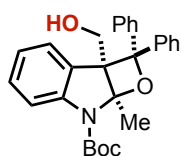
***tert*-butyl-2a,7a-dimethyl-2,2-diphenyl-2a,7a-dihydrooxeto[2,3-*b*]indole-7(2*H*)-carboxylate (29).**



1H -NMR (400 MHz, Acetone- d_6): δ 7.73 (d, J = 8.3 Hz, 2H, Ar), 7.47—7.37 (m, 6H, Ar), 7.25 (t, J = 7.8 Hz, 1H, Ar), 7.02—6.96 (m, 3H, Ar), 6.92—6.84 (m, 2H, Ar), 1.88 (s, 3H, CH_3), 1.64 (s, 9H, $C(CH_3)_3$), 1.45 (s, 3H, CH_3) ppm. **^{13}C -NMR (101 MHz, Acetone- d_6):** δ 152.2, 145.0, 144.7, 133.2, 128.9, 128.8 (x2), 127.8 (x2), 127.6 (x2), 126.9, 126.4 (x2), 126.4 (x2),

126.0, 122.9, 115.6, 102.7, 92.6, 81.6, 59.3, 28.6 (x3), 21.2, 18.0 ppm. **HRMS(ESI-MS)** calculated for $C_{28}H_{30}NO_3^+$ $[M+H]^+$ 428.2197, found 428.2197.

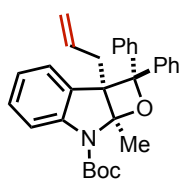
tert-butyl-2a-(hydroxymethyl)-7a-methyl-2,2-diphenyl-2a,7a-dihydrooxeto[2,3-b]indole-7(2H)-carboxylate (30).



85% yield

1H -NMR (400 MHz, Acetone- d_6): δ 7.81 (d, J = 7.6 Hz, 2H, Ar), 7.55 (d, J = 8.1 Hz, 1H, Ar), 7.51 (d, J = 7.6 Hz, 1H, Ar), 7.45 (d, J = 7.6 Hz, 2H, Ar), 7.38 (t, J = 7.6 Hz, 2H, Ar), 7.26 (t, J = 7.3 Hz, 1H, Ar), 7.05—6.97 (m, 3H, Ar), 6.93 (t, J = 7.3 Hz, 1H, Ar), 6.84 (t, J = 7.3 Hz, 1H, Ar), 4.38 (dd, J = 11.4, 4.0 Hz, 1H, $CH_2\alpha$), 3.84 (dd, J = 11.4, 5.6 Hz, 1H, $CH_2\beta$), 3.78 (dd, J = 5.6, 4.0 Hz, 1H, OH), 2.04 (s, 3H, CH_3), 1.65 (s, 9H, $C(CH_3)_3$) ppm. **^{13}C -NMR (101 MHz, Acetone- d_6):** δ 152.3, 146.4, 144.6, 144.1, 130.2, 128.8 (x3), 127.8 (x2), 127.8, 127.3, 126.9, 126.4 (x2), 126.3 (x2), 122.6, 115.6, 101.6, 91.3, 81.6, 63.5, 61.4, 28.6 (x3), 21.9 ppm. **HRMS(ESI-MS)** calculated for $C_{28}H_{30}NO_4^+$ $[M+H]^+$ 444.2169, found 444.2169.

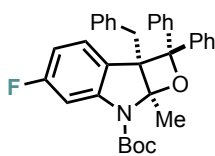
tert-butyl-2a-allyl-7a-methyl-2,2-diphenyl-2a,7a-dihydrooxeto[2,3-b]indole-7(2H)-carboxylate (31).



67% yield

1H -NMR (500 MHz, Acetone- d_6): δ 7.80 (d, J = 8.3 Hz, 2H, Ar), 7.55—7.53 (m, 1H, Ar), 7.45 (d, J = 7.8 Hz, 2H, Ar), 7.42—7.37 (m, 3H, Ar), 7.30—7.26 (m, 1H, Ar), 7.04—6.98 (m, 3H, Ar), 6.92 (t, J = 8.1 Hz, 1H, Ar), 6.85 (t, J = 7.9 Hz, 1H, Ar), 5.37—5.29 (m, 1H, Csp^2H), 5.01 (d, J = 16.0 Hz, 1H, (*E*)- Csp^2H_2), 4.86 (d, J = 11.2 Hz, 1H, (*Z*)- Csp^2H_2), 3.11 (dd, J = 15.0, 6.4 Hz, 1H, $CH_2\alpha$), 2.55 (dd, J = 16.4, 8.6 Hz, 1H, $CH_2\beta$), 1.98 (s, 3H, CH_3), 1.64 (s, 9H, $C(CH_3)_3$) ppm. **^{13}C -NMR (125 MHz, Acetone- d_6):** δ 151.4, 145.0, 143.9, 143.2, 133.9, 129.7, 128.0, 127.9 (x2), 127.0 (x2), 126.4, 126.1, 125.8 (x2), 125.6 (x2), 122.4, 121.8, 117.8, 115.0, 101.4, 91.4, 80.9, 61.7, 36.3, 27.7 (x3), 21.9 ppm. **HRMS(ESI-MS)** calculated for $C_{30}H_{32}NO_3^+$ $[M+H]^+$ 454.5820, found 454.5828.

tert-butyl-2a-benzyl-5-fluoro-7a-methyl-2,2-diphenyl-2a,7a-dihydrooxeto[2,3-b]indole-7(2H)-carboxylate (32).

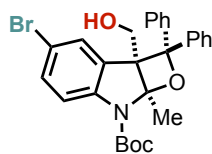


72% yield

1H -NMR (400 MHz, Acetone- d_6): δ 7.91 (d, J = 7.6 Hz, 2H, Ar), 7.53 (d, J = 7.6 Hz, 2H, Ar), 7.48-7.40 (m, 3H, Ar), 7.08 (t, J = 7.6 Hz, 2H, Ar), 7.04-7.03 (m, 3H, Ar), 6.97 (t, J = 7.3 Hz, 1H, Ar), 6.84-6.81 (m, 2H, Ar), 6.55 (td, J = 8.7, 2.4 Hz, 1H, Ar), 3.86 (d, J = 16.2 Hz, 1H, $CH_2\alpha$), 3.22 (d, J = 16.2 Hz, 1H, $CH_2\beta$), 1.92 (s, 3H, CH_3), 1.63 (s, 9H, $C(CH_3)_3$) ppm. **^{13}C -NMR (101 MHz, Acetone- d_6):** δ 163.5 (d, J = 241.0 Hz), 152.2, 147.4 (d, J = 12.7 Hz), 144.7, 143.9, 137.8, 130.6 (x2), 129.0 (x2), 128.7 (x2), 128.7 (d, J = 9.9 Hz), 128.0 (x3), 127.3 (d, J = 2.5 Hz), 127.0 (d, J = 23.7 Hz), 127.0 (x2), 126.5 (x2), 109.0 (d, J = 23.0 Hz),

103.8, 103.5, 102.7, 93.1, 82.6, 63.4, 37.5, 28.5 (x3), 24.2 ppm. $^{19}\text{F-NMR}$ (376 MHz, Acetone- d_6): δ -114.69 (q, J = 10.1 Hz, 1F, C-F Ar) ppm. HRMS(ESI-MS) calculated for $\text{C}_{34}\text{H}_{33}\text{FNO}_3^+$ [$\text{M}+\text{H}^+$] 522.2439, found 522.2445.

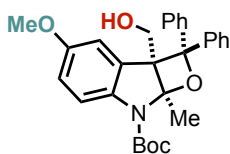
***tert*-butyl-5-bromo-2a-(hydroxymethyl)-7a-methyl-2,2-diphenyl-2a,7a-dihydrooxeto[2,3-*b*]indole-7(2*H*)-carboxylate (33).**



52% yield

$^1\text{H-NMR}$ (500 MHz, Acetone- d_6): δ 7.82 (d, J = 8.0 Hz, 2H, Ar), 7.67 (d, J = 2.2 Hz, 1H, Ar), 7.48–7.44 (m, 3H, Ar), 7.38 (t, J = 8.0 Hz, 2H, Ar), 7.27 (t, J = 7.3 Hz, 2H, Ar), 7.12 (dd, J = 8.7, 2.2 Hz, 1H, Ar), 7.08 (t, J = 8.0 Hz, 2H, Ar), 6.97 (t, J = 7.3 Hz, 1H, Ar), 4.42 (dd, J = 11.7, 4.3 Hz, 1H, $\text{CH}_2\alpha$), 4.04 (dd, J = 5.3, 4.3 Hz, 1H, OH), 3.84 (dd, J = 11.7, 5.3 Hz, 1H, $\text{CH}_2\beta$), 2.02 (s, 3H, CH_3), 1.64 (s, 9H, $\text{C}(\text{CH}_3)_3$) ppm. $^{13}\text{C-NMR}$ (125 MHz, Acetone- d_6): δ 152.0, 145.7, 144.4, 143.7, 133.1, 131.5, 130.3, 128.9 (x2), 128.0 (x2), 128.0, 127.2, 126.4 (x2), 126.3 (x2), 117.1, 114.6, 101.9, 91.3, 82.1, 63.6, 61.1, 28.6 (x3), 21.9 ppm. HRMS(ESI-MS) calculated for $\text{C}_{28}\text{H}_{29}\text{BrNO}_4^+$ [$\text{M}+\text{H}^+$] 522.1274, found 522.1271.

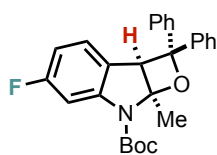
***tert*-butyl-2a-(hydroxymethyl)-4-methoxy-7a-methyl-2,2-diphenyl-2a,7a-dihydrooxeto[2,3-*b*]indole-7(2*H*)-carboxylate (34).**



83% yield

$^1\text{H-NMR}$ (400 MHz, Acetone- d_6): δ 7.81 (d, J = 7.7 Hz, 2H, Ar), 7.48 (d, J = 7.7 Hz, 2H, Ar), 7.44 (d, J = 8.6 Hz, 1H, Ar), 7.38 (t, J = 7.7 Hz, 2H, Ar), 7.25 (t, J = 7.3 Hz, 1H, Ar), 7.13 (d, J = 2.6 Hz, 1H, Ar), 7.05 (t, J = 7.7 Hz, 2H, Ar), 6.94 (t, J = 7.3 Hz, 1H, Ar), 6.55 (dd, J = 8.6, 2.6 Hz, 1H, Ar), 4.40 (q, J = 6.6 Hz, 1H, $\text{CH}_2\alpha$), 3.81 (m, 2H, $\text{CH}_2\beta$ and OH overlapped), 3.70 (s, 3H, OCH_3), 2.01 (s, 3H, CH_3), 1.63 (s, 9H, $\text{C}(\text{CH}_3)_3$) ppm. $^{13}\text{C-NMR}$ (101 MHz, Acetone- d_6): δ 156.1, 152.3, 144.7, 144.2, 140.1, 131.5, 128.8 (x2), 127.9 (x2), 127.8, 127.0, 126.4 (x2), 126.3 (x2), 116.2, 114.2, 113.3, 101.7, 91.2, 81.4, 63.7, 61.5, 55.9, 28.7 (x3), 22.0 ppm. HRMS(ESI-MS) calculated for $\text{C}_{29}\text{H}_{32}\text{NO}_5^+$ [$\text{M}+\text{H}^+$] 474.2275, found 474.2273.

***tert*-butyl-5-fluoro-7a-methyl-2,2-diphenyl-2a,7a-dihydrooxeto[2,3-*b*]indole-7(2*H*)-carboxylate (35).**

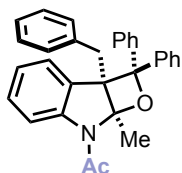


49% yield

$^1\text{H-NMR}$ (400 MHz, Acetone- d_6): δ 7.65 (d, J = 7.7 Hz, 2H, Ar), 7.45 (t, J = 7.7 Hz, 2H, Ar), 7.37–7.31 (m, 2H, Ar), 7.24 (d, J = 7.7 Hz, 2H, Ar), 7.12 (dd, J = 7.7, 6.1 Hz, 1H, Ar), 7.07 (t, J = 7.7 Hz, 2H, Ar), 6.98 (t, J = 7.3 Hz, 1H, Ar), 6.49 (td, J = 8.8, 2.4 Hz, 1H, Ar), 4.75 (s, 1H, CH), 1.92 (s, 3H, CH_3), 1.65 (s, 9H, $\text{C}(\text{CH}_3)_3$) ppm. $^{13}\text{C-NMR}$ (101 MHz, Acetone- d_6): δ 163.5 (d, J = 240.7 Hz), 152.2, 147.0, 143.3, 129.1 (x2), 128.4 (x2), 128.3,

128.2, 128.0, 127.5, 126.6 (x2), 126.3 (x2), 124.3 (d, $J = 2.4$ Hz), 109.2 (d, $J = 22.9$ Hz), 103.6 (d, $J = 29.5$ Hz), 100.2, 89.8, 82.5, 58.0, 30.6, 28.5 (x3), 25.7 ppm. **$^{19}\text{F-NMR}$ (376 MHz, Acetone- d_6):** δ -115.07 (q, $J = 9.7$ Hz, 1F, C-F Ar) ppm. **HRMS(ESI-MS)** calculated for $\text{C}_{27}\text{H}_{27}\text{FNO}_3^+$ [$\text{M}+\text{H}^+$] 432.1969, found 432.1972.

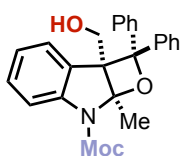
1-(2a-benzyl-7a-methyl-2,2-diphenyl-2a,7a-dihydrooxeto[2,3-*b*]indol-7(2*H*)-yl)ethan-1-one (36).



71% yield

$^1\text{H-NMR}$ (500 MHz, CDCl_3): δ 7.85 (br s, 1H, Ar), 7.73 (d, $J = 7.6$ Hz, 2H, Ar), 7.43 (t, $J = 7.6$ Hz, 2H, Ar), 7.33–7.29 (m, 3H, Ar), 7.13 (d, $J = 7.6$ Hz, 1H, Ar), 7.08–6.95 (m, 7H, Ar), 6.91 (t, $J = 7.6$ Hz, 1H, Ar), 6.68 (d, $J = 7.6$ Hz, 2H, Ar), 3.58 (d, $J = 16.7$ Hz, 1H, $\text{CH}\alpha$), 3.18 (d, $J = 16.7$ Hz, 1H, $\text{CH}\beta$), 2.53 (s, 3H, COCH_3), 1.80 (s, 3H, CH_3) ppm. **$^{13}\text{C-NMR}$ (125 MHz, CDCl_3):** δ 170.1, 146.8, 142.6, 142.4, 136.7, 129.7 (x2), 128.9, 128.5(x2), 128.2 (x2), 127.6, 127.4 (x2), 126.7, 126.3, 126.0 (x2), 125.8 (x2), 123.4, 117.1, 93.6, 63.1, 41.0, 36.9, 24.0 ppm. **HRMS(ESI-MS)** calculated for $\text{C}_{31}\text{H}_{28}\text{NO}_2^+$ [$\text{M}+\text{H}^+$] 446.2115, found 446.2114.

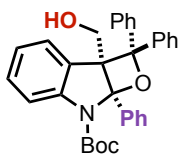
methyl-2a-(hydroxymethyl)-7a-methyl-2,2-diphenyl-2a,7a-dihydrooxeto[2,3-*b*]indole-7(2*H*)-carboxylate (37).



96% yield

$^1\text{H-NMR}$ (200 MHz, Acetone- d_6): δ 7.89 – 7.74 (m, 2H, Ar), 7.64 – 7.47 (m, 2H, Ar), 7.45–7.32 (m, 4H, Ar), 7.31 – 7.18 (m, 1H, Ar), 7.13 – 6.78 (m, 5H, Ar), 3.89 (s, 3H, COOCH_3), 3.82 (dd, $J = 6.7, 4.5$ Hz, 2H, CH_2), 2.02 (s, 3H, CH_3) ppm. **$^{13}\text{C-NMR}$ (50 MHz, Acetone- d_6):** δ 143.3, 142.7, 129.1, 127.6 (x2), 127.5 (x4), 126.6 (x2), 126.6, 126.3, 125.7, 125.0 (x4), 121.7, 114.2, 60.2, 60.0, 51.4, 23.1, 20.2, 16.5 ppm. **HRMS(ESI-MS)** calculated for $\text{C}_{25}\text{H}_{24}\text{NO}_4^+$ [$\text{M}+\text{H}^+$] 402.1700, found 402.1703.

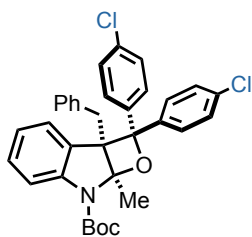
***tert*-butyl-2a-(hydroxymethyl)-2,2,7a-triphenyl-2a,7a-dihydrooxeto[2,3-*b*]indole-7(2*H*)-carboxylate (39).**



22% yield

$^1\text{H-NMR}$ (400 MHz, Acetone- d_6): δ 8.01 (d, $J = 7.8$ Hz, 2H, Ar), 7.69 (d, $J = 7.8$ Hz, 1H, Ar), 7.65 (d, $J = 7.3$ Hz, 1H, Ar), 7.51–7.46 (m, 3H, Ar), 7.41 (t, $J = 7.8$ Hz, 3H, Ar), 7.35–7.24 (m, 4H, Ar), 7.04 (q, $J = 7.3$ Hz, 3H, Ar), 6.92 (t, $J = 7.3$ Hz, 1H, Ar), 6.85 (t, $J = 7.3$ Hz, 1H, Ar), 3.97 (dd, $J = 11.2, 4.2$ Hz 1H, $\text{CH}_2\alpha$), 3.62 (t, $J = 4.2$ Hz, 1H, OH), 3.39 (dd, $J = 11.3, 4.2$ Hz, 1H, $\text{CH}_2\beta$), 1.22 (s, 9H, $\text{C}(\text{CH}_3)_3$) ppm. **$^{13}\text{C-NMR}$ (101 MHz, Acetone- d_6):** δ 151.8, 146.8, 145.0, 144.3, 140.0, 130.8, 130.1, 129.0, 128.8 (x2), 128.8, 128.7, 128.5, 128.3, 128.0 (x2), 127.8, 127.0, 126.5 (x2), 126.3 (x2), 122.8, 114.6, 102.9, 93.3, 81.1, 65.0, 62.4, 28.2 (x3) ppm. **HRMS(ESI-MS)** calculated for $\text{C}_{33}\text{H}_{32}\text{NO}_4^+$ [$\text{M}+\text{H}^+$] 506.2326, found 506.2324.

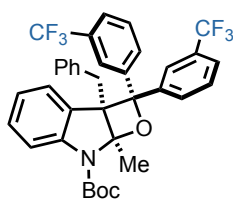
***tert*-butyl-2*a*-benzyl-2,2-bis(4-chlorophenyl)-7*a*-methyl-2*a*,7*a*-dihydrooxeto[2,3-*b*]indole-7(2*H*)-carboxylate (40).**



86% yield

¹H-NMR (400 MHz, Acetone-*d*₆): δ 7.91 (d, *J* = 8.6 Hz, 2H, Ar), 7.60 (d, *J* = 8.6 Hz, 1H, Ar), 7.51 (dd, *J* = 10.7, 8.6 Hz, 4H, Ar), 7.45 (d, *J* = 7.3 Hz, 1H, Ar), 7.09 (d, *J* = 8.6 Hz, 2H, Ar), 7.05–7.00 (m, 4H, Ar), 6.85–6.80 (m, 3H, Ar), 3.88 (d, *J* = 16.0 Hz, 1H, CH₂α), 3.23 (d, *J* = 16.0 Hz, 1H, CH₂β), 1.90 (s, 3H, CH₃), 1.62 (s, 9H, C(CH₃)₃). ppm. **¹³C-NMR (101 MHz, Acetone-*d*₆):** δ 152.3, 146.0, 143.4, 142.6, 137.7, 133.7, 132.7, 130.9, 130.6(x2), 129.3, 129.2 (x2), 128.7 (x2), 128.7 (x2), 128.3 (x2), 128.1 (x2), 127.6, 126.9, 122.9, 116.1, 102.2, 92.4, 82.2, 63.8, 37.4, 28.5 (x3), 24.1 ppm. **HRMS(ESI-MS)** calculated for C₃₄H₃₂Cl₂NO₃⁺ [M+H⁺] 572.1754, found 572.1758.

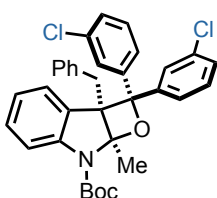
***tert*-butyl-2*a*-benzyl-7*a*-methyl-2,2-bis(3-(trifluoromethyl)phenyl)-2*a*,7*a*-dihydrooxeto[2,3-*b*]indole-7(2*H*)-carboxylate (41).**



53% yield

¹H-NMR (400 MHz, Acetone-*d*₆): δ 8.30 (d, *J* = 7.2 Hz, 1H, Ar), 8.26 (s, 1H, Ar), 7.90 — 7.72 (m, 5H, Ar), 7.58 — 7.55 (m, 2H, Ar), 7.34 — 7.32 (m, 2H, Ar), 7.21 (m, 2H, Ar), 7.04 — 7.00 (m, 4H, Ar), 6.84-6.80 (m, 3H, Ar), 4.06 (d, *J* = 16.0 Hz, 1H, CH₂α), 3.23 (d, *J* = 16.0 Hz, 1H, CH₂β), 1.95 (s, 3H, CH₃), 1.63 (s, 9H, C(CH₃)₃) ppm. **¹³C-NMR (101 MHz, Acetone-*d*₆):** δ 152.2, 146.0, 145.5, 144.8, 137.5, 131.0, 130.6 (x2), 130.5, 130.4, 130.3, 129.5, 129.1, 128.7 (x2), 127.7, 127.0, 125.3 (q), 124.2 (q), 123.4 (q), 123.0, 116.1, 102.5, 92.4, 82.4, 64.1, 37.2, 28.5 (x3), 24.1 ppm. **¹⁹F-NMR (376 MHz, Acetone *d*₆):** δ -63.32 (s, 3F, ArCF₃), -63.47 (s, 3F, ArCF₃) ppm **HRMS(ESI-MS)** calculated for C₃₆H₃₂F₆NO₃⁺ [M+H⁺] 640.2281, found 640.2280.

***tert*-butyl-2*a*-benzyl-2,2-bis(3-chlorophenyl)-7*a*-methyl-2*a*,7*a*-dihydrooxeto[2,3-*b*]indole-7(2*H*)-carboxylate (42).**

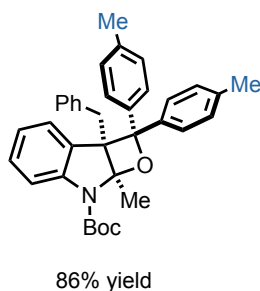


70% yield

¹H-NMR (500 MHz, Acetone-*d*₆): δ 7.95 – 7.88 (m, 2H, Ar), 7.61 (d, *J* = 8.5 Hz, 1H, Ar), 7.59 – 7.57 (m, 2H, Ar), 7.55 – 7.48 (m, 2H, Ar), 7.42 – 7.38 (m, 1H, Ar), 7.13 – 7.08 (m, 1H, Ar), 7.06 – 7.00 (m, 5H, Ar), 6.91 – 6.81 (m, 3H, Ar), 4.01 (d, *J* = 16.1 Hz, 1H, CH₂α), 3.26 (d, *J* = 16.1 Hz, 1H, CH₂β), 1.93 (s, 3H, CH₃), 1.65 (s, 9H, C(CH₃)₃) ppm. **¹³C-NMR (125 MHz, Acetone-*d*₆):** δ 151.4, 145.8, 145.1, 145.0, 136.8, 134.0, 133.0, 130.0, 129.8, 129.7 (x2), 128.9, 128.6, 127.8 (x2), 127.5, 126.8, 126.5, 126.1, 125.8, 125.7,

124.7, 124.4, 122.0, 115.3, 101.5, 91.3, 81.4, 63.0, 36.3, 27.7, 23.2 ppm. **HRMS(ESI-MS)** calculated for $C_{34}H_{32}Cl_2NO_3^+$ $[M+H]^+$ 572.1754, found 572.1755.

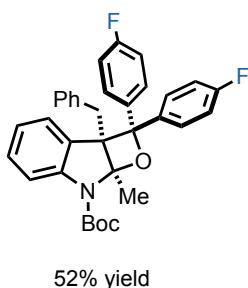
***tert*-butyl-2a-benzyl-7a-methyl-2,2-di-*p*-tolyl-2a,7a-dihydrooxeto[2,3-*b*]indole-7(2*H*)-carboxylate (43).**



1H -NMR (400 MHz, Acetone- d_6): δ 7.75 (d, J = 8.0 Hz, 2H, Ar), 7.59 (d, J = 8.0 Hz, 1H, Ar), 7.41 (d, J = 7.5 Hz, 1H, Ar), 7.37 (d, J = 8.0 Hz, 1H, Ar), 7.25 (d, J = 8.0 Hz, 2H, Ar), 7.01–6.97 (m, 4H, Ar), 6.85 (d, J = 8.0 Hz, 2H, Ar), 6.81–6.76 (m, 3H, Ar), 3.82 (d, J = 16.1 Hz, 1H, $CH_2\alpha$), 3.21 (d, J = 16.1 Hz, 1H, $CH_2\beta$), 2.33 (s, 3H, $ArCH_3$), 2.09 (s, 3H, $ArCH_3$), 1.88 (s, 3H, CH_3) 1.61 (s, 9H, $C(CH_3)_3$) ppm.

^{13}C -NMR (101 MHz, Acetone- d_6): δ 152.5, 146.1, 143.7, 142.2, 141.6, 138.2, 137.3, 136.1, 131.6, 130.7, 130.5 (x2), 129.8, 129.5, 128.9, 128.6 (x2), 128.5 (x2), 127.7, 126.9, 126.8, 126.5, 122.6, 116.1, 101.8, 93.1, 81.8, 63.5, 37.8, 28.6 (x3), 27.4, 21.0, 20.8 ppm. **HRMS(ESI-MS)** calculated for $C_{36}H_{38}NO_3^+$ $[M+H]^+$ 532.2846, found 532.2840.

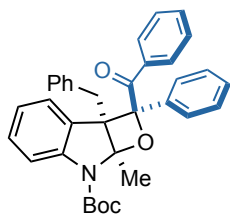
***tert*-butyl-2a-benzyl-2,2-bis(4-fluorophenyl)-7a-methyl-2a,7a-dihydrooxeto[2,3-*b*]indole-7(2*H*)-carboxylate (44).**



1H -NMR (400 MHz, Acetone- d_6): δ 7.93 (dd, J = 8.9, 5.4 Hz, 2H, Ar), 7.59 (d, J = 8.2 Hz, 1H, Ar), 7.53 (dd, J = 8.9, 5.4 Hz, 2H, Ar), 7.41 (d, J = 7.5 Hz, 1H, Ar), 7.23 (t, J = 8.9 Hz, 2H, Ar), 7.04–7.00 (m, 4H, Ar), 6.84–6.79 (m, 5H, Ar), 3.86 (d, J = 16.0 Hz, 1H, $CH_2\alpha$), 3.22 (d, J = 16.0 Hz, 1H, $CH_2\beta$), 1.89 (s, 3H, CH_3), 1.62 (s, 9H, $C(CH_3)_3$) ppm.

^{13}C -NMR (101 MHz, Acetone- d_6): δ 163.0 (d, J = 244.4 Hz), 160.9 (d, J = 244.4 Hz), 152.3, 146.1, 140.8 (d, J = 3.0 Hz), 140.0 (d, J = 3.0 Hz), 137.8, 133.5, 133.4, 131.2, 130.6 (x2), 129.2, 129.1 (d, J = 8.0 Hz), 128.6 (d, J = 8.0 Hz), 128.5 (x2), 127.6, 126.9, 122.8, 116.3 (d, J = 22.1 Hz), 116.1, 115.8 (d, J = 21.5 Hz), 114.7 (d, J = 21.5 Hz), 102.1, 93.0, 82.1, 63.7, 37.5, 30.6, 28.6 (x3), 24.1 ppm. **^{19}F -NMR (376 MHz, Acetone- d_6):** δ -117.51– -117.58 (m, 1F, C-F Ar), -118.43– -118.50 (m, 1F, C-F Ar) ppm. **HRMS(ESI-MS)** calculated for $C_{34}H_{32}F_2NO_3^+$ $[M+H]^+$ 540.2345, found 540.2340.

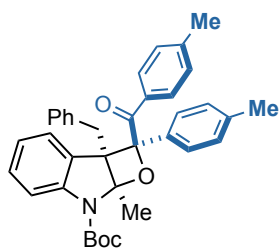
***tert*-butyl-2-benzoyl-2a-benzyl-7a-methyl-2-phenyl-2a,7a-dihydrooxeto[2,3-*b*]indole-7(2*H*)-carboxylate (45).**



>98% yield

¹H-NMR (400 MHz, Acetone-*d*₆): δ 8.04 (d, *J* = 8.3 Hz, 2H, Ar), 7.65 (d, *J* = 7.9 Hz, 1H, Ar), 7.58—7.55 (m, 5H, Ar), 7.49—7.40 (m, 2H, Ar), 7.27 (t, *J* = 8.0 Hz, 2H, Ar), 7.21 (t, *J* = 8.1 Hz, 1H, Ar), 7.09 (t, *J* = 8.1 Hz, 1H, Ar), 7.02-7.00 (m, 3H, Ar), 6.79-6.76 (m, 2H, Ar), 3.54 (d, *J* = 15.7 Hz, 1H, CH₂α), 2.93 (d, *J* = 15.7 Hz, 1H, CH₂β), 1.99 (s, 3H, CH₃), 1.49 (s, 9H, C(CH₃)₃) ppm. **¹³C-NMR (101 MHz, Acetone-*d*₆):** δ 200.8, 152.2, 145.3, 138.2, 137.1, 136.9, 133.2, 130.5 (x2), 129.8 (x2), 129.6, 129.5, 129.4 (x2), 129.3, 128.7 (x2), 128.5 (x2), 127.3 (x2), 127.0, 123.3, 116.2, 102.2, 97.1, 82.3, 64.4, 37.7, 28.4 (x3), 24.0 ppm. **HRMS(ESI-MS)** calculated for C₃₅H₃₄NO₄⁺ [*M*+*H*⁺] 532.6520, found 532.6514.

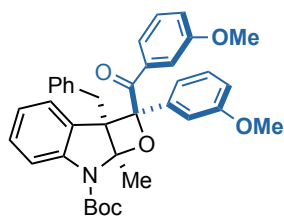
***tert*-butyl-2a-benzyl-7a-methyl-2-(4-methylbenzoyl)-2-(*p*-tolyl)-2a,7a-dihydrooxeto[2,3-*b*]indole-7(2*H*)-carboxylate (46).**



>98 yield

¹H NMR (400 MHz, Acetone-*d*₆): δ 7.88 (d, *J* = 8.0 Hz, 2H, Ar), 7.64 (d, *J* = 8.2 Hz, 1H, Ar), 7.54 (d, *J* = 8.0 Hz, 2H, Ar), 7.37 (d, *J* = 8.1 Hz, 2H, Ar), 7.21–7.11 (m, 3H, Ar), 7.10 – 7.05 (m, 2H, Ar), 7.04 – 6.97 (m, 3H, Ar), 6.80 – 6.76 (m, 2H, Ar) 3.53 (d, *J* = 16.0 Hz, 1H, CH₂α), 2.96 (d, *J* = 16.0 Hz, 1H, CH₂β), 2.40 (s, 3H, CH₃), 2.27 (s, 3H, CH₃), 1.99 (s, 3H, CH₃), 1.52 (s, 9H, C(CH₃)₃) ppm. **¹³C NMR (101 MHz, Acetone-*d*₆):** δ 199.0, 151.3, 144.4, 143.0, 138.0, 136.4, 134.4, 133.3, 129.6 (x2), 129.2 (x2), 129.1 (x2), 128.9, 128.5, 128.3 (x2), 127.8 (x2), 126.4 (x2), 126.0, 125.2, 122.3, 115.3, 101.1, 96.3, 81.3, 63.4, 36.9, 27.5 (x3), 23.1, 20.6, 20.2 ppm. **HRMS(ESI-MS)** calculated for C₃₇H₃₈NO₄⁺ [*M*+*H*⁺] 560.2795, found 560.2796.

***tert*-butyl-2a-benzyl-2-(3-methoxybenzoyl)-2-(3-methoxyphenyl)-7a-methyl-2a,7a-dihydrooxeto[2,3-*b*]indole-7(2*H*)-carboxylate (47).**

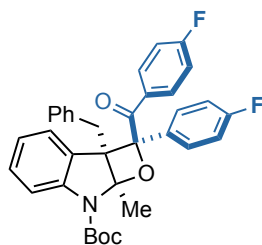


>98% yield

¹H NMR (400 MHz, Acetone-*d*₆): δ 7.66 (d, *J* = 8.2 Hz, 1H, Ar), 7.58 (t, *J* = 6.8 Hz, 3H, Ar), 7.55 – 7.45 (m, 2H, Ar), 7.29 – 7.16 (m, 3H, Ar), 7.13 – 7.04 (m, 3H, Ar), 7.05 – 6.97 (m, 3H, Ar), 6.82 – 6.76 (m, 2H, Ar), 3.91 (s, 3H, OCH₃), 3.73 (s, 3H, OCH₃), 3.58 (d, *J* = 16.0 Hz, 1H, CH₂α), 2.99 (d, *J* = 16.0 Hz, 1H, CH₂β), 2.01 (s, 3H, CH₃), 1.50 (s, 9H, C(CH₃)₃) ppm. **¹³C NMR (101 MHz, Acetone-*d*₆):** δ 199.5, 160.0, 159.0, 151.2, 144.3, 138.8, 137.2, 136.2, 130.4, 129.6 (x3), 128.8, 128.7, 128.6, 127.7 (x2), 126.0, 122.4, 121.2, 118.6, 118.2, 115.3, 113.8, 113.4, 112.3,

101.2, 96.1, 81.3, 63.6, 54.7, 54.6, 36.7, 27.5 (x3), 23.0 ppm. **HRMS(ESI-MS)** calculated for $C_{37}H_{38}NO_6^+$ $[M+H^+]$ 592.2694, found 592.2695.

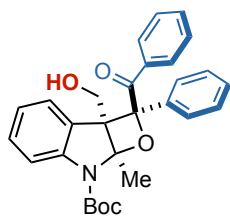
***tert*-butyl-2a-benzyl-2-(4-fluorobenzoyl)-2-(4-fluorophenyl)-7a-methyl-2a,7a-dihydrooxeto[2,3-*b*]indole-7(2*H*)-carboxylate (48).**



>98% yield

1H NMR (400 MHz, Acetone- d_6): δ 8.07 (dd, $J = 7.9, 6.0$ Hz, 2H, Ar), 7.67 (dd, $J = 7.5, 5.9$ Hz, 2H, Ar), 7.62 (d, $J = 8.2$ Hz, 1H, Ar), 7.52 (d, $J = 7.6$ Hz, 1H, Ar), 7.35 (t, $J = 8.7$ Hz, 2H, Ar), 7.19 (t, $J = 7.8$ Hz, 1H, Ar), 7.12 – 6.98 (m, 6H, Ar), 6.79 (d, $J = 4.7$ Hz, 2H, Ar), 3.55 (d, $J = 16.0$ Hz, 1H, $CH_2\alpha$), 2.97 (d, $J = 16.0$ Hz, 1H, $CH_2\beta$), 2.00 (s, 3H, CH_3), 1.52 (s, 9H, $C(CH_3)_3$) ppm. **^{13}C NMR (101 MHz, Acetone- d_6):** δ 198.6, 165.1 (d, $J = 220$.Hz), 162.7 (d, $J = 220$.Hz), 151.1, 144.3, 136.0, 133.1 (d, $J = 2.9$ Hz), 132.4 (d, $J = 3.0$ Hz), 131.9 (d, $J = 9.4$ Hz, x2), 129.6 (x2), 129.2, 128.6 (d, $J = 8.3$ Hz, x2), 128.5 (d, $J = 21.9$ Hz, x2), 127.8 (x2), 126.1, 122.5, 115.3 (d, $J = 21.0$ Hz, x2), 115.2, 114.6 (d, $J = 21.9$ Hz, x2), 101.5, 95.8, 81.5, 63.5, 36.5, 27.5 (x3), 23.0 ppm. **^{19}F -NMR (376 MHz, Acetone- d_6):** δ -107.85 – -107.91 (m, 1F, C-F Ar), -115.89 – -115.95 (m, 1F, C-F Ar) ppm. **HRMS(ESI-MS)** calculated for $C_{35}H_{32}NO_4^+$ $[M+H^+]$ 568.2294, found 568.2297.

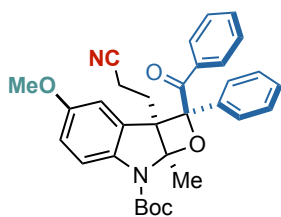
***tert*-butyl-2-benzoyl-2a-(hydroxymethyl)-7a-methyl-2-phenyl-2a,7a-dihydrooxeto[2,3-*b*]indole-7(2*H*)-carboxylate (49).**



85% yield

1H -NMR (400 MHz, Acetone- d_6): δ 7.88 (d, $J = 7.9$ Hz, 2H, Ar), 7.63 (d, $J = 7.9$ Hz, 1H, Ar), 7.59 (d, $J = 7.9$ Hz, 2H, Ar), 7.52–7.47 (m, 3H, Ar), 7.40 (q, $J = 7.2$ Hz, 2H, Ar), 7.26 (t, $J = 7.9$ Hz, 2H, Ar), 7.18 (t, $J = 7.9$ Hz, 1H, Ar), 7.07 (t, $J = 7.9$ Hz, 1H, Ar), 4.08 (dd, $J = 11.3, 3.6$ Hz, 1H, $CH_2\alpha$), 3.70 – 3.59 (m, 2H, $CH_2\beta$ and OH overlapped), 2.10 (s, 3H, CH_3), 1.48 (s, 9H, $C(CH_3)_3$) ppm. **^{13}C -NMR (101 MHz, Acetone- d_6):** δ 199.8, 152.0, 145.6, 137.8, 136.7, 133.2, 129.9 (x2), 129.3 (x2), 129.2, 129.1, 128.5 (x2), 128.5, 126.5 (x2), 123.2, 115.7, 102.1, 95.1, 81.9, 64.1, 61.1, 41.8, 28.4 (x3), 21.9 ppm. **HRMS(ESI-MS)** calculated for $C_{29}H_{30}NO_5^+$ $[M+H^+]$ 472.2118, found 472.2119.

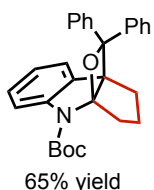
***tert*-butyl-2a-(2-cyanoethyl)-4-methoxy-7a-methyl-2,2-diphenyl-2a,7a-dihydrooxeto[2,3-*b*]indole-7(2*H*)-carboxylate (50).**



79% yield

¹H-NMR (500 MHz, Acetone-*d*₆): δ 7.91 (d, *J* = 7.5 Hz, 2H, Ar), 7.60 — 7.57 (m, 3H, Ar), 7.53 (t, *J* = 7.5 Hz, 2H, Ar), 7.44 — 7.41 (m, 2H, Ar), 7.27 (t, *J* = 7.5 Hz, 2H, Ar), 7.19 (d, *J* = 2.7 Hz, 1H, Ar), 6.81 (dd, *J* = 9.1, 2.7 Hz, 1H, Ar), 3.87 (s, 3H, OCH₃), 2.47 (ddd, *J* = 16.8, 11.2, 5.8 Hz, 1H, CH₂), 2.11 (s, 3H, CH₃), 2.13-2.07 (m, 2H, CH₂) 1.88 (ddd, *J* = 15.7, 10.1, 5.8 Hz, 1H, CH₂), 1.48 (s, 9H, C(CH₃)₃) ppm. **¹³C-NMR (125 MHz, Acetone-*d*₆):** δ 200.0, 156.9, 152.0, 138.7, 137.6, 136.6, 133.4, 129.9 (x2), 129.5 (x2), 129.4, 129.2, 128.6 (x2), 126.9 (x2), 120.0, 117.0, 115.8, 113.9, 102.0, 95.9, 82.0, 63.7, 56.1, 28.4, 27.8 (x3), 22.2, 13.2 ppm. **HRMS(ESI-MS)** calculated for C₃₂H₃₃N₂O₅⁺ [M+H⁺] 525.2384, found 525.2389.

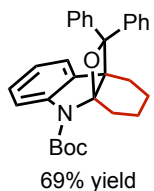
***tert*-butyl-9,9-diphenyl-2,3-dihydro-1*H*,4*H*-3a,8b-(epoxymethano)cyclopenta[*b*]indole-4-carboxylate (51).**



65% yield

¹H-NMR (400 MHz, Acetone-*d*₆): δ 7.72 (d, *J* = 7.9 Hz, 2H, Ar), 7.48 (d, *J* = 7.9 Hz, 2H, Ar), 7.42 — 7.38 (m, 3H, Ar), 7.26 (t, *J* = 7.5 Hz, 1H, Ar), 7.02 — 6.92 (m, 4H, Ar), 6.89 — 6.81 (m, 2H, Ar), 2.70 — 2.61 (m, 2H, CH₂), 1.90 — 1.74 (m, 3H, CH₂), 1.64 (s, 9H, C(CH₃)₃), 1.58 — 1.46 (m, 1H, CH₂) ppm. **¹³C-NMR (101 MHz, Acetone-*d*₆):** δ 152.0, 145.2, 144.4, 132.8, 129.2, 128.7 (x3), 128.6, 128.0 (x2), 127.5, 127.3, 126.9, 126.7, 126.2 (x2), 125.9 (x2), 123.2, 115.1, 91.4, 55.0, 34.1, 28.6 (x3), 28.3, 28.2 ppm. **HRMS(ESI-MS)** calculated for C₂₉H₃₀NO₃⁺ [M+H⁺] 440.2220, found 440.2222.

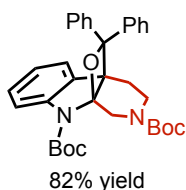
***tert*-butyl-11,11-diphenyl-5,6,7,8-tetrahydro-9*H*-8a,4b-(epoxymethano)carbazole-9-carboxylate (52).**



69% yield

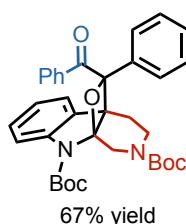
¹H-NMR (400 MHz, Acetone-*d*₆): δ 7.64 (d, *J* = 7.9 Hz, 2H, Ar), 7.44 — 7.37 (m, 6H, Ar), 7.23 (t, *J* = 7.3 Hz, 1H, Ar), 6.97 (q, *J* = 7.3 Hz, 3H, Ar), 6.89 (q, *J* = 7.3 Hz, 2H, Ar), 2.57 — 2.51 (m, 1H, CH₂), 2.25 — 2.21 (m, 1H, CH₂), 2.18 — 2.00 (m, 2H, CH₂), 1.64 (s, 9H, C(CH₃)₃), 1.52 — 1.44 (m, 4H) ppm. **¹³C-NMR (101 MHz, Acetone-*d*₆):** δ 152.0, 145.3, 145.1, 131.8, 129.1, 129.0 (x2), 127.7 (x2), 127.5, 126.7, 126.3 (x2), 126.0 (x2), 125.6, 122.8, 115.0, 101.3, 94.4, 81.4, 58.9, 28.7 (x3), 28.0, 19.9, 19.7 ppm. **HRMS(ESI-MS)** calculated for C₃₀H₃₂NO₃⁺ [M+H⁺] 454.2377, found 454.2375.

di-tert-butyl-11,11-diphenyl-3,4-dihydro-9H-9a,4a-(epoxymethano)pyrido[3,4-b]indole-2,9(1H)-dicarboxylate (53).



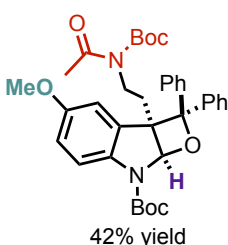
¹H-NMR (400 MHz, Acetone-*d*₆): δ 7.69 (t, J = 7.1 Hz, 2H, Ar), 7.49 – 7.37 (m, 6H, Ar), 7.27 (q, J = 7.1 Hz, 1H, Ar), 7.03 – 6.98 (m, 3H, Ar), 6.93 – 6.86 (m, 2H, Ar), 4.44 (d, J = 14.1 Hz, 1H, CH₂ α), 3.95 (d, J = 14.1 Hz, 1H CH₂ β), 3.34 – 3.24 (m, 1H, CH₂), 2.78 – 2.70 (m, 1H, CH₂), 2.46 – 2.30 (m, 2H, CH₂), 1.68 (s, 9H, C(CH₃)₃), 1.43 (s, 4H, C(CH₃)₃), 1.28 (s, 5H, C(CH₃)₃) ppm. **¹³C-NMR (101 MHz, Acetone-*d*₆):** δ 155.7, 155.0, 151.7, 151.7, 144.6, 144.4, 129.4, 129.3, 129.1 (x2), 128.0, 127.9, 127.8, 127.8, 127.1 (x2), 126.2 (x2), 125.8 (x2), 123.2, 123.1, 115.2, 94.9, 82.0, 79.7, 79.6, 41.8, 40.7, 40.2, 28.7 (x3), 28.6 (x3), 28.6 (x3), 28.5 (x3), 27.3, 26.8, 24.4, 21.3, 17.8 ppm. **HRMS(ESI-MS)** calculated for C₃₄H₃₉N₂O₅⁺ [M+H⁺] 555.2853, found 555.2859.

di-tert-butyl-11-benzoyl-11-phenyl-3,4-dihydro-9H-9a,4a-(epoxymethano)pyrido[3,4-b]indole-2,9(1H)-dicarboxylate (54).



¹H NMR (400 MHz, Acetone-*d*₆): δ 7.84 (d, J = 7.7 Hz, 2H, Ar), 7.60 (t, J = 8.7 Hz, 2H, Ar), 7.52 (t, J = 7.2 Hz, 2H, Ar), 7.49 – 7.41 (m, 4H, Ar), 7.31 (t, J = 7.5 Hz, 2H, Ar), 7.24 (t, J = 7.8 Hz, 1H, Ar), 7.13 (t, J = 7.4 Hz, 1H, Ar), 4.25 (dd, J = 37.5, 14.3 Hz, 2H, CH₂), 3.20 (br, 1H, CH₂), 2.72 (m, 1H, CH₂), 2.19 – 2.10 (m, 2H, CH₂), 1.50 (s, 5H, C(CH₃)₃), 1.47 (s, 9H, C(CH₃)₃), 1.33 (s, 4H, C(CH₃)₃) ppm. **¹³C NMR (101 MHz, Acetone-*d*₆):** δ 199.2, 137.2, 136.0, 132.3, 129.6, 128.9 (x2), 128.8 (x2), 128.7, 128.2, 128.1, 127.7 (x2), 126.7, 125.5 (x2), 123.0, 114.5, 97.6, 45.5, 39.5, 38.9, 27.7 (x3), 27.5 (x3), 26.1, 25.7, 23.5, 16.9, ppm. **HRMS(ESI-MS)** calculated for C₃₅H₃₉N₂O₆⁺ [M+H⁺] 583.2803, found 583.2800.

tert-butyl-2a-(2-(*N*-(tert-butoxycarbonyl)acetamido)ethyl)-4-methoxy-2,2-diphenyl-2a,7a-dihydrooxeto[2,3-*b*]indole-7(2H)-carboxylate (55).

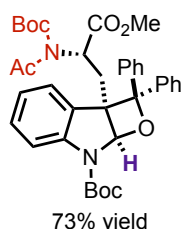


¹H NMR (400 MHz, Acetone-*d*₆): δ 7.85 (d, J = 7.8 Hz, 2H, Ar), 7.56 (d, J = 7.7 Hz, 3H, Ar), 7.44 (t, J = 7.7 Hz, 2H, Ar), 7.30 (t, J = 7.3 Hz, 1H, Ar), 7.16 (t, J = 10.0 Hz, 2H, Ar), 7.07 (d, J = 2.5 Hz, 1H, Ar), 7.03 (t, J = 7.3 Hz, 1H, Ar), 6.66 (dd, J = 8.8, 2.5 Hz, 1H, Ar), 6.54 (br, 1H, CH), 3.73 (s, 3H, OCH₃), 3.32 (ddd, J = 13.3, 10.7, 5.9 Hz, 1H, CH₂), 3.19 – 3.12 (m, 1H, CH₂), 2.50 – 2.38 (m, 1H, CH₂), 2.27 (s, 3H, COCH₃), 1.96 – 1.90 (m, 1H, CH₂), 1.63 (s, 9H, C(CH₃)₃), 1.46 (s, 9H, C(CH₃)₃) ppm. **¹³C NMR (101 MHz, Acetone-*d*₆):** δ 171.6, 155.7, 152.6, 143.3, 128.2 (x4), 127.2 (x4), 127.2, 126.4, 125.9 (x2), 125.5 (x2), 114.1, 112.5, 94.1, 92.5, 82.5, 55.1, 40.9, 39.9, 31.7, 27.6 (x3),

27.2 (x3), 25.9, 23.5, 20.5 ppm. HRMS(ESI-MS) calculated for C₃₆H₄₃N₂O₇⁺ [M+H⁺] 615.3065, found 615.3066.

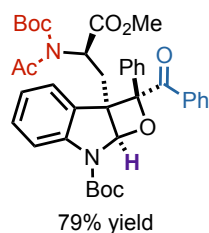
tert-butyl-2a-(2-(N-(tert-butoxycarbonyl)acetamido)-3-methoxy-3-oxopropyl)-2,2-diphenyl-2a,7a-dihydrooxeto[2,3-b]indole-7(2H)-carboxylate (56).

Mixture of diastereoisomers.



¹H NMR (400 MHz, Acetone-d₆): δ 7.84 (d, *J* = 7.8 Hz, 2H, Ar), 7.49 – 7.44 (m, 5H, Ar), 7.37 – 7.25 (m, 2H, Ar), 7.14 – 6.95 (m, 4H, Ar), 6.81 (t, *J* = 7.5 Hz, 1H, Ar), 6.73 (*br*, 1H, CH), 5.28 (t, *J* = 6.4 Hz, 1H, CH), 3.56 (s, 3H, COOCH₃), 2.86 – 2.72 (m, 2H, CH₂), 1.92 (s, 3H, COCH₃), 1.65 (s, 9H, C(CH₃)₃), 1.40 (s, 9H, C(CH₃)₃) ppm. ¹³C NMR (101 MHz, Acetone-d₆): δ 171.3, 170.4, 151.4, 143.3, 143.2, 128.1 (x4), 128.1, 127.2, 127.1, 127.0 (x4), 126.2, 126.1 (x2), 125.6 (x2), 124.2, 122.0, 95.0, 92.3, 83.5, 52.0, 51.5, 32.6, 27.6, 27.0, 25.5 ppm. HRMS(ESI-MS) calculated for C₃₂H₃₃N₂O₅⁺ [M+H⁺] 643.3014, found 643.3016. [α]_D²⁰ = -0.043 (c=0.62, MeOH).

tert-butyl-2-benzoyl-2a-(2-(N-(tert-butoxycarbonyl)acetamido)-3-methoxy-3-oxopropyl)-2-phenyl-2a,7a-dihydrooxeto[2,3-b]indole-7(2H)-carboxylate (57).

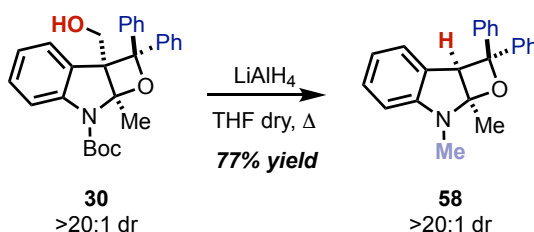


Mixture of diastereoisomers.

¹H NMR (400 MHz, Acetone-d₆): δ 7.94 (t, *J* = 7.0 Hz, 2H, Ar), 7.66 – 7.53 (m, 5H, Ar), 7.52 – 7.37 (m, 2H, Ar), 7.33 – 7.22 (m, 3H, Ar), 7.20 – 7.08 (m, 1H, Ar), 6.84 (s, 1H, CH), 5.16 (t, *J* = 6.8 Hz, 1H, CH), 3.53 (s, 3H, COOCH₃), 2.44 (qd, *J* = 15.1, 6.9 Hz, 2H, CH₂), 2.03 (s, 3H, COCH₃), 1.61 (s, 9H, C(CH₃)₃), 1.39 (s, 9H, C(CH₃)₃) ppm. ¹³C NMR (101 MHz, Acetone-d₆): δ 198.5, 171.2, 151.4, 137.5, 135.2, 133.0, 132.8, 129.3, 129.2, 129.1 (X2), 129.0, 128.8, 128.6, 128.0, 127.9 (x2), 125.9 (x2), 125.7, 122.8, 98.1, 92.5, 83.7, 83.5, 51.8, 51.6, 51.5, 33.0, 27.6 (x3), 27.1 (x3), 30.0, 25.5, 16.9 ppm. HRMS(ESI-MS) calculated for C₃₈H₄₃N₂O₉ [M+H⁺] 671.2963, found 671.2970. [α]_D²⁰ = -0.017 (c=0.38, MeOH).

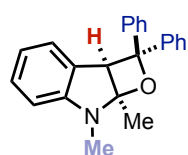
Synthesis and characterization of the PB products manipulations

LiAlH₄ reduction



30 (100 mg, 0.225 mmol, 1 equiv.) was dissolved in 10 mL of anhydrous THF (0.025 M). Subsequently, a 1M solution of LiAlH₄ in THF (1.13 mL, 1.125 mmol, 5 equiv.) was added dropwise, the mixture was stirred at reflux for 4 h. Then, the reaction was quenched with 10 mL of EtOAc at 0°C, 10 mL of a saturated Rochelle salt solution was added, and the mixture was stirred for 30 min. The organic layer was washed with 2x10 mL of Rochelle salt saturated solution and 1x10 mL of a saturated NH₄Cl solution. The organic layer was dried over MgSO₄, filtered and concentrated under reduced pressure, giving **58** as a white solid in 77% yield (56.7 mg, 0.174 mmol).

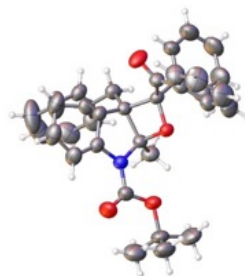
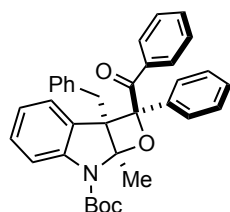
7,7a-dimethyl-2,2-diphenyl-2,2a,7,7a-tetrahydrooxeto[2,3-*b*]indole (**58**).



¹H-NMR (300 MHz, CDCl₃): δ 7.56 (br, 1H, Ar), 7.39—7.36 (m, 1H, Ar), 7.29—7.26 (m, 2H, Ar), 7.23—7.11 (m, 8H, Ar), 7.04—6.90 (m, 2H, Ar), 5.71 (s, 1H, CH), 2.23 (s, 3H, NCH₃), 2.12 (s, 3H, CH₃) ppm. ¹³C-NMR (125 MHz, Acetone-d₆): δ 145.6 (x2), 135.8, 131.0, 129.6, 128.1 (x4), 126.8 (x2), 126.5 (x4), 120.2, 118.2, 117.4, 110.1, 105.7, 75.3, 10.5, 7.7 ppm. HRMS(ESI-MS) calculated for C₂₃H₂₂NO⁺ [M+H⁺] 328.1696, found 328.1672.

X-ray crystallographic analysis of **45**

— X-ray structure of **45** —



Yellow crystals of **45** were grown by slow evaporation of a diethylether solution at ambient temperature. **Mp**: 120-124 °C.

Crystal data: C₃₅H₃₃NO₄

Orthorhombic, *F*2_{dd}, *a*=8.4764(13)Å, *b*=33.008(5)Å, *c*=40.934(6) Å, *V*=11453(3)Å³; *Z*=16; *d*_{calc}=1.233 mg/cm³, *F*(000)= 4512, *μ*=0.080, Tot. refl.= 34654 *hkl* range= -10<*h*<10, -41<*k*<41, -50<*l*<50; Theta max 26.5°, ref.tot.= 5881, number of parameters = 365, GooF= 1.013, *R*=0.0417, *wR*₂=0.0911.

CCDC 1972525 contains the supplementary crystallographic data for this compound. These data can be obtained free of charge from The Cambridge Crystallographic Data Centre via www.ccdc.cam.ac.uk/data_request/cif

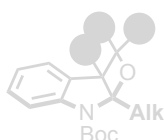
Chapter II – Section 2

Dearomative Paternò-Büchi Reaction – Microfluidic Visible-Light Dearomatization of Oxindole Enol Ethers

Chapter II - Synthetic Transformations Driven by Triplet State Benzophenones

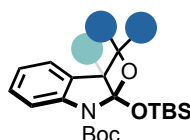
Section 1.

Towards the construction of
Oxeto-Indolinic
Polycycles



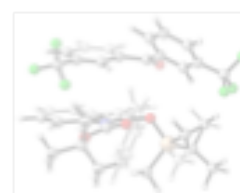
Section 2.

Microfluidic Visible-Light
Dearomatization of
Oxindole Enol Ethers



Section 3.

A Mechanistic Interrogation of the
Process, the Effect of
Visible-Light Irradiation



- To develop a general method to construct oxeto-indolinic polycycles in flow conditions.
- To use oxindole derived silyl enol ether as reaction counterparts in the Paternò-Büchi reaction.²³

²³ The project discussed in this chapter has been conducted in collaboration with Dr. Alberto Vega Peñaloza and Pietro Franceschi (involved in the synthesis and characterization of the starting oxindole derivatives as well as in the final oxeto-indolinic products). I individually prepared several entries of the reaction scope and supervised Pietro Franceschi during his master thesis.

This work has been published: Franceschi, P.; Mateos, J.; Vega-Peñaloza, A.; Dell'Amico, L. *Microfluidic Visible-Light Paternò-Büchi Reaction of Oxindole Enol Ethers*. *Eur. J. Org. Chem.* **2020**, 2020 (43), 6718–6722.

2.2.1 Introduction

The derivatization of biorelevant heterocyclic scaffolds is a valuable target in organic synthesis.²⁴ As described in the previous section with indoles, the oxindole core is also present in numerous naturally occurring compounds and pharmaceutically active ingredients.²⁵ Its structural modification allows the discovery of new drug candidates and the implementation of structure-activity-relationship studies.²⁶ In general, the synthetic methodologies present in literature rely on the pronucleophilic nature of oxindole. This character includes: acylation, alkylation, and condensation reactions with carbonyl compounds.²⁴ For this reason, a broad array of electrophilic partners can be efficiently activated by means of organo- or metal-catalysis (Figure 2.14).²⁷ Recently, the development of new synthetic strategies towards oxindole functionalization has focused on the installation

— classical reactivity of oxindole systems

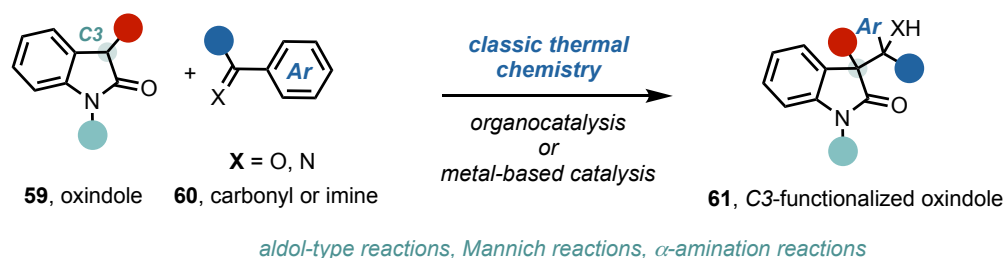


Figure 2.14. - Classical thermal reactivity of oxindole systems.

of the C3 quaternary center, present in a variety of natural alkaloids.^{24,28} Several methods have exploited the reactivity of the corresponding oxindole enolate or enol ether.²⁴⁻²⁷ For example,

²⁴ a) Zhou, F.; Liu, Y.-L.; Zhou, J. Catalytic Asymmetric Synthesis of Oxindoles Bearing a Tetrasubstituted Stereocenter at the C-3 Position. *Adv. Synth. Catal.* **2010**, 352, 1381–1407. b) Russel, J. S. Oxindoles and Spirocyclic Variations: Strategies for C3 Functionalization. In *Heterocyclic Scaffolds II*; Gribble, G. W., Ed.; Topics in Heterocyclic Chemistry; Springer Berlin Heidelberg: Berlin, Heidelberg, **2010**; Vol. 26, pp 397–431.

²⁵ a) Trost, B.; Brennan, M. Asymmetric Syntheses of Oxindole and Indole Spirocyclic Alkaloid Natural Products. *Synthesis* **2009**, 2009, 3003–3025. b) Peddibhotla, S. 3-Substituted-3-Hydroxy-2-Oxindole, an Emerging New Scaffold for Drug Discovery with Potential Anti-Cancer and Other Biological Activities. *CBC* **2009**, 5, 20–38 c) Badillo, J. J.; Hanhan, N. V.; Franz, A. K. Enantioselective Synthesis of Substituted Oxindoles and Spirooxindoles with Applications in Drug Discovery. *Curr. Opin. Drug Discovery Dev.* **2010**, 13, 758–776.

²⁶ Tokunaga, T.; Hume, W. E.; Umezome, T.; Okazaki, K.; Ueki, Y.; Kumagai, K.; Hourai, S.; Nagamine, J.; Seki, H.; Taiji, M.; Noguchi, H.; Nagata, R. Oxindole Derivatives as Orally Active Potent Growth Hormone Secretagogues. *J. Med. Chem.* **2001**, 44, 4641–4649.

²⁷ Bariwal, J.; Voskressensky, L. G.; Van der Eycken, E. V. Recent Advances in Spirocyclization of Indole Derivatives. *Chem. Soc. Rev.* **2018**, 47, 3831–3848.

²⁸ For an example of metal-catalyzed α -arylation see: Taylor, A. M.; Altman, R. A.; Buchwald, S. L. Palladium-Catalyzed Enantioselective α -Arylation and α -Vinylolation of Oxindoles Facilitated by an Axially Chiral P-Stereogenic Ligand. *J. Am. Chem. Soc.* **2009**, 131, 9900–9901.

metal- or organocatalytic approaches, involving aldol-type reactions, or 1,4-additions have been developed using oxindoles as pronucleophiles.^{24, 29}

On the other hand, the introduction of aryl groups at C3 can be accomplished via transition-metal catalysis with aryl electrophiles and arylboronic acids.³⁰ Nevertheless, modern approaches focused on metal-free strategies for the installation of a sp³-sp² bond encompassing the activity of photoexcited EDA complexes (Figure 2.15).³¹

— recent photochemical strategy for oxindole C3 arylation

Selected example: *Chem. Sci.*, **2019**, *10*, 3049–3043

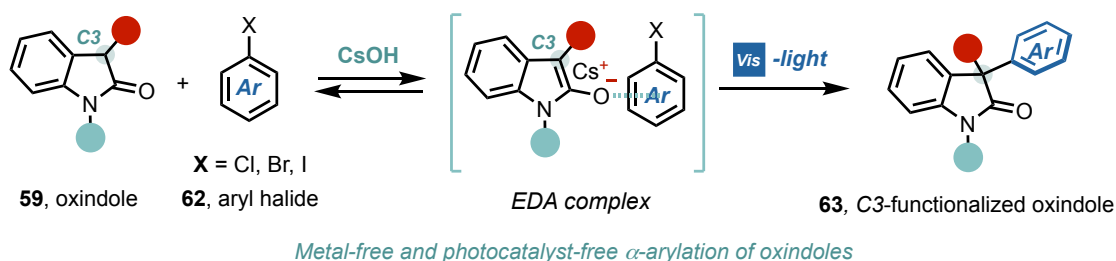


Figure 2.15. - Recent photochemical strategy for the α -arylation of oxindoles.

Despite these recent advancements on the photochemical oxindole functionalization field, the quaternarization at C3 with the concomitant modification at C2 are still rare. Structural modification at both positions will provide complex indolinic polycyclic scaffolds, with wide occurrence in bioactive molecules.²⁵ On the other hand, the installation of an oxetane moiety within the oxindole scaffold is particularly appealing thanks to the biological relevance of this four-membered pharmacophore.^{3,12} However, this represents a challenging synthetic target due to the high ring strain and to the low reactivity at C2. A sustainable strategy to fill this gap can be provided using light-generated radical intermediates.³²

2.2.2 Challenges of the project

As we have previously seen, under light irradiation various heterocyclic systems effectively participate in photocycloaddition transformations with carbonyl compounds.²² We

²⁹ Overman, L. E.; Shin, Y. *Enantioselective Total Synthesis of (+)-Gliocladin C*. *Org. Lett.* **2007**, *9*, 339–341.

³⁰ Shen, K.; Liu, X.; Lin, L.; Feng, X. *Recent Progress in Enantioselective Synthesis of C3-Functionalized Oxindoles: Rare Earth Metals Take Action*. *Chem. Sci.* **2012**, *3*, 327–334.

³¹ Liang, K.; Li, N.; Zhang, Y.; Li, T.; Xia, C. *Transition-Metal-Free α -Arylation of Oxindoles via a Visible-Light-Promoted Electron Transfer*. *Chem. Sci.* **2019**, *10*, 3049–3053.

³² Silvi, M.; Melchiorre, P. *Enhancing the Potential of Enantioselective Organocatalysis with Light*. *Nature* **2018**, *554*, 41–49.

thus wondered if oxindole-derived enol ethers could participate in unprecedented PB processes, delivering a C2-C3 difunctionalized indolinic products.

The effective realization of such a general method is complicated by several synthetic issues, including: *i*) the presence of light-driven side reactions, such as the dimerization of the carbonyl compound enhanced with the use of electron-rich heterocycles, *ii*) the site-, regio- and stereoselectivity of the reaction, *iii*) and the possible desilylation pathways. Additionally, the large-scale synthesis of photochemical reactions is commonly hampered by the need of UV-light sources (Hg or Xe lamps) in batch setups. In this scenario, the combination of visible-light microfluidic photoreactors (MFP) offer decisive advantages to implement safer and general versions of the PB reaction. Indeed, the MFP setup overcomes some fundamental issues related to photochemical batch protocols, such as: scale up, homogeneous irradiation, reproducibility and generality.²⁰

2.2.3 Section overview

In this section, I report the effective realization of a microfluidic photocatalyst-free visible-light PB process between oxindole enol ethers and aromatic ketones under emild reaction conditions and complete atom-economy (Figure 2.16). Strained indolinic polycycles are accessed with excellent site-, regio-, and diastereocontrol. Remarkably, the quaternarization of C3 and the concomitant C2 functionalization is accomplished within a single synthetic operation. The use of visible light guarantees a clean, safe and efficient process. The generality of the microfluidic method is demonstrated for a large variety of substrates (up to >98% yield and >20 : 1 dr). Remarkably, the process can be easily scaled up delivering up to 1.18 g of difunctionalised oxindole product, overcoming the classical limitations of UV-light driven PB procedures.

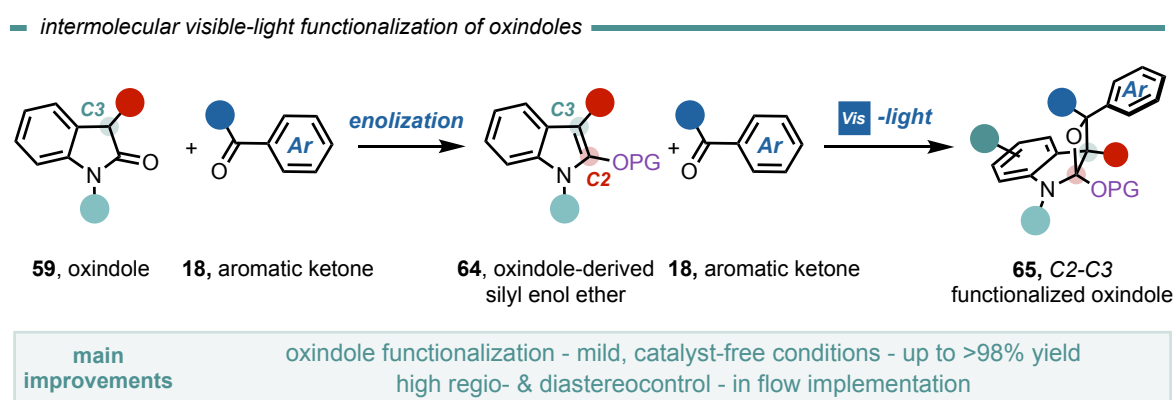
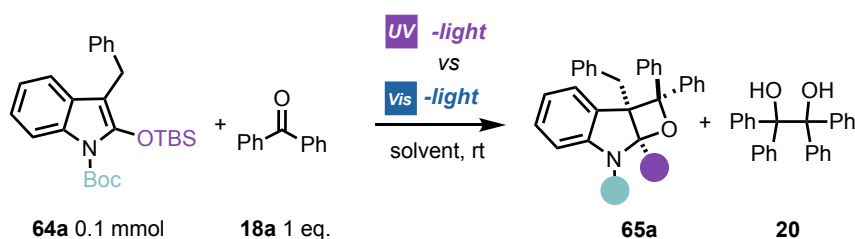


Figure 2.16. - Photochemical strategy developed in this section.

2.2.4 Results and discussion

Reaction optimization

We initiated our studies by testing the silyl enol ether (SEE) **64a** (3 equiv.), derived from the corresponding 3-benzyloxindole, in the presence of benzophenone **18a** under MFP equipped with a 365 nm light source.³³ 3-Benzyl SEE **64a** was selected aiming to generate a valuable *all-carbon* quaternary stereocenter within product **65a**. As expected, when using UV-light sources, we obtained only 12% yield of the product **65a**, along with the undesired benzophenone homodimer **20** (Table 2.7, entry 1). As in this case the used heterocycle **59** is electron-richer than indoles **17** used in Section 1 of this chapter, we slightly modified our optimization strategy. Hence, we investigated how the reagent ratio inferred in the reaction outcome. When **64a** was used in excess, formation of **65a** increased up to a modest 42% yield as single diastereoisomer (entry 2). Regrettably, its purification was complicated by the presence of **20**. As previously stated, a possible solution to circumvent the undesired consumption of benzophenone problem when using electron-rich heterocycles is the use of visible-light emission sources. In fact, the inferior amount of **18a** T₁ excited state, attenuates the ketone homodimerization and channels the reactivity towards the intended PB product **65a**. Irradiation of the same reaction mixture at 405 nm resulted in 96% yield of **65a** (entry 3) and no ketone homodimer was detected. Gratefully, we were able to reduce the residence time up to 12 min. In this case (entry 4), the product **65a** was obtained in excellent yields (98%) as a single diastereoisomer, boosting the performance of the system. Interestingly, when the



entry	light source	ratio 64a:18a	residence time	solvent	(65a) yield %	dr
1	365 nm	3:1	25 min	PhMe	12	>20:1
2	365 nm	1:3	25 min	PhMe	42	>20:1
3	405 nm	1:3	25 min	PhMe	96	>20:1
4	405 nm	1:3	12 min	PhMe	98	>20:1
5	405 nm	1:1	12 min	PhMe	69	>20:1
6	405 nm	1:1	12 min	Acetone	56	>20:1

Table 2.7. - Optimization of the visible-light dearomatization reaction between oxindole-derived silyl enol ethers and benzophenone.

³³ See Chapter III – Section I for more information about the 365 nm photoreactor used in this section.

reaction was performed using an equimolar mixture of reagents, the system maintained decent levels of reactivity (entry 5). Importantly, equimolar mixtures under MFP setups using different solvents such as acetone yielded **65a** in good yields (entry 6, 56% yield).

Generality of the reaction

With the optimized reaction conditions in hand, we next evaluated the generality of the visible-light PB process. As reported in Table 2.8, there is a significant tolerance for structural and electronic variation on the oxindole enol ether. Both electron-withdrawing (EWG) and electron-donating groups (EDGs) at the *ortho*, *meta* and *para* positions of the benzyl ring furnished the corresponding tricyclic products **65-71** in high yields, spanning from 64% to 98% with complete regio- and diastereocontrol. The relative stereochemistry of the products was inferred by X-ray on the single crystal of compound **65**. Also SEE of 3-methyl oxindole resulted in the formation of **72** as single regio- and diastereoisomer in 98% yield.

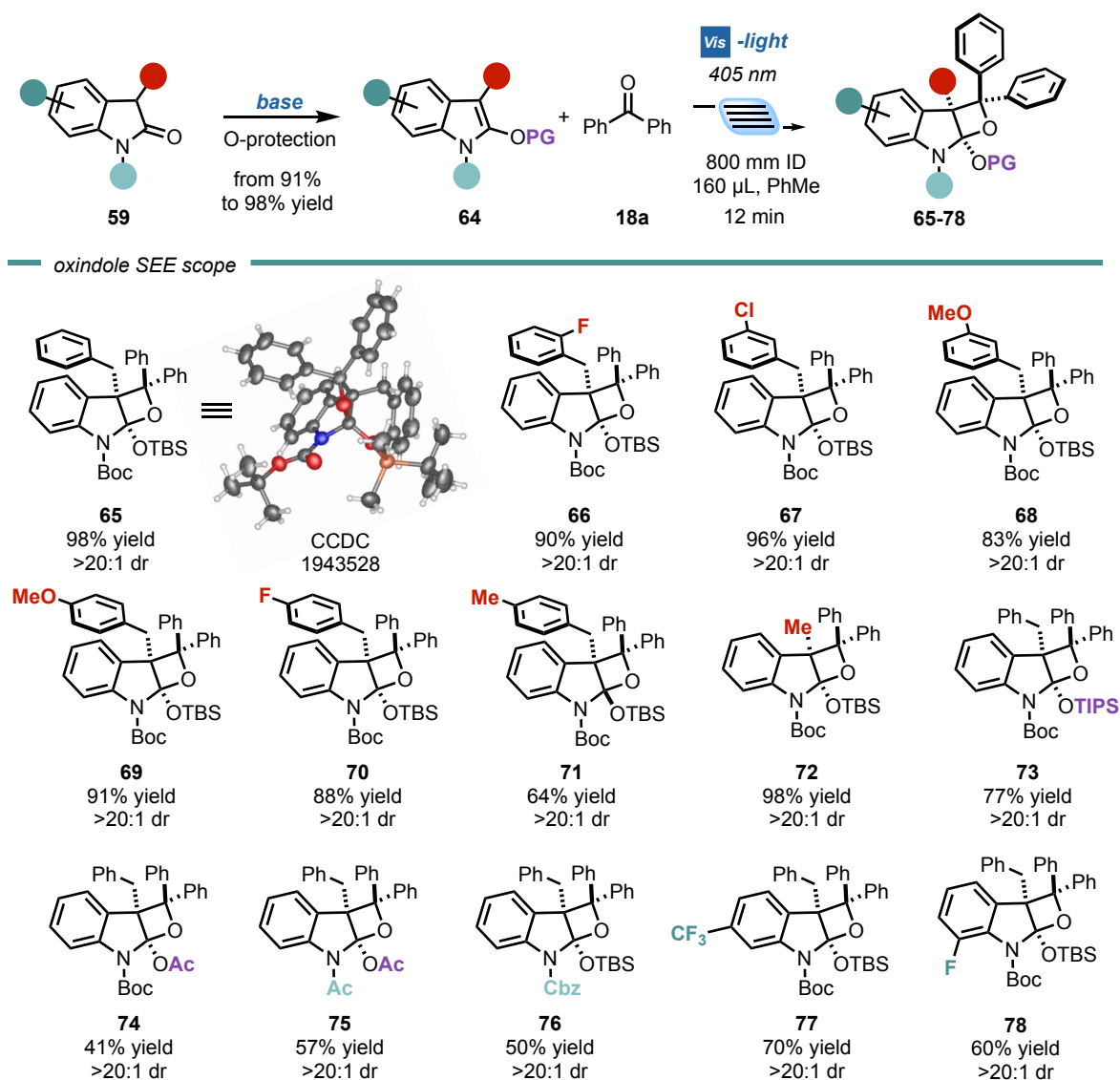


Table 2.8. - Substrate table when using different oxindole-derived silyl enol ether derivatives.

Other types of enol ethers were found competent substrates under these conditions, delivering products **73**, **74** and **75** in 77%, 41% and 57% yield, respectively. Also, different *N*-protected oxindoles can participate in the reported microfluidic PB process, delivering product **76** and **77**, in 57% and 50% yield and with high fidelity (>20:1 dr). Oxindole SEEs bearing both EW- and EDGs at different position of the oxindole core formed the desired PB products **77** and **78** in good chemical yield (70% and 60%).

We next examined the versatility of the reaction with respect to the ketone counterpart (Table 2.9). Remarkably, differently substituted benzophenones with both ED- and EWGs performed well, delivering the corresponding products **79-84** in yields spanning from 41% to >98% and excellent regio- and diastereocontrol (>20:1).

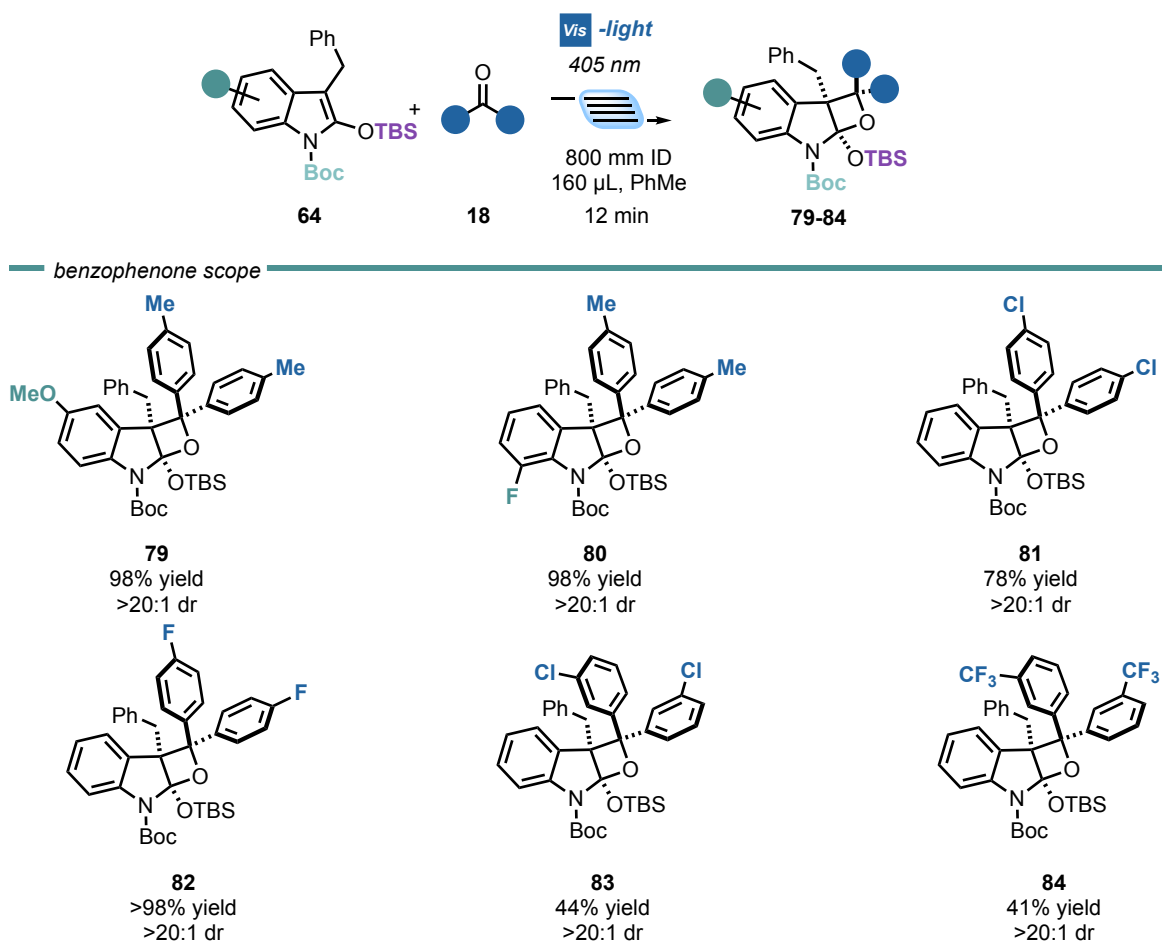


Table 2.9. - Substrate table when using different benzophenone derivatives.

We next assessed substrates with additional reactive double bonds (Figure 2.17). Compound **85**, bearing an allyl functionality, was formed with full site-selectivity (78% yield). This encouraged us to evaluate the possibility of extending the PB reactivity to furan-containing enol ethers. Remarkably, product **86** formed in 74% yield as a single site-, regio- and diastereoisomer. To understand the reason of the observed site-selectivity we performed a competition experiment in the presence of furan **87** (Figure 2.17b). In this case we used 2

equiv. of benzophenone **18a** and 1 equiv. of **64a** and **87**. After 12 min, product **65** formed in 63% yield along with traces of **88**, thus indicating the superior reactivity for the oxindole-SEE double bond, despite its sterically hindered nature.

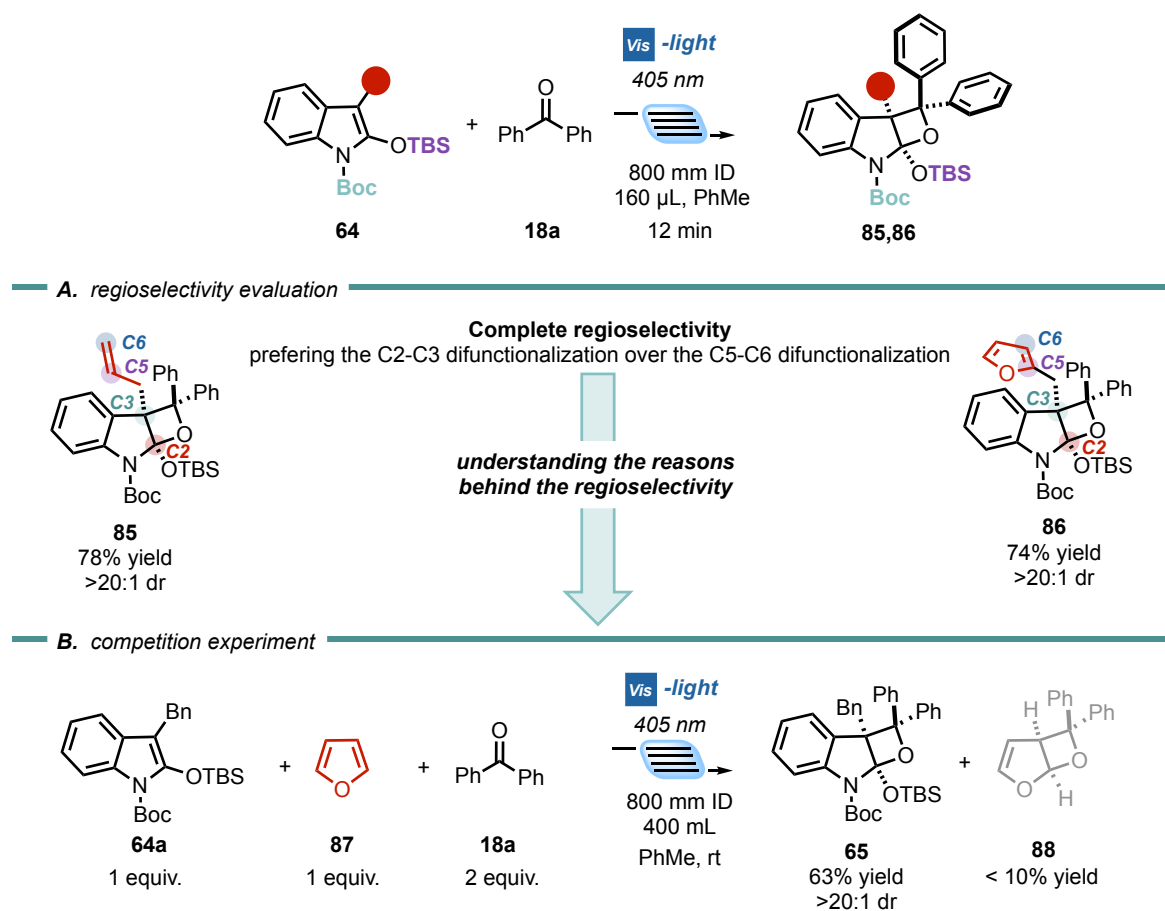
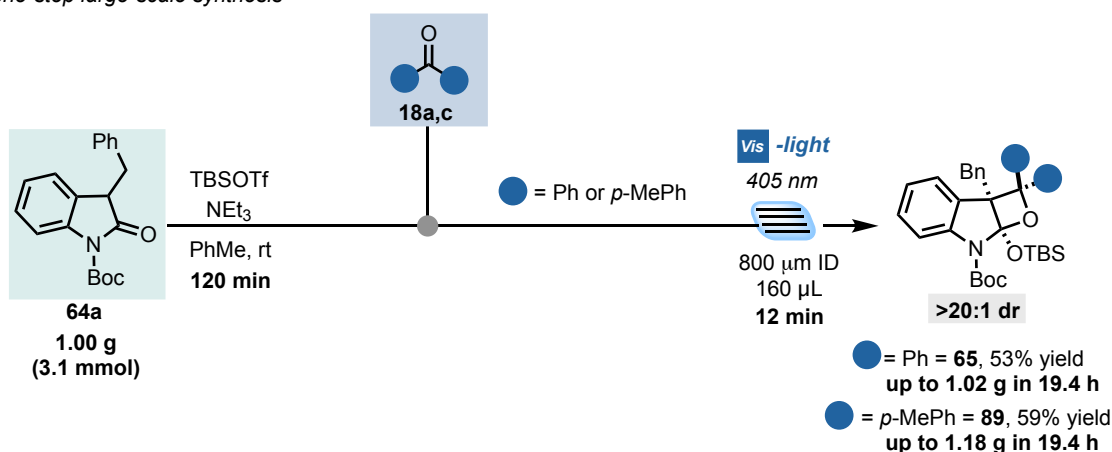


Figure 2.17. - Substrate table with oxindole-derived silyl enol ether containing additional double bonds. a) Regioselectivity evaluation. b) Competition experiment with furan.

Large-scale synthesis

In order to assess the synthetic potential of the presented microfluidic method for the gram-scale functionalization of oxindoles, implementing an in-flow process starting from the simple 3-benzyloxindole precursor **4a** (Scheme 2.3). In this case the crude solution of 3-benzyloxindole **64a** (1.00 g, 3.1 mmol), silylating agent (TBSOTf) and base (NEt_3) in presence of the selected ketones **18a** and **18b** was pumped into two parallel MFPs with a retention time of 12 min over 19.4 h. With our delight, the final oxetane products **65** and **89** were collected in 53% and 59% yield, corresponding respectively to 1.02 g and 1.18 g. Importantly, these experiments proved the robustness of the developed method which can be performed also on crude reaction mixtures, containing organic bases and silylating agents, thus avoiding intermediate purifications.



Scheme 2.4. - Large-scale synthesis of **65** and **89**. Direct functionalization of oxindole.

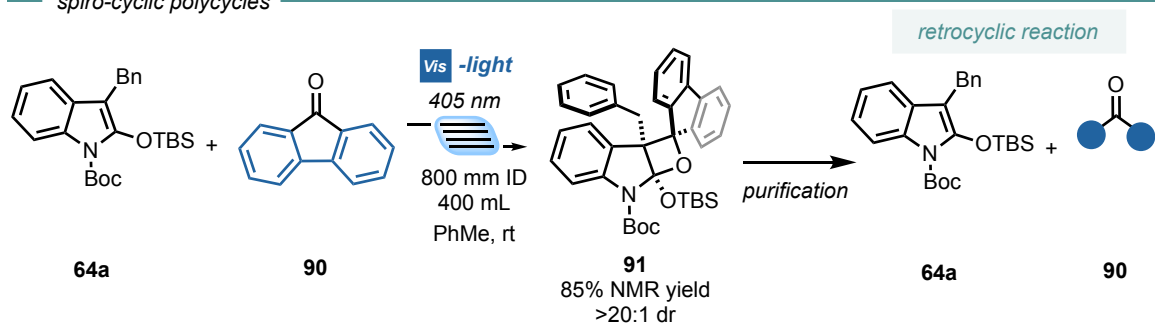
Limitations

This method allows the direct functionalization of oxindole-derived silyl enol ethers in a fast and selective manner. Nevertheless, the use of other electron-rich heterocycles does not prevent the limitations observed when using indole derivatives (Section I of this chapter). Again, acetophenone and benzaldehyde failed to deliver the corresponding oxetane products due to the low absorption under visible light. Hence, the higher-selectivity of MFP setups prevents the use of carbonyl compounds mainly absorbing in the UV-light region.

The two main limitations of this method are the two most promising observations in terms of applications and mechanistic assessment. These limitations can be summarized as following: *i*) the higher-instability of the oxeto-indolinic polycycles; and *ii*) the lower diastereoselectivity observed when using prochiral carbonyl compounds such as benzil.

On one hand, the use of **64a** permits the reaction towards a wider range of carbonyl-compounds (Scheme 2.5). In fact, the reaction is not limited to acyclic benzophenone derivatives but fluorenone **90** is an exceptional reaction partner (the reaction is not limited to fluorenone but xanthone is also well tolerated). The spiro-cyclic polycycle **91** was observed in high NMR yields (85% yield). Interestingly, the formation of these type of polycycles was not observed when using indole derivatives. Hence, we hypothesize that the formation of this product is highly dependent on the indole nature. Unfortunately, the simple solvent removal or the purification by column chromatography furnished the initial starting materials (ascribable to the [2+2]-retrocyclic reaction).

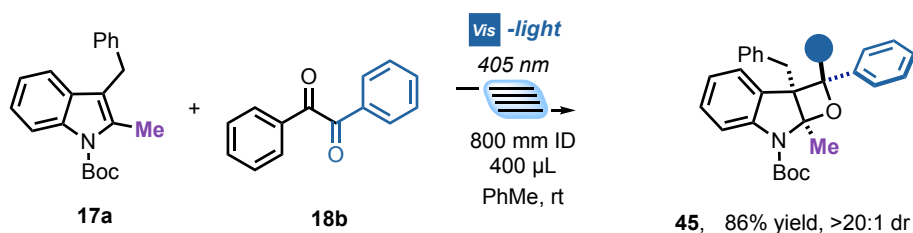
— spiro-cyclic polycycles —



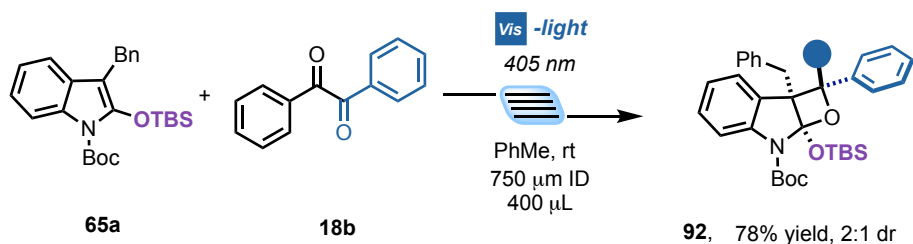
Scheme 2.5. - Formation of spiro-cyclic polycycles.

On the other hand, as already postulated, the selectivity of this PB reaction with benzil **18b** and indoles furnish the corresponding oxeto-indolinic polycycle in exceptional yields and diastereoselectivities (up to >98% yield and >20:1 dr) (Scheme 2.6a). However, the fate of this reaction with oxindole-derived SEE is the same in terms of yields but differs in terms of selectivity (Scheme 2.6b). In fact, the reaction selectivity drops to a poor 2:1 dr. Thus, we hypothesized that using electron-rich indole derivatives has a direct implication in the mechanism taking place in the reaction.

— A. selectivity with indoles —



— B. selectivity with oxindole SEE —



Scheme 2.6. - Selectivity-dependence when using: a) indoles with benzil; or b) oxindole SEE with benzil.

2.2.5 Conclusions

In conclusion, in this section, I disclosed that oxindole enol ethers can engage in visible-light PB processes. Conventional limitations of PB processes such as *i)* the presence of side-reactions, *ii)* the low site-, regio-, and diastereoselectivity, and *iii)* difficult scalability, are overcome thanks to the implementation of a MFP setup. The method is general and can be easily applied to a variety of different substituted oxindole-derivatives and aromatic ketones with yields up to >98% and virtually complete site- regio- and diastereocontrol. Finally, the reaction can be scaled up converting 1 g of 3-benzyloxindole **28** into up to 1.18 g of oxetane product **3**. Despite solving the classical limitations of PB reactions, novel *incognita* were observed.

2.2.6 Experimental Section

The continuous flow reactions were carried out using capillary reactors made with PTFE® tubing (0.8 mm I.D., 1.58 mm O.D.) and fitting connections purchased from Sigma-Aldrich®. Reagents were pumped using a Syrris Atlas pump.

The NMR spectra were recorded on Bruker 400 Avance III HD equipped with a BBI-z grad probe head 5mm and Bruker 500 Avance III equipped with a BBI-ATM-z grad probehead 5mm. The chemical shifts (δ) for ^1H and ^{13}C are given in ppm relative to residual signals of the solvents (CHCl_3 @ 7.26 ppm ^1H NMR, 77.16 ppm ^{13}C NMR, Acetone @ 2.09 ppm ^1H NMR, 30.60 ppm ^{13}C NMR). Coupling constants are given in Hz. The following abbreviations are used to indicate the multiplicity: s, singlet; d, doublet; t, triplet; q, quartet; m, multiplet; br, broad signal.

The ^1H , ^{13}C and ^{19}F NMR spectra are available in literature free of charge.³⁴

High-Resolution Mass Spectra (HRMS) were obtained using Waters GCT gas chromatograph coupled with a time-of-flight mass spectrometer (GC/MS-TOF) with electron ionization (EI).

Chromatographic purification of products was accomplished using flash chromatography on silica gel (SiO_2 , 0.04-0.063 mm) purchased from Machery-Nagel, with the indicated solvent system according to the standard techniques. Thin-layer chromatography (TLC) analysis was performed on pre-coated Merck TLC plates (silica gel 60 GF254, 0.25 mm). Visualization of the developed chromatography was performed by checking UV absorbance (254nm) as well as with aqueous ceric ammonium molybdate and potassium permanganate solutions. Organic solutions were concentrated under reduced pressure on a Büchi rotary evaporator.

Materials: Commercial grade reagents and solvents were purchased at the highest commercial quality from Sigma Aldrich or FluoroChem and used as received, unless otherwise stated.

The diverse reaction set up images are available free of charge in literature.³⁴

Light-sources emission spectra

The following spectra were recorded using an AvaSpec ULS3648 high-resolution fiber-optic spectrometer which was placed at a fixed distance of 0.5 cm from the light source.

(more info at: <https://www.avantes.com/products/spectrometers/starline/item/209-avaspec-uls3648-high-resolution-spectrometer>).

³⁴ Franceschi, P.; Mateos, J.; Vega-Peñalosa, A.; Dell'Amico, L. *Microfluidic Visible-Light Paternò-Büchi Reaction of Oxindole Enol Ethers*. *Eur. J. Org. Chem.* **2020**, 2020, 6718–6722.

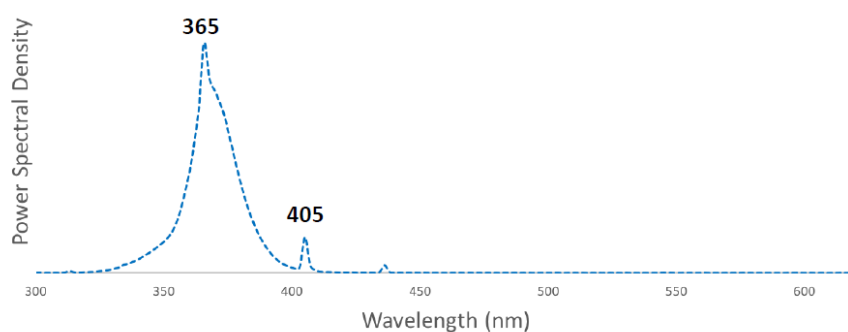


Figure 2.18. - Emission spectra of the 9W 365nm bulb light used in this work.

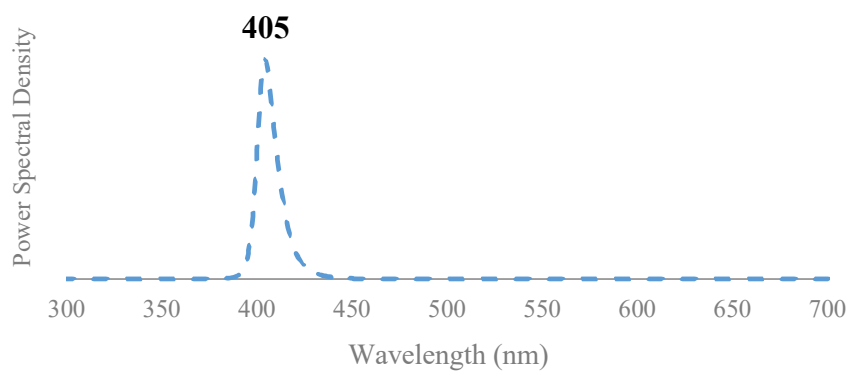
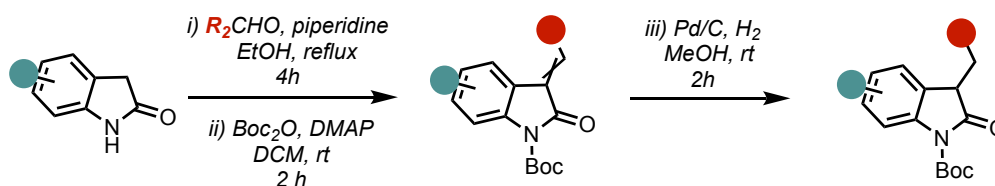


Figure 2.19. - Emission spectra of the 20 W 405 nm LED used in this work.

Synthesis and characterization of the used oxindole silyl enol ether derivatives

Preparation of 3-benzyl oxindoles



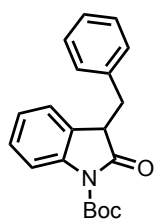
The corresponding aldehyde (4.1 mmol, 1.1 equiv.) and piperidine (0.74 mL, 7.5 mmol, 2.0 equiv.) were added to a suspension of the corresponding oxindole (3.76 mmol, 1.0 equiv.) in ethanol (30 mL, 0.125 M). The resulting mixture was heated to reflux for 4h. The solution was then allowed to cool to room temperature. The precipitate was filtered, washed with cold ethanol and dried to give 3-benzylideneoxindole as a yellow solid, which was used without further purification.

A 1 mmol fraction of the crude 3-benzylideneoxindole was diluted in DCM (3.3 mL, 0.3 M) and DMAP was added portionwise (12 mg, 0.1 mmol, 0.1 equiv.). After 5 min, Boc₂O

(262 mg, 1.2 mmol, 1.2 equiv.) was added. After full consumption of the starting material, monitored by TLC (usually after 2h), the reaction was quenched with 3 mL of cold water. The organic layer was washed with 5 mL of cold water and 5 mL of brine. The combined organic layer was dried with MgSO₄ and concentrated under reduced pressure. The crude of the protected benzylideneoxindole was used without further purification.

The crude product was diluted in a two-neck round-bottom flask in MeOH (10 mL, 0.1 M). Pd/C (10 wt%) was added and the flask was filled with H₂. The mixture was stirred at room temperature until full consumption of the starting material, monitored by TLC (usually after 2-4h). The palladium on carbon was filtered off two filter papers and the solvent was concentrated under reduced pressure. The crude product was purified by column chromatography (9:1, hexane/EtOAc), giving the desired *N*-Boc protected 3-benzyloxindole.

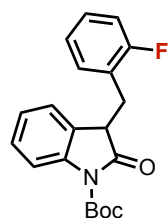
***tert*-butyl 3-benzyl-2-oxindoline-1-carboxylate (64a).**



¹H-NMR (400 MHz, CDCl₃): δ 7.76 (d, J = 8.2 Hz, 1H, Ar), 7.23 – 7.31 (m, 4H, Ar), 7.18 (d, J = 6.9 Hz, 2H, Ar), 7.03 (t, J = 7.5 Hz, 1H, Ar), 6.77 (d, J = 7.5 Hz, 1H, Ar), 3.84 (dd, J = 9.1, 4.4 Hz, 1H, CH₂a), 3.53 (dd, J = 13.9, 4.4 Hz, 1H, CH₂b), 2.98 (dd, J = 13.5, 9.1 Hz, 1H, CH), 1.66 (s, 9H, tBu-Boc) ppm.

¹³C-NMR (101 MHz, CDCl₃): δ 175.5, 149.0, 139.9, 137.3, 129.3, 128.3, 128.1, 127.1, 126.7, 124.3, 123.8, 114.7, 84.2, 47.4, 37.5, 28.0 ppm.

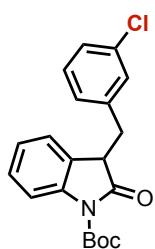
***tert*-butyl 3-(2-fluorobenzyl)-2-oxindoline-1-carboxylate (64b).**



¹H-NMR (400 MHz, CDCl₃): δ 7.77 (d, J = 8.2 Hz, 1H, Ar), 7.31 – 7.13 (m, 3H, Ar), 7.12 – 6.94 (m, 3H, Ar), 6.73 (d, J = 7.5 Hz, 1H, Ar), 3.87 (dd, J = 9.1, 5.2 Hz, 1H, CH₂a), 3.51 (dd, J = 13.9, 5.2 Hz, 1H, CH₂b), 2.98 (dd, J = 13.9, 9.1 Hz, 1H, CH), 1.64 (s, 9H, tBu-Boc) ppm. **¹³C-NMR (101 MHz, CDCl₃):** δ 175.4, 161.4 (d, J = 246.1 Hz), 149.3, 140.1, 131.8 (d, J = 4.5 Hz), 128.9 (d, J = 8.2 Hz), 128.4, 127.2, 124.9 (d, J = 15.2 Hz), 124.5, 124.2 (d, J = 3.7 Hz), 124.1, 115.6 (d, J = 22.0 Hz), 114.9, 84.5, 46.2 (d, J = 1.7 Hz), 31.1 (d, J = 1.9 Hz), 28.2 ppm. **¹⁹F NMR (188 MHz, CDCl₃)** δ -116.88 (dt, J = 12.9, 6.1 Hz, 1F, Ar-F) ppm.

¹³C-NMR (101 MHz, CDCl₃): δ 175.4, 161.4 (d, J = 246.1 Hz), 149.3, 140.1, 131.8 (d, J = 4.5 Hz), 128.9 (d, J = 8.2 Hz), 128.4, 127.2, 124.9 (d, J = 15.2 Hz), 124.5, 124.2 (d, J = 3.7 Hz), 124.1, 115.6 (d, J = 22.0 Hz), 114.9, 84.5, 46.2 (d, J = 1.7 Hz), 31.1 (d, J = 1.9 Hz), 28.2 ppm. **¹⁹F NMR (188 MHz, CDCl₃)** δ -116.88 (dt, J = 12.9, 6.1 Hz, 1F, Ar-F) ppm.

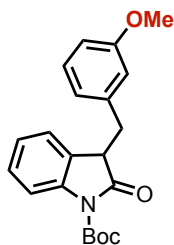
***tert*-butyl 3-(3-chlorobenzyl)-2-oxindoline-1-carboxylate (64c).**



¹H-NMR (400 MHz, CDCl₃): δ 7.73 (d, J = 8.2 Hz, 1H, Ar), 7.25 (q, J = 7.8 Hz, 3H, Ar), 7.15 (d, J = 7.4 Hz, 2H, Ar), 7.00 (t, J = 7.4 Hz, 1H, Ar), 6.74 (d, J = 7.4 Hz, 1H, Ar), 3.82 (dd, J = 9.2, 4.5 Hz, 1H, CH₂a), 3.50 (dd, J = 13.7, 4.5 Hz, 1H, CH₂b), 2.95 (dd, J = 13.7, 9.2 Hz, 1H, CH), 1.63 (s, 9H, tBu-Boc) ppm. **¹³C-NMR (101 MHz, CDCl₃):** δ 175.7, 140.2, 137.5, 130.7, 129.6 (x2),

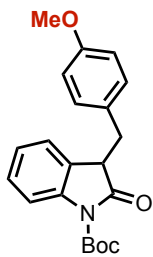
128.6 (x2), 128.3, 127.4, 127.0, 124.6, 124.1, 115.0, 84.5, 47.7, 37.8, 28.3 (x3). ppm. **HRMS (ESI-MS)** calculated for C₂₀H₂₁ClNO₃⁺ [M-H⁺] 358.1204, found 358.1217.

tert-butyl 3-(3-methoxybenzyl)-2-oxoindoline-1-carboxylate (64d).



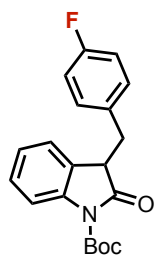
¹H-NMR (400 MHz, CDCl₃): δ = 7.77 (d, J = 8.1 Hz, 1H, Ar), 7.27 (d, J = 7.5 Hz, 1H, Ar), 7.20 (t, J = 7.8 Hz, 1H, Ar), 7.05 (t, J = 7.5 Hz, 1H, Ar), 6.83 – 6.76 (m, 3H, Ar), 6.72 (s, 1H, Ar), 3.85 (dd, J = 8.9, 4.2 Hz, 1H, CH₂a), 3.77 (s, 3H, OCH₃), 3.51 (dd, J = 13.1, 4.2 Hz, 1H, CH₂b), 2.96 (dd, J = 13.1, 8.9 Hz, 1H, CH), 1.66 (s, 9H, tBu-Boc) ppm. **¹³C-NMR (101 MHz, CDCl₃):** δ = 175.5, 159.6, 149.2, 140.0, 138.9, 129.4, 128.2, 127.2, 124.5, 123.9, 121.8, 114.9, 114.7, 112.6, 84.1, 55.2, 47.5, 37.7, 28.1 ppm.

tert-butyl 3-(4-methoxybenzyl)-2-oxoindoline-1-carboxylate (64e).



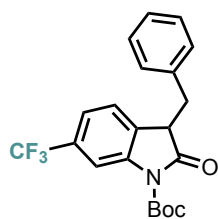
¹H-NMR (400 MHz, CDCl₃): δ 7.75 (d, J = 8.2 Hz, 1H, Ar), 7.28 – 7.24 (m, 1H, Ar), 7.09 – 7.02 (m, 3H, Ar), 6.83 – 6.79 (m, 3H, Ar), 3.81 – 3.78 (dd, J = 13.8, 9.0 Hz, 1H, CH₂a), 3.80 (s, 3H, OCH₃), 3.45 (dd, J = 13.9, 4.6 Hz, 1H, CH₂b), 2.95 (dd, J = 13.8, 9.2 Hz, 1H, CH), 1.65 (s, 9H, tBu-Boc) ppm. **¹³C NMR (101 MHz, CDCl₃)** δ 175.7, 158.6, 149.3, 140.2, 130.6, 129.4, 128.3, 127.5, 124.6, 124.0, 115.0, 113.9, 84.4, 55.4, 47.9, 36.9, 28.3 ppm.

tert-butyl 3-(4-fluorobenzyl)-2-oxoindoline-1-carboxylate (64f).



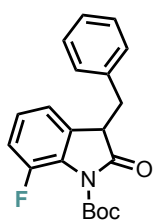
¹H-NMR (400 MHz, CDCl₃): δ 7.72 (d, J = 8.2 Hz, 1H, Ar), 7.25 (t, J = 7.9 Hz, 1H, Ar), 7.00 – 7.11 (m, 3H, Ar), 6.92 (d, J = 8.7 Hz, 2H, Ar), 6.83 (d, J = 7.5 Hz, 1H, Ar), 3.79 (dd, J = 9.1, 4.4 Hz, 1H, CH₂a), 3.42 (dd, J = 13.8, 4.4 Hz, 1H, CH₂b), 3.02 (dd, J = 13.8, 9.1 Hz, 1H, CH), 1.62 (s, 9H, tBu-Boc) ppm. **¹³C-NMR (101 MHz, CDCl₃):** δ 175.3, 161.8 (d, J = 245.1 Hz), 149.0, 140.1, 132.8 (d, J = 3.1 Hz), 130.9 (d, J = 8.0 Hz), 128.3, 126.9, 124.1 (d, J = 25.0 Hz), 115.3, 115.0 (d, J = 16.1 Hz), 84.3, 47.6, 36.7, 28.0 ppm.

tert-butyl 3-benzyl-2-oxo-6-(trifluoromethyl)indoline-1-carboxylate (64g).



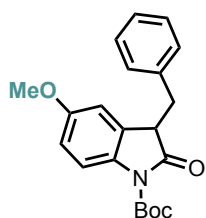
¹H-NMR (600 MHz, CDCl₃): δ 8.09 – 8.09 (m, 1H), 7.32 – 7.27 (m, 4H, Ar), 7.17 – 7.16 (m, 2H, Ar), 6.82 (d, J = 7.8 Hz, 1H, Ar), 3.88 (dd, J = 9.1, 4.4 Hz, 1H, CH₂a), 3.56 (dd, J = 13.8, 4.4 Hz, 1H, CH₂b), 2.98 (dd, J = 13.8, 9.1 Hz, 1H, CH), 1.66 (s, 9H, tBu-Boc) ppm. **¹³C-NMR (151 MHz, CDCl₃):** δ 174.8, 149.0, 140.6, 136.9, 129.5 (x2), 128.8 (x2), 127.3, 124.8, 121.1, 121.0, 112.3, 112.3, 85.2, 47.6, 37.6, 28.2 (x3), 28.1 ppm. **HRMS (ESI-MS)** calculated for C₂₁H₂₁F₃NO₃+ [M-H⁺] 392.1468, found 392.1458.

tert-butyl 3-benzyl-7-fluoro-2-oxoindoline-1-carboxylate (64h).



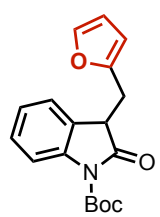
¹H-NMR (600 MHz, CDCl₃): δ 7.29 – 7.24 (m, 3H, Ar), 7.14 (dd, J = 7.9, 1.7 Hz, 2H, Ar), 7.02 – 7.01 (m, 2H, Ar), 6.64 – 6.61 (m, 1H), 3.89 (dd, J = 8.6, 4.5 Hz, 1H, CH₂a), 3.50 (dd, J = 13.8, 4.5 Hz, 1H, CH₂b), 3.06 (dd, J = 13.8, 8.6 Hz, 1H, CH), 1.59 (s, 9H, tBu-Boc).ppm. **¹³C-NMR (151 MHz, CDCl₃):** δ 174.9, 148.7 (d, J = 250.6 Hz), 147.5, 136.8, 130.5, 130.5, 129.5 (x2), 128.6 (x2), 127.1, 125.1 (d, J = 6.9 Hz), 120.4 (d, J = 3.5 Hz), 116.6 (d, J = 20.5 Hz), 84.9, 48.0 (d, J = 1.4 Hz), 37.6, 27.8 (x3) ppm. **HRMS (ESI-MS)** calculated for C₂₀H₂₁FNO₃+ [M-H⁺] 342.1500, found 342.1511.

tert-butyl 3-benzyl-5-methoxy-2-oxoindoline-1-carboxylate (64i).



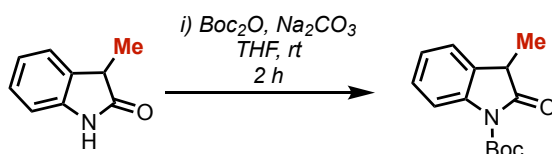
¹H-NMR (400 MHz, CDCl₃): δ 7.69 (d, J = 9.0, 1H, Ar), 7.34 – 7.24 (m, 3H, Ar), 7.21 (d, J = 7.9 Hz, 2H, Ar), 6.79 (dd, J = 2.8, 8.9 Hz, 1H, Ar), 6.36 (d, J = 2.9 Hz, 2H, Ar), 3.81 (dd, J = 4.7; 9.4 Hz, 1H, CH₂a), 3.67 (s, 3H, OCH₃), 3.55 (dd, J = 4.0; 13.5 Hz, 1H, CH₂b), 2.94 (dd, J = 9.4; 13.5, 1H, CH), 1.65 (s, 9H, tBu-Boc) ppm. **¹³C-NMR (101 MHz, CDCl₃):** δ 175.5, 156.2, 149.2, 137.4, 133.4, 129.5, 128.5, 126.9, 115.9, 113.2, 110.5, 84.1, 55.6, 47.8, 37.7, 28.2 ppm.

tert-butyl 3-(furan-2-ylmethyl)-2-oxoindoline-1-carboxylate (64j).



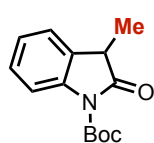
¹H-NMR (400 MHz, CDCl₃): δ 7.79 (d, J = 7.2 Hz, 1H, Ar), 7.31 – 7.37 (m, 1H, Ar), 7.27 (t, J = 7.8 Hz, 1H, Ar), 7.05 (t, J = 7.5 Hz, 1H, Ar), 6.77 (t, J = 7.5 Hz, 1H, Ar), 6.20 – 6.34 (m, 1H, Ar), 6.03 (d, J = 3.2 Hz, 1H, Ar), 3.89 (dd, J = 9.1, 4.4 Hz, 1H, CH₂a), 3.48 (dd, J = 13.9, 4.4 Hz, 1H, CH₂b), 3.00 (dd, J = 13.9, 9.1 Hz, 1H, CH), 1.65 (s, 9H, tBu-Boc) ppm. **¹³C-NMR (101 MHz, CDCl₃):** δ 175.1, 151.5, 149.2, 141.7, 140.0, 128.3, 127.0, 124.3, 124.2, 114.9, 110.5, 107.7, 84.4, 45.2, 29.9, 28.2 ppm.

— Preparation of 3-methyl derived oxindole



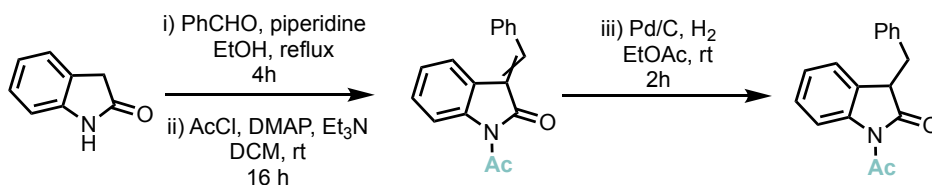
Synthesized following literature procedure starting from 3-methyloxindole (1.47 g, 10 mmol), yielding pure **4h** (colorless oil), in >98% yield (2.74 g, 10 mmol).³⁵

tert-butyl 3-methyl-2-oxindoline-1-carboxylate (64k).



¹H-NMR (400 MHz, CDCl₃): δ 7.74 (d, $J = 8.1$ Hz, 1H, Ar), 7.13 – 7.33 (m, 2H, Ar), 6.99 – 7.13 (m, 1H, Ar), 3.49 (q, $J = 7.5$ Hz, 1H, CH), 1.57 (s, 9H, tBu-Boc), 1.45 (d, $J = 7.5$, 3H, CH₃) ppm. ¹³C-NMR (101 MHz, CDCl₃): δ 176.9, 149.4, 139.8, 129.4, 128.1, 124.3, 123.4, 115.0, 84.3, 41.0, 28.1, 15.9 ppm.

— Preparation of N-Ac protected oxindole



Benzaldehyde (1.7 mL, 17 mmol, 1.13 equiv.) and piperidine (3.0 mL, 30 mmol, 2.0 equiv.) were added to a suspension of 2-oxindole (2.0 g, 15 mmol, 1.0 equiv.) in ethanol (30 mL). The resulting mixture was heated to reflux for 4h. The solution was then allowed to cool to 0 °C. The precipitate was filtered, washed with small amount of cold ethanol and dried to give 3-benzylideneoxindole as a yellow solid, which was used without further purification.

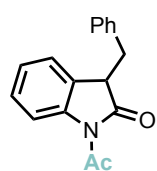
A 1 mmol fraction of the crude benzylideneoxindole was diluted in DCM (10 mL, 0.1 M), DMAP was added portionwise (257 mg, 2.1 mmol, 2.1 equiv.) and Et₃N (293 μ L, 2.1 mmol, 2.1 equiv.). After 5 min, AcCl (149 μ L, 2.1 mmol, 2.1 equiv.) was added dropwise at 0 °C and stirred at rt. After full consumption of the starting material, monitored by TLC (usually after 16h), the reaction was quenched with water. The organic layer was washed with 2x25 mL of water. The organic layer was dried with MgSO₄ and concentrated under reduced

³⁵ Frost, J. R.; Huber, S. M.; Breitenlechner, S.; Bannwarth, C.; Bach, T. *Enantiotopos-Selective C-H Oxygenation Catalyzed by a Supramolecular Ruthenium Complex*. *Angew. Chem. Int. Ed.* **2014**, *54*, 691–695.

pressure. The crude of the protected benzylideneoxindole was used without further purification.

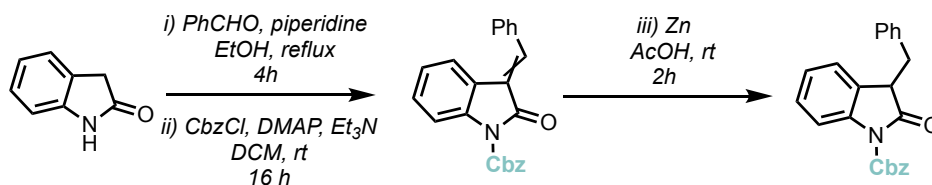
The crude product was diluted in a two-neck round-bottom flask in EtOAc (10 mL, 0.1 M). Pd/C (10 wt%) was added and the flask was filled with H₂. The mixture was stirred at room temperature until full consumption of the starting material, monitored by TLC (usually after 2-4h). The palladium on carbon was filtered and the solvent was concentrated under reduced pressure. The crude product was purified by column chromatography (9:1, hexane/EtOAc), giving the desired N-Ac protected 3-benzyloxindole in 61% yield after 3 consecutive steps.

1-acetyl-3-benzylindolin-2-one (64l).



¹H-NMR (400 MHz, CDCl₃): δ 8.16 (d, J = 8.3 Hz, 1H, Ar), 7.31 – 7.22 (m, 4H, Ar), 7.14 – 7.10 (m, 3H, Ar), 6.91(d, J = 7.5 Hz, 1H, Ar), 3.92 (dd, J = 8.5, 4.7 Hz, 1H, CH₂a), 3.48 (dd, J = 13.7, 4.7 Hz, 1H, CH₂b), 3.09 (dd, J = 13.7, 8.5 Hz, 1H, CH), 2.65 (s, 3H, CH₃-Ac) ppm. **¹³C-NMR (101 MHz, CDCl₃):** δ 177.7, 170.8, 140.5, 136.8, 129.4, 128.4, 128.3, 127.4, 127.0, 124.7, 124.1, 116.4, 47.6, 37.6, 26.7 ppm.

Preparation of N-Cbz protected oxindole



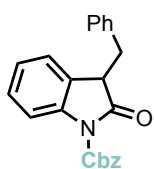
Benzaldehyde (1.7 mL, 17 mmol, 1.13 equiv.) and piperidine (3.0 mL, 30 mmol, 2.0 equiv.) were added to a suspension of 2-oxindole (2.0 g, 15 mmol, 1.0 equiv.) in ethanol (30 mL). The resulting mixture was heated to reflux for 4h. The solution was then allowed to cool to 0 °C. The precipitate was filtered, washed with small amount of cold ethanol and dried to give 3-benzylideneoxindole as a yellow solid, which was used without further purification.

A 1 mmol fraction of the crude benzylideneoxindole was diluted in DCM (10 mL, 0.1 M), DMAP was added portionwise (257 mg, 2.1 mmol, 2.1 equiv.) and Et₃N (293 μL, 2.1 mmol, 2.1 equiv.). After 5 min, CbzCl (300 μL, 2.1 mmol, 2.1 equiv.) was added dropwise at 0 °C and stirred at rt. After full consumption of the starting material, monitored by TLC (usually after 16h), the reaction was quenched with water. The organic layer was washed with 2x25 mL of water. The organic layer was dried with MgSO₄ and concentrated under reduced

pressure. The crude of the protected benzylideneoxindole was used without further purification.

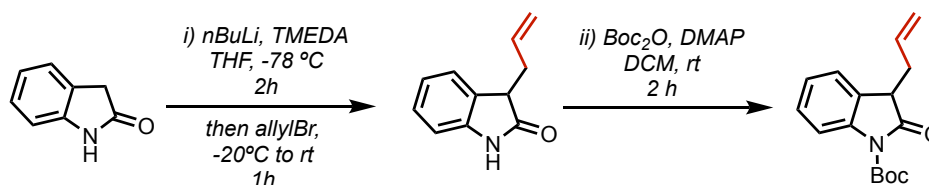
The crude product was diluted in a round-bottom flask in acetic acid (10 mL, 0.1 M). Zn (1.3 g, 20 mmol, 20.0 equiv.) was added. The mixture was stirred at room temperature until full consumption of the starting material, monitored by TLC (usually after 2 h). The Zn was filtered, and the acid was quenched under vigorous stirring at 0 °C with 60 mL of a saturated NaHCO₃ solution. The solution was extracted with 3x20 mL of EtOAc, the combined organic layers were dried over MgSO₄ and concentrated under reduced pressure. The crude product was purified by column chromatography (9:1, hexane/EtOAc), giving the desired *N*-Cbz protected 3-benzyloxindole in 72% yield after three consecutive steps.

benzyl 3-benzyl-2-oxindoline-1-carboxylate (64m).



¹H-NMR (400 MHz, CDCl₃): δ 7.84 (d, *J* = 8.2 Hz, 1H, Ar), 7.54 (d, *J* = 7.8 Hz, 2H, Ar), 7.45 – 7.38 (m, 4H, Ar), 7.29 – 7.25 (m, 3H, Ar), 7.17 – 7.15 (m, 2H, Ar), 7.07 (s, 1H, Ar), 6.83 (d, *J* = 7.5 Hz, 1H, Ar), 5.46 (s, 2H, CH₂), 3.90 (dd, *J* = 8.8, 4.6 Hz, 1H, CH₂a), 3.55 – 3.47 (m, 1H, CH₂b), 3.04 (dd, *J* = 13.7, 8.8 Hz, 1H, CH) ppm. **¹³C-NMR (101 MHz, CDCl₃):** δ 175.1, 150.7, 139.6, 137.1, 135.1, 129.4, 128.7, 128.5, 128.3, 128.1, 127.8, 127.2, 126.9, 124.4, 124.3, 115.0, 68.5, 47.5, 37.6 ppm.

— Preparation of 3-allyl derived oxindole



Following literature procedure, 2-oxindole (4.0 g, 30 mmol) gave the 3-substituted unprotected oxindole in 81% yield (4.2 g, 24.3 mmol).³⁶

The unprotected oxindole (1.1 g, 6.4 mmol, 1.0 equiv.) was diluted in DCM (13 mL, 0.5 M) and DMAP was added portionwise (75 mg, 0.6 mmol, 0.1 equiv.). After 5 min, Boc₂O (2.1 g, 9.6 mmol, 1.5 equiv.) was added. After full consumption of the starting material, monitored by TLC (usually after 2h), the reaction was quenched with a 4M solution of HCl. The organic layer was washed with 2x10 mL of HCl 4M and 2x10 mL NaHCO₃. The

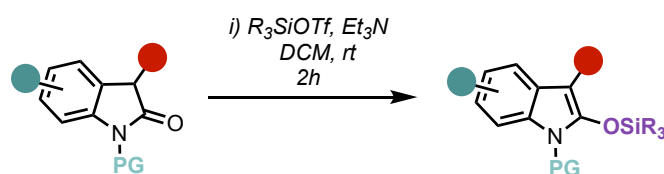
³⁶ Trost, B. M.; Zhang, Y.; Zhang, T. Direct *N*-Carbamoylation of 3-Monosubstituted Oxindoles with Alkyl Imidazole Carboxylates. *J. Org. Chem.* **2009**, *74*, 5115–5117.

combined organic layer was dried with MgSO₄ and concentrated under reduced pressure. Purification through silica gel chromatography (9:1, hexane:EtOAc) gave **64n** in 94% yield.

tert-butyl 3-allyl-2-oxindoline-1-carboxylate (64n).

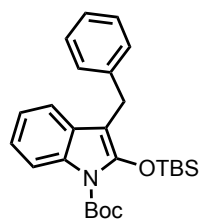
¹H-NMR (400 MHz, CDCl₃): δ 7.83 (d, J = 7.9 Hz, 1H, Ar), 7.34 – 7.28 (m, 2H, Ar), 7.18 – 7.14 (m, 1H, Ar), 5.83 – 5.72 (m, 1H, C(sp²)H), 5.16 – 5.08 (m, 2H, C(sp²)H₂), 3.65 – 3.62 (m, 1H, CH₂a), 2.89 – 2.82 (m, 1H, CH₂b), 2.69 – 2.62 (m, 1H, CH), 1.66 (s, 9H, tBu-Boc) ppm. **¹³C-NMR (101 MHz, CDCl₃):** δ 175.5, 149.2, 140.1, 133.5, 128.2, 127.4, 124.2, 124.0, 118.6, 114.9, 84.3, 45.7, 35.4, 28.1 ppm.

— Preparation of oxindole-derived SEE



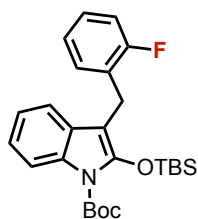
In a round-bottom flask, the *N*-protected oxindole (0.5 mmol, 1.0 equiv.) was dissolved in DCM (1.7 mL, 0.3 M) under Ar atmosphere. Et₃N (139 μL, 1.0 mmol, 2.0 equiv.) was added dropwise at 0 °C. After 5 min, R₃SiOTf (0.75 mmol, 1.5 equiv.) was added dropwise at 0 °C and stirred at room temperature. After full consumption of the starting material, monitored by TLC (usually after 2h), 15 mL of hexane were added. The organic layer was washed with 3x10 mL of a saturated solution of NaHCO₃, dried over MgSO₄ and concentrated under reduced pressure. The crude product was purified by column chromatography (98:2, hexane:EtOAc).

tert-butyl 3-benzyl-2-((tert-butyldimethylsilyl)oxy)-1H-indole-1-carboxylate (65a)



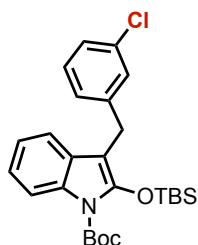
¹H-NMR (400 MHz, CDCl₃): δ 7.86 (d, J = 7.5 Hz, 1H, Ar), 7.29 – 7.26 (m, 4H, Ar), 7.22 – 7.08 (m, 4H, Ar), 4.00 (s, 2H, CH₂), 1.74 (s, 9H, tBu-Boc), 1.09 (s, 9H, tBu-TBS), 0.26 (s, 6H, 2x CH₃-TBS) ppm. **¹³C-NMR (101 MHz, CDCl₃):** δ 149.5, 145.2, 140.2, 131.3, 129.0, 128.6 (x2), 128.4 (x2), 126, 122.5, 122.0, 118.4, 114.6, 100.0, 83.6, 29.2, 28.5 (x3), 26.0 (x3), 18.6, -3.9 (x2) ppm. **HRMS (ESI-MS)** calculated for C₂₆H₃₆NO₃Si⁺ [M-H⁺] 438.2459, found 438.2475.

tert-butyl 2-((tert-butyldimethylsilyloxy)-3-(2-fluorobenzyl)-1H-indole-1-carboxylate (65b)



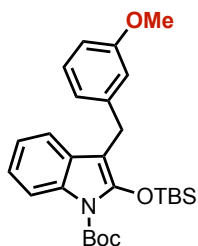
¹H-NMR (400 MHz, CDCl₃): δ 7.86 – 7.84 (m, 1H, Ar), 7.17 – 6.95 (m, 7H, Ar), 4.00 (s, 2H, CH₂), 1.73 (s, 9H, tBu-Boc), 1.07 (s, 9H, tBu-TBS), 0.24 (s, 6H, 2x CH₃-TBS) ppm. **¹³C-NMR (101 MHz, CDCl₃):** δ 161.1 (d, J = 244.3 Hz), 149.4, 145.5, 131.2, 130.6 (d, J = 4.7 Hz), 128.8, 127.6 (d, J = 8.1 Hz), 127.0 (d, J = 15.9 Hz), 124.1 (d, J = 3.5 Hz), 122.7, 122.2, 118.1, 115.0 (d, J = 22.0 Hz), 114.6, 98.5, 83.7, 28.5 (x3), 26.0 (x3), 21.4 (d, J = 4.4 Hz), 18.6, -3.9 (x2) ppm. **¹⁹F-NMR (376 MHz, CDCl₃):** δ - 118.77 (q, J = 8.0 Hz, 1F, Ar-F) ppm. **HRMS (ESI-MS)** calculated for C₂₆H₃₅FNO₃Si⁺ [M-H⁺] 456.2365, found 456.2336.

tert-butyl 2-((tert-butyldimethylsilyloxy)-3-(3-chlorobenzyl)-1H-indole-1-carboxylate (65c).



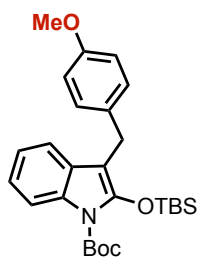
¹H-NMR (400 MHz, CDCl₃): δ 7.84 (d, J = 7.5 Hz, 1H, Ar), 7.30 – 7.24 (m, 3H, Ar), 7.20 – 7.06 (m, 4H, Ar), 3.99 (s, 2H, CH₂), 1.72 (s, 9H, tBu-Boc), 1.08 (s, 9H, tBu-TBS), 0.25 (s, 6H, 2x CH₃-TBS) ppm. **¹³C-NMR (101 MHz, CDCl₃):** δ 149.5, 145.2, 140.2, 131.3, 129.0, 128.6 (x2), 128.4 (x2), 126.0, 122.5, 122.0, 118.4, 114.6, 100.0, 83.6, 29.2, 28.5 (x3), 26.0 (x3), 18.5, -4.0 (x2). ppm. **HRMS (ESI-MS)** calculated for C₂₆H₃₅ClNO₃Si⁺ [M-H⁺] 472.2069, found 471.2746.

tert-butyl 2-((tert-butyldimethylsilyloxy)-3-(3-methoxybenzyl)-1H-indole-1-carboxylate (65d).



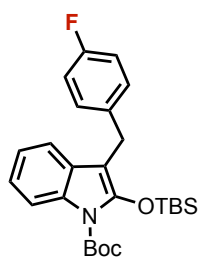
¹H-NMR (400 MHz, CDCl₃): δ 7.84 (d, J = 7.5 Hz, 1H, Ar), 7.20 – 7.09 (m, 4H, Ar), 6.89 – 6.84 (m, 2H, Ar), 6.74 (d, J = 7.7 Hz, 1H, Ar), 3.96 (s, 2H, CH₂), 3.76 (s, 3H, OCH₃), 1.73 (s, 9H, tBu-Boc), 1.08 (s, 9H, tBu-TBS), 0.25 (s, 6H, 2x CH₃-TBS) ppm. **¹³C-NMR (101 MHz, CDCl₃):** δ 159.8, 149.5, 145.1, 141.9, 131.3, 129.4, 128.9, 122.5, 122.0, 121.1, 118.4, 114.5, 114.4, 111.4, 99.8, 83.6, 55.3, 29.3, 28.5 (x3), 26.0 (x3), 18.5, -3.9 (x2) ppm. **HRMS (ESI-MS)** calculated for C₂₇H₃₈NO₄Si⁺ [M-H⁺] 468.2565, found 468.2583.

tert-butyl
carboxylate (65e)



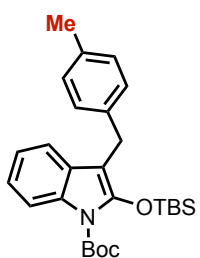
¹H-NMR (400 MHz, CDCl₃): δ 7.82 (d, J = 7.5 Hz, 1H, Ar), 7.18 – 7.05 (m, 5H, Ar), 6.80 (d, J = 7.5 Hz, 2H, Ar), 3.91 (s, 2H, CH₂), 3.77 (s, 3H, OCH₃), 1.71 (s, 9H, tBu-Boc), 1.06 (s, 9H, tBu-TBS), 0.23 (s, 6H, 2x CH₃-TBS) ppm. **¹³C-NMR (101 MHz, CDCl₃):** δ 158.0, 149.5, 145.0, 132.3, 131.3, 129.5 (x2), 129.0, 122.5, 122.0, 118.4, 114.5, 113.9 (x2), 100.3, 83.6, 55.4, 28.5 (x3), 28.4, 26.0 (x3), 18.6, -4.0 (x2) ppm. **HRMS (ESI-MS)** calculated for C₂₇H₃₈NO₄Si⁺ [M-H⁺] 468.2565, found 468.2583.

tert-butyl 2-((tert-butyldimethylsilyloxy)-3-(4-fluorobenzyl)-1H-indole-1-carboxylate (65f).



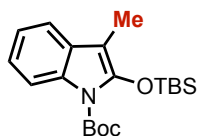
¹H-NMR (400 MHz, CDCl₃): δ 7.84 (d, J = 7.5 Hz, 1H, Ar), 7.18 – 6.94 (m, 7H, Ar), 3.98 (s, 2H, CH₂), 1.71 (s, 9H, tBu-Boc), 1.05 (s, 9H, tBu-TBS), 0.22 (s, 6H, 2x CH₃-TBS) ppm. **¹³C-NMR (101 MHz, CDCl₃):** δ 161.1 (d, J = 244.6 Hz), 149.4, 145.5, 131.2, 130.6 (d, J = 4.4 Hz), 128.8, 127.6 (d, J = 8.0 Hz), 127.0 (d, J = 15.3 Hz), 124.1 (d, J = 3.5 Hz), 122.6, 122.2, 118.1, 115.0 (d, J = 22.0 Hz), 114.6, 98.5, 83.7, 28.5 (x3), 26.0 (x3), 21.4, 18.5, -4.0 (x2) ppm. **¹⁹F-NMR (376 MHz, CDCl₃):** δ -118.7 – -118.8 (m, 1F, Ar-F) ppm. **HRMS (ESI-MS)** calculated for C₂₆H₃₅FNO₃Si⁺ [M-H⁺] 456.2370, found 456.2336.

tert-butyl 2-((tert-butyldimethylsilyloxy)-3-(4-methylbenzyl)-1H-indole-1-carboxylate (65g).



¹H-NMR (400 MHz, CDCl₃): δ 7.81 (d, J = 8.1 Hz, 1H, Ar), 7.14 – 7.04 (m, 6H, Ar), 6.97 (d, J = 7.3 Hz, 1H, Ar), 3.91 (s, 2H, CH₂), 2.28 (s, 3H, CH₃), 1.70 (s, 9H, tBu-Boc), 1.05 (s, 9H, tBu-TBS), 0.22 (s, 6H, 2x CH₃-TBS) ppm. **¹³C-NMR (101 MHz, CDCl₃):** δ 149.5, 145.1, 140.2, 138.0, 131.3, 129.4, 129.0, 128.3, 126.8, 125.7, 122.5, 122.0, 118.5, 114.5, 100.1, 83.6, 29.2, 28.5 (x3), 26.0 (x3), 21.6, 18.6, -3.9 (x2) ppm. **HRMS (ESI-MS)** calculated for C₂₇H₃₈NO₃Si⁺ [M-H⁺] 452.2615, found 452.2613.

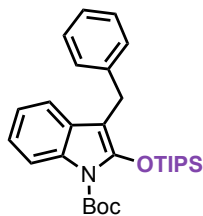
tert-butyl 2-((tert-butyldimethylsilyloxy)-3-methyl-1H-indole-1-carboxylate (65h)



¹H-NMR (400 MHz, CDCl₃): δ 7.81 (d, J = 7.5 Hz, 1H, Ar), 7.32 (d, J = 7.5 Hz, 1H, Ar), 7.21 – 7.13 (m, 2H, Ar), 2.08 (s, 3H, CH₃), 1.68 (s, 9H, tBu-Boc), 1.06 (s, 9H, tBu-TBS), 0.21 (s, 6H, 2x CH₃-TBS) ppm. **¹³C-NMR (101 MHz, CDCl₃):** δ 149.5, 144.3, 131.2, 129.9, 122.5, 122.0, 117.4, 114.5, 96.9,

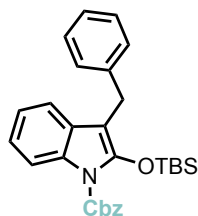
83.4, 28.5 (x3), 26.0 (x3), 18.5, 8.0, -4.1 (x2) ppm. **HRMS (ESI-MS)** calculated for C₂₀H₃₂NO₃Si⁺ [M-H⁺] 362.2146, found 362.2145.

tert-butyl 3-benzyl-2-((triisopropylsilyloxy)-1H-indole-1-carboxylate (65i)



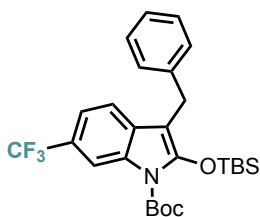
¹H-NMR (400 MHz, CDCl₃): δ 7.78 (d, J = 7.5 Hz, 1H, Ar), 7.26 – 7.02 (m, 8H, Ar), 3.98 (s, 2H, CH₂), 1.69 (s, 9H, tBu-Boc), 1.36 (hept, J = 7.4 Hz, 3H, 3x CH-TIPS), 1.11 (d, J = 7.8 Hz, 18H, (6x CH₃-TIPS) ppm. **¹³C-NMR (101 MHz, CDCl₃):** δ 149.4, 145.8, 140.3, 130.9, 129.1, 128.6 (x2), 128.4 (x2), 126.0, 122.4, 121.8, 118.2, 114.5, 98.9, 83.4, 29.1, 28.5 (x3), 18.1 (x6), 14.0 (x3) ppm. **HRMS (ESI-MS)** calculated for C₂₉H₄₂NO₃Si⁺ [M-H⁺] 480.2928, found 480.2919.

benzyl 3-benzyl-2-((tert-butyldimethylsilyloxy)-1H-indole-1-carboxylate (65j).



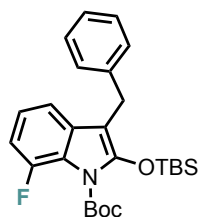
¹H-NMR (400 MHz, CDCl₃): δ 7.95 (d, J = 8.0 Hz, 1H, Ar), 7.53 (d, J = 6.4 Hz, 2H, Ar), 7.41 (q, J = 8.8, 7.6 Hz, 3H, Ar), 7.27 (d, J = 4.4 Hz, 4H, Ar), 7.21 – 7.10 (m, 4H, Ar), 5.48 (s, 2H, CH₂-Cbz), 3.97 (s, 2H, CH₂), 1.03 (s, 9H, tBu-TBS), 0.19 (s, 6H, 2x CH₃-TBS) ppm. **¹³C-NMR (101 MHz, CDCl₃):** δ 151.1, 144.5, 140.0, 135.4, 131.5, 129.1, 128.9 (x2), 128.8 (x2), 128.6 (x2), 128.5 (x2), 126.1, 123.0, 122.5, 118.5, 115.0, 100.3, 68.4, 29.3, 25.9 (x3), 18.5, -3.9 (x2). ppm. **HRMS (ESI-MS)** calculated for C₂₉H₃₄NO₃Si⁺ [M-H⁺] 472.2308, found 472.2304.

tert-butyl 3-benzyl-2-((tert-butyldimethylsilyloxy)-6-trifluoromethyl-1H-indole-1-carboxylate (65k).



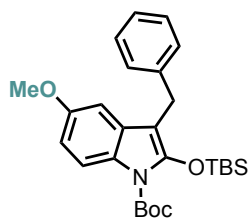
¹H-NMR (400 MHz, CDCl₃): δ 8.14 (s, 1H, Ar), 7.31 – 7.13 (m, 7H, Ar), 3.98 (s, 2H, CH₂), 1.72 (s, 9H, tBu-Boc), 1.06 (s, 9H, tBu-TBS), 0.24 (s, 6H, 2x CH₃-TBS) ppm. **¹³C-NMR (101 MHz, CDCl₃):** δ 148.9, 147.2, 139.7, 131.7, 130.3, 128.6 (x2), 128.5 (x2), 126.3, 126.80 (q, J = 273.3 Hz), 123.9 (q, J = 32.3 Hz), 119.4 (q, J = 3.9, 3.2 Hz), 118.4, 112.15 (q, J = 4.1 Hz), 100.1, 84.6, 29.1, 28.4 (x3), 26.0 (x3), 18.6, -3.9 (x2) ppm. **¹⁹F-NMR (376 MHz, CDCl₃):** δ -61.32 (s, 3F, Ar-CF₃) ppm. **HRMS (ESI-MS)** calculated for C₂₇H₃₅F₃NO₃Si⁺ [M-H⁺] 506.2333, found 506.2368.

tert-butyl 3-benzyl-2-((tert-butyldimethylsilyl)oxy)-7-fluoro-1H-indole-1-carboxylate (65l)



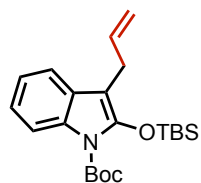
¹H-NMR (400 MHz, CDCl₃): δ 7.26 – 7.14 (m, 5H, Ar), 6.98 – 6.95 (m, 1H, Ar), 6.94 – 6.79 (m, 2H, Ar), 3.95 (s, 2H, CH₂), 1.62 (s, 9H, tBu-Boc), 1.03 (s, 9H, tBu-TBS), 0.25 (s, 6H, 2x CH₃-TBS) ppm. **¹³C-NMR (101 MHz, CDCl₃):** δ 149.33 (d, J = 248.9 Hz), 148.7, 145.8, 140.1, 132.5 (d, J = 3.7 Hz), 128.5 (x2), 128.5 (x2), 126.1, 122.8 (d, J = 7.5 Hz), 118.2 (d, J = 8.7 Hz), 114.2 (d, J = 3.1 Hz), 109.1 (d, J = 21.2 Hz), 98.5, 84.0, 29.3, 27.8 (x3), 26.0 (x3), 18.5, -3.7 (x2) ppm. **¹⁹F-NMR (376 MHz, CDCl₃):** -121.17 (dd, J = 12.3, 3.7 Hz, 1F, Ar-F) ppm. **HRMS (ESI-MS)** calculated for C₂₆H₃₄FNNaO₃Si⁺ [M-Na⁺] 478.2190, found 478.2181.

tert-butyl 3-benzyl-2-((tert-butyldimethylsilyl)oxy)-5-methoxy-1H-indole-1-carboxylate (65m)



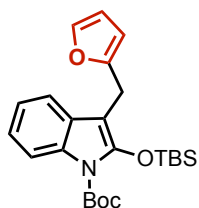
¹H-NMR (400 MHz, CDCl₃): δ 7.74 (d, J = 7.5 Hz, 1H, Ar), 7.29-7.26 (m, 4H, Ar), 7.21-7.18 (m, 1H, Ar), 6.76 (d, J = 7.8 Hz, 1H, Ar), 6.61 (s, 1H, Ar), 3.97 (s, 2H, CH₂), 3.73 (s, 3H, OCH₃), 1.72 (s, 9H, tBu-Boc), 1.09 (s, 9H, tBu-TBS), 0.26 (s, 6H, 2x CH₃-TBS) ppm. **¹³C-NMR (101 MHz, CDCl₃):** δ 155.8, 149.4, 145.8, 140.1, 129.9, 128.6 (x2), 128.4 (x2), 126.1, 125.8, 115.5, 109.5, 102.2, 100.1, 83.3, 55.7, 29.3, 28.5 (x3), 26.0 (x3), 18.6, -3.9 (x2) ppm. **HRMS (ESI-MS)** calculated for C₂₇H₃₈NO₄Si⁺ [M-H⁺] 468.2565, found 468.2566.

tert-butyl 3-allyl-2-((tert-butyldimethylsilyl)oxy)-1H-indole-1-carboxylate (65n)



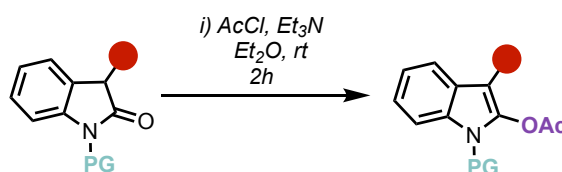
¹H-NMR (200 MHz, CDCl₃): δ 7.81 (dd, J = 6.4, 2.9 Hz, 1H, Ar), 7.39 – 7.35 (m, 1H, Ar), 7.15 (dd, J = 5.9, 3.2 Hz, 2H, Ar), 6.03 – 5.84 (m, 1H, CH), 5.17 – 5.04 (m, 2H, C(sp²)H₂), 3.35 (d, J = 6.0 Hz, 2H, C(sp³)H₂), 1.68 (s, 9H, tBu-Boc), 1.06 (s, 9H, tBu-TBS), 0.22 (s, 6H, 2x CH₃-TBS) ppm. **¹³C-NMR (101 MHz, CDCl₃):** δ 149.5, 144.4, 136.2, 131.3, 129.1, 122.4, 122.0, 118.3, 115.8, 114.5, 98.9, 83.6, 28.5 (x3), 27.6, 26.0 (x3), 18.5, -4.0 (x2). ppm. **HRMS (ESI-MS)** calculated for C₂₂H₃₄NO₃Si⁺ [M-H⁺] 388.2302, found 388.2298.

**tert-butyl
carboxylate (65o)**



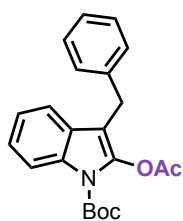
¹H-NMR (400 MHz, CDCl₃): δ 7.83 (d, *J* = 7.5 Hz, 1H, Ar), 7.31 (s, 1H, Ar), 7.25 (d, *J* = 7.5 Hz, 1H, Ar), 7.18 – 7.12 (m, 2H, Ar), 6.26 (d, *J* = 4.1 Hz, 1H, Ar), 5.96 (d, *J* = 1.8 Hz, 1H, Ar), 3.95 (s, 2H, CH₂), 1.70 (s, 9H, tBu-Boc), 1.07 (s, 9H, tBu-TBS), 0.22 (s, 6H, 2x CH₃-TBS) ppm. **¹³C-NMR (101 MHz, CDCl₃):** δ 153.8, 149.4, 145.0, 141.1, 131.2, 128.7, 122.6, 122.1, 118.2, 114.5, 110.4, 106.2, 97.4, 83.7, 28.5 (x3), 26.0 (x3), 22.5, 18.5, -4.1 (x2) ppm. **HRMS (ESI-MS)** calculated for C₂₄H₃₄NO₄Si⁺ [M-H⁺] 428.2252, found 428.2264.

— Preparation of oxindole-derived acetates



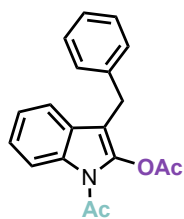
In a round-bottom flask, containing the oxindole **4a**, **4i** (1.0 mmol, 1.0 equiv) was dissolved in Et₂O (5 mL, 0.5 M) under Ar atmosphere. Et₃N (1.4 mL, 10.0 mmol, 10.0 equiv.) was added dropwise at 0 °C. After 5 min, AcCl (356 μL, 5.0 mmol, 5.0 equiv.) was added dropwise at 0 °C and stirred at room temperature. After full consumption of the starting material, monitored by TLC (usually after 2h), the reaction is quenched with water. The organic layer was washed with 3x10 mL of a saturated solution of NaHCO₃, dried over MgSO₄ and concentrated under reduced pressure. The crude product was purified by column chromatography (9:1, hexane:EtOAc).

tert-butyl 2-acetoxy-3-benzyl-1H-indole-1-carboxylate (65p).



¹H-NMR (400 MHz, CDCl₃): δ 8.03 (d, *J* = 7.5 Hz, 1H, Ar), 7.32 – 7.14 (m, 8H, Ar), 3.95 (s, 2H, CH₂), 2.30 (s, 3H, CH₃-Ac), 1.67 (s, 9H, tBu-Boc) ppm. **¹³C-NMR (101 MHz, CDCl₃):** δ 169.0, 149.1, 139.2, 138.8, 132.6, 128.7 (x2), 128.6 (x2), 127.4, 126.4, 124.2, 123.0, 119.2, 115.6, 107.4, 84.3, 28.9, 28.4 (x3), 20.7 ppm. **HRMS (ESI-MS)** calculated for C₂₂H₂₃NNaO₄⁺ [M-Na⁺] 388.1525, found 388.1490.

1-acetyl-3-benzyl-1H-indol-2-yl acetate (65q).



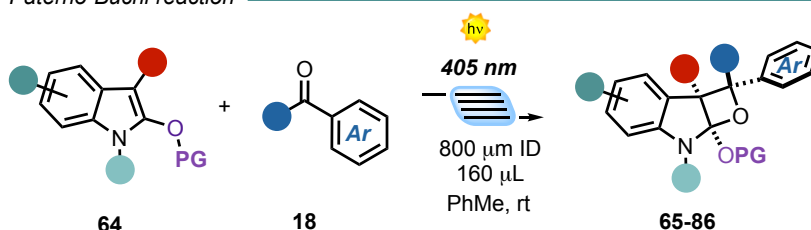
¹H-NMR (300 MHz, CDCl₃): δ 8.27 (d, *J* = 9.1 Hz, 1H, Ar), 7.33 – 7.18 (m, 8H, Ar), 3.91 (s, 2H, CH₂), 2.59 (s, 3H, CH₃-Ac), 2.26 (s, 3H, CH₃-Ac) ppm.

¹³C-NMR (101 MHz, CDCl₃): δ 168.3, 168.2, 138.6, 137.9, 132.9, 128.8 (x2), 128.7 (x2), 127.8, 126.6, 125.0, 123.9, 119.2, 116.3, 108.4, 29.3, 26.2, 20.7 ppm. HRMS (ESI-MS) calculated for C₁₉H₁₈NO₃⁺ [M-H⁺]

308.1281, found 308.1272.

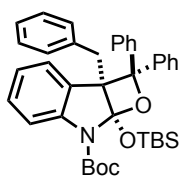
Synthesis and characterization of the PB products

General MFP Paternò-Büchi reaction



In a 4 mL vial, the enol ether (0.2 mmol, 1.0 equiv.) and the benzophenone derivative (0.6 mmol, 3.0 equiv.) were dissolved in toluene (2 mL, 0.1 M) and the reaction mixture was bubbled with Ar for 30 s. Then, the reaction mixture was reacted using the general microfluidic setup of this section. The crude product was purified by chromatography (6:4, hexane:DCM or 98:2 hexane:acetone), giving the oxetane products **65-86** in the stated yields and diastereomeric ratio.

tert-butyl 2a-benzyl-7a-((*tert*-butyldimethylsilyl)oxy)-2,2-diphenyl-2a,7a-dihydrooxeto[2,3-*b*]indole-7(2*H*)-carboxylate (65).

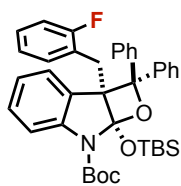


98% yield

¹H-NMR (400 MHz, CDCl₃): δ 7.75 (d, *J* = 7.7 Hz, 2H, Ar), 7.42 (t, *J* = 7.6 Hz, 2H, Ar), 7.35 – 7.27 (m, 3H, Ar), 7.14 (d, *J* = 8.0 Hz, 1H, Ar), 7.02 – 6.93 (m, 8H, Ar), 6.87 (t, *J* = 7.3 Hz, 1H, Ar), 6.77 (d, *J* = 8.0 Hz, 1H, Ar), 6.61 (t, *J* = 7.3 Hz, 1H, Ar), 3.43 (d, *J* = 17.0 Hz, 1H, CH₂*a*), 3.29 (d, *J* = 17.0 Hz, 1H, CH₂*b*), 1.62 (s, 9H, ^tBu-Boc), 0.77 (s, 9H, ^tBu-TBS), 0.60 (s, 3H, CH₃-TBS), 0.24 (s, 3H, CH₃-TBS) ppm. ¹³C-NMR (101 MHz, CDCl₃): δ 150.5, 143.7, 142.4, 142.2, 137.5, 130.0 (x2), 128.4, 128.3 (x2), 127.9, 127.7 (x2), 127.4, 127.0 (x2), 126.4 (x2), 126.3, 126.2 (x2), 125.8, 125.6, 121.5, 114.5, 113.8, 87.2, 81.7, 64.9, 35.3, 28.7 (x3), 26.1 (x3), 18.6, -2.0, -2.2 ppm. HRMS (ESI-MS) calculated for C₃₉H₄₅NNaO₄Si⁺ [M-Na⁺]

642.3016, found 642.3027.

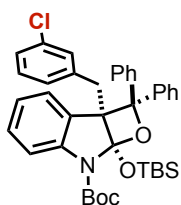
tert-butyl 7a-((tert-butyldimethylsilyl)oxy)-2a-(2-fluorobenzyl)-2,2-diphenyl-2a,7a-dihydrooxeto[2,3-b]indole-7(2H)-carboxylate (66).



90% yield

¹H-NMR (400 MHz, CDCl₃): δ 7.76 (d, *J* = 7.4 Hz, 2H), 7.43 (t, *J* = 7.7 Hz, 2H), 7.36 (d, *J* = 7.2 Hz, 2H), 7.29 (t, *J* = 7.4 Hz, 1H), 7.14 (d, *J* = 8.1 Hz, 1H), 7.01 – 6.94 (m, 4H), 6.90 – 6.85 (m, 4H), 6.68 (dt, *J* = 11.4, 7.6 Hz, 2H), 3.66 (d, *J* = 17.3 Hz, 1H, CH_{2a}), 3.06 (d, *J* = 17.3 Hz, 1H, CH_{2b}), 1.63 (s, 9H, ^tBu-Boc), 0.76 (s, 9H, ^tBu-TBS), 0.63 (s, 3H, CH₃-TBS), 0.23 (s, 3H, CH₃-TBS) ppm. **¹³C-NMR (101 MHz, CDCl₃):** δ 161.3 (d, *J* = 243.6 Hz), 150.5, 143.6, 142.4, 142.1, 131.6 (d, *J* = 3.5 Hz), 128.3 (x2), 128.2, 128.1, 127.4, 127.3 (d, *J* = 8.4 Hz), 127.0 (x2), 126.4, 126.2 (x2), 126.0 (x2), 125.0, 124.8 (d, *J* = 13.8 Hz), 123.5 (d, *J* = 3.4 Hz), 121.8, 114.5, 114.4 (d, *J* = 22.8 Hz), 113.7, 87.1, 81.8, 64.4, 28.6 (x3), 26.6 (d, *J* = 5.0 Hz), 26.1 (x3), 18.5, -2.0, -2.3 ppm. **¹⁹F NMR (376 MHz, CDCl₃)** δ -117.71 – -117.78 (m, 1F, C-F Ar) ppm. **HRMS (ESI-MS)** calculated for C₃₉H₄₅FNO₄Si⁺ [M-H⁺] 638.3096, found 638.3104.

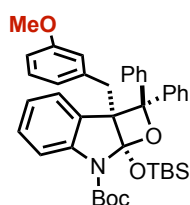
tert-butyl 7a-((tert-butyldimethylsilyl)oxy)-2a-(3-chlorobenzyl)-2,2-diphenyl-2a,7a-dihydrooxeto[2,3-b]indole-7(2H)-carboxylate (67).



96% yield

¹H-NMR (400 MHz, CDCl₃): δ 7.76 (d, *J* = 7.4 Hz, 2H, Ar), 7.43 (t, *J* = 7.8 Hz, 2H, Ar), 7.35 (d, *J* = 7.1 Hz, 2H, Ar), 7.30 (t, *J* = 7.4 Hz, 1H, Ar), 7.15 (d, *J* = 8.1 Hz, 1H, Ar), 7.03 – 6.95 (m, 8H, Ar), 6.88 (t, *J* = 7.8 Hz, 1H, Ar), 6.79 (d, *J* = 7.4 Hz, 1H, Ar), 6.65 (t, *J* = 7.8 Hz, 1H, Ar), 3.45 (d, *J* = 16.9 Hz, 1H, CH_{2a}), 3.30 (d, *J* = 16.9 Hz, 1H, CH_{2b}), 1.63 (s, 9H, ^tBu-Boc), 0.78 (s, 9H, ^tBu-TBS), 0.62 (s, 3H, CH₃-TBS), 0.25 (s, 3H, CH₃-TBS) ppm. **¹³C-NMR (101 MHz, CDCl₃):** δ 150.5, 143.7, 142.4, 142.2, 137.5, 130.0 (x2), 128.3, 128.3 (x2), 127.9, 127.7 (x2), 127.4, 127.0 (x2), 126.4 (x2), 126.3, 126.2 (x2), 125.8, 125.6, 121.5, 114.5, 113.8, 87.2, 81.7, 64.9, 35.2, 28.6 (x3), 26.1 (x3), 18.5, -2.0, -2.2 ppm. **HRMS (ESI-MS)** calculated for C₃₉H₄₅ClNO₄Si⁺ [M-H⁺] 654.2801, found 658.2762.

tert-butyl 7a-((tert-butyldimethylsilyl)oxy)-2a-(3-methoxybenzyl)-2,2-diphenyl-2a,7a-dihydrooxeto[2,3-b]indole-7(2H)-carboxylate (68).

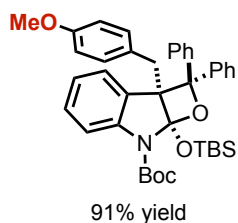


83% yield

¹H-NMR (400 MHz, CDCl₃): δ 7.74 (d, *J* = 8.2 Hz, 2H, Ar), 7.41 (t, *J* = 7.7 Hz, 2H, Ar), 7.34 – 7.29 (m, 4H, Ar), 7.18 (d, *J* = 5.3 Hz, 1H, Ar), 7.13 (d, *J* = 8.2 Hz, 1H, Ar), 7.00 – 6.90 (m, 5H, Ar), 6.86 (t, *J* = 7.7 Hz, 1H, Ar), 6.76 (d, *J* = 7.5 Hz, 1H, Ar), 6.64 (t, *J* = 7.5 Hz, 1H, Ar), 6.57 – 6.49 (m, 2H, Ar), 6.43 (s, 1H, Ar), 3.55 (s, 3H, OCH₃), 3.42 (d, *J* = 14.3 Hz, 1H, CH_{2a}), 3.25 (d, *J* = 14.3 Hz, 1H, CH_{2b}), 1.60 (s, 9H, ^tBu-Boc), 0.74 (s, 9H, ^tBu-TBS), 0.54 (s, 3H, CH₃-TBS), 0.24 (s, 3H, CH₃-TBS) ppm. **¹³C-NMR (101 MHz, CDCl₃):** δ 159.0, 150.6, 143.7, 142.3, 142.2, 139.1, 128.8, 128.6, 128.3 (x2), 128.0, 127.5,

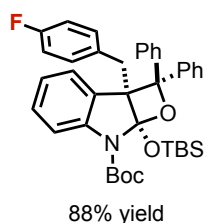
127.4, 127.0 (x2), 126.4 (x2), 126.3 (x2), 125.8, 122.5, 121.6, 115.3, 114.5, 113.7, 111.6, 87.3, 81.7, 64.7, 55.1, 35.2, 28.6 (x3), 26.0 (x3), 18.5, -2.1, -2.3 ppm. **HRMS (ESI-MS)** calculated for $C_{40}H_{48}NO_5Si^+$ $[M-H]^+$ 650.3296, found 650.3250.

tert-butyl 7a-((tert-butyldimethylsilyl)oxy)-2a-(4-methoxybenzyl)-2,2-diphenyl-2a,7a-dihydrooxeto[2,3-b]indole-7(2H)-carboxylate (69).



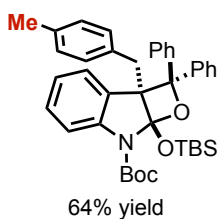
1H -NMR (400 MHz, $CDCl_3$): δ 7.72 (d, $J = 8.0$ Hz, 2H, Ar), 7.40 (t, $J = 7.7$ Hz, 2H, Ar), 7.31 – 7.27 (m, 4H, Ar), 7.18 – 7.17 (m, 2H, Ar), 7.11 (d, $J = 8.9$ Hz, 1H, Ar), 6.98 – 6.91 (m, 4H, Ar), 6.83 (d, $J = 8.7$ Hz, 3H, Ar), 6.74 (d, $J = 6.6$ Hz, 1H, Ar), 6.63 (t, $J = 7.4$ Hz, 1H, Ar), 6.55 (d, $J = 8.7$ Hz, 2H, Ar), 3.66 (s, 3H, OCH_3), 3.35 (d, $J = 14.2$ Hz, 1H, CH_2a), 3.19 (d, $J = 14.5$ Hz, 1H, CH_2b), 1.60 (s, 9H, tBu -Boc), 0.77 (s, 9H, tBu -TBS), 0.57 (s, 3H, CH_3 -TBS), 0.22 (s, 3H, CH_3 -TBS) ppm. **^{13}C -NMR (101 MHz, $CDCl_3$):** δ 157.5, 150.6, 144.3, 143.7, 142.4, 142.2, 131.0 (x2), 129.6, 128.8, 128.4, 128.3 (x2), 127.9, 127.5, 127.3, 127.1, 127.0 (x2), 126.4 (x2), 126.3, 126.3 (x2), 125.9, 121.5, 114.5, 113.8, 113.2, 87.2, 81.7, 65.1, 55.2, 34.4, 28.6 (x3), 26.1 (x3), 18.6, -2.0, -2.1 ppm. **HRMS (ESI-MS)** calculated for $C_{40}H_{48}NO_5Si^+$ $[M-H]^+$ 650.3302, found 650.3250.

tert-butyl 7a-((tert-butyldimethylsilyl)oxy)-2a-(4-fluorobenzyl)-2,2-diphenyl-2a,7a-dihydrooxeto[2,3-b]indole-7(2H)-carboxylate (70).



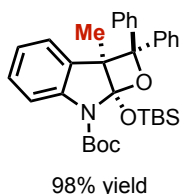
1H -NMR (400 MHz, $CDCl_3$): δ 7.77 (d, $J = 8.0$ Hz, 2H, Ar), 7.44 (t, $J = 7.7$ Hz, 2H, Ar), 7.37 (d, $J = 7.7$ Hz, 2H, Ar), 7.30 (t, $J = 7.3$ Hz, 1H, Ar), 7.15 (d, $J = 8.0$ Hz, 1H, Ar), 6.98 (dt, $J = 15.3, 7.2$ Hz, 4H, Ar), 6.88 (t, $J = 9.8$ Hz, 4H, Ar), 6.72 – 6.66 (m, 2H, Ar), 3.67 (d, $J = 17.3$ Hz, 1H, CH_2a), 3.08 (d, $J = 17.3$ Hz, 1H, CH_2b), 1.64 (s, 9H, tBu -Boc), 0.78 (s, 9H, tBu -TBS), 0.64 (s, 3H, CH_3 -TBS), 0.24 (s, 3H, CH_3 -TBS) ppm. **^{13}C -NMR (101 MHz, $CDCl_3$):** δ 161.4 (d, $J = 243.6$ Hz), 150.5, 143.6, 142.4, 142.1, 131.6 (d, $J = 3.5$ Hz), 128.3 (x2), 128.2, 128.1, 127.4, 127.3 (d, $J = 8.4$ Hz), 127.0 (x2), 126.4, 126.3 (x2), 126.0 (x2), 125.0, 124.8 (d, $J = 13.7$ Hz), 123.5 (d, $J = 3.5$ Hz), 121.8, 114.5, 114.4 (d, $J = 23.0$ Hz), 113.7, 87.2, 81.8, 64.5, 28.6 (x3), 26.57 (d, $J = 5.1$ Hz), 26.1 (x3), 18.5, -2.0, -2.3 ppm. **^{19}F NMR (376 MHz, $CDCl_3$)** δ -117.68 – -117.79 (m, 1F, C-F Ar) ppm. **HRMS (ESI-MS)** calculated for $C_{39}H_{44}FNNaO_4Si^+$ $[M-Na]^+$ 660.2921, found 660.2896.

***tert*-butyl 7a-((*tert*-butyldimethylsilyl)oxy)-2a-(4-methylbenzyl)-2,2-diphenyl-2a,7a-dihydrooxeto[2,3-*b*]indole-7(2*H*)-carboxylate (71).**



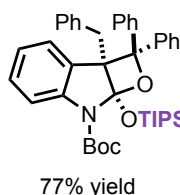
¹H-NMR (400 MHz, CDCl₃) δ 7.76 (d, *J* = 7.5 Hz, 2H, Ar), 7.43 (t, *J* = 7.7 Hz, 2H, Ar), 7.38 – 7.24 (m, 3H, Ar), 7.15 (d, *J* = 8.1 Hz, 1H, Ar), 7.04 – 6.84 (m, 5H, Ar), 6.84 – 6.74 (m, 3H, Ar), 6.71 (d, *J* = 7.7 Hz, 1H, Ar), 6.65 (t, *J* = 7.5 Hz, 1H, Ar), 3.41 (d, *J* = 16.8 Hz, 1H, CH₂*a*), 3.24 (d, *J* = 16.8 Hz, 1H, CH₂*b*), 2.15 (s, 3H, CH₃), 1.63 (s, 9H, ^tBu-Boc), 0.80 (s, 9H, ^tBu-TBS), 0.60 (s, 3H, CH₃-TBS), 0.25 (s, 3H, CH₃-TBS) ppm. **¹³C NMR (101 MHz, CDCl₃)** δ 150.6, 143.7, 142.4, 142.2, 137.4, 137.0, 130.9, 128.5, 128.3 (x2), 127.9, 127.6, 127.4, 127.1, 127.0 (x2), 126.4 (x2), 126.4, 126.3 (x3), 125.9, 121.5, 114.5, 113.7, 87.2, 81.6, 64.9, 35.2, 28.6(x3), 26.1 (x3), 21.5, 18.5, -2.0, -2.2 ppm. **HRMS (ESI-MS)** calculated for C₄₀H₄₈NO₄Si⁺ [M-H⁺] 634.3347, found 634.1819.

***tert*-butyl 7a-((*tert*-butyldimethylsilyl)oxy)-2a-methyl-2,2-diphenyl-2a,7a-dihydrooxeto[2,3-*b*]indole-7(2*H*)-carboxylate (72).**



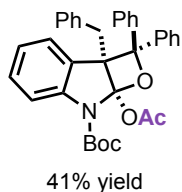
¹H-NMR (400 MHz, CDCl₃): δ 7.63 (d, *J* = 7.3 Hz, 2H, Ar), 7.36 – 7.28 (m, 4H, Ar), 7.24 – 7.15 (m, 4H, Ar), 7.02 – 6.90 (m, 5H, Ar), 1.60 (s, 9H, ^tBu-Boc), 1.35 (s, 3H, CH₃), 0.91 (s, 9H, ^tBu-TBS), 0.21 (s, 3H, CH₃-TBS), 0.07 (s, 3H, CH₃-TBS) ppm. **¹³C-NMR (101 MHz, CDCl₃)**: δ 143.3, 142.7, 142.5, 131.3, 128.8, 128.5, 128.1 (x2), 127.5, 127.1 (x2), 126.4, 126.2 (x2), 125.9 (x2), 124.2, 122.2, 114.9, 113.3, 81.7, 60.9, 53.6, 28.6 (x3), 26.0 (x3), 18.4, 16.5, -2.8, -2.9 ppm. **HRMS (ESI-MS)** calculated for C₃₃H₄₁NNaO₄Si⁺ [M-Na⁺] 566.2703, found 566.2988.

***tert*-butyl 2a-benzyl-2,2-diphenyl-7a-((triisopropylsilyl)oxy)-2a,7a-dihydrooxeto[2,3-*b*]indole-7(2*H*)-carboxylate (73).**



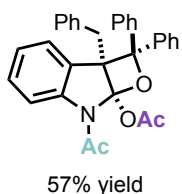
¹H-NMR (400 MHz, CDCl₃): δ 7.80 (d, *J* = 7.4 Hz, 2H, Ar), 7.41 (t, *J* = 7.4 Hz, 2H, Ar), 7.32 – 7.29 (m, 3H, Ar), 7.12 (d, *J* = 8.2 Hz, 1H, Ar), 7.04 – 6.93 (m, 6H, Ar), 6.90 – 6.86 (m, 3H, Ar), 6.63 (d, *J* = 4.4 Hz, 2H, Ar), 3.47 (d, *J* = 16.7 Hz, 1H, CH₂*a*), 3.34 (d, *J* = 16.7 Hz, 1H, CH₂*b*), 1.60 (s, 9H, ^tBu-Boc), 1.42 (hept, *J* = 7.5 Hz, 3H, 3x CH-TIPS), 1.14 (d, *J* = 7.5 Hz, 9H, 3x CH₃-TIPS), 1.08 (d, *J* = 7.5 Hz, 9H, 3x CH₃-TIPS) ppm. **¹³C-NMR (101 MHz, CDCl₃)** δ 150.8, 143.7, 142.3, 142.1, 137.8, 130.3 (x2), 129.0, 128.2 (x2), 127.8, 127.7 (x2), 127.4, 127.0 (x2), 126.9 (x2), 126.7 (x2), 126.5, 126.3, 125.7, 121.6, 115.1, 112.7, 86.8, 81.7, 65.3, 34.9, 28.6 (x3), 18.7 (x3), 18.6 (x3), 14.0 (x3). **HRMS (ESI-MS)** calculated for C₄₂H₅₂NO₄Si⁺ [M-Na⁺] 684.3485, found 684.3482.

tert-butyl 7a-acetoxy-2a-benzyl-2,2-diphenyl-2a,7a-dihydrooxeto[2,3-b]indole-7(2H)-carboxylate (74).



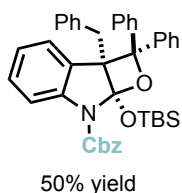
¹H-NMR (400 MHz, CDCl₃): δ 7.83 (d, *J* = 7.9 Hz, 2H, Ar), 7.47 (t, *J* = 7.7 Hz, 2H, Ar), 7.38 (dt, *J* = 14.4, 7.7 Hz, 2H, Ar), 7.29 – 7.26 (m, 3H, Ar), 7.17 – 6.98 (m, 8H, Ar), 6.89 – 6.81 (m, 4H, Ar), 3.71 (d, *J* = 15.1 Hz, 1H, CH₂*a*), 3.17 (d, *J* = 15.1 Hz, 1H, CH₂*b*), 1.98 (s, 3H, CH₃-Ac), 1.63 (s, 9H, ^tBu-Boc) ppm. **¹³C-NMR (101 MHz, CDCl₃):** δ 166.8, 150.3, 144.1, 141.4, 140.9, 136.2, 130.6 (x2), 128.9, 128.4 (x2), 128.1 (x3), 128.0, 127.3 (x2), 127.1 (x2), 126.7, 126.7, 126.5 (x2), 126.2, 121.8, 114.9, 113.8, 91.1, 82.0, 65.5, 35.3, 28.5 (x3), 21.7 ppm. **HRMS (ESI-MS)** calculated for C₃₅H₃₄NO₅⁺ [M-H⁺] 548.2431, found 548.2415.

7-acetyl-2a-benzyl-2,2-diphenyl-2a,7-dihydrooxeto[2,3-b]indol-7a(2H)-yl acetate (75)



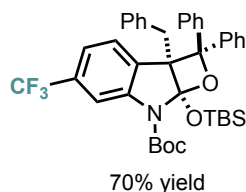
¹H NMR (400 MHz, Toluene-d₈) δ 8.29 (d, *J* = 8.2 Hz, 1H, Ar), 7.85 (d, *J* = 7.2 Hz, 1H, Ar), 7.33 – 7.20 (m, 4H, Ar), 6.96 – 6.82 (m, 7H, Ar), 6.75 (m, 5H, Ar), 3.72 (d, *J* = 15.4 Hz, 1H, CH₂*a*), 3.42 (d, *J* = 15.4 Hz, 1H, CH₂*b*), 2.49 (s, 3H, CH₃-OAc), 1.33 (s, 3H, CH₃-NAc) ppm. **¹³C NMR (101 MHz, Toluene-d₈)** δ 167.0, 165.3, 145.1, 141.4, 140.7, 136.8, 136.1, 135.6, 130.2, 127.1, 127.0, 126.7, 126.4, 126.0, 125.5, 122.4, 116.7, 114.2, 92.0, 65.9, 35.4, 30.0, 23.6 ppm. Overlap with toluene. **HRMS (ESI-MS)** calculated for C₃₂H₂₈NO₄⁺ [M-H⁺] 490.2013, found 490.2023.

benzyl 2a-benzyl-7a-((tert-butyl)dimethylsilyloxy)-2,2-diphenyl-2a,7a-dihydrooxeto[2,3-b]indole-7(2H)-carboxylate (76).



¹H NMR (400 MHz, Acetone-d₆) δ 7.92 – 7.84 (m, 2H, Ar), 7.65 (d, *J* = 7.5 Hz, 2H, Ar), 7.58 – 7.41 (m, 6H, Ar), 7.37 – 7.20 (m, 4H, Ar), 7.08 – 6.95 (m, 5H, Ar), 6.90 – 6.82 (m, 4H, Ar), 6.71 (td, *J* = 7.5, 1.1 Hz, 1H, Ar), 5.79 – 5.66 (d, *J* = 11.5 Hz, 1H, CH₂*a*-Cbz), 5.29 (d, *J* = 11.5 Hz, 1H, CH₂*a*-Cbz), 3.84 (d, *J* = 16.9 Hz, 1H, CH₂*a*), 3.30 (d, *J* = 16.9 Hz, 1H, CH₂*b*), 0.77 (s, 9H, ^tBu-TBS), 0.69 (s, 3H, CH₃-TBS), 0.15 (s, 3H, CH₃-TBS) ppm. **¹³C NMR (101 MHz, Acetone-d₆)** δ 151.7, 142.6, 142.4, 137.4, 137.0, 131.1, 129.6 (x2), 129.2, 128.7, 128.5 (x2), 128.2, 128.1 (x2), 127.8, 127.5 (x2), 127.2, 126.9 (x2), 126.4, 126.1, 125.8 (x2), 125.7 (x2), 125.4, 121.9, 114.2, 113.9, 87.7, 66.3, 65.0, 54.1, 35.0, 25.4 (x3), 17.9, -2.3, -2.9 ppm. **HRMS (ESI-MS)** calculated for C₄₂H₄₄NO₄Si⁺ [M-H⁺] 654.3034, found 654.3024.

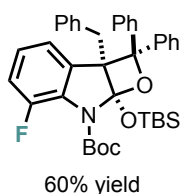
tert-butyl **2a-benzyl-7a-((tert-butyldimethylsilyl)oxy)-2,2-diphenyl-5-(trifluoromethyl)-2a,7a-dihydrooxeto[2,3-*b*]indole-7(2*H*)-carboxylate (77).**



¹H-NMR (400 MHz, CDCl₃): δ 7.75 – 7.73 (m, 2H, Ar), 7.45 – 7.41 (m, 3H, Ar), 7.33 – 7.26 (m, 3H, Ar), 7.04 – 6.93 (m, 8H, Ar), 6.89 (dd, *J* = 7.7, 0.5 Hz, 1H, Ar), 6.83 (d, *J* = 7.7 Hz, 1H), 3.41 (d, *J* = 16.7 Hz, 1H, CH_{2a}), 3.31 (d, *J* = 16.7 Hz, 1H, CH_{2b}), 1.62 (s, 9H, ^tBu-Boc), 0.79 (s, 9H, ^tBu-TBS), 0.61 (s, 3H, CH₃-TBS), 0.25 (s, 3H, CH₃-TBS) ppm.

¹³C-NMR (101 MHz, CDCl₃): δ 150.0, 143.9, 141.8, 141.7, 136.9, 132.3 (q, *J* = 1.4 Hz), 130.0 (q, *J* = 32.0 Hz), 129.9 (x2), 128.4 (x2), 128.0 (x2), 127.6, 127.2 (x2), 126.7, 126.2 (x4), 126.0, 125.9, 124.3 (q, *J* = 273.6 Hz), 118.3 (q, *J* = 3.9 Hz), 113.9, 111.5 (q, *J* = 4.2 Hz), 87.1 (q, *J* = 0.8 Hz), 82.5, 65.0, 35.0, 28.5 (x3), 26.1 (x3), 18.6, -2.0, -2.2 ppm. **¹⁹F-NMR (376 MHz, CDCl₃):** δ -63.05 (s, 3F, Ar-CF₃) ppm. **HRMS (ESI-MS)** calculated for C₄₀H₄₄F₃NNaO₄Si⁺ [M-Na⁺] 710.2889, found 710.2892.

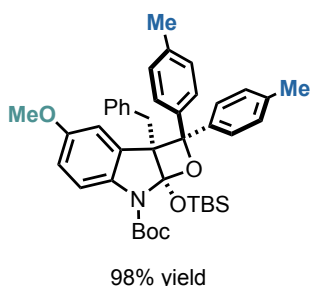
tert-butyl **2a-benzyl-7a-((tert-butyldimethylsilyl)oxy)-6-fluoro-2,2-diphenyl-2a,7a-dihydrooxeto[2,3-*b*]indole-7(2*H*)-carboxylate (78).**



¹H-NMR (400 MHz, CDCl₃) δ 7.76 (d, *J* = 7.9 Hz, 2H, Ar), 7.40 (t, *J* = 7.6 Hz, 2H, Ar), 7.34 – 7.27 (m, 3H, Ar), 7.07 (t, *J* = 7.6 Hz, 2H, Ar), 7.02 – 7.00 (m, 4H, Ar), 6.81 – 6.80 (m, 2H, Ar), 6.66 – 6.57 (m, 2H, Ar), 6.44 (d, *J* = 7.2 Hz, 1H), 3.29 (d, *J* = 16.5 Hz, 1H, CH_{2a}), 3.21 (d, *J* = 16.5 Hz, 1H, CH_{2b}), 1.50 (s, 9H, ^tBu-Boc), 0.83 (s, 9H, ^tBu-TBS), 0.46 (s, 3H, CH₃-TBS),

0.44 (s, 3H, CH₃-TBS) ppm. **¹³C NMR (101 MHz, CDCl₃)** δ 150.6, 150.5 (d, *J* = 250.7 Hz), 141.8, 141.8, 137.3, 133.2 (d, *J* = 2.7 Hz), 131.6 (d, *J* = 9.6 Hz), 129.9 (x2), 128.3 (x2), 127.8 (x2), 127.7, 127.2 (x2), 127.1 (x2), 126.8 (x2), 126.7, 125.9, 123.1 (d, *J* = 7.2 Hz), 122.4 (d, *J* = 3.4 Hz), 115.9 (d, *J* = 21.5 Hz), 114.4, 86.5, 81.4, 65.6, 35.8, 28.1 x3, 26.1 x3, 18.7, -2.3, -2.9. ppm. **¹⁹F NMR (376 MHz, CDCl₃)** δ -117.44 – -117.62 (m, 1F, Ar-F) ppm. **HRMS (ESI-MS)** calculated for C₃₉H₄₅FNO₄Si⁺ [M-H⁺] 638.3096, found 638.3107.

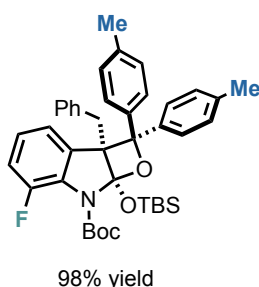
tert-butyl **2a-benzyl-7a-((tert-butyldimethylsilyl)oxy)-4-methoxy-2,2-di-*p*-tolyl-2a,7a-dihydrooxeto[2,3-*b*]indole-7(2*H*)-carboxylate (79).**



¹H NMR (400 MHz, Acetone-d₆) δ 7.79 (d, *J* = 8.3 Hz, 2H, Ar), 7.38 (d, *J* = 8.3 Hz, 2H, Ar), 7.27 (d, *J* = 8.0 Hz, 2H, Ar), 7.14 – 6.96 (m, 6H, Ar), 6.85 (d, *J* = 8.1 Hz, 2H, Ar), 6.81 (d, *J* = 2.7 Hz, 1H, Ar), 6.41 (dd, *J* = 8.9, 2.7 Hz, 1H, Ar), 3.70 (d, *J* = 16.6 Hz, 1H, CH_{2a}), 3.56 (s, 3H, OCH₃), 3.31 (d, *J* = 16.6 Hz, 1H, CH_{2b}), 2.34 (s, 3H, CH₃), 2.11 (s, 3H, CH₃), 1.63 (s, 9H, ^tBu-Boc), 0.79 (s, 9H, ^tBu-TBS), 0.63 (s, 3H, CH₃-TBS), 0.31 (s, 3H, CH₃-TBS)

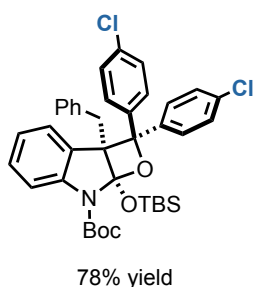
ppm. ^{13}C NMR (101 MHz, Acetone- d_6) δ 154.8, 150.4, 140.3, 139.9, 137.9, 137.2, 136.5, 135.3, 129.8, 129.7 (x2), 128.5 (x2), 127.5 (x2), 127.4 (x2), 126.0 (x2), 125.8 (x2), 125.4, 114.9, 113.9, 113.2, 112.0, 87.1, 80.9, 64.5, 54.9, 35.1, 27.7 (x3), 25.6 (x3), 20.1, 20.0, 18.2, -2.6, -2.7 ppm. HRMS (ESI-MS) calculated for $\text{C}_{42}\text{H}_{52}\text{NO}_5\text{Si}^+$ $[\text{M}-\text{H}^+]$ 678.3609, found 678.3611.

tert-butyl 2a-benzyl-7a-((tert-butyldimethylsilyl)oxy)-6-fluoro-2,2-di-*p*-tolyl-2a,7a-dihydrooxeto[2,3-*b*]indole-7(2*H*)-carboxylate (80)



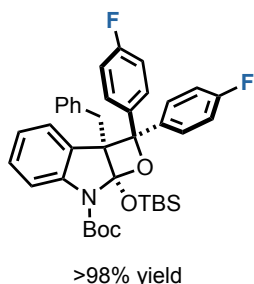
^1H NMR (400 MHz, Acetone- d_6) δ 7.78 (d, $J = 8.3$ Hz, 1H, Ar), 7.37 (d, $J = 8.3$ Hz, 1H, Ar), 7.27 (d, $J = 8.1$ Hz, 1H, Ar), 7.05 – 6.86 (m, 4H, Ar), 6.77 – 6.61 (m, 1H, Ar), 3.52 (d, $J = 16.6$ Hz, 1H, CH_2a), 3.30 (d, $J = 16.6$ Hz, 1H, CH_2b), 2.34 (s, 3H, CH_3), 2.15 (s, 3H, CH_3), 1.54 (s, 9H, $^t\text{Bu-Boc}$), 0.82 (s, 9H, $^t\text{Bu-TBS}$), 0.55 (s, 3H, $\text{CH}_3\text{-TBS}$), 0.50 (s, 3H, $\text{CH}_3\text{-TBS}$) ppm. ^{13}C NMR (101 MHz, Acetone- d_6) δ 150.6, 150.1 (d, $J = 248.3$ Hz), 139.9, 139.4, 137.6, 136.8, 135.6, 133.4 (d, $J = 2.4$ Hz), 131.3 (d, $J = 9.4$ Hz), 129.5 (x2), 128.6 (x2), 127.7 (x2), 127.5 (x2), 126.3 (x2), 126.1 (x2), 125.5, 123.2 (d, $J = 7.1$ Hz), 122.8, 122.8 (d, $J = 3.4$ Hz), 115.5, 115.3, 114.7, 86.3, 80.9, 65.0, 35.5, 27.3 (x3), 25.6 (x3), 18.3, -2.8, -3.5 ppm. ^{19}F NMR (188 MHz, Acetone- d_6) δ -119.28 – -119.45 (m, 1F, Ar-F) ppm. HRMS (ESI-MS) calculated for $\text{C}_{41}\text{H}_{49}\text{FNO}_4\text{Si}^+$ $[\text{M}-\text{H}^+]$ 666.3409, found 666.3398.

tert-butyl 2a-benzyl-7a-((tert-butyldimethylsilyl)oxy)-2,2-bis(4-chlorophenyl)-2a,7a-dihydrooxeto[2,3-*b*]indole-7(2*H*)-carboxylate (81).



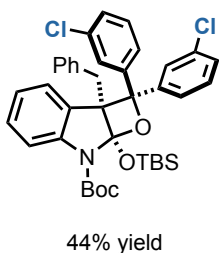
^1H NMR (400 MHz, CDCl_3) δ 7.61 (d, $J = 8.3$ Hz, 2H, Ar), 7.39 (d, $J = 8.2$ Hz, 2H, Ar), 7.21 (d, $J = 8.3$ Hz, 2H, Ar), 7.15 (d, $J = 8.3$ Hz, 1H, Ar), 7.02 – 6.98 (m, 3H, Ar), 6.95 (d, $J = 8.4$ Hz, 2H, Ar), 6.90 – 6.89 (m, 3H, Ar), 6.72 (d, $J = 7.4$ Hz, 1H, Ar), 6.64 (t, $J = 7.4$ Hz, 1H, Ar), 3.32 (d, $J = 16.9$ Hz, 1H, CH_2a), 3.25 (d, $J = 16.9$ Hz, 1H, CH_2b), 1.60 (s, 9H, $^t\text{Bu-Boc}$), 0.74 (s, 9H, $^t\text{Bu-TBS}$), 0.53 (s, 3H, $\text{CH}_3\text{-TBS}$) 0.23 (s, 1H) ppm. ^{13}C NMR (101 MHz, CDCl_3) δ 150.5, 143.6, 140.8, 140.4, 137.0, 133.6, 132.5, 129.9 (x2), 128.7 (x2), 128.4, 127.9 (x2), 127.7, 127.7 (x2), 127.5 (x2), 127.4 (x2), 125.8, 125.7, 121.8, 114.8, 113.7, 86.5, 82.0, 64.8, 35.2, 28.6 (x3), 26.0 (x3), 18.6, -2.1, -2.1 ppm. HRMS (ESI-MS) calculated for $\text{C}_{39}\text{H}_{43}\text{Cl}_2\text{NNaO}_4\text{Si}^+$ $[\text{M}-\text{Na}^+]$ 710.2236, found 710.2236.

tert-butyl 2a-benzyl-7a-((tert-butyldimethylsilyl)oxy)-2,2-bis(4-fluorophenyl)-2a,7a-dihydrooxeto[2,3-b]indole-7(2H)-carboxylate (82).



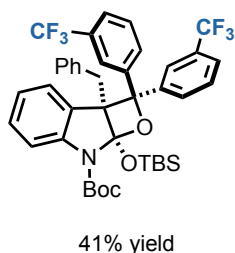
¹H-NMR (400 MHz, CDCl₃) δ 7.68 (dd, *J* = 7.1, 5.2 Hz, 2H, Ar), 7.28 – 7.25 (m, 2H, Ar), 7.14 (q, *J* = 8.2 Hz, 3H, Ar), 7.05 – 7.00 (m, 3H, Ar), 6.92 – 6.88 (m, 3H, Ar), 6.73 – 6.63 (m, 4H, Ar), 3.34 (d, *J* = 16.8 Hz, 1H, CH_{2a}), 3.27 (d, *J* = 16.8 Hz, 1H, CH_{2b}), 1.62 (s, 9H, ^tBu-Boc), 0.77 (s, 9H, ^tBu-TBS), 0.56 (s, 3H, CH₃-TBS), 0.26 (s, 3H, CH₃-TBS) ppm. ¹³C NMR (101 MHz, CDCl₃) δ 162.3 (d, *J* = 246.4 Hz), 160.2 (d, *J* = 245.3 Hz), 150.5, 143.7, 138.1 (d, *J* = 2.9 Hz), 137.9 (d, *J* = 2.9 Hz), 137.2, 129.9 (x2), 128.3, 128.1, 128.0 (x2), 128.0 (d, *J* = 12.3 Hz, x2), 127.8 (x2), 125.7 (d, *J* = 13.6 Hz, x2), 121.7, 115.3 (d, *J* = 21.4 Hz, x2), 114.7, 114.0 (d, *J* = 21.4 Hz, x2), 113.7, 86.7, 81.9, 64.8, 35.2, 28.6 (x3), 26.0 (x3), 18.6, -2.1, -2.2. ppm. ¹⁹F NMR (376 MHz, CDCl₃) δ -115.49 – -115.56 (m, 1F, Ar-F), -116.72 – -116.80 (m, 1F, Ar-F). HRMS (ESI-MS) calculated for C₃₉H₄₃F₂NNaO₄Si⁺ [M-Na⁺] 678.2827, found 678.2852.

tert-butyl 2a-benzyl-7a-((tert-butyldimethylsilyl)oxy)-2,2-diphenyl-2a,7a-dihydrooxeto[2,3-b]indole-7(2H)-carboxylate (83).



¹H-NMR (400 MHz, Acetone-d₆): δ 8.04-7.89 (m, 2H, Ar), 7.74 (m, 1H, Ar), 7.58 – 7.49 (m, 2H, Ar), 7.45 – 7.35 (m, 2H, Ar), 7.29 – 7.11 (m, 4H, Ar), 7.11 – 6.94 (m, 4H, Ar), 6.91 (t, *J* = 7.3 Hz, 1H, Ar), 6.66 (d, *J* = 8.0 Hz, 1H, Ar), 3.79 (d, *J* = 17.0 Hz, 1H, CH_{2a}), 3.33 (d, *J* = 16.6 Hz, 1H, CH_{2b}), 1.67 (s, 9H, ^tBu-Boc), 0.79 (s, 9H, ^tBu-TBS), 0.64 (s, 3H, CH₃-TBS), 0.36 (s, 3H, CH₃-TBS) ppm. ¹³C-NMR (101 MHz, Acetone-d₆): δ 150.4, 144.6, 144.0, 143.2, 137.3, 134.0, 132.6, 130.0, 129.7 (x2), 129.2, 128.9, 128.8, 128.2, 127.5 (x2), 126.6, 126.5, 126.0, 125.7, 125.5, 124.8, 124.7, 121.6, 114.3, 113.6, 86.3, 81.9, 64.8, 34.8, 27.7 (x3), 25.5 (x3), 18.2, -2.7, -2.8. ppm. HRMS (ESI-MS) calculated for C₃₉H₄₃Cl₂NNaO₄Si⁺ [M-Na⁺] 710.2236, found 710.2234.

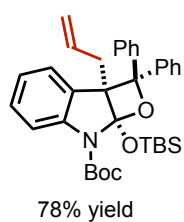
tert-butyl 2a-benzyl-7a-((tert-butyldimethylsilyl)oxy)-2,2-bis(3-(trifluoromethyl)phenyl)-2a,7a-dihydrooxeto[2,3-b]indole-7(2H)-carboxylate (84).



¹H-NMR (400 MHz, CDCl₃): δ 8.11 (s, 1H, Ar), 7.83 (d, *J* = 7.5 Hz, 1H, Ar), 7.62 – 7.52 (m, 4H, Ar), 7.23 (d, *J* = 7.7 Hz, 1H, Ar), 7.15 (t, *J* = 8.5 Hz, 2H, Ar), 7.01 (t, *J* = 7.4 Hz, 3H, Ar), 6.92 (d, *J* = 7.6 Hz, 2H, Ar), 6.87 (t, *J* = 7.8 Hz, 1H, Ar), 6.76 (d, *J* = 7.4 Hz, 1H, Ar), 6.65 (t, *J* = 7.7 Hz, 1H, Ar), 3.33 (d, *J* = 16.7 Hz, 1H, CH_{2a}), 3.27 (d, *J* = 16.7 Hz, 1H, CH_{2b}), 1.61 (s, 9H, ^tBu-Boc), 0.75 (s, 9H, ^tBu-TBS), 0.58 (s, 3H, CH₃-TBS), 0.26 (s, 3H, CH₃-TBS) ppm. ¹³C-NMR (101 MHz, CDCl₃): δ 150.4, 143.5,

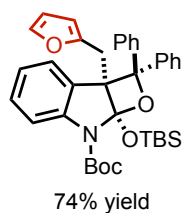
142.9, 142.6, 136.8, 131.2 (q, $J = 32.4$ Hz), 129.9 (x2) 129.7 (q, $J = 32.4$ Hz), 129.6 (q, $J = 1.5$ Hz), 129.5 (q, $J = 1.5$ Hz), 129.0, 128.5, 127.9 (x2), 127.8, 127.3, 126.0, 125.8, 124.7 (q, $J = 3.4$ Hz), 124.3 (q, $J = 273.4$ Hz), 124.0 (q, $J = 272.4$ Hz), 123.7 (q, $J = 4.1$ Hz), 123.3 (p, $J = 4.0$ Hz, x2), 122.0, 114.6, 113.7, 86.5, 82.3, 65.2, 35.3, 28.5 (x3), 26.0 (x3), 18.6, -2.2, -2.3 ppm. **^{19}F -NMR (376 MHz, CDCl_3):** δ -62.98 (s, 3F, Ar- CF_3), -63.07 (s, 3F, Ar- CF_3) ppm. **HRMS (ESI-MS)** calculated for $\text{C}_{41}\text{H}_{43}\text{F}_6\text{NNaO}_4\text{Si}^+$ [M-Na^+] 778.2763, found 778.2758.

***tert*-butyl 2a-allyl-7a-((*tert*-butyldimethylsilyloxy)-2,2-diphenyl-2a,7a-dihydrooxeto[2,3-*b*]indole-7(2*H*)-carboxylate (85).**



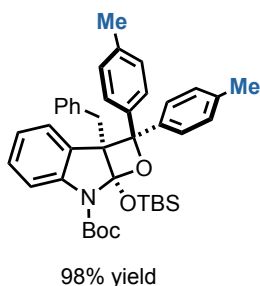
^1H -NMR (500 MHz, CDCl_3): δ 7.68 (d, $J = 7.3$ Hz, 2H, Ar), 7.40 (t, $J = 7.8$ Hz, 2H, Ar), 7.34 (d, $J = 7.3$ Hz, 2H, Ar), 7.29 – 7.25 (m, 1H, Ar), 7.18 (d, $J = 8.1$ Hz, 1H, Ar), 7.14 (d, $J = 7.4$ Hz, 1H, Ar), 7.03 – 6.92 (m, 4H, Ar), 6.88 (t, $J = 7.4$ Hz, 1H, Ar), 5.62 (dddd, $J = 17.2, 10.2, 8.5, 4.7$ Hz, 1H, C(sp²)H), 4.99 (dd, $J = 17.2, 1.2$ Hz, 1H, (E) C(sp²)H₂), 4.91 (dd, $J = 10.2, 1.2$ Hz, (Z)C(sp²)H₂), 2.84 (dd, $J = 15.5, 8.5$ Hz, 1H, CH₂*a*), 2.66 – 2.62 (m, 1H, CH₂*b*), 1.62 (s, 9H, ^tBu-Boc), 0.93 (s, 9H, ^tBu-TBS), 0.56 (s, 3H, CH₃-TBS), 0.30 (s, 3H, CH₃-TBS) ppm. **^{13}C -NMR (126 MHz, CDCl_3)** δ 150.4, 143.8, 142.4, 142.4, 134.7, 128.5, 128.2 (x3), 127.3, 127.1 (x2), 126.4, 126.2 (x2), 125.9 (x2), 125.8, 121.6, 117.7, 114.6, 113.7, 87.1, 81.6, 63.6, 34.6, 28.6 (x3), 26.1 (x3), 18.6, -2.7, -2.9, ppm. **HRMS (ESI-MS)** calculated for $\text{C}_{35}\text{H}_{44}\text{NO}_4\text{Si}^+$ [M-H^+] 570.3034, found 570.3033.

***tert*-butyl 7a-((*tert*-butyldimethylsilyloxy)-2a-(furan-2-ylmethyl)-2,2-diphenyl-2a,7a-dihydrooxeto[2,3-*b*]indole-7(2*H*)-carboxylate (86).**



^1H -NMR (400 MHz, CDCl_3): δ 7.73 (d, $J = 7.6$ Hz, 2H, Ar), 7.41 – 7.36 (m, 4H, Ar), 7.30 – 7.26 (m, 1H, Ar), 7.21 – 7.19 (m, 2H, Ar), 7.05 – 6.96 (m, 5H, Ar), 6.81 (t, $J = 7.6$ Hz, 1H, Ar), 6.06 (dd, $J = 3.0, 1.9$ Hz, 1H, Ar), 5.36 (d, $J = 3.0$ Hz, 1H, Ar), 3.53 (d, $J = 16.8$ Hz, 1H, CH₂*a*), 3.10 (d, $J = 16.8$ Hz, 1H, CH₂*b*), 1.63 (s, 9H, ^tBu-Boc), 0.83 (s, 9H, ^tBu-TBS), 0.49 (s, 3H, CH₃-TBS), 0.27 (s, 3H, CH₃-TBS) ppm. **^{13}C -NMR (101 MHz, CDCl_3)** δ 151.6, 150.5, 143.7, 142.1, 142.1, 140.1, 128.5, 128.4, 128.2 (x2), 127.4, 127.1 (x2), 126.5, 126.4 (x2), 126.3 (x2), 125.5, 121.8, 114.7, 113.2, 110.5, 107.7, 87.3, 81.7, 63.7, 28.8, 28.6 (x3), 26.0 (x3), 18.5, -2.3, -2.4 ppm. **HRMS (ESI-MS)** calculated for $\text{C}_{37}\text{H}_{43}\text{NNaO}_5\text{Si}^+$ [M-Na^+] 632.2808, found 632.2787.

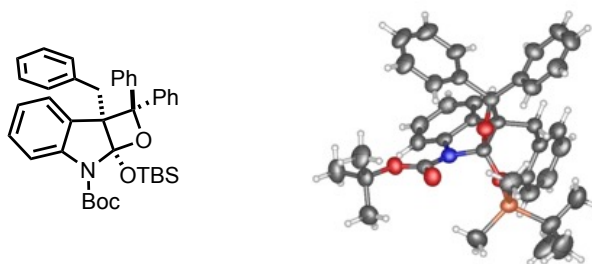
tert-butyl 2a-benzyl-7a-((tert-butyldimethylsilyl)oxy)-2,2-di-p-tolyl-2a,7a-dihydrooxeto[2,3-b]indole-7(2H)-carboxylate (88).



$^1\text{H-NMR}$ (400 MHz, CDCl_3) δ 7.67 (d, $J = 7.9$ Hz, 2H, Ar), 7.32 – 7.22 (m, 5H, Ar), 7.10 – 6.99 (m, 5H, Ar), 6.93 (t, $J = 7.6$ Hz, 1H, Ar), 6.85 – 6.80 (m, 3H, Ar), 6.69 (t, $J = 7.3$ Hz, 1H), 3.47 (d, $J = 16.9$ Hz, 1H, CH_2a), 3.35 (d, $J = 16.9$ Hz, 1H, CH_2a), 2.41 (s, 3H, CH_3), 2.18 (s, 3H, CH_3), 1.69 (s, 9H, $^t\text{Bu-Boc}$), 0.84 (s, 9H, $^t\text{Bu-TBS}$), 0.66 (s, 3H, $\text{CH}_3\text{-TBS}$), 0.31 (s, 3H, $\text{CH}_3\text{-TBS}$) ppm. $^{13}\text{C NMR}$ (101 MHz, CDCl_3) δ 150.6, 143.8, 139.7, 139.6, 137.7, 136.8, 135.6, 130.0 (x2), 128.9 (x2), 128.6, 127.8, 127.7 (x4), 126.1 (x4), 125.8, 125.6, 121.5, 114.6, 113.8, 87.3, 81.6, 64.6, 35.4, 28.7 (x3), 26.1(x3), 21.2, 21.1, 18.6, -2.0, -2.2 ppm. **HRMS (ESI-MS)** calculated for $\text{C}_{41}\text{H}_{50}\text{NO}_4\text{Si}^+$ $[\text{M-H}^+]$ 648.3504, found 648.3505.

X-ray crystallographic analysis of 65

— X-ray structure of 65 —



X-Ray structure of 65.

Colorless crystals of **65** were grown by slow evaporation of a Et_2O solution at ambient temperature.

Crystal data: $\text{C}_{39}\text{H}_{45}\text{NO}_4\text{Si}$

Orthorhombic, $P2_12_12_1$, $a=10.1848(8)\text{\AA}$, $b=16.7586(14)\text{\AA}$, $c=20.4119(18)\text{\AA}$, $V=3484.0(5)\text{\AA}^3$; $Z=4$; $d_{\text{calc}}=1.182\text{mg/cm}^3$, $F(000)=1328$, $\mu=0.906$, Tot. refl.= 38933, hkl range= $-12 < h < 12$, $-16 < k < 20$, $-25 < l < 25$; Theta max 73.1° , ref.tot.= 6856, number of parameters = 414, GooF= 1.086, $R=0.0611$, $wR_2=0.1761$.

CCDC 1943528 contains the supplementary crystallographic data for this compound. These data can be obtained free of charge from The Cambridge Crystallographic Data Centre via www.ccdc.cam.ac.uk/data_request/cif



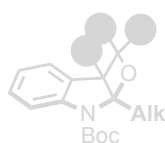
Chapter II – Section 3

Dearomative Paternò-Büchi Reaction – The Effect of Visible-Light Irradiation on the Reaction Manifold

Chapter II - Synthetic Transformations Driven by Triplet State Benzophenones

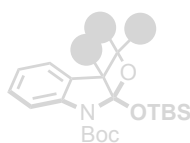
Section 1.

Towards the construction of
Oxeto-Indolinic
Polycycles



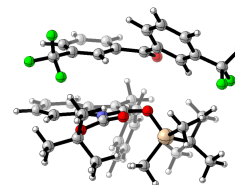
Section 2.

Microfluidic Visible-Light
Dearomatization of
Oxindole Enol Ethers



Section 3.

A Mechanistic Interrogation of the
Process, the Effect of
Visible-Light Irradiation



- To disclose the different mechanistic scenarios of the reaction between indoles and aryl ketones.
- To control the diastereoselectivity of the Paternò-Büchi reaction when using different prochiral carbonyls.³⁷

³⁷ The project discussed in this chapter has been conducted in collaboration with Dr. Francesco Rigodanza (involved in the photochemical and electrochemical characterization of the reaction), Prof. Mirco Natali from the University of Ferrara (involved in the characterization of the transient intermediates by Laser Flash Photolysis), Dr. Paolo Costa and Prof. Andrea Sartorel (involved in the DFT modelling of the reaction complex interactions). I individually performed the reaction kinetics and studied the reaction mechanism by using LFER techniques.

This work has been submitted recently as: Mateos, J.; Rigodanza, F.; Natali, M.; Costa, P.; Sartorel, A.; Bonchio, M.; Dell'Amico, L. *A Mechanistic Interrogation of the Paternò-Büchi Reaction. The Impact of Visible-Light Irradiation on the Diastereoselectivity Prediction*. Submitted manuscript

2.3.1 Introduction

Given the limitations observed in both previous sections, we decided to carefully investigate the mechanisms governing the selectivity of the Paternò-Büchi process between indoles and aryl ketones.

In the recent years the general perception that radical species are difficult-to-handle intermediates has been progressively cleared away.³⁸ For this reason, the development of novel and selective visible-light synthetic methods has tracked the rapid development of photochemistry.³⁹ To this regard, the Paternò-Büchi reaction has been a long-standing case of study.^{1,2} Diverse reaction mechanisms and predicting models have been proposed over the years (Figure 2.20).⁴⁰

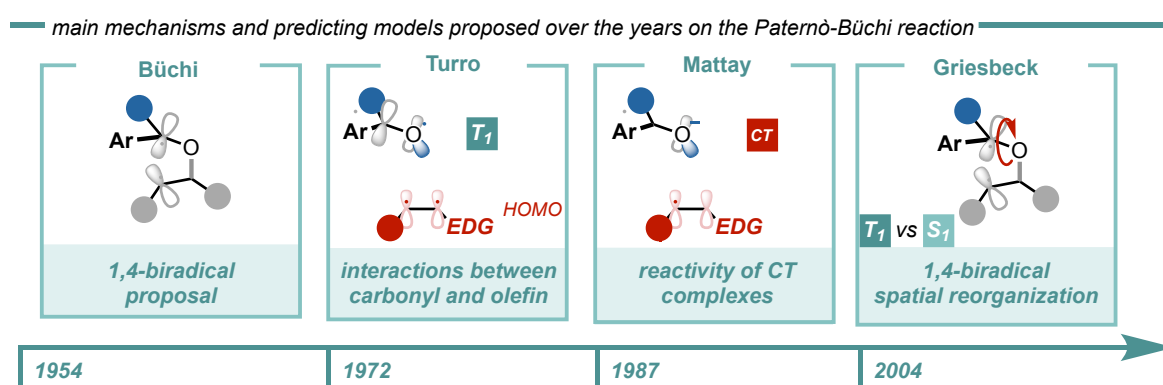


Figure 2.20. - Timescale of the main predicting models proposed over the years on the Paternò-Büchi reaction.

Since the initial studies of Büchi on the characterization of the 1,4-biradical intermediate, many groups directed their efforts towards the topic.^{40a} Indeed, Griesbeck

³⁸ a) Minisci, F.; Vismara, E.; Morini, G.; Fontana, F.; Levi, S.; Serravalle, M.; Giordano, C. *Polar Effects in Free-Radical Reactions. Selectivity and Reversibility in the Homolytic Benzoylation of Protonated Heteroaromatic Bases.* *J. Org. Chem.* **1986**, *51*, 476–479. b) Yan, M.; Lo, J. C.; Edwards, J. T.; Baran, P. S. *Radicals: Reactive Intermediates with Translational Potential.* *J. Am. Chem. Soc.* **2016**, *138*, 12692–12714

³⁹ Shaw, M. H.; Twilton, J.; MacMillan, D. W. C. *Photoredox Catalysis in Organic Chemistry.* *J. Org. Chem.* **2016**, *81*, 6898–6926

⁴⁰ The chronological order of the different models proposed over the years depicted in Figure 2.20 is the following: a) Büchi, G.; Inman, C. G.; Lipinsky, E. S. *Light-Catalyzed Organic Reactions. I. The Reaction of Carbonyl Compounds with 2-Methyl-2-Butene in the Presence of Ultraviolet Light.* *J. Am. Chem. Soc.* **1954**, *76*, 4327–4331. b) Turro, N. J.; Dalton, J. C.; Dawes, K.; Farrington, G.; Hautala, R.; Morton, D.; Niemczyk, M.; Schore, N. *Molecular Photochemistry. L. Molecular Photochemistry of Alkanones in Solution. a-Cleavage, Hydrogen Abstraction, Cycloaddition, and Sensitization Reactions.* *Acc. Chem. Res.* **1972**, *5*, 92–101. c) Gersdorf, J.; Mattay, J.; Goerner, H. *Radical Cations. 3. Photoreactions of Biacetyl, Benzophenone, and Benzil with Electron-Rich Alkenes.* *J. Am. Chem. Soc.* **1987**, *109*, 1203–1209. d) Griesbeck, A. G.; Abe, M.; Bondock, S. *Selectivity Control in Electron Spin Inversion Processes: Regio- and Stereochemistry of Paternò-Büchi Photocyclo-Additions as a Powerful Tool for Mapping Intersystem Crossing Processes.* *Acc. Chem. Res.* **2004**, *37*, 919–928.

clarified how the spatial reorganization of this intermediate leads to a loss of diastereocontrol depending on the spin multiplicity of the excited carbonyl (Figure 2.21).^{40d} When using diarylketones, leading to long-lived triplet 1,4-biradical intermediates **II** (1-10 ns) that must undergo a spin change required for the following radical recombination, major diastereoselectivity issues are observed. Contrarily, the use of aliphatic ketones **III** that generally form short-lived singlet biradical intermediates, the oxetane product is commonly yielded in high diastereoselectivities due to the concerted radical recombination.

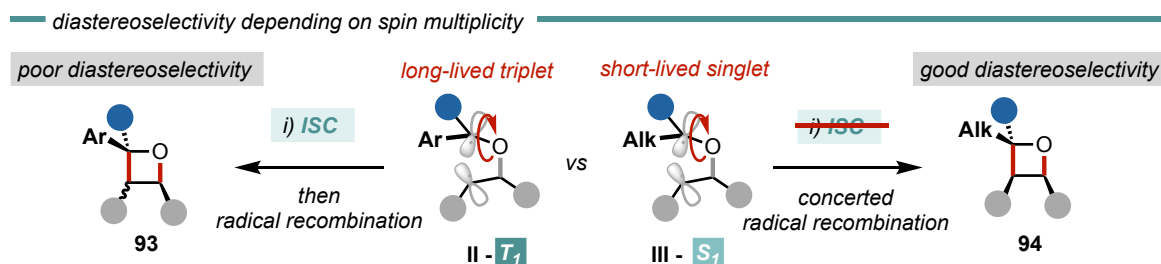


Figure 2.21. - Griesbeck spatial reorganization of 1,4-biradicals.

Analogously to singlet biradicals pathways, the CT processes can occur by-passing the diastereocontrol loss through concerted or quasi-concerted mechanisms. Specifically, Turro and Mattay comprehended the different interactions of excited carbonyls arising charge-transfer processes.^{40b,c} They postulated that in this case, different interactions occur in the course of the reaction. Commonly, no interaction occurs in the ground state but after carbonyl excitation. Is in this case that the biradical triplet intermediate forms an exciplex between the half-filled n_p orbital and the electron-rich π -system. After CT, the electrostatic interactions trigger the reaction through a more selective concerted or quasi-concerted mechanism (Figure 2.22).⁴¹

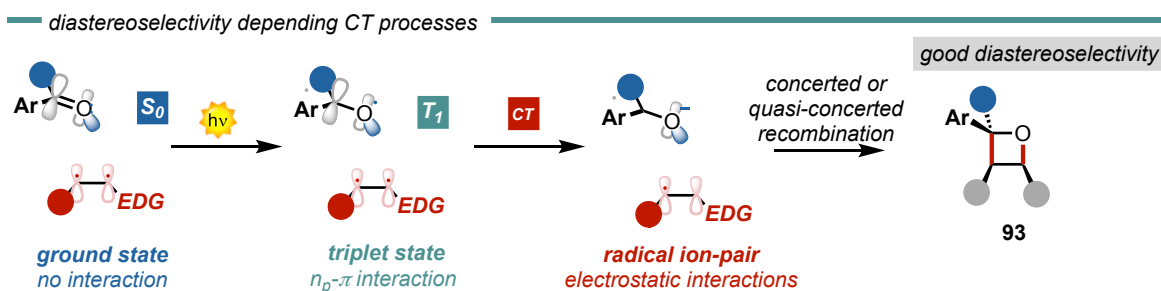


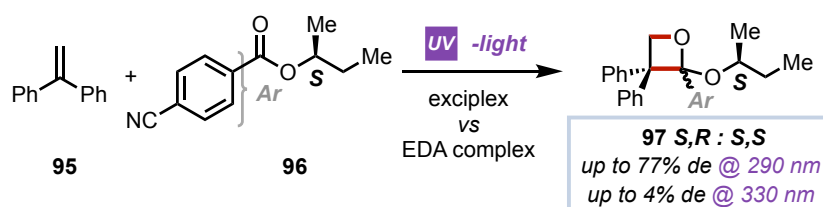
Figure 2.22. - Diastereoselectivity dependent on CT processes.

⁴¹ Mateos, J.; Cuadros, S.; Vega-Peñaloza, A.; Dell'Amico, L. *Unlocking the Synthetic Potential of Light-Excited Aryl Ketones: Applications in Direct Photochemistry and Photoredox Catalysis*. *Synlett* **2021**. <https://doi.org/10.1055/a-1403-4613>

In the PB reaction, the CT state conventionally originates from an exciplex between an electron-rich olefin and the ketone. However, a CT state can in principle evolve also from a ground state interaction (*e.g.* through an EDA complex).⁴² Importantly, the spatial arrangement of the reagents determine the geometries of the CT states and the final oxetane stereochemistry. In their seminal work, Mori, Inoue and co-workers demonstrated that by changing the irradiation wavelength from 290 to 330 nm it was possible to irradiate a CT band, channeling the system towards an EDA-complex-based pathway.⁴³ Thus, the diastereomeric excess (*de*)⁴⁴ of the PB reaction of chiral alkyl benzoates **96** moved from 77% to 3% upon changing the irradiation wavelength (Figure 2.23). Likewise, the wavelength selection in visible-light-driven PB processes⁴⁵ can have an even more relevant impact on the stereochemical outcome.

— seminal report of PB diastereodifferentiation process

Selected example: *J. Am. Chem. Soc.*, **2009**, *121*, 17076—17077



Light stereodifferentiation principle — diastereoselectivity changes with the wavelength

Figure 2.23. - Seminal report of Mori, Inoue and co-workers on the light stereodifferentiation principle.

⁴² Crisenza, G. E. M.; Mazzarella, D.; Melchiorre, P. *Synthetic Methods Driven by the Photoactivity of Electron Donor–Acceptor Complexes*. *J. Am. Chem. Soc.* **2020**, *142*, 5461–5476

⁴³ Matsumura, K.; Mori, T.; Inoue, Y. *Wavelength Control of Diastereodifferentiating Paternò–Büchi Reaction of Chiral Cyanobenzoates with Diphenylethene through Direct versus Charge-Transfer Excitation*. *J. Am. Chem. Soc.* **2009**, *131*, 17076–17077.

⁴⁴ The term *de* is restricted to the use of a chiral auxiliary, being the *de* directly related to the enantiomeric excess (*ee*) once the auxiliary is removed. Hence, the obtained *de* value is the same than the posterior *ee* value. Nevertheless, in this chapter no chiral auxiliaries have been used. For clarity and to favour the comparison with the previously reported light stereodifferentiation methods we will use the *de* term instead of *dr* (diastereomeric ratio).

⁴⁵ For the seminal works discussing the role of light source in the Paternò–Büchi reaction regioselectivity see: **a)** Sun, D.; Hubig, S. M.; Kochi, J. K. *Oxetanes from [2+2] Cycloaddition of Stilbenes to Quinone via Photoinduced Electron Transfer*. *J. Org. Chem.* **1999**, *64*, 2250–2258. **b)** Zhang, Y.; Xue, J.; Gao, Y.; Fun, H.-K.; Xu, J.-H. *Photoinduced [2+2] Cycloadditions (the Paternò–Büchi Reaction) of 1-Acetylisatin with Enol Ethers—Regioselectivity, Diastereoselectivity and Acid Catalysed Transformations of the Spirooxetane Products*. *J. Chem. Soc., Perkin Trans.1* **2002**, *3*, 345–353.

2.3.2 Challenges of the project

Given the novelty of the PB reaction between indoles and carbonyl compounds under visible-light irradiation, the parameters governing the diastereoselectivity of the reaction are unknown. This fact, combined with the limited knowledge about light stereodifferentiation reactions, challenged us to understand the selectivity outcome of the system.

2.3.3 Section overview

Based on detailed mechanistic investigations, we herein report new predicting models capable of anticipating the stereochemical outcome of visible-light PB reactions. Our study includes biorelevant indole heterocycles and aromatic ketones. We used various spectroscopic techniques, including laser flash photolysis (LFP), absorption and emission spectroscopy, as well as DFT calculations to rationalize the activity of two stereodivergent reaction manifolds (Figure 2.24). Remarkably, acting on specific physicochemical parameters (*e.g.* light source, stereoelectronic factors) the diastereoselectivity of the process can be deliberately modulated towards unprecedented light stereodifferentiation processes or triggering the diastereoinversion in visible-light PB reactions.

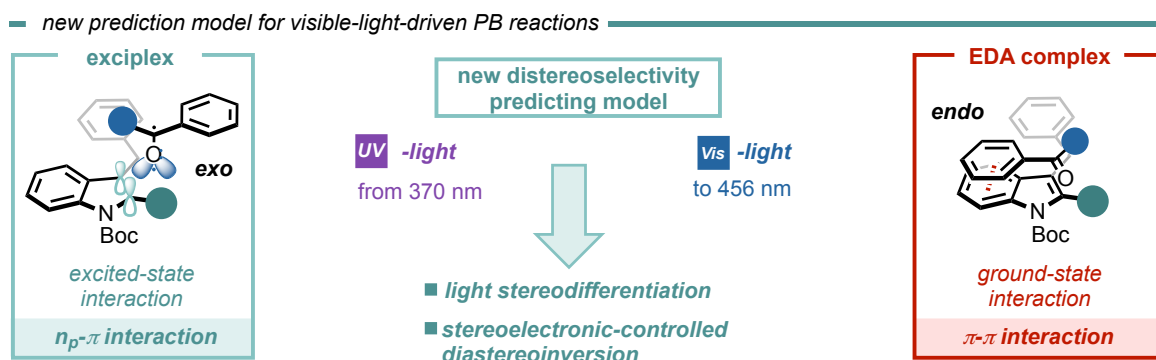


Figure 2.24. - New diastereoselectivity predicting model based diverse interactions between indole-derivatives and carbonyl compounds.

2.3.4 Results and discussion

Characterization of the reaction pathways

We first selected as a mechanistic probe the reaction between indoles **17a** and **65a** and aryl ketones **18a** and **18d** (described in section I and section II of this chapter), where no diastereoselection is envisaged due to the symmetrical nature of the ketone (up to >98% yield). Interestingly, this reaction is passing through three alternative reaction manifolds by modifying the substitution pattern in the *C2* position of the indole and the *C3* position of the benzophenone. This synergistic pathways have been previously described in literature for

different systems and confirmed herein by a specific spectroscopic and photophysical evidence.⁶

Conventional pure triplet pathway I (Figure 2.25)

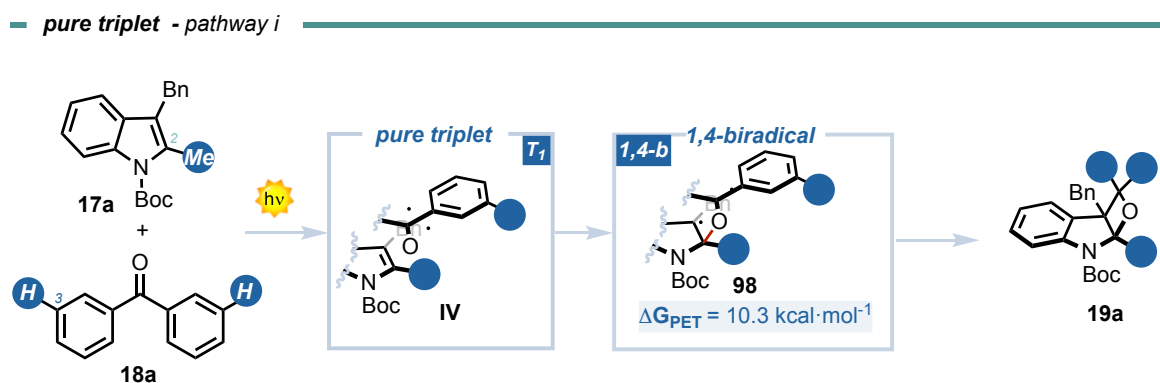


Figure 2.25. - Intermediates of the pure triplet pathway.

When indole **17a** ($C2=Me$) and benzophenone **18a** ($C3 = H$) are involved, a conventional radical trapping mechanism is observed.^{7c} This PB process is commonly mediated by a UV-light source (250–360 nm). Specifically, the direct carbonyl excitation leads to the generation of the first singlet state (S_1) that efficiently undergoes ISC to the long-lived T_1 , which is then trapped by the olefin, in this case **17a** (Figure 2.25), generating the corresponding 1,4-biradical **98**.

This mechanism was confirmed by LFP and UV-Vis experiments (Figure 2.26). In fact, by LFP we observed the decay of the T_1 (max abs. at 525 nm) along with the concomitant appearance of the 1,4-biradical **98** (max abs. at 390 nm).⁴⁶ This transient intermediate leads to the oxetane product **19a** within a hundred ns (up to 400 ns). The experimental data clearly suggest a pure-triplet mechanism as the only operative pathway, as no traces of a radical ion-pair (IP) were detected by LFP and no ground state interaction was observed by UV-Vis. Additionally, alternative PET pathways can be excluded owing to the endergonicity of the electron-transfer process ($\Delta G_{PET} = 10.3 \text{ kcal}\cdot\text{mol}^{-1}$).^{47,48}

⁴⁶ Freilich, S. C.; Peters, K. S. Observation of the 1,4 Biradical in the Paterno-Buchi Reaction. *J. Am. Chem. Soc.* **1981**, *103*, 6255–6257.

⁴⁷ Rehm, D.; Weller, A. Kinetics of Fluorescence Quenching by Electron and H-Atom Transfer. *Isr. J. Chem.* **1970**, *8*, 259–271

⁴⁸ The ΔG_{PET} was calculated by using the modified Rehm-Weller equation for PET as reported in: **a**) Mattay, J.; Runsink, J.; Rumbach, T.; Ly, C.; Gersdorf, J. Selectivity and Charge Transfer in Photoreactions of Donor-Acceptor Systems. 5. Selectivity and Charge Transfer in Photoreactions of α,α,α -Trifluorotoluene with Olefins. *J. Am. Chem. Soc.* **1985**, *107*, 2557–2558 **b**) Mattay, J.; Gersdorf, J.; Buchkremer, K. Photoreactions of Biacetyl with Electron-Rich Olefins. An Extended Mechanism. *Chem. Ber.* **1987**, *120*, 307–318.

— pure triplet - pathway i

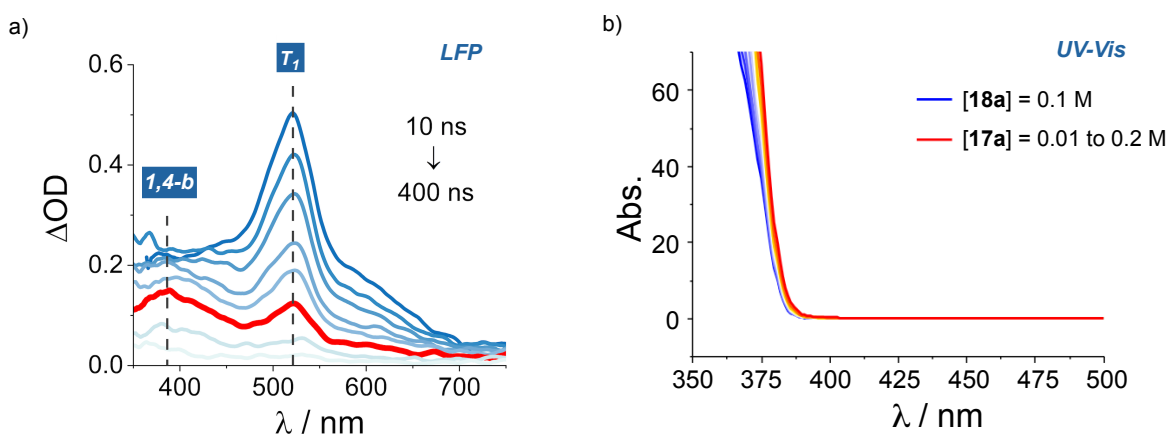


Figure 2.26. - Spectroscopic experiments. a) LFP – identification of the 1,4-biradical intermediate and the triplet state of **18a**. b) UV-Vis – no ground interaction observed.

Exciplex-based pathway ii (Figure 2.27)

— exciplex - pathway ii

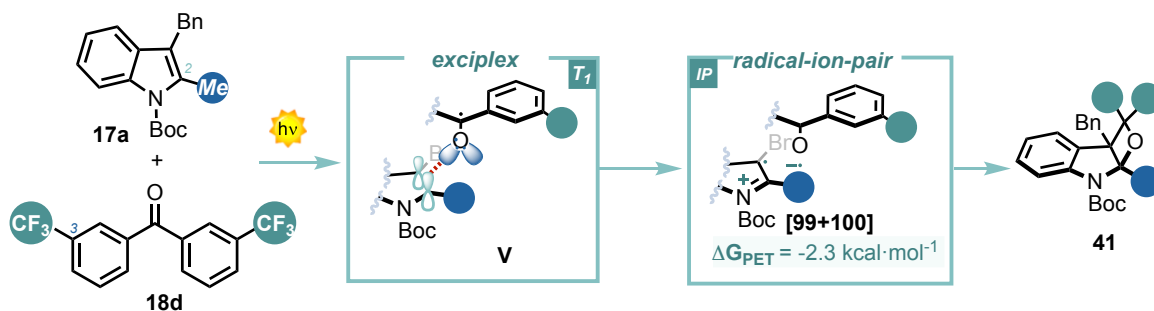


Figure 2.27. - Intermediates of the exciplex pathway.

In the presence of a more electron-deficient ketone such as **18d** ($C3=CF_3$), an alternative mechanism is unlocked (Figure 2.27). Analogously to *pathway i*, no ground state interactions between **17a** and **18d** were detected as UV-Vis spectroscopy signature for an EDA complex (Figure 2.28b). Nevertheless, LFP experiments revealed the appearance of the transient radical IP (**99+100**) upon T_1 decay, as supported by the spectral changes at $\lambda > 700$ nm characteristic of the benzophenone radical anion (Figure 2.29a). Additionally, no traces of the biradical **98** were detected, suggesting that the radical IP evolves through a concerted or quasi-concerted mechanism to the oxetane product **41** in 10 ns. This data implies that after the ketone excitation, the T_1 state of **18d** associates with the indole generating the exciplex **V**. The exciplex **V** possesses a charge transfer character which is consistent with the exergonicity of the photoinduced electron transfer (PET) process ($\Delta G_{PET} = -2.3 \text{ kcal}\cdot\text{mol}^{-1}$).

— exciplex - pathway ii

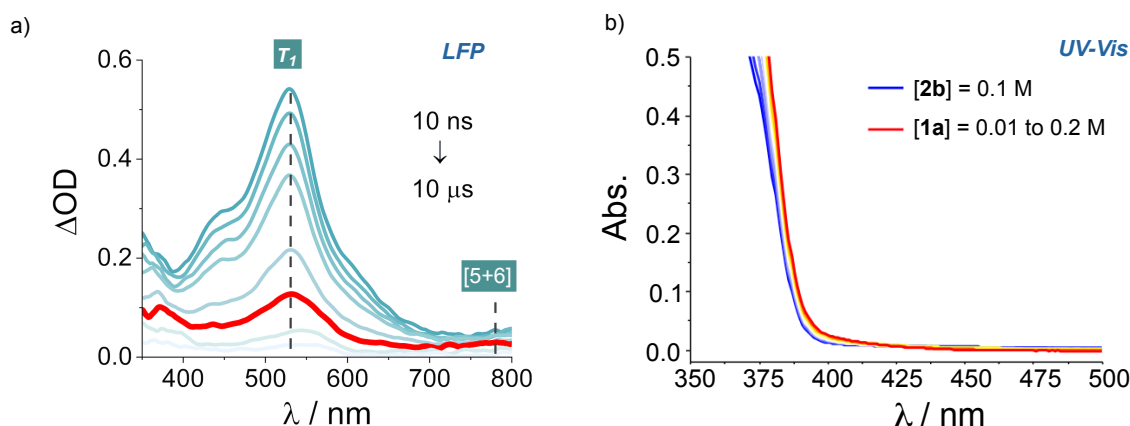


Figure 2.28. - Spectroscopic experiments. a) LFP – identification of the radical ion-pair intermediate and the triplet state of **18d**. b) UV-Vis – no ground state interaction observed.

EDA complex-based pathway iii (Figure 2.29)

— EDA complex - pathway iii

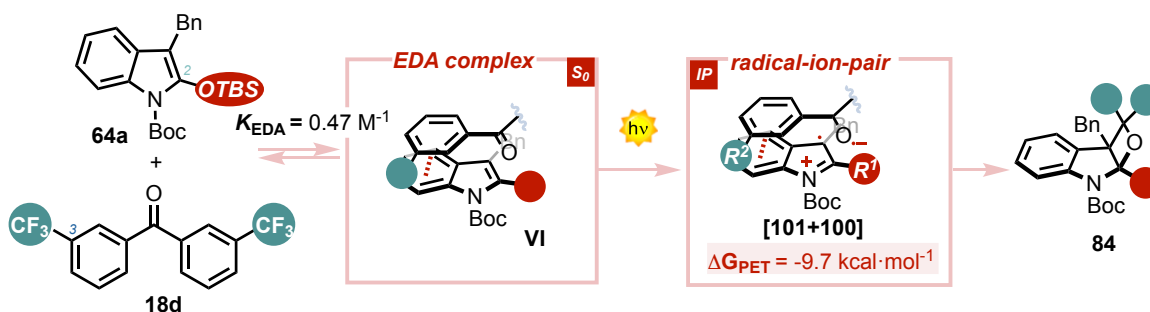


Figure 2.29. - Intermediates of the EDA complex pathway.

This pathway foresees the interaction of the two reactants at the ground state level into an EDA complex. UV-titration experiments with the electron-rich indole **64a**, and the electron-poor benzophenone **18d**, revealed the appearance of a red-shifted CT band (Figure 2.30b). The EDA complex was found to have a modest binding constant ($K_{\text{EDA}} = 0.47 \text{ M}^{-1}$, in acetone at $25 \text{ }^{\circ}\text{C}$). Within this framework, a radical IP is directly produced upon light-excitation of the complex. As monitored by LFP, a favorable PET process ($\Delta G_{\text{PET}} = -9.7 \text{ kcal}\cdot\text{mol}^{-1}$) occurs delivering the radical IP (Figure 2.30a). This species decays with a time-constant of 180 ns to the oxetane product. In this case, however, the orbital interaction differs from *pathways i* and *ii* due to the lack of the initial overlap of the π orbital of the indole with the half-filled n_p molecular orbital of the ketone.

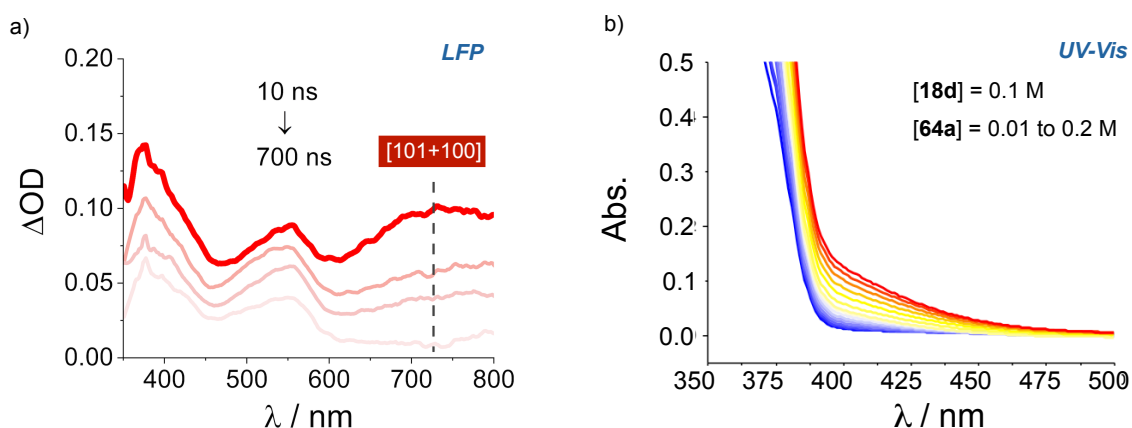


Figure 2.30. - Spectroscopic experiments. a) LFP – identification of the radical ion-pair intermediate. b) UV-Vis –new CT-band observed indicating the formation of an EDA complex.

Exciplex vs EDA complex. DFT models.

Having identified three alternative reaction manifolds, we focused our attention on the exciplex-based *pathway ii* and EDA-complex *pathway iii*, where the stereochemistry is preserved to the oxetane product without geometry reorganization. Here, we can consider that, when using a red-shifted wavelength and irradiating the CT band, the EDA-complex *pathway iii* is favored. On the other hand, the use of a UV-light source will also promote the direct excitation of the free ketone **18d**, guiding the reaction through the exciplex *pathway ii*. Hence, by selecting the light source we can deliberately channel the system towards the intended PET-based pathway ii or iii. To gain insight on the spatial arrangements involved in the two PET-based pathways, we used DFT calculations (Figure 2.31).⁴³

The M06-2X/6-311++ level of theory, including dispersion corrections,⁴⁹ allowed us to model two different orientations between the carbonyl and the indole. In the exciplex (Figure 2.31a), the oxygen atom of the T₁ **18d** and the C2 position of **64a** are in close proximity (n_p-π interaction, 3.66 Å). Additionally, to confirm the biradical nature of the intermediate we depicted the spin density map of the reaction couple. This map confirmed that the spin density is still located in **18d** while interacting with the electron-rich π orbital of **64a**. On the other

⁴⁹ a) Spicher, S.; Grimme, S. Efficient Computation of Free Energy Contributions for Association Reactions of Large Molecules. *J. Phys. Chem. Lett.* **2020**, *11*, 6606–6611. b) Gutiérrez-Hernández, A.; Richaud, A.; Chacón-García, L.; Cortés-García, C. J.; Méndez, F.; Contreras-Celedón, C. A. Deep Eutectic Solvent Choline Chloride *p*-Toluenesulfonic Acid and Water Favor the Enthalpy-Driven Binding of Arylamines to Maleimide in Aza-Michael Addition. *J. Org. Chem.* **2021**, *86*, 223–234.

hand, the EDA complex (Figure 2.31b), **18d** and **64a** interact through a π - π stacking (π - π interaction 3.35 Å).⁵⁰

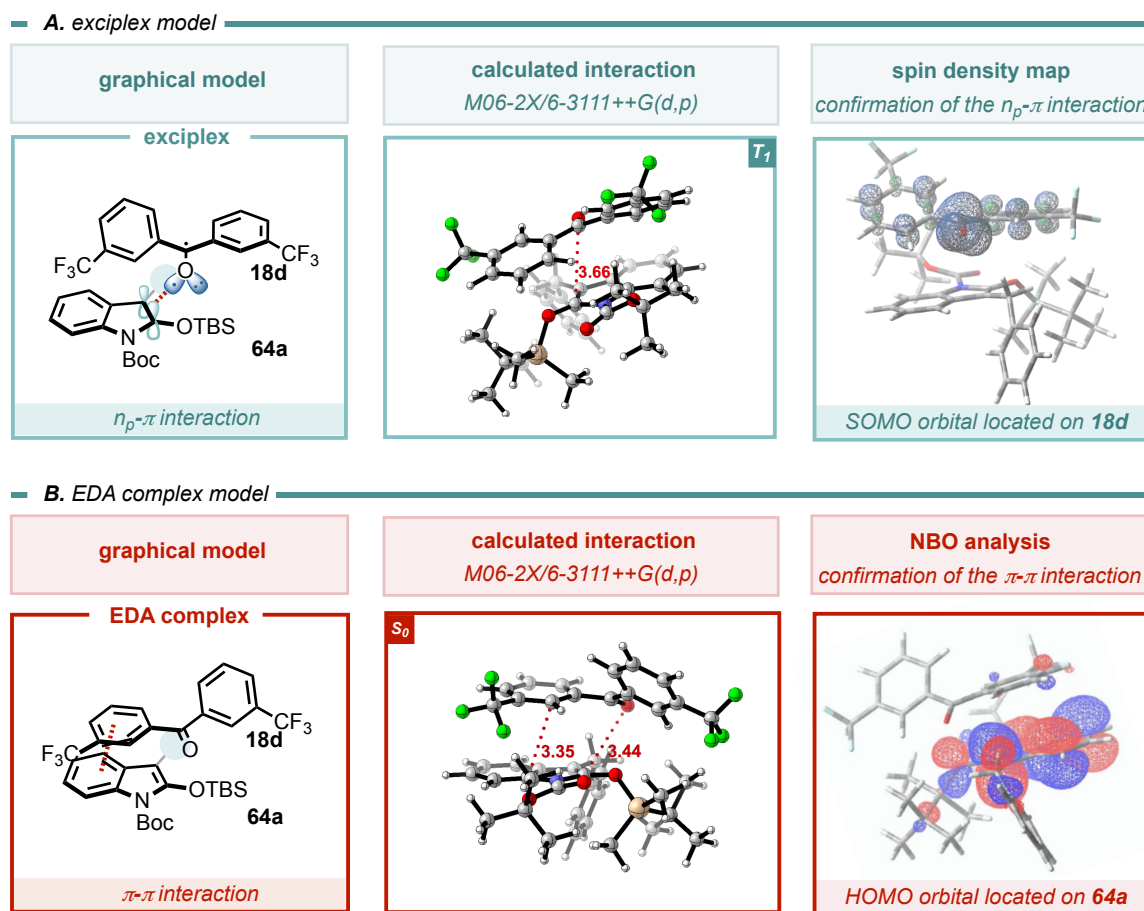


Figure 2.31. - Graphical and DFT models of the diverse interactions. a) n_p - π interaction in pathway ii. b) π - π interaction in pathway iii.

Based on the different geometries determined by DFT calculations, it is possible to represent the two alternative reaction manifolds by using a simplified potential energy surface diagram (Figure 2.32).²² It is worth reminding that these spatial arrangements are retained and directly transferred to the final oxetane product due to the fast radical recombination happening by the IP. For instance, when the reaction mixture is irradiated at 405 nm, the CT-band of the EDA complex is directly excited. This selective irradiation leads to the formation of a radical IP with a preferred π - π interaction. On the other hand, **18d** can be directly excited at 370 nm. In this case the n_p - π interaction will govern the spatial arrangement of the IP. Thus,

⁵⁰ The modelling of the EDA-complex and exciplex was also accomplished with a simplified model involving 3,5-CF₃benzophenone as the ketone **18d** and an *N*-Moc indole where R² = R³ = Me. For this model system, several conformers of the EDA were obtained with slightly different energies (0.1 to 0.2 kcal·mol⁻¹). For the real case study, involving indole **64a** (*N*-Boc, R² = OTBS, R³ = Bn), we considered the EDA complex having a proper orientation of the functional groups matching with the observed experimental results.

a light stereodifferentiation processes (stereoselection caused by different wavelengths) can in principle occur when passing from UV- to visible-light. Yet, the energy barrier resulting from the potential energy surface crossing in the excited state determines the interconversion from one spatial organization to the other one.

— Simplified potential energy surface

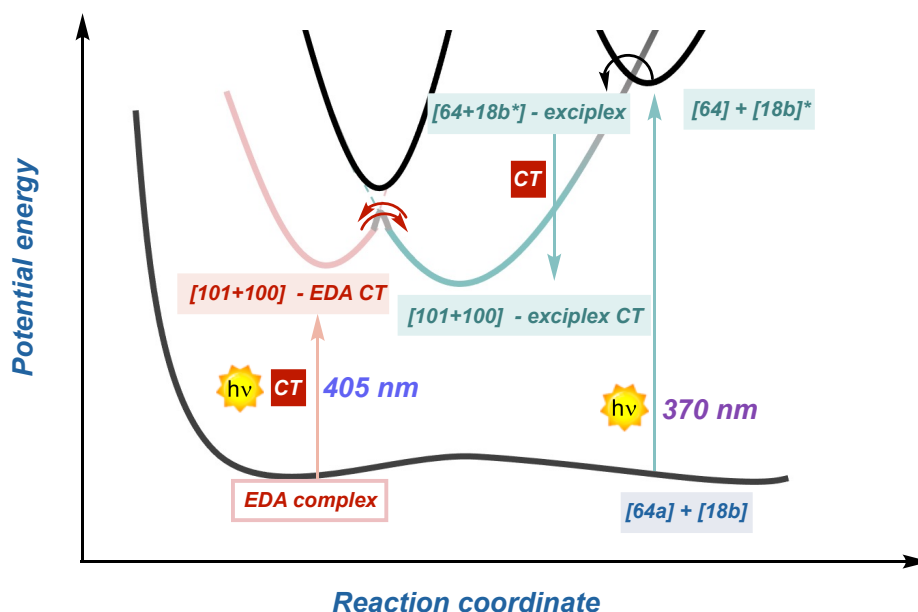


Figure 2.32. - Simplified potential energy surface of the light stereodifferentiation between pathway ii and pathway iii.

Experimental assessment of the developed model with benzil

The two alternative sets of interactions determined by DFT calculations and explained through PES, which do not result in any product diversification when using symmetric benzophenones, are crucial when moving to prochiral carbonyls such as 1,2 diketones or α -ketoesters. For this reason, we applied the developed model to benzil **18b**, that represents a class of synthetically relevant prochiral carbonyls used in several polar and radical reactions.⁵¹ We anticipate that the *endo/exo* selectivity⁵² of the reaction will depend on the competition

⁵¹ Trost, B. M.; Dong, G.; Vance, J. A. Cyclic 1,2-Diketones as Core Building Blocks: A Strategy for the Total Synthesis of (-)-Terpestacin. *Chem. Eur. J.* **2010**, *16*, 6265–6277.

⁵² The *endo/exo* selectivity notation has been widely used in the Paternò-Büchi transformation. It refers to the initial approach of the aryl group of the carbonyl to the alkene. For an example see: Buschmann, H.; Scharf, H.-D.; Hoffmann, N.; Esser, P. *The Isoinversion Principle—a General Model of Chemical Selectivity*. *Angew. Chem. Int. Ed.* **1991**, *30*, 477–515.

between the two alternative reaction manifolds (exciplex *versus* EDA complex in Figure 2.33).

— Paternò-Büchi reaction between benzil and indole derivatives

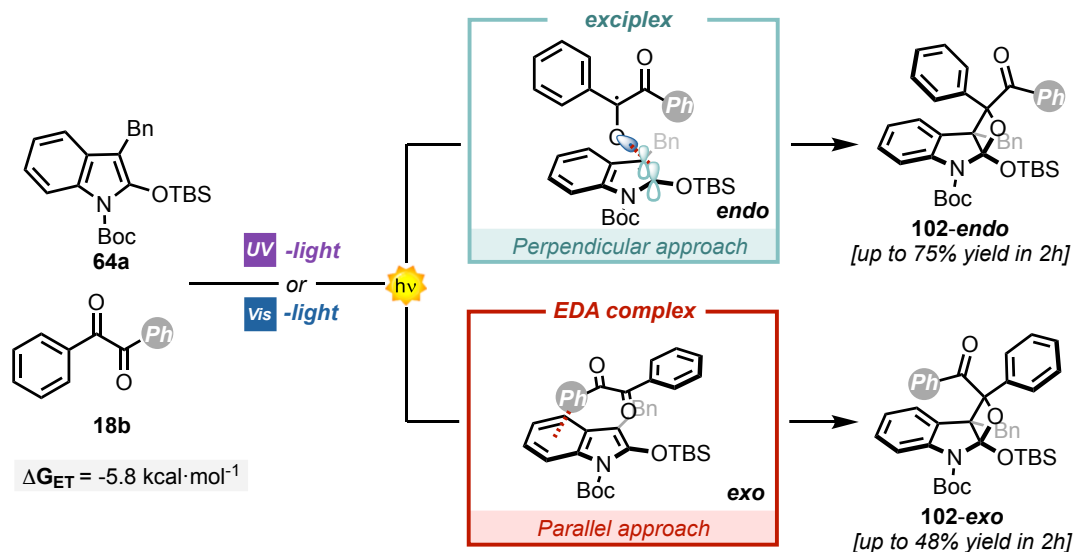


Figure 2.33. - Light stereodifferentiation between **18b** and **64a**.

Initially, we ruled out the conventional pure-triplet mechanism (*pathway i*) when looking at the LFP experiments of **18b** with **64a** (Figure 2.34a) which confirm the photogeneration of the radical IP in agreement with a favorable ΔG_{ET} ($-5.8 \text{ kcal}\cdot\text{mol}^{-1}$). Thus, by altering the parameters that influence the formation of the EDA complex as well as the irradiation wavelength, the *endo/exo* selectivity can be deliberately altered in a light stereodifferentiation process. In fact, the **102-endo** will be the preferred product in an exciplex-based mechanism, while the **102-exo** product will be favored following an EDA complex pathway.

— spectroscopic evidences

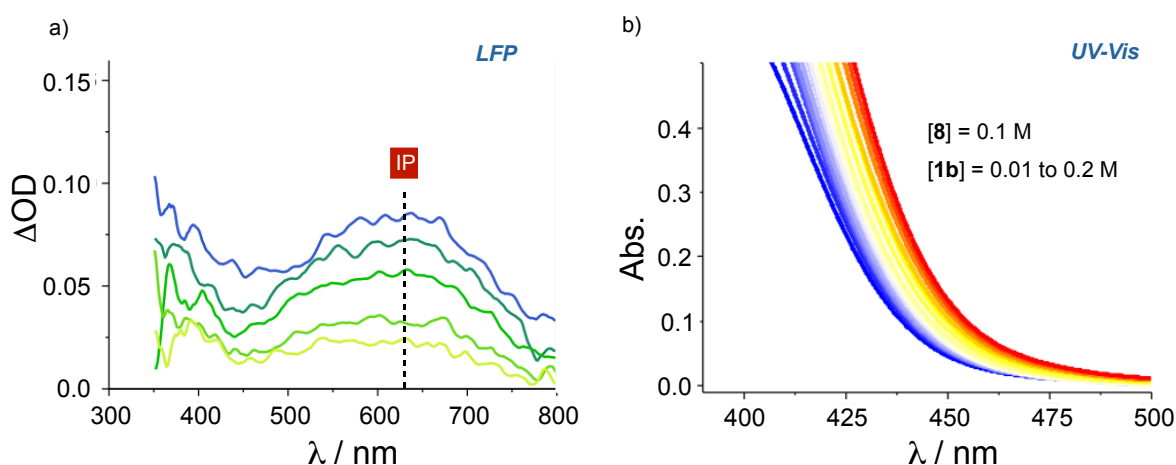
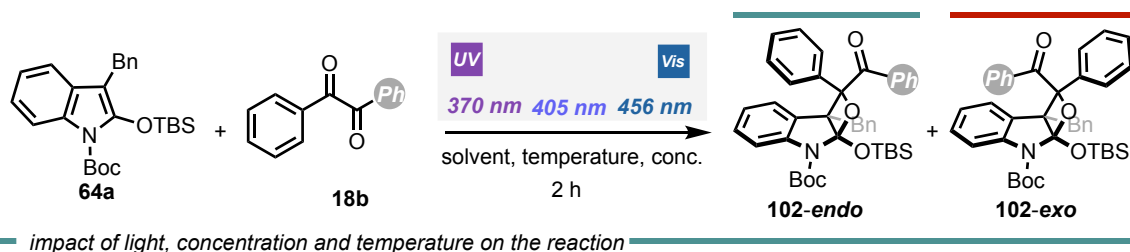


Figure 2.34. - Spectroscopic evidences of the reaction between benzil **18b** and **64a**. a) LFP – identification of the radical ion-pair. b) UV-Vis – observation of a novel CT band indicating the formation of an EDA complex.

In fact, when running the reaction at 370 nm we observed the formation of **102-endo** as a single diastereoisomer (>98% de, acetone-d₆, 370 nm Table 2.10). The endo selectivity results from the direct excitation of the free ketone **18b**, participating into an exciplex with **64a**. As hypothesized, when moving to less energetic 405 and 456 nm irradiation wavelengths the endo-selectivity decreases with the de moving to 28% (456 nm Table 2.10). This is in line with the activity of the EDA complex, and it is confirmed by the UV-titration experiments of benzil **18b** with the indole **64a** (Figure 2.34b). Increasing the concentration from 0.01 to 0.1 M favors the EDA complex pathway resulting in a *de* of 86% and 35% upon irradiation at 370 and 405 nm, respectively. No significant variation was observed at 456 nm, indicating that 28% *de* is the limit value under these reaction conditions.



diastereoselectivity				yield - ¹ H NMR (CH ₂ Br ₂)					
light source	Ace-d ₆ de (%)	0.1 M de (%)	-78 °C de (%)	light source	Ace-d ₆ de (%)	0.1 M de (%)	-78 °C de (%)	C ₆ D ₆ de (%)	yield (%)
370 nm	>98	86	>98	370 nm	-	51	39	>98	75
405 nm	54	35	36	405 nm	52	58	-	59	>98
456 nm	28	28	4	456 nm	84	69	>98	50	>98

Table 2.10. - Effect of light, concentration, temperature and solvent on the diastereoselectivity and the yields of the reaction between **18b** and **64a**.

We next reasoned that performing the reaction under reduced temperature should inhibit the interconversion between the two reaction manifolds, thus magnifying the observed light stereodifferentiation process.⁵³ Indeed, when running the reaction at -78 °C, the *de* passed from >98% at 370 nm, to 4% at 456 nm. Remarkably, this *de* variation, is one of the highest ever registered for PB light-diastereodifferentiation processes.⁵⁴ Furthermore, these

⁵³ For the effect of temperature variation in light stereodifferentiation processes see e.g. : Matsumura, K.; Mori, T.; Inoue, Y. *Solvent and Temperature Effects on Diastereodifferentiating Paternó-Büchi Reaction of Chiral Alkyl Cyanobenzoates with Diphenylethene upon Direct versus Charge-Transfer Excitation*. *J. Org. Chem.* **2010**, *75*, 5461–5469.

⁵⁴ For previous examples of light stereodifferentiation reactions see: a) Saito, H.; Mori, T.; Wada, T.; Inoue, Y. *Diastereoselective [2 + 2] Photocycloaddition of Stilbene to Chiral Fumarate. Direct versus Charge-Transfer Excitation*. *J. Am. Chem. Soc.* **2004**, *126*, 1900–1906. b) Aoki, Y.; Matsuki, N.; Mori, T.; Ikeda, H.; Inoue, Y. *Exciplex Ensemble Modulated by Excitation Mode in Intramolecular Charge-Transfer Dyad: Effects of [...]*

experimental data, while confirming the robustness of the proposed model giving always synthetically useful yields (from 51 to >98%), reveals that the choice of the light is crucial.

Reproducibility issues in diastereoselective PB processes involving heterocyclic systems can be now rationalized and possibly resolved by selecting the proper light source.⁴ As a control experiment performed a reaction in an aromatic solvent, capable of interfering with the π - π interactions in the EDA complex. Accordingly, when using C₆D₆ as solvent we observed a reduced activity of the EDA-complex pathway, resulting in a *de*% no lower than 50% at 465 nm (Table 2.10). Additionally to this control experiment, the reaction kinetics were followed at different wavelengths. In all the cases the oxetane product was stable overtime, maintaining constant the ratio of the two formed diastereoisomers as followed by ¹H-NMR measurements.

Experimental assessment of the developed model with α -ketoesters

Having assessed the potential of the developed model to predict light stereodifferentiation events, we next investigated how these mechanistic tools can be generally extended to other prochiral carbonyls. Specifically, we selected α -ketoesters **103** as a molecular probe to monitor the impact of steric and electronic parameters on the reaction outcome (Figure 2.35).

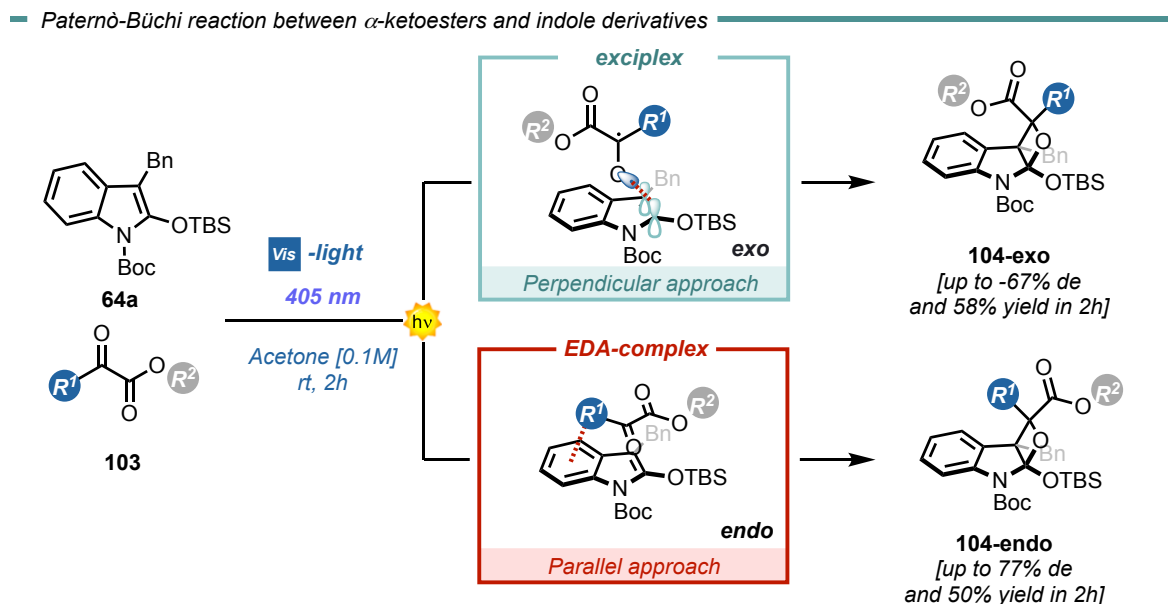


Figure 2.35. - Reaction between **64a** and α -ketoesters **103**.

[...] Temperature, Solvent Polarity, and Wavelength on Photochemistry and Photophysics of Tethered Naphthalene-Dicyanoethene System. *Org. Lett.* **2014**, 16, 4888–4891. c) Nagasaki, K.; Inoue, Y.; Mori, T. Entropy-Driven Diastereoselectivity Improvement in the Paternò-Büchi Reaction of 1-Naphthyl Aryl Ethenes with a Chiral Cyanobenzoate through Remote Alkylation. *Angew. Chem. Int. Ed.* **2018**, 57, 4880–4885.

Specifically, the steric repulsion between R² and the substituent at the C2 of the indole **64a** (OTBS) will favor a carbonyl perpendicular orientation in the exciplex, leading to **104-exo** (Figure 2.35, exciplex box). On the other hand, the **104-endo** selectivity will be favored in the presence of a π - π interaction, that stabilizes the parallel approach in the EDA complex (Figure 2.35, EDA complex box).

We began our experiments by evaluating the impact of the electronic factors on the reaction outcome. First, we selected various α -ketoesters recording the corresponding UV-Vis spectra in order to assess their ability to generate an EDA complex with indole **64a** (Figure 2.36).

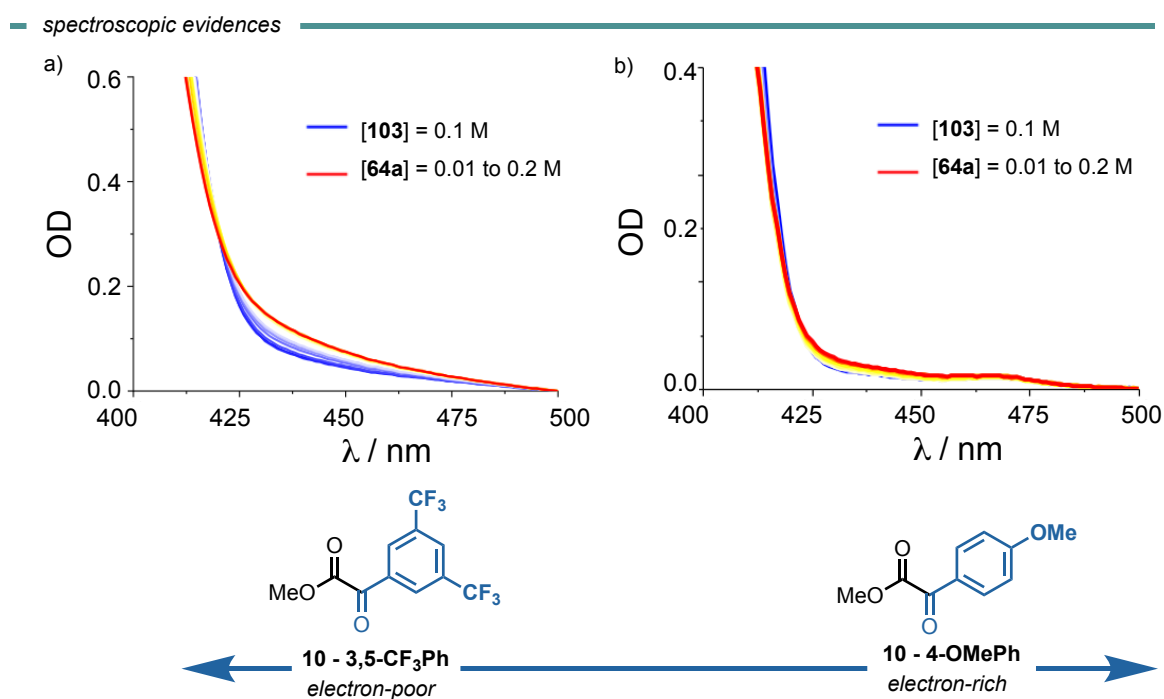


Figure 2.36. - Identification of EDA complexes with diverse α -ketoesters. a) UV-Vis – observation of a novel CT band indicating the formation of an EDA complex. b) UV-Vis – no ground state interaction observed.

When R¹ = 3,5-CF₃Ph, we observed a red-shifted CT band (Figure 2.37a), while measuring a $\Delta G_{\text{PET}} = -17.1$ kcal·mol⁻¹, associated to the formation of an EDA complex. The PB reaction with this electron-deficient α -ketoester resulted highly *endo*-selective (67% *de*, Table 2.11). On the other hand, all the other α -ketoesters did not show any ground-state association with **64a**, while maintaining high level of exergonicity (ΔG_{PET} in the range of -6.0 to -9.5 kcal·mol⁻¹ for R¹ = 4-OMePh, 4-MePh, Ph and 4-CF₃Ph, Table 2.11).^{40b, 48} These data suggested for all the other α -ketoesters the activity of an exciplex-based manifold since no EDA complex was observed in any case. Accordingly, the reaction performed with the different α -ketoesters furnished the product with similar diastereoselectivity (from 41 to 48%

de in favor of the *endo*). Interestingly, the observed differences in the reactivity could be also graphically represented by plotting the obtained experimental *de*% versus the E_{red} of the α -ketoesters, highlighting the diverse behavior of the 3,5-CF₃Ph α -ketoester (Table 2.11, right).

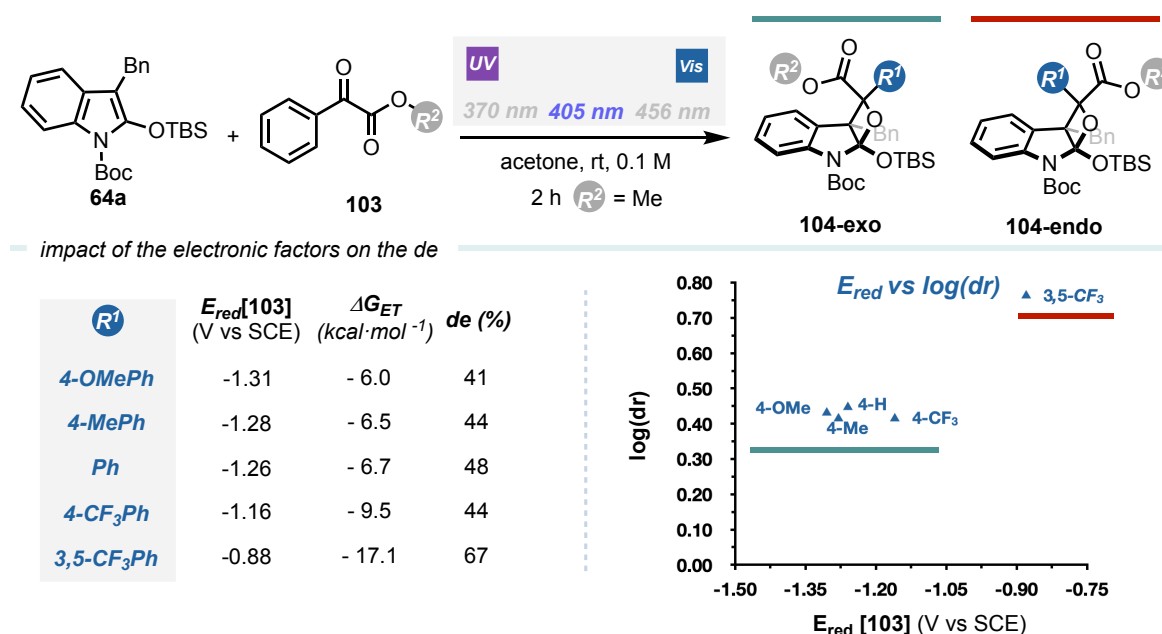
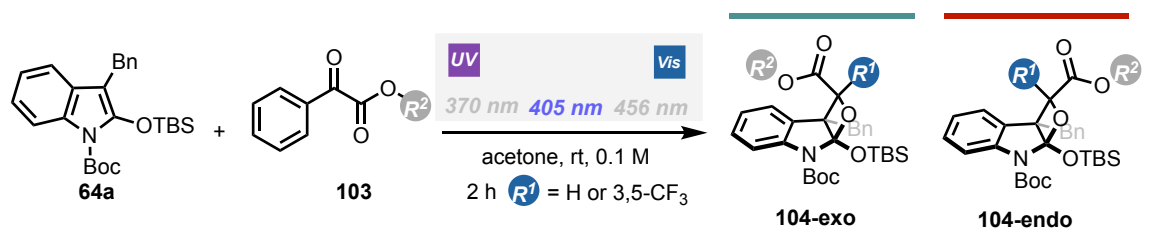


Table 2.11. - Effect of electronic factors on the diastereoselectivity of the reaction between **14a** and **103**.

Thereafter, we investigated the role of the steric factors tuning the R^2 group within the α -ketoester **103** (Table 2.12). In this case, a Charton analysis allowed us to compare the sensitivities (ψ) of the two different manifolds (EDA complex vs exciplex).⁵⁵ When increasing the R^2 bulkiness (from Me to Cy), the *endo/exo* selectivity is reversed passing from 48% to -12% *de* in the case of R^1 =Ph (exciplex manifold), and from 67% to -7% *de* in the case of R^1 = 3,5-CF₃Ph (EDA complex manifold). The observed trend can be rationalized by means of an increased steric repulsion between the R^2 and the OTBS group of the indole, favoring the perpendicular approach. Nevertheless, the EDA complex manifold experiences a 1.5 higher sensitivity (ψ = -1.51 vs ψ = -2.23 for the exciplex and EDA manifolds, respectively), in agreement with a higher dependence of the parallel approach towards steric variations.

⁵⁵ For examples of the application of the Charton analysis see: **a)** Sigman, M. S.; Miller, J. J. Examination of the Role of Taft-Type Steric Parameters in Asymmetric Catalysis. *J. Org. Chem.* **2009**, *74*, 7633–7643. **b)** Harper, K. C.; Bess, E. N.; Sigman, M. S. Multidimensional Steric Parameters in the Analysis of Asymmetric Catalytic Reactions. *Nature Chem* **2012**, *4*, 366–374.



— impact of sterics on the de

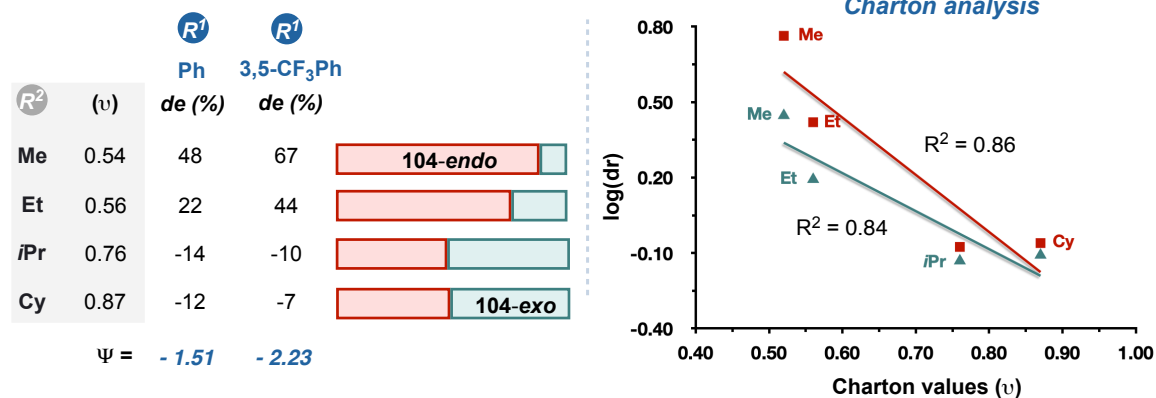


Table 2.12. - Effect of steric factors on the diastereoselectivity of the reaction between **64a** and **103**.

We finally sought to capitalize this valuable information to deliberately alter the diastereoselective outcome of the PB process by acting on the stereoelectronic factors and without changing the light-source.⁵⁶ In order to do so, we decided to run the reaction under 405 nm irradiation. The choice of using a visible-light source was crucial, allowing the activity of both the exciplex and the EDA-complex pathway (Figure 2.38).

— diastereoselectivity inversion

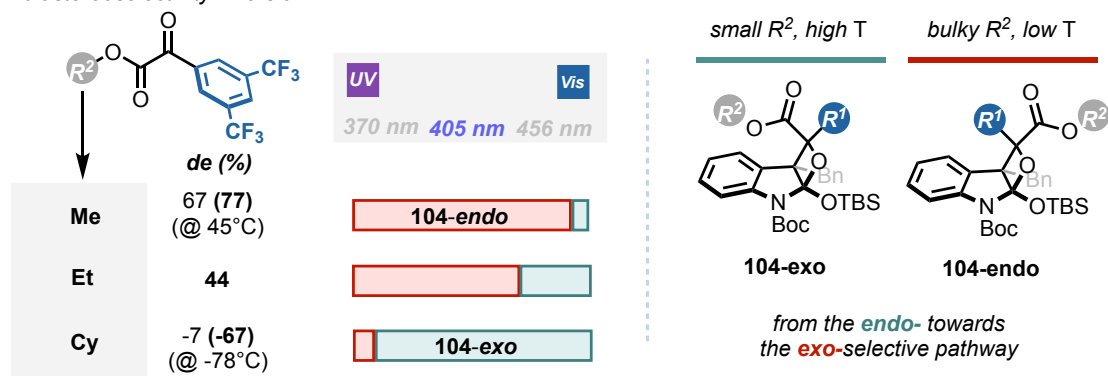


Figure 2.37. - Inversion of the diastereoselectivity by tuning the steric and electronic factors of the α -ketoester.

⁵⁶ The use of more selective light sources such as lasers would probably result in even more selective reaction pathways. However, over all the experiments we have decided to use cheaper and readily available light sources (Kessil lamp, LEDs), increasing the reproducibility of the reactions and their utilization for synthetic purposes.

We thus selected the 3,5-CF₃Ph α -ketoester **103** being the only substrate showing a clear CT band with **64a**. In this case we observed an initial *de* of 67% in favor of the *endo* product. Interestingly, running the reaction at higher temperature (45°C), the *de* was enhanced to 77%.^{43, 54} When passing from R¹ = Me, to R¹ = Et the *de* decreased to 44%. Remarkably, when using the bulkier Cy substituent, the *de* was inverted up to -7% and further magnified to -67% when lowering the temperature (-78°C).^{43, 54} We were thus able to isolate and characterized also the elusive *exo*-isomer of oxetane **104** in synthetically useful yield (58%). These results demonstrate the importance of the proper light-source selection in PB processes to unlock the activity of alternative reaction manifolds. Moreover, we further confirmed the generality of the developed models to rationally gain control over the reaction outcome by acting on the stereoelectronic parameters.

Limitations

The model described in this section resulted to have high fidelity on the diastereoselectivity prediction when indole and 1,2-diketones or α -ketoesters were used. However, few limitations were observed when using different systems (Figure 2.38).

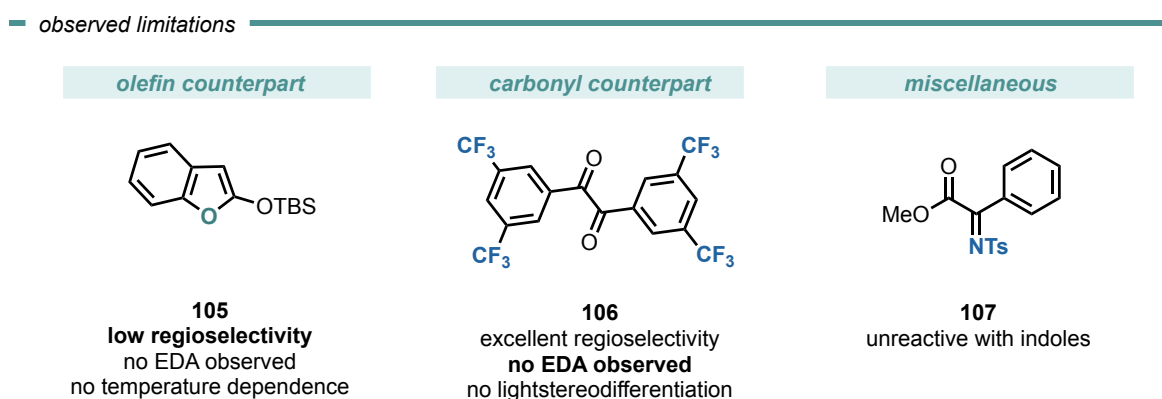


Figure 2.38. - Limitations of the diastereoselectivity prediction model.

i) Diverse bicyclic scaffolds such as benzofuran-derived SEE **105** were tested. In this case, low regioselectivity was observed. Surprisingly, no EDA complex was observed at room temperature with acetone despite being electron-richer than the *N*-Boc protected indole derivative. For these two reasons, all the attempts to tune the diastereoselectivity while changing diverse reaction parameters failed.

ii) When substituting benzil with diverse groups, such as 3,5-CF₃ moieties in both electronic rings **106**, the reaction performed well in excellent regioselectivities. Nevertheless, no EDA complex was observed at room temperature in acetone despite being electron-poorer than **18b**. Thus, no light stereodifferentiation was observed in this case.

iii) When using tosylimines **107**, known to generate exciplexes with electron-rich olefins (in aza-Paternò-Büchi reactions), **no reaction was observed**.⁵⁷ Thus, limiting our model to carbonyl compounds.

2.3.5 Conclusions

In conclusion, we have developed new models for the diastereoselectivity prediction of PB processes of indoles and aromatic ketones. These models are based on the study of the reaction mechanism and photodynamics, analyzed by UV-Vis, LFP-experiments and supported by DFT calculations. With a rational approach, we have revealed the competent role of an EDA complex manifold that can channel the reactivity towards the unconventional *exo*-selectivity. The often-overlooked effect of the light-source variation was exploited to the development of new light-stereodifferentiation reactions (*de* from >98 to 4%). On the other hand, the careful modulation of the stereoelectronic parameters of the starting ketone allows access to unprecedented diastereoinversion events under visible-light irradiation (*de* from 77 to -67%). Our study demonstrates how the fine mechanistic understanding of light-driven processes can increase their synthetic potential, opening the way to previously inaccessible structural targets.

⁵⁷ Given the lack of reactivity, this observation could be ascribed to the limitations of Chapter II – Section 2. Nevertheless, the importance of this reagents in exciplex-type manifolds make such compounds an important case of study in mechanistic investigations. For a recent example of exciplex-type reactivity in aza-Paternò-Büchi reactions see: Sakamoto, R.; Inada, T.; Sakurai, S.; Maruoka, K. [2 + 2] Photocycloadditions between the Carbon–Nitrogen Double Bonds of Imines and Carbon–Carbon Double Bonds. *Org. Lett.* **2016**, *18*, 6252–6255.

2.3.6. Experimental Section

Light sources: The used light sources used in this work are the following and were purchased from Kessil and Amazon webpages.

- **370 nm:** Kessil lamp **PR160L-370 (43W)**
(<https://www.kessil.com/science/PR160L.php>)
- **405 nm:** JUNERAIN lamp 2nn5lm2af5sx9vw4D02 **(6W)**
(<https://www.amazon.it/JUNERAIN-Lampada-fotopolimerizzante-Stampante-fotosensibile/dp/B07KJH2ZPK>)
- **427 nm:** Kessil lamp **PR160L-427 (45W)**
(<https://www.kessil.com/science/PR160L.php>)
- **456 nm:** Kessil lamp **PR160L-456 (50W)**
(<https://www.kessil.com/science/PR160L.php>)

NMR experiments: NMR spectra were recorded on Bruker 400 Avance III HD equipped with a BBI-z grad probe head 5mm and Bruker 500 Avance III equipped with a BBI-ATM-z grad probehead 5mm. The chemical shifts (δ) for ^1H and ^{13}C are given in ppm relative to residual signals of the solvents (CHCl_3 @ 7.26 ppm ^1H NMR, 77.16 ppm ^{13}C NMR). Coupling constants are given in Hz. The following abbreviations are used to indicate the multiplicity: s, singlet; d, doublet; t, triplet; q, quartet; m, multiplet; bs, broad signal. NMR yields were calculated by using trichloroethylene as internal standard.

High-Resolution Mass Spectra (HRMS): were obtained using Waters GCT gas chromatograph coupled with a time-of-flight mass spectrometer (GC/MS-TOF) with electron ionization (EI).

Chromatographic purification of products was accomplished using flash chromatography on silica gel (SiO_2 , 0.04-0.063 mm) purchased from Machery-Nagel, with the indicated solvent system according to the standard techniques. Thin-layer chromatography (TLC) analysis was performed on pre-coated Merck TLC plates (silica gel 60 GF254, 0.25 mm). Visualization of the developed chromatography was performed by checking UV absorbance (254nm) as well as with aqueous ceric ammonium molybdate and potassium permanganate solutions. Organic solutions were concentrated under reduced pressure on a Büchi rotary evaporator.

Time dependent density functional calculations (TD-DFT) were used to support the attribution of transient absorption signals. TD-DFT were performed at the B3LYP/6-311+g(d,p) level of theory, including a polarizable continuum model in solvent (acetone). Frequencies were calculated in order to ensure that the species are actual relative minima of energy

Density functional calculations (DFT) were used to model the geometry of EDA and exciplex complexes between carbonyl compounds and indoles. In this case, calculations were performed at the M06-2X/6-311++ level of theory, where the functional includes dispersion corrections that allow a proper description of charge-transfer complexes. Frequencies were calculated in order to ensure that the species are actual relative minima of energy.

Steady-state absorption spectroscopy: the studies have been performed at room temperature on a Varian Cary 5000 UV-Vis double beam spectrophotometer; 300 μm path length Hellma Analytics quartz cuvettes have been used.

Steady-state fluorescence spectra: room-temperature luminescence measurements were recorded on a Varian Cary Eclipse Fluorescence spectrometer, while emission spectra at 77 K were measured using an Edinburgh instrument spectrofluorometer equipped with a cryostat; 10 mm path length Hellma Analytics 117.100F QS quartz cuvettes were used.

Electrochemical characterizations: were carried out in acetonitrile (MeCN)/0.1 M tetrabutylammonium hexafluorophosphate (TBAPF₆) at room temperature, on an Autolab 302N electrochemical workstation (Metrohm, The Netherlands) in a glass cell. A typical three-electrode cell was employed, which was composed of glassy carbon (GC) working electrode (3 mm diameter), a platinum wire as counter electrode and a saturated calomel electrode (SCE) as reference electrode (RE). Oxygen was removed by purging the MeCN solution with high-purity Nitrogen. The potential of ferrocenium/ferrocene (Fc/Fc⁺) couple was measured and found to be 0.45 V vs SCE, in agreement with the value reported in literature (in MeCN).⁵⁸ The GC electrode was polished before any measurement with diamond paste and ultrasonically rinsed with deionized water for 15 minutes. The electrode was electrochemically activated in the background solution by means of several voltammetric cycles at 100 mV/s between the anodic and cathodic solvent/electrolyte discharges.

Nanosecond laser flash photolysis: Nanosecond transient measurements were performed with a custom laser spectrometer comprised of a *Continuum Surelite II* Nd:YAG laser (FWHM 6-8 ns) with frequency tripled (355 nm) option, an *Applied Photophysics* xenon light source including a mod. 720 150 W lamp housing, a mod. 620 power-controlled lamp supply and a mod. 03 –102 arc lamp pulser. Laser excitation was provided at 90° with respect to the white light probe beam. Light transmitted by the sample was focused onto the entrance slit of a 300 mm focal length *Acton SpectraPro 2300i* triple grating, flat field, double exit monochromator equipped with a photomultiplier detector (*Hamamatsu R3896*) and a *Princeton Instruments PIMAX II* gated intensified CCD camera, using an *RB Gen II* intensifier, a ST133 controller and a PTG pulser. Signals from the photomultiplier (kinetic

⁵⁸ Lewandowski, A.; Waligora, L.; Galinski, M. Ferrocene as a Reference Redox Couple for Aprotic Ionic Liquids. *Electroanalysis* **2009**, *21*, 2221–2227.

traces) were processed by means of a *TeledyneLeCroy 604Zi* (400 MHz, 20 GS/s) digital oscilloscope. Transient absorption measurements were performed on argon-purged solutions using quartz cuvettes with 2-mm path length. These cuvettes were put in the sample holder at a 45° geometry with respect to both excitation and analysis beams.

Materials: Commercial grade reagents and solvents were purchased at the highest commercial quality from Sigma Aldrich or FluoroChem and used as received, unless otherwise stated. Benzophenone **18a**, benzil **18b**, 3,3'-bis(trifluoromethyl)benzophenone **18d**, methylphenyl glyoxylate **103** – H and ethyl benzoylformate **103** – H – Et were purchased from Sigma-Aldrich and used as received.

Light-sources emission spectra

The light emission spectra of Kessil lamps can be found at: <https://www.kessil.com/science/PR160L.php>

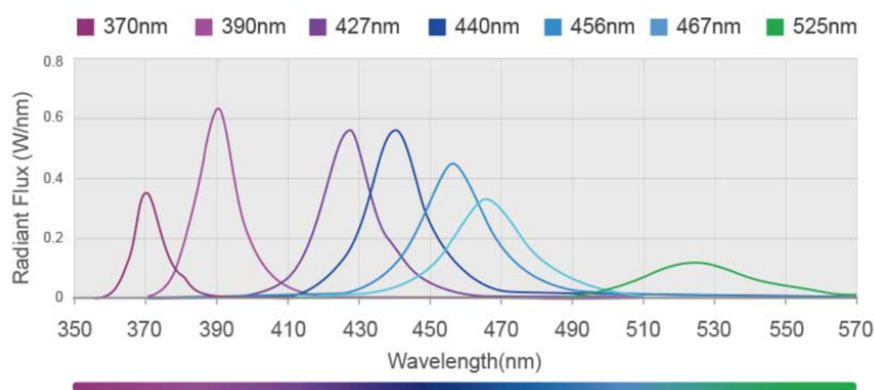


Figure 2.39. - Emission spectra of Kessil PR160L lamps, obtained from: <https://www.kessil.com/science/PR160L.php>

The light emission spectra of JUNERAIN lamp 2nn5lm2af5sx9vw4D02 was recorded by an AvaSpec ULS3648 high-resolution fiber-optic spectrometer which was placed at a fixed distance of 0.5 cm from the light source.

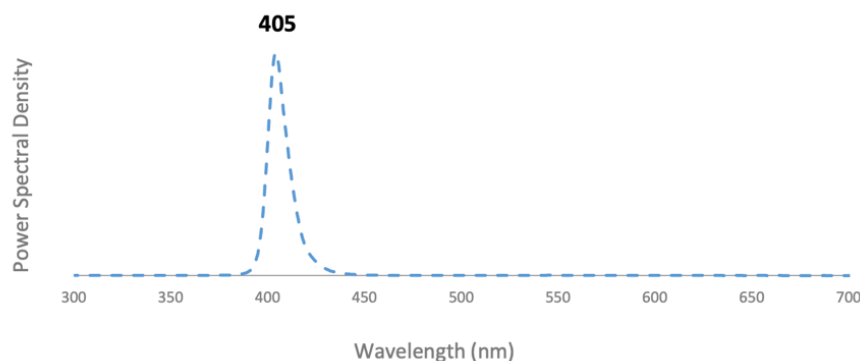
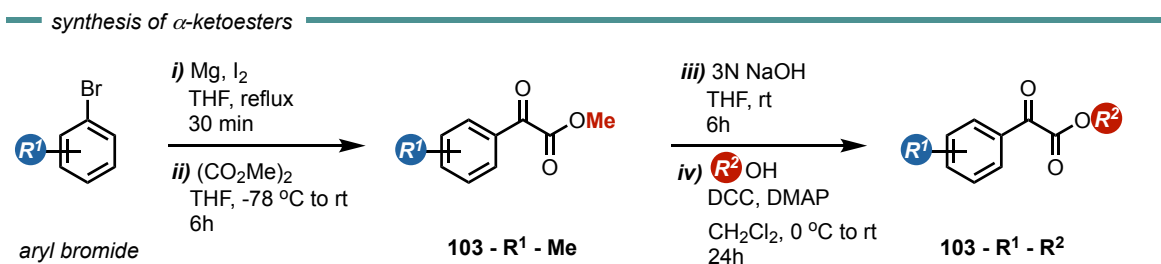


Figure 2.40. - Emission spectra of the 405 nm (JUNERAIN lamp) used in this study.

General Synthetic Procedures for the Synthesis of Starting Materials



α -Ketoester derivatives **103** were prepared following a modified procedure reported in literature.⁵⁹

First step: Magnesium turnings (11.0 mmol, 1.1 equiv.) were heated for 10 min in a three neck round flask with condenser and dropping funnel. After cooling to room temperature, THF (20 mL) was added followed by I₂ (0.01 mmol, 0.01 equiv.). The corresponding aryl bromide (10 mmol, 1.0 equiv.) dissolved in THF (10 mL, 1M) was added dropwise and heated to reflux for 30 min.

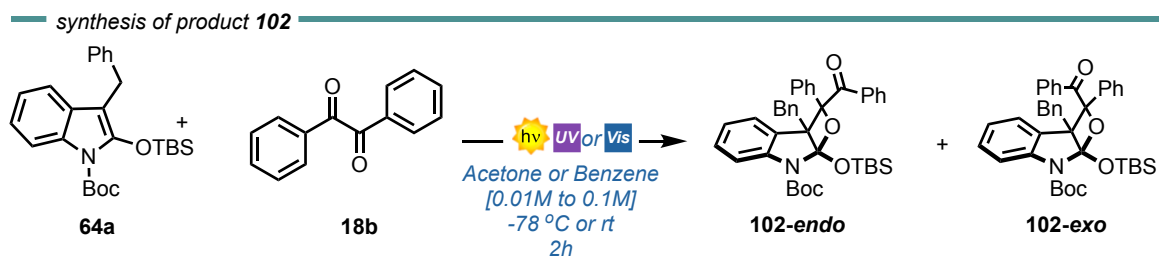
Second step: The Grignard reagent was added over 1 h to a solution of dimethyl oxalate (10.0 mmol, 1.0 equiv.) in THF (10 mL) at -78 °C. After 1 h at -78 °C, the reaction mixture was warmed to 0 °C. The mixture was quenched with aqueous saturated NH₄Cl, extracted with Et₂O, washed with brine and dried over MgSO₄. The combined organic layer was filtered and the solvent evaporated at reduced pressure. The crude product was purified by flash column chromatography (Hexane/AcOEt = 20/1 to 10/1) to afford pure methyl substituted α -ketoester derivatives **103 - R¹ - Me**.

Third step: **103 - R¹ - Me** (5 mmol, 1.0 equiv.) was hydrolyzed with 3N NaOH in THF:H₂O (1:1 ratio, 50 mL) at reflux for 6 h. The solution was cooled down to room temperature and THF was evaporated at reduced pressure. The aqueous residue was cooled to 0 °C and acidified with 6N HCl. Then, extracted with 3x50 mL of EtOAc. The combined organic layers were washed with brine and dried over MgSO₄. The solvent was filtered and reevaporated at reduced pressure to afford crude glyoxylic acid derivatives as brown solids.

Fourth step: In a round-bottom flask, crude glyoxylic acid derivatives (1.4 mmol, 1.0 equiv.) were dissolved in CH₂Cl₂ (4 mL). Then, DMAP (0.14 mmol, 0.1 equiv.) and the corresponding alcohol (R²OH, 2.1 mmol, 1.5 equiv.) were added. The reaction mixture was cooled to 0 °C and dicyclohexylcarbodiimide (DCC, 1.5 mmol, 1.1 equiv.) was added portionwise at this temperature. After 1h, the reaction was allowed to warm up to room temperature and stirred for 23h. After full consumption of the starting material (monitored by

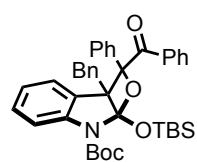
⁵⁹ Shirai, T.; Ito, H.; Yamamoto, Y. Cationic Ir/Me-BIPAM-Catalyzed Asymmetric Intramolecular Direct Hydroarylation of α -Ketoamides. *Angew. Chem. Int. Ed.* **2014**, *53*, 2658–2661.

TLC) The suspension was filtered through Celite and washed with brine (3x15 mL). The combined organic layers were filtered and evaporated under reduced pressure. The crude product was purified by flash column chromatography (Hexane/AcOEt = 20/1 to 10/1) to afford pure R² substituted α -ketoester derivatives **103** – **R¹** – **R²**.



In a 4 mL vial, the indole **64a** (0.05 mmol, 1.0 equiv.) and **18b** (0.05 mmol, 1.0 equiv.) were added. The two reagents were dissolved in acetone-d₆ (0.5 mL, 0.1 M) and the reaction mixture was bubbled with argon for one minute. Then, CH₂Br₂ was added (0.1 mmol, 2.0 equiv.) as the internal standard. The vial was placed in front of the selected light source and irradiated for 2 hours. The reaction crude was then transferred to an NMR tube and the ¹H NMR spectra was recorded.

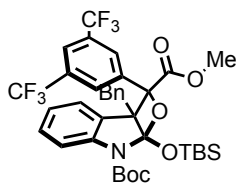
tert-butyl-2-benzoyl-2a-benzyl-7a-((tert-butyl(dimethylsilyloxy)oxy)-2-phenyl-2a,7a-dihydrooxeto[2,3-*b*]indole-7(2*H*)-carboxylate (102-endo**).**



¹H-NMR (500 MHz, Acetone-d₆): δ 7.96 (d, J = 8.0 Hz, 2H, Ar), 7.62 (t, J = 7.8 Hz, 1H, Ar), 7.55 – 7.49 (m, 3H, Ar), 7.19—7.11 (m, 5H, Ar), 7.06—7.01 (m, 3H, Ar), 6.96 (t, J = 8.4 Hz, 1H, Ar), 6.78 (t, J = 8.1 Hz, 2H, Ar), 6.51 (t, J = 8.0 Hz, 1H, Ar), 4.13 (d, J = 14.9 Hz, 1H, CH₂a), 3.58 (d, J = 14.9 Hz, 1H, CH₂b), 1.68 (s, 9H, C(CH₃)₃), 0.69 (s, 9H, SiC(CH₃)₃), 0.29 (s, 3H, SiCH₃), -0.13 (s, 3H, SiCH₃) ppm. ¹³C-NMR (125 MHz, Acetone-d₆): δ 198.9, 150.3, 143.2, 137.5, 137.2, 135.5, 133.2, 129.8, 129.7, 129.6, 129.3, 128.2, 127.9, 127.7, 127.6, 127.5, 127.2, 125.9, 125.6, 125.6, 121.7, 113.9, 113.8, 90.3, 81.9, 67.3, 34.2, 31.7, 27.7, 25.5, 18.0, -3.2 ppm. HRMS calculated for C₄₀H₄₅NO₅Si+Na, 670.2964; found, 670.3045.

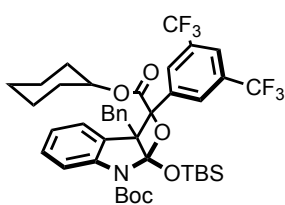
*The same procedure was used for the synthesis of products **104***

7-(*tert*-butyl) 2-methyl-2a-benzyl-2-(3,5-bis(trifluoromethyl)phenyl)-7a-((*tert*-butyldimethylsilyl)oxy)-2a,7a-dihydrooxeto[2,3-*b*]indole-2,7(2H)-dicarboxylate (104-*endo*).



¹H-NMR (500 MHz, Acetone-*d*₆): δ 8.58 (s, 2H, Ar), 8.20 (s, 1H, Ar), 7.55 (d, *J* = 8.4 Hz, 1H, Ar), 7.22 – 7.17 (m, 2H, Ar), 7.04–6.98 (m, 5H, Ar), 6.84 (t, *J* = 8.0 Hz, 1H, Ar), 3.46 (d, *J* = 14.9 Hz, 1H, CH₂a), 3.25 (s, 3H, COOCH₃), 3.02 (d, *J* = 14.9 Hz, 1H, CH₂b), 1.72 (s, 9H, C(CH₃)₃), 0.75 (s, 9H, SiC(CH₃)₃), 0.54 (s, 3H, SiCH₃), 0.41 (s, 3H, SiCH₃) ppm. **¹³C-NMR (125 MHz, Acetone-*d*₆):** δ 168.9, 150.7, 143.8, 139.0, 136.1, 131.2, 130.8, 129.6, 129.4, 129.0, 128.1, 128.0, 127.6, 126.6, 126.4, 125.9, 122.2, 114.8, 114.0, 86.1, 82.3, 64.5, 52.0, 34.1, 31.4, 27.8, 27.3, 25.4, 22.4, 18.3, -2.9, -3.3 ppm. **¹⁹F-NMR (188 MHz, Acetone-*d*₆):** δ -63.55 ppm. **HRMS** calculated for C₃₇H₄₁F₆NO₆Si+Na, 760.2505; found, 760.2756.

7-(*tert*-butyl) 2-cyclohexyl-2a-benzyl-2-(3,5-bis(trifluoromethyl)phenyl)-7a-((*tert*-butyldimethylsilyl)oxy)-2a,7a-dihydrooxeto[2,3-*b*]indole-2,7(2H)-dicarboxylate (104-*exo*).



¹H-NMR (500 MHz, Acetone-*d*₆): δ 8.04 (s, 2H, Ar), 8.77 (s, 1H, Ar), 7.21 (d, *J* = 8.4 Hz, 1H, Ar), 7.16 (d, *J* = 8.0 Hz, 1H, Ar), 7.08 (t, *J* = 7.9 Hz, 2H, Ar), 7.04 – 6.99 (m, 2H, Ar), 6.86–6.81 (m, 1H, Ar), 6.57 (t, *J* = 8.0 Hz, 1H, Ar), 5.06–4.99 (m, 1H, CHCy), 4.03 (d, *J* = 14.9 Hz, 1H, CH₂a), 3.86 (d, *J* = 14.9 Hz, 1H, CH₂b), 1.64 (s, 9H, C(CH₃)₃), 1.61–1.26 (m, 9H, CHCy), 0.88 (s, 9H, SiC(CH₃)₃), 0.67 (s, 3H, SiCH₃), 0.41 (s, 3H, SiCH₃) ppm. **¹³C-NMR (125 MHz, Acetone-*d*₆):** δ 167.5, 145.0, 142.9, 140.5, 136.5, 130.3, 129.8, 128.7, 127.8, 127.2, 126.0, 126.0, 125.7, 124.7, 121.9, 113.9, 82.4, 75.7, 65.8, 33.3, 31.3, 31.1, 27.5, 25.8, 25.0, 23.4, 23.3, 18.2, -2.7, -2.8 ppm. **¹⁹F-NMR (188 MHz, Acetone-*d*₆):** δ -63.83 ppm. **HRMS** calculated for C₄₂H₄₉F₆NO₆Si+Na +Na, 828.3131; found, 828.3402.



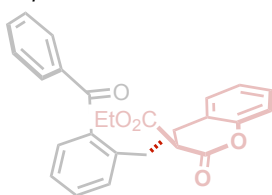
Chapter III

Synthetic Transformations Driven by Triplet State *o*-Alkyl Substituted Benzophenones

Chapter III - Synthetic Transformations Driven by Triplet State *o*-Alkyl Substituted Benzophenones

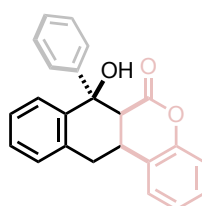
Section 1.

A microfluidic photoreactor enables 2-methylbenzophenone light-driven reactions with superior performances



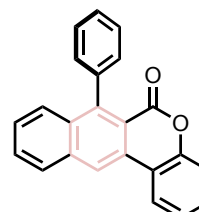
Section 2.

Microfluidic light-driven synthesis of tetracyclic molecular architectures



Section 3.

Synthesis and characterization of naphthochromenones as new potential organic photocatalysts



Goals:

- Development of simple microfluidic photoreactors that enable 2-methylbenzophenone reactivity with superior performances
- To exploit the utilization of this type of microfluidic photoreactors for the construction of tetracyclic architectures
- To study, characterize and perform the large-scale synthesis of the products obtained from the reaction between 2-methylbenzophenone and coumarin derivatives

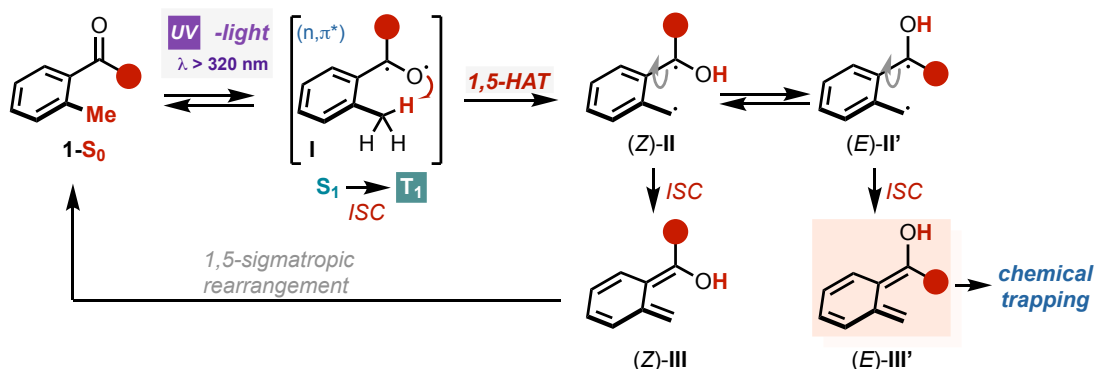
Publications:

- Section 1:** Mateos, J.; Cherubini-Celli, A.; Carofiglio, T.; Bonchio, M.; Marino, N.; Companyó, X.; Dell'Amico, L. A Microfluidic Photoreactor Enables 2-Methylbenzophenone Light-Driven Reactions with Superior Performance. *Chem. Commun.* **2018**, 54, 6820–6823.
- Section 2:** Mateos, J.; Meneghini, N.; Bonchio, M.; Marino, N.; Carofiglio, T.; Companyó, X.; Dell'Amico, L. Microfluidic Light-Driven Synthesis of Tetracyclic Molecular Architectures. *Beilstein J. Org. Chem.* **2018**, 14, 2418–2424.
- Section 3:** Mateos, J.; Rigodanza, F.; Vega-Peñaloza, A.; Sartorel, A.; Natali, M.; Bortolato, T.; Pelosi, G.; Companyó, X.; Bonchio, M.; Dell'Amico, L. Naphthochromenones: Organic Bimodal Photocatalysts Engaging in Both Oxidative and Reductive Quenching Processes. *Angew. Chem. Int. Ed.* **2020**, 59, 1302–1312.

3. The photoenolization process

In contrast with the photoreactivity of benzophenone described in the previous chapter, the light-excitation of *ortho*-alkyl substituted aryl ketones (**1-S₀**, Figure 3.1a) triggers the rapid formation of highly reactive hydroxy-*ortho*-quinodimethanes (**III'**).¹ These intermediates are also known as *photoenols*. Since the discovery of this photochemical process in 1961,² diverse independent studies have characterized all the transient species leading to **III'**.³

A. The photoenolization process - 1961 Yang and Rivas



B. The reactivity of the photoenol **III'**

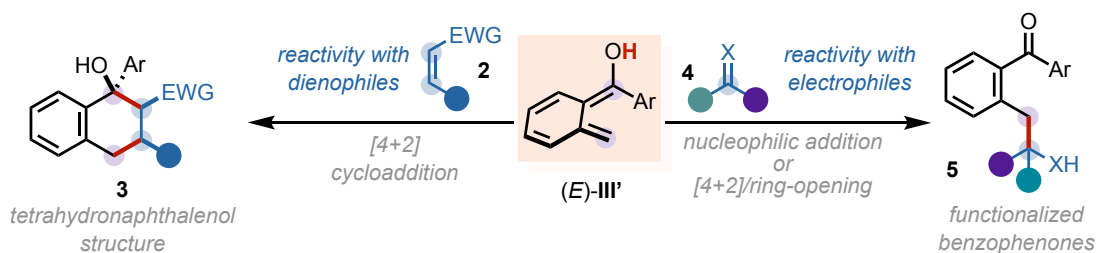


Figure 3.1. - Light-triggered 2-alkylbenzophenones reactivity. a) The photoenolization process. b) Reactivity with dienophiles and electrophiles.

¹ Sammes, P. G. Photoenolisation. *Tetrahedron* **1976**, 32, 405–422.

² Yang, N. C.; Rivas, C. A New Photochemical Primary Process, the Photochemical Enolization of *o*-Substituted Benzophenones. *J. Am. Chem. Soc.* **1961**, 83, 2213–2213.

³ a) Zwicker, E. F.; Grossweiner, L. I.; Yang, N. C. The Role of $n \rightarrow \pi^*$ Triplet in the Photochemical Enolization of *o*-Benzylbenzophenone. *J. Am. Chem. Soc.* **1963**, 85, 2671–2672. b) Huffman, K. R.; Loy, M.; Ullman, E. F. Photoenolization of Some Photochromic Ketones. The Scope and Mechanism of the Reaction. *J. Am. Chem. Soc.* **1965**, 87, 5417–5423. c) Porter, G.; Tchir, M. F. Flash Photolysis of an *Ortho*-Alkyl-Benzophenone. *J. Chem. Soc. D* **1970**, 20, 1372. d) Lutz, H.; Br  h  ret, E.; Lindqvist, L. Photoenolization of *Ortho*-Methyl-Substituted Acetophenones: Solvent Effects on the Triplet State Reactivity. *J. Chem. Soc., Faraday Trans. 1* **1973**, 69, 2096–2102. e) Wagner, P. J.; Chen, C. P. A Rotation-Controlled Excited-State Reaction. The Photoenolization of *Ortho* Alkyl Phenyl Ketones. *J. Am. Chem. Soc.* **1976**, 98, 239–241. f) Scaiano, J. C. Laser Flash Photolysis Studies of the Reactions of Some 1,4-Biradicals. *Acc. Chem. Res.* **1982**, 15, 252–258. g) Netto-Ferreira, J. C.; Wintgens, V.; Scaiano, J. C. Laser Flash Photolysis Study of the Photoenols Generated from *Ortho*-Benzylbenzophenone in Different Solvents. *Can. J. Chem.* **1994**, 72 (6), 1565–1569. h) Suzuki, T.; Omori, T.; Ichimura, T. Excited-State Reaction of Short-Lived 2-Methylbenzophenone Enols Studied by Stepwise Two-Color Excitation Time-Resolved Thermal Lensing Technique. *J. Phys. Chem. A* **2000**, 104, 11671–11676.

The mechanism of photoenolization is initiated by the absorption of a photon by the carbonyl group in **1**, producing an electronically excited singlet state **1^{*}-S₁**. This state is generally of $n\pi^*$ character and rapidly decays to a triplet $n\pi^*$ state (**1^{*}-T₁**) by an ISC process. Then, the half-filled $n\pi$ orbital of **1^{*}-T₁** state is prone to undergo a 1,5-HAT from the C-H σ -orbital, leading to the formation of the conjugated 1,4-biradical (*Z*)-**II** (Norrish-type II reactivity). This latter species is in fast equilibrium with its conformer (*E*)-**II**, and both can relax to the corresponding ground state (*Z*)-**III'** and (*E*)-**III'** enols through a second ISC process. While the (*Z*)-**III'** returns faster to the starting ketone **1** through an intramolecular 1,5-sigmatropic rearrangement, the (*E*)-**III'** enol requires an intermolecular proton transfer mediated by a molecule of acid or solvent. This fact confers a higher lifetime to the (*E*)-**1'** photoenol ($\tau = 1 \cdot 10^{-6}$ s),¹ thus being the principal species involved in subsequent chemical trapping events.⁴

The reactive photoenol (*E*)-**III'** has been traditionally exploited as diene in [4+2]-cycloaddition reactions with dienophiles **2**, giving access to biologically relevant tetrahydronaphthalenol derivatives **3** (Figure 3.2b, left pathway).⁵ More recently, it has been disclosed that the use of other type of electrophiles **4**, such as α,β -unsaturated carbonyl compounds,⁶ activated imines,⁷ α -fluoroketones⁸ or CO₂,⁹ can lead to the exclusive formation of functionalized benzophenones **45** (Figure 3.1b, right pathway).¹⁰ Overall, the photoenolization process enables the straightforward access to a versatile intermediate (**1'**)

⁴ Klán, P.; Wirz, J.; Gudmundsdottir, A. *Photoenolization and its Applications*, CRC Handbook of Organic Photochemistry and Photobiology, ed. A. Griesbeck, CRC Press, United States, 3rd edn, **2012**, ch. 26, pp. 627–652

⁵ **a)** Nicolaou, K. C.; Gray, D.; Tae, J. *Total Synthesis of Hamigerans: Part 1. Development of Synthetic Technology for the Construction of Benzannulated Polycyclic Systems by the Intramolecular Trapping of Photogenerated Hydroxy-*o*-quinodimethanes and Synthesis of Key Building Blocks*. *Angew. Chem., Int. Ed.*, **2001**, *40*, 3675–3679. **b)** *Total Synthesis of Hamigerans: Part 2. Implementation of the Intramolecular Diels–Alder Trapping of Photochemically Generated Hydroxy-*o*-quinodimethanes; Strategy and Completion of the Synthesis*, *Angew. Chem. Int. Ed.*, **2001**, *40*, 3679–3683.

⁶ **a)** Dell'Amico, L.; Fernández-Alvarez, V. M.; Maseras, F.; Melchiorre, P. *Light-Driven Enantioselective Organocatalytic β -Benzoylation of Enals*. *Angew. Chem. Int. Ed.* **2017**, *56*, 3304–3308. **b)** Paria, S.; Carletti, E.; Marcon, M.; Cherubini-Celli, A.; Mazzanti, A.; Rancan, M.; Dell'Amico, L.; Bonchio, M.; Companyó, X. *Light-Triggered Catalytic Asymmetric Allylic Benzoylation with Photogenerated C-Nucleophiles*. *J. Org. Chem.* **2020**, *85*, 4463–4474

⁷ Hepburn, H.; Magagnano, G.; Melchiorre, P. *Light-Triggered Enantioselective Organocatalytic Mannich-Type Reaction*. *Synthesis* **2016**, *49*, 76–86.

⁸ Cuadros, S.; Dell'Amico, L.; Melchiorre, P. *Forging Fluorine-Containing Quaternary Stereocenters by a Light-Driven Organocatalytic Aldol Desymmetrization Process*. *Angew. Chem. Int. Ed.* **2017**, *56*, 11875–11879.

⁹ Masuda, Y.; Ishida, N.; Murakami, M. *Light-Driven Carboxylation of *o*-Alkylphenyl Ketones with CO₂*. *J. Am. Chem. Soc.* **2015**, *137*, 14063–14066.

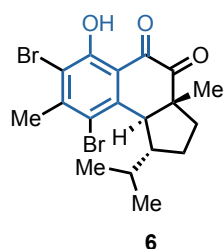
¹⁰ Cuadros, S.; Melchiorre, P. *Organocatalytic Strategies to Stereoselectively Trap Photochemically Generated Hydroxy-*o*-Quinodimethanes*: *Eur. J. Org. Chem.* **2018**, *2018*, 2884–2891.

that can be exploited in alternative synthetic scenarios, including natural product synthesis⁵, macromolecule linkage¹¹ or polymer chemistry (Figure 3.2).¹²

— Photoenols in natural product synthesis, macromolecule linkage and polymer chemistry

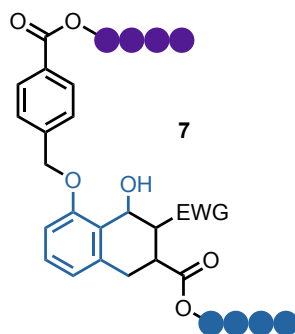
Natural product synthesis

5-epi-4-bromohamigeran B
moderate cytotoxicity against
P-388 leukemia cells



Macromolecule linkage

Linkage of polymers



Polymerization

Ligation of RAFT polymers
photo-conjugation of dithiobenzoate
end-capped polymer

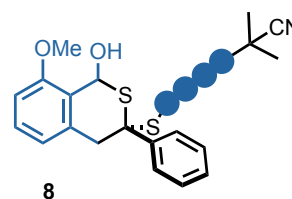


Figure 3.2. - Applications of the photoenol intermediate in natural product synthesis, macromolecule synthesis and polymer chemistry.

¹¹ Hildebrandt, K.; Elies, K.; D'hooge, D. R.; Blinco, J. P.; Barner-Kowollik, C. A Light-Activated Reaction Manifold. *J. Am. Chem. Soc.* **2016**, 138, 7048–7054.

¹² Oehlenschlaeger, K. K.; Mueller, J. O.; Heine, N. B.; Glassner, M.; Guimard, N. K.; Delaitre, G.; Schmidt, F. G.; Barner-Kowollik, C. Light-Induced Modular Ligation of Conventional RAFT Polymers. *Angew. Chem. Int. Ed.* **2013**, 52, 762–766.

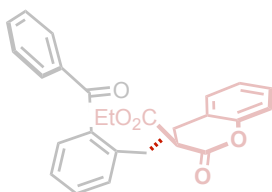
Chapter III – Section 1

Microfluidic Photoreactors – Unveiling the Superior Performances of 2- Methylbenzophenone Light-Driven Reactions

— Chapter III - Synthetic Transformations Driven by Triplet State *o*-Alkyl Substituted Benzophenones —

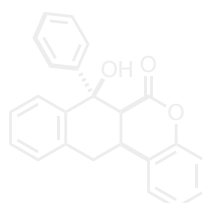
Section 1.

A microfluidic photoreactor enables 2-methylbenzophenone light-driven reactions with superior performances



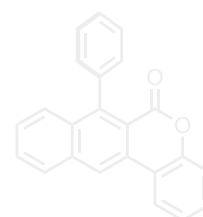
Section 2.

Microfluidic light-driven synthesis of tetracyclic molecular architectures



Section 3.

Synthesis and characterization of naphthochromenones as new potential organic photocatalysts



- To develop of novel and versatile microfluidic photoreactors
- To study the performance of 2-methylbenzophenone photoreactions with previously known reaction partners as well as with new challenging substrates.¹³

¹³ The project discussed in this section has been conducted in collaboration with Dr Alessio Cherubini-Celli (involved in the synthesis and characterization the coumarin-derived products as well as in the quantum yield measurments), Dr Xavier Companyó (involved in the photostability studies and the reaction kinetics) and Prof. Tommaso Carofiglio (involved in the design of the photoreactor). I individually optimized the reaction conditions for the seven different reactions described in this section as well as I performed the reaction kinetics, photophysical studies and prepared several entries of the reaction scope.

This work has been published: Mateos, J.; Cherubini-Celli, A.; Carofiglio, T.; Bonchio, M.; Marino, N.; Companyó, X.; Dell'Amico, L. A Microfluidic Photoreactor Enables 2-Methylbenzophenone Light-Driven Reactions with Superior Performance. *Chem. Commun.* **2018**, 54, 6820–6823.

3.1.1 Introduction

As discussed also in the previous chapter, synthetic photochemistry has recently emerged as a key enabling technology for the construction of complex molecular architectures (e.g. oxeto-indolinic polycycles) using light as a green energy source.¹⁴ By exploiting the unprecedented reactivity of organic molecules, an increased number of synthetic strategies paved the way towards unexplored reaction pathways.¹⁵ In this scenario, the implementation of novel technologies such as microfluidic photoreactors (MFP) served as an invaluable ally to reach the main goal of a synthetic chemist: the development of unprecedented reactions in high yields and efficiencies. This decisive potential is directly related to the disadvantages of photochemical batch protocols (Figure 3.3 and *Chapter I, section II*).¹⁶ MFPs have a definite advantage considering: *i*) the enhanced surface-to-volume ratio; *ii*) uniform irradiation and increased light penetration depth; *iii*) short diffusion distance for efficient mass and photon transfer; *iv*) favorable heat dissipation and gas–liquid interfacial areas; and *v*) synthetic up-scaling by continuous flow parallelization.¹⁷ Thus, MFP likely impact both the reaction kinetics and the selectivity of the transformations, deactivating undesired pathways and avoiding common overirradiation issues.^{16,17}

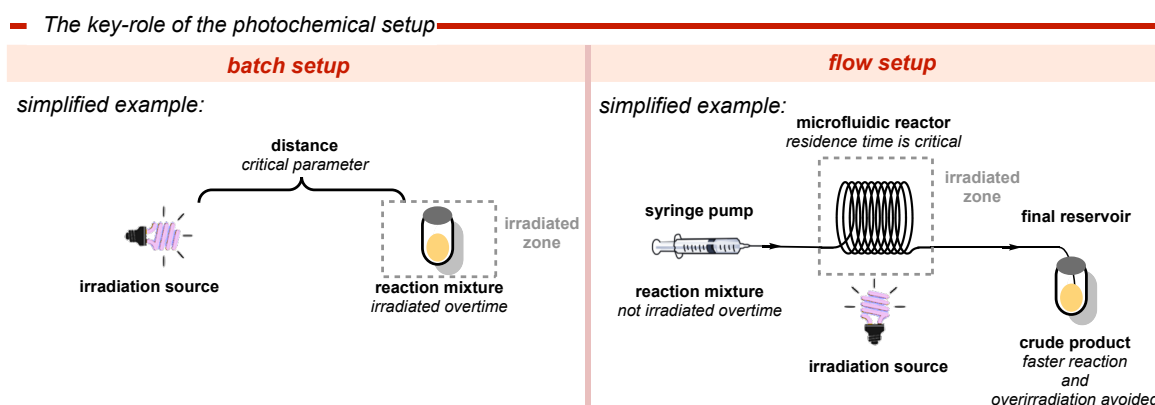


Figure 3.3. - The key-role of the photochemical setup. Simplified graphical representations of batch (left) and flow (right) protocol.

¹⁴ For a recent review on the topic see: Ravelli, D.; Protti, S.; Fagnoni, M. *Carbon–Carbon Bond Forming Reactions via Photogenerated Intermediates*. *Chem. Rev.* **2016**, *116*, 9850–9913.

¹⁵ Fagnoni, M.; Dondi, D.; Ravelli, D.; Albini, A. *Photocatalysis for the Formation of the C–C Bond*. *Chem. Rev.* **2007**, *107*, 2725–2756.

¹⁶ Plutschack, M. B.; Pieber, B.; Gilmore, K.; Seeberger, P. H. *The Hitchhiker’s Guide to Flow Chemistry*. *Chem. Rev.* **2017**, *117*, 11796–11893.

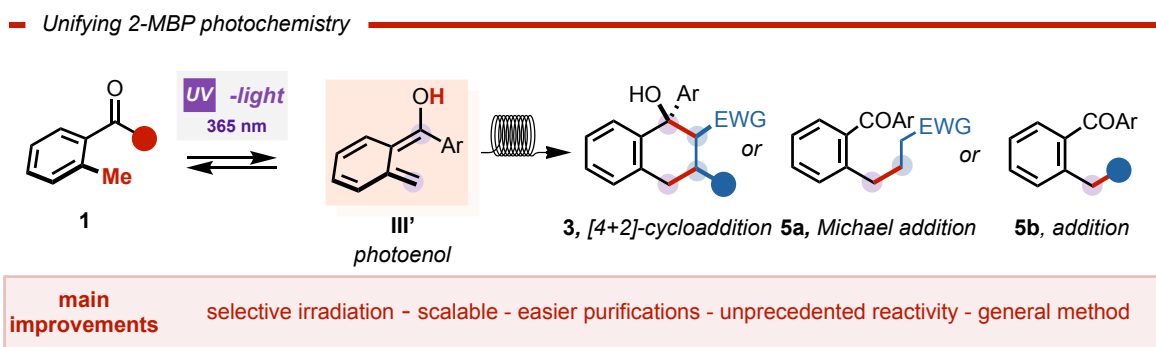
¹⁷ Cambié, D.; Bottecchia, C.; Straathof, N. J. W.; Hessel, V.; Noël, T. *Applications of Continuous-Flow Photochemistry in Organic Synthesis, Material Science, and Water Treatment*. *Chem. Rev.* **2016**, *116*, 10276–10341.

3.1.2 Challenges of the project

Despite the significant efforts devoted to the photochemistry of 2-methylbenzophenone (2-MBP), a unifying and general synthetic platform was not available. This fact precluded the facile discovery of light-driven transformations where the *photoenol* was involved. In addition, the lack of reproducibility of this type of chemistry impeded the implementation of these transformation in lab-scale and to a further extent to industrial-scale transformations. The main challenge of this section targets the development of a simple MFP setup for 2-MBP photoreactions.

3.1.3 Section overview

Herein, I report how 2-MBP light-driven reactions proceed within a MFP setup leading to higher production rates when compared to the conventional batch protocols (Scheme 3.1). Additionally, outstanding product selectivity is obtained. This strategy serves as a simple junction protocol for the previous 2-MBP photoreaction methods which used a myriad of dangerous and expensive light-sources. Interestingly, this unification strategy also enhanced the synthetic potential of *photoenols*, engaging in previously unexplored reactions with coumarin derivatives, advancing the state-of-the-art synthetic scope and overtaking batch setups.



Scheme 3.1. - General method for the application of 2-MBP photochemistry described in this section

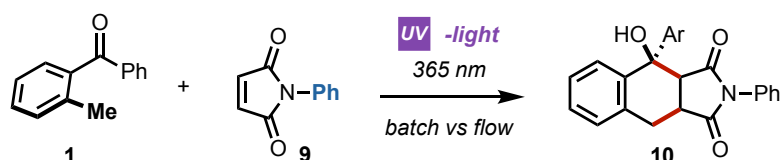
3.1.4 Results and discussion

Optimization of the microfluidic photoreactor

Initially, the MFP was designed by screening the performance of a benchmark reaction. For this reason, we chose the classical [4+2]-photocycloaddition reaction between 2-MBP **1** and *N*-phenylmaleimide **9**, furnishing the tetrahydronaphthalenol scaffold **10** (Figure 3.4a). After testing different setups and light sources, two home-made reactors were selected to

optimize the reaction outcome that was further compared with the performance of a common batch protocol at room temperature (Figure 3.4b, A). The first flow reactor (Figure 3.4b, B), consisted of a 3D-printed reactor with 12x365 nm LEDs of 3W and a PTFE tubing with a total volume of 400 μ L. The second (Figure 3.4b, C), consisted of a 9W 365 nm bulb with a wrapped PTFE tubing with a total volume of 400 μ L.

A. [4+2]-cycloaddition reaction



B. reaction setups

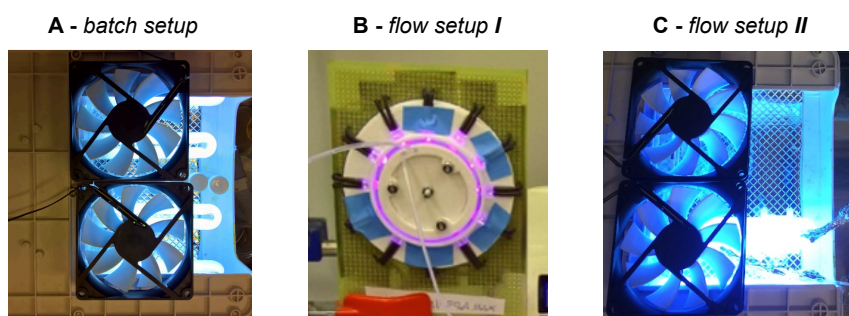
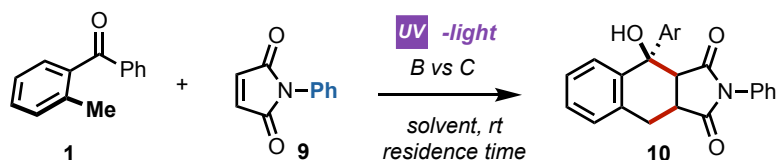


Figure 3.4. - Benchmarking the protocol. a) [4+2]-cycloaddition reaction between 2-MBP and *N*-phenylmaleimide. b) Reaction setups used in this section.

As depicted in Table 3.1, the benchmark reaction was optimized by screening different reaction conditions. The solvent combined with the equivalents of 9 and the reactor choice resulted to be pivotal for an excellent reaction outcome.



entry	reactor	equivalents (9)	solvent	residence time (min)	conversion (%)	yield % (10)
1	B	10	PhMe	80	>99	94
2	B	10	PhMe	8	20	-
3	B	2	PhMe	80	>99	95
4	B	1	PhMe	80	>99	95
5	C	1	PhMe	10	>99	>98
6	C	1	PhCl	10	93	89
7	C	1	DMSO	10	89	86

Table 3.1. - Initial optimization of the benchmark reaction.

Altogether, allowed us to reduce the reaction time to 10 minutes, yielding **10** as a single diastereoisomer in quantitative yields and high purities after simple solvent removal.

This optimization procedure allowed us to compare the productivity of the reaction when irradiated in batch conditions. Interestingly, reactor A furnished **10** in 95% yield after 480 minutes. This encouraging result clashed with the even better result obtained when using flow conditions (reactors B and C). Figure 3.5, clearly shows that despite obtaining **10** in excellent yields in all the cases, the MFP system C produces the tetrahydronaphthalenol product in higher rates. Hence, the different performances of the photochemical protocols are highlighted by the relative productivity rates ($\text{mmol}\cdot\text{h}^{-1}$)¹⁸ whereby the MFP C system outcompetes the conventional photoreactor A by a 20-fold enhancement (0.012 vs 0.240 $\text{mmol}\cdot\text{h}^{-1}$).

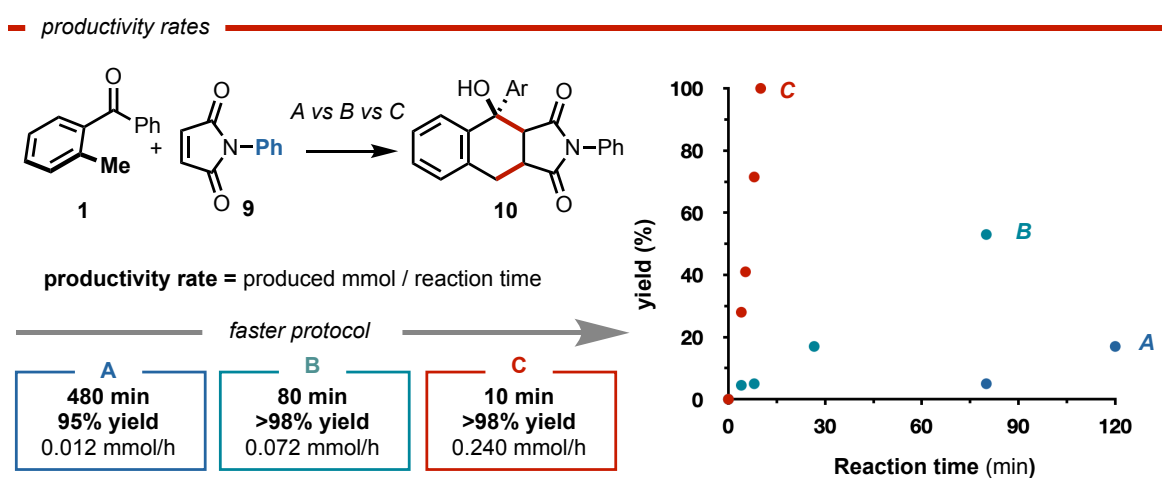


Figure 3.5. - Comparison of productivity rates between the three different setups discussed in this section.

Application of the MFP to previously developed systems

Having a powerful but simple MFP in hand, we screened diverse transformations previously developed and compared the productivity rates (Table 3.2). The aim of this process was to unify all the methods in terms of light sources and reaction setups, avoiding all the reproducibility issues associated with the use of special protocols. We thus selected different reaction partners, exploiting the reaction manifolds 2-MBP offers. For this reason, three [4+2]-cycloaddition reactions (Table 3.2, A, B and C) and two nucleophilic additions (Table 3.2, D and E) were tested.

¹⁸ For an example of the use of space-time-yield metrics for the evaluation of MFP see: Meyer, S.; Tietze, D.; Rau, S.; Schäfer, B.; Kreisel, G. *Photosensitized Oxidation of Citronellol in Microreactors. Journal of Photochemistry and Photobiology A: Chemistry* **2007**, *186*, 248–253.

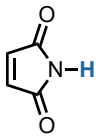
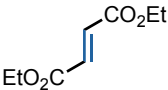

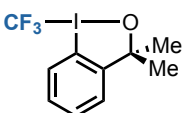

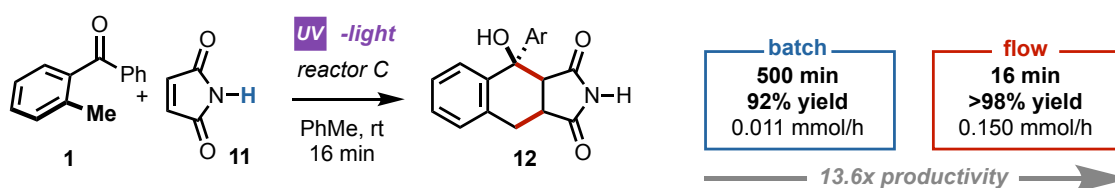
reaction partner	reaction conditions	irradiation source	yield (%)	productivity rate (mmol·h ⁻¹)
A  <i>Angew. Chem. Int. Ed.</i> , 2016 , <i>55</i> , 3313.	Solvent: CyH/PhMe (1mL) Conc.: 0.1 M Reaction time: 24 h 3 equiv. of 1 used	Single black LED plate (365 nm)	72	0.003
B  <i>J. Chem. Soc. Perkin Trans.</i> 1973 , <i>1</i> , 308.	Solvent: PhH (120 mL) Conc.: 0.17 M Reaction time: 24 h	Hanovia 8A-1 high-pressure Hg lamp	58	0.493
C  <i>Can. J. Chem.</i> , 1995 , <i>73</i> , 1454	Solvent: PhH Conc.: not given Reaction time: 2 h 1.7 equiv. of 1 used	450 W Hanovia medium-pressure Hg lamp	82	nd
D  <i>Org. Lett.</i> , 2017 , <i>19</i> , 4452	Solvent: DMSO (1mL) Conc.: 0.03 M Reaction time: 1 h 3 equiv. of 1 used	Reylon LED lamp (3W 365 nm)	98	0.029
E  <i>JACS</i> , 2015 , <i>137</i> , 14063	Solvent: DMSO (1mL) Conc.: 0.04 M Reaction time: 2 h 1 atm. of CO ₂ used	CCS, 8332AAC8361 (lamp composed by 100x365 nm LEDs)	89	0.089

Table 3.2. - Selected transformations previously reported with 2-MBP and different reaction conditions.

When using unprotected maleimide **11** (Scheme 3.2), it turned to be less reactive than the *N*-Ph counterpart **9**. Nevertheless, product **12** was obtained in quantitative yield (>98%) after 16 minutes (0.150 mmol·h⁻¹), outcompeting the corresponding batch control reaction in a 13.6-time folded productivity. The classical protocol showed full conversion after 500 minutes (92% isolated yield, 0.011 mmol·h⁻¹).

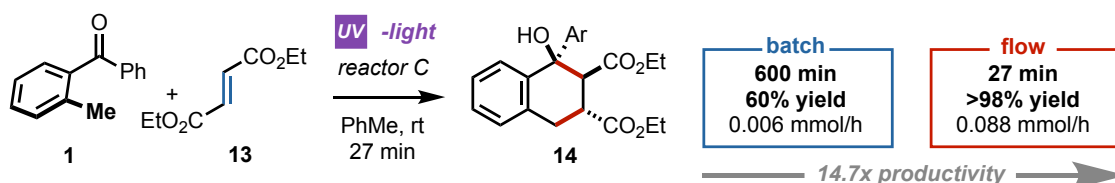
— productivity rate comparison —



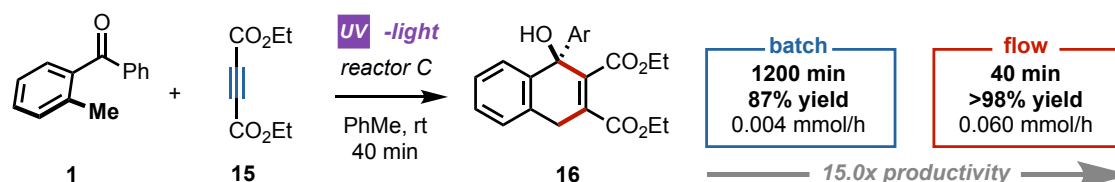
Scheme 3.2. - Productivity rates when using **11**.

Quantitative transformations were also obtained with acyclic trans-diethyl fumarate **13** and diethyl acetylenedicarboxylate **15** (Scheme 3.3). The desired benzannulated products **14** and **16** were formed in excellent yields (>98%) and rates of production (0.088 and 0.060 mmol·h⁻¹, respectively). Meanwhile, the performances of the batch reactions were again remarkably lower, forming the corresponding products in 60% and 87% yields, respectively (0.006 mmol·h⁻¹ for **14** and 0.004 mmol·h⁻¹ for **16**).

A. productivity rates comparison



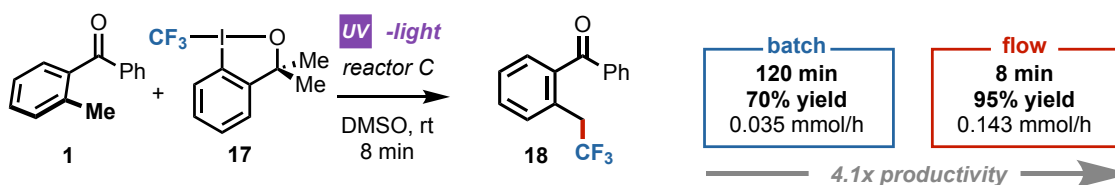
B. productivity rates comparison



Scheme 3.3. - Productivity rates when using a) **13** and b) **15**.

Photo-assisted trifluoromethylation of 2-MBP provided a further synthetic paragon.¹⁹ Under MFP conditions, using the commercially available Togni's reagent I **17**,²⁰ **18** was obtained in 8 minutes (95% yield) with a production rate of 0.143 mmol·h⁻¹ (Scheme 3.4), thus registering a consistent 4-times folded improvement in terms of productivity with respect to the batch control reaction (in 0.035 mmol·h⁻¹ in Table 3.2).

productivity rate comparison

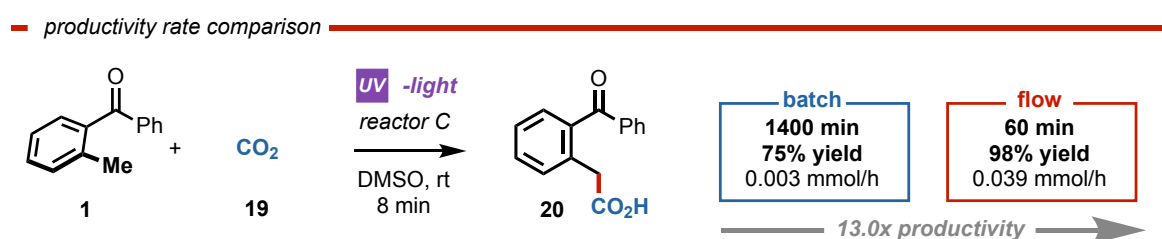


Scheme 3.4. - Productivity rates when using **17**.

¹⁹ Ide, T.; Masuda, S.; Kawato, Y.; Egami, H.; Hamashima, Y. *Benzyl C–H Trifluoromethylation via Photoenol*. *Org. Lett.* **2017**, *19*, 4452–4455.

²⁰ Charpentier, J.; Früh, N.; Togni, A. *Electrophilic Trifluoromethylation by Use of Hypervalent Iodine Reagents*. *Chem. Rev.* **2015**, *115*, 650–682.

It is noteworthy that the MFP setup was also effective for the light-driven carboxylation of 2-MBP with CO₂ **19**.⁹ In the original work, a very energetic light source was required (Table 3.2). Under the present MFP setup, using the simpler 9 W 365 nm bulb the carboxylated benzophenone **20** was obtained in excellent yield (98%) with a productivity rate as good as 0.039 mmol·h⁻¹ (Scheme 3.5). It should be noted that pure **20** was isolated after a simple extraction work-up, making this transformation appealing for large-scale continuous-flow production. On the other hand, the batch reaction furnished **20** in 75% yield, with a poor productivity rate (0.003 mmol·h⁻¹).



Scheme 3.5. - Productivity rates when using CO₂.

Reactivity with challenging substrates

In order to expand the scope of the 2-MBP photochemistry in flow, we decided to use challenging light-absorbing reagents. In this regard, the developed MFP platform turned out to be excellent for coumarin functionalization. Coumarins²¹ and chromanones²² are biologically active compounds with a distinctive photochemistry, as many widely used as organic dyes embody the coumarin scaffold. Indeed, the selective addition of 2-MBP **1** to coumarins represent an innovative entry for the direct assembly of benzylated chromanones. However, photo-excitation of coumarins **21** ($\lambda > 320$ nm) is known to promote self [2+2]-cycloaddition reaction, yielding cyclobutanes **22** generally formed as a complex mixture of regio- and stereoisomers (Figure 3.6).²³

²¹ On the natural importance of coumarins and chromanones: a) Kontogiorgis, C. A.; Hadjipavlou-Litina, D. J. Synthesis and Antiinflammatory Activity of Coumarin Derivatives. *J. Med. Chem.* **2005**, *48*, 6400–6408. b) Medina, F. G.; Marrero, J. G.; Macías-Alonso, M.; González, M. C.; Córdova-Guerrero, I.; Teissier García, A. G.; Osegueda-Robles, S. Coumarin Heterocyclic Derivatives: Chemical Synthesis and Biological Activity. *Nat. Prod. Rep.* **2015**, *32*, 1472–1507.

²² Feng, L.; Maddox, M. M.; Alam, Md. Z.; Tsutsumi, L. S.; Narula, G.; Bruhn, D. F.; Wu, X.; Sandhaus, S.; Lee, R. B.; Simmons, C. J.; Tse-Dinh, Y.-C.; Hurdle, J. G.; Lee, R. E.; Sun, D. Synthesis, Structure–Activity Relationship Studies, and Antibacterial Evaluation of 4-Chromanones and Chalcones, as Well as Olympicin A and Derivatives. *J. Med. Chem.* **2014**, *57*, 8398–8420.

²³ Wolff, T.; Görner, H. Photodimerization of Coumarin Revisited: Effects of Solvent Polarity on the Triplet Reactivity and Product Pattern. *Phys. Chem. Chem. Phys.* **2004**, *6*, 368–376.

- why coumarins are challenging substrates?

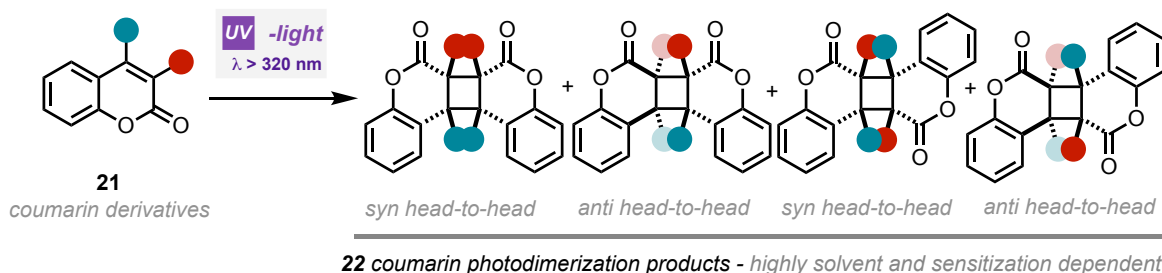


Figure 3.6. - Coumarin photodimerization products under UV-light irradiation.

As shown in Figure 3.7, the absorption of ethyl-3-coumarincarboxylate **23** and 2-methylbenzophenone **1** overlap at 0.1M concentrations. Therefore, the irradiation at 365 nm will favor the [2+2]-cycloaddition of **23**, precluding the intended Michael-type addition reaction in synthetically useful yields.

- reaction mixture absorption

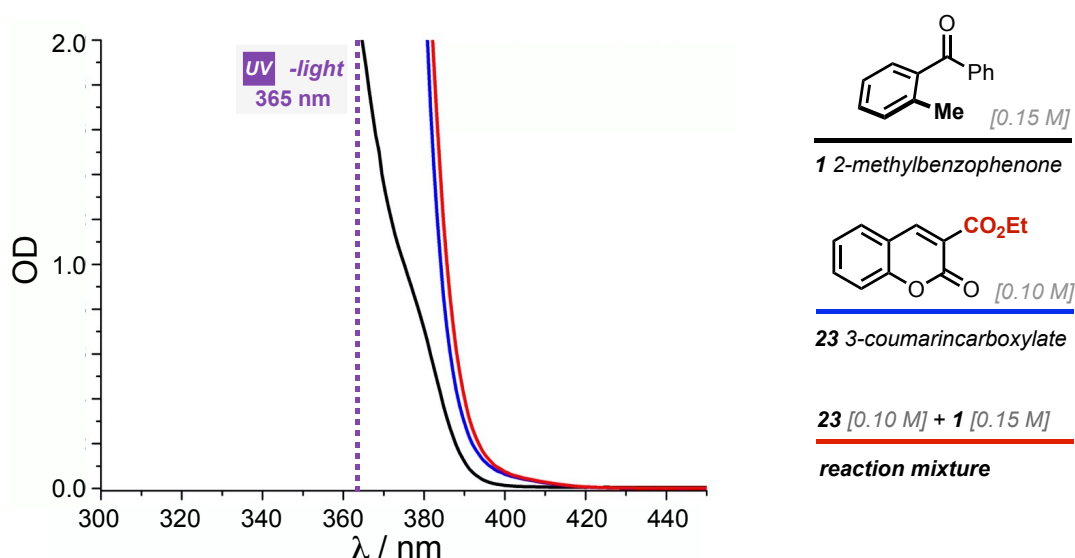
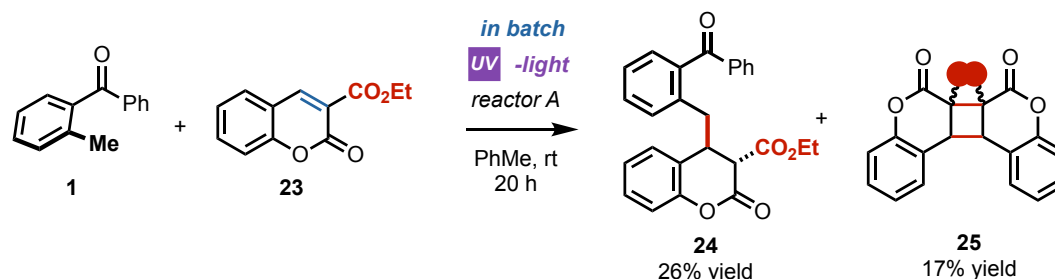
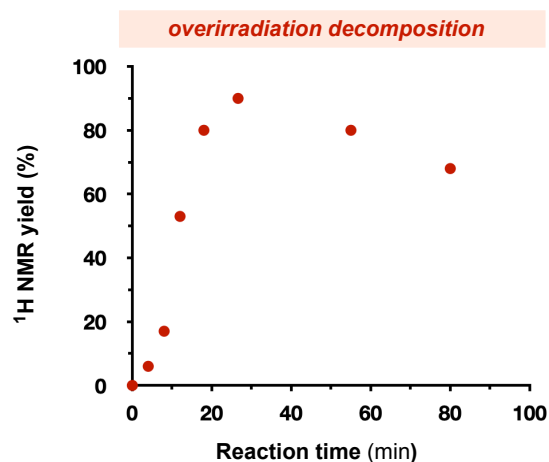
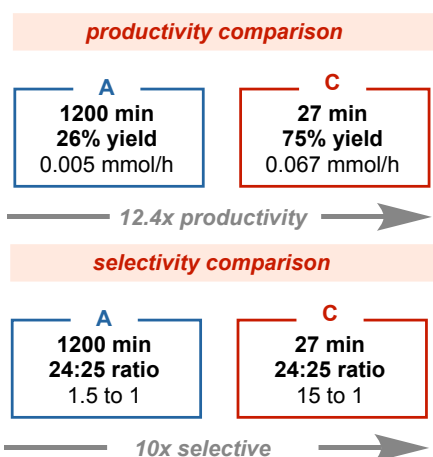
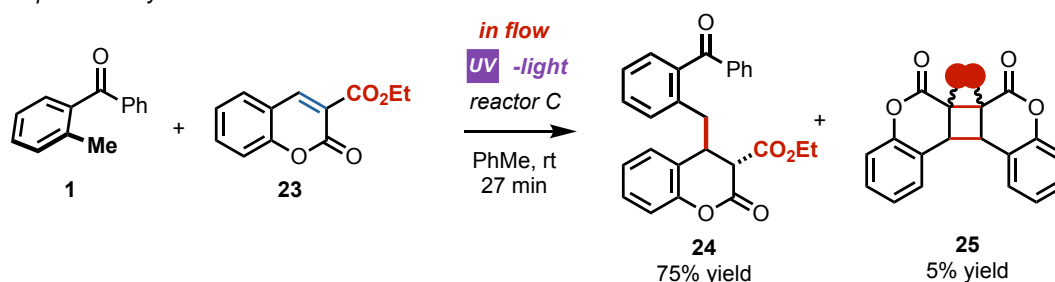


Figure 3.7. - Absorption of the reaction mixture containing **1** and **23**.

To our delight, within the MFP setup, irradiation of a reaction mixture containing 1.5 equivalents of **1** and coumarin **23** yielded the unprecedented 4-benzylated chromanone **24** in 75% yield (Figure 3.8a). Remarkably, only 5% of the photo-dimerization side product **25** was formed. Thus, showing a 15 to 1 ratio of **24** over **25**. Additionally, the reaction kinetics showed a decrease of **24** for when the reaction mixture was kept for longer periods of irradiation. This experimental fact highlights the importance of the residence time selection due to the presence of the diaryl ketone moiety in **24** which decomposes overtime when irradiated. For this reason, when the same reaction is performed in batch, it furnishes **24** in a decreased 26% yield along with 17% of **25** (Figure 3.8b). This comparison allow us to conclude that MFP protocols allow

the development of previously inaccessible transformations in 12.4-times folded productivity rates and 10-time folded selectivities when compared with batch reaction setups.²⁴

A. photo-benylation of coumarins in flow



B. photo-benylation of coumarins in batch

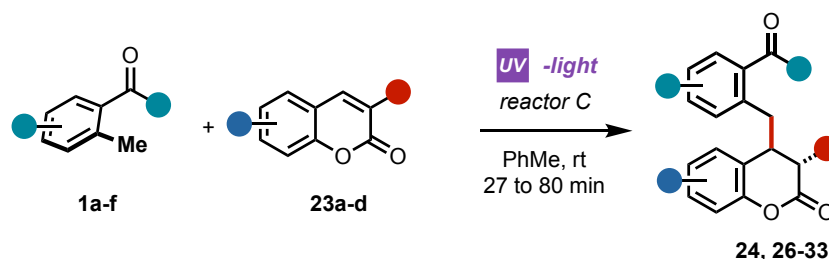
Figure 3.8. - Photo-benylation reaction in a) flow conditions; and b) batch conditions. Evidence of a higher production rate and a higher selectivity due to overirradiation issues.

Generality of the method

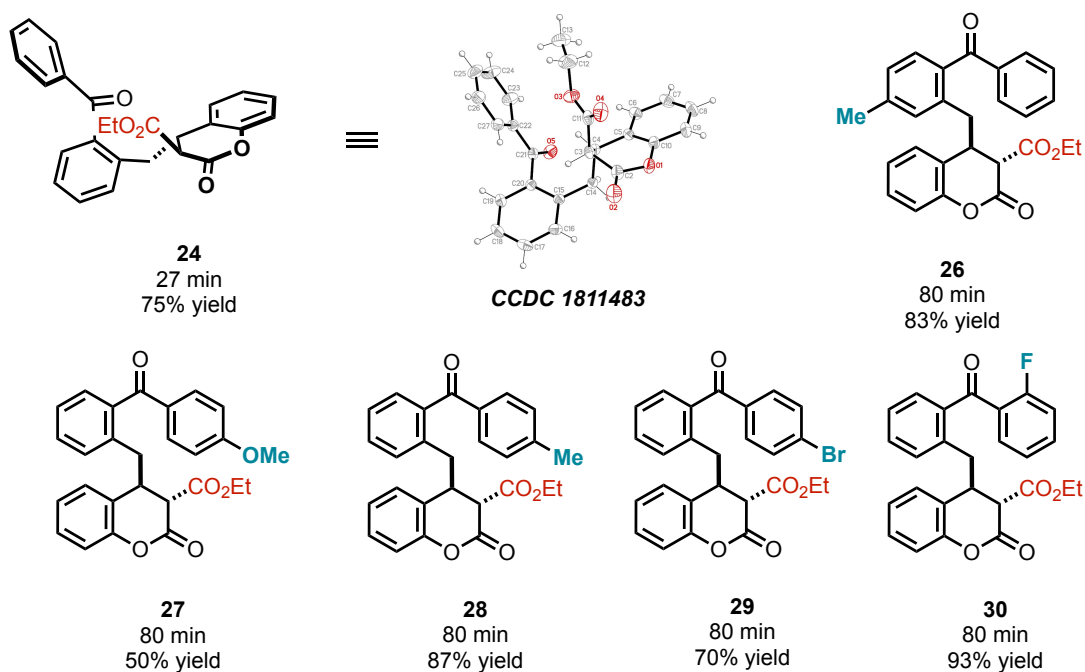
The generality of the microfluidic photo-benylation reaction of coumarins was subsequently assessed by varying the substitution pattern on both aromatic rings of 2-MBP as

²⁴ Under MFP conditions, cyclobutene **25** does not reversibly decompose to coumarin **23**. Control experiments rule out a direct addition of photoenol **III'** to cyclobutane **25**.

well as on the coumarin scaffold (Table 3.3). Electron-donating and electron-withdrawing substituents were well tolerated, affording the corresponding benzylated chromanones **26–33** with yields in the range of 50–93% and complete diastereocontrol.



— 2-methylbenzophenone scope



— coumarin scope

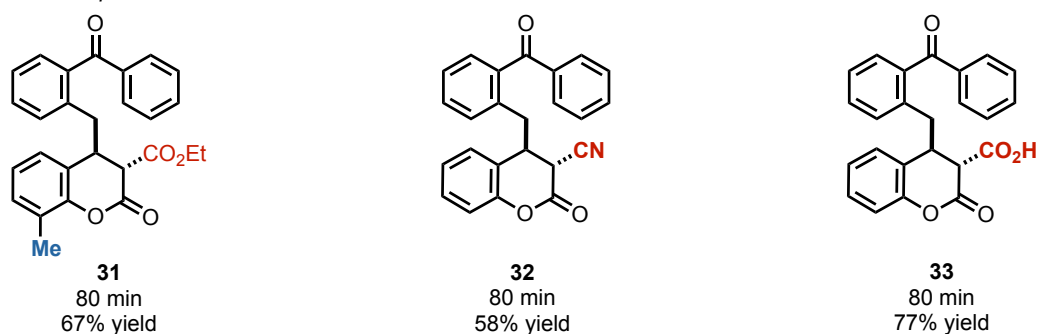


Table 3.3. - Substrate scope of the photo-benzylation reaction.

The use of different coumarin scaffolds was also evaluated. 8-Methylcoumarin performed smoothly, leading to product **31** in 67% yield. Interestingly, products **32** and **33** were obtained from 3-cyanocoumarin and coumarin-3-carboxylic acid in 58% and 77%

yields, respectively, in 80 min albeit with diverse distereocontrol (4 : 1 dr for **32** and >20 : 1 dr for **33**).

Reasons behind the enhanced performances

In order to gain insight into the reasons behind the enhanced performances of reactor C, the photon flow of both setups (A and C) were measured using 2-nitrobenzaldehyde **34** as a chemical actinometer (Figure 3.9).²⁵ Indeed, the UV-light mediated isomerization of **34**, yielding 2-nitrosobenzoic acid **35** in a $\phi=0.5 \text{ mol} \cdot \text{Einstein}^{-1}$ at 365 nm, allowed us to quantify the photon flux by measuring the pH of the system at different times. Hence, the registered photon flux density under the MFP setup protocol C (L_{MFP}), outcompetes by 20 times the value obtained for the batch setup A (L_{B}).²⁶

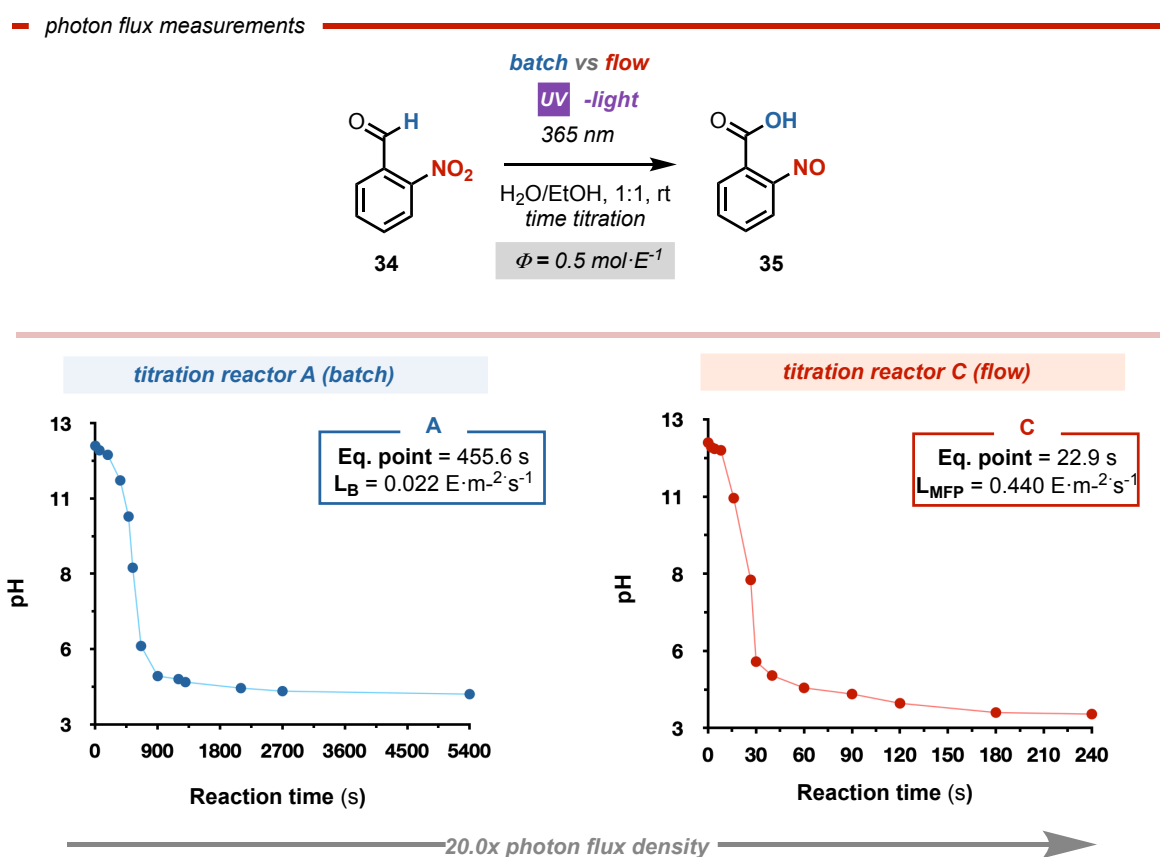



Figure 3.9. - Measurements of the photon flux density by comparing the reactivity of 2-nitrobenzaldehyde in reactors A and C.

²⁵ De la Cruz, N.; Romero, V.; Dantas, R. F.; Marco, P.; Bayarri, B.; Giménez, J.; Esplugas, S. *o*-Nitrobenzaldehyde Actinometry in the Presence of Suspended TiO_2 for Photocatalytic Reactors. *Catalysis Today* **2013**, 209, 209–214.

²⁶ For previous studies on the photon flux comparison between MFP see: Aillet, T.; Loubiere, K.; Dechy-Cabaret, O.; Prat, L. *Accurate Measurement of the Photon Flux Received Inside Two Continuous Flow Microphotoreactors by Actinometry*. *International Journal of Chemical Reactor Engineering* **2014**, 12, 257–269.



Thus, the enhanced reactivity is ascribed to the higher photon flux,²⁷ correlated with an increased concentration of the *photoenol* intermediate **III'** in the reaction media. Also, the fine control over the residence time and hence the time of irradiation successfully prevent the light-promoted product decomposition. We believe that the combination of these elements together with the more uniform irradiation surface and the shorter diffusion distance are the basis of the observed performance enhancement of the MFP setup described herein.

Limitations

Despite the highly improved productivity rates as well as the increased photon flux density observed with this unified protocol, some issues associated to the use of MFPs are commonly observed. In fact, when using polar reagents and/or highly concentrated solutions, system can easily get clogged due to the higher polarity of the obtained product. For this reason, I recommend using low concentrations with this method.

On the other hand, when looking at the newly developed photo-benzoylation reactivity, the method presents few limitations. In addition to the already commented overirradiation issues, that can be easily solved by tuning the residence time, coumarin carboxylates with higher absorptions at 365 nm (such as the dye “Coumarin 343”) cannot get benzoylated in the *C4* position.

3.1.5 Conclusions

In conclusion, a novel, simple and powerful MFP protocol was conveniently applied to photoreactions of 2-methylbenzophenones, outperforming the conventional batch protocols in terms of selectivity, yield and productivity rate. Among the seven different classes of photoreactions successfully implemented, in five cases the corresponding reaction products were isolated in pure forms after simple solvent evaporation, because of enhanced selectivity and negligible side-product formation. Also, the new MFP platform was pivotal to access the direct photobenzoylation of coumarincarboxylates, which represent a new class of reaction partners for 2-MBPs. In this regard, coumarin dimerization was successfully circumvented under MFP conditions, selectively yielding a broad range of 4-benzoylated-2-chromanones with high diastereocontrol and up to 93% isolated yield.

²⁷ To see the reason behind accelerated photochemical transformations in flow check: Su, Y.; Straathof, N. J. W.; Hessel, V.; Noël, T. Photochemical Transformations Accelerated in Continuous-Flow Reactors: Basic Concepts and Applications. *Chem. Eur. J.* **2014**, *20*, 10562–10589.

3.1.6 Experimental Section

The continuous flow reactions were carried out using capillary reactors made with PTFE tubing (0.75 mm I.D., 1.58 mm O.D.) and fitting connections purchased from SigmaAldrich. Reagents were pumped using a Syrris Asia pump (<https://syrris.com/modules/asia-syringe-pump/>). LEDs were purchased from Roithner LaserTechnik GmbH (model LED365-06Z 5.5 mW <http://www.roithnerlaser.com/index.html>). 26 W black bulb and 9W 365 nm bulb lamps were purchased from Amazon (<https://www.amazon.it/Foxnovo-sostituzione-lampadina-essiccatorrelampada/dp/B00JKE1T70>).

The NMR spectra were recorded on Bruker 400 Avance III HD equipped with a BBI-z grad probehead 5mm, Bruker 500 Avance III equipped with a BBI-ATM-z grad probehead 5mm and Bruker DMX 600 equipped with a BBI z-grad probehead 5mm. The chemical shifts (δ) for ^1H and ^{13}C are given in ppm relative to residual signals of the solvents (CHCl_3 @ 7.26 ppm ^1H NMR, 77.16 ppm ^{13}C NMR). Coupling constants are given in Hz. The following abbreviations are used to indicate the multiplicity: s, singlet; d, doublet; t, triplet; q, quartet; m, multiplet; bs, broad signal. NMR yields were calculated by using trichloroethylene as internal standard.

The ^1H , ^{13}C and ^{19}F NMR spectra are available in literature free of charge.²⁸

High-Resolution Mass Spectra (HRMS) were obtained using Waters GCT gas chromatograph coupled with a time-of-flight mass spectrometer (GC/MS-TOF) with electron ionization (EI) or MicroTOF II (Bruker Daltonics): HPLC-MS-TOF (ESI). Chromatographic purification of products was accomplished using flash chromatography on silica gel (SiO_2 , 0.04-0.063 mm) purchased from Machery-Nagel, with the indicated solvent system according to the standard techniques. Thin-layer chromatography (TLC) analysis was performed on pre-coated Merck TLC plates (silica gel 60 GF254, 0.25 mm). Visualization of the developed chromatography was performed by checking UV absorbance (254nm) as well as with aqueous ceric ammonium molybdate and potassium permanganate solutions. Organic solutions were concentrated under reduced pressure on a Büchi rotary evaporator.

Materials: Commercial grade reagents and solvents were purchased at the highest commercial quality from Sigma Aldrich or FluoroChem and used as received, unless otherwise stated.

The diverse reaction set up images, quantum yield measurements and photophysical studies are available free of charge in literature.²⁸

²⁸ Mateos, J.; Cherubini-Celli, A.; Carofiglio, T.; Bonchio, M.; Marino, N.; Companyó, X.; Dell'Amico, L. A Microfluidic Photoreactor Enables 2-Methylbenzophenone Light-Driven Reactions with Superior Performance. *Chem. Commun.* **2018**, 54, 6820–6823.

Light sources emission spectra

The following spectra were recorded using an AvaSpec ULS3648 high-resolution fiber-optic spectrometer which was placed at a fixed distance of 0.5 cm from the light source.

(more info at: <https://www.avantes.com/products/spectrometers/starline/item/209-avaspec-uls3648-high-resolution-spectrometer>).

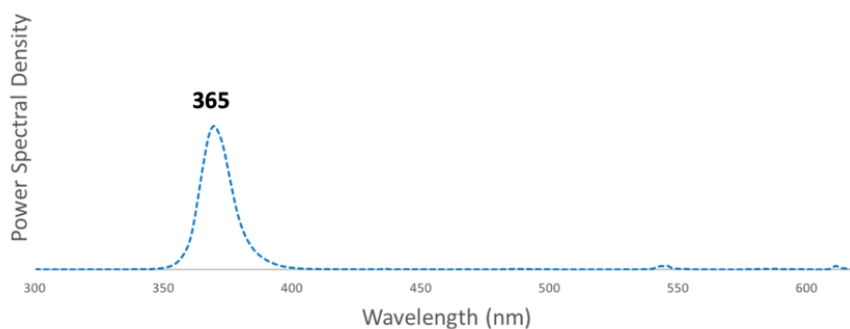


Figure 3.10. - Emission spectra of the Roithner LaserTechnik 365 nm LEDs used in this section.

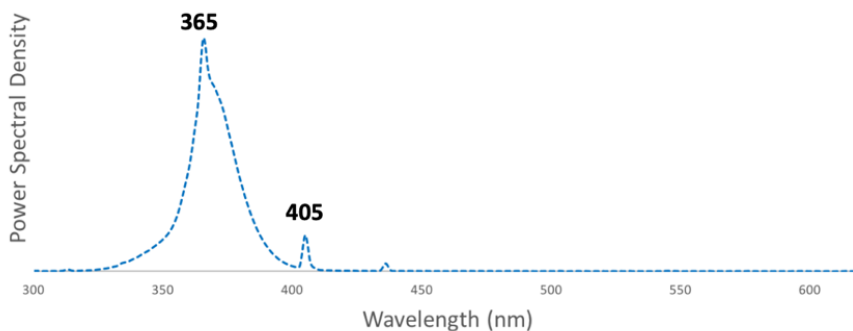


Figure 3.11. - Emission spectra of the 365 nm 9W bulbs used in this section.

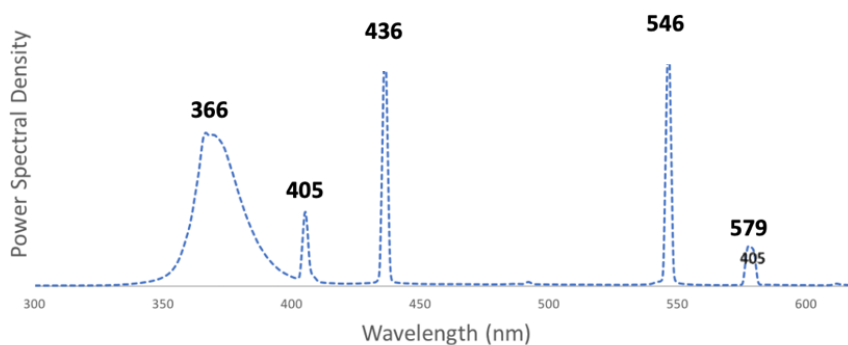
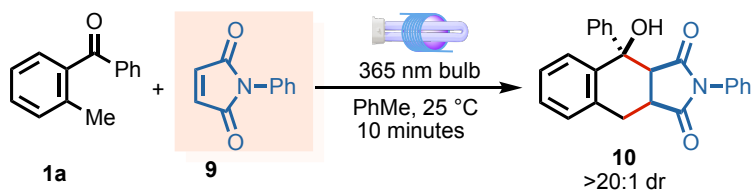


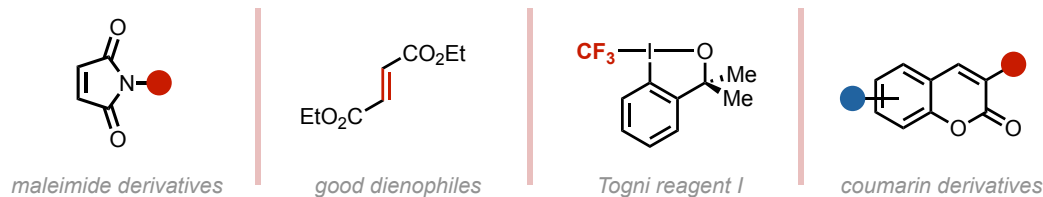
Figure 3.12. - Emission spectra of the 23 W black light bulb (BLB) used in this section.

General procedure for the microfluidic reactions

General procedure for solid reagents



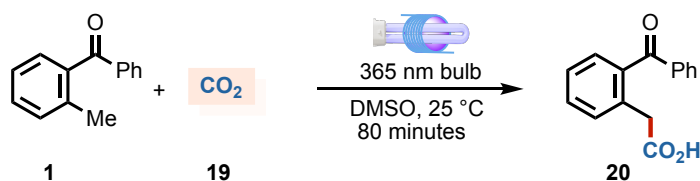
Solid reagents used in this section



Example with maleimide derivatives:

N-Phenylmaleimide **9** (173.2 mg, 1 equivalent, 1.0 mmol) was introduced into a 12 mL vial under nitrogen atmosphere and dissolved with 10 mL of degassed toluene. Then, 2-methylbenzophenone **1** (196.2 mg, 1 equivalent, 1.0 mmol) was added in one portion and the solution was further bubbled with nitrogen for 5 minutes. The resultant solution was pumped into the MFP irradiated by a 9W 365nm bulb with a residence time of 10 minutes. The product solution was collected into a round bottom flask. Subsequently, the solvent was removed by rotary evaporation furnishing **3a** (white solid) as a single diastereoisomer in >98% yield (365.7 mg, 0.989 mmol).

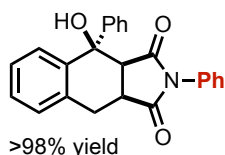
General procedure with carbon dioxide



DMSO (5 mL) was bubbled with carbon dioxide **19** in a 12 mL vial for 10 minutes. Then, 2-methylbenzophenone **1** (39.2 mg, 0.2 mmol) was added in one portion and the solution was bubbled again with carbon dioxide for 5 minutes. The resultant solution was pumped into the MFP with a residence time of 80 minutes. The product solution was collected into a round bottom flask. The crude reaction mixture was diluted with EtOAc (5 mL) and poured into a saturated aqueous solution of NH₄Cl. The aqueous layer was extracted with EtOAc (x3). The combined organic layers were dried with anhydrous MgSO₄ and the solvent was removed

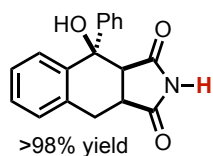
under rotary evaporation to afford the pure product **20** as a white solid in >98% of yield (47.5 mg, 0.197 mmol).

4-hydroxy-2,4-diphenyltetrahydro-1H-benzo[*f*]isoindole-1,3(2H)-dione (**10**).



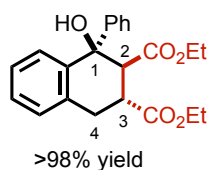
¹H-NMR (400 MHz, CDCl₃): 7.90 (d, *J* = 7.4 Hz, 1H, Ar), 7.45 (t, *J* = 7.6 Hz, 1H, Ar), 7.37–7.32 (m, 7H, Ar), 7.28–7.26 (m, 2H, Ar), 7.15 (d, *J* = 7.4 Hz, 1H, Ar), 6.81–6.79 (m, 2H, Ar), 5.46 (s, 1H, OH), 4.18 (d, *J* = 9.0 Hz, 1H, H₂), 3.40 (td, *J* = 8.8, 1.3 Hz, 1H, H₃), 3.01 (d, *J* = 15.2 Hz, 1H, H_{4α}), 2.64 (dd, *J* = 15.2, 8.7 Hz, 1H, H_{4β}) ppm. **¹³C-NMR (100 MHz, CDCl₃):** δ 179.6, 178.4, 141.0, 140.9, 134.2, 132.8, 131.1, 129.2, 129.0, 128.8, 128.5, 128.4, 128.2, 128.0, 126.9, 126.3, 126.1, 125.3, 48.3, 39.4, 30.4 ppm. **HRMS calculated for [C₂₄H₁₉NO₃+H]⁺:** 370.1365, found: 370.1415.

4-hydroxy-4-phenyltetrahydro-1H-benzo[*f*]isoindole-1,3(2H)-dione (**12**).



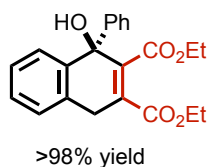
¹H-NMR (400 MHz, CDCl₃): δ 8.22 (br s, 1H, NH), 7.83 (d, *J* = 7.4 Hz, 1H, Ar), 7.41 (t, *J* = 7.6 Hz, 1H, Ar), 7.35–7.28 (m, 4H, Ar), 7.21–7.17 (m, 2H, Ar), 7.12 (d, *J* = 7.4 Hz, 1H, Ar), 5.25 (s, 1H, OH), 4.01 (d, *J* = 9.0 Hz, 1H, H₂), 3.23 (td, *J* = 8.8, 1.3 Hz, 1H, H₃), 2.92 (d, *J* = 15.2 Hz, 1H, H_{4α}), 2.54 (dd, *J* = 15.2, 8.7 Hz, 1H, H_{4β}) ppm. **¹³C-NMR (100 MHz, CDCl₃):** δ 180.3, 179.1, 140.9, 140.7, 132.8, 128.7, 128.4, 128.4 (x2), 127.9, 126.8, 125.3, 76.2, 49.3, 40.2, 29.6 ppm.

Diethyl-1-hydroxy-1-phenyltetrahydronaphthalene-2,3-dicarboxylate (**14**).



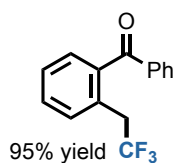
¹H-NMR (400 MHz, CDCl₃): δ 7.40 (t, *J* = 7.4 Hz, 2H, Ar), 7.36 (d, *J* = 7.4 Hz, 2H, Ar), 7.33–7.30 (m, 1H, Ar), 7.24–7.21 (m, 2H, Ar), 7.11 (t, *J* = 7.4 Hz, 1H, Ar), 6.84 (d, *J* = 7.4 Hz, 1H, Ar), 4.29–4.15 (m, 2H, COOCH₂CH₃), 4.01–3.84 (m, 2H, COOCH₂CH₃), 3.71 (td, *J* = 12.0, 5.4 Hz, 1H, H₃), 3.43 (d, *J* = 11.9 Hz, 1H, H₂), 3.39 (dd, *J* = 15.9 Hz, 5.4 Hz, 1H, H_{4α}), 3.23 (dd, *J* = 16.5, 12.1 Hz, 1H, H_{4β}), 1.32 (t, *J* = 7.1 Hz, 3H, COOCH₂CH₃), 0.88 (t, *J* = 7.1 Hz, 3H, COOCH₂CH₃) ppm. **¹³C-NMR (100 MHz, CDCl₃):** δ 174.1, 173.81, 145.0, 139.9, 133.9, 129.7, 128.6, 128.2, 127.8, 127.8, 127.2, 126.8, 126.6, 126.6, 76.1, 61.1, 60.83, 54.41, 39.66, 32.41, 14.16, 13.58 ppm.

Diethyl-1-hydroxy-1-phenyltetrahydronaphthalene-2,3-dicarboxylate (16).



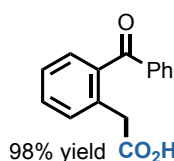
¹H-NMR (400 MHz, CDCl₃): δ 7.44-7.40 (m, 3H, Ar), 7.31 (t, *J* = 7.4 Hz, 2H, Ar), 7.27-7.21 (m, 4H, Ar), 4.32 (qd, *J* = 7.1, 1.9 Hz, 2H, COOCH₂CH₃), 4.24 (br s, 1H, OH), 4.19-4.05 (m, 2H, COOCH₂CH₃), 3.91 (s, 2H, CH₂), 1.37 (t, *J* = 7.1 Hz, 3H, COOCH₂CH₃), 1.09 (t, *J* = 7.1 Hz, 3H, COOCH₂CH₃) ppm. **¹³C-NMR (100 MHz, CDCl₃):** δ 167.5, 167.7, 145.1, 138.8, 131.9, 130.0, 128.1, 127.8, 127.5, 127.5, 127.3, 127.2, 125.7, 74.2, 61.6, 30.8, 14.0, 13.6 ppm.

Phenyl[2-(trifluoroethyl)phenyl]methanone (18).



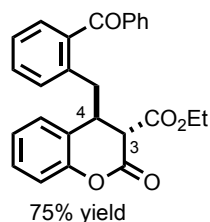
¹H-NMR (400 MHz, CDCl₃): δ 7.80 (m, 2H, Ar), 7.57 (m, 1H, Ar), 7.51 (m, 1H, Ar), 7.47 (m, 3H, Ar), 7.40 (m, 2H, Ar), 3.74 (q, *J* = 10.9 Hz, 2H, CH₂) ppm. **¹³C-NMR (150 MHz, CDCl₃):** δ 197.7, 139.5, 137.4, 133.3, 132.4, 130.7, 130.4, 129.8, 129.5 (q, *J* = 2.4 Hz), 128.4, 127.4, 125.7 (q, *J* = 277.1 Hz), 36.1 ppm (q, *J* = 29.4 Hz). **¹⁹F-NMR (376 MHz, CDCl₃):** δ -65.0 ppm (t, *J* = 10.9 Hz).

2-(2-benzoylphenyl)acetic acid (320)



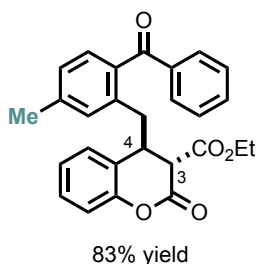
¹H-NMR (400 MHz, CDCl₃): δ 7.81 (m, 2H, Ar), 7.61 (1H, Ar), 7.48 (m, 5H, Ar), 7.35 (m, 1H, Ar), 3.83 (s, 2H) ppm. **¹³C-NMR (100 MHz, CDCl₃):** δ 199.1, 174.6, 137.5, 137.2, 133.9, 133.5, 131.9, 131.7, 130.7, 128.4, 126.7, 39.7 ppm.

Ethyl-4-(2-benzoylbenzyl)-2-oxochromane-3-carboxylate (24).



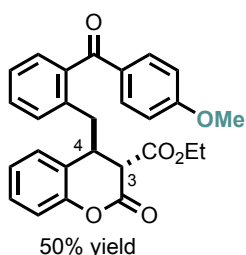
¹H-NMR (400 MHz, CDCl₃): 7.77 (d, *J* = 8.5 Hz, 2H, Ar), 7.60 (t, *J* = 7.4 Hz, 1H, Ar), 7.47 (t, *J* = 7.4 Hz, 2H, Ar), 7.43-7.40 (m, 2H, Ar), 7.35-7.31 (m, 1H, Ar), 7.24-7.20 (m, 1H, Ar), 7.10 (d, *J* = 7.6 Hz, 1H, Ar), 7.04 (d, *J* = 8.1 Hz, 1H, Ar), 7.01 (m, 2H, Ar), 4.01-3.90 (m, 2H, COOCH₂CH₃), 3.82-3.79 (m, 2H, C₃H & C₄H), 3.16 (dd, *J* = 13.6 Hz, 6.7 Hz, 1H, CH₂α), 2.77 (dd, *J* = 13.9 Hz, 8.8 Hz, 1H, CH₂β), 0.96 (t, *J* = 7.2 Hz, COOCH₂CH₃) ppm. **¹³C-NMR (100 MHz, CDCl₃):** δ 198.0, 166.8, 166.4, 164.4, 137.1, 133.2, 132.0, 120.8, 130.3, 130.2, 128.9, 128.5, 126.5, 124.7, 123.3, 116.8, 62.0, 50.8, 41.5, 38.6, 13.7 ppm. **HRMS calculated for [C₂₆H₂₂O₅+H]⁺:** 415.1467, found: 415.1460.

Ethyl-4-(2-benzoyl-5-methylbenzyl)-2-oxochromane-3-carboxylate (26).



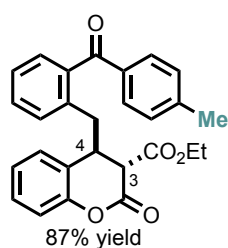
¹H-NMR (400 MHz, CDCl₃): 7.76 (d, *J* = 8.5 Hz, 2H, Ar), 7.58 (t, *J* = 7.6 Hz, 1H, Ar), 7.46 (t, *J* = 7.4 Hz, 2H, Ar), 7.33 (d, *J* = 7.8 Hz, 1H, Ar), 7.21 (m, 2H, Ar), 7.12 (d, *J* = 7.7 Hz, 1H, Ar), 7.07-7.00 (m, 3H, Ar), 6.90 (s, 1H, Ar), 4.21-3.92 (m, 2H, COOCH₂CH₃), 3.82-3.79 (m, 2H, C₃H & C₄H), 3.21 (dd, *J* = 13.6 Hz, 6.7 Hz, 1H, CH₂α), 2.74 (dd, *J* = 13.9 Hz, 8.8 Hz, 1H, CH₂β), 2.37 (s, 3H, Ar-CH₃), 0.96 (t, *J* = 7.2 Hz, COOCH₂CH₃) ppm. **¹³C-NMR (100 MHz, CDCl₃):** δ 198.2, 167.1, 164.7, 164.4, 150.8, 141.7, 138.6, 137.7, 135.2, 131.2, 130.3, 129.1, 128.5, 127.2, 124.9, 124.1, 116.9, 62.2, 50.9, 41.6, 38.9, 21.6, 14.4 ppm. **HRMS calculated for [C₂₇H₂₄O₅+H]⁺:** 429.1624, found: 429.1623.

Ethyl-4-[2-(4-methoxybenzoyl)benzyl]-2-oxochromane-3-carboxylate (27).



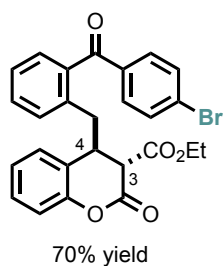
¹H-NMR (400 MHz, CDCl₃): 7.77 (d, *J* = 8.5 Hz, 2H, Ar), 7.41-7.37 (m, 2H, Ar), 7.34-7.28 (m, 2H, Ar), 7.24-7.19 (m, 2H, Ar), 7.08-6.98 (m, 3H, Ar), 6.93 (d, *J* = 7.6 Hz, 1H, Ar), 4.01-3.91 (m, 2H, COOCH₂CH₃), 3.88 (s, 3H, OCH₃), 3.80-3.75 (m, 2H, C₃H & C₄H), 3.10 (dd, *J* = 13.6 Hz, 6.7 Hz, 1H, CH₂α), 2.74 (dd, *J* = 13.9 Hz, 8.8 Hz, 1H, CH₂β), 0.95 (t, *J* = 7.2, COOCH₂CH₃) ppm. **¹³C-NMR (100 MHz, CDCl₃):** δ 196.8, 167.0, 164.6, 163.9, 150.8, 139.0, 136.7, 132.7, 131.9, 130.7, 130.4, 129.0, 126.6, 124.8, 124.0, 116.9, 113.9, 62.2, 55.7, 51.0, 45.4, 41.6, 38.7, 13.8 ppm. **HRMS calculated for [C₂₇H₂₄O₆+H]⁺:** 445.1573, found: 445.1576.

Ethyl-4-[2-(4-methylbenzoyl)benzyl]-2-oxochromane-3-carboxylate (28).



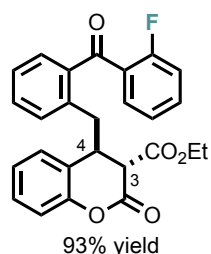
¹H-NMR (400 MHz, CDCl₃): 7.71 (d, *J* = 8.5 Hz, 2H, Ar), 7.41 (d, *J* = 7.4 Hz, 2H, Ar), 7.36 (d, *J* = 7.4 Hz, 1H, Ar), 7.30-7.23 (m, 3H, Ar), 7.12-7.03 (m, 4H, Ar), 4.04-3.94 (m, 2H, COOCH₂CH₃), 3.82-3.79 (m, 2H, C₃H & C₄H), 3.16 (dd, *J* = 13.6 Hz, 6.7 Hz, 1H, CH₂α), 2.79 (dd, *J* = 13.9 Hz, 8.8 Hz, 1H, CH₂β), 2.46 (s, 3H, Ar-CH₃), 0.98 (t, *J* = 7.2, COOCH₂CH₃) ppm. **¹³C-NMR (100 MHz, CDCl₃):** δ 197.9, 167.0, 164.6, 150.8, 144.4, 138.7, 137.0, 135.4, 132.0, 130.7, 130.6, 130.3, 129.3, 129.0, 126.6, 124.9, 124.0, 116.9, 62.2, 51.0, 41.6, 38.8, 21.9, 13.9 ppm. **HRMS calculated for [C₂₇H₂₄O₅+H]⁺:** 429.1624, found: 429.1629.

Ethyl-4-[2-(4-bromobenzoyl)benzyl]-2-oxochromane-3-carboxylate (29).



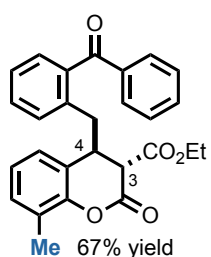
¹H-NMR (500 MHz, CDCl₃): δ 7.66–7.58 (m, 4H, Ar), 7.44 (td, *J* = 7.4, 1.5 Hz, 1H, Ar), 7.40–7.31 (m, 2H, Ar), 7.22 (td, *J* = 7.6, 2.2 Hz, 1H, Ar), 7.13 (d, *J* = 7.5 Hz, 1H, Ar), 7.07–6.97 (m, 3H, Ar), 4.06–3.90 (m, 2H, COOCH₂CH₃), 3.82–3.74 (m, 2H, C₃H & C₄H), 3.16 (dd, *J* = 13.7, 6.8 Hz, 1H, CH₂α), 2.79 (dd, *J* = 13.7, 9.2 Hz, 1H, CH₂β), 0.96 (t, *J* = 7.1 Hz, 3H, COOCH₂CH₃) ppm. **¹³C-NMR (125 MHz, CDCl₃):** δ 196.80, 166.79, 164.35, 150.71, 137.61, 137.28, 136.59, 132.08, 131.78, 131.67, 131.06, 130.18, 128.92, 128.85, 126.55, 124.74, 123.66, 116.86, 62.09, 50.86, 41.52, 38.51, 29.69, 13.71 ppm. **HRMS *m/z* calculated for [C₂₆H₂₁BrO₅+H]⁺:** 493.0645, found: 493.0644.

Ethyl-4-[2-(2-fluorobenzoyl)benzyl]-2-oxochromane-3-carboxylate (30).



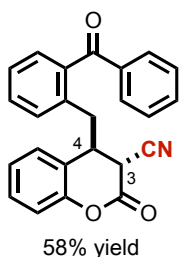
¹H-NMR (400 MHz, CDCl₃): 7.63 (t, *J* = 7.3 Hz, 1H, Ar), 7.56 (q, *J* = 6.9 Hz, 1H, Ar), 7.45 (m, 2H, Ar), 7.33–7.24 (m, 3H, Ar), 7.15 (d, *J* = 7.4 Hz, 2H, Ar), 7.11–7.03 (m, 3H, Ar), 4.04–3.93 (m, 2H, COOCH₂CH₃), 3.87 (t, *J* = 7.8 Hz, 1H, C₃H), 3.80 (s, 1H, C₄H), 3.36 (dd, *J* = 13.6 Hz, 6.7 Hz, 1H, CH₂α), 2.91 (dd, *J* = 13.9 Hz, 8.8 Hz, 1H, CH₂β), 0.98 (t, *J* = 7.2, COOCH₂CH₃) ppm. **¹³C NMR (100 MHz, CDCl₃):** δ 193.4, 167.1, 164.8, 150.9, 138.0, 134.1, 132.7, 132.1, 131.8, 131.4, 129.2, 129.0, 127.2, 125.0, 124.6, 124.5, 124.2, 117.0, 62.2, 51.0, 41.4, 39.2, 14.1 ppm. **HRMS calculated for [C₂₆H₂₁FO₅+H]⁺:** 433.1373, found: 433.1361.

Ethyl-4-(2-benzoylbenzyl)-8-methyl-2-oxochromane-3-carboxylate (31).



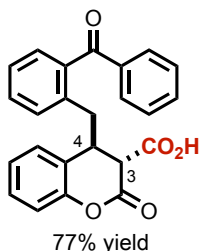
¹H-NMR (400 MHz, CDCl₃): 7.76 (d, *J* = 7.5 Hz, 2H, Ar), 7.59 (t, *J* = 7.4 Hz, 1H, Ar), 7.48–7.39 (m, 4H, Ar), 7.33 (t, *J* = 7.5 Hz, 1H, Ar), 7.13 (d, *J* = 7.5 Hz, 1H, Ar), 7.05 (d, *J* = 7.5 Hz, 1H, Ar), 6.90 (t, *J* = 7.5 Hz, 1H, Ar), 6.81 (d, *J* = 7.5 Hz, 1H, Ar), 4.01–3.90 (m, 2H, COOCH₂CH₃), 3.76–3.73 (m, 2H, C₃H & C₄H), 3.16 (dd, *J* = 13.6 Hz, 6.7 Hz, 1H, CH₂α), 2.77 (dd, *J* = 13.9 Hz, 8.8 Hz, 1H, CH₂β), 2.28 (s, 3H, ArCH₃) 0.94 (t, *J* = 7.2, COOCH₂CH₃) ppm. **¹³C-NMR (100 MHz, CDCl₃):** δ 198.0, 166.9, 164.7, 149.0, 138.2, 137.9, 137.2, 133.2, 132.0, 130.8, 130.3, 130.2, 128.4, 126.4, 126.4, 124.3, 123.5, 61.9, 50.8, 41.6, 38.5, 15.6 13.7 ppm. **HRMS calculated for [C₂₇H₂₄O₅+H]⁺:** 429.1624, found: 429.1627.

4-(2-benzoylbenzyl)-2-oxochromane-3-carbonitrile (32).



¹H-NMR (400 MHz, CDCl₃): 7.73 (d, $J = 8.1$ Hz, 2H, Ar), 7.60 (t, $J = 7.6$ Hz, 1H, Ar), 7.47–7.38 (m, 5H, Ar), 7.34–7.30 (m, 2H, Ar), 7.07 (d, $J = 8.2$ Hz, 1H, Ar), 6.94 (t, $J = 7.6$ Hz, 1H, Ar), 6.86–6.84 (m, 1H, Ar), 6.63 (d, $J = 7.4$ Hz, 1H, Ar), 4.03 (d, $J = 5.1$ Hz, 1H, C₃H), 3.91 (dt, $J = 9.8$ Hz, 5.6 Hz, 1H, C₄H), 3.39 (dd, $J = 13.2$ Hz, 5.8 Hz, 1H, CH₂α), 2.90 (dd, $J = 13.4$ Hz, 10.2 Hz, 1H, CH₂β) ppm. **¹³C-NMR (100 MHz, CDCl₃):** δ 198.0, 160.9, 151.9, 150.4, 138.7, 137.5, 135.8, 135.7, 133.6, 132.4, 130.5, 130.0, 129.8, 128.9, 128.6, 126.9, 125.8, 125.0, 122.8, 117.3, 113.5, 40.5, 38.8, 35.8 ppm. **HRMS calculated for [C₂₄H₁₇NO₃+H]⁺:** 368.1208, found: 368.1268.

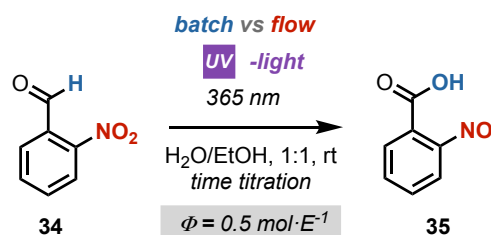
4-(2-benzoylbenzyl)-2-oxochromane-3-carboxylic acid (33).



¹H-NMR (400 MHz, CDCl₃): 7.77 (d, $J = 8.5$ Hz, 2H, Ar), 7.60 (t, $J = 7.4$ Hz, 1H, Ar), 7.48–7.40 (m, 5H, Ar), 7.33 (d, $J = 7.5$ Hz, 1H, Ar), 7.10–6.99 (m, 4H, Ar), 3.86–3.82 (m, 2H, C₃H & C₄H), 3.13 (dd, $J = 13.6$ Hz, 6.7 Hz, 1H, CH₂α), 2.77 (dd, $J = 13.9$ Hz, 8.8 Hz, 1H, CH₂β). **¹³C-NMR (100 MHz, CDCl₃):** δ 198.1, 169.3, 164.4, 150.7, 138.2, 137.9, 137.1, 133.2, 132.0, 130.8, 130.3, 130.2, 129.0, 128.9, 128.5, 127.4, 126.5, 124.7, 123.7, 117.0, 50.6, 41.2, 38.9, 29.7. **HRMS calculated for [C₂₄H₁₈O₅+H]⁺:** 387.1154, found: 387.1244.

Photon flux density measurements

— photon flux measurements



A measurement of the photon flow (ϕ) through batch and microreactor setups was performed, in order to prove that the difference in the reactivity across the two setups is to be attributed only to their different nature, and not to their ability to interact with radiation. As it was shown by De la Cruz et al.,²⁵ the photon flow (ϕ) can be easily measured through the use of a 2-nitrobenzaldehyde (NBA) actinometer **34**. When exposed to UV-light, NBA isomerises to 2-nitrosobenzoic acid (HNB) **35**, that can be detected through a pH-meter.

The actinometry experiments were conducted using the setups A and C and an *XS Instruments*® pH 80 pH-meter.

During the actinometric runs, the pH of the actinometric solution (0.1 M NBA, 0.005 M NaOH in H₂O/EtOH 1:1) was measured at different residence times. Plotting the pH against time, a titration curve was obtained. Hence, the equivalence point was determined as where $\Delta^2\text{pH}/\Delta t^2$ crosses the y=0 axis.

The time to reach the equivalence point of the titration was chosen as a parameter to compare the two systems. The microreactor had a total volume of 0.4 mL, while the batch vial was holding 1.5 mL. The equivalence point for the microreactor was at $2.0 \cdot 10^{-6}$ moles of HNB produced, while for the batch reactor was at $7.5 \cdot 10^{-6}$ moles of HNB produced. The NBA actinometer has a quantum yield (ϕ) of 0.5 across the 290-400 nm range. Thus, the photon flow (ϕ) was calculated in the following equations for the C and A respectively, obtaining

$$\begin{aligned}\phi_{MFP} &= \frac{\text{moles of HNB produced}}{\phi \cdot t(\text{end point})} = \frac{2.0 \cdot 10^{-6} \text{ mol}}{0.5 \text{ mol Einstein}^{-1} \cdot 23 \text{ s}} \\ &= 1.74 \cdot 10^{-7} \text{ Einstein s}^{-1}\end{aligned}$$

$$\begin{aligned}\phi_B &= \frac{\text{moles of HNB produced}}{\phi \cdot t(\text{end point})} = \frac{7.5 \cdot 10^{-6} \text{ mol}}{0.5 \text{ mol Einstein}^{-1} \cdot 456 \text{ s}} \\ &= 3.29 \cdot 10^{-8} \text{ Einstein s}^{-1}\end{aligned}$$

The photon flow in Einstein s⁻¹ was then converted to W m⁻². Using the Planck equation $E = h\nu$, an irradiation wavelength of 365 nm has an energy of $5.45 \cdot 10^{-19}$ J photon⁻¹, equivalent to $3.28 \cdot 10^5$ J Einstein⁻¹. The cross-section of the microreactor was calculated as the product of its length, 1.00 m, times the width of the tubing, 0.75 mm, which gives 7.5 cm². The cross-section of the batch vial was equal to the product of its width, 1.0 cm, times 1.4 cm (the height of 1.5 mL of liquid), which gives 1.4 cm². The photon flow in W m⁻² was calculated in the following equations for the C and A respectively, obtaining:

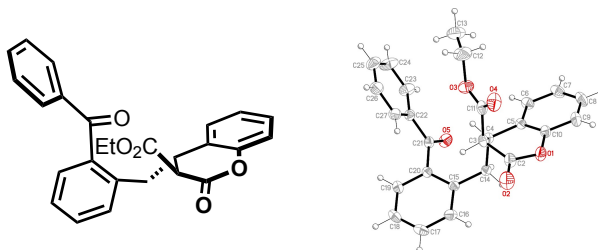
$$\frac{1.74 \cdot 10^{-7} \text{ Einstein s}^{-1} \cdot 3.28 \cdot 10^5 \text{ J Einstein}^{-1}}{7.5 \cdot 10^{-4} \text{ m}^2} = 76 \text{ W m}^{-2}$$

$$\frac{3.29 \cdot 10^{-8} \text{ Einstein s}^{-1} \cdot 3.28 \cdot 10^5 \text{ J Einstein}^{-1}}{1.4 \cdot 10^{-4} \text{ m}^2} = 77 \text{ W m}^{-2}$$

As expected from using the very same apparatus for both the microreactor and the batch, the flow of photons was similar across the two setups. Thus, the differences in reactivity and selectivity can be attributed only to the superior performances of the microreactor setup.

X-ray crystallographic analysis of 24

— X-Ray structure of 24



Crystal data: C₂₆H₂₂O₅

Formula	C ₂₆ H ₂₂ O ₅
fw	414.43
Crystal system	Triclinic
Space group	<i>P</i> -1
Unit cell dimensions	a = 8.58811(15) Å a = 89.0458(13)° b = 9.78515(16) Å b = 80.7673(14)° c = 13.2312(2) Å g = 86.3224(14)°
<i>V</i>	1095.21(3) Å ³
<i>Z</i>	2
Density (calculated)	1.257 g/cm ³
Absorption coefficient	0.087 mm ⁻¹
<i>F</i> (000)	436
Crystal size	0.650 x 0.400 x 0.300 mm ³
Reflections collected	24550
Independent reflections	5384 [<i>R</i> (int) = 0.0218]
Completeness to theta = 25.242°	99.9 %

Data / restraints / parameters	5384 / 467 / 292
Goodness-of-fit on F^2	1.047
Final R indices $[I > 2\sigma(I)]^{a,b}$	$R_1 = 0.0452, wR_2 = 0.1117$
R indices (all data) ^{a,b}	$R_1 = 0.0602, wR_2 = 0.1220$
$\Delta\rho_{\max, \min}$	0.161/-0.185 e \AA^{-3}

^a $R_1 = \sum ||F_o| - |F_c|| / \sum |F_o|$. ^b $wR_2 = \{\sum w(F_o^2 - F_c^2)^2 / \sum [w(F_o^2)^2]\}^{1/2}$ and $w = 1 / [\sigma^2(F_o)^2 + (mP)^2 + nP]$ with $P = (F_o^2 + 2F_c^2) / 3$, $m = 0.0513$ and $n = 0.1878$.

CCDC 1811483 contains the supplementary crystallographic data for this compound. These data can be obtained free of charge from The Cambridge Crystallographic Data Centre via www.ccdc.cam.ac.uk/data_request/cif

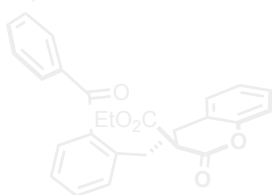
Chapter III – Section 2

Microfluidic Photoreactors – Light-Driven Synthesis of Tetracyclic Molecular Architectures

Chapter III - Synthetic Transformations Driven by Triplet State *o*-Alkyl Substituted Benzophenones

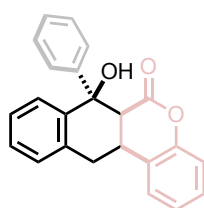
Section 1.

A microfluidic photoreactor enables 2-methylbenzophenone light-driven reactions with superior performances



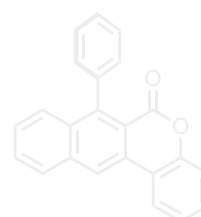
Section 2.

Microfluidic light-driven synthesis of tetracyclic molecular architectures



Section 3.

Synthesis and characterization of naphthochromenones as new potential organic photocatalysts



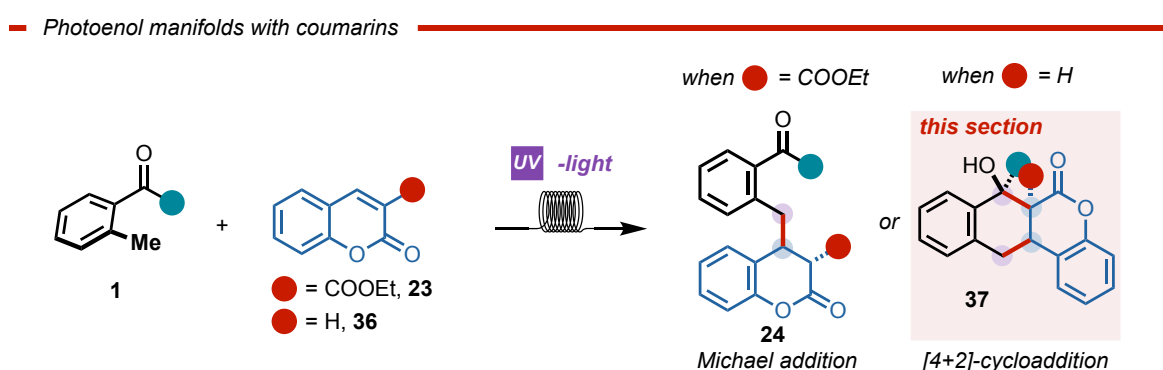
- To apply the developed microfluidic photoreactors towards previously unaccessible scaffolds.
- To study the reactivity of coumarins and chromones with 2-methylbenzophenone in photochemically-driven flow reactions.²⁹

²⁹ The project discussed in this chapter has been conducted in collaboration with Nicholas Meneghini (involved in the synthesis and characterization the coumarin-derived products). I individually optimized the reaction conditions and prepared several entries of the reaction scope.

This work has been published: Mateos, J.; Meneghini, N.; Bonchio, M.; Marino, N.; Carofiglio, T.; Companyó, X.; Dell'Amico, L. Microfluidic Light-Driven Synthesis of Tetracyclic Molecular Architectures. *Beilstein J. Org. Chem.* **2018**, *14*, 2418–2424.

3.2.1 Introduction

The sophistication of synthetic photochemistry offers new avenues for unexplored reactivities.³⁰ In this regard, the use of MFPs revealed to be a key enabling technology for diverse photochemical processes.³¹ As described in the last section, the increased light penetration together with a more uniform and effective irradiation of the reaction system highly improved the synthetic performances of 2-methylbenzophenone photochemistry when compared to classical batch protocols. This synthetic approach was used to disclose the photobenzoylation of 3-coumarincarboxylates through a Michael-type addition manifold.²⁸ Nevertheless, the reaction modes of 2-MBP are not restricted to the nucleophilic addition of the *photoenol* intermediate but to [4+2]-cycloaddition reactions as well (Scheme 3.6).



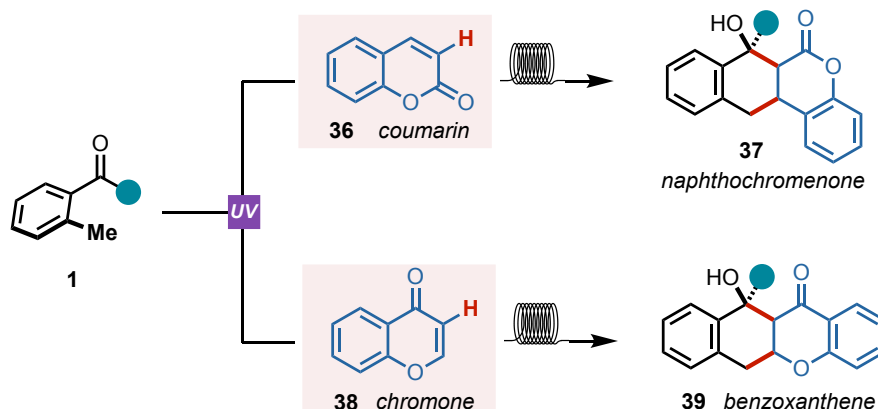
Scheme 3.6. - Photoenol manifolds with diversely substituted coumarins.

Prompted by the interest of developing novel light-driven microfluidic methods for the construction of biologically relevant molecular scaffolds, we investigated the reaction between 2-MBP **1** and 3-unsubstituted coumarin **36** and chromone **38** (Scheme 3.7). It was anticipated that the successful development of these photoreactions would generate valuable privileged scaffolds, namely: naphthochromenones **37** and benzoxanthenes **39**, through a diastereoselective light-driven [4+2]-cycloaddition manifold. Interestingly, the tetracyclic scaffolds **37** and **39** are embodied in different biologically active molecules, with diverse pharmacological activities.³²

³⁰ Buglioni, L.; Raymenants, F.; Slattery, A.; Zondag, S. D. A.; Noël, T. *Technological Innovations in Photochemistry for Organic Synthesis: Flow Chemistry, High-Throughput Experimentation, Scale-up, and Photoelectrochemistry*. *Chem. Rev.* **2021**, DOI: 10.1021/acs.chemrev.1c00332.

³¹ Rehm, T. H. *Flow Photochemistry as a Tool in Organic Synthesis*. *Chem. Eur. J.* **2020**, *26*, 16952–16974.

³² Wright, P. M.; Seiple, I. B.; Myers, A. G. *The Evolving Role of Chemical Synthesis in Antibacterial Drug Discovery*. *Angew. Chem. Int. Ed.* **2014**, *53*, 8840–8869.



Scheme 3.7. - Photoenol reactivity with C3 unsubstituted coumarins and chromones.

3.2.2 Challenges of the project

Even if the construction of the fully aromatized naphthochromenone scaffold can be achieved under oxidative conditions (e.g. photocatalysis or electrochemistry),³³ to the best of our knowledge, no diastereoselective methods for the direct construction of **37** were reported in literature prior to this work. On the other hand, the construction of the benzoxanthene scaffold **39**, relies on the use of harsh reaction conditions (e.g. 250 °C), leading to a mixture of regio- and diastereoisomers in moderate yields.³⁴ Hence, the development of an efficient synthetic method to access these privileged scaffolds still represented an unsolved problem in synthetic chemistry.

3.2.3 Section overview

In this section, you will find the optimization and generality evaluation of a new photochemical method suited for the modification of a broad range of coumarins **36** and chromones **37**, used as precursors for the direct generation of the tetracyclic scaffolds, with high synthetic performances (up to >98% yield) and complete diastereocontrol (>20:1). Noteworthy, the photoreactions presented in this section do not proceed under conventional batch conditions, thus highlighting the importance of the MFP protocol to enable novel light-driven synthetic transformations.

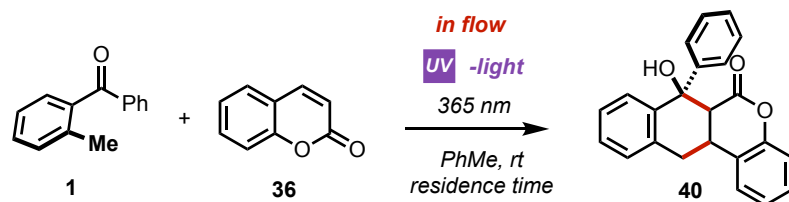
³³ Su, W.; Xu, P.; Ritter, T. Decarboxylative Hydroxylation of Benzoic Acids. *Angew. Chem. Int. Ed.* **2021**, DOI: 10.1002/anie.202108971.

³⁴ Sandulache, A.; Silva, A. M. S.; Cavaleiro, J. A. S. Diels–Alder Reactions of Chromone-3-Carboxaldehydes with Ortho-Benzoquinodimethane. *New Synthesis of Benzo[b]Xanthenes. Tetrahedron* **2002**, 58, 105–114.

3.2.4 Results and discussion

Reaction optimization

The reaction between 2-methylbenzophenone **1** and coumarin **36** was initially screened using the conditions reported in Section 1 of this chapter. A MFP of 400 μL volume was used, adding 1.5 equiv. of **1** and a residence time of 26.6 min (Table 3.4). Under these reaction conditions, product **40** was formed in 70% yield as a single diastereoisomer with a production of 0.063 $\text{mmol}\cdot\text{h}^{-1}$ (entry 1). Interestingly, when the volume size was increased, despite the reaction yield dropped to 57%, the productivity was enhanced to 0.128 $\text{mmol}\cdot\text{h}^{-1}$ (entry 2). Hence, our goal was to reach quantitative yields in preparative useful productions ($>0.1 \text{ mmol}\cdot\text{h}^{-1}$). Reversing the reagents ratio, *i.e.* using an excess of coumarin **36** (3 equiv.), turned out to be highly beneficial, yielding the cyclized product **40** in 83% yield (entry 3). Decreasing the reaction concentration and further enhancing the equivalents of **40** turned to be detrimental for the success of the reaction (entries 4 and 5). Nevertheless, the optimal reaction conditions for the light-driven [4+2]-cycloaddition were achieved within a 1000 μL MFP, with a residence time set at 35 min and a decreased concentration (entry 6). Indeed, product **40** formed in quantitative yield, complete diastereocontrol and a productivity of 0.102 $\text{mmol}\cdot\text{h}^{-1}$. On the contrary, when the same reaction was performed under a batch setup, the expected [4+2]-cycloaddition product **4a** was only formed in trace amounts along with extensive coumarin photodimerization product (entry 7).

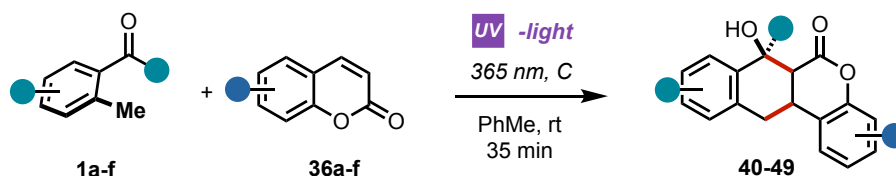


entry	reactor volume (μL)	reagent ratio (1:36)	conc. (M)	residence time (min)	productivity rate ($\text{mmol}\cdot\text{h}^{-1}$)	yield % (10)
1	400	1.5:1	0.10	26.6	0.063	70
2	1000	1.5:1	0.10	26.6	0.128	57
3	1000	1:3	0.10	26.6	0.187	83
4	1000	1:3	0.06	26.6	0.114	77
5	1000	1:5	0.06	26.6	0.114	77
6	1000	1:5	0.06	35.0	0.102	>98
7	batch	1:5	0.06	35.0	-	nr

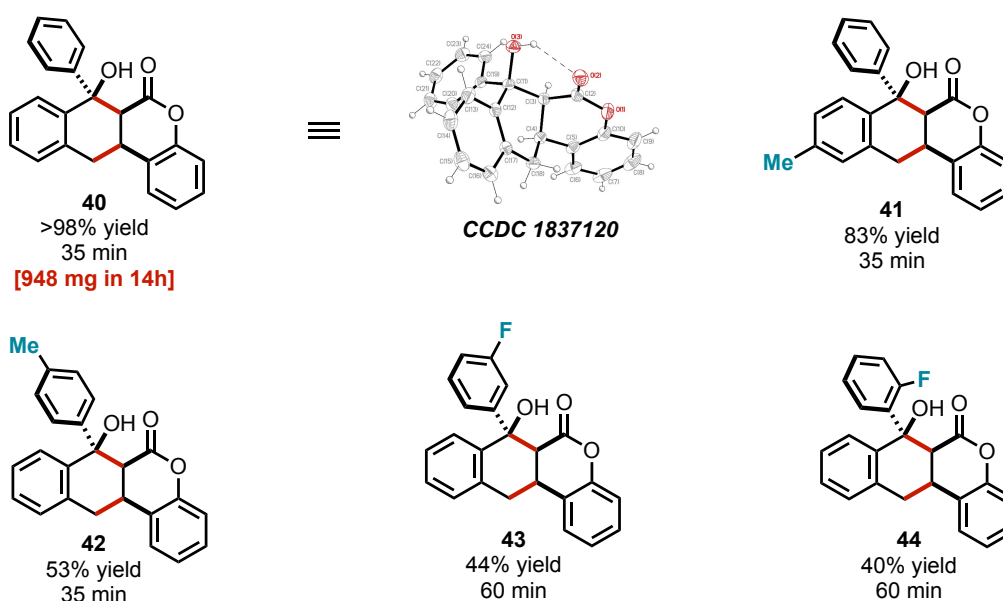
Table 3.4. - Optimization table of the [4+2]-cycloaddition reaction with coumarins.

The enhanced reactivity under the MFP compared to the batch setup (entry 6 vs entry 7) is again attributed to the more efficient illumination and the shorter irradiation time within the MFP,³⁵ successfully preventing the light-promoted side-reactions.³⁶

Generality of the reaction with coumarins (Table 3.5)



2-methylbenzophenone scope



coumarin scope

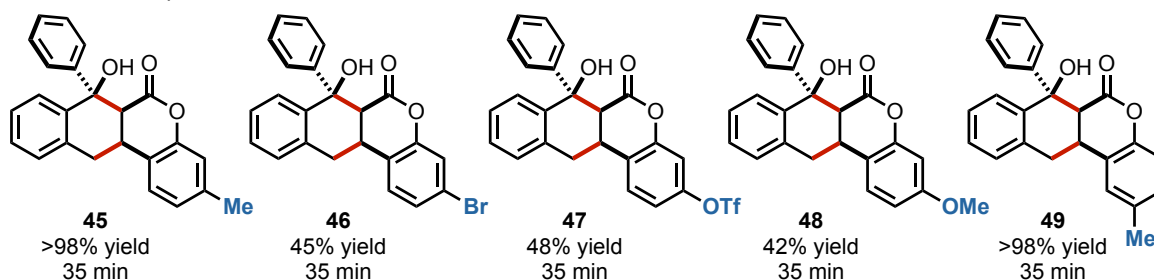


Table 3.5. - Substrate scope of the [4+2]-cycloaddition reaction between 2-MBP and coumarins.

³⁵ The optimization of the MFP used in this section has been previously described in this chapter, see Chapter III – Section 1.

³⁶ The batch reaction was performed using the same light source employed for the MFP setup and stopped at different reaction times. When the batch reaction was stopped at short reaction time (e.g., 2 h) the product 40 was only detected in low amount (<10%) along with recovery of the unreacted starting material, 1, 36 and high amounts of the coumarin dimerization products.

With the optimal reaction conditions in hand, we explored the generality and limits of the photochemical transformation. First, different substitutions on the 2-MBP scaffold were evaluated (Table 3.5, middle). Electron-donating substituents on both aromatic rings gave excellent results, furnishing the corresponding naphthochromenones **41-42** as single diastereoisomers (>20:1 dr), with yields spanning from 53% to 83% and short residence times (35 min). On the contrary, electron-withdrawing substituents resulted in inferior synthetic performances. Compounds **43** and **44** were isolated in 44% and 40% respectively within 60 min.

The optimized reaction conditions were also amenable to diverse coumarin scaffolds. 6- and 7-substituted coumarins furnished the corresponding cyclic products **45-49** in moderate to excellent yields (41->98%) and spanning synthetically useful functionalities such as halides and pseudo-halides (compounds **46** and **47**, in Table 3.5 down).

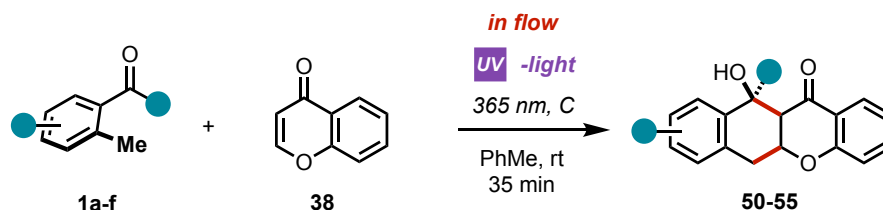
Additionally, and to demonstrate the easy scalability of the present method we applied the parallelization strategy. Hence, by placing two MFPs in parallel, 948 mg of **40** were obtained after 14 h. This experimental trend highlights the preparative nature of the protocols thanks to the increased productivity rate (0.196 mmol·h⁻¹).³⁷

Generality of the reaction with chromones

Next, the chromone scaffold **37**, which is a precursor of diverse classes of biologically active molecules,³⁸ was evaluated under the developed MFP setup. Notably, the [4+2]-cycloaddition product **50** formed in 72% yield and >20:1 dr, without the need of further condition adjustments. The relative *syn* configuration within **50** was confirmed by x-ray analysis on its single crystal (Table 3.6). Noteworthy, different 2-MBPs bearing-electron donating or electron-withdrawing groups underwent light-driven [4+2]-cycloaddition, affording the corresponding tetracyclic products **5b-f** with excellent dr and in good yields spanning from 41% to 72%.

³⁷ Su, Y.; Kuijpers, K.; Hessel, V.; Noël, T. A Convenient Numbering-up Strategy for the Scale-up of Gas-Liquid Photoredox Catalysis in Flow. *React. Chem. Eng.* **2016**, *1*, 73–81.

³⁸ Bauvois, B.; Puiffe, M.-L.; Bongui, J.-B.; Paillat, S.; Monneret, C.; Dauzonne, D. *Synthesis and Biological Evaluation of Novel Flavone-8-Acetic Acid Derivatives as Reversible Inhibitors of Aminopeptidase N/CD13*. *J. Med. Chem.* **2003**, *46*, 3900–3913.



— 2-methylbenzophenone scope

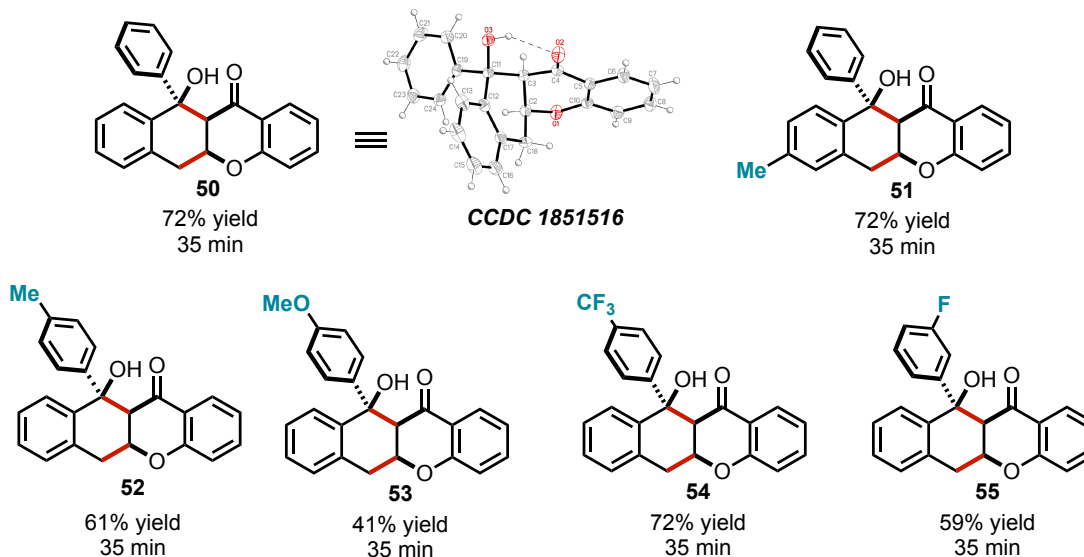


Table 3.6. - Substrate scope of the [4+2]-cycloaddition reaction between 2-MBP and chromone **38**.

Limitations

The present microfluidic photochemical method presents wide limitations in terms of reactivity when using coumarin derivatives with higher absorption at 365 nm (Figure 3.13). In fact, thioxocoumarin **56** showed poor reactivity under the titled reaction conditions, producing only traces of the expected sulphur-containing cycloadduct. As a matter of fact, compound **56** showed high tendency to undergo light-promoted [2+2]-dimerisation reaction, thus preventing the productive [4+2]-cycloaddition pathway. The same fate had the 2-quinolone derivative **57**. The irradiation of a reaction mixture containing **1** and **57** provided highly luminescent crudes with no traces of the product.

— Limitations of this protocol

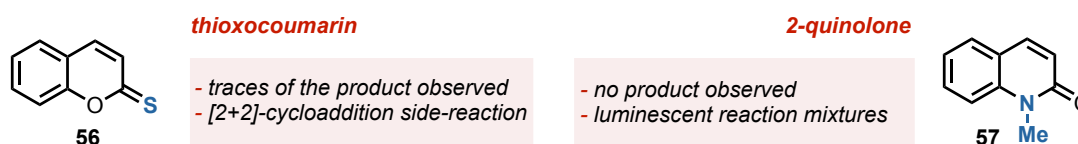


Figure 3.13. - Limitations of the [4+2]-cycloaddition protocol presented in this section.



3.2.5 Conclusions

In conclusion we developed an effective light-driven microfluidic method for the synthesis of valuable tetracyclic molecular architectures using commercially available precursors and common 365 nm bulbs. The reaction does not proceed under conventional batch conditions, highlighting the essential role of the developed MFP. A wide series of naphthochromenones and benzoxanthenes were synthesized in high yields and excellent diastereoselectivity. Finally, the large-scale production of product **40** demonstrated the high synthetic appeal of the present MFP method, which can be well suited for the construction of diverse biologically active molecules.

3.2.6 Experimental Section

The continuous flow reactions were carried out using capillary reactors made with PTFE tubing (0.75 mm I.D., 1.58 mm O.D.) and fitting connections purchased from SigmaAldrich. Reagents were pumped using a Syrris Asia pump (<https://syrris.com/modules/asia-syringe-pump/>). LEDs were purchased from Roithner LaserTechnik GmbH (model LED365-06Z 5.5 mW <http://www.roithnerlaser.com/index.html>). 26 W black bulb and 9W 365 nm bulb lamps were purchased from Amazon (<https://www.amazon.it/Foxnovo-sostituzione-lampadina-essiccatorrelampada/dp/B00JKE1T70>).

The NMR spectra were recorded on Bruker 400 Avance III HD equipped with a BBI-z grad probehead 5mm, Bruker 500 Avance III equipped with a BBI-ATM-z grad probehead 5mm and Bruker DMX 600 equipped with a BBI z-grad probehead 5mm. The chemical shifts (δ) for ^1H and ^{13}C are given in ppm relative to residual signals of the solvents (CHCl_3 @ 7.26 ppm ^1H NMR, 77.16 ppm ^{13}C NMR). Coupling constants are given in Hz. The following abbreviations are used to indicate the multiplicity: s, singlet; d, doublet; t, triplet; q, quartet; m, multiplet; bs, broad signal. NMR yields were calculated by using trichloroethylene as internal standard.

The ^1H , ^{13}C and ^{19}F NMR spectra are available in literature free of charge.³⁹

High-Resolution Mass Spectra (HRMS) were obtained using Waters GCT gas chromatograph coupled with a time-of-flight mass spectrometer (GC/MS-TOF) with electron ionization (EI) or MicroTOF II (Bruker Daltonics): HPLC-MS-TOF (ESI). Chromatographic purification of products was accomplished using flash chromatography on silica gel (SiO_2 , 0.04-0.063 mm) purchased from Machery-Nagel, with the indicated solvent system according to the standard techniques. Thin-layer chromatography (TLC) analysis was performed on pre-coated Merck TLC plates (silica gel 60 GF254, 0.25 mm). Visualization of the developed chromatography was performed by checking UV absorbance (254nm) as well as with aqueous ceric ammonium molybdate and potassium permanganate solutions. Organic solutions were concentrated under reduced pressure on a Büchi rotary evaporator.

Materials: Commercial grade reagents and solvents were purchased at the highest commercial quality from Sigma Aldrich or FluoroChem and used as received, unless otherwise stated.

The diverse reaction set up images and photophysical studies are available free of charge in literature.²⁸

³⁹ Mateos, J.; Meneghini, N.; Bonchio, M.; Marino, N.; Carofiglio, T.; Companyó, X.; Dell'Amico, L. *Microfluidic Light-Driven Synthesis of Tetracyclic Molecular Architectures*. *Beilstein J. Org. Chem.* **2018**, *14*, 2418–2424.

Light sources emission spectra

The following spectra were recorded using an AvaSpec ULS3648 high-resolution fiber-optic spectrometer which was placed at a fixed distance of 0.5 cm from the light source.

(more info at: <https://www.avantes.com/products/spectrometers/starline/item/209-avaspec-uls3648-high-resolution-spectrometer>).

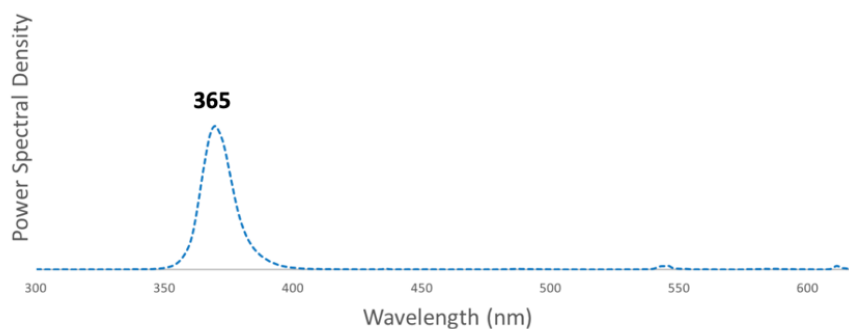


Figure 3.14. - Emission spectra of the Roithner LaserTechnik 365 nm LEDs used in this section.

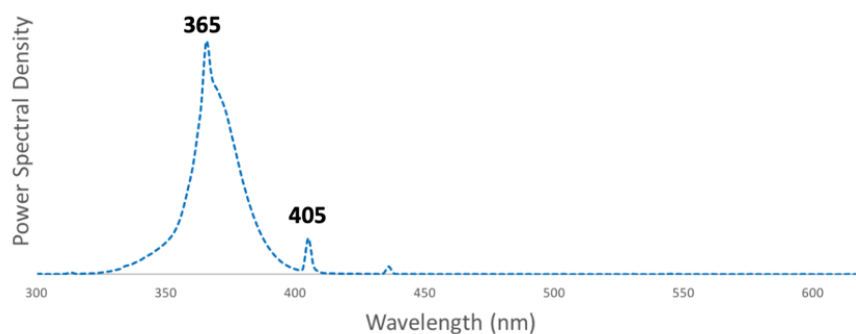
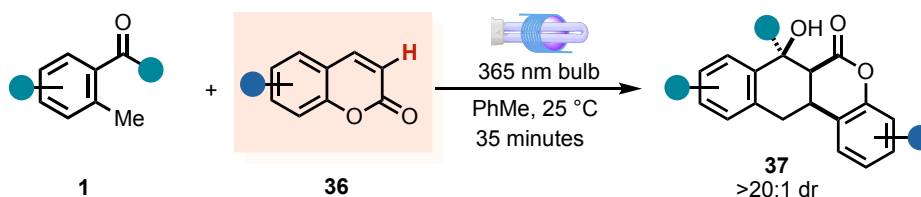


Figure 3.15. - Emission spectra of the 365 nm 9W bulbs used in this section.

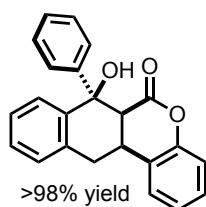
General procedure for the microfluidic reactions with coumarins

General procedure with coumarin derivatives



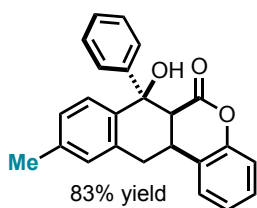
Coumarin (**36**, 219.2 mg, 5 equiv, 1.5 mmol) was introduced into a 12 mL vial under nitrogen atmosphere and dissolved in 5 mL of degassed toluene. Then, 2-methylbenzophenone (**1**, 55 μ L, 1 equiv, 0.3 mmol) was added in one portion and the solution was further bubbled with nitrogen for 5 min. The resultant solution was pumped into the MFP and irradiated by a 9 W 365 nm bulb with a residence time of 35 min. The product solution was collected into a 7 mL vial. Subsequently, the solvent was removed by rotary evaporation and the crude subjected to flash column chromatography on silica gel (9:1 hexane/EtOAc) yielding pure **37** (white solid), as a single diastereoisomer in >98% yield (100.1 mg, 0.293 mmol).

7-Hydroxy-7-phenyl-6a,7,12,12a-tetrahydro-6H-naphtho[2,3-c]chromen-6-one (**40**).



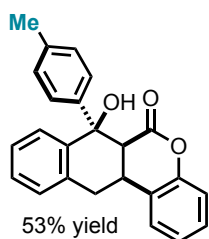
¹H-NMR (400 MHz, CDCl₃): 7.71 (d, $J = 7.5$ Hz, 1H, Ar), 7.37-7.27 (m, 6H, Ar), 7.19 (d, $J = 7.7$ Hz, 2H, Ar), 7.16–7.09 (m, 4H, Ar), 5.47 (br s, 1H, OH), 3.35 (d, $J = 4.5$ Hz, 1H, CH 2), 3.22 (dt, $J = 12.8, 6.5$, 2H, CH₂ 4), 2.90 (dd, $J = 19.4, 13.6$, 1H, CH 3) ppm. **¹³C-NMR (100 MHz, CDCl₃):** δ 171.0 (COO), 150.5 (Cq Ar), 146.2 (Cq Ar), 139.4 (Cq Ar), 133.3 (Cq Ar), 128.7 (CH Ar), 128.0 (CH Ar), 128.0 (CH Ar x2), 127.7 (CH Ar), 127.7 (CH Ar), 127.7 (Cq Ar), 127.4 (CH Ar), 127.3 (CH Ar x2), 127.1 (CH Ar), 124.8 (CH Ar), 117.0 (CH Ar), 76.2 (Cq I), 50.61 (CH), 33.4 (CH₂), 33.2 (CH) ppm.

7-Hydroxy-10-methylphenyl-6a,7,12,12a-tetrahydro-6H-naphtho[2,3-c]chromen-6-one (**41**).



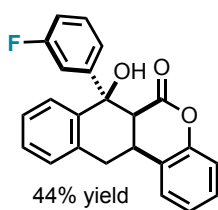
¹H-NMR (400 MHz, CDCl₃): 7.47 (d, $J = 8.2$ Hz, 1H, Ar), 7.23-7.14 (m, 4H, Ar), 7.10-6.98 (m, 6H, Ar), 6.84 (s, 1H, Ar), 5.30 (br s, 1H, OH), 3.20 (d, $J = 4.4$ Hz, 1H, C₂H), 3.11-3.01 (m, 2H, C₄H₂), 2.74 (dd, $J = 15.4, 7.0$, 1H, C₃H), 2.27 (s, 3H, CH₃) ppm. **¹³C-NMR (100 MHz, CDCl₃):** δ 171.2 (COO), 150.7 (Cq Ar), 146.4 (Cq Ar), 137.9 (Cq Ar), 136.6 (Cq Ar), 133.3 (Cq Ar), 128.9 (CH Ar), 128.6 (CH Ar), 128.4 (CH Ar), 128.2 (CH Ar x2), 128.1 (CH Ar), 128.0 (Cq Ar), 127.9 (CH Ar), 127.5 (CH Ar x2), 127.3 (CH Ar), 124.9 (CH Ar), 117.1 (CH Ar), 76.3 (Cq I), 50.9 (CH 2), 33.5 (CH₂ 4), 33.5 (CH 3), 21.3 (CH₃) ppm. **HRMS (MALDI)** calculated for [C₂₄H₂₀O₃+Na]⁺: 379.1305, found: 379.1307.

7-Hydroxy-7-(*p*-tolyl)-6a,7,12,12a-tetrahydro-6*H*-naphtho[2,3-*c*]chromen-6-one (42).



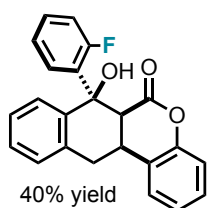
¹H-NMR (400 MHz, CDCl₃): 7.64 (dd, *J* = 7.32, 1.78, 1H, Ar), 7.33-7.18 (m, 3H, Ar), 7.11- 6.94 (m, 8H, Ar), 5.37 (br s, 1H, OH), 3.25 (d, *J* = 3.44 Hz, 1H, CH), 3.23-3.14 (m, 2H, CH₂), 2.81 (td, *J* = 14.78, 5.92 Hz, 1H, CH), 2.28 (s, 3H, CH₃) ppm. **¹³C-NMR (100 MHz, CDCl₃):** δ 171.3 (COO), 150.7 (Cq Ar) 143.5 (Cq Ar), 139.8 (Cq Ar), 137.6 (Cq Ar), 133.4 (Cq Ar), 128.9 (CH Ar x3), 128.2 (CH Ar), 128.1 (CH Ar), 127.9 (Cq Ar), 127.9 (CH Ar), 127.5 (CH Ar), 127.4 (CH Ar x2), 127.3 (CH Ar), 124.9 (CH Ar), 117.1 (CH Ar), 76.2 (Cq *I*), 50.8 (CH 2), 33.5 (CH₂ 4), 33.4 (CH 3), 21.2 (CH₃) ppm. **HRMS (MALDI)** calculated for [C₂₄H₂₀O₃+Na]⁺: 379.1305, found: 379.1305.

7-(3-Fluorophenyl)-7-hydroxy-6a,7,12,12a-tetrahydro-6*H*-naphtho[2,3-*c*]chromen-6-one (43).



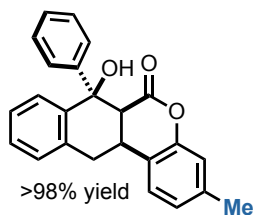
¹H-NMR (400 MHz, CDCl₃): 7.59-7.57 (m, 1H, Ar), 7.26-7.14 (m, 4H, Ar), 7.05-7.01 (m, 4H, Ar), 6.90–6.80 (m, 3H, Ar), 5.39 (br s, 1H, OH), 3.20 (d, *J* = 4.9 Hz, 1H, CH 2), 3.14-3.07 (m, 2H, CH₂ 4), 2.78 (dd, *J* = 19.9, 13.7 Hz, 1H, CH 3) ppm. **¹³C-NMR (100 MHz, CDCl₃):** δ 171.0 (COO), 150.6 (Cq Ar), 139.1 (Cq Ar), 133.4 (Cq Ar), 129.7 (Cq Ar), 129.7, 129.1 (CH Ar), 128.6, 128.1, 128.1, 127.8, 127.7, 127.4 (CH Ar), 125.1 (CH Ar), 123.4, 123.3, 117.2, 115.1, 114.9, 76.1 (Cq *I*), 50.7 (CH 2), 33.5 (CH₂ 4), 33.4 (CH 3) ppm. **HRMS (MALDI)** calculated for [C₂₃H₁₇FO₃+Na]⁺: 383.1054, found: 383.1051.

7-(2-Fluorophenyl)-7-hydroxy-6a,7,12,12a-tetrahydro-6*H*-naphtho[2,3-*c*]chromen-6-one (44).



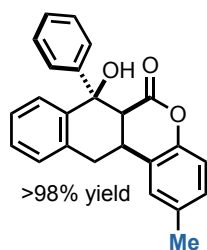
¹H-NMR (400 MHz, CDCl₃): 7.64-7.62 (m, 1H, Ar), 7.27-7.19 (m, 4H, Ar), 7.06-7.01 (m, 5H, Ar), 6.90 (t, *J* = 8.4 Hz, 1H, Ar), 6.51 (t, *J* = 7.8 Hz, 1H, Ar), 4.88 (br s, 1H, OH), 3.76 (d, *J* = 4.8 Hz, 1H, CH 2), 3.14-3.06 (m, 2H, CH₂ 4), 2.83 (dd, *J* = 19.7, 12.8 Hz, 1H, CH 3) ppm. **¹³C-NMR (100 MHz, CDCl₃):** δ 170.7 (COO), 161.7 (Cq Ar), 159.7 (Cq Ar), 150.9 (Cq Ar), 139.2, 133.4, 131.0, 130.3, 128.9, 128.5, 128.3, 128.2, 127.6, 127.5, 127.1, 125.0, 123.7, 117.2, 117.1, 75.6 (Cq *I*), 48.1 (CH 2), 33.6 (CH₂ 4), 33.1 (CH 3) ppm. **HRMS (MALDI)** calculated for [C₂₃H₁₇FO₃+Na]⁺: 383.1054, found: 383.1052.

7-Hydroxy-3-methyl-7-phenyl-6a,7,12,12a-tetrahydro-6H-naphtho[2,3-c]chromenone (45).



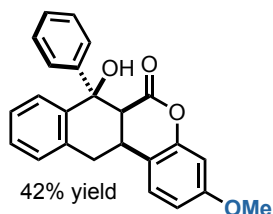
¹H-NMR (400 MHz, CDCl₃): 7.65-7.41 (m, 1H, Ar), 7.25-7.13 (m, 5H, Ar), 7.06 (dd, *J* = 7.7, 2.0 Hz, 2H, Ar), 7.02 (dd, *J* = 6.5, 2.2 Hz, 1H, Ar), 6.97 (dd, *J* = 8.3, 1.7 Hz, 1H, Ar), 6.88 (d, *J* = 8.3 Hz, 1H, Ar), 6.77 (d, *J* = 1.8 Hz, 1H, Ar), 5.39 (br s, 1H, OH), 3.19 (d, *J* = 3.2 Hz, 1H, CH 2), 3.12-3.00 (m, 2H, CH₂ 4), 2.75 (td, *J* = 15.8, 7.1 Hz, 1H, CH 3), 2.18 (s, 3H, CH₃) ppm. **¹³C-NMR (100 MHz, CDCl₃):** δ 171.1 (COO), 148.2 (Cq Ar) 146.1 (Cq Ar), 139.3 (Cq Ar), 134.4 (Cq Ar), 133.2 (Cq Ar), 128.9 (CH Ar), 127.9 (CH Ar x4), 127.6 (Cq Ar), 127.5 (CH Ar), 127.4 (CH Ar), 127.2 (CH Ar), 127.2 (CH Ar x3), 116.5 (CH Ar), 76.1 (Cq I), 50.5 (CH 2), 33.3 (CH₂ 4), 33.0 (CH 3), 20.5 (CH₃) ppm. **HRMS (MALDI)** calculated for [C₂₄H₂₀O₃+Na]⁺: 379.1305, found: 379.1302.

7-Hydroxy-2-methyl-7-phenyl-6a,7,12,12a-tetrahydro-6H-naphtho[2,3-c]chromen-6-one (46).



¹H-NMR (400 MHz, CDCl₃): 7.59 (dd, *J* = 7.3, 2.0, 1H, Ar), 7.27-7.13 (m, 5H, Ar), 7.06 (dd, *J* = 7.7, 2.0 Hz, 2H, Ar), 7.02 (dd, *J* = 6.6, 2.05 Hz, 1H, Ar), 6.89-6.77 (m, 3H, Ar), 5.37 (br s, 1H, OH), 3.19 (d, *J* = 4.7 Hz, 1H, CH 2), 3.11-2.98 (m, 2H, CH₂ 4), 2.74 (td, *J* = 19.7, 13.8 Hz, 1H, CH 3), 2.25 (s, 3H, CH₃) ppm. **¹³C-NMR (100 MHz, CDCl₃):** δ 171.8 (COO), 150.9 (Cq Ar) 146.8 (Cq Ar), 140.0 (Cq Ar), 139.6 (Cq Ar), 133.9 (Cq Ar), 128.5 (CH Ar x4), 128.2 (CH Ar), 128.2 (CH Ar), 127.8 (CH Ar x3), 127.3 (CH Ar), 125.9 (CH Ar), 125.1 (Cq Ar), 117.9 (CH Ar), 76.7 (Cq I), 51.3 (CH 2), 34.0 (CH₂ 4), 33.4 (CH 3), 21.6 (CH₃) ppm. **HRMS (MALDI)** [C₂₄H₂₀O₃+Na]⁺: 379.1305, found: 379.1307.

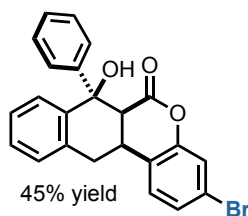
7-Hydroxy-3-methoxy-7-phenyl-6a,7,12,12a-tetrahydro-6H-naphtho[2,3-c]chromen-6-one (47).



¹H-NMR (400 MHz, CDCl₃): 7.59 (d, *J* = 7.5 Hz, 1H, Ar), 7.25-7.18 (m, 5H, Ar), 7.08 (dd, *J* = 7.8, 2.4 Hz, 2H, Ar), 7.03 (dd, *J* = 7.7, 2.4 Hz, 1H, Ar), 6.88 (d, *J* = 7.5, 1H, Ar), 6.57-6.52 (m, 2H, Ar), 5.33 (br s, 1H, OH), 3.71 (s, 3H, OMe), 3.21 (d, *J* = 4.0 Hz, 1H, CH 2), 3.12-3.02 (m, 2H, CH₂ 4), 2.74 (td, *J* = 19.7, 13.8 Hz, 1H, CH 3) ppm. **¹³C-NMR (100 MHz, CDCl₃):** δ 171.2 (COO), 160.1 (Cq Ar) 151.4 (Cq Ar), 146.4 (Cq Ar), 139.6 (Cq Ar), 133.6 (Cq Ar), 128.2 (CH Ar x4), 127.9 (CH Ar), 127.9 (CH Ar), 127.8 (CH Ar), 127.5 (CH Ar x3), 119.9 (Cq Ar), 110.7 (CH Ar), 102.9 (CH Ar), 76.4 (Cq I), 55.8

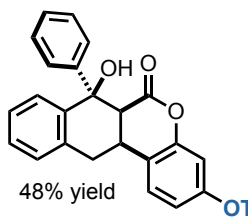
(OMe), 51.1 (CH 2), 33.9 (CH2 4), 32.7 (CH 3) ppm. **HRMS (MALDI)** [C₂₄H₂₀O₄+Na]⁺: 395.1254, found: 395.1257.

3-bromo-7-hydroxy-7-phenyltetrahydro-6H-naphtho[2,3-c]chromen-6-one (48).



¹H-NMR (400 MHz, CDCl₃): δ 7.69 (d, *J* = 7.5 Hz, 1H, Ar), 7.33-7.25 (m, 6H, Ar), 7.24-7.15 (m, 3H, Ar), 6.97 (d, *J* = 7.8 Hz, 1H, Ar), 5.32 (s, 1H, OH), 3.351(d, *J* = 4.7 Hz, 1H, CH 2), 3.18 (dt, *J* = 12.2, 6.9, 2H, CH₂ 4), 2.85 (dd, *J* = 19.4, 12.8, 1H, CH 3) ppm. **¹³C-NMR (100 MHz, CDCl₃):** δ 170.2 (COO), 151.0 (Cq Ar), 146.0 (Cq Ar), 139.2 (Cq Ar), 133.3 (Cq Ar), 132.9(CH Ar), 128.4 (CH Ar), 128.2 (CH Ar x2), 128.1 (CH Ar), 128.0 (CH Ar), 127.9 (CH Ar), 127.8 (Cq Ar), 127.3 (CH Ar x2), 126.7 (CH Ar x2), 121.5 (CH Ar), 120.3 (CH Ar), 76.1 (Cq 1), 50.5 (CH), 33.2 (CH₂), 33.0 (CH) ppm. **HRMS** calculated for [C₂₃H₁₇BrO₃+H]⁺: 421.0361, found: 421.0359.

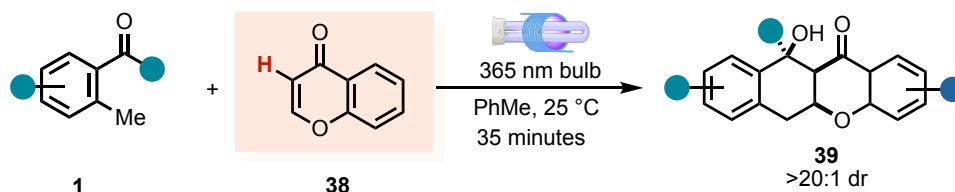
7-hydroxy-7-phenyltetrahydro-6H-naphtho[2,3-c]chromen-3-yltrifluoromethanesulfonate (49).



¹H-NMR (400 MHz, CDCl₃): δ 7.59 (d, *J* = 8.2 Hz, 1H, Ar), 7.25-7.19 (m, 5H, Ar), 7.09-7.03 (m, 4H, Ar), 6.97-6.92 (m, 2H, Ar), 5.11 (br s, 1H, OH), 3.24 (d, *J* = 3.7 Hz, 1H, C₂H), 3.18-3.07 (m, 2H, C₄H₂), 2.76 (dd, *J* = 16.7, 10.7, 1H, C₃H) ppm. **¹³C-NMR (100 MHz, CDCl₃):** δ 169.7 (COO), 151.3 (Cq Ar), 148.9 (Cq Ar), 145.9 (Cq Ar), 139.2 (Cq Ar), 132.8 (Cq Ar), 128.7 (CH Ar), 128.5 (CH Ar), 128.4 (CH Ar x 2), 128.2 (CH Ar), 127.9 (CH Ar), 127.5 (Cq Ar), 127.9 (CH Ar), 117.8 (CH Ar), 111.03 (CH Ar) 76.2 (Cq 1), 50.4 (CH 2), 33.3 (CH₂ 4), 33.1 (CH 3), 21.3 (CH₃) ppm. **¹⁹F-NMR (376 MHz, CDCl₃):** δ -73.07 (s, 3F, CF₃) ppm. **HRMS (ESI-MS)** calculated for [C₂₄H₁₇F₃O₆S+H]⁺: 491.0698, found: 491.0702.

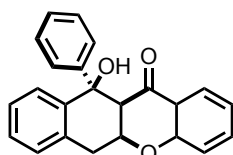
General procedure for the microfluidic reactions with chromones

— General procedure with chromone derivatives



Chromone (**38**, 219.2 mg, 5 equiv, 1.5 mmol) was introduced into a 12 mL vial under nitrogen atmosphere and dissolved in 5 mL of degassed toluene. Then, 2-methylbenzophenone (**1**, 55 μ L, 1 equiv, 0.3 mmol) was added in one portion and the solution was further bubbled with nitrogen for 5 min. The resultant solution was pumped into the MFP and irradiated by a 9 W 365 nm bulb with a residence time of 35 min. The product solution was collected into a 7 mL vial. Subsequently, the solvent was removed by rotary evaporation and the crude subjected to flash column chromatography on silica gel (9:1 hexane/EtOAc) yielding pure **39** (white solid), as a single diastereoisomer in >98% yield (100.1 mg, 0.293 mmol).

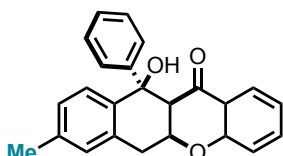
11-Hydroxy-11-phenyl-5a,6,11,11a-tetrahydro-12H-benzo[b]xanthen-12-one (**50**).



72% yield

¹H-NMR (400 MHz, CDCl₃): 7.74 (dd, $J = 7.5, 1.9$ Hz, 1H, Ar), 7.53-7.49 (m, 1H, Ar), 7.40 (ddd, $J = 15.6, 7.4, 2.0$ Hz, 1H, Ar), 7.24-7.15 (m, 5H, Ar), 7.07-7.00 (m, 3H, Ar), 6.91 (t, $J = 7.4$ Hz, 1H, Ar), 6.83 (d, $J = 8.4$ Hz, 1H, Ar), 5.67 (br s, 1H, OH), 4.71 (ddd, $J = 9.5, 7.1, 5.1$ Hz, 1H, CH 3), 3.57 (d, $J = 5.8$ Hz, 1H, CH 2), 3.22 (dd, $J = 17.5, 9.5$ Hz, 1H, CH2 4a), 3.22 (dd, $J = 17.5, 7.0$ Hz, 1H, CH2 4b) ppm. **¹³C-NMR (100 MHz, CDCl₃):** δ 196.0 (C=O), 159.7 (Cq Ar), 146.4 (Cq Ar), 140.5 (Cq Ar), 137.3 (CH Ar), 132.4 (Cq Ar), 128.8 (CH Ar), 128.7 (CH Ar x2), 128.6 (CH Ar x2), 128.2 (CH Ar), 127.9 (CH Ar), 127.5 (CH Ar x2), 127.3 (CH Ar), 121.8 (CH Ar), 121.3 (Cq Ar), 118.8 (CH Ar), 78.3 (Cq 1), 74.2 (CH 2), 55.4 (CH 3), 30.8 (CH2 4) ppm. **HRMS (MALDI)** calculated for [C₂₃H₁₈O₃+Na]⁺: 365.1154, found: 365.1158.

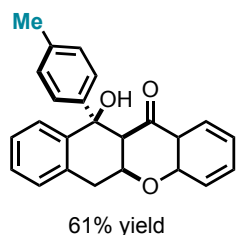
11-Hydroxy-8-methyl-11-phenyl-5a,6,11,11a-tetrahydro-12H-benzo[b]xanthen-12-one (**51**).



72% yield

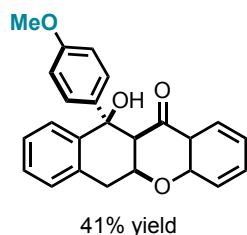
¹H-NMR (400 MHz, CDCl₃): 7.73 (d, $J = 7.5$ Hz, 1H, Ar), 7.43-7.36 (m, 2H, Ar), 7.26-7.13 (m, 3H, Ar), 7.06 (d, $J = 7.5$ Hz, 2H, Ar), 7.00 (d, $J = 7.8$ Hz, 1H, Ar), 6.90 (t, $J = 7.4$ Hz, 1H, Ar), 6.83-6.81 (m, 2H, Ar), 5.53 (br s, 1H, OH), 4.77 (ddd, $J = 9.5, 7.1, 5.1$ Hz, 1H, CH 3), 3.53 (d, $J = 5.8$ Hz, 1H, CH 2), 3.17 (dd, $J = 17.5, 9.5$ Hz, 1H, CH2 4a), 3.09 (dd, $J = 17.5, 7.0$ Hz, 1H, CH2 4b), 2.24 (s, 3H, CH3) ppm. **¹³C-NMR (100 MHz, CDCl₃):** δ 195.5 (C=O), 159.3 (Cq Ar), 146.2 (Cq Ar), 138.0 (Cq Ar), 137.3 (Cq Ar), 136.9 (CH Ar), 131.8 (Cq Ar), 128.8 (CH Ar), 128.6 (CH Ar), 128.2 (CH Ar), 128.1 (CH Ar x2), 127.7 (CH Ar), 127.2 (CH Ar x2), 127.0 (CH Ar), 121.4 (CH Ar), 121.0 (Cq Ar), 118.3 (CH Ar), 77.7 (Cq 1), 73.2 (CH 2), 55.1 (CH 3), 30.4 (CH2 4), 21.2 (CH3) ppm. **HRMS (MALDI)** calculated for [C₂₄H₂₀O₃+Na]⁺: 365.1310, found: 365.1315.

11-Hydroxy-11-(*p*-tolyl)phenyl-5a,6,11,11a-tetrahydro-12*H*-benzo[*b*]xanthen-12-one (52).



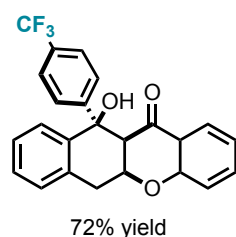
¹H-NMR (400 MHz, CDCl₃): 7.73 (dd, *J* = 7.2, 2.1 Hz, 1H, Ar), 7.53-7.49 (m, 1H, Ar), 7.40 (ddd, *J* = 15.6, 7.4, 2.0 Hz, 1H, Ar), 7.20–7.14 (m, 2H, Ar), 7.03-6.98 (m, 3H, Ar), 6.94-6.88 (m, 3H, Ar), 6.83 (d, *J* = 8.3 Hz, 1H, Ar), 5.62 (br s, 1H, OH), 4.80 (ddd, *J* = 9.5, 7.1, 5.1 Hz, 1H, CH 3), 3.55 (d, *J* = 5.8 Hz, 1H, CH 2), 3.21 (dd, *J* = 17.5, 9.5 Hz, 1H, CH2 4a), 3.13 (dd, *J* = 17.5, 7.0 Hz, 1H, CH2 4b), 2.24 (s, 3H, CH₃) ppm. **¹³C-NMR (100 MHz, CDCl₃):** δ 195.6 (C=O), 159.3 (Cq Ar), 143.2 (Cq Ar), 140.4 (Cq Ar), 137.4 (Cq Ar), 136.9 (CH Ar), 132.0 (Cq Ar), 128.9 (CH Ar x2), 128.3 (CH Ar), 128.3 (CH Ar), 128.2 (CH Ar), 127.5 (CH Ar), 127.0 (CH Ar x2), 126.9 (CH Ar), 121.4 (CH Ar), 120.9 (Cq Ar), 118.4 (CH Ar), 77.7 (Cq 1), 73.8 (CH 2), 55.1 (CH 3), 30.4 (CH2 4), 21.1 (CH₃) ppm. **HRMS (MALDI)** calculated for [C₂₄H₂₀O₃+Na]⁺: 365.1315, found: 365.1319.

11-Hydroxy-11-(4-methoxy)phenyl-5a,6,11,11a-tetrahydro-12*H*-benzo[*b*]xanthen-12-one (53)



¹H-NMR (400 MHz, CDCl₃): 7.73 (dd, *J* = 7.5, 1.9 Hz, 1H, Ar), 7.55-7.53 (m, 1H, Ar), 7.42 (ddd, *J* = 15.6, 7.4, 2.0 Hz, 1H, Ar), 7.22–7.15 (m, 2H, Ar), 7.04-7.00 (m, 1H, Ar), 7.97-6.88 (m, 3H, Ar), 6.84 (d, *J* = 7.4 Hz, 1H, Ar), 6.73 (d, *J* = 8.4 Hz, 1H, Ar), 5.67 (br s, 1H, OH), 4.80 (ddd, *J* = 9.5, 7.1, 5.1 Hz, 1H, CH 3), 3.71 (s, 3H, OMe), 3.57 (d, *J* = 5.8 Hz, 1H, CH 2), 3.20 (dd, *J* = 17.5, 9.5 Hz, 1H, CH2 4a), 3.12 (dd, *J* = 17.5, 7.0 Hz, 1H, CH2 4b) ppm. **¹³C-NMR (100 MHz, CDCl₃):** δ 195.7 (C=O), 159.3 (Cq Ar), 159.1 (Cq Ar), 140.3 (Cq Ar), 138.4 (Cq Ar), 137.0 (CH Ar), 132.0 (Cq Ar), 128.4 (CH Ar x3), 128.3 (CH Ar), 128.2 (CH Ar x3), 121.4 (CH Ar), 120.9 (Cq Ar), 118.4 (CH Ar), 113.5 (CH Ar x2), 77.7 (Cq 1), 73.8 (CH 2), 55.4 (OMe), 55.42 (CH 3), 30.3 (CH2 4) ppm. **HRMS (MALDI)** calculated for [C₂₄H₂₀O₄+Na]⁺: 395.1259, found: 395.1262.

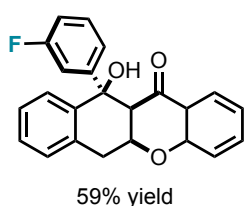
11-Hydroxy-11-(4-trifluoromethyl)phenyl-5a,6,11,11a-tetrahydrobenzo[*b*]xanthen-12-one (54).



¹H-NMR (400 MHz, CDCl₃): 7.74 (dd, *J* = 7.5, 1.9 Hz, 1H, Ar), 7.50-7.36 (m, 4H, Ar), 7.24–7.14 (m, 4H, Ar), 7.09-7.04 (m, 1H, Ar), 6.92 (t, *J* = 7.5 Hz, 1H, Ar), 6.83 (d, *J* = 8.4 Hz, 1H, Ar), 5.45 (br s, 1H, OH), 4.77 (ddd, *J* = 9.5, 7.1, 5.1 Hz, 1H, CH 3), 3.46 (d, *J* = 6.0 Hz, 1H, CH 2), 3.26 (dd, *J* = 17.5, 9.5 Hz, 1H, CH2 4a), 3.17 (dd, *J* = 17.5, 7.0 Hz, 1H, CH2 4b) ppm. **¹³C-NMR (100 MHz, CDCl₃):** δ 194.8 (C=O), 159.4

(Cq Ar), 150.1 (Cq Ar), 139.6 (Cq Ar), 137.0 (CH Ar), 131.2 (Cq Ar), 128.7 (CH Ar), 128.7 (CH Ar), 128.4 (CH Ar), 127.8 (CH Ar), 127.6 (CH Ar x4), 127.0 (CH Ar), 125.3 (CF₃), 121.8 (CH Ar), 121.0 (Cq Ar), 118.4 (CH Ar), 77.3 (Cq I), 73.7 (CH 2), 54.8 (CH 3), 30.7 (CH₂ 4) ppm. **HRMS (MALDI)** calculated for [C₂₄H₁₇F₃O₃+Na]⁺: 433.1023, found: 433.1025.

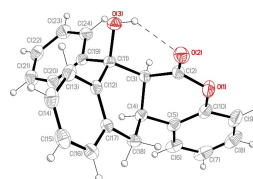
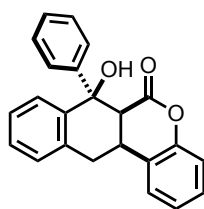
11-(3-Fluorophenyl)-11-hydroxyphenyl-5a,6,11,11a-tetrahydrobenzo[*b*]xanthen-12-one (55).



¹H-NMR (400 MHz, CDCl₃): 7.74 (dd, *J* = 7.5, 1.9 Hz, 1H, Ar), 7.50–7.47 (m, 1H, Ar), 7.44 (ddd, *J* = 15.3, 7.5, 2.0 Hz, 1H, Ar), 7.24–7.15 (m, 3H, Ar), 7.07–7.03 (m, 1H, Ar), 6.97–6.78 (m, 5H, Ar), 6.83 (d, *J* = 8.4 Hz, 1H, Ar), 5.68 (br s, 1H, OH), 4.80 (ddd, *J* = 9.4, 7.2, 5.1 Hz, 1H, CH 3), 3.54 (d, *J* = 5.8 Hz, 1H, CH 2), 3.25 (dd, *J* = 17.5, 9.5 Hz, 1H, CH₂ 4a), 3.18 (dd, *J* = 17.5, 7.0 Hz, 1H, CH₂ 4b) ppm. **¹³C-NMR (100 MHz, CDCl₃):** δ 195.3 (C=O), 163.7 (Cq Ar), 161.7 (Cq Ar), 159.2 (Cq Ar), 148.6, 148.6, 139.5, 137.1, 131.9, 129.7, 128.2, 127.7, 127.0, 122.9, 121.6, 120.7, 118.4, 114.8, 114.4, 77.5 (Cq I), 73.6 (CH 2), 54.7 (CH 3), 30.3 (CH₂ 4) ppm. **HRMS (MALDI)** calculated for [C₂₃H₁₇FO₃+Na]⁺: 383.1059, found: 383.1063.

X-ray crystallographic analysis of 40

— X-Ray data of 40 —



Empirical formula	C ₂₃ H ₁₈ O ₃
Formula weight	342.37
Temperature	293(2) K
Wavelength	0.71073 Å
Crystal system	Orthorhombic
Space group	<i>Pbca</i>

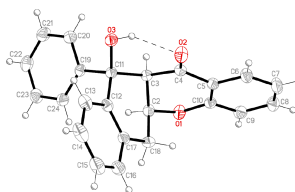
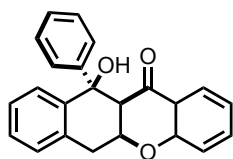
Unit cell dimensions	$a = 14.6629(5) \text{ \AA}$	$\alpha = 90^\circ$.
	$b = 7.5142(2) \text{ \AA}$	$\beta = 90^\circ$.
	$c = 30.7557(9) \text{ \AA}$	$\gamma = 90^\circ$.
Volume	3388.69(18) \AA^3	
Z	8	
Density (calculated)	1.342 g/cm ³	
Absorption coefficient	0.088 mm ⁻¹	
$F(000)$	1440	
Theta range for data collection	2.649 to 28.213°.	
Index ranges	-19 ≤ h ≤ 17, -9 ≤ k ≤ 9, -38 ≤ l ≤ 40	
Reflections collected	21025	
Independent reflections	3774 [$R(\text{int}) = 0.0420$]	
Completeness to theta = 25.242°	99.9 %	
Data / restraints / parameters	3774 / 0 / 235	
Goodness-of-fit on F^2	1.064	
Final R indices [$I > 2\sigma(I)$]	$R_1 = 0.0475$, $wR_2 = 0.0948$	
R indices (all data)	$R_1 = 0.0818$, $wR_2 = 0.1103$	
Largest diff. peak and hole	0.198 and -0.163 e. \AA^{-3}	

^a $R_1 = \sum ||F_o| - |F_c|| / \sum |F_o|$. ^b $wR_2 = \{ \sum w(F_o^2 - F_c^2)^2 / \sum [w(F_o^2)]^{1/2} \}$ and $w = 1 / [\sigma^2(F_o)^2 + (mP)^2 + nP]$ with $P = (F_o^2 + 2F_c^2) / 3$, $m = 0.0398$ and $n = 0.5786$.

CCDC 1837120 contains the supplementary crystallographic data for this compound. These data can be obtained free of charge from The Cambridge Crystallographic Data Centre via www.ccdc.cam.ac.uk/data_request/cif

X-ray crystallographic analysis of 50

— X-Ray data of 50



Empirical formula	C ₂₃ H ₁₈ O ₃	
Formula weight	342.37	
Temperature	298(2) K	
Wavelength	1.54184 Å	
Crystal system	Orthorhombic	
Space group	<i>P</i> 2 ₁ 2 ₁ 2 ₁	
Unit cell dimensions	<i>a</i> = 10.008942(16) Å	$\alpha = 90^\circ$.
	<i>b</i> = 11.49917(17) Å	$\beta = 90^\circ$.
	<i>c</i> = 14.7105(2) Å	$\gamma = 90^\circ$.
Volume	1693.18(5) Å ³	
<i>Z</i>	4	
Density (calculated)	1.343 g/cm ³	
Absorption coefficient	0.707 mm ⁻¹	
<i>F</i> (000)	720	
Reflections collected	13333	
Independent reflections	3362 [<i>R</i> (int) = 0.0276]	
Completeness to theta = 25.242°	99.9 %	
Data / restraints / parameters	3362 / 0 / 236	
Goodness-of-fit on <i>F</i> ²	1.066	
Final <i>R</i> indices [<i>I</i> > 2σ(<i>I</i>)]	<i>R</i> 1 = 0.0359, <i>wR</i> 2 = 0.0948	
<i>R</i> indices (all data)	<i>R</i> 1 = 0.0369, <i>wR</i> 2 = 0.0956	

Largest diff. peak and hole

0.223 and -0.200 e.Å⁻³

^a $R_1 = \sum ||F_o| - |F_c|| / \sum |F_o|$. ^b $wR_2 = \{ \sum w(F_o^2 - F_c^2)^2 / \sum [w(F_o^2)^2] \}^{1/2}$ and $w = 1 / [\sigma^2(F_o)^2 + (mP)^2 + nP]$ with $P = (F_o^2 + 2F_c^2) / 3$, $m = 0.0624$ and $n = 0.1241$.

CCDC 1851516 contains the supplementary crystallographic data for this compound. These data can be obtained free of charge from The Cambridge Crystallographic Data Centre via www.ccdc.cam.ac.uk/data_request/cif

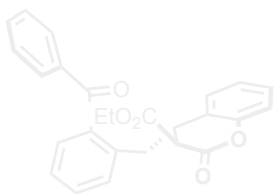
Chapter III – Section 3

Microfluidic Photoreactors – Light-Driven Construction of Naphthochromenones as a New Potential Class of Photocatalysts

— Chapter III - Synthetic Transformations Driven by Triplet State *o*-Alkyl Substituted Benzophenones —

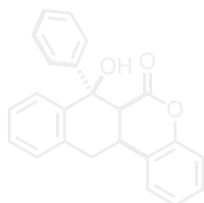
Section 1.

A microfluidic photoreactor enables 2-methylbenzophenone light-driven reactions with superior performances



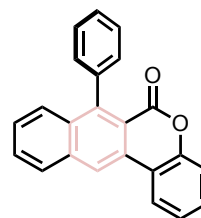
Section 2.

Microfluidic light-driven synthesis of tetracyclic molecular architectures



Section 3.

Synthesis and characterization of naphthochromenones as new potential organic photocatalysts



- To study the reactivity of the obtained products.
- To characterize the naphthochromenone scaffold and investigate its possible applications.⁴⁰

⁴⁰ The project discussed in this chapter has been conducted in collaboration with Dr. Alberto Vega-Peñaloza (involved in the synthesis and manipulation of the naphthochromenone-derived products) and Dr. Francesco Rigodanza (involved in the photophysical and electrochemical characterization of the compounds). I individually optimized the reaction conditions of diverse reactions as well as I prepared and characterized several entries of the reaction scope.

This work is part of the published work: Mateos, J.; Rigodanza, F.; Vega-Peñaloza, A.; Sartorel, A.; Natali, M.; Bortolato, T.; Pelosi, G.; Companyó, X.; Bonchio, M.; Dell'Amico, L. Naphthochromenones: Organic Bimodal Photocatalysts Engaging in Both Oxidative and Reductive Quenching Processes. *Angew. Chem. Int. Ed.* **2020**, *59*, 1302–1312.

3.3.1 Introduction

The development of novel synthetic methodologies is commonly guided by several factors.⁴¹ Such purposes span from the development of general catalysts to the design of versatile reagents. Regardless the motivation, the goal is generally common: the expansion of the synthetic chemist toolbox.⁴² For this reason, the focus on developing new methodologies for the development of specific drugs and enriched materials is key. Given the generality of the MFP method developed in the previous sections, together with the biorelevant properties of naphthochromenone scaffolds, we decided to focus our attention on the applications of the obtained product. For this reason, we decided to explore the flexibility of **40** in terms of manipulability. In fact, the presence of functional groups such as the lactone ring and the tertiary alcohol in a tetracyclic scaffold enlarged the possibilities of naphthochromenones as chromophoric cores.

3.3.2 Challenges of the project

Finding a general application to novel methodologies is not a trivial task. In fact, a clear application has to be envisaged in order to achieve the goal. For this reason, and seizing the distinctive absorptions of benzophenones and coumarins in the UV-light zone, we started looking towards possible applications in light-related fields of NTC scaffolds. Such applications could span from the development of light-responsive materials to versatile photocatalysts.

3.3.3 Section overview

In this section I detail the different types of manipulations of the naphthochromenone core **40**, with a special focus on the derivatization of product **61** as a potential class of organic photocatalyst (Figure 3.16). On one hand, when looking at the modification of the lactone ring, we report diverse ring opening reactions. Through different nucleophilic additions and reduction reactions products **58**, **59** and **60** were obtained in high yields (up to >98% yield) and excellent diastereoselectivities (>20:1 dr). On the other hand, when investigating at the tertiary alcohol moiety, we report an elimination/aromatization sequence. The obtained product **61**, possess interesting photo- and electro-chemical properties. For this reason, we

⁴¹ Ball, P. *Chemistry: Why Synthesize?* *Nature* **2015**, 528, 327–329.

⁴² Boström, J.; Brown, D. G.; Young, R. J.; Keserü, G. M. *Expanding the Medicinal Chemistry Synthetic Toolbox*. *Nat Rev Drug Discov* **2018**, 17, 709–727.

further investigated how the different functionalities (12 different naphthochromenones were synthesized) impact on the physicochemical properties.

— Manipulations of the naphthochromenone core

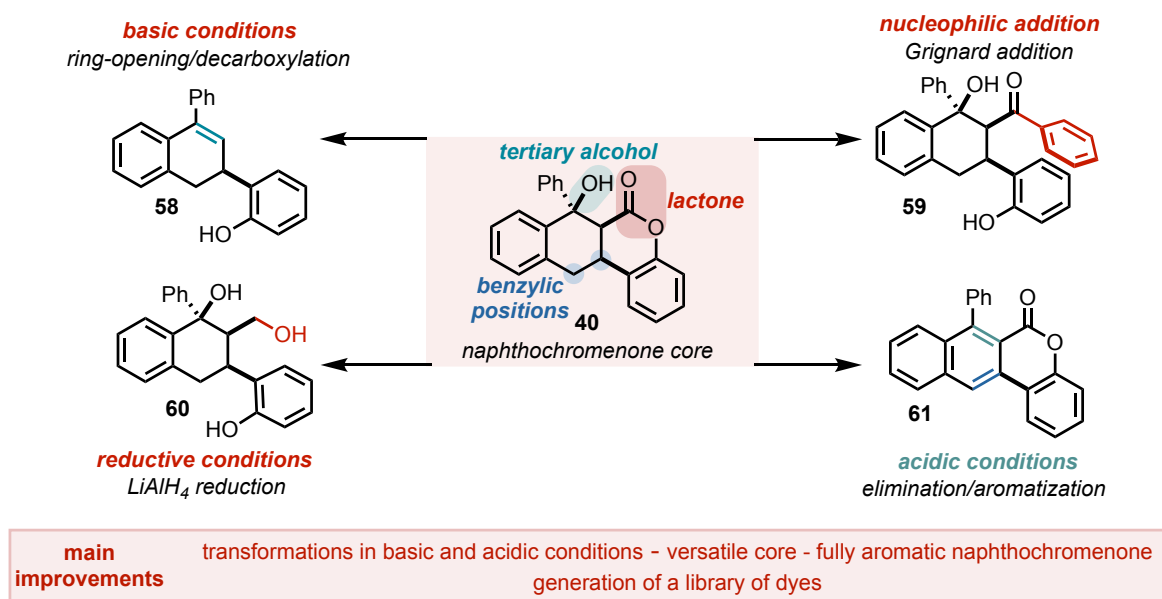


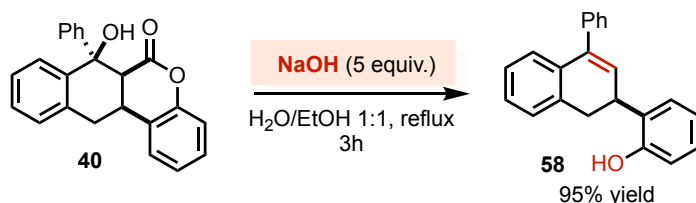
Figure 3.16. - Manipulations of the naphthochromenone core described in this section.

3.3.4 Results and discussion

Lactone ring-opening reactions (Scheme 3.8)

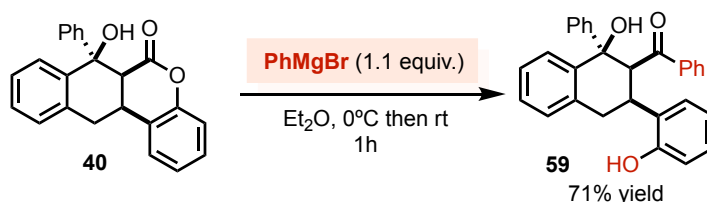
— A. Decarboxylation/Elimination sequence

basic conditions



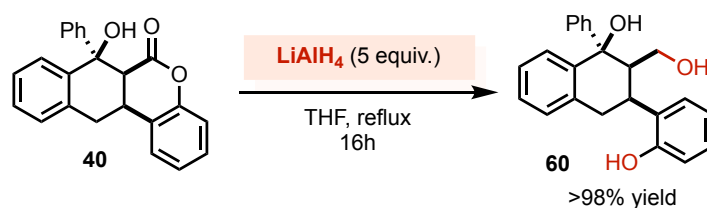
— B. Grignard addition

nucleophilic addition



— C. LiAlH_4 reduction

reductive conditions



Scheme 3.8. - Lactone-ring manipulation reactions. a) Decarboxylation/elimination sequence in basic conditions. b) Nucleophilic addition using Grignard reagents. c) Reduction with LiAlH₄.

The lactone ring possesses a myriad of opportunities when looking at its manipulation possibilities. Herein, I describe the: *i*) basic ring-opening reaction; *ii*) the Grignard addition; and *iii*) the reduction with LiAlH₄ (Scheme 3.8).

- The treatment of **40** with a solution of sodium hydroxide in water promoted a quantitative lactone-opening/decarboxylation cascade sequence, yielding 2,4-dihydronaphthalene **58** in quantitative yield without the need of chromatographic purification (Scheme 3.8a). Interestingly, scaffold **58** is a valuable intermediate for the synthesis of biologically active natural compounds⁴³ and industrially relevant drugs⁴⁴ reminiscent of the bioactive tetralinolic pharmacophoric core.⁴⁵
- The treatment of **40** with PhMgBr, converting the lactone moiety into the corresponding aryl ketone **59** (Scheme 3.8b). **59** was formed in 71% yield without diastereoisomeric loss. Nevertheless, the product obtained resulted to be highly unstable at room temperature without protection of light irradiation.
- Finally, LiAlH₄ reduction of **40** furnished bicyclic 1,3-diol **60** in quantitative yield without the need of chromatographic purification (Scheme 3.8c).

Noteworthy, compounds **58-60** embody different functionalities which can be suited for additional synthetic transformations.

Tertiary alcohol elimination reaction

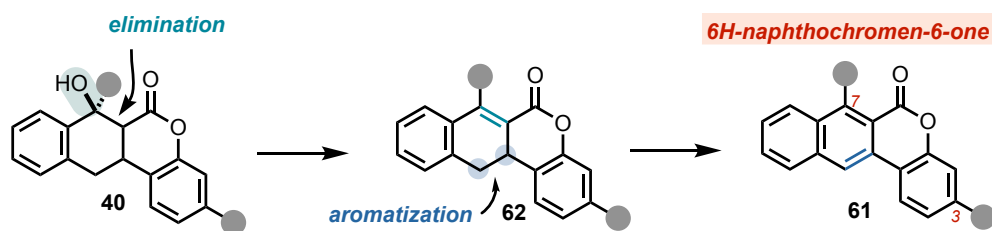
Analogously to the lactone motif, the tertiary alcohol is also a versatile functional group when thinking in thermal chemistry transformations. For this reason, we envisaged on the obtention of the fully aromatic molecule **61** through an elimination/aromatization sequence (Scheme 3.9).

⁴³ Lantaño, B.; Aguirre, J. M.; Drago, E. V.; de la Faba, D. J.; Pomilio, N.; Mufato, J. D. *Effect of Methoxyl Groups on the NMR Spectra: Configuration and Conformation of Natural and Synthetic Indanic and Tetralinic Structures: Effect of Methoxyl Groups on the NMR Spectra of Indanic and Tetralinic Structures.* *Magn. Reson. Chem.* **2017**, *55*, 619–633.

⁴⁴ Park, O. S.; Jang, B. S. *Synthesis of 4-Hydroxycoumarin Derivatives-1: An Efficient Synthesis of Floccoumafen.* *Arch. Pharm. Res.* **1995**, *18*, 277–281.

⁴⁵ Hanaya, K.; Onodera, S.; Ikegami, Y.; Kudo, H.; Shimaya, K. *The Hydrogen-Stretching Absorptions and Conformations of Tetralin-1-ol, Chroman-4-ol, Thiochroman-4-ol, and Indan-1-ol Derivatives.* *J. Chem. Soc., Perkin Trans. 2* **1981**, No. 6, 944.

— Elimination/aromatization strategy



Scheme 3.9. - Elimination/aromatization strategy adopted for the obtention of **61**.

Considering that both starting materials for the preparation of **40** (benzophenone **1** and coumarin **36**) have distinctive absorptions under the UV region,¹¹ we hypothesized a possible absorption at longer wavelengths of the more conjugated naphthochromenone scaffold. However, **61** was not obtained on purpose at the first attempts (Figure 3.17). Serendipitously, the acidic treatment of **40** at high temperatures with an air leak in the Argon atmosphere, generated the corresponding fully-aromatic core in a one-pot trend without traces of the α,β -unsaturated molecule **62**. Despite challenging, the purification furnished a fluorescent compound with potential light-related applications (see Chapter IV for the applications of naphthochromenones as versatile organic photocatalysts).

— Serendipitous obtention of **61**

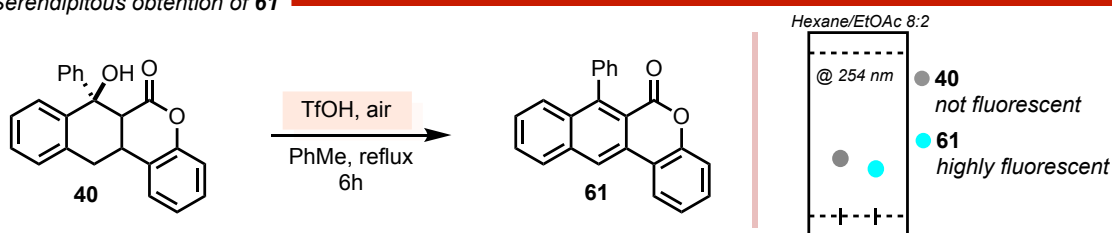
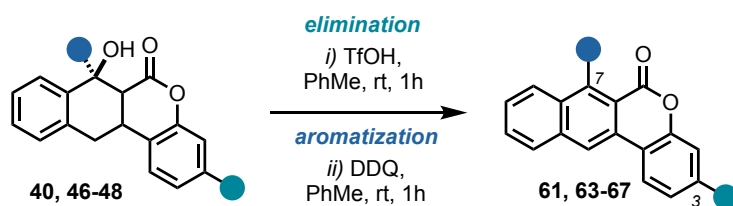


Figure 3.17. - Serendipitous obtention of **61** in a one-pot fashion.

Generality of the method

Once **60** was fully characterized, we designed a general and milder synthetic strategy (Table 3.7). The method consists of a two-step procedure. First, the acidic elimination of the tertiary alcohol at room temperature furnishes **62** in quantitative yields. Then, the aromatization of **62** with DDQ, yields NTCs in excellent yields (up to 91% yield over two consecutive steps). Additionally, when carrying out the reaction in multi-mmol scale, the recrystallization furnishes the product in high yields and purities.



— Substrate scope

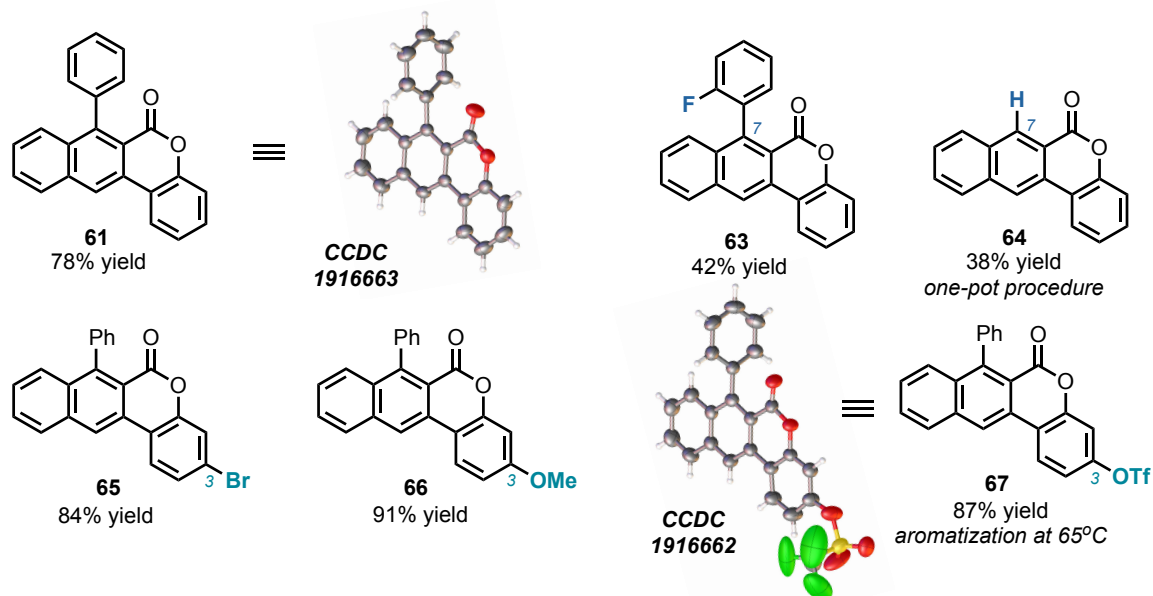


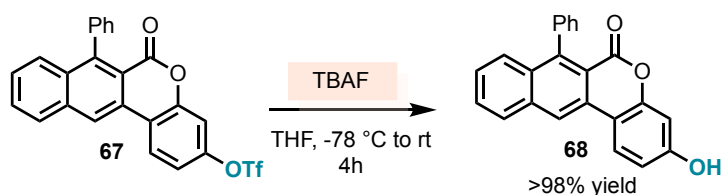
Table 3.7. - Substrate scope of the elimination/aromatization sequence.

These reaction conditions were applied to diverse readily available starting materials **43**, **46-48** (prepared in the previous section), allowing the easy tuning of the NTC scaffold at positions *C3* and *C7* (Table 3.7). When different groups were placed in the *C7* position, the yields were moderate (**63** and **64**). However, the substitution at *C3* furnished diversely functionalized naphthochromenones in high yields over two steps (up to 91%, **65-67**). This tunability allowed us to define structure-property relationships while generating a library of highly fluorescent compounds (see Chapter IV for a complete table with these properties).

Post-modification reactions

Prompted by the simple synthetic route which allows the fast and effective synthesis of diverse scaffolds **61**, we explored the impact of diverse structural post-functionalization. We identified **67**, bearing a pseudohalide group at position 3, a versatile precursor to diverse extended conjugation compounds. On the one hand, the hydroxyl functionality was easily deprotected by treatment with tetrabutylammonium fluoride (TBAF) solution, delivering **68** in quantitative yield (Scheme 3.10).

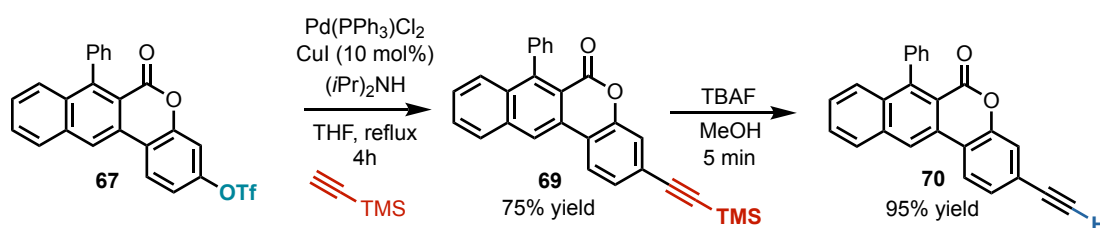
- Triflate deprotection



Scheme 3.10. - Deprotection of **67**.

Next, **69** was synthesized (95% yield) to evaluate the effect of an increased π -conjugation (Table 3.8). Hence, after a simple desilylation step, **70** was obtained in high yield. At this juncture, diverse aromatic substituents bearing electron withdrawing or electron donating groups were introduced by a simple synthetic operation. PCs **71-74** were synthesized in excellent yields spanning from 81% to 91% by using **70** and selected aryl halides through a Sonogashira cross-coupling.

- extension of the π -conjugation



- Sonogashira cross-couplings

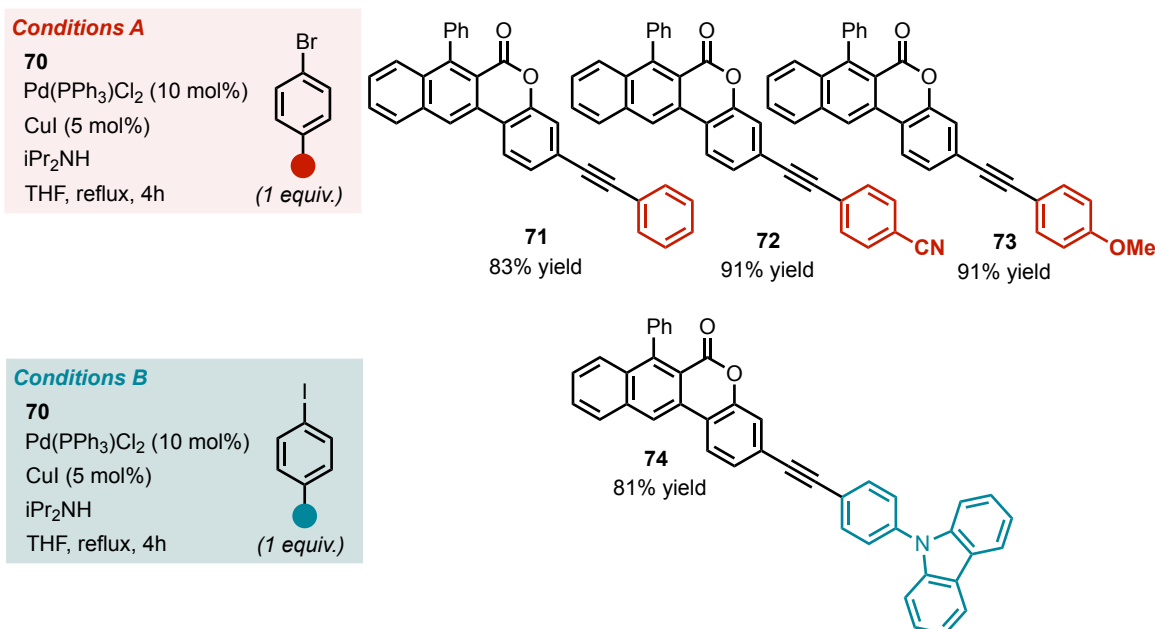


Table 3.8. - Extension of the π -conjugation in naphthochromenone scaffolds.

Limitations

While looking at the manipulations of the naphthochromenone scaffold, we identified two main limitations.

- i) As commented in the section 2 of this chapter there is a lack of generality, as the initial [4+2]-cycloaddition reaction only proceeds well with the reported coumarins, no substitution is tolerated in the reactive aromatic ring of the 2-MBP. Hence, naphthochromenone scaffolds decorated in this part cannot be obtained by this method. Indeed, the only NTC dye obtained decorated in this zone, is **75** but in a 5% overall yield after three consecutive steps (Figure 3.18).
- ii) In the post-modification section, the cross-couplings reported are limited to Sonogashira reactions. When the direct construction of a C-N bond was attempted through a Buchwald-Hartwig amination, the desired product **76** was observed in traces. Nevertheless, further optimization of the process must be evaluated.

— Limitations of this protocol

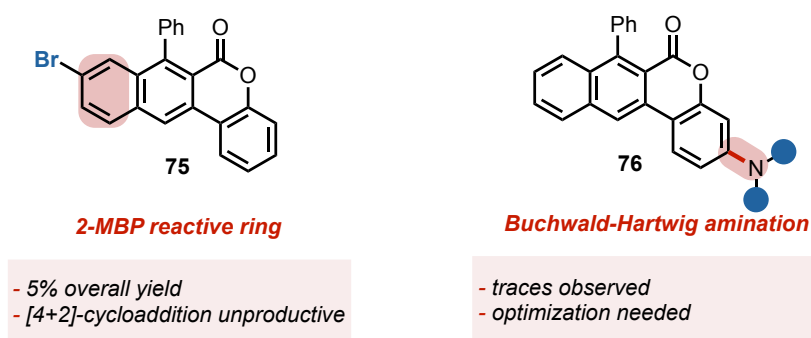


Figure 3.18. - Limitations of the method described in this section.

3.3.5 Conclusions

In conclusion, in this section I discussed the applications of the obtained naphthochromenone scaffolds (reported in section II) by means of different manipulation reactions. The lactone-ring as well as the tertiary alcohol were seized to prepare diverse tetralinolic and fully aromatic scaffolds, respectively. Indeed, the fully aromatic naphthochromenone family turned to be easily tunable at different ring positions. Thus, a family of 12 different highly luminescent compounds with potential applications as organic photoredox catalysts was achieved successfully in high yields. This fact paved the way to study structure-activity relationships of this family of compounds.

3.3.6 Experimental Section

The NMR spectra were recorded on Bruker 400 Avance III HD equipped with a BBI-z grad probehead 5mm, Bruker 500 Avance III equipped with a BBI-ATM-z grad probehead 5mm and Bruker DMX 600 equipped with a BBI z-grad probehead 5mm. The chemical shifts (δ) for ^1H and ^{13}C are given in ppm relative to residual signals of the solvents (CHCl_3 @ 7.26 ppm ^1H NMR, 77.16 ppm ^{13}C NMR). Coupling constants are given in Hz. The following abbreviations are used to indicate the multiplicity: s, singlet; d, doublet; t, triplet; q, quartet; m, multiplet; bs, broad signal. NMR yields were calculated by using trichloroethylene as internal standard.

The ^1H , ^{13}C and ^{19}F NMR spectra are available in literature free of charge.⁴⁶

High-Resolution Mass Spectra (HRMS) were obtained using Waters GCT gas chromatograph coupled with a time-of-flight mass spectrometer (GC/MS-TOF) with electron ionization (EI) or MicroTOF II (Bruker Daltonics): HPLC-MS-TOF (ESI). Chromatographic purification of products was accomplished using flash chromatography on silica gel (SiO_2 , 0.04-0.063 mm) purchased from Machery-Nagel, with the indicated solvent system according to the standard techniques. Thin-layer chromatography (TLC) analysis was performed on pre-coated Merck TLC plates (silica gel 60 GF254, 0.25 mm). Visualization of the developed chromatography was performed by checking UV absorbance (254nm) as well as with aqueous ceric ammonium molybdate and potassium permanganate solutions. Organic solutions were concentrated under reduced pressure on a Büchi rotary evaporator.

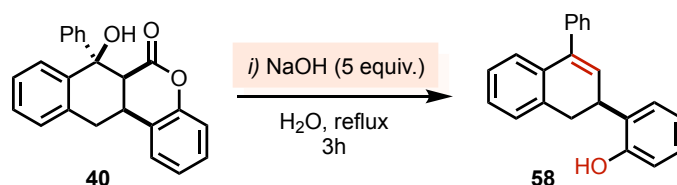
Materials: Commercial grade reagents and solvents were purchased at the highest commercial quality from Sigma Aldrich or FluoroChem and used as received, unless otherwise stated.

The diverse reaction set up images and photophysical studies are available free of charge in literature.²⁸

⁴⁶ Mateos, J.; Rigodanza, F.; Vega-Peñaloza, A.; Sartorel, A.; Natali, M.; Bortolato, T.; Pelosi, G.; Companyó, X.; Bonchio, M.; Dell'Amico, L. *Naphthochromenones: Organic Bimodal Photocatalysts Engaging in Both Oxidative and Reductive Quenching Processes*. *Angew. Chem. Int. Ed.* **2020**, *59*, 1302–1312.

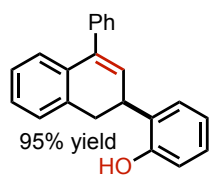
General procedures for the nucleophilic modification of **40** in the lactone motif

— Decarboxylation in basic conditions with NaOH



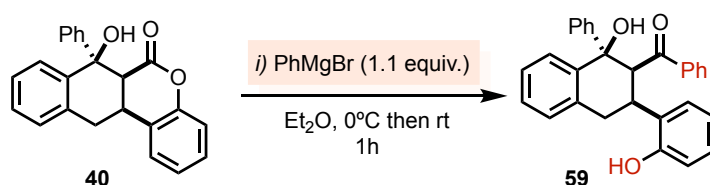
Tetrahydronaphthochromenone **40** (200 mg, 1 equivalent, 0.60 mmol) was dissolved in H₂O (3 mL). To the resulting heterogenous solution, NaOH (120 mg, 5 equivalents, 3 mmol) was added portion wise under vigorous stirring at room temperature. The solution was then heated to reflux. After 3h, full conversion was observed by TLC analysis. The reaction was cooled down to room temperature and extracted with 3x10 mL of DCM. The combined organic phases were dried over MgSO₄ and the solvent was removed by rotary evaporation. Concentration under high vacuum yielded 2-(4-phenyldihydronaphthalen-2-yl)phenol **58** (white solid), in 95% yield (170 mg, 0.576 mmol).

2-(4-phenyl-1,2-dihydronaphthalen-2-yl)phenol



¹H-NMR (400 MHz, CDCl₃): 7.46-7.35 (m, 5H, Ar), 7.30 (dd, *J* = 7.5, 1.6 Hz, Ar), 7.25-7.09 (m, 5H, Ar), 6.91 (dt, *J* = 7.5, 1.1 Hz, 1H, Ar), 6.83 (dd, *J* = 7.9, 1.1 Hz), 6.18 (d, *J* = 3.5 Hz, 1H, Csp²), 4.98 (br s, 1H, OH), 4.22 (ddd, *J* = 8.5, 3.5, 3.1 Hz, 1H, CH), 3.16-3.14 (m, 2H, CH₂) ppm. **¹³C-NMR (100 MHz, CDCl₃):** δ 153.5 (Cq Ar), 141.2 (Cq Ar), 140.5 (Cq Ar), 136.1 (Cq Ar), 134.6 (Cq Ar), 130.9 (CH Ar), 130.4 (Cq Ar), 129.2 (CH Ar), 129.0 (CH Ar x2), 128.5 (CH Ar x2), 128.1 (CH Ar), 127.9 (CH Ar), 127.7 (CH Ar), 127.6 (CH Ar), 126.7 (CH Ar), 125.9 (CH Ar), 121.2 (CH Ar), 115.9 (CH sp²), 35.6 (CH), 35.3 (CH₂) ppm. **HRMS (MALDI)** calculated for [C₂₂H₁₈O+H]⁺: 321.1250, found: 321.1114.

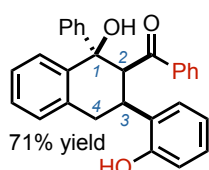
— Grignard addition



Tetrahydronaphthochromenone **40** (200 mg, 1 equivalent, 0.60 mmol) was dissolved in dry Et₂O (8 mL) under inert atmosphere. To the resulting solution, PhMgBr (1.0 M in THF; 768 μL, 1.1 equivalents, 0.768 mmol) was added dropwise under vigorous stirring at 0 °C. The solution was then stirred for 1h at room temperature. After 1h, full conversion was observed by TLC analysis. 8 mL of a saturated solution of NH₄Cl were added dropwise. The

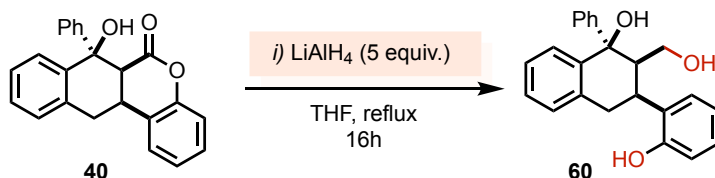
reaction was extracted with 3x10 mL of Et₂O. The combined organic phases were dried over MgSO₄ and the solvent was removed by rotary evaporation. After flash column chromatography (9:1 Hexane/EtOAc) **59** (transparent oil) was obtained in 71% yield, in 71% yield (209.2 mg, 0.496 mmol).

1-hydroxy-3-(2-hydroxyphenyl)-1-phenyl-1,2,3,4-tetrahydronaphthalen-2-yl)(phenyl)methanone



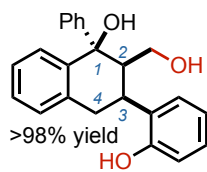
¹H-NMR (400 MHz, CDCl₃): 7.41-7.35 (m, 3H, Ar), 7.27-7.19 (m, 9H, Ar), 7.05 (t, *J* = 7.8, 2H, Ar), 6.79 (t, *J* = 7.0 Hz, 1H, Ar), 6.60 (d, *J* = 7.0 Hz, 1H, Ar), 6.47 (d, *J* = 7.4 Hz, 1H, Ar), 6.39 (t, *J* = 7.3 Hz, 1H, Ar), 4.62 (d, *J* = 3.9 Hz, 1H, CH 2), 3.79 (dt, *J* = 12.8, 3.9 Hz, 1H, CH 3), 3.39 (dd, *J* = 16.4, 12.1 Hz, 1H, CH₂ 4a), 2.88 (dd, *J* = 16.4, 4.9 Hz, 1H, CH₂ 4b) ppm. **¹³C-NMR (100 MHz, CDCl₃):** δ 204.0 (C=O), 153.2 (Cq Ar), 148.1 (Cq Ar), 140.9 (Cq Ar), 139.0 (Cq Ar), 136.9 (Cq Ar), 132.8 (CH Ar), 130.4 (Cq Ar), 128.5 (CH Ar), 128.1 (CH Ar x4), 128.0 (CH Ar x2), 127.8 (CH Ar), 127.7 (CH Ar x2), 127.7 (CH Ar x2), 127.6 (CH Ar), 127.5 (CH Ar), 127.2 (CH Ar), 124.8 (Cq Ar), 120.8 (CH Ar), 115.3 (CH Ar), 78.5 (Cq), 57.1 (CH 2), 34.1 (CH 3), 30.3 (CH₂ 4) ppm. **HRMS (MALDI)** calculated for [C₂₉H₂₄O₃+Na]⁺: 443.1618, found: 443.1657.

— LiAlH₄ reduction



Tetrahydronaphthochromenone **40** (200 mg, 1 equivalent, 0.60 mmol) was dissolved in dry THF (6 mL) under inert atmosphere. To the resulting solution, LiAlH₄ (1.0 M in THF; 3 mL, 5 equivalents, 3.0 mmol) was added dropwise under vigorous stirring at 0 °C. The solution was then heated to reflux. After 16h, full conversion was observed by TLC analysis. The reaction was cooled down to room temperature and EtOAc was added dropwise. The reaction was extracted with 3x10 mL of EtOAc. The combined organic phases were dried over MgSO₄ and the solvent was removed by rotary evaporation. Concentration under high vacuum yielded **60** (white solid), in >98% yield (201.2 mg, 0.6 mmol).

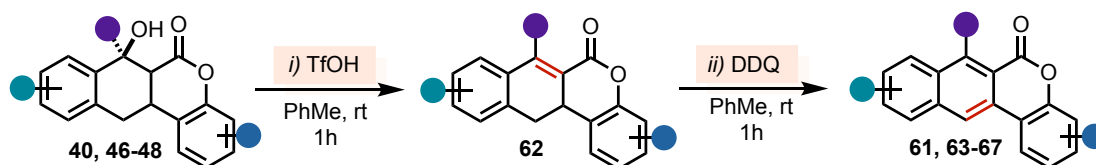
2-(hydroxymethyl)-3-(2-hydroxyphenyl)-1-phenyl-1,2,3,4-tetrahydronaphthalen-1-ol



¹H-NMR (400 MHz, CDCl₃): 7.38-7.24 (m, 9H, Ar), 7.14-7.07 (m, 2H, Ar), 6.84 (t, *J*= 7.6 Hz, 1H, Ar), 6.78 (d, *J*= 8.0 Hz, 1H, Ar), 3.82 (dd, *J*= 11.3, 6.8 Hz, 1H, CH₂OH a), 3.76 (dd, *J*= 11.4, 6.8 Hz, 1H, CH₂OH b), 3.69 (td, *J*= 6.7, 3.3 Hz, 1H, CH₂), 3.34 (dd, *J*= 17.0, 7.1 Hz, 1H, CH₂ 4), 3.27 (dd, *J*= 17.0, 6.3 Hz, 1H, CH₂ 4), 2.85 (td, *J*= 6.7, 3.3 Hz, 1H, CH 3) ppm. **¹³C-NMR (125 MHz, MeOD-d₄):** δ 155.2 (Cq Ar), 149.1 (Cq Ar), 140.4 (Cq Ar), 136.5 (Cq Ar), 128.8 (CH Ar), 128.7 (CH Ar), 127.9 (CH Ar), 127.7 (CH Ar x2), 127.0 (CH Ar), 126.9 (CH Ar x2), 126.5 (CH Ar), 126.1 (CH Ar), 118.6 (CH Ar), 114.6 (CH Ar), 80.8 (Cq), 60.8 (CH), 49.5 (CH) 32.1 (CH₂), 29.2 (CH₂) ppm. **HRMS (MALDI)** calculated for [C₂₃H₂₂O₃+Na]⁺: 369.1461, found: 369.1453.

General procedures for the obtention of the naphthochromenone scaffold

— Two-step procedure (personally preferred) —

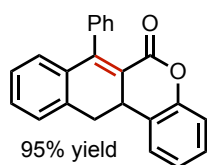


Step i: Trifluoromethanesulfonic acid elimination

Tetrahydronaphthochromenone **40** (200 mg, 1 equivalent, 0.60 mmol) was dissolved in dry toluene (6 mL) under inert atmosphere. To the resulting solution, TfOH (160 μL, 3 equivalents, 1.8 mmol) was added dropwise under vigorous stirring at 0 °C. The solution was stirred for 1h at 0 °C and allowed to gradually warm up to room temperature. After 3h, full conversion was observed by TLC analysis and quenched with NaHCO₃. The reaction was extracted with 3x10 mL of DCM. The combined organic phases were dried over MgSO₄ and the solvent was removed by rotary evaporation. Concentration under high vacuum yielded 7-phenyldihydronaphtho[2,3-*c*]chromenone **62** (white solid), in 95% yield (170 mg, 0.572 mmol).

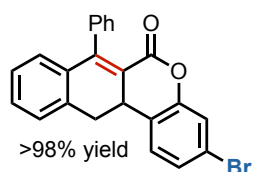
I personally prefer this procedure. The final purification step becomes easier and yield the naphthochromenone scaffold in higher purity than when doing in a single step. In addition, the two-step procedure is fast and only needs a final recrystallization.

7-phenyl-6H-dihydronaphtho[2,3-c]chromen-6-one (62).



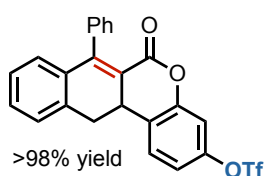
¹H-NMR (400 MHz, CDCl₃): 7.49-7.41 (m, 4H, Ar), 7.39-7.27 (m, 4H, Ar), 7.23-7.14 (m, 3H, Ar), 7.07 (dd, *J* = 8.2, 1.2 Hz, 1H, Ar), 6.89 (d, *J* = 7.8 Hz, 1H, Ar), 4.30 (dd, *J* = 15.9, 6.4 Hz, 1H, CH₂ a), 3.52 (dd, *J* = 15.9, 6.2 Hz, 1H, CH₂ b), 3.21 (t, *J* = 15.4 Hz, 1H, CH) ppm. **¹³C-NMR (100 MHz, CDCl₃):** δ 160.2 (COO), 153.2 (Cq Ar), 150.6 (Cq Ar), 139.1 (Cq Ar), 135.7 (CH Ar), 135.5 (Cq Ar), 130.4 (CH Ar), 129.5 (CH Ar), 129.2 (Cq), 128.7 (CH Ar), 128.4 (Cq Ar), 128.3 (CH Ar), 127.7 (CH Ar), 127.5 (CH Ar), 127.4 (CH Ar), 126.6 (CH Ar), 125.5 (Cq), 124.5 (CH Ar), 123.2 (CH Ar), 119.4 (CH Ar), 117.2 (CH Ar), 34.6 (CH), 34.2 (CH₂) ppm. **HRMS (MALDI)** calculated for [C₂₃H₁₆O₃+Na]⁺: 347.1043, found: 343.1258.

3-bromo-7-phenyl-6H-dihydronaphtho[2,3-c]chromen-6-one (62b).



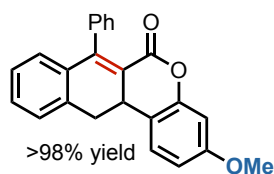
¹H-NMR (400 MHz, CDCl₃): δ 7.78 (d, *J* = 8.2, 1H, Ar), 7.47-7.40 (m, 3H, Ar), 7.37-7.33 (m, 4H, Ar), 7.28-7.17 (m, 3H, Ar), 6.89 (d, *J* = 8.2, 1H, Ar), 4.24 (dd, *J* = 15.9, 6.4 Hz, 1H, CH₂ a), 3.48 (dd, *J* = 15.9, 6.2 Hz, 1H, CH₂ b), 3.20 (t, *J* = 15.4 Hz, 1H, CH) ppm. **¹³C-NMR (100 MHz, CDCl₃):** δ 159.3 (COO), 153.9 (Cq Ar), 151.0 (Cq Ar), 140.7 (Cq Ar), 138.7 (Cq Ar), 138.3 (Cq Ar), 137.9 (Cq Ar), 135.3 (CH Ar), 135.2 (CH Ar), 133.1 (CH Ar), 129.5 (CH Ar), 128.4 (CH Ar), 127.8 (CH Ar), 127.4 (CH Ar), 125.4 (CH Ar), 122.1 (CH Ar), 120.2 (CH Ar), 118.3 (CH Ar), 119.4 (CH Ar), 117.2 (CH Ar), 34.3 (CH), 34.1 (CH₂) ppm. **HRMS (ESI-MS)** calculated for [C₂₃H₁₅BrO₂+H]⁺: 403.0255, found: 403.0256.

7-phenyl-6H-dihydronaphtho[2,3-c]chromenon-3-yltrifluoromethanesulfonate (62c).



¹H-NMR (400 MHz, CDCl₃): 7.54-7.52 (m, 1H, Ar), 7.51-7.42 (m, 3H, Ar), 7.37-7.35 (m, 2H, Ar), 7.19-7.11 (m, 3H, Ar), 7.00 (d, *J* = 8.2, 1H, Ar), 6.88 (d, *J* = 7.8 Hz, 1H, Ar), 4.30 (dd, *J* = 15.9, 6.4 Hz, 1H, CH₂ a), 3.48 (dd, *J* = 15.9, 6.2 Hz, 1H, CH₂ b), 3.22 (t, *J* = 15.4 Hz, 1H, CH) ppm. **¹³C-NMR (100 MHz, CDCl₃):** δ 158.6 (COO), 154.6 (Cq Ar), 151.3 (Cq Ar), 148.7 (Cq Ar), 138.5 (Cq Ar), 135.2 (Cq Ar), 135.1 (Cq Ar), 130.6 (CH Ar), 129.7 (CH Ar), 128.1 (CH Ar), 127.7 (CH Ar x2), 127.6 (CH Ar x2), 127.5 (CH Ar), 123.6 (CH Ar), 117.5 (CH Ar), 117.1 (CH Ar), 110.5 (CH Ar), 34.3 (CH), 34.2 (CH₂) ppm. **¹⁹F-NMR (376 MHz, CDCl₃):** δ -73.07 (s, 3F, CF₃) ppm. **HRMS (ESI-MS)** calculated for [C₂₄H₁₅F₃O₅S+H]⁺: 473.0592, found: 473.0588.

3-methoxy-7-phenyl-6H-dihydronaphtho[2,3-c]chromen-6-one (62d).

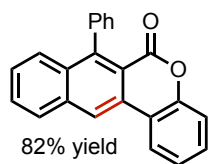


¹H-NMR (400 MHz, CDCl₃): δ 7.48-7.43 (m, 3H, Ar), 7.36-7.34 (m, 3H, Ar), 7.20-7.16 (m, 2H, Ar), 6.99 (d, *J* = 8.2, 1.2 Hz, 1H, Ar), 6.79 (dd, *J* = 7.8 Hz, 1.2 Hz, 1H, Ar), 6.62 (d, *J* = 1.2 Hz, 1H, Ar), 4.24 (dd, *J* = 15.9, 6.4 Hz, 1H, CH₂ a) 3.83 (s, 3H, OMe), 3.48 (dd, *J* = 15.9, 6.2 Hz, 1H, CH₂ b), 3.17 (t, *J* = 15.4 Hz, 1H, CH) ppm. **¹³C-NMR (100 MHz, CDCl₃):** δ 160.0 (COO), 159.8 (Cq Ar), 153.2 (Cq Ar), 151.1 (Cq Ar), 139.0 (Cq Ar), 135.8 (Cq Ar), 135.4 (Cq Ar), 130.2 (CH Ar), 129.4 (CH Ar), 128.1 (Cq), 127.5 (CH Ar x2), 127.4 (CH Ar x2), 127.2 (CH Ar), 127.2 (CH Ar), 119.3 (CH Ar), 114.8 (Cq Ar), 111.0 (CH Ar), 101.8 (CH Ar), 117.2 (CH Ar), 55.6 (OMe), 34.5 (CH), 33.9 (CH₂) ppm. **HRMS (ESI-MS)** calculated for [C₂₄H₁₈O₃+H]⁺: 355.1256, found: 355.1257.

Step ii – Aromatization with DDQ

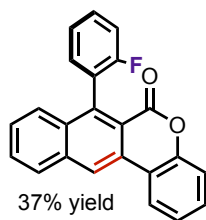
The 7-phenyl-6H-dihydronaphtho[2,3-c]chromen-6-one crude (102.7 mg, 1 equivalent, 0.3 mmol) was dissolved in dry toluene (5 mL) under argon atmosphere. To the resulting solution, DDQ (77.2 mg, 1.2 equivalents, 0.36 mmol) was added portion wise under vigorous stirring at 0 °C. The solution was stirred for 1h at room temperature, after this time full conversion was observed by TLC analysis. The reaction was quenched with 5 mL of a saturated solution of NaHCO₃ and 20 mL of EtOAc were added. Then, the organic phase was washed with a saturated solution of NaHCO₃ (3x15 mL). The organic phase was dried over MgSO₄. Subsequently, the solvent was removed by rotary evaporation and the crude subjected to flash column chromatography on silica gel (9:1 Hexane/EtOAc) yielding pure **5a** 7-phenyl-6H-naphtho[2,3-c]chromen-6-one (yellowish solid) was obtained in 85% yield, (156.7 mg, 0.486 mmol).

7-phenyl-6H-naphtho[2,3-c]chromen-6-one (61).



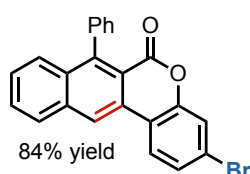
¹H-NMR (400 MHz, CDCl₃): δ 8.55 (s, 1H, Ar), 8.18 (dd, *J* = 8.0 Hz, 1.5 Hz, 1H, Ar), 7.94 (dd, *J* = 8.0 Hz, 1.5 Hz, 1H, Ar), 7.55 (t, *J* = 7.0 Hz, 1H, Ar), 7.46-7.39 (m, 4H, Ar), 7.36-7.30 (m, 2H, Ar), 7.26-7.15 (m, 4H, Ar) ppm. **¹³C-NMR (100 MHz, CDCl₃):** δ 159.5 (COO), 151.0 (Cq Ar), 147.1 (Cq Ar), 139.7 (Cq Ar), 135.6 (Cq Ar), 133.3 (Cq Ar), 130.3 (Cq Ar), 130.2 (CH Ar), 129.2 (CH Ar), 128.6 (CH Ar), 128.6 (CH Ar x2), 128.2 (CH Ar x2), 128.0 (CH Ar), 127.3 (CH Ar), 126.9 (CH Ar), 124.3 (CH Ar), 123.0 (CH Ar), 121.0 (CH Ar), 118.9 (Cq Ar), 117.6 (CH Ar), 116.9 (CH Ar) ppm. **HRMS (ESI-MS)** calculated for [C₂₃H₁₄O₂+H]⁺: 323.0994, found: 323.0996.

7-(2-fluorophenyl)-6H-naphtho[2,3-c]chromen-6-one (63).



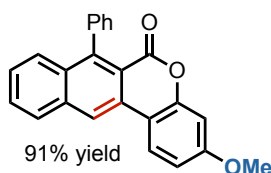
¹H-NMR (400 MHz, CDCl₃): δ 8.70 (s, 1H, Ar), 8.28 (dd, *J* = 8.0 Hz, 1.5 Hz, 1H, Ar), 8.06 (dd, *J* = 8.0 Hz, 1.5 Hz, 1H, Ar), 7.68 (t, *J* = 7.0 Hz, 1H, Ar), 7.58-7.47 (m, 4H, Ar), 7.40-7.25 (m, 5H, Ar) ppm. **¹³C-NMR (100 MHz, CDCl₃):** δ 159.4 (COO), 150.7, 140.2, 135.7, 130.7, 130.6, 130.3, 130.2, 129.7, 129.6, 129.3, 128.3, 127.8, 127.3, 124.4, 124.0, 124.0, 123.0, 121.7, 118.3, 117.6, 115.6, 115.4 ppm. **¹⁹F-NMR (376 MHz, CDCl₃):** -115.51 (d, *J* = 6.9 Hz, F) ppm. **HRMS (ESI-MS)** calculated for [C₂₃H₁₃FO₂+H]⁺: 341.0900, found: 341.0899.

3-bromo-7-phenyl-6H-naphtho[2,3-c]chromen-6-one (65).



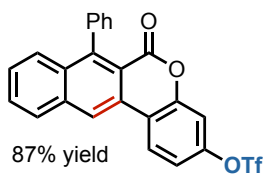
¹H-NMR (400 MHz, CDCl₃): δ 8.52 (s, 1H, Ar), 8.05 (d, *J* = 8.0 Hz, 1H, Ar), 7.96 (d, *J* = 8.0 Hz, 1H, Ar), 7.61 (t, *J* = 7.5 Hz, 1H, Ar), 7.60-7.44 (m, 4H, Ar), 7.42-7.37 (m, 3H, Ar), 7.19 (dd, *J* = 8.0 Hz, 1.5 Hz, 2H, Ar) ppm. **¹³C-NMR (100 MHz, CDCl₃):** δ 158.8 (COO), 151.3 (Cq Ar), 147.5 (Cq Ar), 139.3 (Cq Ar), 135.6 (Cq Ar), 133.4 (Cq Ar), 129.5 (CH Ar), 128.7 (CH Ar), 128.5 (CH Ar x2), 128.4 (CH Ar x2), 128.2 (CH Ar), 128.0 (CH Ar), 127.6 (CH Ar), 127.4 (CH Ar), 127.2 (CH Ar), 124.3 (CH Ar), 123.2 (Cq Ar), 121.0 (Cq Ar), 120.7 (CH Ar), 117.6 (Cq Ar), 116.5 (Cq Ar) ppm. **HRMS (ESI-MS)** calculated for [C₂₃H₁₃BrO₂+H]⁺: 401.0099, found: 401.0101.

3-methoxy-7-phenyl-6H-naphtho[2,3-c]chromen-6-one (66).



¹H-NMR (400 MHz, CDCl₃): δ 8.51 (s, 1H, Ar), 8.17 (dd, *J* = 8.0 Hz, 1.5 Hz, 1H, Ar), 8.00 (dd, *J* = 8.0 Hz, 1.5 Hz, 1H, Ar), 7.64 (t, *J* = 7.0 Hz, 1H, Ar), 7.56-7.50 (m, 4H, Ar), 7.43-7.38 (m, 1H, Ar), 7.31-7.28 (m, 2H, Ar), 6.96 (dd, *J* = 8.8, 2.6 Hz, 1H, Ar), 6.84 (d, *J* = 2.6 Hz), 3.91 (s, 1H, OCH₃) ppm. **¹³C-NMR (100 MHz, CDCl₃):** δ 161.3 (COO), 159.7 (Cq Ar), 152.2 (Cq Ar), 147.1 (Cq Ar), 139.7 (Cq Ar), 135.8 (Cq Ar), 132.7 (Cq Ar), 130.6 (Cq Ar), 129.1 (CH Ar), 128.6 (CH Ar), 128.6 (CH Ar x2), 128.1 (CH Ar x2), 127.8 (CH Ar), 127.3 (CH Ar), 126.4 (CH Ar), 124.1 (CH Ar), 119.8 (CH Ar), 116.2 (Cq Ar), 112.4 (CH Ar), 111.4 (Cq Ar), 101.3 (CH Ar), 55.7 (OCH₃) ppm. **HRMS (ESI-MS)** calculated for [C₂₄H₁₆O₃+H]⁺: 356.1099, found: 356.1098.

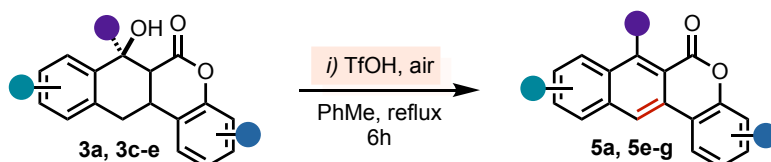
7-phenyl-6H-naphtho[2,3-c]chromenon-3-yltrifluoromethanesulfonate (67).



*In this case, the aromatization **does not** reach full conversion at room temperature. I recommend warming up the solution to 65 °C for 2h.*

¹H-NMR (400 MHz, CDCl₃): δ 8.62 (s, 1H, Ar), 8.36 (d, *J* = 8.0 Hz, 1H, Ar), 8.08 (dd, *J* = 8.0 Hz, 1H, Ar), 7.72 (t, *J* = 7.0 Hz, 1H, Ar), 7.60-7.47 (m, 5H, Ar), 7.32-7.28 (m, 4H, Ar) ppm. ¹³C-NMR (100 MHz, CDCl₃): δ 158.3 (COO), 151.5 (Cq Ar), 149.6 (Cq Ar), 147.4 (Cq Ar), 139.1 (Cq Ar), 135.6 (Cq Ar), 133.7 (Cq Ar), 129.6 (CH Ar), 128.8 (CH Ar), 128.7 (Cq Ar), 128.5 (CH Ar x2), 128.2 (CH Ar x2), 128.1 (CH Ar), 127.6 (CH Ar), 124.8 (CH Ar), 121.6 (CH Ar), 119.0 (CH Ar), 116.2 (Cq Ar), 110.9 (CH Ar) ppm. ¹⁹F-NMR (376 MHz, CDCl₃): -72.97 ppm. HRMS (ESI-MS) calculated for [C₂₄H₁₃F₃O₅S+H]⁺: 471.4182, found: 471.4180.

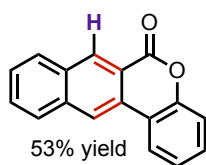
— One-pot procedure —



Tetrahydronaphthochromenone **3a** (200 mg, 1 equivalent, 0.60 mmol) was dissolved in dry toluene (6 mL). To the resulting solution, trifluoromethanesulfonic acid (160 μL, 3 equivalents, 1.8 mmol) was added dropwise under vigorous stirring at 0 °C. The solution was stirred for 6h at reflux. After this time full conversion was observed by TLC analysis. The reaction was quenched with 5 mL of a saturated solution of NaHCO₃ and 20 mL of EtOAc were added. The organic phase was washed with a saturated solution of NaHCO₃ (3x15 mL). The organic phase was dried over MgSO₄. Subsequently, the solvent was removed by rotary evaporation and the crude subjected to flash column chromatography on silica gel (9:1 Hexane/EtOAc) yielding 7-phenylnaphthochromenone **5a** (yellowish solid), in 75% yield (145.0 mg, 0.450 mmol).

The reaction works for all the naphthochromenones reported, but I only recommend doing it in the following case:

6H-naphtho[2,3-c]chromen-6-one (64).



¹H-NMR (400 MHz, CDCl₃): δ 8.55 (s, 1H, Ar), 8.43 (dd, J = 7.9, 1.0 Hz, 1H, Ar), 8.30 (d, J = 8.1 Hz, 1H, Ar), 7.95 (dd, J = 8.1, 0.6 Hz, 1H, Ar), 7.90-7.82 (m, 2H, Ar), 7.76 (s, 1H, Ar), 7.60 (ddd, J = 7.6, 7.5, 1.1 Hz, 1H, Ar), 7.53 (dd, J = 8.1, 1.4 Hz, 1H, Ar), 7.50 (dd, J = 8.1, 1.4 Hz, 1H, Ar) ppm. **¹³C NMR (100 MHz, CDCl₃):** δ 161.1 (COO), 148.8 (Cq Ar), 134.9 (CH Ar), 134.7 (Cq Ar), 134.1 (Cq Ar), 130.8 (CH Ar), 130.3 (Cq Ar), 129.1 (CH Ar), 128.3 (CH Ar), 127.7 (CH Ar), 127.3 (CH Ar), 125.8 (CH Ar), 122.6 (CH Ar), 122.1 (CH Ar), 121.5 (Cq Ar), 118.2 (Cq Ar), 113.6 (CH Ar) ppm. **HRMS (ESI-MS)** calculated for [C₁₇H₁₀O₂+H]⁺: 247.0681, found: 247.0678.

Multi-gram scale reaction

Compound **61** has been also prepared according to *the two-step procedure* with identical overall yield (82%) but in reduced time (40 h): 2.5 g (7.5 mmol) of 7-hydroxy-7-phenyl-6H-tetrahydro[2,3-c]naphthochromen-6-one **40** were dissolved in 50 mL of toluene. Then, trifluoromethanesulfonic acid (2 mL, 3 equivalents, 22.5 mmol) were added dropwise at 0 °C. The solution was stirred for 1h at room temperature. The reaction was quenched with 20 mL of a saturated solution of NaHCO₃ and 100 mL of EtOAc were added. Subsequently, the organic phase was washed with a saturated solution of NaHCO₃ (3x30 mL). The combined organic phase was dried over MgSO₄. Subsequently, the solvent was removed by rotary evaporation yielding 7-phenyl-6H-dihydro[2,3-c]naphthochromen-6-one **62** (white solid), in 99% yield (2.4 g., 7.5 mmol). The resulting crude product was used without further purification.

The 7-phenyl-6H-dihydro[2,3-c]naphthochromen-6-one crude (2.4 g, 1 equivalent, 7.5 mmol) was dissolved in dry toluene (50 mL) under argon atmosphere. To the resulting solution, DDQ (77.2 mg, 1.2 equivalents, 0.36 mmol) was added portion wise under vigorous stirring at 0 °C. The solution was stirred for 3h at room temperature. The reaction was quenched with 20 mL of a saturated solution of NaHCO₃ and 100 mL of EtOAc were added. Then, the reaction crude was washed with a saturated solution of NaHCO₃ (3x50 mL). The organic phase was dried over MgSO₄. Subsequently, the solvent was removed by rotary evaporation. After recrystallization in MeCN 7-phenyl-6H-naphtho[2,3-c]chromen-6-one crystals (yellowish solid) were obtained in 82% yield, (1.98 g, 6.15 mmol).

4+2 cycloaddition reaction step: 99% yield – 35 minutes residence time – 26.5 h in total

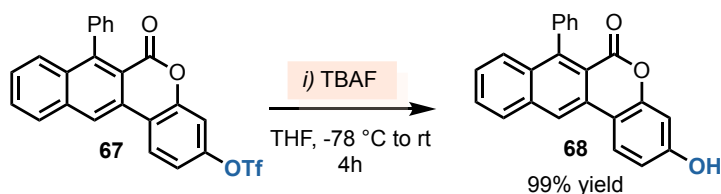
Elimination step: 99% yield – 1 h

Aromatization step: 82% yield after recrystallization – 3 h

Overall yield after three steps in gram scale: 82% yield – 40 h

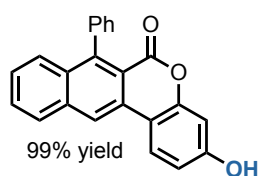
Manipulations of the naphthochromenone scaffold

Triflate deprotection



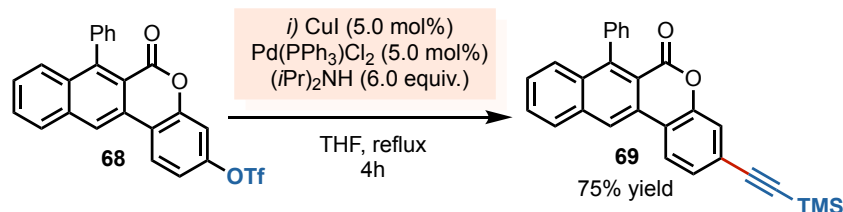
In a round-bottom flask, compound **67** (114 mg, 1.0 equivalent, 0.24 mmol) was dissolved in 4 mL of THF under argon atmosphere. Tetrabutylammonium fluoride (4.8 ml of a [0.1 M] THF solution, 2.0 equivalents, 0.48 mmol) was added dropwise at -78 °C. The reaction mixture was stirred for 2 hours at this temperature and then allowed to warm up to room temperature. After 2 addition hours, the reaction was quenched with a saturated solution of NH₄Cl (3 mL). The aqueous phase was extracted with ethyl acetate (3x10 mL), the combined organic layers were dried over MgSO₄ and the solvent was removed by reduced pressure evaporation. The residue was purified by column chromatography over silica gel (Hexane/EtOAc 7:3 to 1:1) to afford 81.1 mg of compound **68** as a yellow solid (>98%).

3-hydroxy-7-phenyl-6H-naphtho[2,3-c]chromen-6-one (**68**).



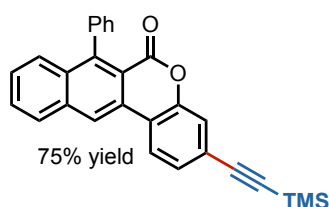
¹H-NMR (400 MHz, Acetone-d₆): δ 8.99 (s, 1H, Ar-OH), 8.67 (s, 1H, Ar), 8.19 (d, *J* = 8.0 Hz, 1H, Ar), 8.00 (d, *J* = 8.0 Hz, 1H, Ar), 7.55 (dt, *J* = 8.0, 1.5 Hz, 1H, Ar), 7.41-7.26 (m, 5H, Ar), 7.16-7.13 (m, 2H, Ar), 6.80 (dd, *J* = 8.0, 2.6 Hz, 1H, Ar), 6.60 (d, *J* = 2.6 Hz) ppm. **¹³C-NMR (100 MHz, CDCl₃):** δ 159.6 (COO), 158.7 (Cq Ar), 152.3 (Cq Ar), 146.5 (Cq Ar), 140.1 (Cq Ar), 136.1 (Cq Ar), 132.5 (Cq Ar), 131.0 (Cq Ar), 129.0 (CH Ar), 128.7 (CH Ar x2), 128.0 (CH Ar x2), 127.9 (CH Ar x2), 126.9 (CH Ar), 126.4 (CH Ar), 124.9 (CH Ar), 120.0 (CH Ar), 116.1 (Cq Ar), 112.9 (CH Ar), 110.5 (Cq Ar), 102.8 (CH Ar) ppm. **HRMS (ESI-MS)** calculated for [C₂₃H₁₄O₃+H]⁺: 339.0943, found: 339.0939.

Sonogashira reaction



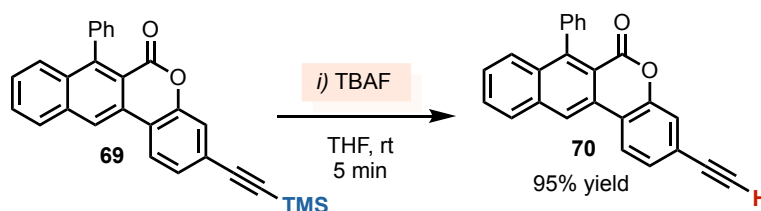
In a two-necked round-bottom flask a mixture of **68** (190 mg, 1.0 equivalent, 0.40 mmol), PdCl₂(PPh₃)₂ (14 mg, 0.05 equivalents, 0.02 mmol), CuI (4 mg, 0.05 equivalents, 0.02 mmol) and ethynyltrimethylsilane (84 μL, 1.5 equivalents, 0.60 mmol) were dissolved with anhydrous THF (5 mL). Subsequently, 0.34 mL of diisopropylamine (0.34 mL, 6.0 equivalents, 2.4 mmol) were added at room temperature. The reaction was stirred at 70 °C for 4 h under nitrogen atmosphere. After this time, the reaction was allowed to reach room temperature and subsequently quenched with a saturated solution of NH₄Cl (5 mL). The aqueous phase was extracted with ethyl acetate (3x10 mL). The combined organic layers were dried over MgSO₄ and the solvent was removed by reduced pressure evaporation. The residue was purified by column chromatography over silica gel (Hexane/EtOAc 9:1 to 8:2) to afford **15 69** as brownish solid in 75% yield (117 mg, 0.30 mmol).

7-phenyl-3-((trimethylsilyl)ethynyl)-6H-naphtho[2,3-c]chromen-6-one (**69**).



¹H-NMR (400 MHz, CDCl₃): δ 8.53 (s, 1H, Ar), 8.10 (dd, *J* = 8.0 Hz, 1.5 Hz, 1H, Ar), 7.95 (dd, *J* = 8.0 Hz, 1.5 Hz, 1H, Ar), 7.58 (t, *J* = 7.0 Hz, 1H, Ar), 7.46-7.42 (m, 4H, Ar), 7.39-7.32 (m, 3H, Ar), 7.21-7.18 (m, 2H, Ar), 0.24 (s, 9H, TMS) ppm. **¹³C-NMR (100 MHz, CDCl₃):** δ 159.2 (COO), 150.6 (Cq Ar), 147.3 (Cq Ar), 139.5 (Cq Ar), 135.6 (Cq Ar), 133.4 (Cq Ar), 129.7 (Cq Ar), 129.3 (Cq Ar), 128.7 (CH Ar), 128.5 (CH Ar), 128.2 (CH Ar x2), 128.1 (CH Ar), 127.9 (CH Ar), 127.2 (CH Ar), 124.8 (CH Ar), 122.9 (CH Ar), 121.4 (CH Ar), 120.7 (CH Ar), 118.7 (CH Ar), 116.7 (Cq Ar), 103.7 (Csp q), 97.0 (Csp q), -0.1 (TMS) ppm. **HRMS (ESI-MS)** calculated for [C₂₈H₂₂O₂Si+H]⁺: 419.1389, found: 419.1391.

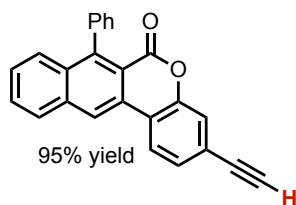
— Desilylation reaction



69 (100 mg, 1.0 equivalent, 0.24 mmol) was dissolved in 2.5 ml of THF. Tetrabutylammonium fluoride (0.48 ml of a [1.0 M] THF solution, 2.1 equivalents, 0.48 mmol) was added dropwise at room temperature. Immediately after the addition, the reaction solution turned dark blue and the reaction was stirred for 5 minutes. The reaction was quenched with a saturated solution of NH₄Cl (3 mL). The aqueous phase was extracted with ethyl acetate (3x10 mL), the combined organic layers were dried over MgSO₄ and the solvent was removed by reduced pressure evaporation. The residue was purified by column

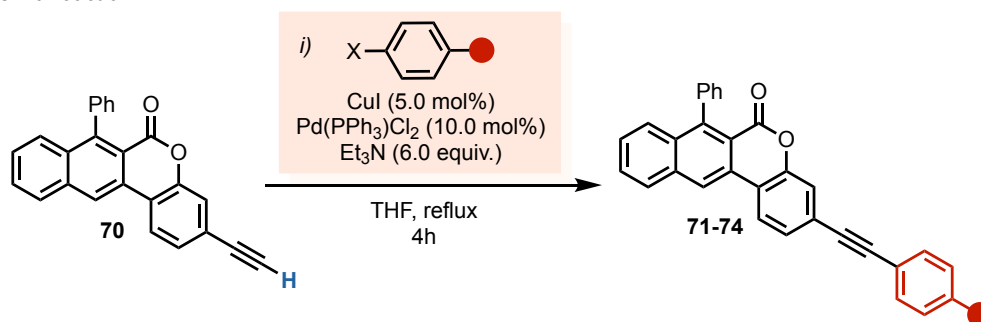
chromatography over silica gel (Hexane/EtOAc 8:2) to afford **70** as a white solid in 95% yield (78 mg, 0.23 mmol).

3-ethynyl-7-phenyl-6*H*-naphtho[2,3-*c*]chromen-6-one (**70**).



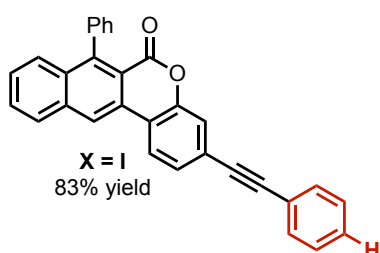
¹H-NMR (400 MHz, CDCl₃): δ 8.54 (s, 1H, Ar), 8.12 (dd, *J* = 8.0 Hz, 1.5 Hz, 1H, Ar), 7.96 (dd, *J* = 8.0 Hz, 1.5 Hz, 1H, Ar), 7.59 (t, *J* = 7.0 Hz, 1H, Ar), 7.47-7.43 (m, 4H, Ar), 7.40-7.35 (m, 3H, Ar), 7.21-7.19 (m, 2H, Ar), 3.15 (s, 1H, CH) ppm. **¹³C-NMR (100 MHz, CDCl₃):** δ 159.0 (COO), 150.6 (Cq Ar), 147.4 (Cq Ar), 139.4 (Cq Ar), 135.6 (Cq Ar), 133.5 (Cq Ar), 129.6 (Cq Ar), 129.4 (Cq Ar), 128.7 (CH Ar), 128.5 (CH Ar), 128.2 (CH Ar x2), 128.1 (CH Ar), 128.0 (CH Ar), 127.4 (CH Ar), 127.3 (CH Ar), 123.8 (CH Ar), 121.4 (CH Ar), 121.0 (CH Ar), 119.1 (CH Ar), 116.7 (Cq Ar) 82.5 (Csp q), 79.4 (Csp CH) ppm. **HRMS (ESI-MS)** calculated for [C₂₅H₁₄O₂+H]⁺: 347.0994, found: 347.0997.

— Sonogashira reaction —



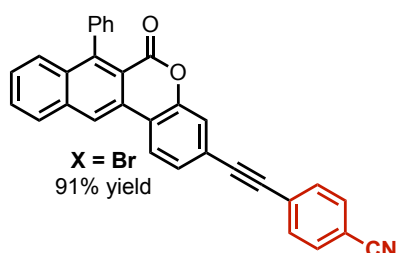
In a two-necked round-bottom flask, a mixture of **70** (1.0 equivalent), PdCl₂(PPh₃)₂ (0.10 equivalents), CuI (0.05 equivalents) and the corresponding aryl halide (1.0 equivalent) were dissolved in anhydrous THF [0.03 M]. Subsequently, triethylamine (6.0 equivalents) was added. The reaction was stirred vigorously at 70 °C for 12 h under nitrogen atmosphere. After this time, the reaction was allowed to reach room temperature and quenched with a saturated solution of NH₄Cl. The aqueous phase was extracted with ethyl acetate (3x10 mL). The combined organic layers were dried over MgSO₄ and the solvent was removed by reduced pressure evaporation. The residue was purified by column chromatography over silica gel.

7-phenyl-3-(phenylethynyl)-6*H*-naphtho[2,3-*c*]chromen-6-one (71).



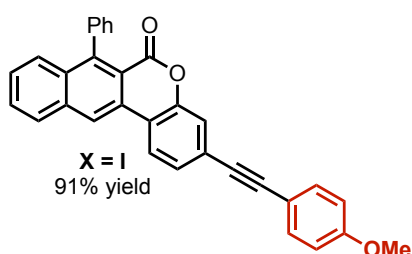
¹H-NMR (400 MHz, CDCl₃): δ 8.52 (s, 1H, Ar), 8.13 (dd, *J* = 8.0 Hz, 1.5 Hz, 1H, Ar), 7.94 (dd, *J* = 8.0 Hz, 1.5 Hz, 1H, Ar), 7.57 (t, *J* = 7.0 Hz, 1H, Ar), 7.50-7.36 (m, 9H, Ar), 7.30-7.28 (m, 3H, Ar), 7.20-7.19 (m, 2H, Ar) ppm. **¹³C-NMR (100 MHz, CDCl₃):** δ 159.1 (COO), 150.8 (Cq Ar), 147.3 (Cq Ar), 139.5 (Cq Ar), 135.6 (Cq Ar), 133.4 (Cq Ar), 131.8 (Cq Ar), 129.8 (Cq Ar), 129.3 (Cq Ar), 128.7 (CH Ar), 128.7 (CH Ar), 128.6 (CH Ar), 128.5 (CH Ar), 128.2 (CH Ar x2), 128.1 (CH Ar), 127.6 (CH Ar), 127.4 (CH Ar), 127.2 (CH Ar), 125.1 (CH Ar), 123.1 (CH Ar), 122.8 (CH Ar), 121.3 (CH Ar), 120.3 (CH Ar), 118.5 (CH Ar), 116.7 (Cq Ar), 91.8 (Csp q), 88.4 (Csp q) ppm. **HRMS (ESI-MS)** calculated for [C₃₁H₁₈O₂+H]⁺: 422.1307, found: 422.1307.

4-((7-phenyl-6*H*-naphthochromen-3-yl)ethynyl)benzonitrile (72).



¹H-NMR (400 MHz, CDCl₃): δ 8.52 (s, 1H, Ar), 8.13 (dd, *J* = 8.0 Hz, 1.5 Hz, 1H, Ar), 7.94 (dd, *J* = 8.0 Hz, 1.5 Hz, 1H, Ar), 7.57 (t, *J* = 7.0 Hz, 1H, Ar), 7.50-7.36 (m, 8H, Ar), 7.30-7.28 (m, 3H, Ar), 7.20-7.19 (m, 2H, Ar) ppm. **¹³C-NMR (100 MHz, CDCl₃):** δ 159.0 (COO), 150.8 (Cq Ar), 147.5 (Cq Ar), 139.4 (Cq Ar), 135.6 (Cq Ar), 134.9 (Cq Ar), 134.8 (Cq Ar), 133.6 (Cq Ar), 132.2 (Cq Ar), 130.8 (Cq Ar), 129.5 (Cq Ar), 128.7 (CH Ar), 128.5 (CH Ar), 128.2 (CH Ar), 128.1 (CH Ar), 128.0 (CH Ar), 128.0 (CH Ar), 127.9 (CH Ar), 127.7 (CH Ar), 127.6 (CH Ar), 123.8 (CH Ar), 123.3 (CH Ar), 121.5 (CH Ar), 120.6 (CH Ar), 119.4 (CH Ar), 116.6 (CH Ar), 116.7 (Cq Ar), 111.9 (CN), 92.5 (Csp q), 89.8 (Csp q) ppm. **HRMS (ESI-MS)** calculated for [C₃₂H₁₇NO₂+H]⁺: 448.1259, found: 448.1254.

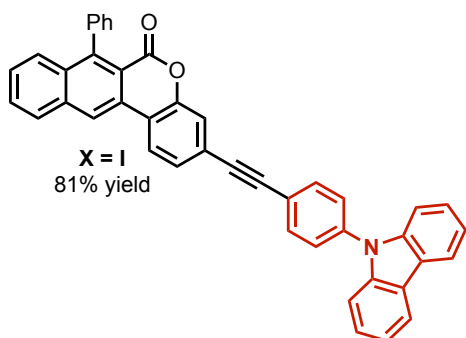
3-((4-methoxyphenyl)ethynyl)-7-phenyl-6*H*-naphtho[2,3-*c*]chromen-6-one (73).



¹H-NMR (400 MHz, CDCl₃): δ 8.54 (s, 1H, Ar), 8.14 (dd, *J* = 8.0 Hz, 1.5 Hz, 1H, Ar), 7.96 (dd, *J* = 8.0 Hz, 1.5 Hz, 1H, Ar), 7.59 (t, *J* = 7.0 Hz, 1H, Ar), 7.49-7.35 (m, 9H, Ar), 7.21-7.19 (m, 3H, Ar), 6.83 (d, *J* = 7.0 Hz, 2H, Ar), 3.77 (s, 3H, OMe) ppm. **¹³C-NMR (100 MHz, CDCl₃):** δ 160.0 (COO), 159.2 (Cq Ar), 150.8 (Cq Ar), 147.3 (Cq Ar), 139.5 (Cq Ar), 135.6 (Cq Ar), 133.4 (Cq Ar), 133.3 (CH Ar x2), 129.9 (Cq Ar), 129.3 (Cq Ar), 128.7 (Cq Ar), 128.6 (CH Ar x2), 128.2 (CH Ar), 128.1 (CH Ar x2), 127.4 (CH Ar), 127.4 (CH Ar), 127.1 (CH Ar), 125.5 (CH Ar), 123.0 (CH Ar), 121.2 (CH Ar), 120.0 (CH

Ar), 118.1 (CH Ar), 116.7 (CH Ar x2), 114.8 (CH Ar), 114.1 (CH Ar), 91.9 (Csp q), 87.2 (Csp q), 55.7 (OMe) ppm. **HRMS (ESI-MS)** calculated for $[C_{32}H_{20}O_3+H]^+$: 453.1412, found: 453.1413.

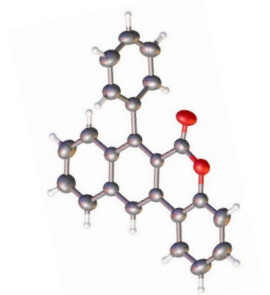
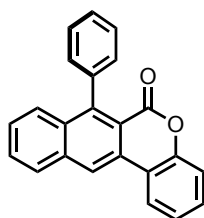
3-((4-(9H-carbazolyl)phenyl)ethynyl)-7-phenyl-6H-naphtho[2,3-c]chromen-6-one (74).



1H -NMR (400 MHz, $CDCl_3$): δ 8.66 (s, 1H, Ar), 8.28 (dd, $J = 8.0$ Hz, 1.5 Hz, 1H, Ar), 8.18 (d, $J = 8.2$ Hz, 2H, Ar), 8.07 (dd, $J = 8.0$ Hz, 1.5 Hz, 1H, Ar), 7.82 (d, $J = 8.3$ Hz, 2H, Ar), 7.69 (t, $J = 7.1$ Hz, 1H, Ar), 7.64-7.62 (m, 2H, Ar), 7.58-7.54 (m, 5H, Ar), 7.50-7.46 (m, 5H, Ar), 7.36-7.31 (m, 4H, Ar) ppm. **^{13}C -NMR (100 MHz, $CDCl_3$):** δ 159.1 (COO), 150.8, 147.4, 140.5, 139.5, 138.0, 135.6, 133.4, 133.3, 129.7, 129.4, 128.7, 128.6, 128.2, 128.1, 127.6, 127.4, 127.2, 126.9, 123.6, 123.2, 121.7, 121.4, 120.4, 120.3, 118.7, 116.7, 114.8, 109.8, 91.0 (Csp q), 89.3 (Csp q) ppm. **HRMS (ESI-MS)** calculated for $[C_{43}H_{25}NO_2+H]^+$: 588.1885, found: 588.1885.

X-ray crystallographic analysis of 61

— X-ray structure of 61



Empirical formula	$C_{23}H_{14}O_2$
Formula weight	323.10
Temperature	298(2) K
Crystal system	Triclinic
Space group	$P-1$
Unit cell dimensions	$a=11.029(4)\text{\AA}$, $\alpha=74.662(5)^\circ$, $b=11.142(4)\text{\AA}$, $\beta=70.798(5)^\circ$,

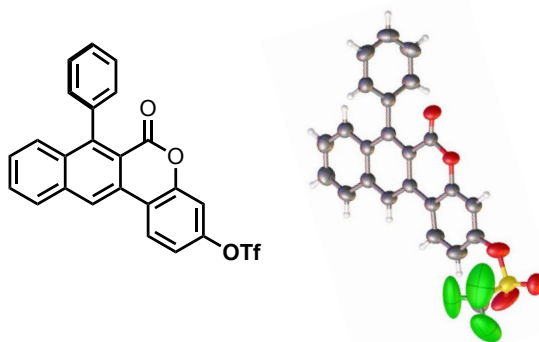
	$c=14.956(5) \text{ \AA}$, $\gamma=68.562(5)^\circ$,
Volume	$1593.7(9) \text{ \AA}^3$
Z	2
Density (calculated)	1.343 g/cm^3
$F(000)$	672
Theta max	26.4° ,
Index ranges	$-13 < h < 13, -13 < k < 13, -18 < l < 18$
Reflections collected	19967

^a $R_1 = \sum ||F_o| - |F_c|| / \sum |F_o|$. ^b $wR_2 = \{ \sum w(F_o^2 - F_c^2)^2 / \sum [w(F_o^2)] \}^{1/2}$ and $w = 1 / [\sigma^2(F_o)^2 + (mP)^2 + nP]$ with $P = (F_o^2 + 2F_c^2) / 3$

CCDC 1916662 contains the supplementary crystallographic data for this compound. These data can be obtained free of charge from The Cambridge Crystallographic Data Centre via www.ccdc.cam.ac.uk/data_request/cif

X-ray crystallographic analysis of 67

— X-ray structure of 67 —



Empirical formula	$C_{24}H_{13}F_3O_5S$
Formula weight	471.42
Temperature	298(2) K
Crystal system	Monoclinic
Space group	$P2_1/n$
Unit cell dimensions	$a = 16.286(9) \text{ \AA}$,

	$b=6.323(3)\text{\AA}$, $\beta=105.86(1)^\circ$,
	$c=20.408(11)\text{\AA}$,
Volume	$2022(2)\text{\AA}^3$;
Z	4
Density (calculated)	1.546 mg/cm^3
$F(000)$	960
Reflections collected	16616
Hkl range	$-20 < h < 20$, $-7 < k < 7$, $-22 < l < 25$

^a $R_1 = \sum ||F_o| - |F_c|| / \sum |F_o|$. ^b $wR_2 = \{ \sum w(F_o^2 - F_c^2)^2 / \sum [w(F_o^2)^2] \}^{1/2}$ and $w = 1 / [\sigma^2(F_o)^2 + (mP)^2 + nP]$ with $P = (F_o^2 + 2F_c^2) / 3$

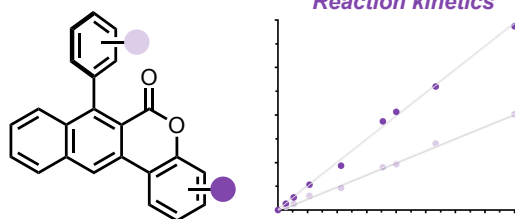
CCDC 1916663 contains the supplementary crystallographic data for this compound. These data can be obtained free of charge from The Cambridge Crystallographic Data Centre via www.ccdc.cam.ac.uk/data_request/cif

The Evolution of Aryl Ketone-Derived Products – Applications in Organophotoredox Catalysis

— Chapter IV - The Evolution of Aryl Ketone-Derived Products – Applications in Organophotoredox Catalysis —

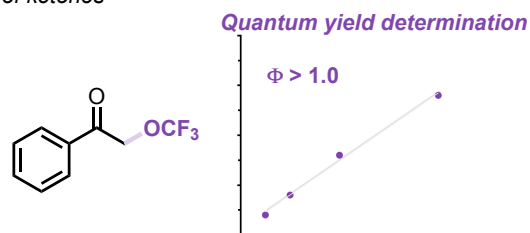
Section 1.

Organophotoredox catalysis - structure-activity relationships in organic photoredox catalysts



Section 2.

Photoredox catalysis - Radical α -trifluoromethoxylation of ketones



Goals:

- Determine structure-activity relationships in organophotoredox catalysis.
- Develop novel methods for the radical trifluoromethoxylation of ketones using organic photocatalysts.

Publications:

Introduction: Vega-Peñaloza, A.; Mateos, J.; Companyó, X.; Escudero-Casao, M.; Dell'Amico, L. *A Rational Approach to Organo-Photocatalysis: Novel Designs and Structure-Property Relationships*. *Angew. Chem. Int. Ed.* **2021**, *60*, 1082–1097

Section 1: Mateos, J.; Rigodanza, F.; Vega-Peñaloza, A.; Sartorel, A.; Natali, M.; Bortolato, T.; Pelosi, G.; Companyó, X.; Bonchio, M.; Dell'Amico, L. *Naphthochromenones: Organic Bimodal Photocatalysts Engaging in Both Oxidative and Reductive Quenching Processes*. *Angew. Chem. Int. Ed.* **2020**, *59*, 1302–1312.

Section 2: Duhail, T.; Bortolato, T.; Mateos, J.; Anselmi, E.; Jelier, B.; Togni, A.; Magnier, E.; Dagousset, G.; Dell'Amico, L. *Radical α -Trifluoromethoxylation of Ketones under Batch and Flow Conditions by Means of Organic Photoredox Catalysis*. *Org. Lett.* **2021**, *23*, 7088–7093

4. Introduction to photocatalysis¹

The driving force of modern photochemistry has been the development of new photocatalytic methods.² Indeed, pioneering contributions have involved the use of metal-based photocatalysts (PCs),³ which have clearly demonstrated the synthetic potential of photoredox catalysis towards novel reactivity, inaccessible by means of conventional thermal chemistry.⁴ As a result,⁵ photocatalysis, previously mastered only by few specialized research groups, have rapidly become a widely used tool in synthetic chemistry. Over the last decade, major efforts have been devoted to the development of new light-driven synthetic methods, often at the expense of an accurate study of the photocatalytic system. More recently, with the consolidated knowledge acquired,⁶ the field has moved towards a more conscious approach, which relies on the tuning of the PC physicochemical properties.⁷ Apart from being a cheaper and more sustainable option with respect to metal-based PCs, organic PCs offer an increasing number of modular scaffolds, characterized by peculiar and tuneable physicochemical features. In this chapter, I summarize the efforts that have involved me and my research group in the field of photo-organocatalysis, both in terms of photocatalyst design, characterization and development of new methodologies.

Organophotocatalysis

The aim of this small section is to provide a “beginners” toolbox to know which parameters to consider when designing and evolving organic PCs (figure 4.1). This task will be addressed by analyzing how diverse structural changes alter the key physicochemical properties, which finally impact on the synthetic performances.

¹ I recommend reading carefully this section to fully understand the rest of the chapter. This fact derives from the large quantity of parameters, properties and symbols commonly used to describe a photocatalytic system.

² Prier, C. K.; Rankic, D. A.; MacMillan, D. W. C. *Visible Light Photoredox Catalysis with Transition Metal Complexes: Applications in Organic Synthesis*. *Chem. Rev.* **2013**, *113*, 5322–5363.

³ Hossain, A.; Bhattacharyya, A.; Reiser, O. Copper's Rapid Ascent in Visible-Light Photoredox Catalysis. *Science* **2019**, *364*, eaav9713.

⁴ Marzo, L.; Pagire, S. K.; Reiser, O.; König, B. *Visible-Light Photocatalysis: Does It Make a Difference in Organic Synthesis?* *Angew. Chem. Int. Ed.* **2018**, *57*, 10034–10072.

⁵ Bach, T.; Hehn, J. P. *Photochemical Reactions as Key Steps in Natural Product Synthesis*. *Angew. Chem. Int. Ed.* **2011**, *50*, 1000–1045.

⁶ Xuan, J.; Xiao, W.-J. *Visible-Light Photoredox Catalysis*. *Angew. Chem. Int. Ed.* **2012**, *51*, 6828–6838.

⁷ a) Romero, N. A.; Nicewicz, D. A. *Organic Photoredox Catalysis*. *Chem. Rev.* **2016**, *116*, 10075–10166. b) Vega-Peñalosa, A.; Mateos, J.; Companyó, X.; Escudero-Casao, M.; Dell'Amico, L. *A Rational Approach to Organophotocatalysis: Novel Designs and Structure-Property Relationships*. *Angew. Chem. Int. Ed.* **2021**, *60*, 1082–1097.

Basic principles of organic photocatalysis

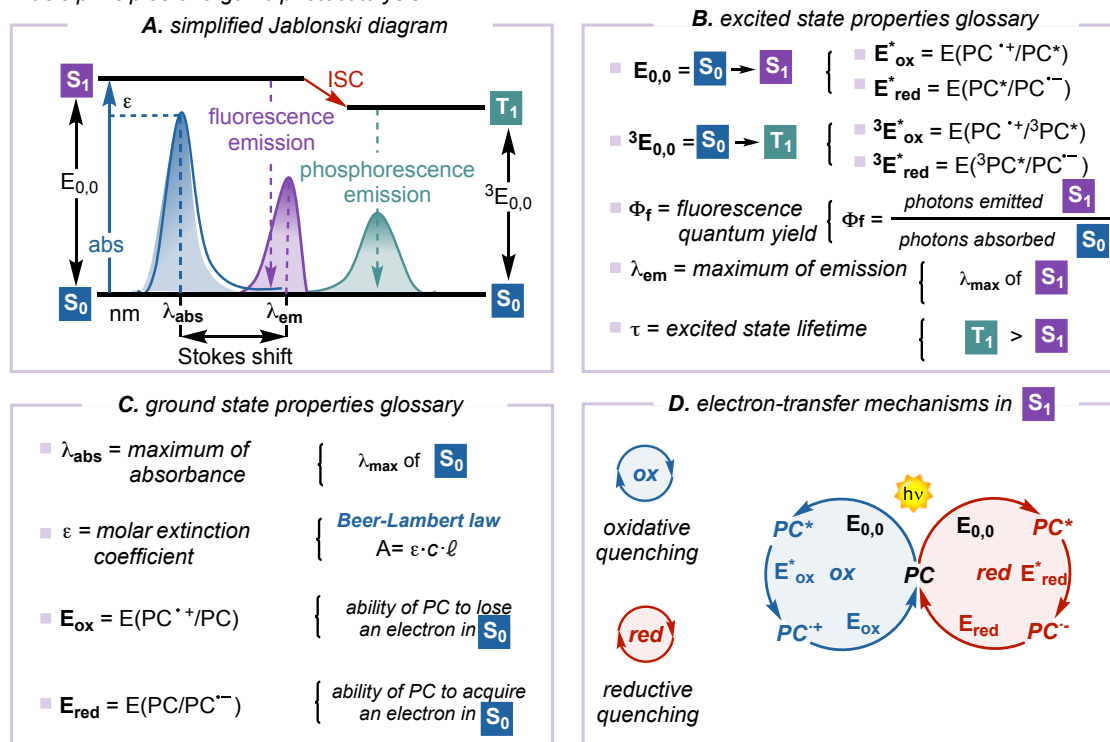


Figure 4.1. - Basic principles of organic photocatalysis. a) simplified Jablonski diagram. b) glossary of excited state properties crucial in photocatalysis. c) glossary of ground state properties crucial in photocatalysis. d) common electron-transfer mechanisms involved in photocatalytic cycles.

A summary of the main PC properties to consider when designing organic dyes are the following:

- Considering the reactivity in the **excited state** of a PC:

the energy of the first singlet state (S_1) is defined by its $E_{0,0}$ (see simplified Jablonski diagram in Figure 4.1a). This energy is reflected into the excited state reduction (E_{red}^*) and oxidation potentials (E_{ox}^*), which can be tuned by rational structural modifications (Figure 4.1b). In organic PCs, the excited species involved in the photocatalytic cycle is usually the singlet (S_1) state, but in some cases this species rapidly decays to the triplet state (T_1), by intersystem crossing (ISC).⁸ In these cases, the energy of the T_1 (${}^3E_{0,0}$), determines the reduction (${}^3E_{red}^*$) and oxidation potential (${}^3E_{ox}^*$). In general, we can assume that when the T_1 is the reactive photocatalytic species, the τ (lifetime) of the S_1

⁸ Strieth-Kalthoff, F.; James, M. J.; Teders, M.; Pitzer, L.; Glorius, F. *Energy Transfer Catalysis Mediated by Visible Light: Principles, Applications, Directions*. *Chem. Soc. Rev.* **2018**, *47*, 7190–7202.

is shorter, its emission prevented, and its fluorescence quantum yield (Φ_f) lowered.

Another property that should be mentioned is the excited state charge transfer (CT) character. Similarly to the metal to ligand CT (MLCT) in metal complexes, some organic PCs are able to access excited states where the electron-density is transferred from an electron-rich portion to an electron-deficient moiety. This charge movement is dictated by the electron-accepting and electro-donating ability, as well as the structural surroundings. It is possible to roughly estimate the CT experimentally by looking at the **Stokes shift** and the Φ_f . The higher the Stokes shift the stronger the CT.⁹ In most of the cases, when the CT is effective, a new S₁-CT or T₁-CT excited state is generated. In some cases, this phenomenon is desired to generate a long-lived CT excited species; in other cases, is detrimental to the reactivity, reducing the excited state reductive/oxidative power.

- Considering the reactivity in the **ground state** of a PC:

along with the mentioned excited state properties, we also must consider the key PC ground state (S₀) parameters (Figure 4.1c). Indeed, structural changes also alter the absorption spectra of the dye. Such parameters are the maximum absorption (λ) and the molar extinction coefficient at a certain wavelength (ϵ).

Particularly relevant are also the ground state E_{red} , which represents the tendency of a PC to acquire one electron from an electrode, and the ground state E_{ox} which represents the tendency to lose one electron to an electrode. While the excited state potentials are generally responsible for the initiation of the photocatalytic cycle, the E_{red} or E_{ox} is essential to close the cycle, restoring the PC ground state (Figure 4.1d).²

In fact, different organic PCs, with exquisite parameter design, have proved the synthetic potential and versatility of the most used metal-complexes.⁷ These dyes can be divided in three sections such as: strongly oxidant, strongly reducing and bimodal photocatalysts (Figure 4.2). This differentiation is made based on the excited state reduction and oxidation potentials. Thus, strongly oxidative photocatalysts possess an $*E_{red} > +1.8$ V vs SCE and the main example of this class of sensitizers is the acridinium family, mainly engaging in reductive

⁹ Lakowicz, J. R. Principles of Fluorescence Spectroscopy, 3. ed.; Springer: New York, 2010.

quenching cycles. Contrarily, strongly reductive photocatalysts possess an $*E_{ox} > -1.8$ V vs SCE, engaging in oxidative quenching cycles. In this group we can mainly find phenoxazines and phenothiazines. Finally, bimodal or redox-balanced photocatalysts are represented by cyanoarenes. In fact, this family of PCs recently found numerous applications in synthetic chemistry acting in both oxidative and reductive quenching cycles. Its versatility derives from its $*E_{ox} < -1.8$ V vs SCE and $*E_{red} < +1.8$ V vs SCE.

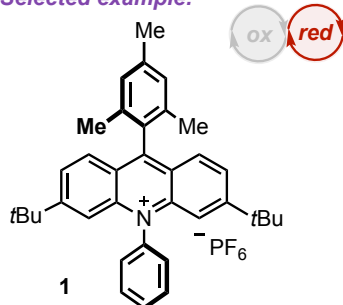
— Classes of organic photocatalysts

Strongly oxidant

Acridinium salts

E^*_{red} up to 2.32 V vs SCE and
 E^*_{ox} up to -0.57 V vs SCE

Selected example:

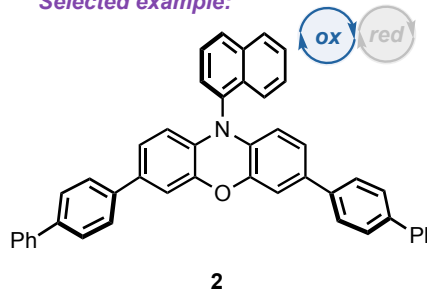


Strongly reducing

Phenoxazines

E^*_{red} up to 0.62 V vs SCE and
 E^*_{ox} up to -2.36 V vs SCE

Selected example:



Bimodal

Cyanoarenes

E^*_{red} up to 1.82 V vs SCE and
 E^*_{ox} up to -1.74 V vs SCE

Selected example:

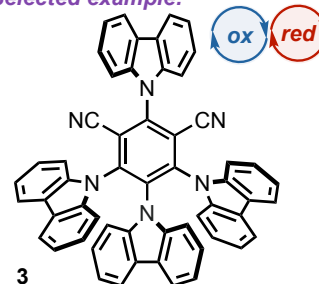


Figure 4.2. - Classes of organic photocatalysts based on their redox properties.

A summary of the properties of the naphthochromenone photocatalysts prepared in Chapter III – Section 3 and used along Chapter IV is depicted in the following pages:

— Naphthochromenone photocatalysts

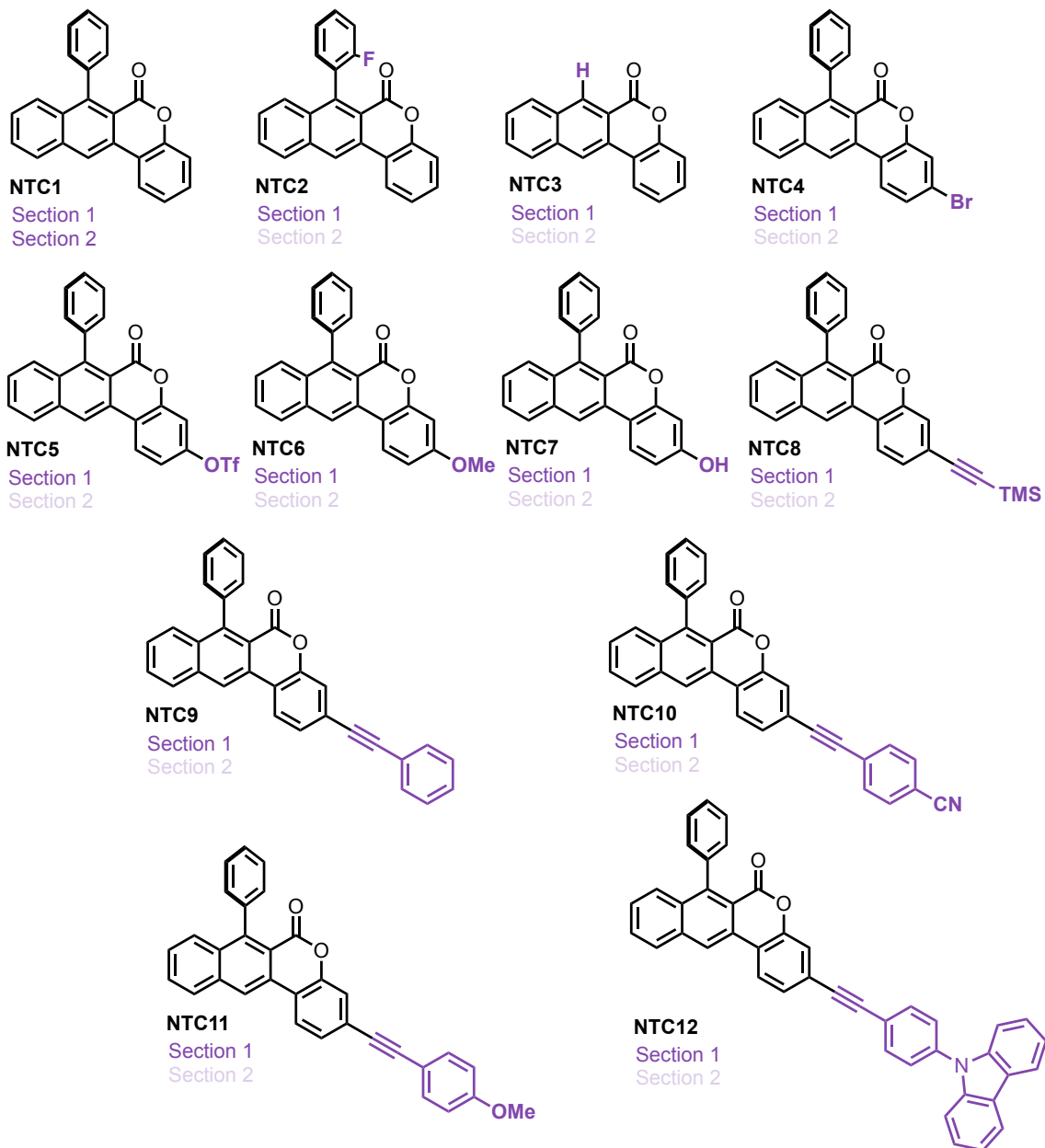
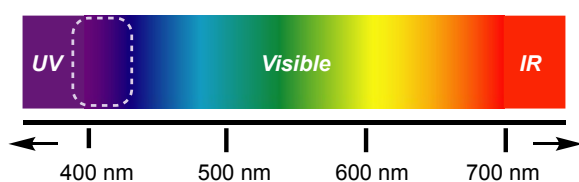
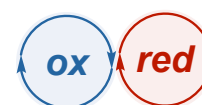


Table 4.1. - Naphthochromenone photocatalysts used in this chapter.

Preferred wavelength



Electron-transfer active mechanisms



PC	λ_{max} emission (nm)	$E_{0,0}$ (eV)	Φ_f (%)	τ (ns)	E_{red} (V vs SCE)	E_{ox} (V vs SCE)	$*E_{red}$ (V vs SCE)	$*E_{ox}$ (V vs SCE)
NTC1	421	3.02	4	1.44	-1.74	1.75	1.28	-1.27
NTC2	421	3.15	9	2.07	-1.68	1.81	1.47	-1.34
NTC3	411	3.22	8	3.86	-1.67	1.80	1.55	-1.42
NTC4	421	3.16	5	1.49	-1.61	1.78	1.55	-1.38
NTC5	413	3.20	4	0.81	-1.55	1.86	1.65	-1.34
NTC6	462	2.97	20	7.78	-1.76	1.47	1.21	-1.50
NTC7	461	2.89	12	8.50	-1.89	1.44	1.00	-1.45
NTC8	426	3.13	15	2.53	-1.71	1.73	1.42	-1.40
NTC9	434	3.12	17	3.34	-1.70	1.64	1.42	-1.48
NTC10	427	3.14	23	3.05	-1.58	1.69	1.56	-1.45
NTC11	449	3.08	16	4.21	-1.65	1.44	1.43	-1.64
NTC12	459	3.12	6	2.49	-1.59	1.35	1.53	-1.77

Table 4.2. - Excited- and ground-state photoredox values of naphthochromenone photocatalysts.¹⁰

¹⁰ Mateos, J.; Rigodanza, F.; Vega-Peñaloza, A.; Sartorel, A.; Natali, M.; Bortolato, T.; Pelosi, G.; Companyó, X.; Bonchio, M.; Dell'Amico, L. *Naphthochromenones: Organic Bimodal Photocatalysts Engaging in Both Oxidative and Reductive Quenching Processes*. *Angew. Chem. Int. Ed.* **2020**, *59*, 1302–1312.



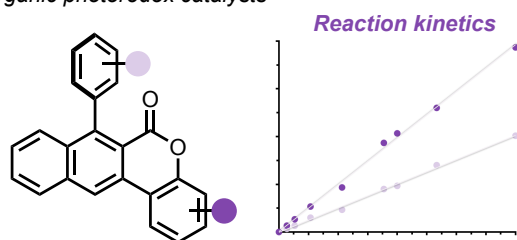
Chapter IV – Section 1

Structure-Activity Relationships in Organic Photoredox Catalysts

— Chapter IV - The Evolution of Aryl Ketone-Derived Products – Applications in Organophotoredox Catalysis —

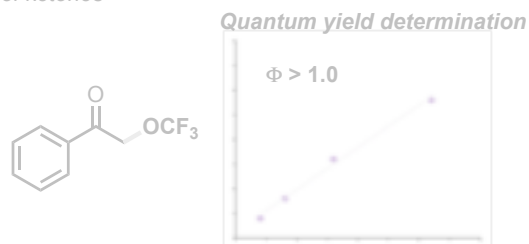
Section 1.

Organophotoredox catalysis - structure-activity relationships in organic photoredox catalysts



Section 2.

Photoredox catalysis - Radical α -trifluoromethoxylation of ketones



- To determine the structure-activity relationships when using naphthochromenones as photocatalysts.
- To use naphthochromenone derivatives in diverse photocatalyzed reactions.¹¹

¹¹ The project discussed in this chapter has been conducted in collaboration with Dr. Francesco Rigodanza (involved in the photophysical characterization of the photocatalysts), Dr. Alberto Vega Peñalosa, Tommaso Bortolato (involved in the synthesis of the photocatalysts), Prof. Andrea Sartorel (involved in the DFT calculations of the photocatalysts) and Prof. Mirco Natali (involved in the measurement of the photocatalyst lifetimes). I individually performed the reaction kinetics as well as the different reactions with the photocatalysts.

This work has been published: Mateos, J.; Rigodanza, F.; Vega-Peñalosa, A.; Sartorel, A.; Natali, M.; Bortolato, T.; Pelosi, G.; Companyó, X.; Bonchio, M.; Dell'Amico, L. *Naphthochromenones: Organic Bimodal Photocatalysts Engaging in Both Oxidative and Reductive Quenching Processes*. *Angew. Chem. Int. Ed.* **2020**, *59*, 1302–1312.

4.1.1 Introduction

The conversion of light into diverse energy forms is at the forefront of intense research in diverse scientific areas from biology to engineering.¹² The chemical community, playing a central role across disciplines, has devoted enormous efforts towards the identification of more efficient molecules that can act as photocatalysts (PCs). This class of compounds is capable of performing numerous light-driven transformations under catalytic conditions.²⁻⁷ Their utilization has a direct impact on our everyday life, spanning from the synthesis of polymers¹³ to more recent applications towards natural product synthesis or drug development.^{5,14} Recently, the identification of novel photocatalytic systems¹⁵ has become an extremely active field of research.¹⁶ Indeed, new directions are pointing towards the identification of more sustainable purely organic molecules.^{7,17}

4.1.2 Challenges of the project

The paradigm of organic PCs is the use of a single family of dyes for the largest number of mechanistically diverse reactions in a selective and efficient manner. This property encompasses a balanced distribution of the excited-state photoredox properties of the sensitizer in the excited state (Figure 4.3). In fact, PCs undergoing both oxidations and reductions upon light irradiation are still limited (4CzIPN **3** is the main example). This bimodal mode of action is rare in organic photocatalysis, especially in combination with wide excited-state energies ($E_{0,0} > 2.5$ eV).⁷ The large majority of organic PCs with $E_{0,0} > 2.5$ eV are

¹² a) Seath, C. P.; Trowbridge, A. D.; Muir, T. W.; MacMillan, D. W. C. *Reactive Intermediates for Interactome Mapping*. *Chem. Soc. Rev.* **2021**, *50*, 2911–2926. b) Buglioni, L.; Raymenants, F.; Slattery, A.; Zondag, S. D. A.; Noël, T. *Technological Innovations in Photochemistry for Organic Synthesis: Flow Chemistry, High-Throughput Experimentation, Scale-up, and Photoelectrochemistry*. *Chem. Rev.* **2021**, DOI: 10.1021/acs.chemrev.1c00332.

¹³ Corrigan, N.; Shanmugam, S.; Xu, J.; Boyer, C. *Photocatalysis in Organic and Polymer Synthesis*. *Chem. Soc. Rev.* **2016**, *45*, 6165–6212.

¹⁴ Michelin, C.; Hoffmann, N. *Photocatalysis Applied to Organic Synthesis – A Green Chemistry Approach*. *Current Opinion in Green and Sustainable Chemistry* **2018**, *10*, 40–45.

¹⁵ McAtee, R. C.; McClain, E. J.; Stephenson, C. R. J. *Illuminating Photoredox Catalysis*. *Trends in Chemistry* **2019**, *1*, 111–125.

¹⁶ For a selected example of novel innovative strategies in photocatalysis see: Ravetz, B. D.; Pun, A. B.; Churchill, E. M.; Congreve, D. N.; Rovis, T.; Campos, L. M. *Photoredox Catalysis Using Infrared Light via Triplet Fusion Upconversion*. *Nature* **2019**, *565*, 343–346.

¹⁷ Selected examples of the development of novel organic photocatalysts: a) McCarthy, B. G.; Pearson, R. M.; Lim, C.-H.; Sartor, S. M.; Damrauer, N. H.; Miyake, G. M. *Structure–Property Relationships for Tailoring Phenoxazines as Reducing Photoredox Catalysts*. *J. Am. Chem. Soc.* **2018**, *140*, 5088–5101. b) Joshi-Pangu, A.; Lévesque, F.; Roth, H. G.; Oliver, S. F.; Campeau, L.-C.; Nicewicz, D.; DiRocco, D. A. *Acridinium-Based Photocatalysts: A Sustainable Option in Photoredox Catalysis*. *J. Org. Chem.* **2016**, *81*, 7244–7249. c) Speckmeier, E.; Fischer, T. G.; Zeitler, K. *A Toolbox Approach To Construct Broadly Applicable Metal-Free Catalysts for Photoredox Chemistry: Deliberate Tuning of Redox Potentials and Importance of Halogens in Donor–Acceptor Cyanoarenes*. *J. Am. Chem. Soc.* **2018**, *140*, 15353–15365.

able to catalyze either oxidative or reductive photoreactions with extreme thermodynamic requirements (e.g., the acridinium salt **1** and phenoxazine **2**). This fact forces the user to move from one class of PCs to another one when changing the operative reaction mechanism. Thus increasing the cost of the optimization process due to the screening of two, or more different dyes. For this reason, the combination of a strongly oxidative excited state and equally strong reductive excited state under visible-light excitation (≥ 400 nm) within a single molecule will define an ideal class of bimodal organic PCs, capable of performing both oxidative and reductive thermodynamically challenging processes in a catalytic routine.

— Paradigm of organic photocatalysis

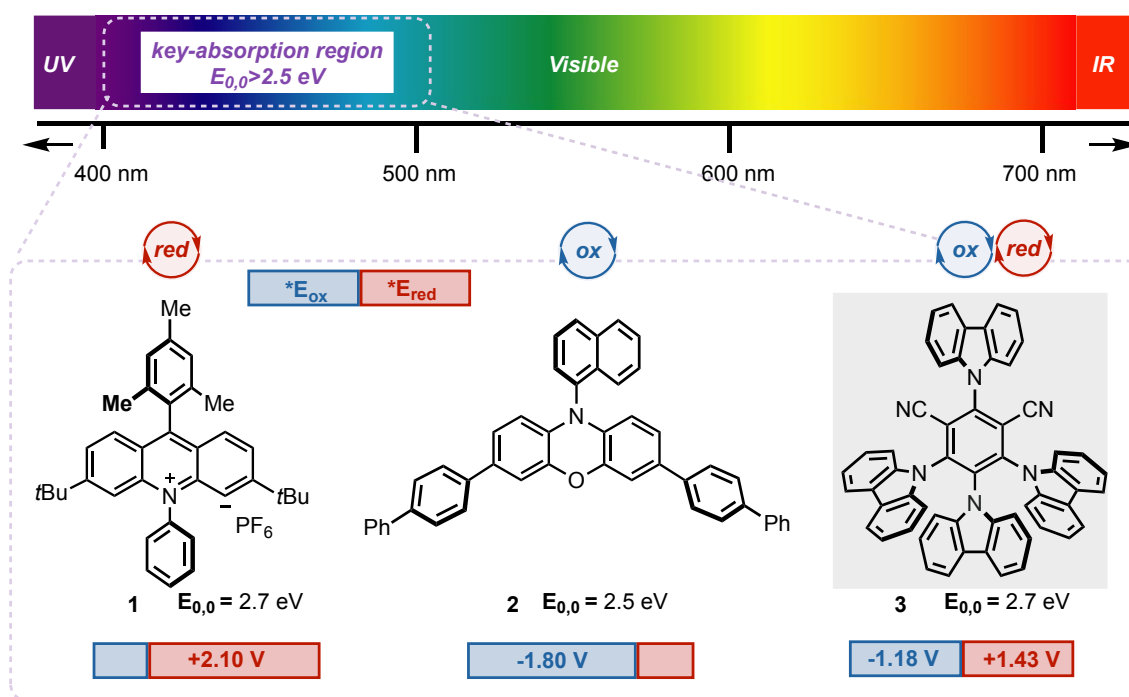


Figure 4.3. - 4CzIPN as the paradigm of a balanced organic photocatalysis.

4.1.3 Section overview

In this section, I outline the identification and performance of *6H*-naphthochromen-6-one (**4**, NTC) scaffolds in a novel family of bimodal organic PCs (Figure 4.4). NTCs absorb visible light towards the lower-wavelength edge, which guarantees access to high-energy excited states ($E_{0,0}$ up to 3.22 eV) with the use of visible-light sources, maintaining both strongly oxidative and strongly reductive properties, with $*E_{red}$ up to 1.65 V and $*E_{ox}$ up to -1.77 V vs SCE. Indeed, some structure–activity relationships were assessed when modifying the structure. Additionally, the synthetic potential of this new class of PCs is demonstrated in a variety of mechanistically diverse transformations (oxidative and reductive quenching processes) classically promoted by either UV- or visible-light-absorbing PCs.

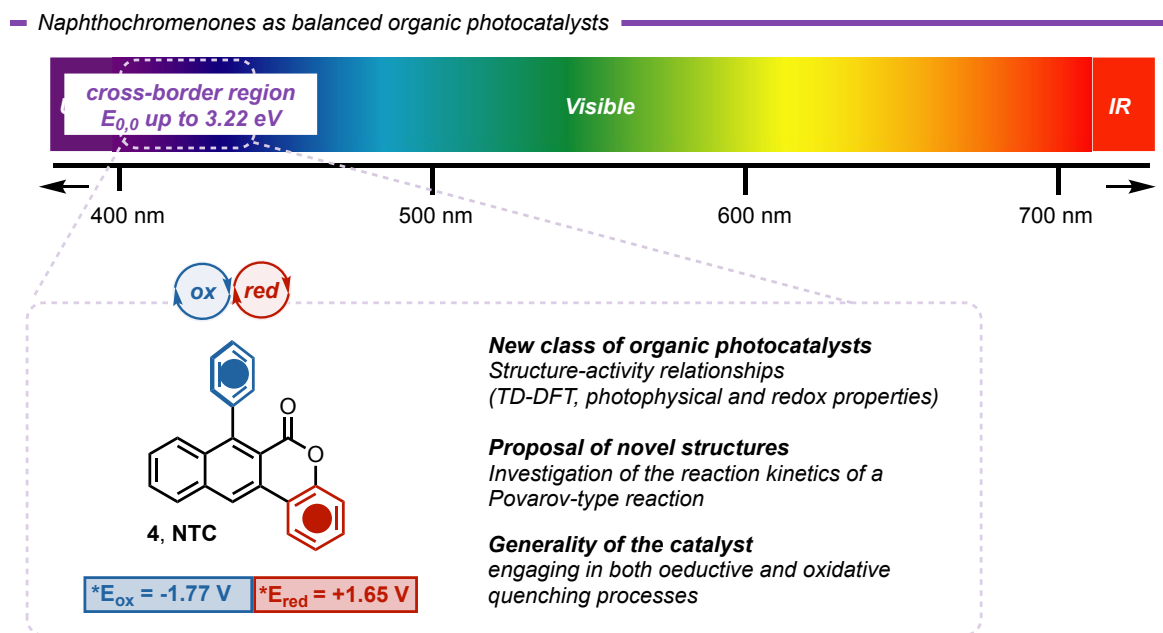


Figure 4.4. - This section: utilization of naphthochromenones as balanced organic photocatalysts.

4.1.4 Results and discussion

Structure-properties relationships – photoredox properties

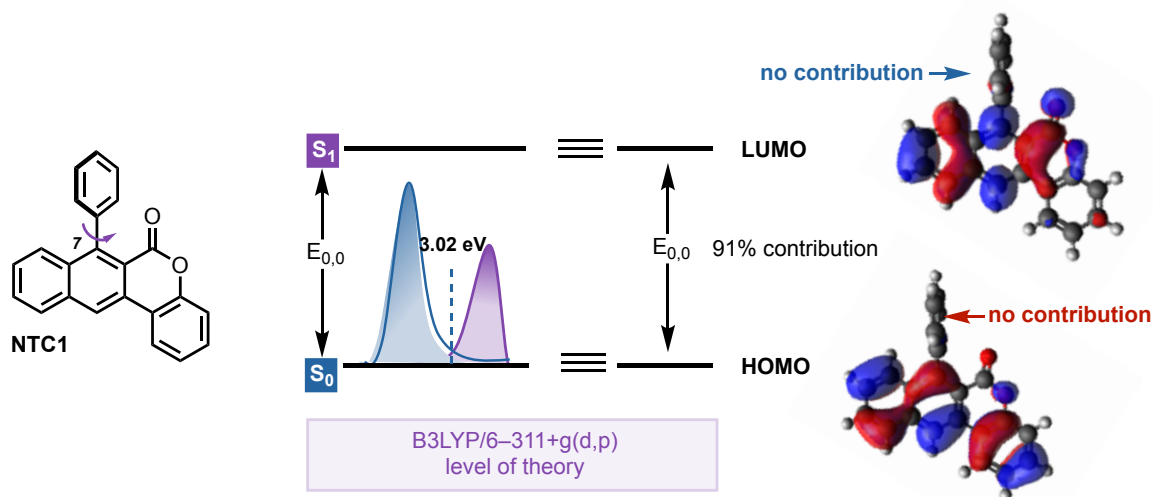
The identification of NTC scaffold **4** as a potential organic PC was inspired by the promising properties and tuneability observed during its synthesis (*see Chapter III – Section 3*). For this reason, we first investigated the properties of naphthochromenones in both the excited and ground state, crucial in affecting the photocatalytic performance. For organic PCs, the S_1 is the easiest reactive state to compare when confronted with T_1 states which generally need transient studies. Additionally, the S_1 is also the most likely to react in bimolecular reactions due to the generally short lifetimes of organic molecules. Indeed, S_1 reacts upon excitation in PET processes.¹⁸ Therefore, the characterization of the S_1 state in terms of decay and its lifetime is instrumental to anticipate its photoreactivity. From a simplistic point of view, high $E_{0,0}$ and a bimodal way of action can indicate that the high reactivity of the PC for a myriad of reactions. Simultaneously, longer lifetimes lead to greater chances of encountering the desired substrate.

¹⁸ For all twelve the NTC photocatalysts, we have calculated the T_1 excited-state energies and the corresponding lifetimes. Nevertheless, the resulting T_1 potentials are unable to drive the reactions herein discussed (*see below*). In agreement with the lower T_1 excited-state potentials, none of the compounds used in the Povarov-type reaction were not able to quench **NTC1-T₁**, ruling out the hypothesis of T_1 catalyzed processes. See: V. Balzani, P. Ceroni, A. Juris, *Photochemistry and Photophysics: Concepts, Research, Applications*, 1st ed., Wiley-VCH, Weinheim, 2014.

Substitution in position C7 of the NTC scaffold

Initially, we started our analysis of NTCs by looking at the effect of different substitutions patterns on the S_1 properties. Thus, we initiated investigating the effects of the aromatic ring in the C7 position (Figure 4.5).

A. Effects of the C7 aromatic ring, TD-DFT calculations



B. Experimental trends

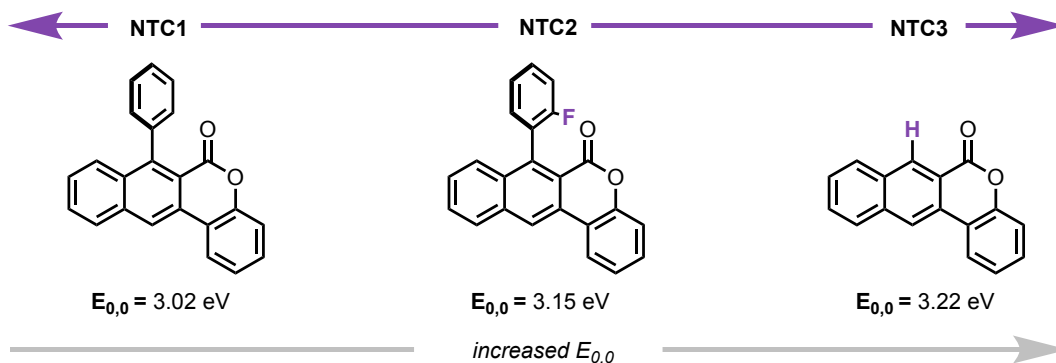


Figure 4.5. - Effects and structure-activity relationships when modifying in position C7. a) TD-DFT calculations. b) Experimental trends observed.

NTC1 has an emission maximum at 421 nm, which is consistent with an $E_{0,0}$ of 3.02 eV. Interestingly, when looking at the electronic transitions responsible for the absorption of this compound (HOMO→LUMO 91% contribution as calculated using the TD-DFT theory at the B3LYP/6-311+g(d,p) level of theory, Figure 4.5a) no contribution of the aromatic ring at position 7 was observed. This fact is also in agreement with the lack of conjugation of this ring in the X-Ray structure of **NTC1**. For this reason, substituting this ring with electron-withdrawing groups (**NTC2**) do not significantly alter the emission properties of the dye but the $E_{0,0}$ energy is slightly increased to 3.15 eV (Figure 4.5b). On the other hand, removing this phenyl ring (**NTC3**) leads to an emission shift of 10 nm to more energetic wavelengths thus increasing the $E_{0,0}$ to 3.22 eV, the highest in the series.

Substitution in position C3 of the NTC scaffold

Then, we analyzed the impact of the substitution pattern in the C3 position of the scaffold. Again, when looking at the electronic transitions responsible for the absorption of **NTC1**, the electron density of the HOMO orbital is mainly located in the coumarin-derived part of the scaffold (Figure 4.6). Hence, the modification of this part will have an increased implication in the photophysical and redox properties of the dyes.

— Effects of the C3 position, TD-DFT calculations

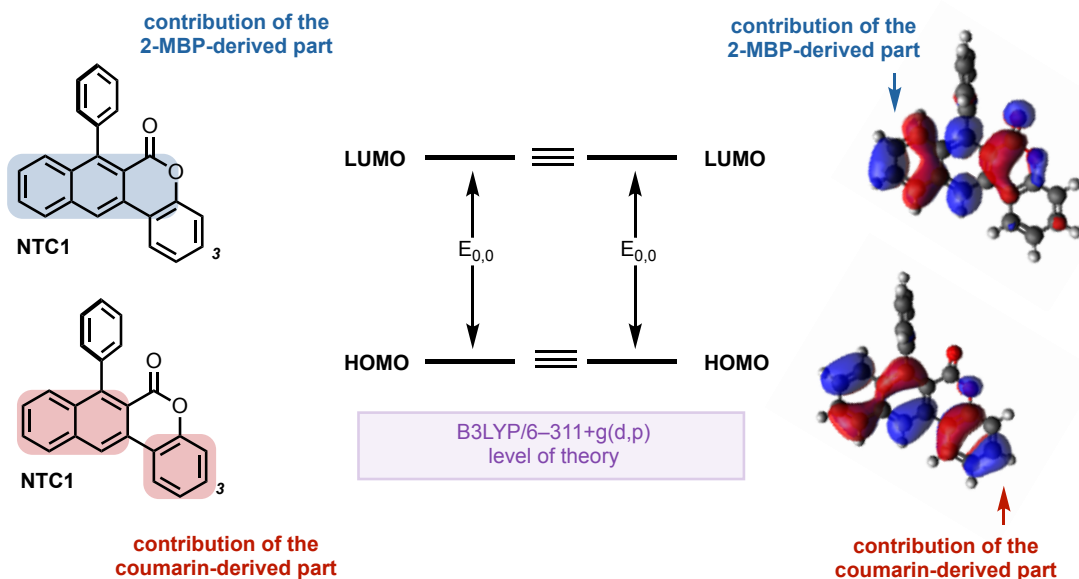


Figure 4.6. - Orbital contributions in the naphthochromenone scaffold.

On one hand, when adding halogen or electron-withdrawing groups (**NTC4** and **NTC5**, respectively) one can expect to lower the HOMO energy (Figure 4.7). This fact is experimentally translated to wider excited-state energy windows ($E_{0,0} = 3.16$ eV for **NTC4** and $E_{0,0} = 3.20$ eV for **NTC5**), emissions shifted towards the UV zone ($\lambda_{\max} = 421$ nm for **NTC4** and $\lambda_{\max} = 413$ nm for **NTC5**) and increased reduction potentials due to the greater ability of accepting an electron (E_{ox} **NTC5** = 1.86 V vs SCE). On the other hand, when adding electron-donating substituents such as the methoxy- and the hydroxy- groups (**NTC6** and **NTC7**, respectively) one can expect the opposite trend. Indeed, the increase of the HOMO energy leads to shorter $E_{0,0}$ windows (up to 2.97 eV), visible light shifted emissions and increased oxidation potentials. Indeed, **NTC6** and **NTC7** have a marked blue-light emission spectra ($\lambda_{\max} =$ up to 462 nm) while being good oxidants (E_{red} **NTC7** = -1.89 V vs SCE). Hence, these PCs are very good candidates for demanding PET processes.

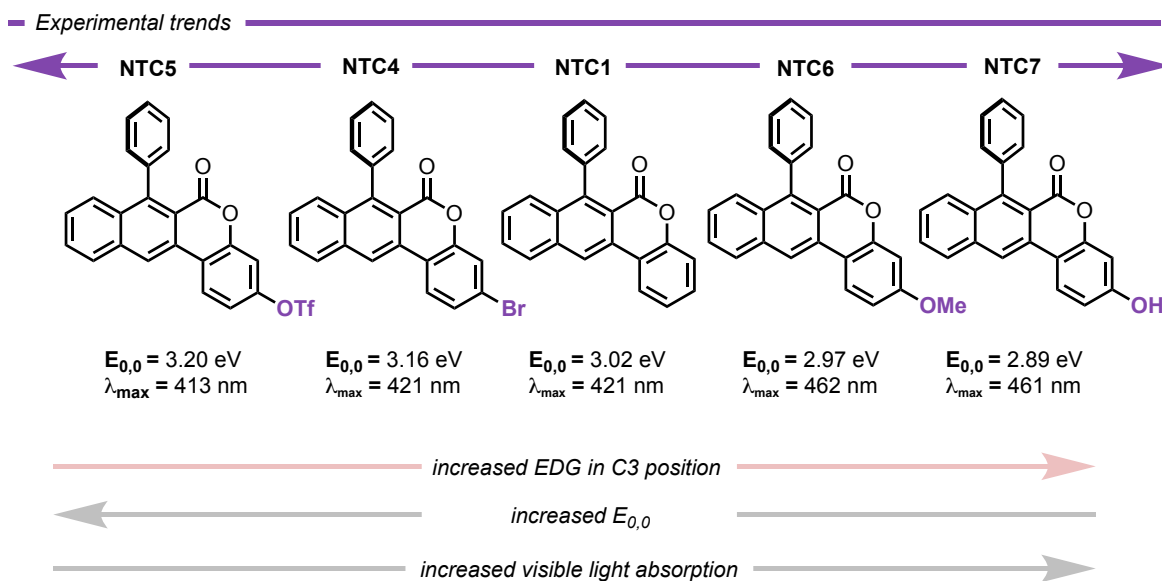


Figure 4.7. - Experimental trends observed when varying the substitution pattern in the C3 position.

An additional computational comparison between the parent **NTC1** and **NTC6** bearing an electron-donating group to better understand the structure-activity-relationships previously assessed (Figure 4.8). In fact, TD-DFT calculations confirmed the enhanced absorption in the visible region for **NTC6**. Analogously, when focusing on the HOMO transition, significant effects were observed, where a 0.2–0.3 eV increase in the orbital energy was noted, consistent with the electron-donating character of the methoxy in position 3.

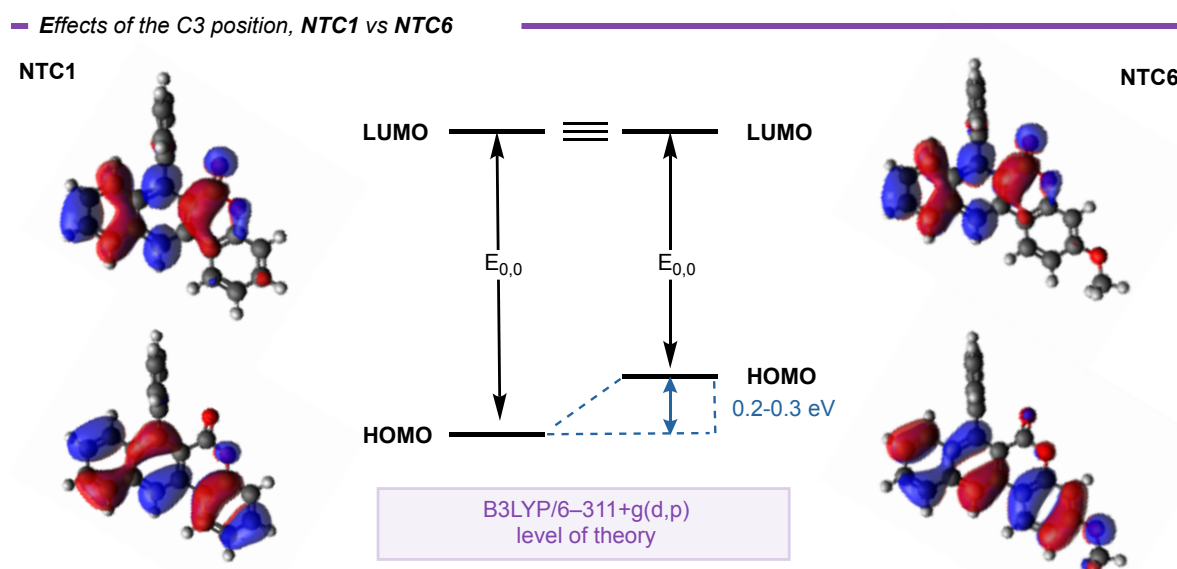


Figure 4.8. - Orbitals comparison between **NTC1** and **NTC6**.

Increasing the π -conjugation

Finally, increasing the π -conjugation with a triple bond can also impact the photophysical properties of the dyes.¹⁹ Thus, by attaching EDG to the sp-hybridized carbon, the spatial separation of the HOMO-LUMO orbitals can be achieved, leading to intramolecular CT complexes when excited (Figure 4.9). Indeed, **NTC12** has a distinctive HOMO that is higher in energy and located predominantly on the carbazole (Cz) moiety, suggesting an intramolecular charge transfer contribution.

Intramolecular CT

NTC12

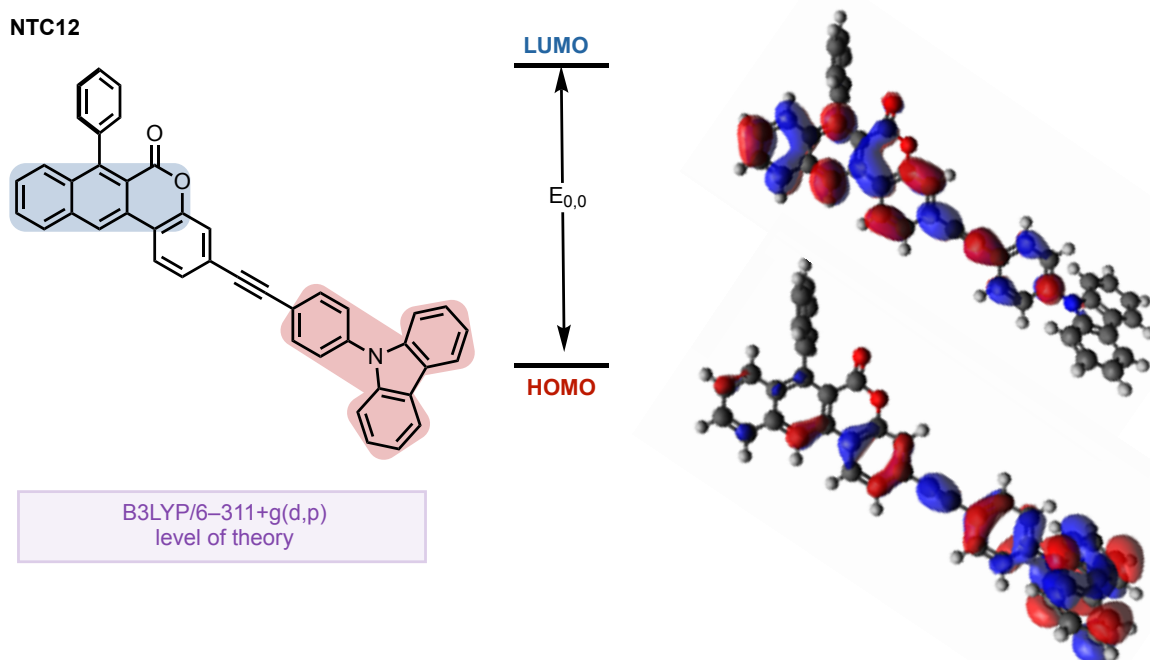


Figure 4.9. - Intramolecular CT character of compound **NTC12**.

When looking at the measured properties, the emission maximum was observed in the range from 427 nm (**NTC11**, bearing an electron-withdrawing group) to 459 nm (**NTC12**, bearing an electron-donating group) passing by 434 nm (**NTC10**, with unsubstituted aryl rings). Additionally, the quantum yields were determined to be 15–23 % and the lifetimes of the excited state were generally longer than 2 ns, overpassing the properties of the parent **NTC1**.

¹⁹ Bureš, F.; Čermáková, H.; Kulhánek, J.; Ludwig, M.; Kuznik, W.; Kityk, I. V.; Mikysek, T.; Růžička, A. *Structure-Property Relationships and Nonlinear Optical Effects in Donor-Substituted Dicyanopyrazine-Derived Push-Pull Chromophores with Enlarged and Varied π -Linkers*. *Eur. J. Org. Chem.* **2012**, 2012, 529–538.

Effects in the redox properties

One of the advantages of the NTCs is their wide redox window, which allows for both highly demanding reductive and oxidative quenching cycles. **NTC1** undergoes reversible reduction at -1.74 V vs SCE and oxidation at 1.75 V vs SCE. Moreover, the calculated potentials of the excited states of 1.28 V ($*E_{\text{red}}$) and -1.27 V ($*E_{\text{ox}}$) are well suited for a variety of different photoreactions requiring strong oxidative or reductive power.

As we have observed, by modulating the substituents within the NTC core, it is possible to reach more negative E values ($*E_{\text{ox}}$) with electron-donating groups in position 3, as shown for **NTC6** (-1.50 V vs SCE) and **NTC7** (-1.45 V vs. SCE). Even more negative values were registered for PCs with extended conjugation, ranging from -1.45 V for **NTC10** up to a remarkable -1.77 V for **NTC12** (Figure 4.10).

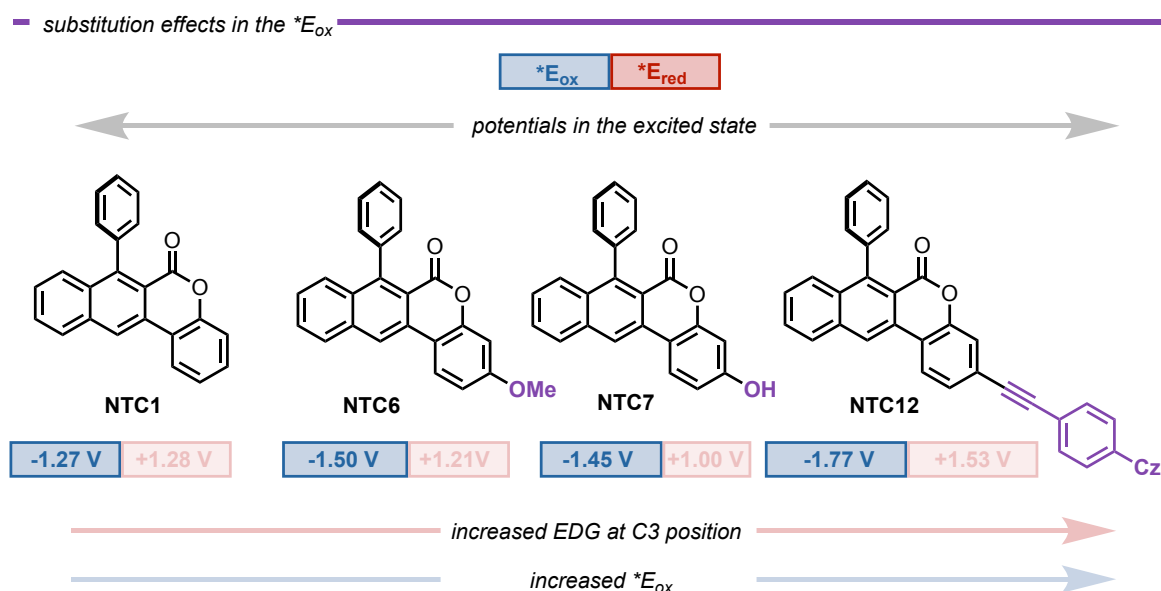


Figure 4.10. - Impact of the substitution at the C3 position in the oxidation potential in the excited state.

Moving to the reductive process ($*E_{\text{red}}$), we immediately discerned the wider variability of the PCs covering the window from 1.00 V vs SCE for **NTC7** to 1.65 V vs SCE for **NTC5** (Figure 4.11). Indeed, the addition of EWGs as in **NTC2**, **NTC5**, and **NTC10** stabilizes the HOMO of the PCs, bringing the potential to above 1.65 V vs SCE.

substitution effects in the ${}^*E_{red}$

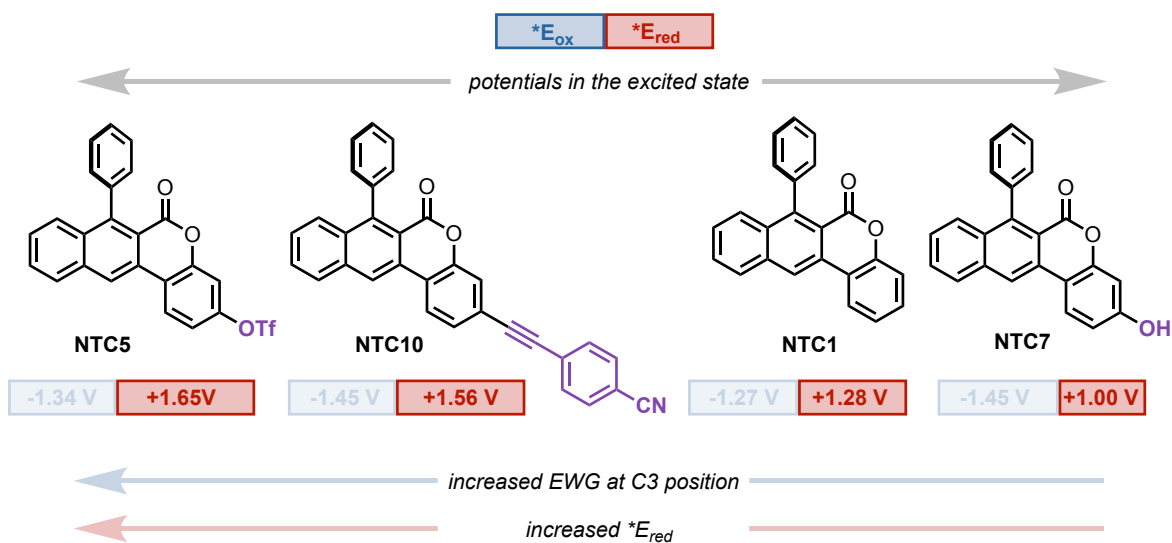
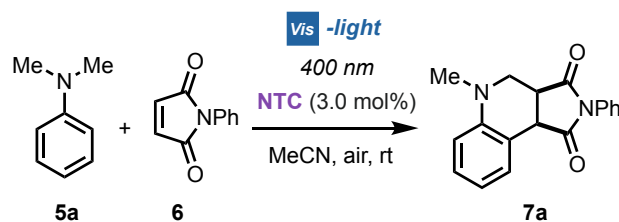


Figure 4.11. - Impact of the substitution at the C3 position in the reduction potential in the excited state.



benchmark reaction, reactivity & mechanism

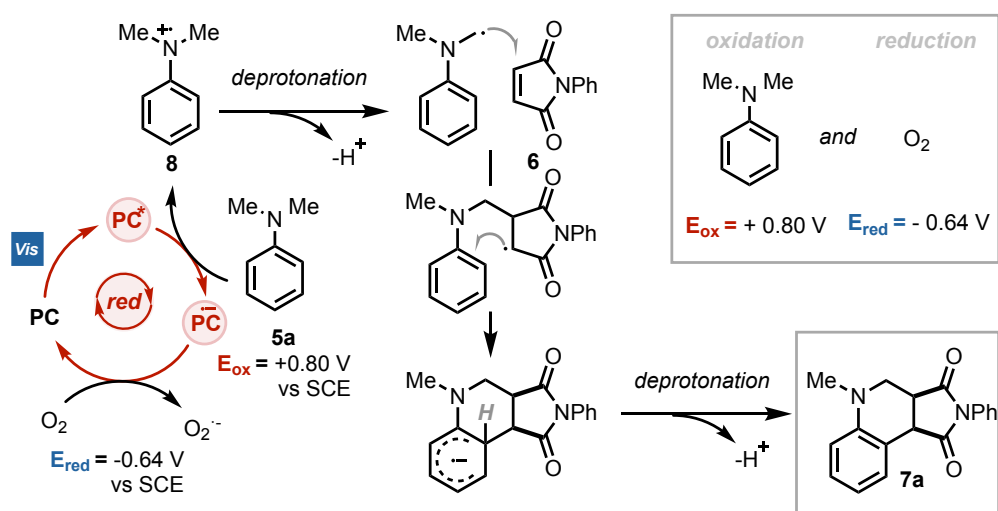


Figure 4.12. - Povarov-type cycloaddition as benchmark reaction for the determination of SARs with Naphthochromenone PCs.

Structure-activity relationships – Reaction kinetics vs Quenching kinetics

After having established general structure–*property* relationships, we wanted to address a more challenging issue and determine structure-*activity* relationships in photoredox catalysis across the twelve PCs. The determination of such type of relationships still remains to limited PC structures.²⁰ For this reason, we evaluated the photocatalytic performances of NTC PCs in a benchmark reaction. We chose the Povarov-type addition of *N,N*-dimethylaniline (**5a**) to phenylmaleimide (**6**; Figure 4.12).

This photoreaction was chosen based on two main considerations:

- i) the reaction mechanism is well known and has been studied for both metal complexes²¹ and organic PCs,²² facilitating comparisons.
- ii) the redox potentials of **6a** ($E_{\text{ox}}(\mathbf{6a}^+/\mathbf{6a})=+0.80$ V vs SCE) and O_2 ($E_{\text{red}}(\text{O}_2/\text{O}_2^{\cdot-})=-0.64$ V vs. SCE)²³ are within the operational windows of the twelve developed PCs, thus enabling their comparison.

This transformation was evaluated by its reaction kinetics and Stern–Volmer analysis. In Figure 4.13, these two processes are shown for NTC1. Interestingly, the reaction proceeds in a pseudo-zero order regime at the beginning of the reaction, which allows an easy comparison between PCs at the initial reaction rate (k_0).²⁴ Additionally, considering a purely dynamic quenching, the slope (K_{PC}) of the Stern–Volmer plot is defined as $K_{\text{PC}}=k_q\tau_{\text{PC}}$,²⁵ where k_q is the bimolecular rate constant and τ_{PC} the excited-state lifetime of the photocatalyst. Hence, we hypothesized the comparison of the initial reaction rate constant (k_0) and the k_q as key to assess unexplored SAR in photoredox catalysis.

²⁰ Li, X.; Maffettone, P. M.; Che, Y.; Liu, T.; Chen, L.; Cooper, A. I. *Combining Machine Learning and High-Throughput Experimentation to Discover Photocatalytically Active Organic Molecules*. *Chem. Sci.* **2021**, *12*, 10742–10754.

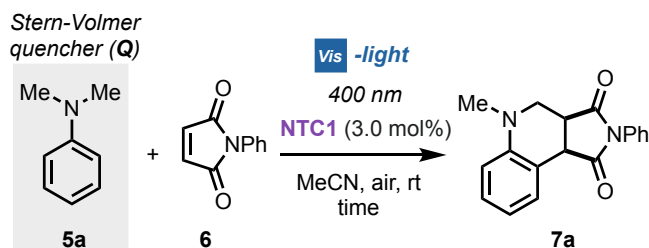
²¹ Ju, X.; Li, D.; Li, W.; Yu, W.; Bian, F. *The Reaction of Tertiary Anilines with Maleimides under Visible Light Redox Catalysis*. *Adv. Synth. Catal.* **2012**, *354*, 3561–3567.

²² Liang, Z.; Xu, S.; Tian, W.; Zhang, R. *Eosin Y-Catalyzed Visible-Light-Mediated Aerobic Oxidative Cyclization of *N,N*-Dimethylanilines with Maleimides*. *Beilstein J. Org. Chem.* **2015**, *11*, 425–430.

²³ Singh, P. S.; Evans, D. H. *Study of the Electrochemical Reduction of Dioxygen in Acetonitrile in the Presence of Weak Acids*. *J. Phys. Chem. B* **2006**, *110*, 637–644.

²⁴ Ollis, D. F. *Kinetics of Photocatalyzed Reactions: Five Lessons Learned*. *Front. Chem.* **2018**, *6*, 378.

²⁵ Gehlen, M. H. *The Centenary of the Stern-Volmer Equation of Fluorescence Quenching: From the Single Line Plot to the SV Quenching Map*. *Journal of Photochemistry and Photobiology C: Photochemistry Reviews* **2020**, *42*, 100338.



initial rate vs Stern-Volmer quenching

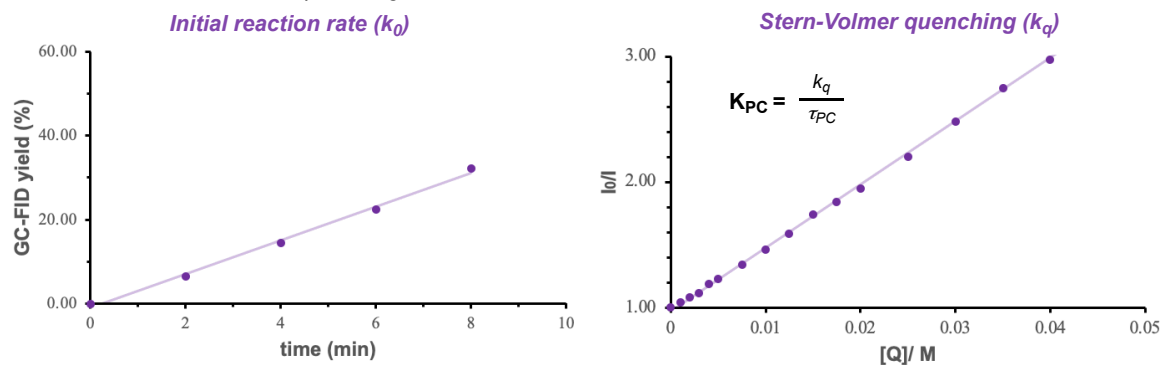


Figure 4.13. - Initial reaction rate (k_0) and Stern-Volmer quenching constant (k_q) as parameters to assess SAR in organic photoredox catalysis.

k_0 vs k_q when substitution in position C7 of the NTC scaffold

Interestingly, the k and k_q values of the different NTCs fall in a narrow range. Thus, a comparison with the parent NTC1 can be done considering the diverse substitution patterns. When substituting at the C7 position (Figure 4.14):

- i)* When comparing k_0 , NTC1 presented the highest initial reaction rate. Indeed, NTC2 and NTC3 showed an inferior rate. Remarkably, these rates followed the same trend observable for the PC lifetime, compact NTC3 showed the longer lifetime in the series (3.86 ns) but the lowest k_0 . At the same time, NTC1 with the shortest excited-state lived lifetime (1.44 ns) showed the highest rate in the series. This strange observation is in contrast with what it was expected. In fact, long-lived photocatalyst quench better the reactive species and this could also be translated to higher reaction rates.
- ii)* When comparing the Stern-Volmer quenching constants, NTC2 and NTC3 showed enhanced rates (1.04 times-folded and 1.42 times-folded, respectively). This perfectly matches with the lifetimes trend, where the longest-lived excited state shows the higher k_q .

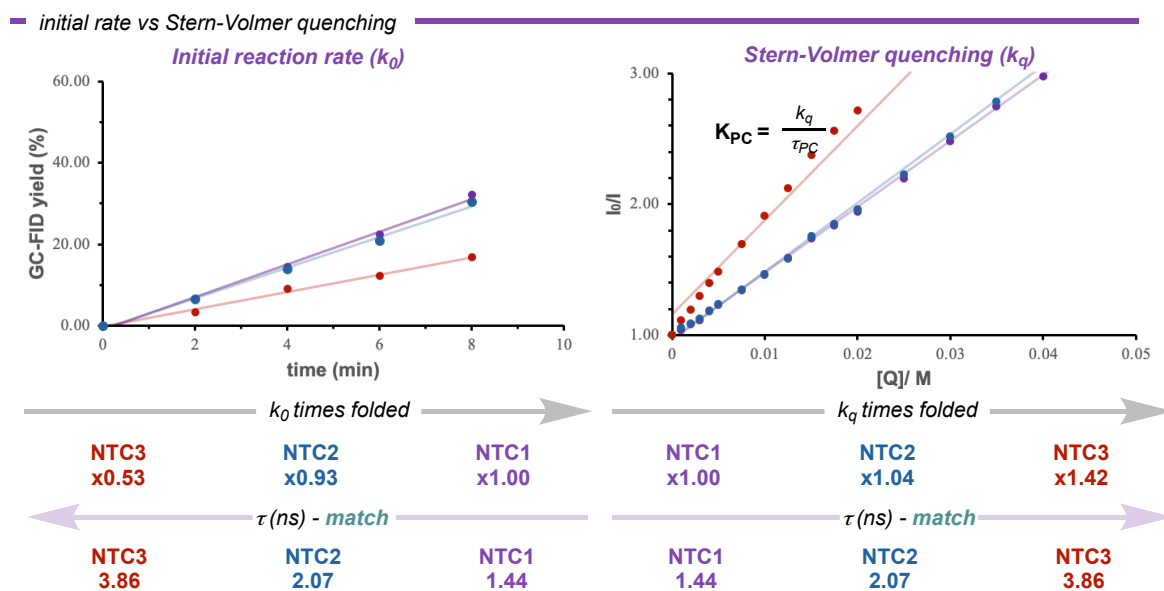
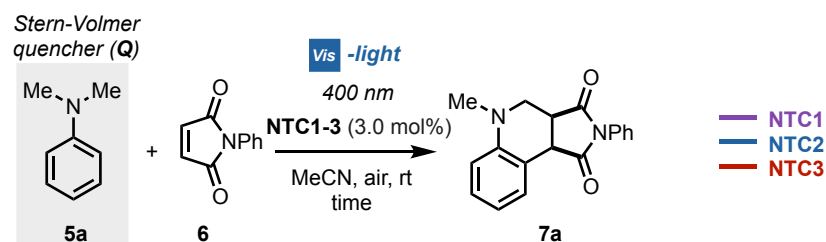


Figure 4.14. - Initial reaction rate (k_0) and Stern-Volmer quenching constant (k_q) comparison with NTC1 when varying the C7 position.

k_0 vs k_q when substitution in position C3 of the NTC scaffold

When moving to the substitution pattern in position C3 the comparison becomes more complex. Indeed, no simple correlations are observed for this type of NTCs (Figure 4.15).

- i) In the comparison of the k_0 between NTC4-7 and NTC1, electron-rich substituted PCs clearly showed an enhanced rate (NTC6 with a methoxy- group and NTC7 with an hydroxy- group). Following this trend, one could expect to have decreased k_0 with EWG in this position. Nevertheless, this hypothesis is only true for NTC5 (triflate-substituted NTCs). Interestingly, NTC4 outcompeted NTC6. This fact indicates that the k_0 is related to more than one parameter.
- ii) The application of the previous comparison (k_q vs τ), failed for this type of NTCs. Indeed, NTC6 and NTC7 present the higher lifetimes of the series (7.78 ns and 8.50 ns, respectively) being the latter the longest-lived one. Nevertheless, NTC6 outcompeted NTC7 in terms of k_q . Additionally, this unexpected outcome is also observed for the other three PCs used in this study.

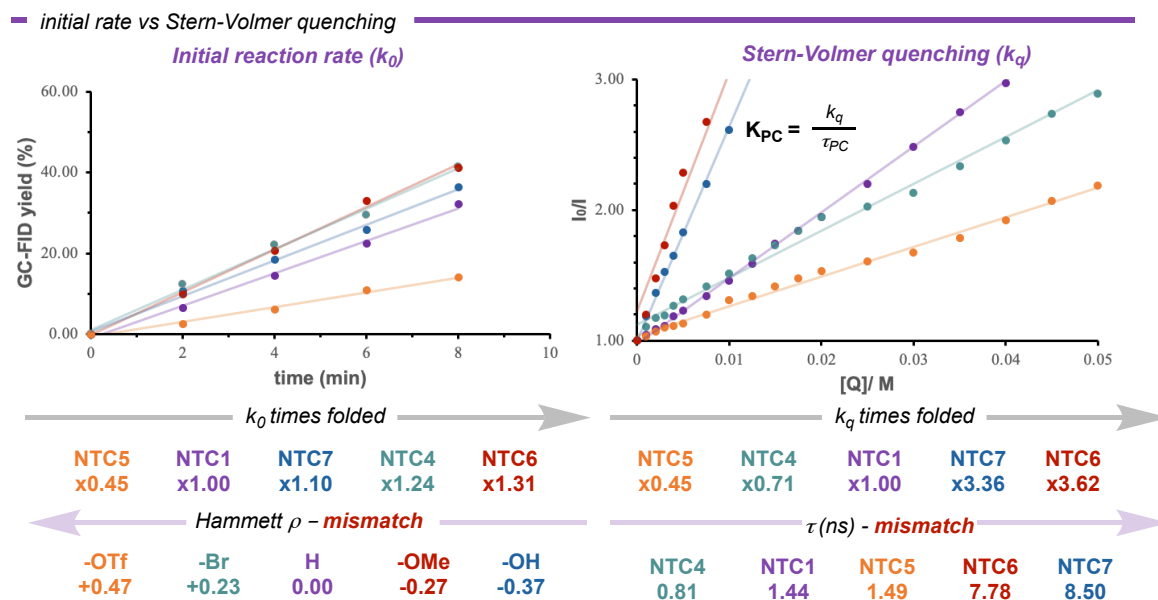
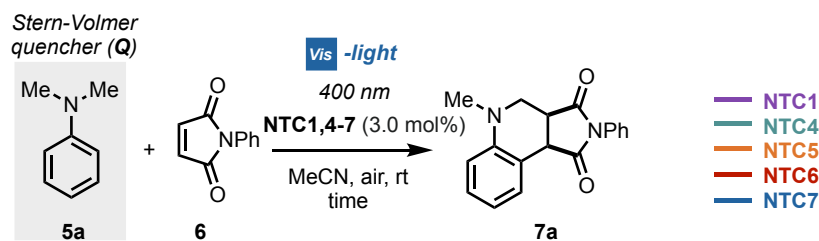


Figure 4.15. - Initial reaction rate (k_0) and Stern-Volmer quenching constant (k_q) comparison between NTC1 when varying the C3 position.

k_0 vs k_q when a π -extended conjugation is present with the NTC scaffold

Finally, when moving to NTCs with an increased π -conjugation no correlations were observed (Figure 4.15).

- i) When comparing the k_0 between NTC9-12 and NTC1, no big differences were obtained (from 0.67 to 1.26 times-folded NTC1 k_0). Again, the electronic effects occurring in the additional aryl ring does not have a linear impact within the initial reaction rate.
- ii) When k_q was compared with the PCs lifetimes, it showed an order mismatch as well. Indeed, NTC10 and NTC12 have longer lifetimes (along the series $\tau=3.05$ and 2.49 ns, respectively) than NTC1 but the measured k_q were inferior to the parent NTC scaffold (0.83 and 0.81 times different, respectively). Hence, the properties governing this comparison are not restricted only to these parameters.

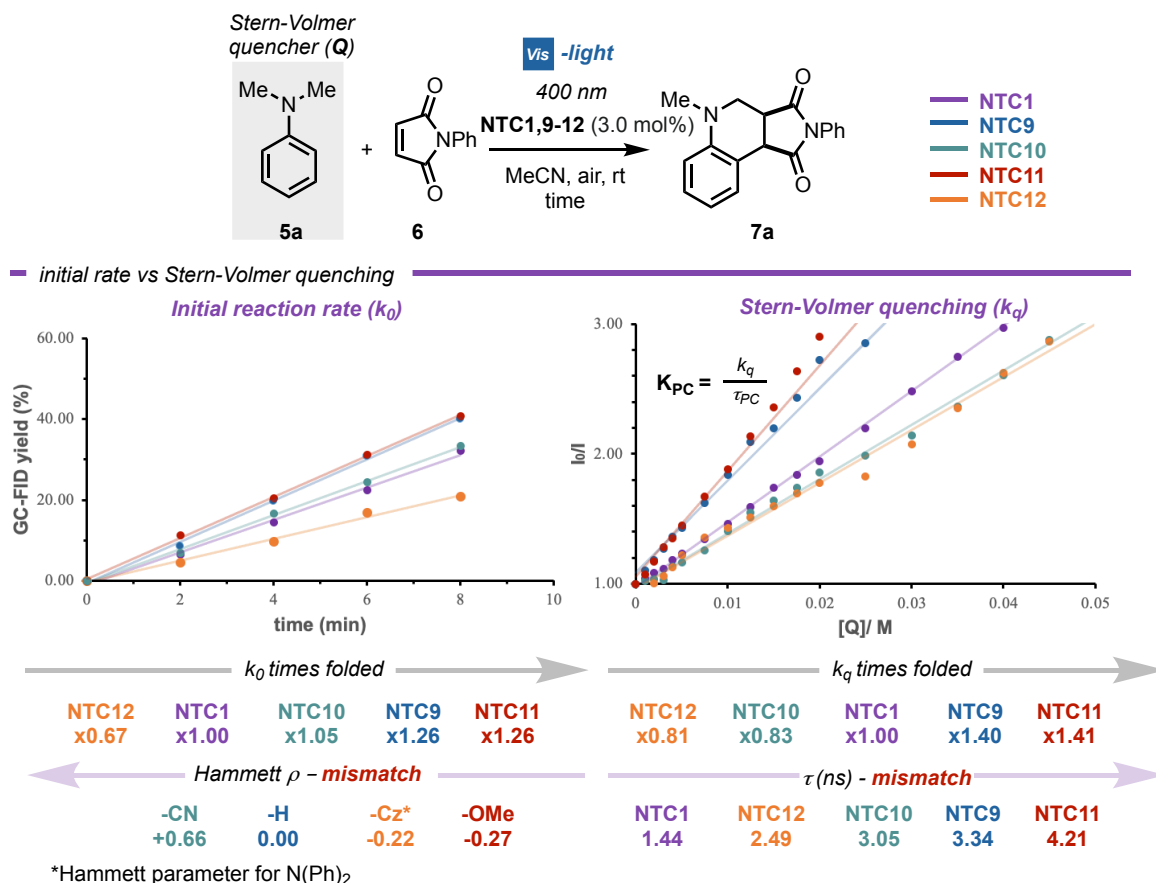


Figure 4.16. - Initial reaction rate (k_0) and Stern-Volmer quenching constant (k_q) comparison between NTC1 when increasing the conjugation.

Generality of the photocatalysts

Reductive quenching: Povarov-type reaction

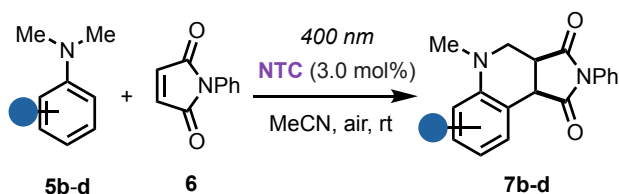
Having defined structure-*property* relationships and having useful information in hand to assess structure-*activity* relationships for the naphthochromenone PC family, we evaluated the synthetic application of such sensitizers. With this aim, we next selected substrates **5b–d** because of their high oxidation potentials (E_{ox} =1.05–1.33 V vs. SCE, Table 4.3).

Because of their thermodynamically demanding oxidation, these compounds are beyond the state-of-the-art synthetic applications reported thus far, catalyzed by Ru,²¹ Cu,²⁶ Co,²⁷ Ir,²⁸ and

²⁶ Nicholls, T. P.; Constable, G. E.; Robertson, J. C.; Gardiner, M. G.; Bissember, A. C. Brønsted Acid Cocatalysis in Copper(I)-Photocatalyzed α -Amino C–H Bond Functionalization. *ACS Catal.* **2016**, *6*, 451–457.

²⁷ Yang, X.-L.; Guo, J.-D.; Lei, T.; Chen, B.; Tung, C.-H.; Wu, L.-Z. Oxidative Cyclization Synthesis of Tetrahydroquinolines and Reductive Hydrogenation of Maleimides under Redox-Neutral Conditions. *Org. Lett.* **2018**, *20* (10), 2916–2920.

²⁸ Peng, F.; Zhi, P.; Ji, H.; Zhao, H.; Kong, F.-Y.; Liang, X.-Z.; Shen, Y.-M. Visible Light Mediated Cyclization of Tertiary Anilines with Maleimides Using a Supported Iridium Complex Catalyst. *RSC Adv.* **2017**, *7*, 19948–19953.



substrate	E_{ox} (vs SCE)	product	NTC	isol. yield			
 5b	1.05 V	 7b	NTC1	42			
			NTC2	43			
			NTC4	33			
			NTC5	25			
			NTC6	50			
			NTC7	67			
			NTC10	16			
			NTC11	63			
			 5c	1.12 V	 7c	NTC1	41
						NTC2	52
						NTC4	24
NTC5	23						
NTC6	36						
NTC7	49						
NTC10	17						
NTC11	61						
 5d	1.33 V	 7d				NTC1	50
						NTC2	63
						NTC4	51
			NTC5	42			
			NTC6	29			
			NTC7	17			
			NTC10	36			
			NTC11	70			

Table 4.3. - NTC performance in Povarov-type reaction with *N,N*-maleimide with high oxidation potentials.

Pt- complexes,²⁹ eosin Y,²² different supported metal oxides including TiO₂³⁰ and more recently, aldehydes.³¹

We started using **5b**, bearing an ester group at the *para* position ($E_{\text{ox}}=1.05$ V vs. SCE). Two of the best performances were registered for **NTC6** and **NTC7**, with 50 % and 67 % yield, respectively. Remarkably, the highly oxidizing **NTC11** ($*E_{\text{red}} = 1.56$ V vs SCE) furnished the product in 63 % yield. Subsequently, **5c** was selected not only for the higher oxidation potential ($E_{\text{ox}}=1.12$ V vs SCE), but also for the presence of an aldehyde moiety, which is particularly sensitive to chemical oxidants. Gratefully, PCs **NTC2** and **NTC11**, characterized by high excited-state reduction potentials, delivered **7c** in 52 and 61 % yield, respectively. Additional experiments were carried out with **5d** ($E_{\text{ox}}=1.33$ V vs SCE), bearing two CF₃ groups in the 3,5-positions. The most oxidant PCs exhibited the best performances, with **NTC11** furnishing **5d** in 70 % yield. It is interesting to note how PCs **NTC6** and **NTC7** ($*E_{\text{red}} = 1.21$ and 1.00 V vs SCE, respectively) showed inferior performances when moving from **5a,b** to the more oxidizing substrate **5d**. This fact indicates the increased impact of the excited-state oxidative power (**NTC***/**NTC⁻**) upon moving towards the thermodynamic oxidation limits of the PC. On the other hand, the more oxidizing PCs **NTC2** and **NTC11** ($*E_{\text{ox}} = 1.47$ and 1.56 V vs SCE) resulted in improved performances. Eosin Y, the previous PC of choice for this type of reaction, turned out to be completely inefficient.

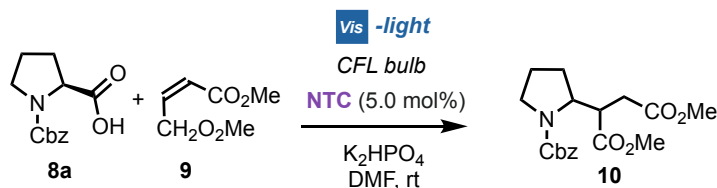
Reductive quenching: Giese-type reaction

At this juncture, we decided to evaluate **NTCs** in diverse photochemical transformations. We started by testing their performance under reductive quenching methods, in the decarboxylative Giese-type addition of protected proline **8a** and dimethyl maleate **9** (Figure 4.17).

²⁹ Ranieri, A. M.; Burt, L. K.; Stagni, S.; Zacchini, S.; Skelton, B. W.; Ogden, M. I.; Bissember, A. C.; Massi, M. Anionic Cyclometalated Platinum(II) Tetrazolato Complexes as Viable Photoredox Catalysts. *Organometallics* **2019**, *38*, 1108–1117.

³⁰ Tang, J.; Grampp, G.; Liu, Y.; Wang, B.-X.; Tao, F.-F.; Wang, L.-J.; Liang, X.-Z.; Xiao, H.-Q.; Shen, Y.-M. Visible Light Mediated Cyclization of Tertiary Anilines with Maleimides Using Nickel(II) Oxide Surface-Modified Titanium Dioxide Catalyst. *J. Org. Chem.* **2015**, *80*, 2724–2732.

³¹ Nikitas, N. F.; Theodoropoulou, M. A.; Kokotos, C. G. Photochemical Reaction of *N,N*-Dimethylanilines with *N*-Substituted Maleimides Utilizing Benzaldehyde as the Photoinitiator. *Eur. J. Org. Chem.* **2021**, 2021, 1168–1173.



— Giese-type reaction, reactivity & mechanism

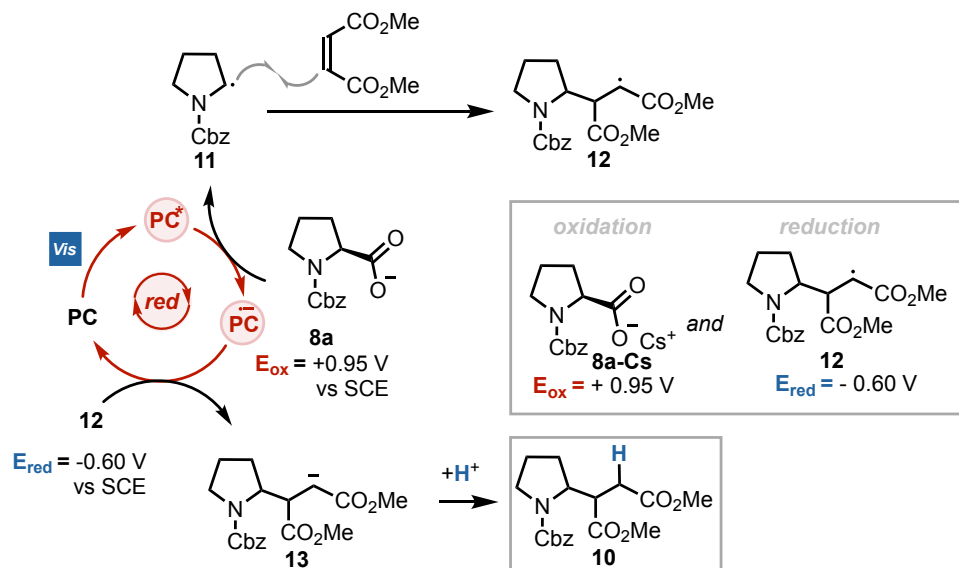


Figure 4.17. - Giese-type reaction as example of challenging reductive quenching process.

This reaction has been used to evaluate the synthetic performance of diverse photocatalytic systems, including Ir-based PCs,³² acridinium salts,^{17b} and cyanoarenes.^{17c} This transformation is difficult to be efficiently catalyzed because of the need for an optimal balance between the oxidative excited-state properties of the PC and the reductive power of its radical anion. It is important to ensure that:

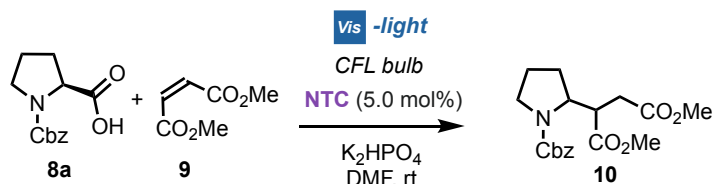
- i) the decarboxylation step is efficient (by PC* reductive quenching, **8a-Cs**: $E_{\text{ox}} = +0.95 \text{ V vs. SCE}$)³² generating the reactive α -amino radical **11**.
- ii) the reduction of the formed C-centered radical **12** ($E_{\text{red}} = -0.60 \text{ V vs. SCE}$)³² is fast, thus closing the photocatalytic cycle.

It is worth mentioning that only specific Ir-based and organic PCs have been able to catalyze this transformation.^{17b,32} In fact, diverse PCs turned out to be highly inefficient, despite suitable redox potentials.

PCs **NTC2** and **NTC4** furnished the product in reduced yields of 48 % and 53 %, respectively (Table 4.4 entries 2 and 3). Inferior results were obtained for **NTC5** (entry 4), in

³² Chu, L.; Ohta, C.; Zuo, Z.; MacMillan, D. W. C. Carboxylic Acids as A Traceless Activation Group for Conjugate Additions: A Three-Step Synthesis of (\pm)-Pregabalin. *J. Am. Chem. Soc.* **2014**, *136*, 10886–10889.

agreement with its very short excited-state lifetime of 0.81 ns. **NTC6**, with inferior excited-state reduction potential ($*E_{\text{red}}=+1.21$ V) and superior τ (7.78 ns), performed well, giving the desired product in 62 % yield (entry 5). Finally, PCs with extended conjugation such as **NTC11** and **NTC12** efficiently catalyzed this reaction to give product **10** in 75 % and 70 % yield, respectively. In particular **NTC11** with $*E_{\text{red}}=+1.56$ V and $\tau=3.05$ ns was the best of the series (entry 6). Selected metal-based PCs were also compared under the same reaction conditions, but gave poor results (entries 8–10).³²



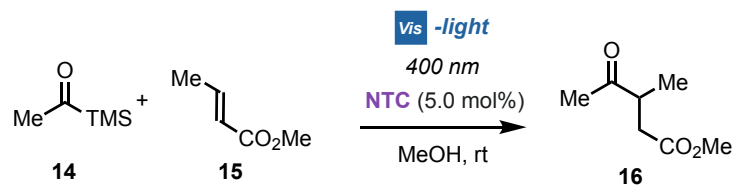
entry	PC	$*E_{\text{red}}$ (V vs SCE)	E_{red} (V vs SCE)	τ (ns)	$^1\text{H NMR}$ yield
1	NTC1	1.28	-1.74	1.44	66
2	NTC2	1.47	-1.68	2.07	48
3	NTC4	1.55	-1.61	1.49	53
4	NTC5	1.55	-1.55	0.81	62
5	NTC11	1.43	-1.65	4.21	77
6	NTC12	1.53	-1.59	2.49	72
7	$\text{Ru}(\text{bpy})_2\text{Cl}_2$	0.77	-1.33	1100.00	16
8	<i>fac</i> - $\text{Ir}(\text{ppy})_3$	0.55	-1.95	1900.00	<5
9	<i>fac</i> - $\text{Ir}(\text{dFppy})_3$	1.06	-1.77	1600.00	<5
10 ^a	$[\text{Ir}(\text{dF}(\text{CF}_3)\text{ppy})_2(\text{dtbbpy})]\text{PF}_6$	1.45	-1.13	2300.00	10

Table 4.4. - NTC performance in the Giese-type reaction with proline and dimethyl maleate.

Reductive quenching: Acylation of ethyl crotonate

To expand the repertoire of reactions catalyzed by NTCs with respect to reductive quenching, we explored a synthetically valuable light-driven acylation reaction (Figure 4.18). The mechanism involves the oxidation of acyl silane **14** ($E_{\text{ox}}=1.46$ V vs SCE)³³ by PC^* , generating the reactive acyl radical **18** after silyl group cleavage. Trapping of **18** by methyl crotonate **15** and reduction of the formed radical **19** by the reduced form of the photocatalyst (PC^-), delivers the β -ketoester product **16**.

³³ Capaldo, L.; Riccardi, R.; Ravelli, D.; Fagnoni, M. Acyl Radicals from Acylsilanes: Photoredox-Catalyzed Synthesis of Unsymmetrical Ketones. *ACS Catal.* **2018**, *8*, 304–309.



— Acylation reaction, reactivity & mechanism

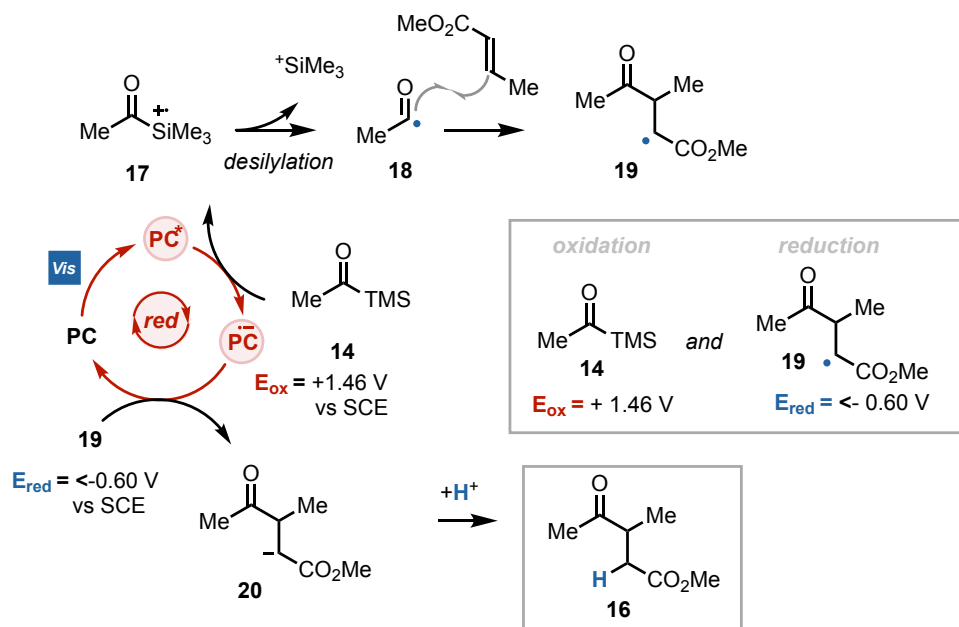
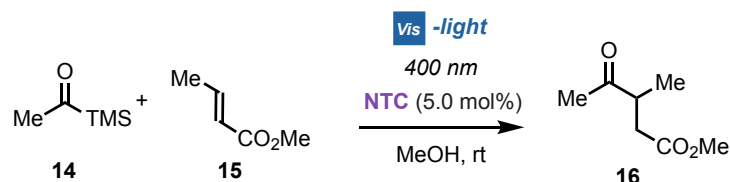


Figure 4.18. - Acylation reaction as example of challenging reductive quenching process.



entry	PC	$^*E_{red}$ (V vs SCE)	E_{red} (V vs SCE)	τ (ns)	1H NMR yield
1	NTC1	1.28	-1.74	1.44	69
2	NTC2	1.47	-1.68	2.07	70
3	NTC5	1.55	-1.55	0.81	66
4	NTC6	1.21	-1.76	7.78	28
5	NTC11	1.43	-1.65	4.21	88
6	NTC12	1.53	-1.59	2.49	43
7 ^a	TBADT @ 310 nm	2.44	-0.97	51.5	60

^a As reported in reference 33

Table 4.5. - NTC performance in the acylation reaction with acyl silanes and methyl crotonate.

The reaction has significant thermodynamic restrictions, it requires an excited-state PC reduction potential $>+ 1.46$ V vs SCE and a ground-state reduction potential of <-0.6 V vs SCE.^{32,33} Remarkably, different NTCs performed well (Table 4.5), with **NTC11** ($*E_{\text{ox}} = 1.56$ V vs SCE and $E_{\text{red}} = -1.45$ V vs SCE) delivering the product in 85 % yield. Metal-based and acridinium PCs were completely unproductive (entries 7–10). Previous to this method, only tetrabutylammonium decatungstate (TBADT= $(n\text{Bu}_4\text{N})_4[\text{W}_{10}\text{O}_{32}]$) was used with this purpose under deep-UV irradiation (310 nm; 60 % yield).³³

Oxidative quenching: Benzylhalide dehalogenation

To further evaluate the generality of the NTCs in mechanistically reversed photochemical methods, we assessed them under oxidative quenching processes, and selected diverse benzyl halides **21** (Figure 4.19).

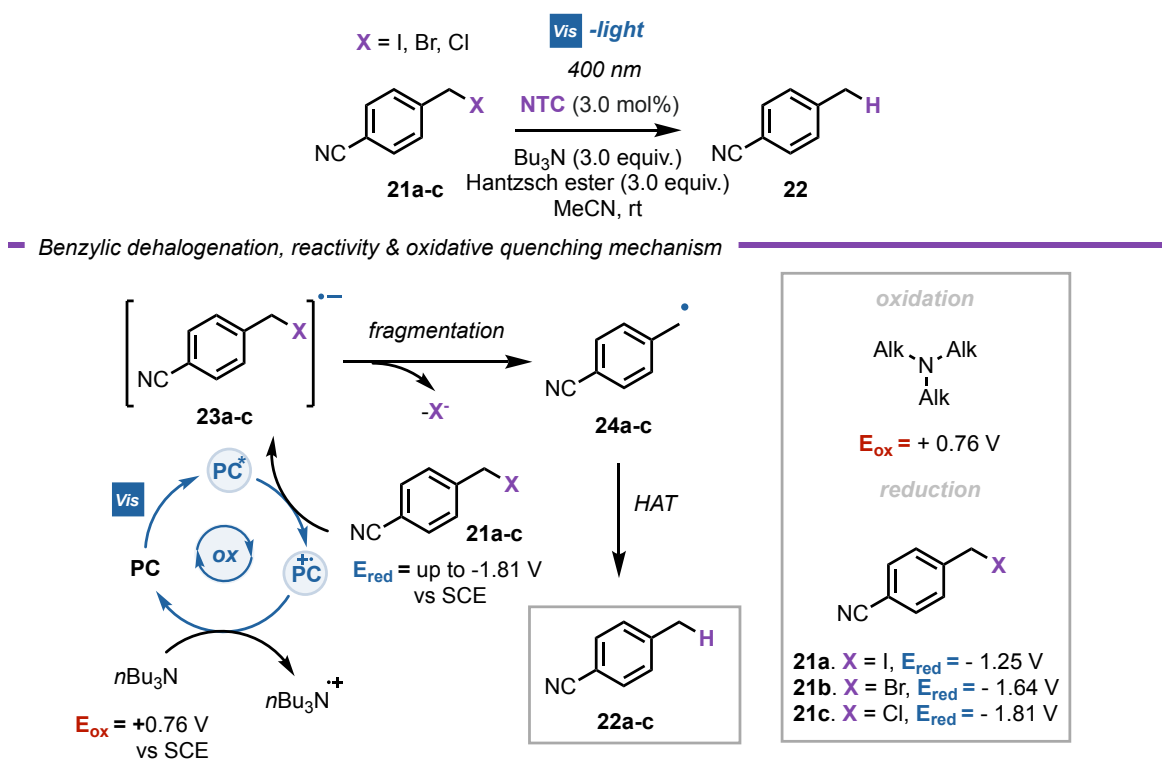


Figure 4.19. - Benzylic dehalogenation reaction as example of challenging oxidative quenching process.

Following previous reports on dehalogenation reactions,³⁴ we assumed the reaction to proceed through a single-electron reduction of **21** by **PC***.³⁵

³⁴ Nguyen, J. D.; D'Amato, E. M.; Narayanam, J. M. R.; Stephenson, C. R. J. *Engaging Unactivated Alkyl, Alkenyl and Aryl Iodides in Visible-Light-Mediated Free Radical Reactions*. *Nature Chem* **2012**, *4*, 854–859.

³⁵ Stern–Volmer experiments indicate that **NTC1** is quenched by both the benzyl halide and the amine. The ambivalent oxidative and reductive powers of the developed PCs **NTC1** allow both reductive and oxidative quenching cycles to be operative with definite advantages for the overall reactivity of the system.

The use of **NTC1** with a 400 nm irradiation source, furnished the reduction product of benzyl iodide **21a** ($E_{\text{red}} = -1.25$ V vs. SCE) and benzyl bromide **21b** ($E_{\text{red}} = -1.64$ V vs. SCE) in 87 % and 82 % yield, respectively (Table 4.6, entries 1 and 2).



entry	X	PC	* E_{ox} (V vs SCE)	E_{ox} (V vs SCE)	τ (ns)	GC-FID yield
1	I	NTC1	-1.27	1.75	1.44	87
2	Br	NTC1	-1.27	1.75	1.44	82
3	Br	NTC5	-1.34	1.86	0.81	9
4	Br	NTC6	-1.50	1.47	7.78	68
5	Br	NTC11	-1.64	1.44	4.21	62
6	Br	NTC12	-1.77	1.35	2.49	46
7	Cl	NTC1	-1.27	1.75	1.44	15
8	Cl	NTC6	-1.50	1.47	7.78	48
9	Cl	NTC11	-1.64	1.44	4.21	54
10	Cl	NTC12	-1.77	1.35	2.49	48
11	Cl	Ru(bpy) ₃ Cl ₂	-0.81	1.29	1100.00	-
12	Cl	<i>fac</i> -Ir(ppy) ₃	-1.49	1.01	1900.00	<5
13	Cl	<i>fac</i> -Ir(dFppy) ₃	-1.24	1.52	1600.00	19

Table 4.6. - NTC performance in the benzylic dehalogenation reaction.

As expected (considering an oxidative quenching cycle), the less reductive **NTC5** gave much inferior results while the more reducing **NTC6** and **NTC12** performed well, delivering **22** in 68 % and 62 % yield, respectively (entries 4 and 5). We next examined benzyl chloride **21b** ($E_{\text{red}} = -1.81$ V vs. SCE). Importantly, benzyl chlorides are generally inexpensive and readily available starting materials but their use in photocatalysis is often restricted by their difficult single-electron reduction. Notably, when the reaction was performed in the presence of **NTC1**, product **22** was formed in a poor 15 % yield. This prompted us to screen other PCs

³⁵ Nevertheless, this process became controversial in the recent years. A report from Juliá, Leonori and co-workers, suggests that the dehalogenation of this type of substrates proceed through an halogen atom transfer (XAT) mechanism derived from the excess of alkyl amine used in the reaction. (1)

Constantin, T.; Zanini, M.; Regni, A.; Sheikh, N. S.; Juliá, F.; Leonori, D. *Aminoalkyl Radicals as Halogen-Atom Transfer Agents for Activation of Alkyl and Aryl Halides*. *Science* **2020**, *367*, 1021–1026.

in this unprecedented process. The most reducing PCs **NTC6**, **NTC11**, and **NTC12** gave promising results, with yields of 47 %, 51 %, and 45 %, respectively (entries 8–10).

Oxidative quenching: Dehalogenation of arylhalides

Prompted by the results obtained for the reduction of benzylic chlorides, we next examined an additional oxidative quenching-based reaction: the deiodination of arenes (Figure 4.20). With methyl 4-iodobenzoate (**25**; $E_{\text{red}} = -1.96$ V vs SCE), we further challenged the reductive excited-state potential of NTCs.

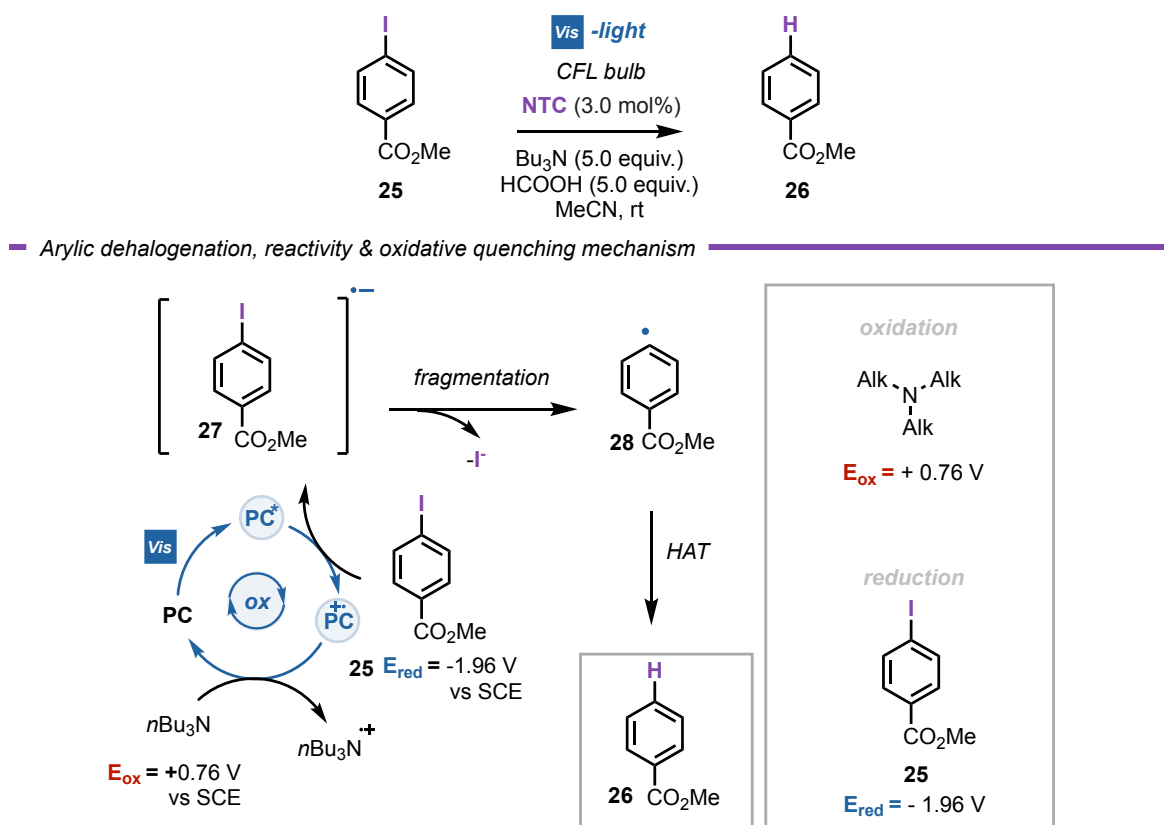
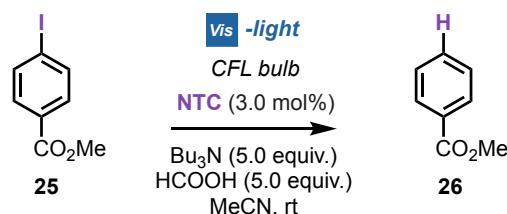


Figure 4.20. - Arylic dehalogenation reaction as example of challenging oxidative quenching process.

Interestingly, **NTC1** performed well, delivering **26** in 83 % yield (Table 4.7, entry 1). Less reducing PCs, such as **NTC5**, gave **26** in poor yields (entry 2). On the contrary, the highly reducing PC **NTC6** and **NTC12** produced **26** in 81 % and 93 % yield, respectively (entries 3 and 4), outperforming more expensive metal complexes (entries 5 and 6). It should be noted that this type of reactions can be catalyzed only by precious-metal Ir complexes³⁴

unbalanced phenothiazine PCs absorbing in the UV-light region,³⁶ or through reductive chain propagations.³⁷ Thanks to their ambivalent oxidative/reductive nature, NTC photocatalysts represent a new convenient option also towards the development of light-driven reductive processes.³⁸



entry	PC	*E _{ox} (V vs SCE)	E _{ox} (V vs SCE)	τ (ns)	GC-FID yield
1	NTC1	-1.27	1.75	1.44	86
2	NTC5	-1.34	1.86	0.81	13
3	NTC6	-1.50	1.47	7.78	81
4	NTC12	-1.77	1.35	2.49	96
5	Ru(bpy) ₃ Cl ₂	-0.81	1.29	1100.00	<5
6 ^a	fac-Ir(ppy) ₃	-1.49	1.01	1900.00	92

^a As reported in reference 32

Table 4.7. - NTC performance in the aryl dehalogenation reaction with methyl iodobenzoate.

Limitations

NTCs revealed a high synthetic potential. Furthermore, they are cheap, easy to prepare and versatile PCs. Additionally, structure-*property* relationships were easily assessed by measuring the most useful properties and the rationalization with frontier orbitals analysis. However, the assignment of single-variable structure-*activity* relationships remained an unsolved puzzle. For this reason, further investigations using the collected data in combination with computable parameters as well as modern techniques, such as artificial intelligence²⁰ or multivariate analysis³⁹ is an ongoing work. This approach could improve the activity of such class of catalysts as well as other well-known families of catalysts.

³⁶ Discekici, E. H.; Treat, N. J.; Poelma, S. O.; Mattson, K. M.; Hudson, Z. M.; Luo, Y.; Hawker, C. J.; de Alaniz, J. R. *A Highly Reducing Metal-Free Photoredox Catalyst: Design and Application in Radical Dehalogenations*. *Chem. Commun.* **2015**, 51, 11705–11708.

³⁷ Constantin, T.; Juliá, F.; Sheikh, N. S.; Leonori, D. *A Case of Chain Propagation: α-Aminoalkyl Radicals as Initiators for Aryl Radical Chemistry*. *Chem. Sci.* **2020**, 11, 12822–12828.

³⁸ Ghosh, I.; Ghosh, T.; Bardagi, J. I.; König, B. *Reduction of Aryl Halides by Consecutive Visible Light-Induced Electron Transfer Processes*. *Science* **2014**, 346, 725–728.

³⁹ Santiago, C. B.; Guo, J.-Y.; Sigman, M. S. *Predictive and Mechanistic Multivariate Linear Regression Models for Reaction Development*. *Chem. Sci.* **2018**, 9, 2398–2412.

4.1.5 Conclusions

In conclusion, we identified naphthochromenones as a new class of versatile organic PCs with wide redox windows (up to 3.22 eV) and superior excited-state potentials ranging from -1.77 V to 1.65 V vs SCE. Because of this unique feature, both thermodynamically demanding oxidative and reductive light-driven transformations can be catalyzed by these compounds. The elucidated structure–property relationships were supported by DFT calculations. Finally, the synthetic potential of the NTCs was confirmed in five diverse photoreactions, characterized by strong and opposite thermodynamic requirements (from $E_{\text{ox}}=1.46$ V to $E_{\text{red}}=-1.96$ V vs SCE), thus covering a vast application spectrum. Interestingly, NTCs outperformed diverse well-established PCs, including eosin Y, acridinium salts, and Ru and Ir complexes, while efficiently catalyzing unprecedented Povarov-type reactions with electron-deficient dimethylanilines and the photo-dehalogenation of benzyl chlorides. The merging of a large redox window with the ambivalent oxidative/reductive nature enables NTC photocatalysts to unlock previously inaccessible light-driven reactivity.

4.1.6 Experimental Section

The NMR spectra were recorded on Bruker 400 Avance III HD equipped with a BBI-z grad probe head 5mm and Bruker 500 Avance III equipped with a BBI-ATM-z grad probehead 5mm. The chemical shifts (δ) for ^1H and ^{13}C are given in ppm relative to residual signals of the solvents (CHCl_3 @ 7.26 ppm ^1H NMR, 77.16 ppm ^{13}C NMR). Coupling constants are given in Hz. The following abbreviations are used to indicate the multiplicity: s, singlet; d, doublet; t, triplet; q, quartet; m, multiplet; bs, broad signal. NMR yields were calculated by using trichloroethylene as internal standard.

The ^1H , ^{13}C and ^{19}F NMR spectra are available in literature free of charge.¹⁰

High-Resolution Mass Spectra (HRMS) were obtained using Waters GCT gas chromatograph coupled with a time-of-flight mass spectrometer (GC/MS-TOF) with electron ionization (EI).

Chromatographic purification of products was accomplished using flash chromatography on silica gel (SiO_2 , 0.04-0.063 mm) purchased from Machery-Nagel, with the indicated solvent system according to the standard techniques. Thin-layer chromatography (TLC) analysis was performed on pre-coated Merck TLC plates (silica gel 60 GF254, 0.25 mm). Visualization of the developed chromatography was performed by checking UV absorbance (254nm) as well as with aqueous ceric ammonium molybdate and potassium permanganate solutions. Organic solutions were concentrated under reduced pressure on a Büchi rotary evaporator.

All calculations were performed using Gaussian 16 software package; structures were optimized at the B3LYP/6-311+g(d,p) level of theory including a polarizable continuum model (PCM) of water solvent. 50 states were then included in the TD-DFT to calculate absorption properties.

Steady-state absorption spectroscopy studies have been performed at room temperature on a Varian Cary 1000 UV-Vis double beam spectrophotometer; 10 mm path length Hellma Analytics 100 QS quartz cuvettes have been used.

Steady-state fluorescence spectra have been recorded on a Varian Cary Eclipse Fluorescence spectrophotometer; 10 mm path length Hellma Analytics 117.100F QS quartz cuvettes have been used.

The electrochemical characterizations were carried out in acetonitrile and 0.1 M tetrabutylammonium hexafluorophosphate (TBAPF_6) at room temperature, on an Autolab 302N electrochemical workstation (Metrohm, The Netherlands) in a glass cell. A typical three-electrode cell was employed, which was composed of glassy carbon working electrode (3 mm diameter), a platinum wire as counter electrode and a saturated calomel electrode (SCE) as reference electrode. Oxygen was removed by purging the MeCN solution with high-purity nitrogen. The potential of ferrocenium/ferrocene (Fc/Fc^+) couple was measured and

found to be 0.45 V vs SCE, in agreement with the value reported in literature (in MeCN).⁴⁰ The GC electrode was polished before any measurement with diamond paste and ultrasonically rinsed with deionized water for 15 minutes. The electrode was electrochemically activated in the background solution by means of several voltammetric cycles at 100 mV/s between the anodic and cathodic solvent/electrolyte discharges.

The quantum yield measurements were performed with quinine sulphate in 0.10 M H₂SO₄ (literature quantum yield 0.54 at 360 nm) as the standard. The fluorescence quantum yields were calculated according to equation:

$$\Phi_x = \Phi_{st} \cdot \frac{I_x}{I_{st}} \cdot \frac{f_{st}}{f_x} \cdot \frac{\eta_x^2}{\eta_{st}^2}$$

I is the measured integrated fluorescence emission intensity, f is the absorption factor, η is the refractive index of the solvent and Φ is the quantum yield. I_x denotes the sample and the I_{st} denotes the standard.

The diverse reaction set up images, quantum yield measurements, triplet energies, photocatalysts lifetimes, Stern-Volmer analysis of all the reactions and molecular coordinates of the DFT calculations are available free of charge in literature.¹⁰

⁴⁰ Lewandowski, A.; Waligora, L.; Galinski, M. Ferrocene as a Reference Redox Couple for Aprotic Ionic Liquids. *Electroanalysis* **2009**, *21*, 2221–2227.

Light sources emission spectra

The following spectra were recorded using an AvaSpec ULS3648 high-resolution fiber-optic spectrometer which was placed at a fixed distance of 0.5 cm from the light source.

(more info at: <https://www.avantes.com/products/spectrometers/starline/item/209-avaspec-uls3648-high-resolution-spectrometer>).

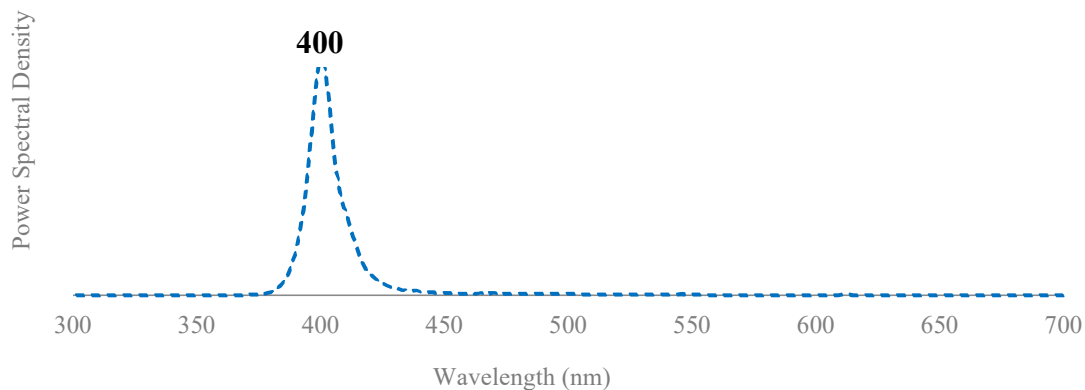


Figure 4.21. - Emission spectra of the 400 nm LED strips used in this section.

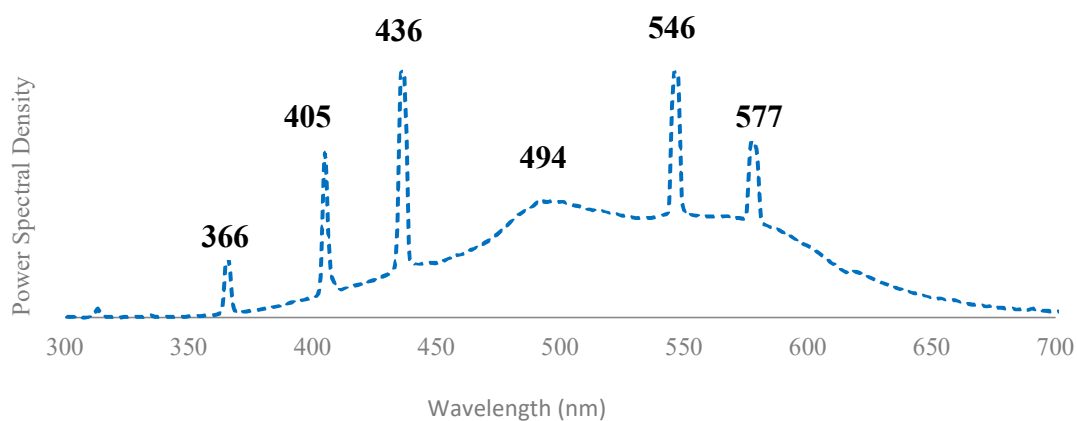
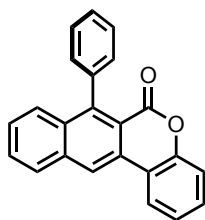


Figure 4.22. - Emission spectra of the 40W CFL bulbs used in this study.

Photophysical characterization of the naphthochromenones

NTC1



$$E_{1/2}(PC^{\bullet+}/PC^*) = -1.54 \text{ V vs SCE}$$

$$E_{1/2}(PC^*/PC^{\bullet-}) = 1.55 \text{ V vs SCE}$$

$$E_{1/2}(PC^{\bullet+}/PC) = 1.75 \text{ V vs SCE}$$

$$E_{1/2}(PC/PC^{\bullet-}) = -1.74 \text{ V vs SCE}$$

Redox potentials

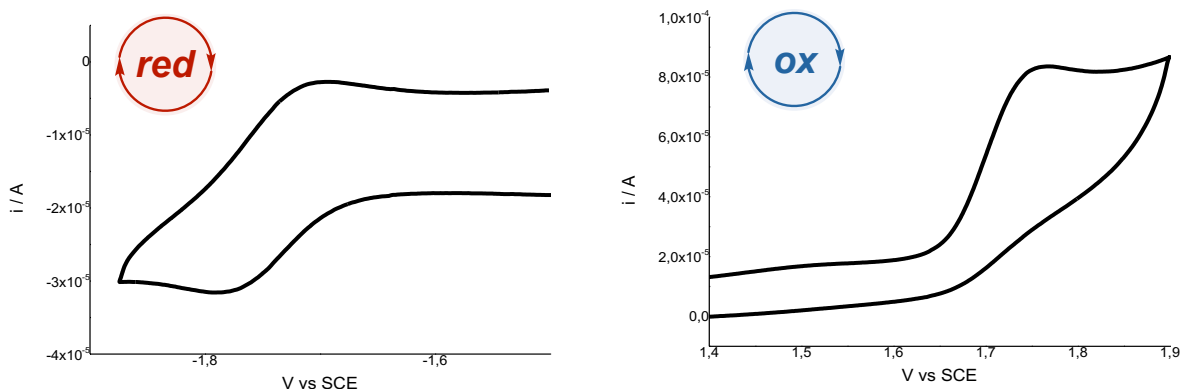


Figure 4.23. - **Left:** Anodic, **Right:** Cathodic CV of NTC1 in 0.1 TBAPF₆ MeCN solution. GCelectrode.

Scan rate: 100 mV/s, potential referred to SCE at room temperature using a platinum wire as counter electrode.

Absorption/Emission

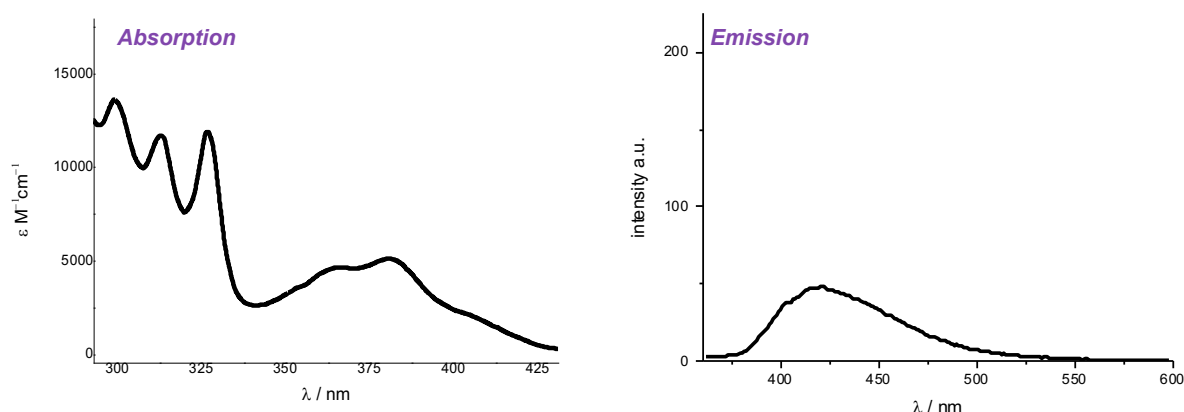
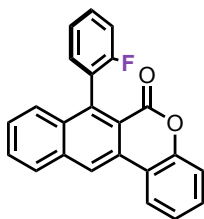


Figure 4.24. - **Left:** Extinction coefficient (ϵ) of NTC1 estimated from 3 spectra at different concentrations in MeCN.

Right: Emission spectrum of NTC1 in MeCN. ($\lambda_{\text{ex}}=350 \text{ nm}$).

NTC2



$$E_{1/2}(PC^{\bullet+}/PC^*) = -1.49 \text{ V vs SCE}$$

$$E_{1/2}(PC^*/PC^{\bullet-}) = 1.62 \text{ V vs SCE}$$

$$E_{1/2}(PC^{\bullet+}/PC) = 1.81 \text{ V vs SCE}$$

$$E_{1/2}(PC/PC^{\bullet-}) = -1.68 \text{ V vs SCE}$$

Redox potentials

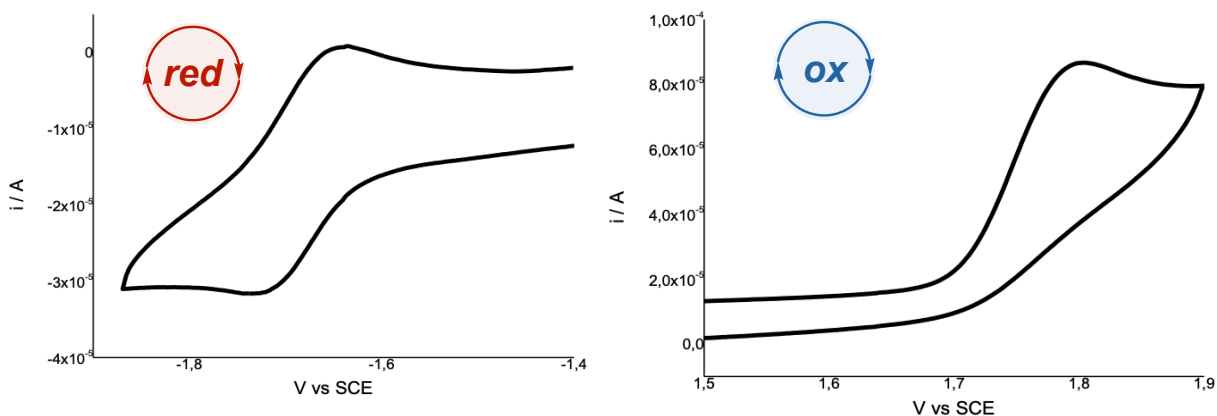


Figure 4.25. - **Left:** Anodic, **Right:** Cathodic CV of NTC2 in 0.1 TBAPF₆ MeCN solution. GCelectrode.

Scan rate: 100 mV/s, potential referred to SCE at room temperature using a platinum wire as counter electrode.

Absorption/Emission

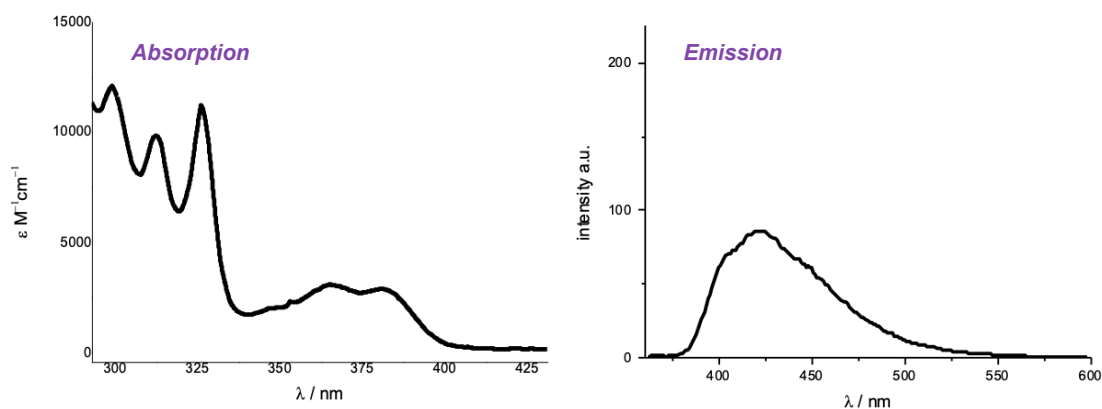
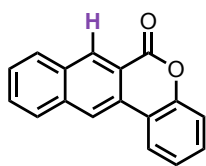


Figure 4.26. - **Left:** Extinction coefficient (ϵ) of NTC2 estimated from 3 spectra at different concentrations in MeCN.

Right: Emission spectrum of NTC2 in MeCN. ($\lambda_{\text{ex}}=350 \text{ nm}$).

NTC3



$$E_{1/2}(PC^{\bullet+}/PC^*) = -1.55 \text{ V vs SCE}$$

$$E_{1/2}(PC^*/PC^{\bullet-}) = 1.68 \text{ V vs SCE}$$

$$E_{1/2}(PC^{\bullet+}/PC) = 1.80 \text{ V vs SCE}$$

$$E_{1/2}(PC/PC^{\bullet-}) = -1.67 \text{ V vs SCE}$$

Redox potentials

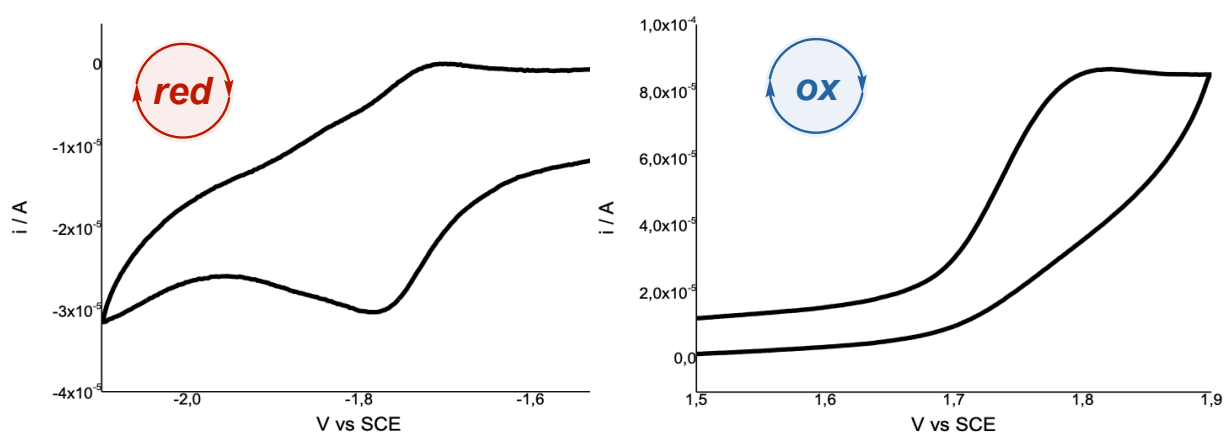


Figure 4.27. - **Left:** Anodic, **Right:** Cathodic CV of NTC3 in 0.1 TBAPF₆ MeCN solution. GCelectrode.

Scan rate: 100 mV/s, potential referred to SCE at room temperature using a platinum wire as counter electrode.

Absorption/Emission

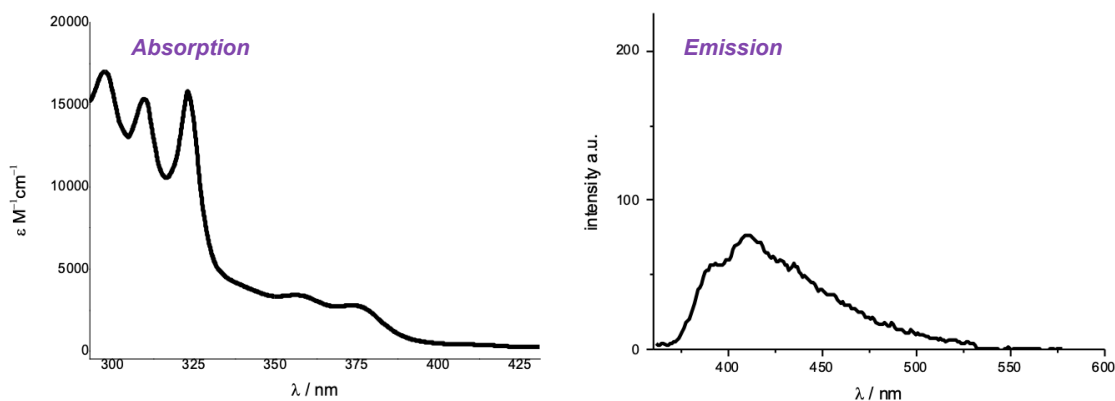
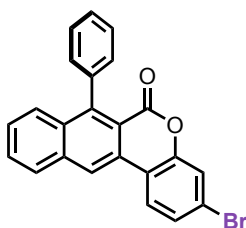


Figure 4.28. - **Left:** Extinction coefficient (ϵ) of NTC3 estimated from 3 spectra at different concentrations in MeCN.

Right: Emission spectrum of NTC3 in MeCN. ($\lambda_{\text{ex}}=350 \text{ nm}$).

NTC4



$$E_{1/2}(PC^{\bullet+}/PC^*) = -1.48 \text{ V vs SCE}$$

$$E_{1/2}(PC^*/PC^{\bullet-}) = 1.65 \text{ V vs SCE}$$

$$E_{1/2}(PC^{\bullet+}/PC) = 1.78 \text{ V vs SCE}$$

$$E_{1/2}(PC/PC^{\bullet-}) = -1.61 \text{ V vs SCE}$$

Redox potentials

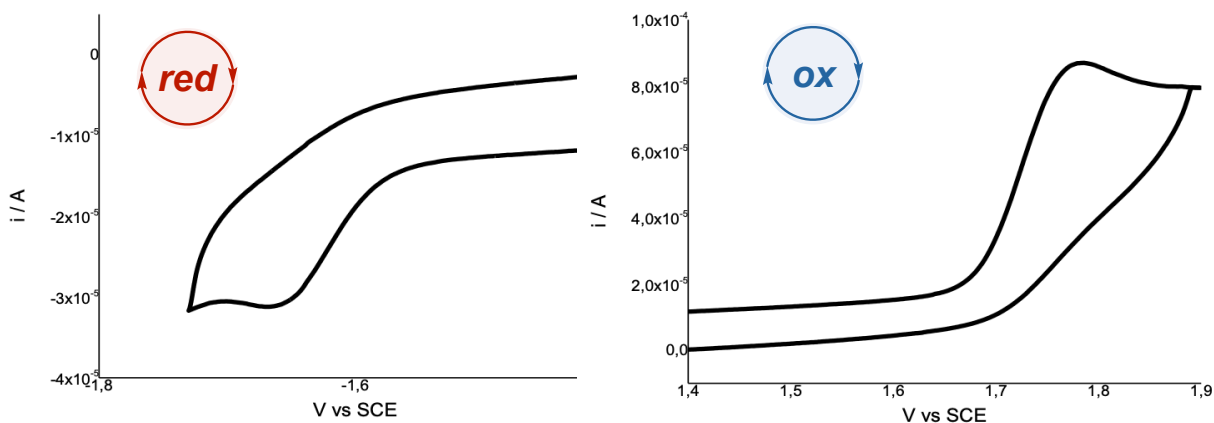


Figure 4.29. - Left: Anodic, Right: Cathodic CV of NTC4 in 0.1 TBAPF₆ MeCN solution. GCelectrode.

Scan rate: 100 mV/s, potential referred to SCE at room temperature using a platinum wire as counter electrode.

Absorption/Emission

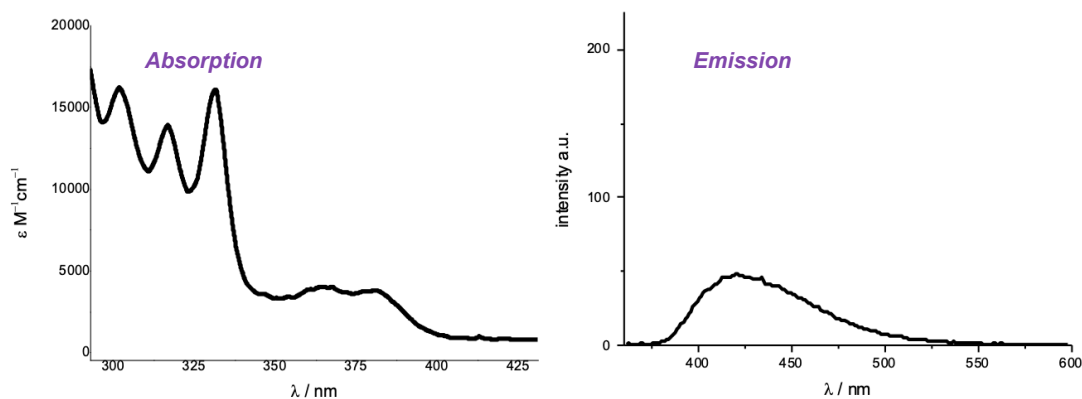
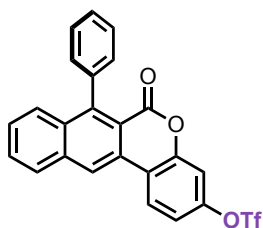


Figure 4.30. - Left: Extinction coefficient (ϵ) of NTC4 estimated from 3 spectra at different concentrations in MeCN.

Right: Emission spectrum of NTC4 in MeCN. ($\lambda_{ex}=350 \text{ nm}$).

NTC5



$$E_{1/2}(PC^{\bullet+}/PC^*) = -1.43 \text{ V vs SCE}$$

$$E_{1/2}(PC^*/PC^{\bullet-}) = 1.74 \text{ V vs SCE}$$

$$E_{1/2}(PC^{\bullet+}/PC) = 1.86 \text{ V vs SCE}$$

$$E_{1/2}(PC/PC^{\bullet-}) = -1.55 \text{ V vs SCE}$$

Redox potentials

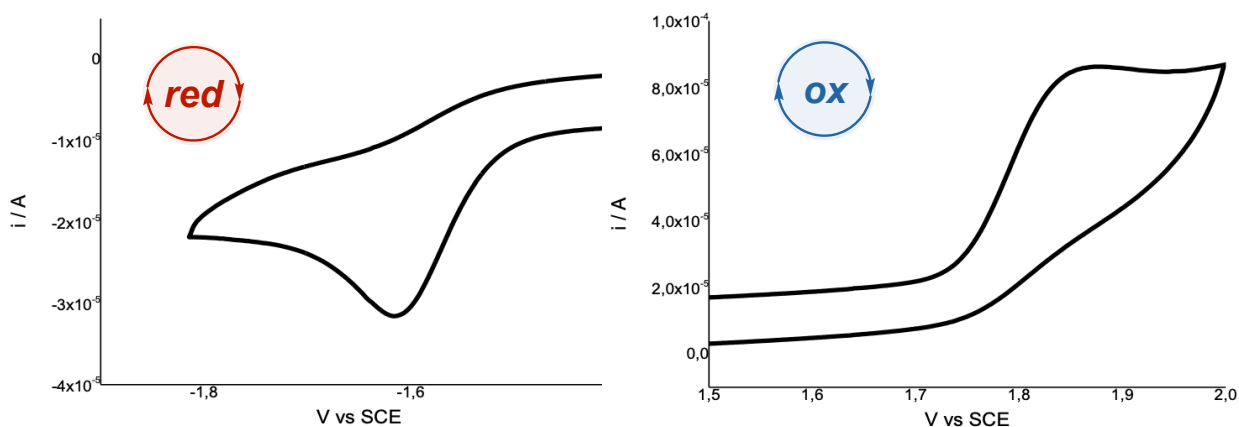


Figure 4.31. - Left: Anodic, Right: Cathodic CV of NTC5 in 0.1 TBAPF₆ MeCN solution. GCelectrode.

Scan rate: 100 mV/s, potential referred to SCE at room temperature using a platinum wire as counter electrode.

Absorption/Emission

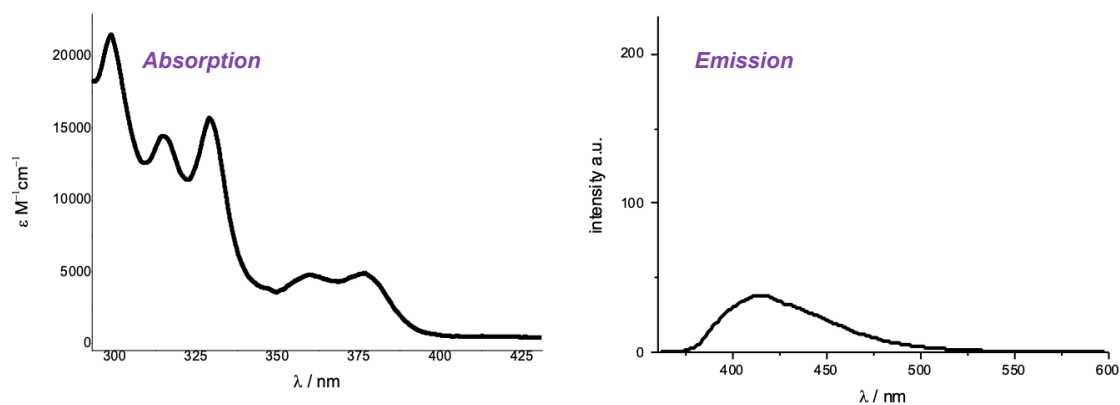
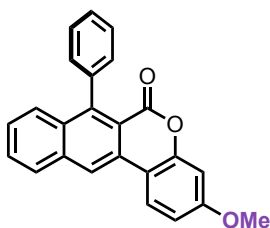


Figure 4.32. - Left: Extinction coefficient (ϵ) of NTC5 estimated from 3 spectra at different concentrations in MeCN.

Right: Emission spectrum of NTC5 in MeCN. ($\lambda_{\text{ex}}=350 \text{ nm}$).

NTC6



$$E_{1/2}(PC^{\bullet+}/PC^*) = -1.60 \text{ V vs SCE}$$

$$E_{1/2}(PC^*/PC^{\bullet-}) = 1.31 \text{ V vs SCE}$$

$$E_{1/2}(PC^{\bullet+}/PC) = 1.47 \text{ V vs SCE}$$

$$E_{1/2}(PC/PC^{\bullet-}) = -1.76 \text{ V vs SCE}$$

Redox potentials

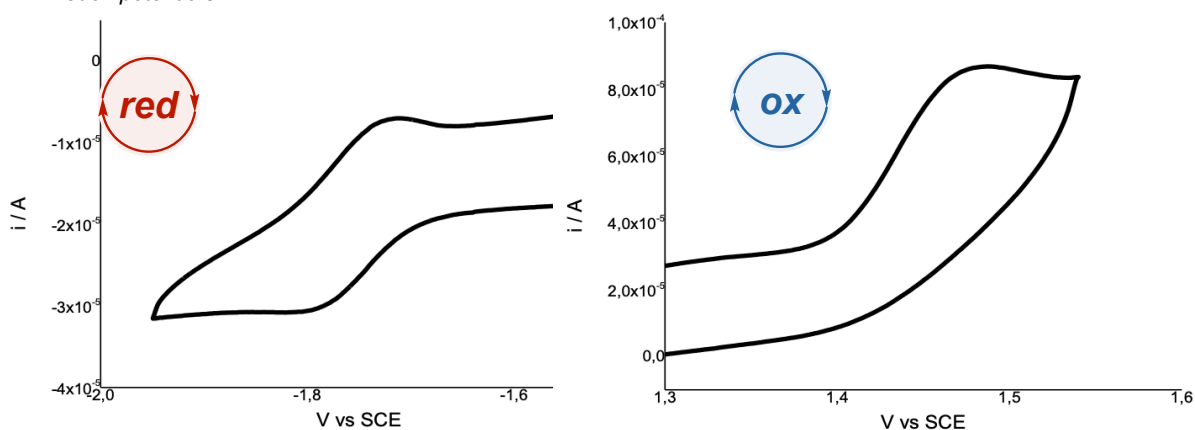


Figure 4.33. - **Left:** Anodic, **Right:** Cathodic CV of NTC6 in 0.1 TBAPF₆ MeCN solution. GCelectrode.

Scan rate: 100 mV/s, potential referred to SCE at room temperature using a platinum wire as counter electrode.

Absorption/Emission

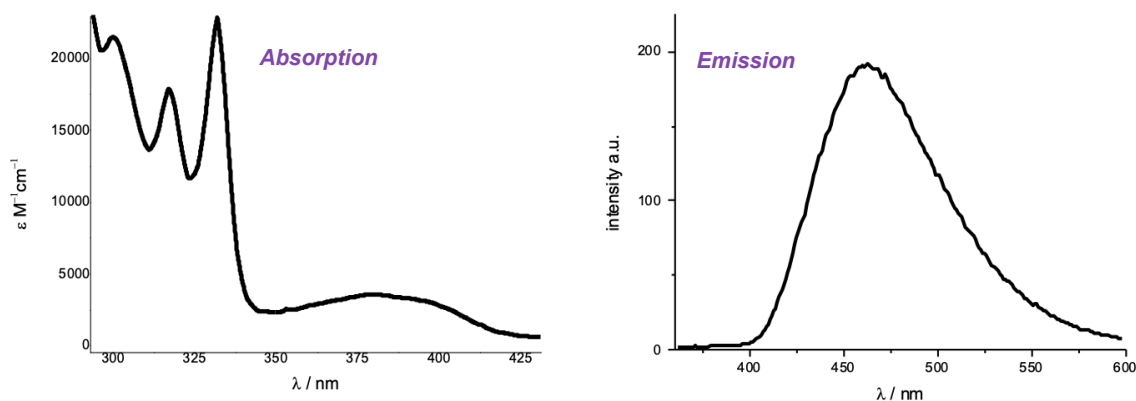
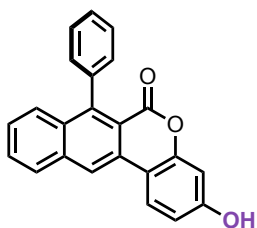


Figure 4.34. - **Left:** Extinction coefficient (ϵ) of NTC6 estimated from 3 spectra at different concentrations in MeCN.

Right: Emission spectrum of NTC6 in MeCN. ($\lambda_{\text{ex}}=350 \text{ nm}$).

NTC7



$$E_{1/2}(PC^{\bullet+}/PC^*) = -1.63 \text{ V vs SCE}$$

$$E_{1/2}(PC^*/PC^{\bullet-}) = 1.18 \text{ V vs SCE}$$

$$E_{1/2}(PC^{\bullet+}/PC) = 1.44 \text{ V vs SCE}$$

$$E_{1/2}(PC/PC^{\bullet-}) = -1.89 \text{ V vs SCE}$$

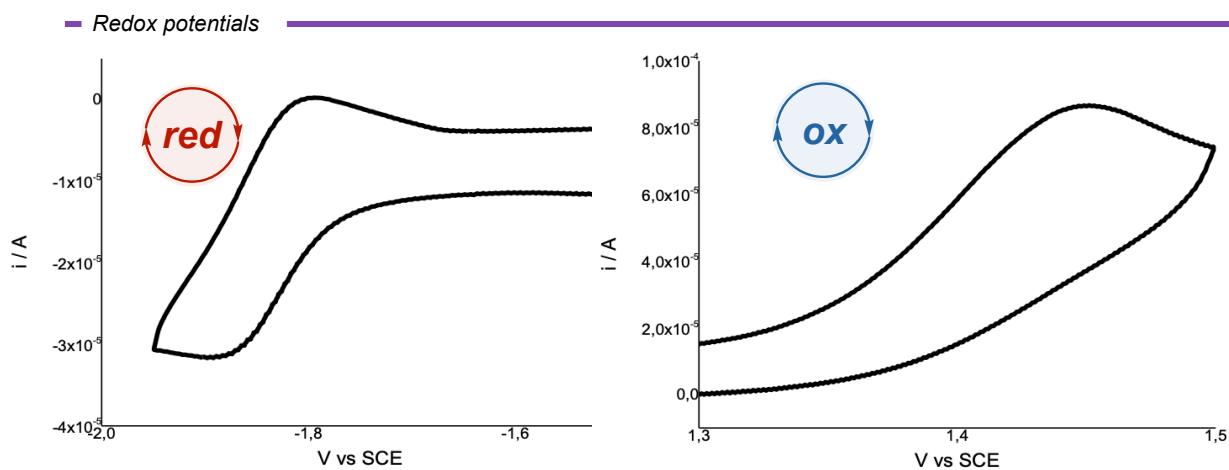


Figure 4.35. - Left: Anodic, Right: Cathodic CV of NTC7 in 0.1 TBAPF₆ MeCN solution. GCelectrode.

Scan rate: 100 mV/s, potential referred to SCE at room temperature using a platinum wire as counter electrode.

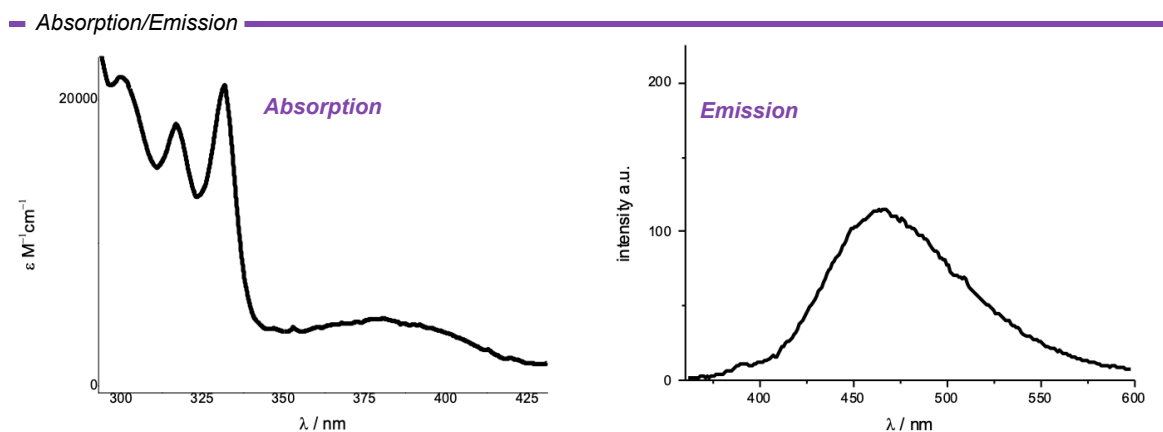
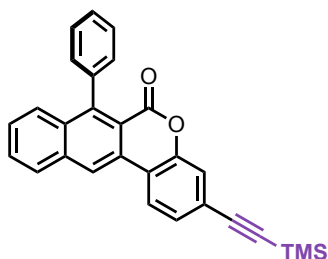


Figure 4.36. - Left: Extinction coefficient (ϵ) of NTC7 estimated from 3 spectra at different concentrations in MeCN.

Right: Emission spectrum of NTC7 in MeCN. ($\lambda_{\text{ex}}=350 \text{ nm}$).

NTC8



$$E_{1/2}(PC^{\bullet+}/PC^*) = -1.49 \text{ V vs SCE}$$

$$E_{1/2}(PC^*/PC^{\bullet-}) = 1.51 \text{ V vs SCE}$$

$$E_{1/2}(PC^{\bullet+}/PC) = 1.73 \text{ V vs SCE}$$

$$E_{1/2}(PC/PC^{\bullet-}) = -1.73 \text{ V vs SCE}$$

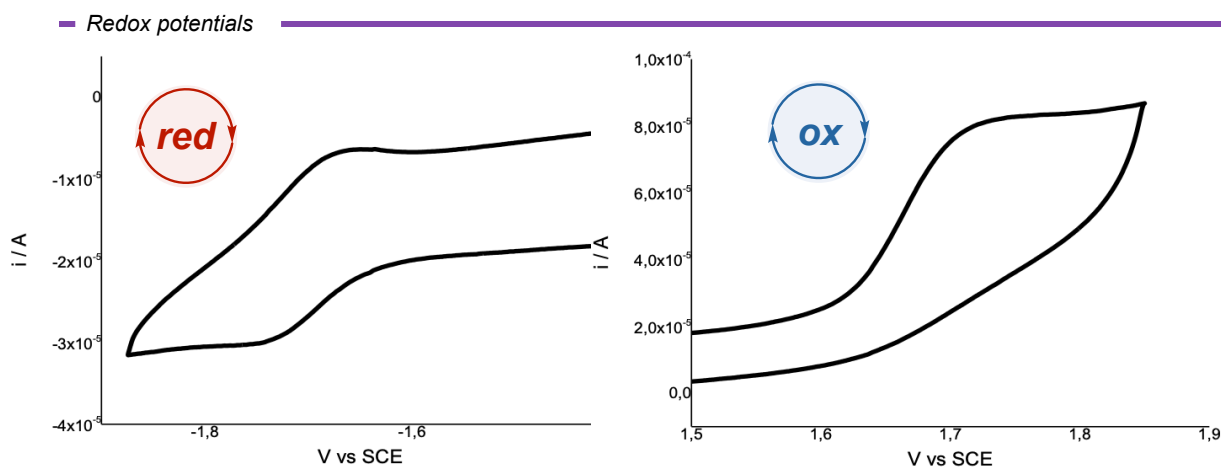


Figure 4.37. - **Left:** Anodic, **Right:** Cathodic CV of NTC8 in 0.1 TBAPF₆ MeCN solution. GCelectrode.

Scan rate: 100 mV/s, potential referred to SCE at room temperature using a platinum wire as counter electrode.

— Absorption/Emission

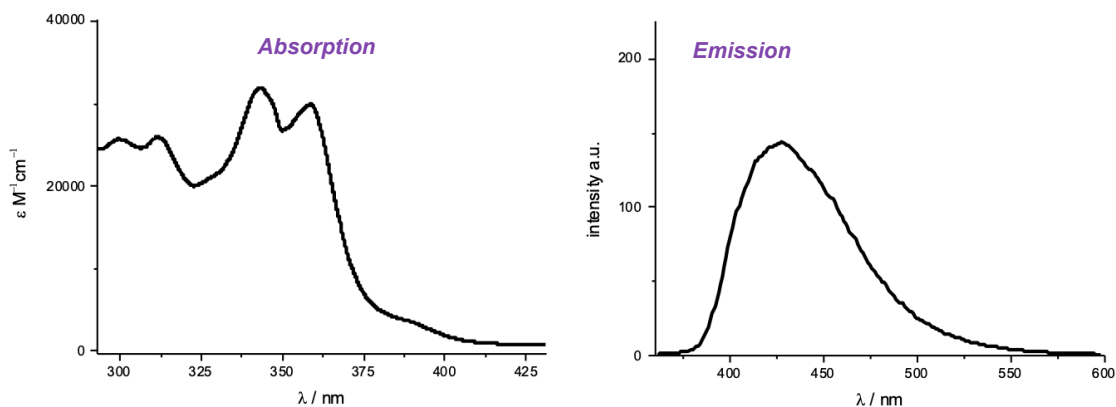
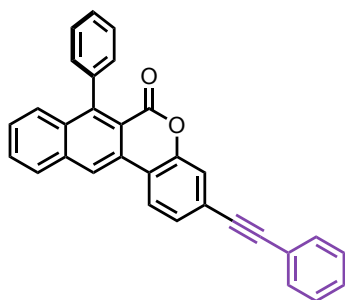


Figure 4.38. - **Left:** Extinction coefficient (ϵ) of NTC8 estimated from 3 spectra at different concentrations in MeCN.

Right: Emission spectrum of NTC8 in MeCN. ($\lambda_{\text{ex}}=350 \text{ nm}$).

NTC9



$$E_{1/2}(PC^{\bullet+}/PC^*) = -1.56 \text{ V vs SCE}$$

$$E_{1/2}(PC^*/PC^{\bullet-}) = 1.50 \text{ V vs SCE}$$

$$E_{1/2}(PC^{\bullet+}/PC) = 1.67 \text{ V vs SCE}$$

$$E_{1/2}(PC/PC^{\bullet-}) = -1.70 \text{ V vs SCE}$$

Redox potentials

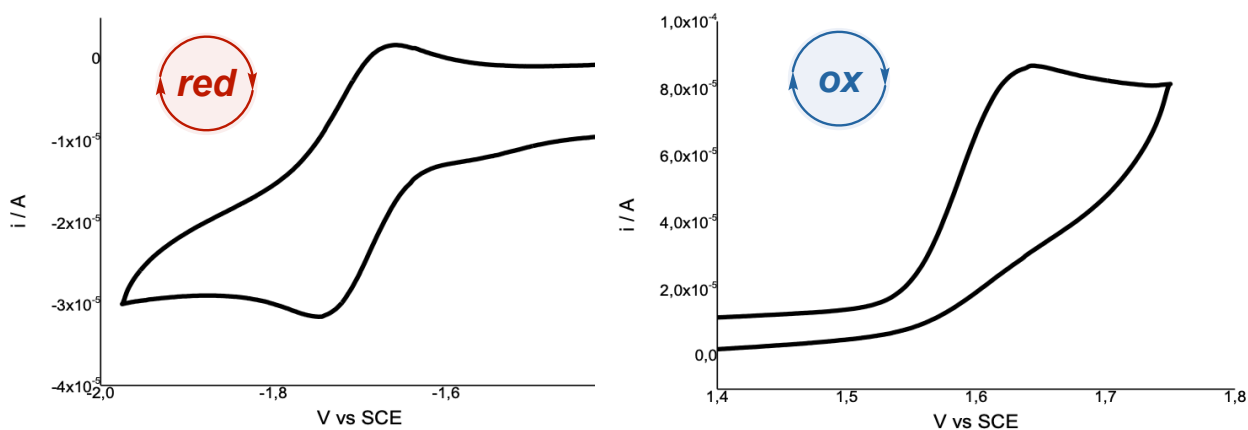


Figure 4.39. - Left: Anodic, Right: Cathodic CV of NTC9 in 0.1 TBAPF₆ MeCN solution. GCelectrode.

Scan rate: 100 mV/s, potential referred to SCE at room temperature using a platinum wire as counter electrode.

Absorption/Emission

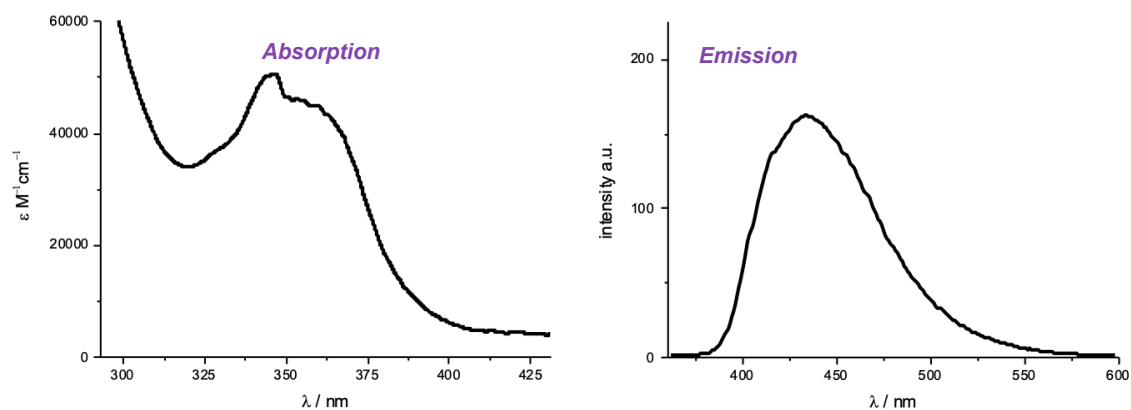
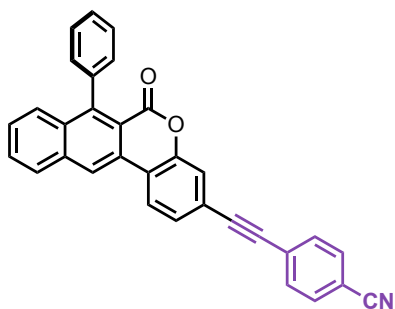


Figure 4.40. - Left: Extinction coefficient (ϵ) of NTC9 estimated from 3 spectra at different concentrations in MeCN.

Right: Emission spectrum of NTC9 in MeCN. ($\lambda_{\text{ex}}=350 \text{ nm}$).

NTC10



$$E_{1/2}(PC^{\bullet+}/PC^*) = -1.54 \text{ V vs SCE}$$

$$E_{1/2}(PC^*/PC^{\bullet-}) = 1.65 \text{ V vs SCE}$$

$$E_{1/2}(PC^{\bullet+}/PC) = 1.69 \text{ V vs SCE}$$

$$E_{1/2}(PC/PC^{\bullet-}) = -1.58 \text{ V vs SCE}$$

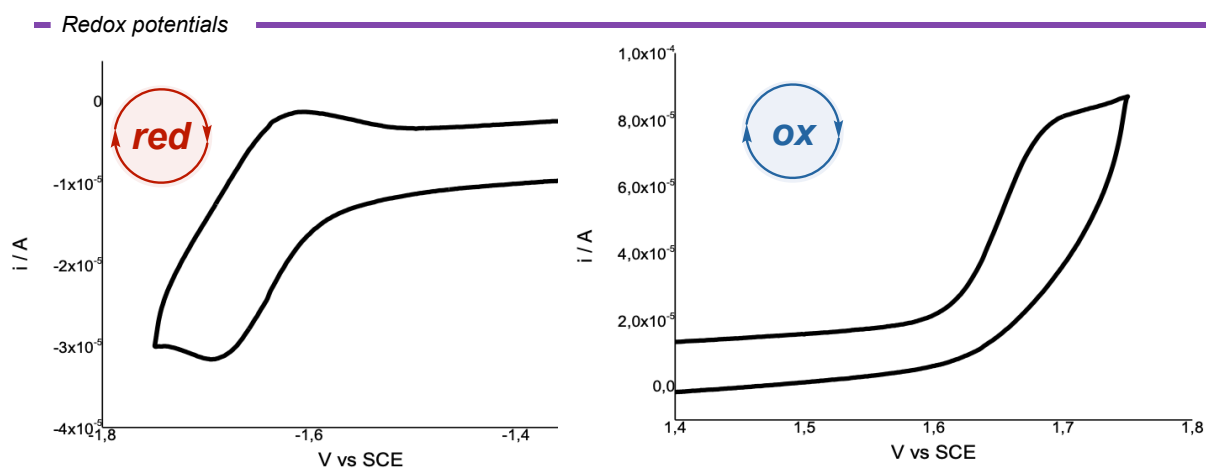


Figure 4.41. - **Left:** Anodic, **Right:** Cathodic CV of NTC10 in 0.1 TBAPF₆ MeCN solution. GCelectrode.

Scan rate: 100 mV/s, potential referred to SCE at room temperature using a platinum wire as counter electrode.

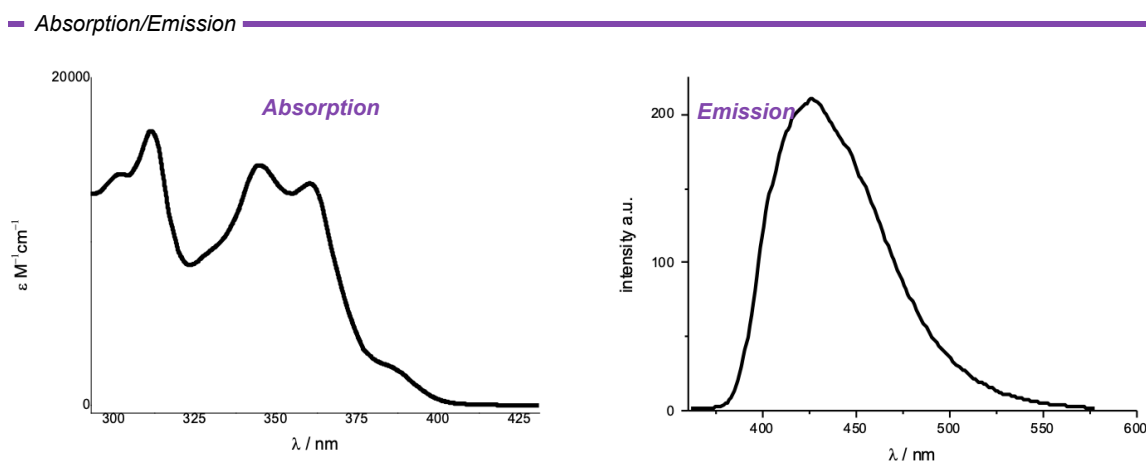
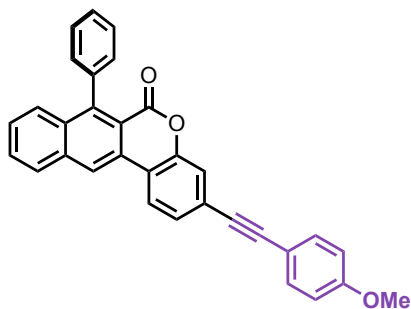


Figure 4.42. - **Left:** Extinction coefficient (ϵ) of NTC10 estimated from 3 spectra at different concentrations in MeCN.

Right: Emission spectrum of NTC10 in MeCN. ($\lambda_{\text{ex}}=350 \text{ nm}$).

NTC11



$$E_{1/2}(PC^{\bullet+}/PC^*) = -1.71 \text{ V vs SCE}$$

$$E_{1/2}(PC^*/PC^{\bullet-}) = 1.50 \text{ V vs SCE}$$

$$E_{1/2}(PC^{\bullet+}/PC) = 1.44 \text{ V vs SCE}$$

$$E_{1/2}(PC/PC^{\bullet-}) = -1.65 \text{ V vs SCE}$$

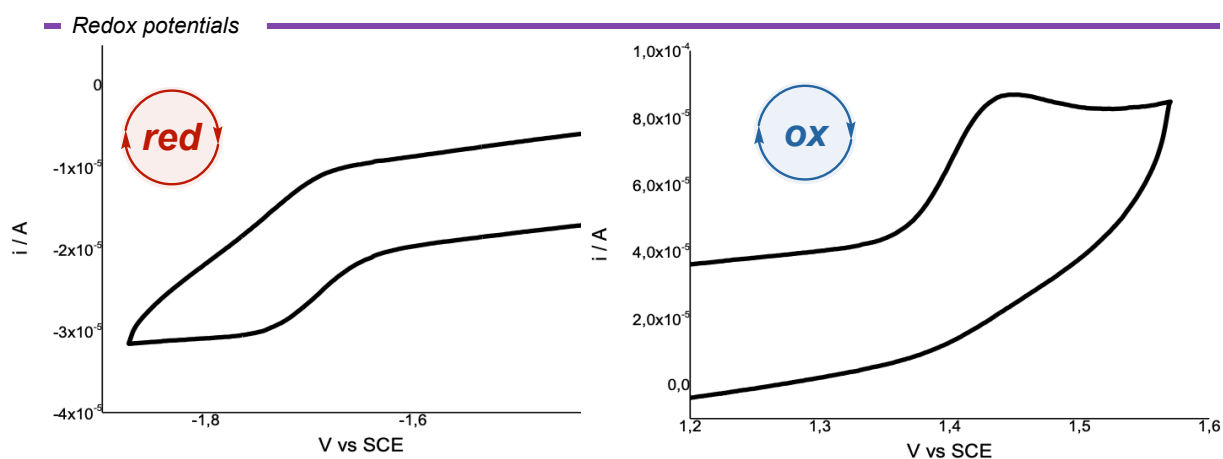


Figure 4.43. - **Left:** Anodic, **Right:** Cathodic CV of NTC11 in 0.1 TBAPF₆ MeCN solution. GC electrode.

Scan rate: 100 mV/s, potential referred to SCE at room temperature using a platinum wire as counter electrode.

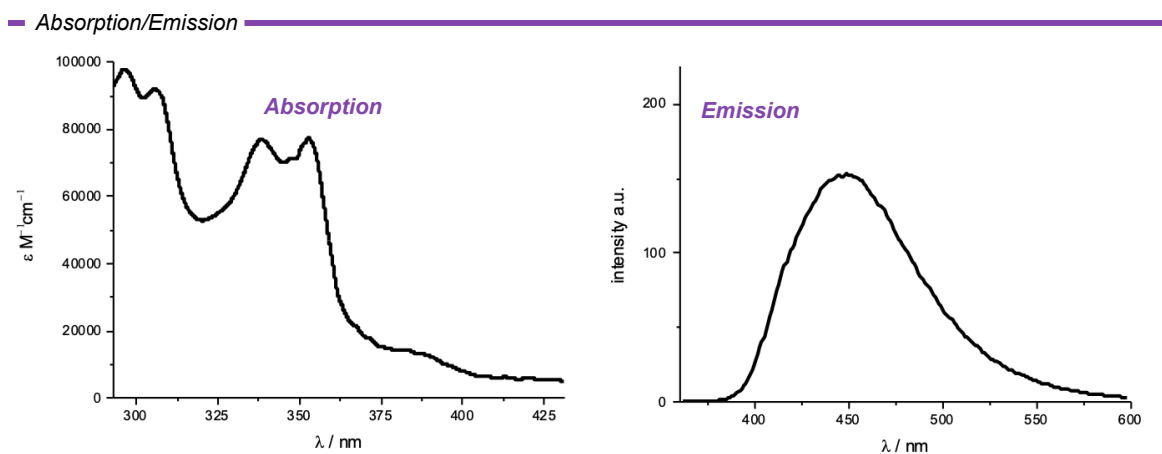
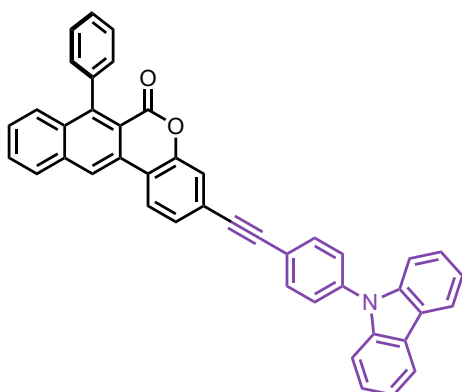


Figure 4.44. - **Left:** Extinction coefficient (ϵ) of NTC11 estimated from 3 spectra at different concentrations in MeCN.

Right: Emission spectrum of NTC11 in MeCN. ($\lambda_{\text{ex}}=350 \text{ nm}$).

NTC12



$$E_{1/2}(PC^{\bullet+}/PC^*) = -1.83 \text{ V vs SCE}$$

$$E_{1/2}(PC^*/PC^{\bullet-}) = 1.59 \text{ V vs SCE}$$

$$E_{1/2}(PC^{\bullet+}/PC) = 1.35 \text{ V vs SCE}$$

$$E_{1/2}(PC/PC^{\bullet-}) = -1.59 \text{ V vs SCE}$$

Redox potentials

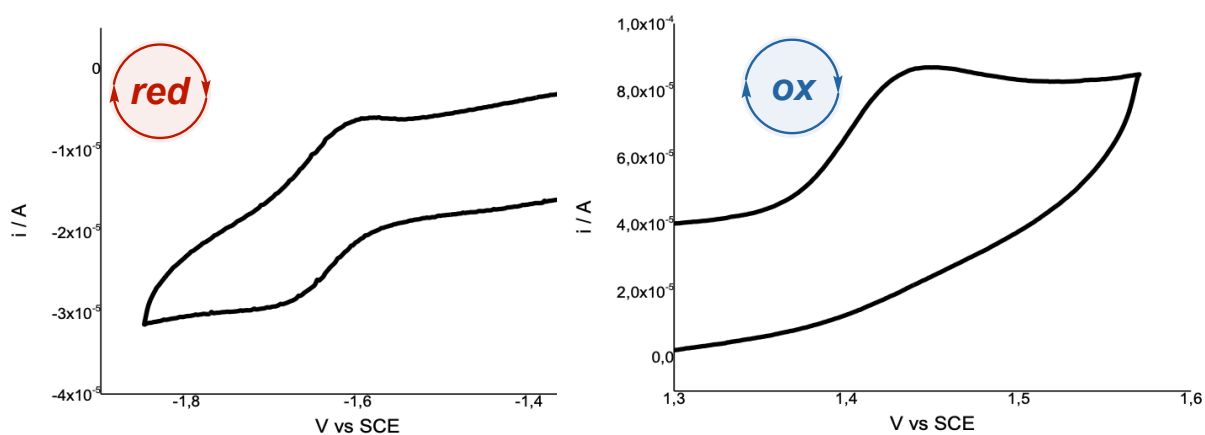


Figure 4.45. - Left: Anodic, Right: Cathodic CV of NTC12 in 0.1 TBAPF₆ MeCN solution. GCElectrode.

Scan rate: 100 mV/s, potential referred to SCE at room temperature using a platinum wire as counter electrode.

Absorption/Emission

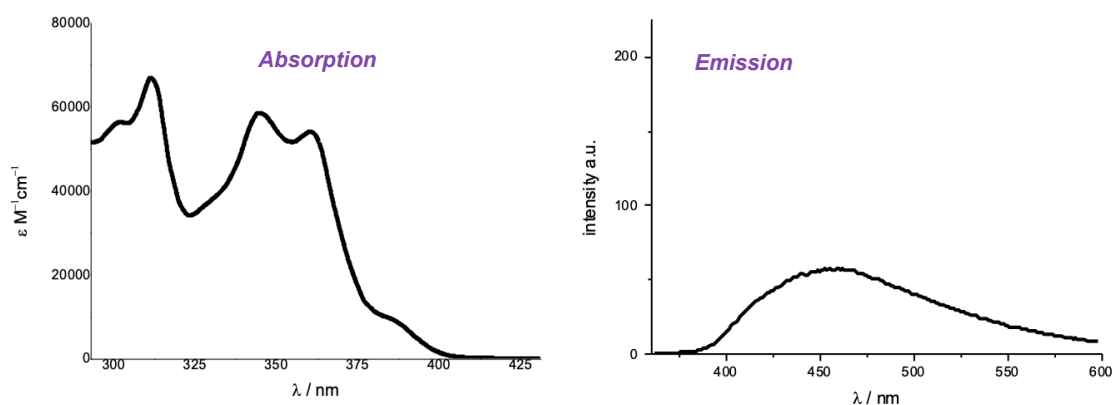
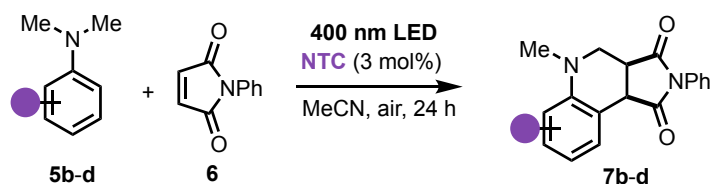


Figure 4.46. - Left: Extinction coefficient (ϵ) of NTC12 estimated from 3 spectra at different concentrations in MeCN.

Right: Emission spectrum of NTC12 in MeCN. ($\lambda_{\text{ex}}=350 \text{ nm}$).

Applications towards photoredox-catalyzed reactions

Povarov-type reaction



The reactions were carried out using the general procedure previously described in literature.²¹ *N*-phenylmaleimide **6** (17.3 mg, 1 equivalent, 0.10 mmol) was dissolved in dry MeCN (0.9 mL). To the resulting solution, *N,N*-dimethylaniline **5a** (25 μ L, 2 equivalents, 0.2 mmol) was added dropwise under vigorous stirring at room temperature. Then, 0.3 mL of a stock solution of the selected photocatalyst (5 mM in MeCN, 3.0 mol% catalyst loading) were added. The solution (0.083 M) was stirred at room temperature and irradiated using a 400 nm LED. Once the reaction reached full conversion, the solvent was removed by reduced pressure evaporation and the crude was subjected to flash column chromatography yielding product **7a**.

The reactions were monitored by GC-FID using mesitylene as internal standard.

Oxidation potentials of *N,N*-dimethylanilines

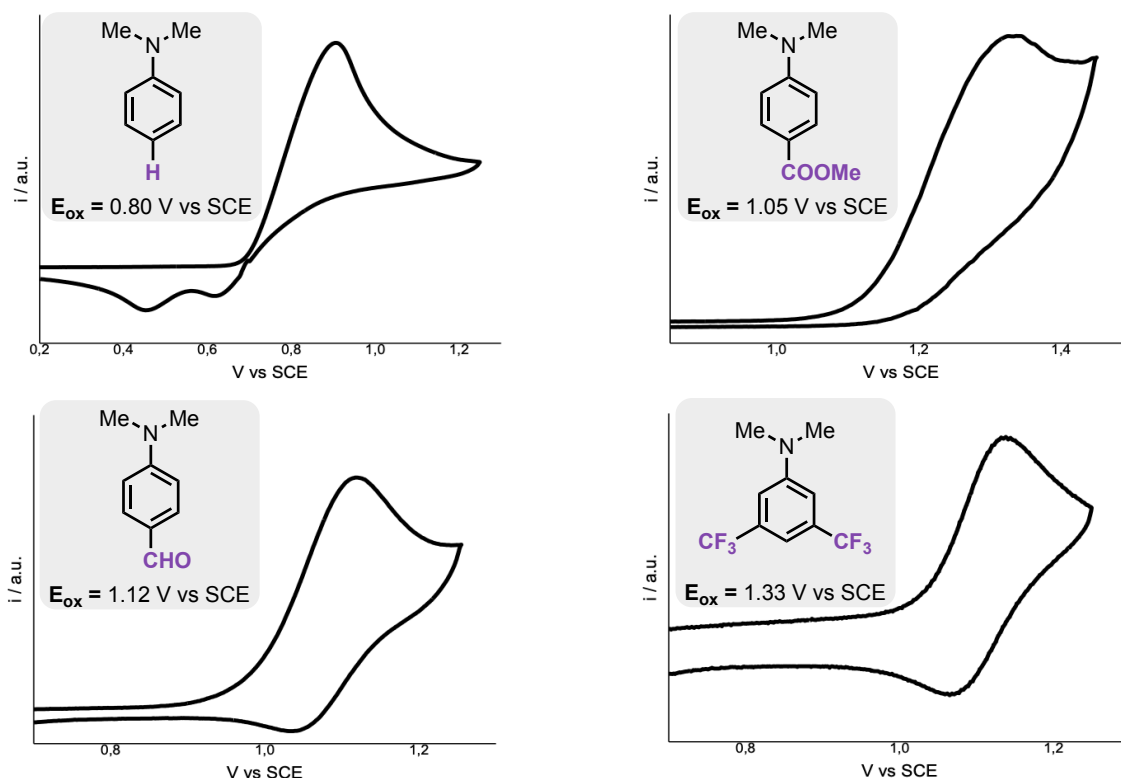
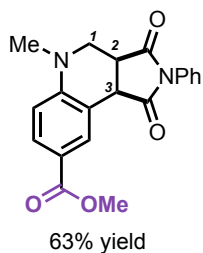


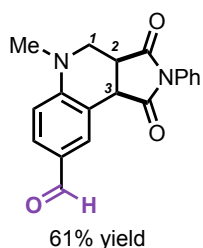
Figure 4.47. - Cathodic CVs of *N,N*-dimethylaniline derivatives in 0.1 TBAPF₆ MeCN solution. GCelectrode. Scan rate: 100 mV/s, potential referred to SCE at room temperature using a platinum wire as counter electrode.

Methyl 5-methyl-1,3-dioxo-2-phenylhexahydro-1H-pyrrolo[3,4-c]quinoline-8-carboxylate (7b).



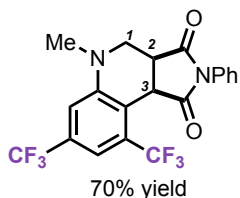
¹H-NMR (400 MHz, CDCl₃): δ 8.23 (s, 1H, Ar), 7.93 (d, *J* = 8.0 Hz, 1H, Ar), 7.46-7.35 (m, 4H, Ar), 7.27-7.26 (m, 1H, Ar), 6.75 (d, *J* = 8.7 Hz, 1H, Ar), 4.21 (d, *J* = 10.0 Hz, 1H, CH 3), 3.89 (s, 1H, COOCH₃), 3.68 (dd, *J* = 11.8, 3.0 Hz, 1H, CH 1a), 3.60 (ddd, *J* = 11.8, 3.0, 4.4 Hz 1H, CH 2), 3.26 (dd, *J* = 11.8, 4.4 Hz, 1H, CH 1b), 2.94 (s, 3H, CH₃) ppm. **¹³C-NMR (100 MHz, CDCl₃):** δ 170.6 (CON), 175.2 (CON), 168.9 (COO), 151.7 (Cq Ar), 132.0 (CH Ar), 130.7 (CH Ar), 129.0 (CH Ar x2), 128.6 (CH Ar), 126.3 (CH Ar x2), 120.8 (Cq Ar), 117.3 (Cq Ar), 112.0 (CH Ar), 110.7 (CH Ar), 51.8, 49.7, 43.1, 41.7, 39.4 ppm. **HRMS (ESI-MS)** calculated for [C₂₀H₁₈N₂O₄+H]⁺: 351.1267, found: 351.1266.

5-methyl-1,3-dioxo-2-phenylhexahydro-1H-pyrrolo[3,4-c]quinoline-8-carbaldehyde (7c).



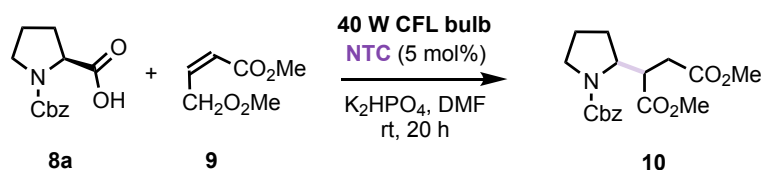
¹H-NMR (400 MHz, CDCl₃): δ 9.83 (s, 1H, CHO), 8.05 (s, 1H, Ar), 7.78 (d, *J* = 8.0 Hz, 1H, Ar), 7.46-7.33 (m, 4H, Ar), 7.27-7.25 (m, 1H, Ar), 6.82 (d, *J* = 8.7 Hz, 1H, Ar), 4.23 (d, *J* = 10.0 Hz, 1H, CH 3), 3.72 (dd, *J* = 11.8, 3.0 Hz, 1H, CH 1b), 3.58 (ddd, *J* = 11.8, 3.0, 4.4 Hz 1H, CH 2), 3.72 (dd, *J* = 11.8, 4.4 Hz, 1H, CH 1a), 2.99 (s, 3H, CH₃) ppm. **¹³C-NMR (100 MHz, CDCl₃):** δ 190.4 (CHO), 176.8 (CON), 175.1 (CON), 152.7 (Cq Ar), 133.0 (Cq Ar), 131.7 (CH Ar), 130.5 (Cq Ar), 129.1 (CH Ar x2), 128.7 (CH Ar), 128.1 (CH Ar), 126.3 (CH Ar x2), 117.4 (Cq Ar), 112.4 (CH Ar), 49.2, 42.0, 41.4, 39.4 ppm. **HRMS (ESI-MS)** calculated for [C₁₉H₁₆N₂O₃+H]⁺: 321.1161, found: 321.1162.

5-methyl-2-phenyl-7,9-bis(trifluoromethyl)tetrahydro-1H-pyrrolo[3,4-c]quinoline-1,3(2H)-dione (7d).



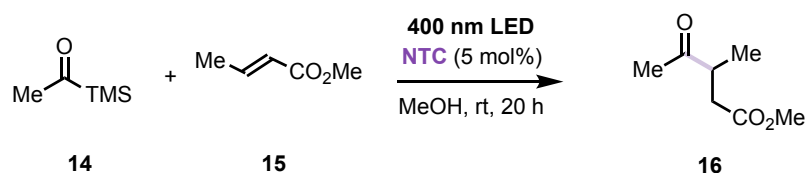
¹H-NMR (400 MHz, CDCl₃): δ 7.58 (s, 1H, Ar), 7.49-7.41 (m, 3H, Ar), 7.31 (d, *J* = 7.8 Hz, 2H, Ar), 7.21 (s, 1H, Ar) 4.76 (d, *J* = 10.0 Hz, 1H, CH 3), 3.67-3.62 (m, 2H, CH 1a + CH 2), 3.04 (dd, *J* = 11.8, 4.4 Hz 1H, CH 1b), 2.91 (s, 3H, CH₃) ppm. **¹³C-NMR (100 MHz, CDCl₃):** 177.5 (CON), 173.4 (CON), 152.5 (Cq Ar), 131.8 (Cq Ar), 131.6 (q, ²*J*_{C-F} = 30.6 Hz, Cq Ar-CF₃), 130.8 (q, ²*J*_{C-F} = 32.7 Hz, Cq Ar-CF₃), 129.1 (CH Ar x2), 128.9 (CH Ar), 126.2 (CH Ar x2), 124.2 (CH Ar), 123.4 (q, ¹*J*_{C-F} = 275.0 Hz, CF₃), 123.3 (q, ¹*J*_{C-F} = 275.0 Hz, CF₃), 114.9 (m, CH Ar), 112.9 (Cq Ar), 53.8, 45.9, 40.0 (q, ⁴*J*_{C-F} = 1.8 Hz, C 3), 39.7 ppm. **¹⁹F-NMR (376 MHz, CDCl₃):** δ -58.35 (s, 3F, CF₃), -63.46 (s, 3F, CF₃) ppm. **HRMS (ESI-MS)** calculated for [C₂₀H₁₄F₆N₂O₂+H]⁺: 429.0959, found: 429.0959.

— Giese-type addition



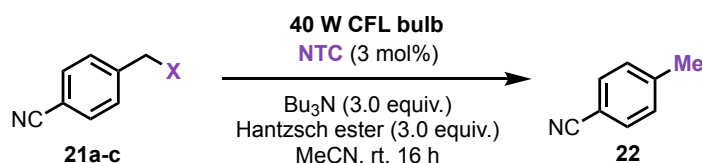
The reactions were carried out using the general procedure previously described in literature.³² An oven-dried 10 mL Schlenk flask with a glass cap and a magnetic stir bar was charged with the selected photocatalyst (0.005 mmol, 5 mol% cat. loading), Cbz-Pro-OH **8a** (0.2 mmol, 1.0 equiv), methyl fumarate **9** (0.2 mmol, 1.0 equiv), K₂HPO₄ (0.24 mmol, 1.2 equiv), and 0.5 mL of DMF. The reaction mixture was degassed by using the freeze-pump-thaw technique, then irradiated with the 40W CFL bulb. After 20h, the reaction mixture was diluted with saturated aqueous NaHCO₃ solution and extracted with Et₂O (3 × 5 mL). The combined organic extracts were washed with water and brine, dried over MgSO₄ and concentrated in vacuo. Purification of the crude product by flash chromatography on silica gel afforded the desired product.

— Acylation reaction



A 4 mL vial with a magnetic stir bar was charged with ethyl crotonate **15** (0.10 mmol, 1.0 equiv), the corresponding photocatalyst (0.005 mmol, 5.0 mol% cat. loading), 1 mL of methanol (0.1 M) degassed with argon and acetyltrimethylsilane **14** (0.15 mmol, 1.5 equiv). Then, the reaction mixture was irradiated and stirred for 15 h with a 400 nm LED reactor. The β -ketoester **16** was obtained as a colorless oil in up to 85% yield (12.3 mg, 0.09 mmol). The spectroscopic data of **16** were in accordance with the data reported in the literature.³³

Dehalogenation of benzylhalides



An oven-dried 10 mL Schlenck with a glass cap and a magnetic stir bar was charged with the corresponding benzylhalide **21a-c** (0.10 mmol, 1.0 equiv), MeCN (1.0 mL), tributylamine (0.30 mmol, 3.0 equiv), formic acid (0.30 mmol, 3.0 equiv) and the corresponding photocatalyst (0.003 mmol, 3.0 mol% cat. loading). The reaction mixture was degassed by using the freeze-pump-thaw technique, then irradiated with a 400 nm LED reactor. The reaction mixture was stirred 16 h.

The reactions were monitored by GC-FID using mesitylene as internal standard.

Reduction potentials of benzylhalides

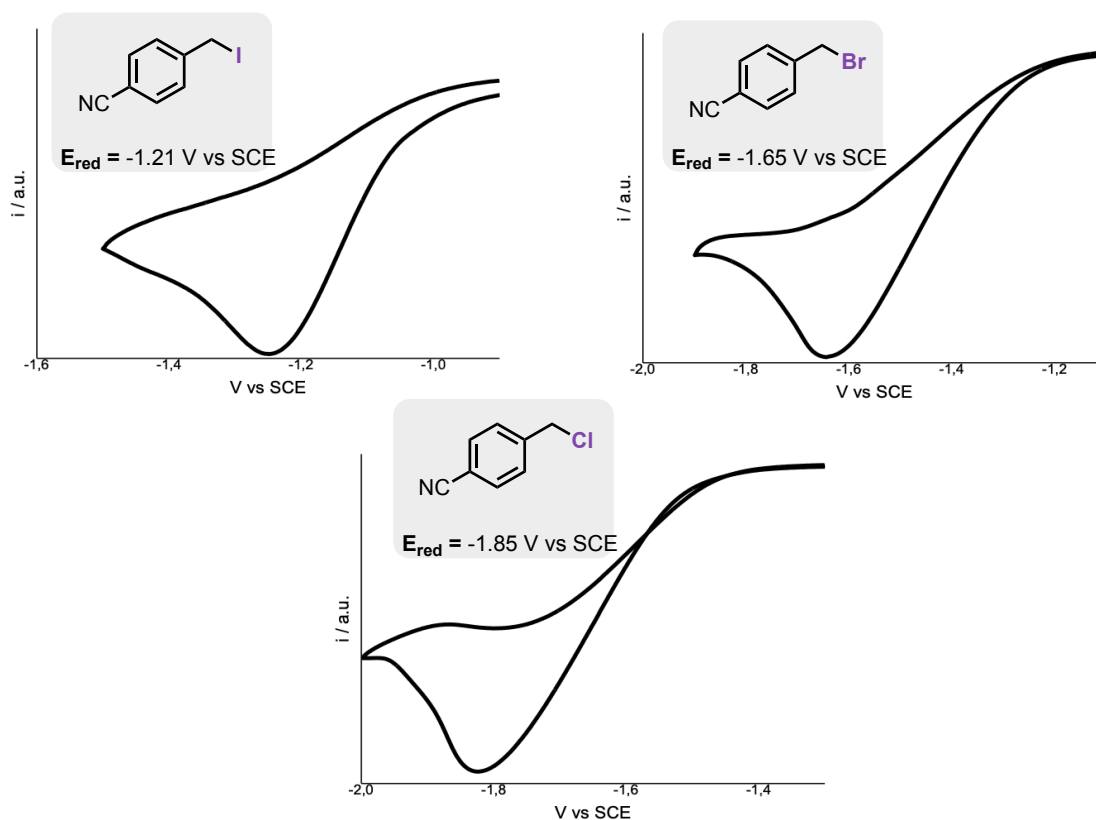
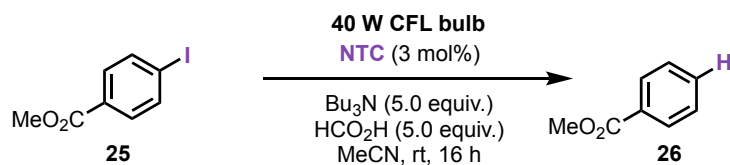


Figure 4.48. - Anodic CVs of benzylhalides in 0.1 TBAPF₆ MeCN solution. GCelectrode. Scan rate: 100 mV/s, potential referred to SCE at room temperature using a platinum wire as counter electrode.



The reactions were carried out using the general procedure previously described in literature.³⁴ An oven-dried 10 mL Schlenk with a glass cap and a magnetic stir bar was charged with 4-iodomethylbenzoate **25** (0.10 mmol, 1.0 equiv), MeCN (1.0 mL), tributylamine (0.30 mmol, 3.0 equiv), formic acid (0.30 mmol, 3.0 equiv) and the used photocatalyst (0.005 mmol, 5.0 mol% cat. loading). The reaction mixture was degassed by using the freeze-pump-thaw technique, then irradiated with the 40W CFL bulb. The reaction mixture was stirred 20 h, then 0.1 mL of product solution were introduced into an NMR tube with, diluted with CDCl_3 and analyzed by ^1H NMR to calculate the NMR yield using trimethoxybenzene as internal standard.

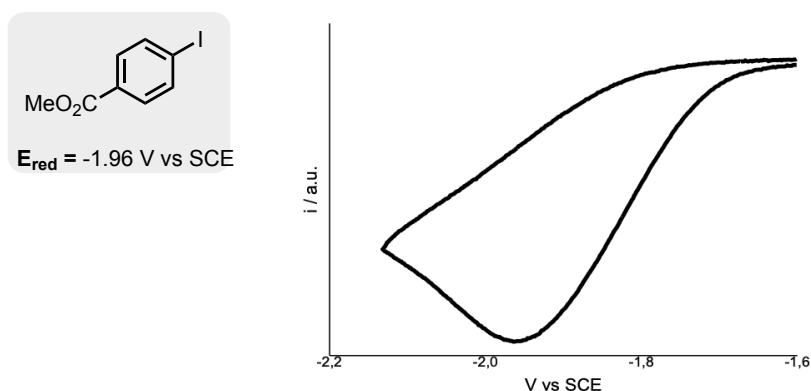


Figure 4.49. - Anodic CVs of methyl iodobenzoate in 0.1 TBAPF_6 MeCN solution. GCelectrode. Scan rate: 100 mV/s, potential referred to SCE at room temperature using a platinum wire as counter electrode.



Chapter IV – Section 2

Photoredox Catalysis –

Radical α -Trifluoromethoxylation of Ketones

Chapter IV - The Evolution of Aryl Ketone-Derived Products – Applications in Organophotoredox Catalysis

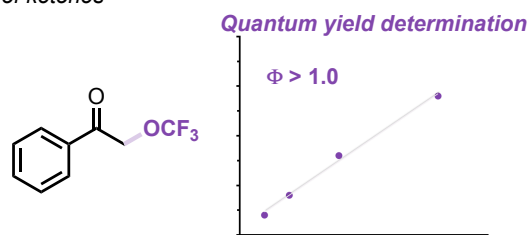
Section 1.

Organophotoredox catalysis -
structure-activity relationships in
organic photoredox catalysts



Section 2.

Photoredox catalysis -
Radical α -trifluoromethoxylation
of ketones



- To expand the chemistry of the trifluoromethoxy radical.
- To study the reasons behind the low yields of the studied reaction.⁴¹

⁴¹ The project discussed in this chapter is fruit of an international collaboration with the groups of Prof. Emmanuel Magnier (CNRS-Paris, France) and Prof. Antonio Togni (ETH Zürich, Switzerland). The work conducted in Padova has been done in collaboration with Tommaso Bortolato (involved in the optimization of the photocatalyzed reaction, the demonstration of the generality of the reaction and mechanistic investigation). I individually found the initial reactivity through EDA complex reactivity, performed the initial optimization process, studied the mechanism of the reaction and prepared several entries of the reaction scope.

This work has been published: Duhail, T.; Bortolato, T.; Mateos, J.; Anselmi, E.; Jelier, B.; Togni, A.; Magnier, E.; Dagousset, G.; Dell'Amico, L. *Radical α -Trifluoromethoxylation of Ketones under Batch and Flow Conditions by Means of Organic Photoredox Catalysis*. *Org. Lett.* **2021**, DOI: 10.1021/acs.orglett.1c02494

4.2.1 Introduction

The utilization of organic photocatalysis is not restricted to the development of novel photocatalysts but to previously unknown transformations.⁵ When looking at this type of reactivity, the attachment of perfluorinated groups has been widely studied. Nevertheless, the introduction of the OCF₃ (trifluoromethoxy-) moiety, which occupies a special place due to its interesting physicochemical properties, is underdeveloped.⁴² Indeed, these remarkable properties associated with good metabolic stability and unique conformational properties make this group particularly attractive for the life sciences.⁴³ Despite this, the number of marketed pharmaceutical and agrochemical products containing OCF₃ remains low (Figure 4.50). To date, only four of the 340 identified drugs containing at least one fluorine atom bear a OCF₃ group.⁴⁴ One example of such drugs is Riluzole **29**, a widely used medication for the treatment of amyotrophic lateral sclerosis (ALS) that can delay up to five months the tracheotomy intervention.⁴⁵ But not only the presence of the OCF₃ moiety is limited in drugs, among the 424 fluoro-agrochemicals, only ten bearing an OCF₃ moiety are listed.⁴⁶ As an example of this class of compounds, flucarbazone **30** is listed. Indeed, it is used to treat wheat, avoiding the appearance of wild oat in the soil.⁴⁷ Given the importance of these molecules, it should also be pointed out that the OCF₃ group is always attached to an aromatic ring. This contrasting situation (interesting physicochemical properties but low amount of marketed compounds) is mainly due to the small number of existing methods capable of delivering these target under selective conditions at the intermediate- or late-stage phase of a synthetic route.

⁴² a) Tang, P.; Jiang, X. *Emerging Fluorinated Motifs Synthesis, Properties, and Applications*; Oxygen-Linked Fluorine-Containing Motifs, Cahard, D. and Ma, J.-A., Ed. Wiley-VCH Weinheim, Germany, **2020**; pp 195–224. b) Toulgouat, F.; Liger, F.; Billard, T. *Organofluorine Chemistry, Synthesis, Modeling, and Applications*, Szabó, K.-J. and Selande, N., Ed. Wiley-VCH Weinheim, Germany, **2020**; pp 49–97.

⁴³ a) Klocker, J.; Karpfen, A.; Wolschann, P. *On the Structure and Torsional Potential of Trifluoromethoxybenzene: an ab Initio and Density Functional Study*. *Chem. Phys. Lett.* **2003**, *367*, 566–575. b) Klocker, J.; Karpfen, A.; Wolschann, P. *Trends in the Torsional Potentials of Methoxy and Trifluoromethoxy Groups: An ab Initio and Density Functional Study on the Structure of para-Substituted Pyridines and Pyridinium Cations*. *J. Chem. Phys. A.* **2003**, *107*, 23652–23668. c) Manteau, B.; Genix, P.; Brelot, L.; Vors, J.-P.; Pazenok, S.; Giornal, F.; Leuenberger, C.; Leroux, F. R. *A General Approach to (Trifluoromethoxy)pyridines: First X-ray Structure Determinations and Quantum Chemistry Studies*. *Eur. J. Org. Chem.* **2010**, 6043–6066.

⁴⁴ Inoue, M.; Sumii, Y.; Shibata, N. *Contribution of Organofluorine Compounds to Pharmaceuticals*. *ACS Omega*, **2020**, *19*, 10633–10640.

⁴⁵ Bensimon, G.; Lacomblez, L.; Meininger, V. *A Controlled Trial of Riluzole in Amyotrophic Lateral Sclerosis*. *N Engl J Med* **1994**, *330*, 585–591.

⁴⁶ Ogawa, Y.; Tokunaga, E.; Kobayashi, O.; Hirai, K.; Shibata, N. *Current Contributions of Organofluorine Compounds to the Agrochemical Industry*. *iScience* **2020**, *23*, 101467

⁴⁷ *The 1999 Brighton Conference - Weeds: Proceedings of an International Conference Held at the Brighton Metropole Hotel, Brighton, UK, 15-18 November 1999*; British Crop Protection Council, Ed.; British Crop Protection Council: Farnham, **1999**.

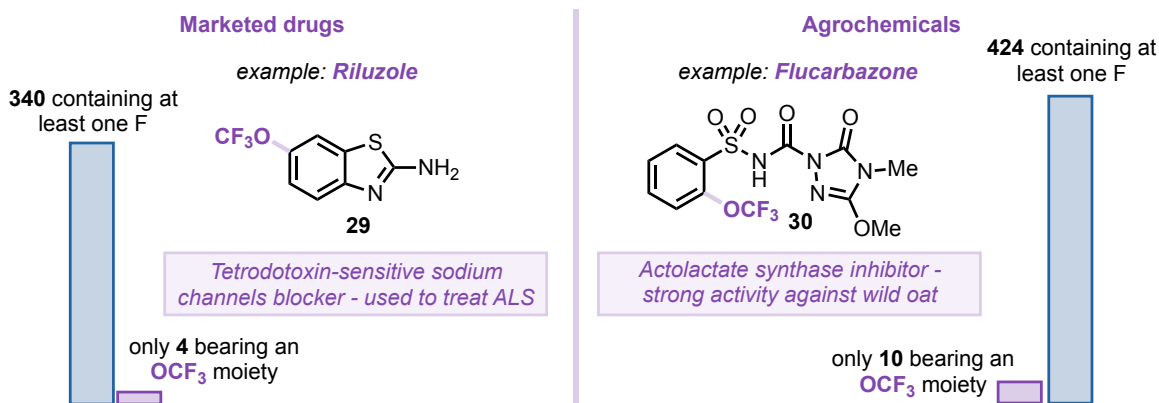


Figure 4.50. - Marketed drugs and agrochemicals containing an OCF₃ moiety.

4.2.2 Challenges of the introduction of OCF₃ moieties

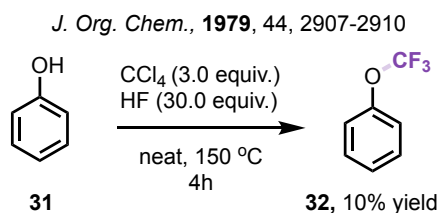
Due to the venerable properties of this moiety, diverse elegant alternatives for accessing trifluoromethoxylated compounds have been proposed over the years. Indeed, the most straightforward process is the direct introduction of the OCF₃ functionality. However, despite the wide advantages of this strategy, several limitations are observed nowadays.

O-CF₃ bond formation (Figure 4.51)

Limitations of the O-CF₃ bond formation

Selected example

i) direct O-CF₃ bond formation using HF:



Selected example

ii) direct O-CF₃ bond formation using hypervalent iodine reagents:

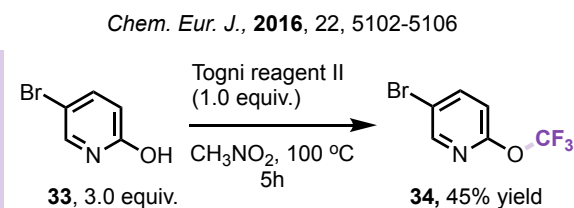


Figure 4.51. - Examples of direct O-CF₃ bond formation.

Many works focused on the construction of the O-CF₃ bond from the already installed OH group (mainly in phenols), via *i*) multistep processes, requiring harsh conditions and toxic reagents (e.g., HF and SF₄),⁴⁸ or *ii*) direct electrophilic trifluoromethylation of alcohols, either with hypervalent iodine reagents that require large excesses of alcohol (5–75 equiv) to achieve

⁴⁸ For reviews, see a) Tlili, A.; Toulgoat, F.; Billard, T. *Synthetic Approaches to Trifluoromethoxy-Substituted Compounds*. *Angew. Chem. Int. Ed.* **2016**, 55, 11726–11735. b) Zhang, X.; Tang, P. *Recent Advances in New Trifluoromethoxylation Reagents*. *Sci. China Chem.* **2019**, 62, 525–532.

reasonable yields or with an unstable oxonium salt. Despite recent improvements,⁴⁹ such approaches are still limited in practicality and scope.

Direct OCF₃ introduction (Figure 4.52)

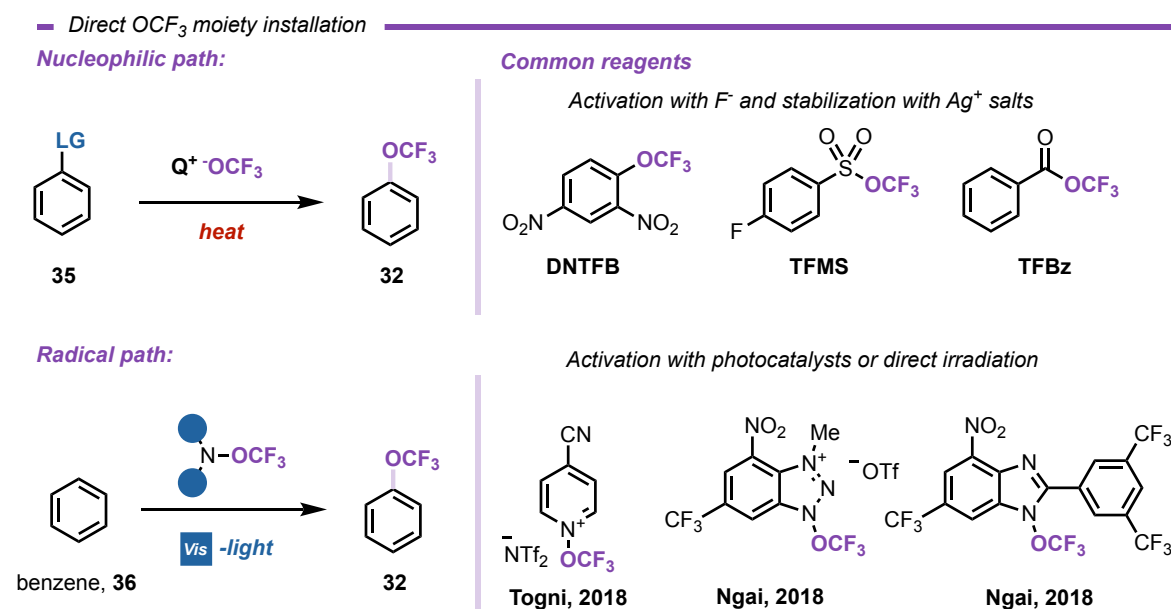


Figure 4.52. - Strategies and reagents used for the direct installation of the OCF₃ moiety.

Nucleophilic path: nucleophilic routes have been proposed, with recent leading advances involving the description of new sources of the trifluoromethoxide anion or new methods for its *in situ* formation (Figure 4.52 top).⁵⁰ However, the use of this approach is hampered by: *i*) the need for prefunctionalized starting materials; *ii*) the innate instability of the OCF₃ anion; and *iii*) the low chemo- and regioselectivity.

⁴⁹ a) Yoritata, M.; Londregan, A. T.; Lian, Y.; Hartwig, J. F. *Sequential Xanthalation and O-Trifluoromethylation of Phenols: A Procedure for the Synthesis of Aryl Trifluoromethyl Ethers*. *J. Org. Chem.* **2019**, *84*, 15767–15776. b) Kalim, J.; Duhail, T.; Pietrasiak, E.; Anselmi, E.; Magnier, E.; Togni, A. *Direct Trifluoromethylation of Alcohols Using a Hypervalent Iodosulfoximine Reagent*. *Chem. Eur. J.* **2021**, *67*, 2638–2642. c) Liang, A.; Han, S.; Liu, Z.; Wang, L.; Li, J.; Zou, D.; Wu, Y.; Wu, Y. *Regioselective Synthesis of N-Heteroaromatic Trifluoromethoxy Compounds by Direct O–CF₃ Bond Formation*. *Chem. Eur. J.* **2016**, *22*, 5102–5106.

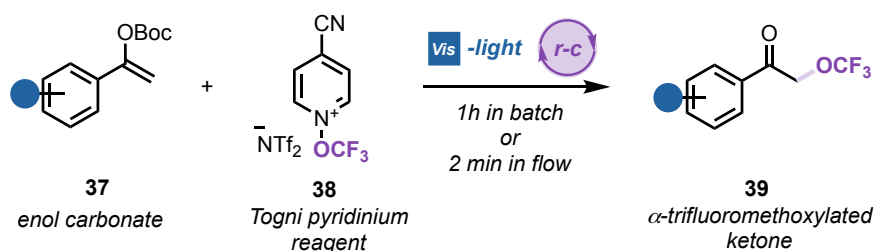
⁵⁰ Selected recent examples: a) Huang, C.; Liang, T.; Harada, S.; Lee, E.; Ritter, T. *Silver-Mediated Trifluoromethoxylation of Aryl Stannanes and Arylboronic Acids*. *J. Am. Chem. Soc.* **2011**, *133*, 13308–13310. b) Guo S.; Cong, F.; Guo, R.; Wang, L.; Tang, P. *Asymmetric Silver-Catalysed Intermolecular Bromotrifluoromethoxylation of Alkenes with a New Trifluoromethoxylation Reagent*. *Nat. Chem.* **2017**, *9*, 546–551. c) Zhou, M.; Ni, C.; Zeng, Y.; Hu, J. *Trifluoromethyl Benzoate: A Versatile Trifluoromethoxylation Reagent*. *J. Am. Chem. Soc.* **2018**, *140*, 6801–6805. d) Tursoy, A.; Scattolin, T.; Bouayad-Gervais, S.; Schoenebeck, F. *Facile Access to AgOCF₃ and Its New Applications as a Reservoir for OCF₂ for the Direct Synthesis of N–CF₃, Aryl or Alkyl Carbamoyl Fluorides*. *Chem. Eur. J.* **2020**, *26*, 2183–2186. e) Li, Y.; Yang, Y.; Tang, P. *Nucleophilic Trifluoromethoxylation of Alkyl Halides without Silver*. *Nat. Chem.* **2020**, *11*, 755–762.

Radical path: Previously unknown, the radical approach emerged in 2018 and has seen rapid development,⁵¹ in particular with the development of three new reagents (Figure 4.52 down). The Togni group designed a pyridine *N*-oxide reagent,⁵² and the Ngai group reported the use of azole-based compounds.⁵³ Under photoredox conditions, these three reagents proved to be efficient for the catalytic C–H trifluoromethoxylation of arenes and heteroarenes.⁵⁴ To date, their scope has not been extended beyond (hetero)aromatic substrates. This fact represents an unprecedented challenge, the success of which would provide access to new or hitherto poorly described molecules due to their cumbersome synthesis.

4.2.3 Section overview

In this section, I report a mild visible-light-driven strategy for tackling an unsolved synthetic issue, the direct α -trifluoromethoxylation of ketones. We identified enol carbonates as substrates for their peculiar stereoelectronic properties, their ease of preparation, and the molecular diversity they offer. Mechanistic investigations pointed out towards a radical-chain propagation path which is general for the trifluoromethoxylation of structurally diverse ketones (Figure 4.53).

— **This section:** mild light-driven α -trifluoromethoxylation of ketones



main improvements

high selectivity - scalable - mild method - unprecedented reactivity - general method

Figure 4.53. - α -trifluoromethoxylation of ketones reported in this section.

⁵¹ Selected reviews: **a)** Ghiazza, C.; Billard, T.; Tlili, A. Merging Visible-Light Catalysis for the Direct Late-Stage Group-16–Trifluoromethyl Bond Formation. *Chem. Eur. J.* **2019**, *25*, 6482–6495. **b)** Lee, J. W.; Lee, K. N.; Ngai, M. Synthesis of Tri- and Difluoromethoxylated Compounds by Visible-Light Photoredox Catalysis. *Angew. Chem. Int. Ed.* **2019**, *58*, 11171–11181.

⁵² Jelier, B. J.; Tripet, P. F.; Pietrasiak, E.; Franzoni, I.; Jeschke, G.; Togni, A. Radical Trifluoromethoxylation of Arenes Triggered by a Visible-Light-Mediated N–O Bond Redox Fragmentation. *Angew. Chem. Int. Ed.* **2018**, *57*, 13784–13789.

⁵³ **a)** Zheng, W.; Morales-Rivera, C.-A.; Lee, J. W.; Liu, P.; Ngai, M.-Y. Catalytic C–H Trifluoromethoxylation of Arenes and Heteroarenes. *Angew. Chem. Int. Ed.* **2018**, *57*, 9645–9649. **b)** Zheng, W.; Lee, J. W.; Morales-Rivera, C. A.; Liu, P.; Ngai, M.-Y. Redox-Active Reagents for Photocatalytic Generation of the OCF₃ Radical and (Hetero)Aryl C–H Trifluoromethoxylation. *Angew. Chem. Int. Ed.* **2018**, *57*, 13795–13799.

⁵⁴ **a)** Yang, S.; Chen, M.; Tang, P. Visible-Light Photoredox-Catalyzed and Copper-Promoted Trifluoromethoxylation of Arenediazonium Tetrafluoroborates. *Angew. Chem. Int. Ed.* **2019**, *58*, 7840–7844. **b)** Dix, S.; Golz, P.; Schmid, J. R.; Riedel, S.; Hopkinson, M. N. Radical C–H Trifluoromethoxylation of (Hetero)arenes with Bis(trifluoromethyl)peroxide. *Chem. Eur. J.* **2021**, doi: 10.1002/chem.202101621.

4.2.4 Results and discussion

Reaction optimization

EDA complex approach

The discovery of the α -trifluoromethoxylation reaction began with a simpler initial observation. Indeed, when studying the reaction between enol acetate **40** (1 equiv., 0.1 M) and the *N*-trifluoromethoxypyridinium **38**, commercially available as NTf₂⁻ salt, we observed a change of color of the reaction mixture (Figure 4.54, macroscopic observation). For this reason, we initially evaluated the possibility of exploiting an EDA complex irradiation between these two reagents.⁵⁵ UV-Vis absorption measurements, clearly showed a formed CT band (purple line Figure 4.55 left). Irradiation of the CT band at 400 nm delivered the trifluoromethoxylated target **41**. Unexpectedly, product **42** was accompanied by the undesired side-product **4**, where the OCF₃ group was introduced onto the aromatic ring.⁵² We reasoned that the low chemoselectivity of the process could be overcome by channeling the transformation towards a photoredox process.

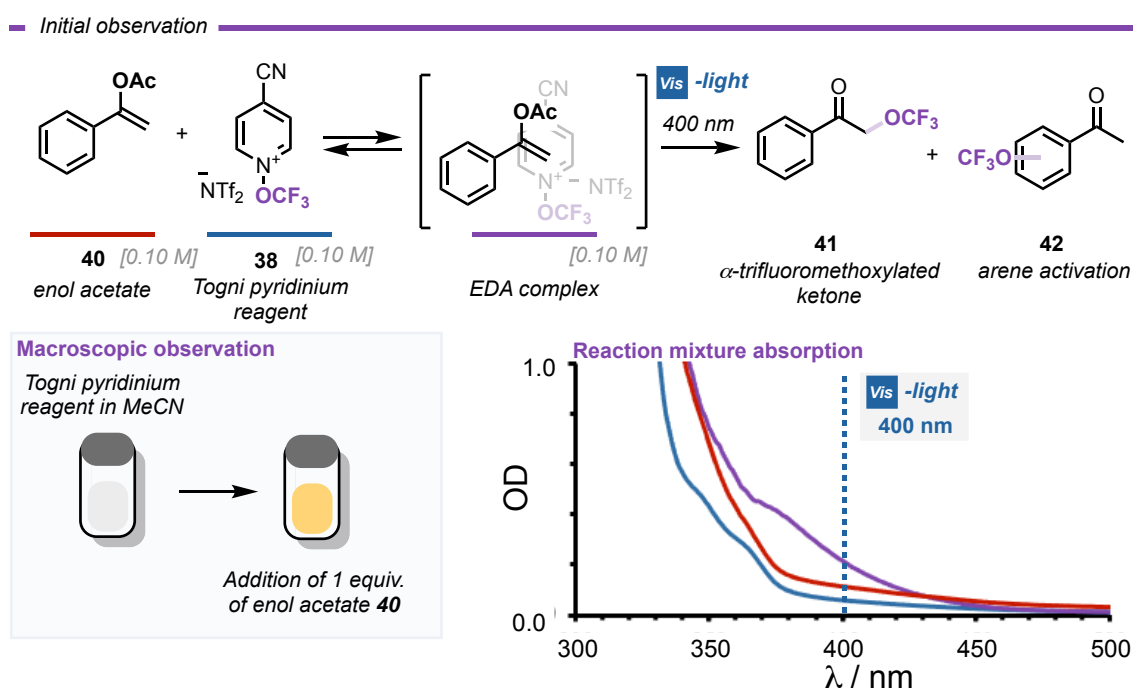


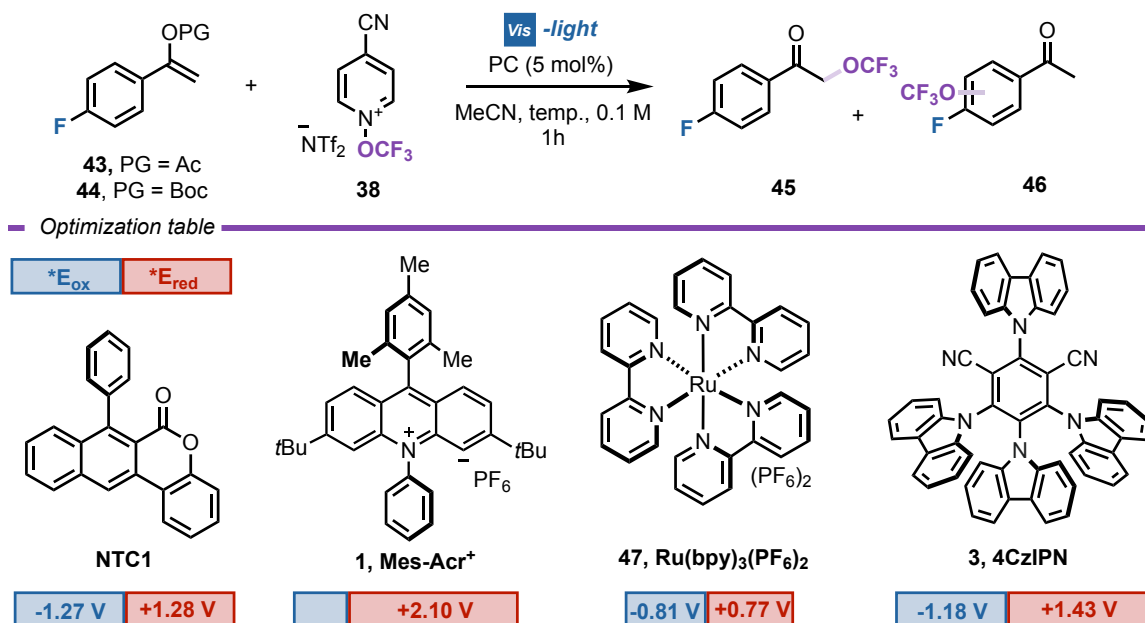
Figure 4.54. - Initial observation of an EDA complex between enol acetate **40** and pyridinium reagent **38**.

Photocatalyzed approach

Subsequently, we started our optimization by moving from the direct excitation of the reaction mixture towards a photocatalyzed reaction manifold. We screened various

⁵⁵ Crisenza, G. E. M.; Mazzarella, D.; Melchiorre, P. *Synthetic Methods Driven by the Photoactivity of Electron Donor–Acceptor Complexes*. *J. Am. Chem. Soc.* **2020**, *142*, 5461–5476

photocatalysts characterized by diverse redox and photochemical properties.^{2,7} Naphthochromenone (NTC1, Table 4.8, entry 2) resulted in only slight improvements when compared with the uncatalyzed approach (20% yield and 12:1 ratio, entry 2 vs 1).¹⁰



entry	1 (equiv.)	PG	PC	light source (nm)	temperature (°C)	1:2 ratio	¹⁹ F NMR yield 1 (%)
1	10	Ac	-	400	rt	8:1	17
2	10	Ac	NTC1	400	rt	13:1	20
3	10	Ac	Mes-Acr ⁺	456	rt	9:1	7
4	10	Ac	Ru(bpy) ₃ (PF ₆) ₂	456	rt	12:1	33
5	10	Ac	4CzIPN	456	rt	>20:1	37
6	10	Ac	4CzIPN	456	50	>20:1	41
7 ^a	10	Ac	4CzIPN	456	50	>20:1	44
8 ^a	10	Boc	4CzIPN	456	50	>20:1	52
9 ^a	5	Boc	4CzIPN	456	50	>20:1	50
10 ^a	1.5	Boc	4CzIPN	456	50	>20:1	30
11 ^a	5	Boc	4CzIPN	-	50	-	-

^a Concentration = 0.01 M

Table 4.8. - Reaction optimization table.

This fact could result from the close to the UV-light irradiation used (400 nm). We thus selected a red-shifted light source (456 nm). In this case, no reaction was observed using NTC1, so we evaluated the performance of diverse PCs such as Mes-Acr⁺ **1**, Ru(bpy)₃(PF₆)₂ **47** and 4CzIPN **3**. The low yield (7%) and chemoselectivity (9:1) obtained with the highly oxidizing Mes-Acr⁺ is attributed to the oxidation of **1a**.⁷ On the other hand, Ru(bpy)₃(PF₆)₂

and 4CzIPN, delivered the product **45** in promising yield and selectivity, up to 37% and >20:1, respectively (entries 4 and 5). Remarkably, when using 4CzIPN, **46** was not detected. We observed additional improvements by increasing the temperature in a more diluted medium (entries 6 and 7). Finally, replacing the acetyl group (Ac) for a *tert*-butyloxycarbonyl (Boc) group led to 52% yield in only 1h reaction time (entry 8). Under these conditions, we were able to halve the substrate loading with minimal yield erosion (entry 9). Further decreasing the amount of **44** resulted in 30% yield (entry 10). It is worth noting that we were able to recover, after purification, more than 80% of the unreactive starting material **44**. Finally, the reaction did not proceed in the absence of light irradiation (entry 11).

Mechanistic investigations

In order to gain insights about the modest yields observed after optimizing the reaction, we decided to decipher the operative mechanism of this transformation. This procedure allowed us to understand the impact of alternative reaction manifolds on the reaction outcome when using trifluoromethoxy radicals.

EDA complex manifold

We started our investigations by studying the intermediates related to the EDA-based pathway. The poor chemoselectivity was ascribed to the rapid *in situ* deprotection of **1b**, promoted by its single-electron oxidation and the following trifluoromethoxylation of the resulting acetophenone (Figure 4.55).⁵² This observation was supported by the fact that more diluted conditions disfavored the EDA complex formation. Nevertheless, quantum yield measurements at 0.01 M supported a short chain-propagation mechanism ($\Phi=0.88$).³⁷

— Low selectivity in the EDA complex pathway —

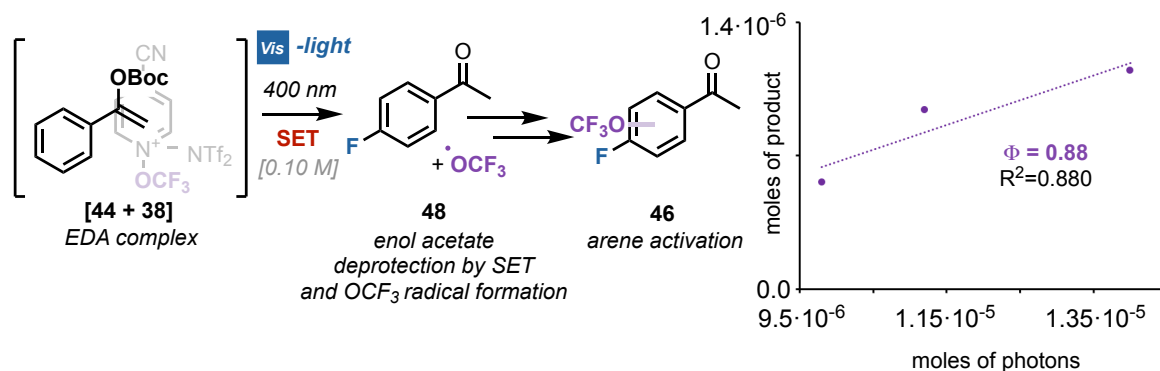


Figure 4.55. - Mechanistic investigations on the EDA complex path.

Radical-chain propagation manifold

To corroborate the chain-propagation hypothesis we started studying the reactivity with Mes-Acr⁺. Indeed, the initial oxidation of **43** is detrimental to the reaction outcome. Hence, the available concentration of **43** in the reaction mixture is a key parameter to channel the reactivity towards the intended α -trifluoromethoxylation. Interestingly, the identification of enol carbonate **44** was key to increase the overall reactivity of the system. We speculated that the use of the Boc group facilitates the formation of the final product by exploiting the driving force for CO₂ and isobutylene formation.

The higher reactivity observed under the optimized reaction conditions led us to depict the mechanistic scenario shown in Figure 4.56. Upon excitation, the PC reaches an electronically excited state that reduces **38** by SET, with the generation of the OCF₃ radical, and the formation of the PC^{•+} radical cation. The OCF₃ radical is readily intercepted by **44**, with the formation of the C-O bond within **49**. At this juncture, **49** can reduce a second molecule of **38**, in a radical-chain process which delivers carbocation **50**. This intermediate, rapidly evolves to the final product **45** with the formation of CO₂ and isobutylene. Finally, the chain process is terminated by the oxidation of **49** by PC^{•+}.

Proposed radical chain propagation mechanism

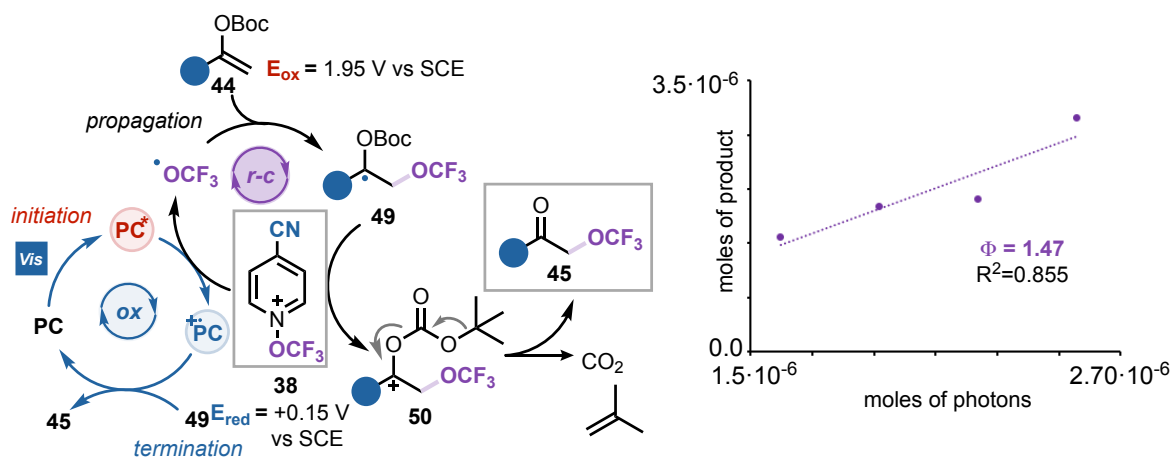


Figure 4.56. - Proposed reaction mechanism engaging a radical-chain propagation path.

Photocatalyzed manifold

To prove the importance of the radical-chain propagation manifold, we confronted it with a classic photocatalyzed manifold (Figure 4.57). Indeed, by measuring the quantum yield in the presence of different trifluoromethoxylating agents **38** and **51** we were able to rule out the different pathways. When using the easily reducible **38** (E_{red} = +0.15V vs SCE) we

measured a quantum yield of 1.47, indicating that a chain propagation is operative.⁵⁶ Contrarily, when using the more electron-rich **51** ($E_{\text{red}} = -0.70\text{V}$ vs SCE) the quantum yield dropped drastically to less than 0.01, indicating that intermediate **49** is not able to reduce this pyridinium reagent and the mechanism switches to a classic photoredox cycle. Additionally, the reaction appeared much slower affording in 1h product **45** in 12% yield instead of 50%.

— Proposed photoredox path

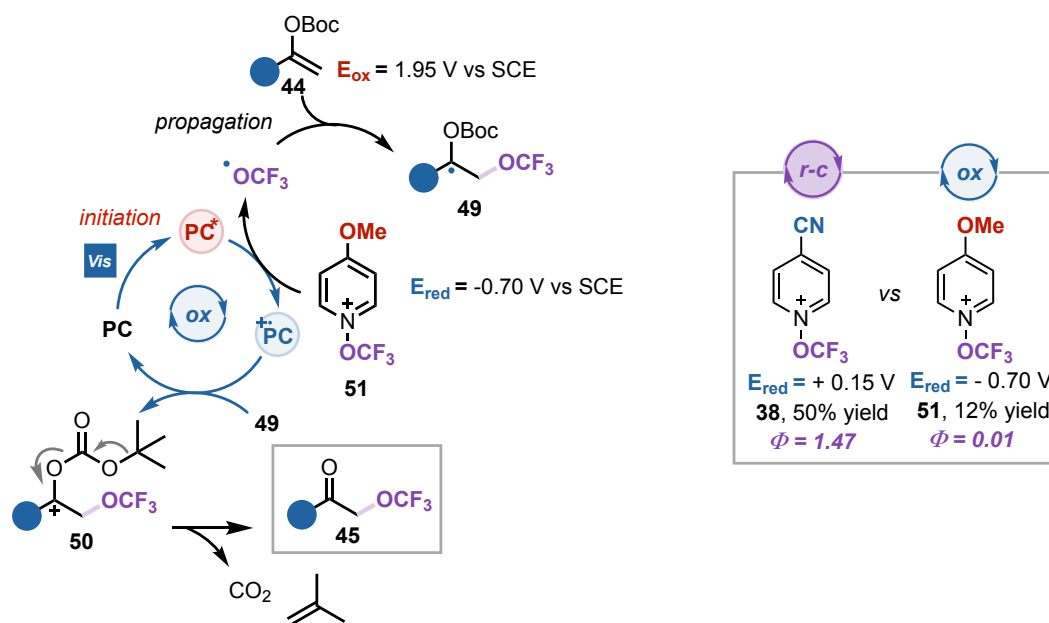
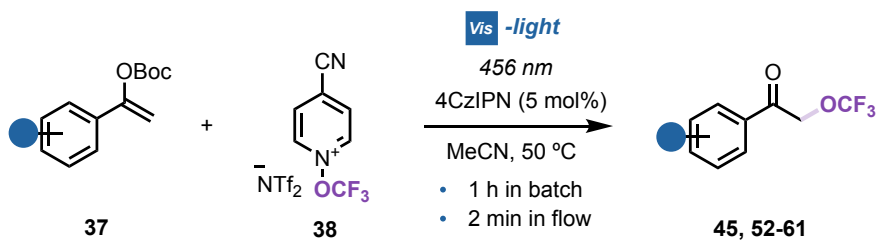


Figure 4.57. - Proposed reaction mechanism engaging a purely photoredox path.

Generality of the reaction

Having deciphered the operative reaction manifold, we tested the generality of the developed trifluoromethoxylation method (Table 4.9). We were pleased to see that substitutions on all the positions of the aromatic ring were tolerated. Alkyl substituents (**52-54**) gave comparable results with yields up to 46%. Interestingly, the OCF_3 group was also readily installed on enol carbonates bearing electron-withdrawing functionalities (CN, Ac, CF_3 , Br), affording the corresponding products **55-61** in up to 46% yield in 1h. Remarkably, the reaction was easily transferred into a flow photoreactor without any significant yield erosion (48% for **45**, 50% for **55**, for 41% for **61**), allowing a very short reaction time of only 2 min.

⁵⁶ Cismesia, M. A.; Yoon, T. P. *Characterizing chain processes in visible light photoredox catalysis*. *Chem. Sci.* **2015**, *6*, 5426–5434.



— Reaction scope with aryl substituted enol carbonates

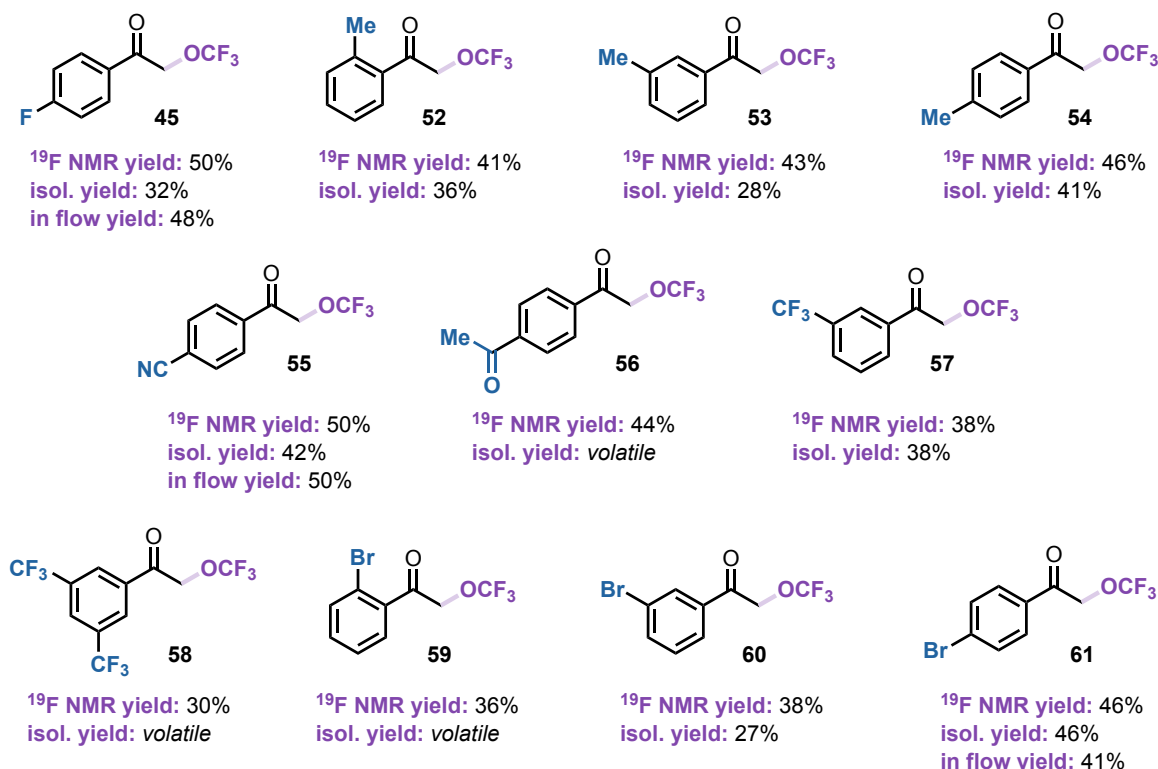
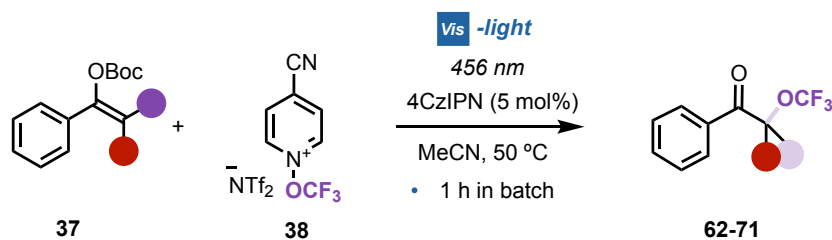


Table 4.9. - Reaction scope when using aryl substituted substrates.

It is worth noting that this mild photoredox-catalyzed protocol is not limited to terminal enol carbonates, and that trifluoromethoxylated ketones (Table 4.10, **62-63**) bearing a methyl, or benzyl group at the α position can also be prepared. We then turned our attention to cyclic ketones. Thus, 1-Indanone-derived enol carbonates (**64-65**) and benzosuberone (**66**) were also trifluoromethoxylated under our conditions.

Synthetically appealing difluorinated enol carbonates were also investigated. Remarkably, the unprecedented perfluoroalkylated ketones **67** and **68** were easily obtained. We then evaluate the use of challenging enol carbonates derived from aliphatic ketones and enones. We were pleased to see that the intended trifluoromethoxylated ketones (**69-71**) were still successfully produced, in spite of a less important stabilization of the corresponding radical intermediate. Noteworthy, **70** and **71** were formed as single regioisomers despite the presence of two conjugated double bonds.



— Reaction scope with α -substituted enol carbonates

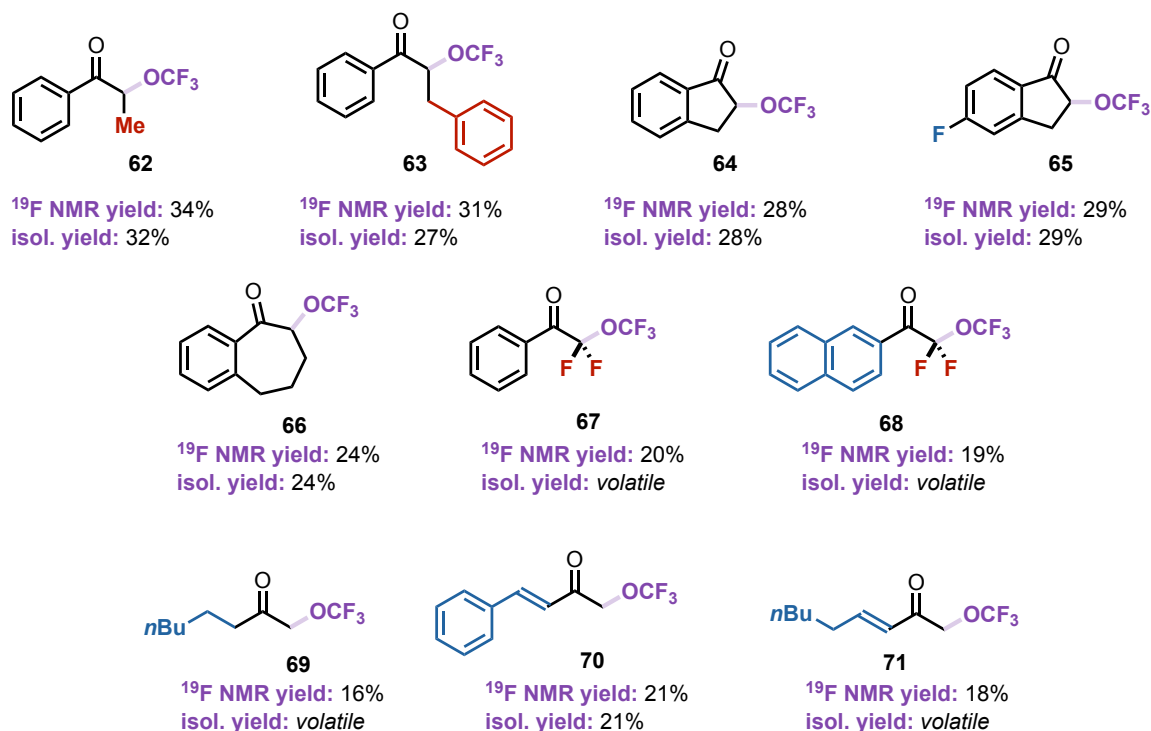
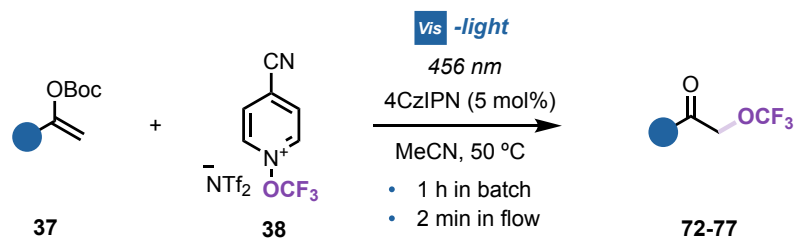


Table 4.10. - Reaction scope when using α -substituted enol carbonates.

We next tested the versatility of the developed method for the mild late stage trifluoromethoxylation of biorelevant targets (Table 4.11). To our delight, α -OCF₃ ketones **72-74** derived from fixolide, Musk ketone and Celestolide were readily obtained. Remarkably, even the structurally complex bioactive natural products α -ionone, and pregnenolone participated in the developed trifluoromethoxylation process although with inferior results (**75-76**). Despite the presence of several double bonds, full chemoselectivity was observed in all these reactions, while preserving the fragile nature of these complex natural scaffolds. Encouraged by these results, we attempted the installation of the OCF₃ fragment into the testosterone scaffold. In this case, two conjugated double bonds are present in the starting material, possibly leading to the formation of two diverse regioisomers (α - vs γ -OCF₃). We were pleased to see that the trifluoromethoxylation occurred selectively at the vinylogous γ -position, furnishing **77** exclusively, in 11% isolated yield.



— Reaction scope with natural products and drugs

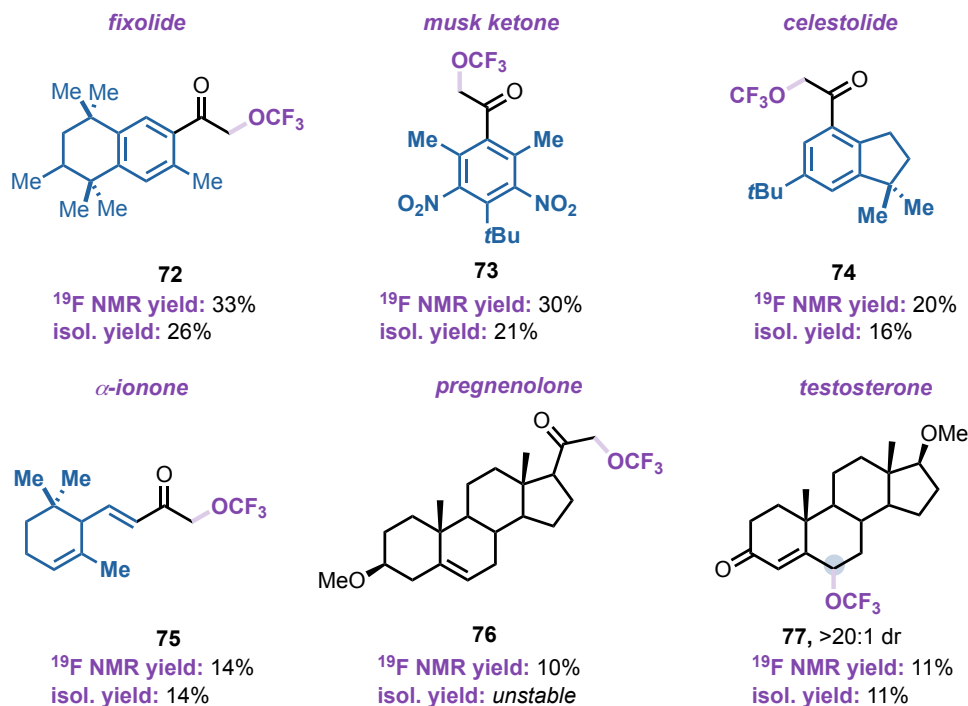


Table 4.11. - Reaction scope when using biorelevant enol carbonates.

Limitations

The method shown in this section, represents the first α -trifluoromethoxylation of ketones, which has been an important challenge over the years in organofluorine chemistry. Nevertheless, the transformation is far from solving all the issues related to generality, efficiency and ease of preparation of trifluoromethoxylated compounds (Figure 4.58).

— limitations of the method

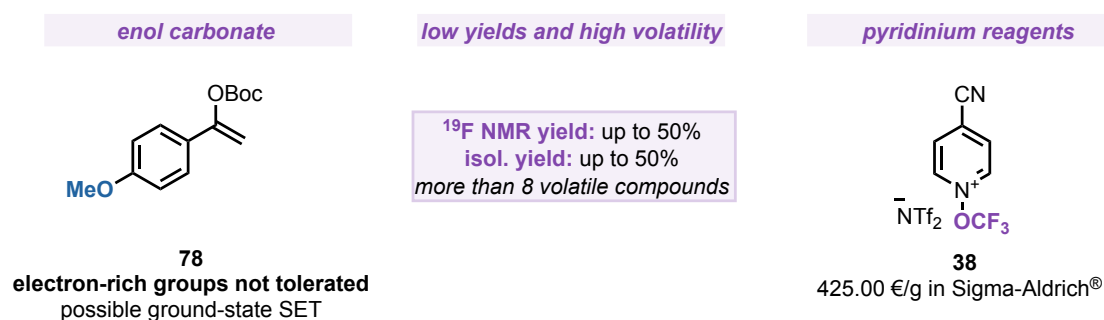


Figure 4.58. - Main limitations of the method presented in this section.

- i)* On the one hand, enol carbonates bearing electron-rich substituents in the aromatic ring are not tolerated (such as **78** in Figure 4.58). This fact can derive from the use of a good oxidant (pyridinium reagent) in the presence of easy to oxidize reagents. Hence, ground-state reactivity can take place, degrading the OCF₃ reagent and preventing radical-chain propagation processes.
- ii)* On the other hand, the reaction yields are low to moderate mainly due to the high volatility of the formed products. However, these yields are comparable to the ones obtained for the direct addition of the OCF₃ fragment to aryl groups.⁵²
- iii)* Finally, the use of such pyridinium reagents is still expensive in 2021.⁵⁷ Nonetheless, I foresee a bright future for improved versions of this type of reagents. Thus, the determination of radical chain-propagation mechanisms could pave the way to upgraded versions of this type of pyridiniums.

4.2.5 Conclusions

In conclusion, a mild and selective visible-light method for the α -trifluoromethoxylation of ketones has been described in this section. The process uses a commercially available trifluoromethoxylating reagent, an organic photocatalyst and a wide range of structurally diverse enol carbonates. Mechanistic investigations revealed that a radical chain mechanism is essential to access the desired trifluoromethoxylated products in useful synthetic yields. The easy in-flow upscaling of the products make of this methodology an unprecedented tool for the incorporation of the OCF₃ fragment into synthetically and biologically relevant targets.

⁵⁷ Sigma-Aldrich® price on the 7th of September of 2021 = 425.00€/g

4.2.6 Experimental Section

The NMR spectra were recorded on Bruker 400 Avance III HD equipped with a BBI-z grad probe head 5mm and Bruker 500 Avance III equipped with a BBI-ATM-z grad probehead 5mm. The chemical shifts (δ) for ^1H and ^{13}C are given in ppm relative to residual signals of the solvents (CHCl_3 @ 7.26 ppm ^1H NMR, 77.16 ppm ^{13}C NMR). Coupling constants are given in Hz. The following abbreviations are used to indicate the multiplicity: s, singlet; d, doublet; t, triplet; q, quartet; m, multiplet; bs, broad signal. NMR yields were calculated by using trichloroethylene as internal standard.

The ^1H , ^{13}C and ^{19}F NMR spectra are available in literature free of charge.⁵⁸

High-Resolution Mass Spectra (HRMS) were obtained using Waters GCT gas chromatograph coupled with a time-of-flight mass spectrometer (GC/MS-TOF) with electron ionization (EI).

Chromatographic purification of products was accomplished using flash chromatography on silica gel (SiO_2 , 0.04-0.063 mm) purchased from Machery-Nagel, with the indicated solvent system according to the standard techniques. Thin-layer chromatography (TLC) analysis was performed on pre-coated Merck TLC plates (silica gel 60 GF254, 0.25 mm). Visualization of the developed chromatography was performed by checking UV absorbance (254nm) as well as with aqueous ceric ammonium molybdate and potassium permanganate solutions. Organic solutions were concentrated under reduced pressure on a Büchi rotary evaporator.

Steady-state absorption spectroscopy studies have been performed at room temperature on a Varian Cary 1000 UV-Vis double beam spectrophotometer; 10 mm path length Hellma Analytics 100 QS quartz cuvettes have been used.

The diverse reaction set up images and mechanistic investigations are available free of charge in literature.⁵⁸

⁵⁸ Duhaill, T.; Bortolato, T.; Mateos, J.; Anselmi, E.; Jelier, B.; Togni, A.; Magnier, E.; Dagousset, G.; Dell'Amico, L. *Radical α -Trifluoromethoxylation of Ketones under Batch and Flow Conditions by Means of Organic Photoredox Catalysis*. *Org. Lett.* **2021**, *23*, 7088 - 7093.

Light sources emission spectra

The following spectra were recorded using an AvaSpec ULS3648 high-resolution fiber-optic spectrometer which was placed at a fixed distance of 0.5 cm from the light source.

(more info at: <https://www.avantes.com/products/spectrometers/starline/item/209-avaspec-uls3648-high-resolution-spectrometer>).

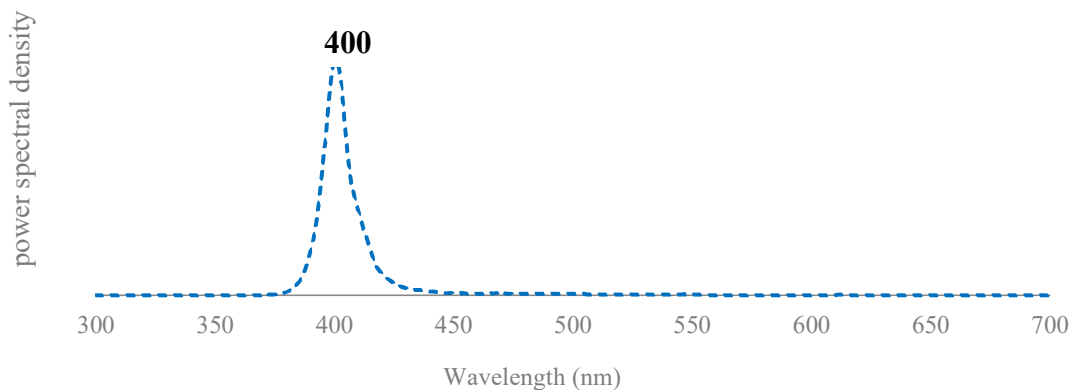


Figure 4.59. - Emission spectra of the 400 nm LED strips used in this section.

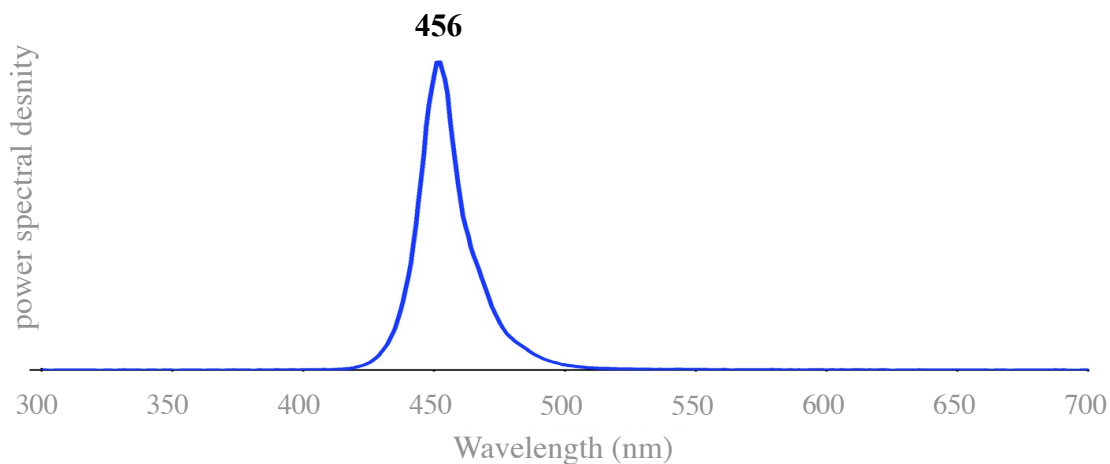
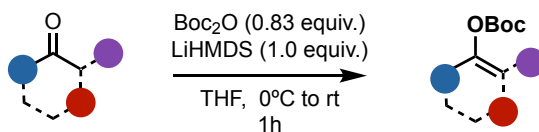


Figure 4.60. - Emission spectra of the 456 nm LEDs used in this study.

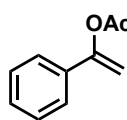
General procedures for the synthesis of starting materials

General procedure A



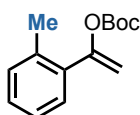
A round-bottomed flask was charged with the required ketone (3.2 mmol, 1.2 equiv.) and suspended in THF (5 mL, 0.6M) at 0°C under argon atmosphere. LiHMDS (1.06 M in THF, 3.0 mL, 1.2 equiv.) was added at once to this suspension, which was then stirred for 5 mins at 0°C . Boc_2O (600 μL , 2.6 mmol, 1 equiv.) was then added and the reaction medium was stirred for 1h at room temperature. The resulting mixture was then quenched with water (20 mL) and extracted with CH_2Cl_2 (3x20mL). The organic phases were then dried over MgSO_4 and concentrated under vacuum. Corresponding enol carbonates were isolated by column chromatography on silica gel (Pentane/EtOAc 95/5).

1-(4-fluorophenyl)ethenyl acetate (43)



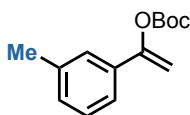
1-(4-fluorophenyl)ethenyl acetate **1a** was synthesized according to a procedure reported in the literature. The spectral data matched with those reported in the literature.

tert-butyl (1-(o-tolyl)vinyl) carbonate (44b)



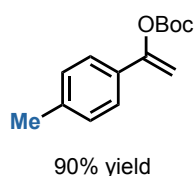
^1H NMR (300 MHz, CDCl_3) δ 7.40 (d, $J = 7.0$ Hz, 1H), 7.29 – 7.14 (m, 3H), 5.25 (s, 1H), 4.97 (s, 1H), 2.44 (s, 3H), 1.44 (s, 9H) ppm. **^{13}C NMR (75 MHz, CDCl_3)** δ 154.1, 151.1, 136.0, 135.2, 130.6, 129.0, 128.8, 125.7, 104.9 (s, C=CH₂), 83.1 (s, 1C, O-C-(CH₃)₃), 27.7 (s, 3C, C-(CH₃)₃), 20.5 ppm. **HRMS (ASAP +)** Calcd for $\text{C}_{14}\text{H}_{18}\text{O}_3\text{Na}^+$ $[\text{M} + \text{Na}]^+$: 257.1148. Found: 257.1156.

tert-butyl (1-(m-tolyl)vinyl) carbonate (44c)



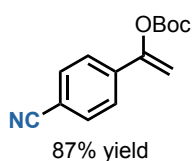
^1H NMR (300 MHz, CDCl_3) δ 7.35 (d, $J = 7.6$ Hz, 2H), 7.28 (t, $J = 7.6$ Hz, 1H), 7.18 (d, $J = 7.5$ Hz, 1H), 5.43 (d, $J = 2.2$ Hz, 1H), 5.12 (d, $J = 2.3$ Hz, 1H), 2.40 (s, 3H), 1.55 (s, 9H) ppm. **^{13}C NMR (75 MHz, CDCl_3)** δ 153.6, 151.5, 138.2, 134.4, 129.8, 128.5, 125.6, 122.0, 101.4 (s, C=CH₂), 83.2 (s, 1C, O-C-(CH₃)₃), 27.7 (s, 3C, C-(CH₃)₃), 21.5 ppm. **HRMS (ASAP +)** Calcd for $\text{C}_{14}\text{H}_{18}\text{O}_3\text{Na}^+$ $[\text{M} + \text{Na}]^+$: 257.1148. Found: 257.1154.

tert-butyl (1-(*p*-tolyl)vinyl) carbonate (44d)



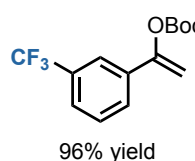
$^1\text{H NMR}$ (300 MHz, CDCl_3) δ 7.40 (d, $J = 8.5$ Hz, 2H), 7.17 (d, $J = 8.1$ Hz, 2H), 5.36 (d, $J = 2.4$ Hz, 1H), 5.04 (d, $J = 2.5$ Hz, 1H), 2.35 (s, 3H), 1.50 (s, 9H) ppm. $^{13}\text{C NMR}$ (75 MHz, CDCl_3) δ 153.5, 151.6, 139.1, 131.7, 129.4, 124.9, 100.9 (s, $\text{C}=\text{CH}_2$), 83.3 (s, 1C, O-C-(CH_3) $_3$), 27.8 (s, 3C, C-(CH_3) $_3$), 21.4 ppm. **HRMS (ASAP +)** Calcd for $\text{C}_{14}\text{H}_{18}\text{O}_3\text{Na}^+$ [$\text{M} + \text{Na}$] $^+$: 257.1148. Found: 257.1153.

tert-butyl (1-(4-cyanophenyl)vinyl) carbonate (44e)



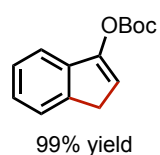
$^1\text{H NMR}$ (300 MHz, CDCl_3) δ 7.66 (d, $J = 8.1$ Hz, 2H), 7.59 (d, $J = 8.3$ Hz, 2H), 5.53 (s, 1H), 5.28 (s, 1H), 1.50 (s, 9H) ppm. $^{13}\text{C NMR}$ (75 MHz, CDCl_3) δ 151.8, 151.2, 139.0, 132.6, 125.6, 118.6, 112.6, 105.0 ($\text{C}=\text{CH}_2$), 84.2 (O-C-(CH_3) $_3$), 27.8 (C-(CH_3) $_3$) ppm. **MP** 59-61°C. **HRMS (ASAP +)** Calcd for $\text{C}_{14}\text{H}_{16}\text{NO}_3^+$ [$\text{M} + \text{H}$] $^+$: 246.1125. Found: 246.1119.

tert-butyl (1-(3-(trifluoromethyl)phenyl)vinyl) carbonate (44f)



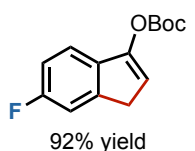
$^1\text{H NMR}$ (300 MHz, CDCl_3) δ 7.74 (s, 1H), 7.67 (d, $J = 8.0$ Hz, 1H), 7.57 (d, $J = 7.9$ Hz, 1H), 7.45 (t, $J = 7.8$ Hz, 1H), 5.47 (s, 1H), 5.20 (s, 1H), 1.49 (s, 5H) ppm. $^{13}\text{C NMR}$ (75 MHz, CDCl_3) δ 152.1, 151.3, 135.5, 131.2 (q, $J = 32.5$ Hz), 129.2, 128.2, 125.6 (q, $J = 3.8$ Hz), 124.0 (q, $J = 272.3$ Hz, CF_3), 121.7 (q, $J = 3.9$ Hz), 103.1 (s, $\text{C}=\text{CH}_2$), 83.8 (s, 1C, O-C-(CH_3) $_3$), 27.5 (s, 3C, C-(CH_3) $_3$) ppm. $^{19}\text{F NMR}$ (188 MHz, CDCl_3) δ -63.4 ppm. **HRMS (ASAP +)** Calcd for $\text{C}_{14}\text{H}_{16}\text{F}_3\text{O}_3^+$ [$\text{M} + \text{H}$] $^+$: 289.1046. Found: 289.1060.

tert-butyl 1H-inden-3-yl carbonate (44g)



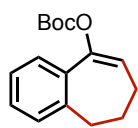
$^1\text{H NMR}$ (300 MHz, CDCl_3) δ 7.45 (dd, $J = 15.5, 7.3$ Hz, 2H), 7.39 – 7.27 (m, 2H), 6.34 (s, 1H), 3.44 (s, 2H), 1.62 (s, 9H) ppm. $^{13}\text{C NMR}$ (75 MHz, CDCl_3) δ 150.9, 149.6, 142.0, 139.0, 126.4, 125.8, 124.2, 118.3, 114.6, 83.7 (s, 1C, O-C-(CH_3) $_3$), 34.9, 27.8 (s, 3C, C-(CH_3) $_3$) ppm.

tert-butyl (6-fluoro-1H-inden-3-yl) carbonate (44h)



$^1\text{H NMR}$ (300 MHz, CDCl_3) δ 7.34 – 7.25 (m, 3H), 7.15 (d, $J = 8.8$ Hz, 1H), 7.03 (t, $J = 8.9$ Hz, 1H), 6.28 (s, 1H), 3.39 (s, 2H), 1.59 (s, 9H) ppm. $^{13}\text{C NMR}$ (75 MHz, CDCl_3) δ 163.8, 160.5, 150.8, 148.9, 144.0 (d, $J = 8.8$ Hz, 1C), 135.0 (d, $J = 2.2$ Hz, 1C), 119.1 (d, $J = 8.9$ Hz, 1C), 114.0 (d, $J = 3.8$ Hz, 1C), 112.70 (dd, $J = 121.1, 23.3$ Hz), 83.8 (s, 1C, O-C-(CH_3) $_3$), 34.9 (d, $J = 2.4$ Hz, 1C), 27.8 (s, 3C, C-(CH_3) $_3$) ppm. $^{19}\text{F NMR}$ (188 MHz, CDCl_3) δ -117.84 (td, $J = 9.0, 5.0$ Hz, 1F) ppm.

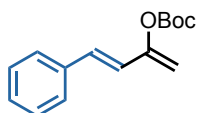
tert-butyl (6,7-dihydro-5H-benzo[7]annulen-9-yl) carbonate (44i)



92% yield

$^1\text{H NMR}$ (300 MHz, CDCl_3) δ 7.47 – 7.34 (m, 1H), 7.27 – 7.16 (m, 3H), 5.93 (t, $J = 6.1$ Hz, 1H), 2.83 (t, $J = 6.0$ Hz, 2H), 2.18 (q, $J = 6.5$ Hz, 2H), 2.13 – 7.02 (m, 2H), 1.47 (s, 9H) ppm. $^{13}\text{C NMR}$ (75 MHz, CDCl_3) δ 152.3, 146.2, 141.8, 134.5, 129.2, 128.2, 126.2, 125.3, 119.3, 82.9 (s, 1C, O-C-(CH_3)₃), 33.8, 31.1, 27.8 (s, 3C, C-(CH_3)₃), 25.3 ppm.

(E)-tert-butyl (4-phenylbuta-1,3-dien-2-yl) carbonate (44j)



63% yield

Stored at -20°C , decomposition was noticed after few days in the fridge.

$^1\text{H NMR}$ (300 MHz, CDCl_3) δ 7.44 (d, $J = 7.5$ Hz, 2H), 7.40 – 7.27 (m, 3H), 6.70 (dd, $J = 16.1, 11.3$ Hz, 2H), 5.10 (d, $J = 8.7$ Hz, 2H), 1.58 (s, 9H) ppm. $^{13}\text{C NMR}$ (75 MHz, CDCl_3) δ 152.3, 136.2, 130.1, 128.8, 128.4, 127.0, 122.6, 105.7 (s, C= CH_2), 83.4 (s, 1C, O-C-(CH_3)₃), 27.8 (s, 3C, C-(CH_3)₃) ppm.

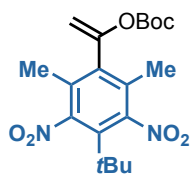
(E)-tert-butyl nona-1,3-dien-2-yl carbonate (44k)



99% yield

$^1\text{H NMR}$ (300 MHz, CDCl_3) δ 5.99 – 5.78 (m, 2H), 4.83 (s, 2H), 2.10 (q, $J = 7.0$ Hz, 2H), 1.52 (s, 9H), 1.40 (t, $J = 7.0$ Hz, 2H), 1.29 (s, 4H), 0.92 – 0.82 (t, $J = 6.7$ Hz, 3H) ppm. $^{13}\text{C NMR}$ (75 MHz, CDCl_3) δ 152.2, 151.4, 132.9, 124.0, 102.8 (s, C= CH_2), 82.8 (s, 1C, O-C-(CH_3)₃), 32.2, 31.3, 28.6, 27.6 (s, 3C, C-(CH_3)₃), 22.5, 14.0 ppm. **HRMS (ASAP +)** Calcd for $\text{C}_{14}\text{H}_{24}\text{NaO}_3^+$ [M + Na]⁺: 263,1613. Found: 263,1618.

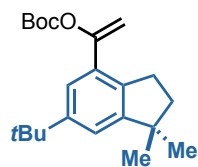
tert-butyl (1-(4-(tert-butyl)-2,6-dimethyl-3,5-dinitrophenyl)vinyl) carbonate (44l)



99% yield

$^1\text{H NMR}$ (300 MHz, CDCl_3) δ 5.56 (s, 1H), 4.94 (s, 1H), 2.28 (s, 6H), 1.48 (s, 9H), 1.44 (s, 9H) ppm. $^{13}\text{C NMR}$ (75 MHz, CDCl_3) δ 150.4, 148.6, 136.8, 131.9, 131.8, 108.2 (s, C= CH_2), 84.2 (s, 1C, O-C-(CH_3)₃), 37.5, 30.5, 27.7 (s, 3C, C-(CH_3)₃), 16.1 ppm. **HRMS (ASAP +)** Calcd for $\text{C}_{19}\text{H}_{27}\text{N}_2\text{O}_7^+$ [M + H]⁺: 395.1813. Found: 395.1813.

***tert*-butyl (1-(6-(*tert*-butyl)-1,1-dimethyl-2,3-dihydro-1H-inden-4-yl)vinyl) carbonate (44m)**

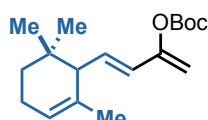


70% yield

$^1\text{H NMR}$ (300 MHz, CDCl_3) δ 7.28 (s, 1H), 7.14 (s, 1H), 5.16 (d, $J = 9.7$ Hz, 2H), 2.96 (t, $J = 7.1$ Hz, 2H), 1.93 (t, $J = 7.2$ Hz, 2H), 1.45 (s, 9H), 1.32 (s, 9H), 1.26 (s, 6H) ppm. $^{13}\text{C NMR}$ (75 MHz, CDCl_3) δ 153.9, 153.5, 151.4, 150.0, 137.3, 130.7, 121.5, 119.6, 103.8 (s, $\text{C}=\text{CH}_2$), 83.1 (s, 1C, $\text{O}-\text{C}-(\text{CH}_3)_3$), 43.9, 41.6, 34.8, 31.7, 30.1, 28.8, 27.8 (s, 3C, $\text{C}-(\text{CH}_3)_3$) ppm.

HRMS (ASAP +) Calcd for $\text{C}_{34}\text{H}_{50}\text{O}_2^+ [2(\text{M} - \text{Boc} + \text{H}) + \text{H}]^+$: 489.3727. Found: 489.3726.

(*E*)-*tert*-butyl (4-(2,6,6-trimethylcyclohex-2-en-1-yl)buta-1,3-dien-2-yl) carbonate (44n)

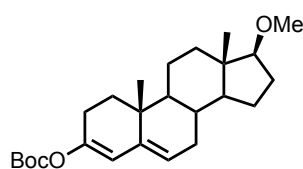


72% yield

$^1\text{H NMR}$ (300 MHz, CDCl_3) δ 5.91 (d, $J = 15.6$ Hz, 1H), 5.64 (dd, $J = 15.4, 9.4$ Hz, 1H), 5.34 (d, $J = 36.8$ Hz, 1H), 4.84 (s, 2H), 2.16 (d, $J = 9.5$ Hz, 1H), 1.98 (s, 2H), 1.55 (s, 3H), 1.49 (s, 9H), 1.42 – 1.32 (m, 1H), 1.23 – 1.09 (m, 1H), 0.88 (s, 3H), 0.80 (s, 3H) ppm. $^{13}\text{C NMR}$ (75 MHz, CDCl_3) δ 152.2, 151.4, 133.8, 133.6, 125.2, 121.5, 103.3 (s, $\text{C}=\text{CH}_2$), 82.9 (s, 1C, $\text{O}-\text{C}-(\text{CH}_3)_3$), 54.1, 32.6, 31.7, 27.7 (s, 3C, $\text{C}-(\text{CH}_3)_3$), 27.5, 27.1, 23.1, 23.0 ppm.

HRMS (ASAP +) Calcd for $\text{C}_{13}\text{H}_{21}\text{O}^+ [\text{M} - \text{Boc} + \text{H}]^+$: 193.1587. Found: 193.1586.

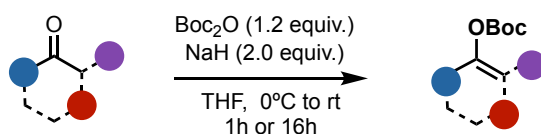
***tert*-butyl (-17-methoxy-10,13-dimethyl-dodecahydro-1H-cyclopenta[*a*]phenanthren-3-yl) carbonate (44o)**



76% yield

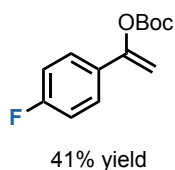
$^1\text{H NMR}$ (300 MHz, CDCl_3) δ 5.38 (s, 1H), 5.25 (s, 1H), 3.33 (s, 3H), 3.20 (t, $J = 8.3$, 1H), 2.23 (t, $J = 7.7$ Hz, 4H), 2.05 – 1.85 (m, 2H), 1.74 – 1.55 (m, 2H), 1.49 (d, 9H), 1.46 – 1.35 (m, 4H), 1.33 – 1.07 (m, 3H), 1.00 – 0.90 (m, 5H), 0.77 (s, 3H) ppm. $^{13}\text{C NMR}$ (75 MHz, CDCl_3) δ 152.0, 149.5, 145.1, 115.6, 107.2, 90.8, 82.9

(s, 1C, $\text{O}-\text{C}-(\text{CH}_3)_3$), 58.0, 54.7, 50.9, 43.0, 38.1, 38.0, 37.2, 36.2, 31.2, 30.8, 27.9, 27.8 (s, 3C, $\text{C}-(\text{CH}_3)_3$), 23.6, 21.4, 17.5, 11.6 ppm. **HRMS (ASAP +)** Calcd for $\text{C}_{25}\text{H}_{38}\text{O}_4\text{Na}^+ [\text{M} + \text{Na}]^+$: 425.2662. Found: 425.2677.



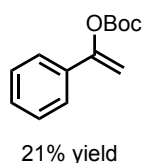
A round-bottomed flask was charged with the required ketone (5 mmol, 1 equiv.) and dissolved in dry THF (5 mL, 1M) at 0°C under nitrogen atmosphere. NaH (60% dispersion in mineral oil, 400 mg, 10 mmol, 2 equiv.) was added portionwise to the reaction mixture, which was then stirred for 15 mins at 0°C. Boc₂O (1.38 mL, 6 mmol, 1.2 equiv.) was then added dropwise and the reaction mixture was stirred for 16h at room temperature. The resulting mixture was then quenched with water (20 mL) and DMAP (61 mg, 0.5 mmol, 0.1 equiv.) was added and the reaction mixture stirred for 2 hours. The crude was then diluted with CH₂Cl₂ (50 mL) and washed with brine (3x20 mL). The organic phase was then dried over MgSO₄ and concentrated under vacuum. Corresponding enol carbonates were isolated by column chromatography on silica gel with the indicated eluent system.

***tert*-butyl (1-(4-fluorophenyl)vinyl) carbonate (44a)**



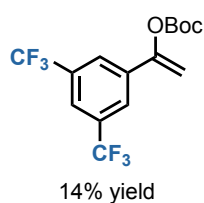
¹H NMR (500 MHz, CDCl₃) δ 7.50 – 7.44 (m, 2H), 7.06 – 7.00 (m, 2H), 5.32 (d, *J* = 2.4 Hz, 1H), 5.07 (d, *J* = 2.4 Hz, 1H), 1.49 (s, 9H) ppm. ¹³C NMR (126 MHz, CDCl₃) δ 163.2 (d, *J* = 248.7 Hz, C-F), 152.5, 151.4, 130.8 (d, *J* = 3.4 Hz), 126.9 (d, *J* = 8.2 Hz), 115.6 (d, *J* = 21.9 Hz), 101.4 (d, *J* = 1.7 Hz, C=CH₂), 83.4 (O-C-(CH₃)₃), 27.6 (C-(CH₃)₃) ppm. ¹⁹F NMR (188 MHz, ¹H decoupled, CDCl₃) δ -112.84 ppm. HRMS (ESI+) Calcd. for C₈H₆F⁺ [M - OBoc]⁺: 121.0448. Found: 121.0409.

***tert*-butyl (1-phenylvinyl) carbonate (44p)**



The spectral data matched with those reported in the literature.

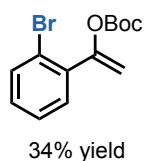
1-(3,5-bis(trifluoromethyl)phenyl)vinyl *tert*-butyl carbonate (44q)



$^1\text{H NMR}$ (400 MHz, CDCl_3) δ 7.92 (s, 2H), 7.84 (s, 1H), 5.58 (d, $J = 2.9$ Hz, 1H), 5.34 (d, $J = 2.9$ Hz, 1H), 1.51 (s, 9H) ppm. $^{13}\text{C NMR}$ (101 MHz, CDCl_3) δ 151.1, 150.8, 136.9, 132.3 (q, $J = 33.5$ Hz, C-CF₃), 125.1 (d, $J = 2.7$ Hz), 123.2 (q, $J = 272.9$ Hz, C-CF₃), 122.6 (p, $J = 7.1, 3.7, 3.4$ Hz), 104.9 (C=CH₂), 84.5 (O-C-(CH₃)₃), 27.7 (C-(CH₃)₃) ppm. $^{19}\text{F NMR}$ (188

MHz, ^1H decoupled, CDCl_3) δ -63.6 ppm. HRMS (ASAP +) Calcd for C₁₀H₇F₆O⁺ [M - Boc + H]⁺: 257.0396. Found: 257.0390.

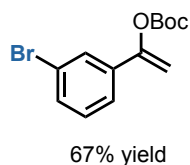
1-(2-bromophenyl)vinyl *tert*-butyl carbonate (44r)



$^1\text{H NMR}$ (500 MHz, CDCl_3) δ 7.57 (dd, $J = 8.0, 1.2$ Hz, 1H), 7.44 (dd, $J = 7.7, 1.7$ Hz, 1H), 7.29 (td, $J = 7.5, 1.2$ Hz, 1H), 7.17 (ddd, $J = 8.0, 7.4, 1.7$ Hz, 1H), 5.32 (d, $J = 2.0$ Hz, 1H), 5.16 (d, $J = 2.0$ Hz, 1H), 1.44 (s, 9H) ppm. $^{13}\text{C NMR}$ (126 MHz, CDCl_3) δ 152.4, 150.8, 136.4, 133.4, 130.8, 130.1, 127.3, 121.5,

106.3 (C=CH₂), 83.3 (O-C-(CH₃)₃), 27.7 (C-(CH₃)₃) ppm. HRMS (ESI+) Calcd. for C₈H₆Br⁺ [M - OBoc]⁺: 180.9647. Found: 180.9623.

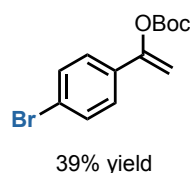
1-(3-bromophenyl)vinyl *tert*-butyl carbonate (44s)



$^1\text{H NMR}$ (500 MHz, CDCl_3) δ 7.64 (t, $J = 1.9$ Hz, 1H), 7.45 (ddd, $J = 7.9, 2.0, 1.0$ Hz, 1H), 7.42 (ddd, $J = 7.9, 1.8, 1.0$ Hz, 1H), 7.21 (t, $J = 7.9$ Hz, 1H), 5.41 (d, $J = 2.5$ Hz, 1H), 5.14 (d, $J = 2.5$ Hz, 1H), 1.50 (s, 9H) ppm.

$^{13}\text{C NMR}$ (126 MHz, CDCl_3) δ 152.0, 151.3, 136.6, 132.0, 130.1, 128.1, 123.5, 122.8, 102.9 (C=CH₂), 83.7 (O-C-(CH₃)₃), 27.7 (C-(CH₃)₃) ppm. HRMS (ASAP +) Calcd for C₈H₈BrO⁺ [M - Boc + H]⁺: 198.9753. Found: 198.9759.

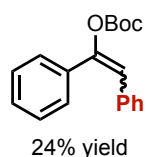
1-(4-bromophenyl)vinyl *tert*-butyl carbonate (44t)



$^1\text{H NMR}$ (500 MHz, CDCl_3) δ 7.48 (d, $J = 8.7$ Hz, 2H), 7.36 (d, $J = 8.7$ Hz, 2H), 5.40 (d, $J = 2.4$ Hz, 1H), 5.12 (d, $J = 2.4$ Hz, 1H), 1.50 (s, 9H) ppm.

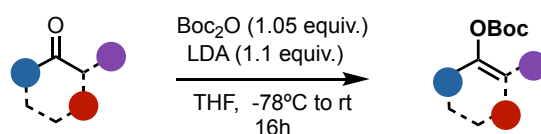
$^{13}\text{C NMR}$ (126 MHz, CDCl_3) δ 152.5, 151.4, 133.6, 131.8, 126.6, 123.2, 102.4 (C=CH₂), 83.7 (O-C-(CH₃)₃), 27.8 (C-(CH₃)₃) ppm. HRMS (ESI+) Calcd. for C₁₃H₁₅BrO₃Na⁺ [M + Na]⁺: 321.0102. Found: 321.0110.

tert-butyl (1-phenylprop-1-en-1-yl) carbonate (44w)



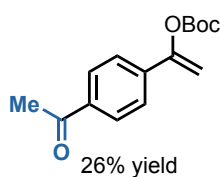
$^1\text{H NMR}$ (500 MHz, CDCl_3) δ 7.37 – 7.32 (m, 1H), 7.27 – 7.21 (m, 2H), 7.20 – 7.15 (m, 1H), 5.75 (q, $J = 7.0$ Hz, 1H), 1.69 (d, $J = 7.0$ Hz, 3H), 1.42 (s, 9H) ppm. $^{13}\text{C NMR}$ (126 MHz, CDCl_3) δ 151.2, 147.4, 135.4, 128.6, 128.1, 124.4, 112.7 (C=CHR), 83.1 (O-C-(CH₃)₃), 27.8 (C-(CH₃)₃), 11.4 ppm. HRMS

(ESI+) Calcd. for C₉H₉⁺ [M - OBoc]⁺: 117.0699. Found: 117.0701.



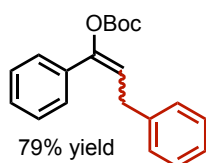
A flame-dried, nitrogen flushed round-bottomed flask was charged with the required ketone (5 mmol, 1 equiv.) and dissolved in dry THF (5 mL, 1M) under nitrogen atmosphere. A freshly prepared solution of LDA (0.5 M in THF, 11 mL, 5.5 mmol, 1.1 equiv.) was dropwise at -78°C to the reaction mixture, which was then stirred for 90 minutes at -78°C . Boc_2O (1.21 mL, 5.25 mmol, 1.05 equiv.) was then added dropwise and the reaction medium was stirred for 30 minutes at -78°C and at room temperature for 16 hours. The resulting mixture was then quenched with water (20 mL), DMAP (61 mg, 0.5 mmol, 0.1 equiv.) was added and the resulting mixture stirred for 2 hours. The crude was then diluted with CH_2Cl_2 (50mL) and washed with brine (3x20 mL). The organic phase was then dried over MgSO_4 and concentrated under vacuum. Corresponding enol carbonates were isolated by column chromatography on silica gel with the indicated eluent system.

1-(4-acetylphenyl)vinyl *tert*-butyl carbonate (44x)



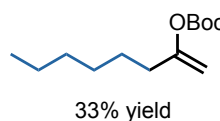
$^1\text{H NMR}$ (400 MHz, CDCl_3) δ 7.98 – 7.90 (m, 2H), 7.61 – 7.53 (m, 2H), 5.52 (d, $J = 2.5$ Hz, 1H), 5.22 (d, $J = 2.5$ Hz, 1H), 2.59 (s, 3H), 1.49 (s, 9H) ppm. $^{13}\text{C NMR}$ (101 MHz, CDCl_3) δ 197.4, 152.5, 151.3, 138.9, 137.2, 128.8, 125.1, 104.1 (C=CH₂), 83.8 (O-C-(CH₃)₃), 27.7 (C-(CH₃)₃), 26.7 ppm. **HRMS (ESI+)** Calcd. for $\text{C}_{15}\text{H}_{19}\text{O}_4\text{H}^+$ [$\text{M} + \text{H}$]⁺: 263.1278. Found: 263.1286.

tert-butyl (1,3-diphenylprop-1-en-1-yl) carbonate (44y)



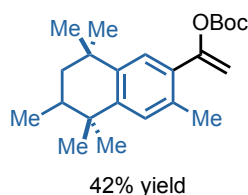
$^1\text{H NMR}$ (500 MHz, CDCl_3) δ 7.41 – 7.35 (m, 2H), 7.28 – 7.15 (m, 7H), 7.16 – 7.09 (m, 1H), 5.82 (t, $J = 7.5$ Hz, 1H), 3.48 (d, $J = 7.5$ Hz, 2H), 1.41 (s, 9H) ppm. $^{13}\text{C NMR}$ (126 MHz, CDCl_3) δ 151.3, 147.0, 139.8, 135.2, 128.7, 128.6, 128.6, 128.4, 126.4, 124.6, 116.8 (C=CHR), 83.4 (O-C-(CH₃)₃), 32.3, 27.7 (C-(CH₃)₃) ppm. **HRMS (ESI+)** Calcd. for $\text{C}_{15}\text{H}_{13}^+$ [$\text{M} - \text{OBoc}$]⁺: 193.1012. Found: 193.1002.

tert-butyl oct-1-en-2-yl carbonate (44z)



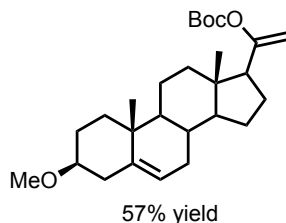
$^1\text{H NMR}$ (400 MHz, CDCl_3) δ 4.75 – 4.67 (m, 1H), 4.62 – 4.56 (m, 1H), 2.21 – 2.10 (m, 2H), 1.43 (s, 9H), 1.41 – 1.38 (m, 4H), 1.24 – 1.21 (m, 4H), 0.83 – 0.80 (m, 3H) ppm. $^{13}\text{C NMR}$ (101 MHz, CDCl_3) δ 156.6, 151.46, 100.4 (C=CH₂), 82.4 (O-C-(CH₃)₃), 33.1, 31.6, 28.6, 27.6 (C-(CH₃)₃), 26.4, 22.5, 14.0 ppm. **HRMS (ESI+)** Calcd. for $\text{C}_{13}\text{H}_{24}\text{O}_3\text{Na}^+$ [$\text{M} + \text{Na}$]⁺: 251.1618. Found: 251.1596.

tert-butyl 1-(3,5,5,6,8,8-hexamethyl-5,6,7,8-tetrahydronaphthalen-2-yl)vinyl carbonate (44aa)



$^1\text{H NMR}$ (500 MHz, CDCl_3) δ 7.29 (s, 1H), 7.15 (s, 1H), 5.21 (d, $J = 1.6$ Hz, 1H), 4.96 (d, $J = 1.6$ Hz, 1H), 2.39 (s, 3H), 1.85 (dq, $J = 13.5, 6.8, 2.6$ Hz, 1H), 1.61 (t, $J = 13.2$ Hz, 1H), 1.43 (s, 9H), 1.36 (dd, $J = 13.5, 2.6$ Hz, 1H), 1.31 (s, 3H), 1.27 (s, 3H), 1.23 (s, 3H), 1.06 (s, 3H), 0.98 (d, $J = 6.8$ Hz, 3H) ppm. $^{13}\text{C NMR}$ (126 MHz, CDCl_3) δ 153.9, 151.2, 146.8, 142.3, 132.8, 132.4, 129.3, 126.5, 104.3 ($\text{C}=\text{CH}_2$), 83.0 ($\text{O}-\text{C}-(\text{CH}_3)_3$), 43.8, 37.7, 34.7, 34.1, 32.5, 32.1, 28.7, 27.8 ($\text{C}-(\text{CH}_3)_3$), 25.0, 20.5, 17.0 ppm. **HRMS (ESI+)** Calcd. for $\text{C}_{18}\text{H}_{25}^+$ [$\text{M} - \text{OBoc}$] $^+$: 241.1951. Found: 241.1967.

tert-butyl (1-(3-methoxy-10,13-dimethyl-tetradecahydro-1H-cyclopenta[a]phenanthren-17-yl)vinyl carbonate (44ab)

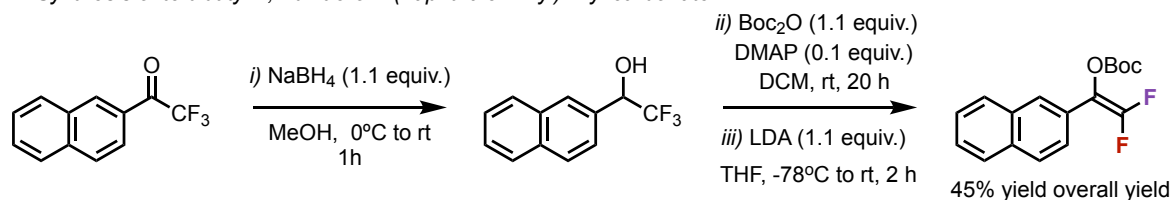


Pregnenolone methyl ether was synthesized according to a literature procedure. Spectral data matched with those reported in the literature.

$^1\text{H NMR}$ (500 MHz, CDCl_3) δ 5.34 (dt, $J = 5.4, 2.1$ Hz, 1H), 4.85 (dd, $J = 1.9, 1.0$ Hz, 1H), 4.74 (t, $J = 1.7$ Hz, 1H), 3.34 (s, 3H), 3.04 (tt, $J = 11.4, 4.6$ Hz, 1H), 2.43 – 2.31 (m, 2H), 2.19 – 2.10 (m, 1H), 2.02 – 1.94 (m, 2H), 1.93 – 1.81 (m, 2H), 1.74 – 1.64 (m, 2H), 1.58 – 1.50 (m, 2H), 1.49 (s, 9H), 1.45 – 1.35 (m, 2H), 1.25 (ddd, $J = 18.7, 9.0, 4.6$ Hz, 2H), 1.21 – 1.14 (m, 2H), 1.14 – 1.02 (m, 2H), 0.99 (s, 3H), 0.65 (s, 3H). $^{13}\text{C NMR}$ (126 MHz, CDCl_3) δ 157.6, 151.8, 141.1, 121.4, 101.8 ($\text{C}=\text{CH}_2$), 82.6 ($\text{O}-\text{C}-(\text{CH}_3)_3$), 80.4, 56.1, 55.7, 53.3, 50.3, 43.1, 38.8, 38.0, 37.3, 37.1, 32.3, 31.9, 28.1, 27.9 ($\text{C}-(\text{CH}_3)_3$), 24.9, 24.3, 21.1, 19.5, 12.7 ppm. **HRMS (ESI+)** Calcd. for $\text{C}_{27}\text{H}_{42}\text{O}_4\text{Na}^+$ [$\text{M} + \text{Na}$] $^+$: 453.2975. Found: 453.2980.

tert-butyl 2,2-difluoro-1-(naphthalen-2-yl)vinyl carbonate (44ac)

— Synthesis of tert-butyl 2,2-difluoro-1-(naphthalen-2-yl)vinyl carbonate



2,2,2-trifluoro-1-(naphthalen-2-yl)ethan-1-one was synthesized according to a reported literature procedure.^[8] The spectral data matched with those reported in the literature.

2,2,2-trifluoro-1-(naphthalen-2-yl)ethan-1-one (433 mg, 1.93 mmol, 1 equiv.) was dissolved in MeOH (5 mL, 0.4M) at 0°C. NaBH₄ (80 mg, 2.12 mmol, 1.1 equiv.) was then added portionwise and the reaction stirred for 1h at room temperature. The reaction was then cooled to 0°C, quenched with sat. NH₄Cl until gas evolution stopped and evaporated to dryness. The crude residue was diluted with DCM (20 mL) and washed with brine (3x 10 mL). The organic phase was then dried over MgSO₄ and concentrated under reduced pressure. The crude 2,2,2-trifluoro-1-(naphthalen-2-yl)ethan-1-ol product was used in the subsequent step without further purification.

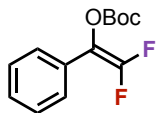
Crude 2,2,2-trifluoro-1-(naphthalen-2-yl)ethan-1-ol (340 mg) was dissolved in MeCN (7 mL) and DMAP (18.3 mg, 0.15 mmol) was added. Boc₂O (517 μL, 2.25 mmol) was then added dropwise and the reaction mixture stirred for 20h, after which time the mixture was concentrated under reduced pressure. The residue was filtered on silica using DCM as eluent and the eluted solution evaporated under reduced pressure. The crude tert-butyl (2,2,2-trifluoro-1-(naphthalen-2-yl)ethyl) carbonate product was used in the subsequent step without further purification.

To a solution of crude tert-butyl (2,2,2-trifluoro-1-(naphthalen-2-yl)ethyl) carbonate (485 mg) in dry THF (7 mL) at -78 °C was added dropwise a freshly prepared solution of LDA (0.7 M, 3.21 mL). After stirring for 1h at -78 °C, the reaction mixture was stirred for an additional 1 h at room temperature. The reaction mixture was then diluted with water (10 mL) and extracted with EtOAc (3 × 10 mL), dried over anhydrous MgSO₄, and the solvent evaporated to give a residue. Finally, the residue was purified by silica gel chromatography (hexane/EtOAc 97/3) to give tert-butyl 2,2-difluoro-1-(naphthalen-2-yl)vinyl carbonate **1t** in 45% yield over 3 steps (266 mg, 0.87 mmol).

¹H NMR (500 MHz, CDCl₃) δ 7.92 – 7.88 (m, 1H), 7.89 – 7.79 (m, 3H), 7.56 (dt, *J* = 8.7, 1.8 Hz, 1H), 7.54 – 7.47 (m, 2H), 1.53 (s, 9H) ppm. ¹³C NMR (126 MHz, CDCl₃) δ 155.2 (dd, *J* = 292.4, 290.5 Hz, (C=CF₂)), 151.0 (dd, *J* = 3.5, 2.3 Hz), 133.2 (d, *J* = 10.5 Hz), 128.6, 128.4, 127.8, 126.9, 126.9, 126.8, 126.8, 125.1 (t, *J* = 5.3 Hz), 122.9 (dd, *J* = 7.0, 2.3 Hz), 113.4 (dd, *J* = 38.8, 19.5 Hz, C=CF₂), 84.7 (O-C-(CH₃)₃), 27.7 (C-(CH₃)₃) ppm. ¹⁹F NMR

(188 MHz, CDCl₃) δ -92.4 (d, J = 46.6 Hz), -103.9 (d, J = 46.6 Hz) ppm. HRMS (ASAP +) Calcd for C₁₂H₉F₂O⁺ [M - Boc + H]⁺: 207.0616. Found: 207.0621.

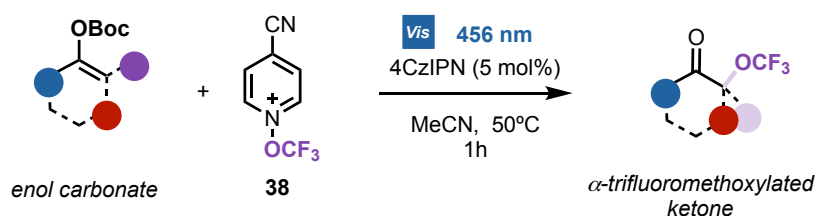
tert-butyl 2,2-difluoro-1-phenylvinyl carbonate (44ad)



tert-butyl 2,2-difluoro-1-phenylvinyl carbonate 1s was synthesized according to a procedure reported in the literature.

General procedures for the synthesis of α -trifluoromethoxylated ketones

Synthesis of α -trifluoromethoxylated ketones



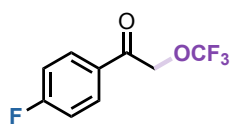
A sealable tube surrounded by blue LEDs with a watertight protection, purged with argon and equipped with a cap was charged with 4-cyano-1-(trifluoromethoxy)pyridin-1-ium bis((trifluoromethyl)sulfonyl)amide **38** (46.9 mg, 0.1 mmol, 1 equiv.), the desired enol carbonate (0.5 mmol, 5 equiv.) and 4CzIPN (3.9 mg, 0.005 mmol, 0.05 equiv.). Dry acetonitrile (10 mL, 0.01 M) was finally added and the reaction medium purged with argon again. The resulting mixture in the sealable tube was placed in a water bath and allowed to stir vigorously for 1h at 50°C under irradiation of the blue LEDs.

Depending on the substrate two different purification procedures were applied:

i) The crude was then concentrated under vacuum. α -trifluoromethoxylated ketones were isolated by preparative thin layer chromatography (PTLC).

ii) The crude reaction mixture was then quenched with sat. NaHCO₃ until gas evolution stopped, diluted with DCM (30 mL) and washed with brine (3x10 mL). The organic phase was dried over MgSO₄ and concentrated under vacuum. Corresponding alpha-trifluoromethoxylated ketones were isolated by column chromatography on silica gel.

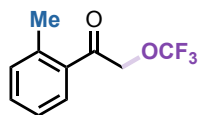
1-(4-fluorophenyl)-2-(trifluoromethoxy)ethanone (45)



32% yield

¹H NMR (300 MHz, CDCl₃) δ 8.02 – 7.89 (m, 1H), 7.19 (t, *J* = 8.4 Hz, 1H), 5.13 (s, 1H) ppm. **¹³C NMR (75 MHz, CDCl₃)** δ 188.9 (C=O), 166.5 (d, *J* = 257.2 Hz, C1), 130.9 (d, *J* = 9.5 Hz, C2), 130.4 (d, *J* = 3.1 Hz, C4), 121.8 (q, *J* = 256.6 Hz, ROCF₃), 116.48 (d, *J* = 22.2 Hz, C3), 68.3 (q, *J* = 2.9 Hz, RCH₂-OCF₃) ppm. **¹⁹F NMR (188 MHz, CDCl₃)** δ -61.56 (s, 3F), -102.88 (m, 1F) ppm. **HRMS (ASAP +)** Calcd for C₉H₇F₄O₂⁺ [M + H]⁺: 223.0377. Found: 223.0386.

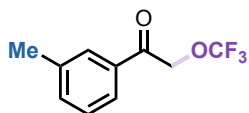
1-(*o*-tolyl)-2-(trifluoromethoxy)ethanone (52)



36% yield

¹H NMR (300 MHz, CDCl₃) δ 7.54 (d, *J* = 7.7 Hz, 1H), 7.46 (t, *J* = 7.6 Hz, 1H), 7.31 (d, *J* = 8.0 Hz, 2H), 5.04 (s, 2H), 2.54 (s, 3H) ppm. **¹³C NMR (75 MHz, CDCl₃)** δ 193.6, 139.7, 133.8, 132.8, 132.7, 128.3, 126.0, 121.8 (q, *J* = 256 Hz, ROCF₃), 69.3 (q, *J* = 2.9 Hz, RCH₂-OCF₃), 21.4 ppm. **¹⁹F NMR (188 MHz, CDCl₃)** δ -61.40 ppm. **HRMS (ASAP +)** Calcd for C₁₀H₁₀F₃O₂⁺ [M + H]⁺: 219.0627. Found: 219.0634.

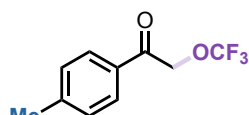
1-(*m*-tolyl)-2-(trifluoromethoxy)ethanone (53)



28% yield

¹H NMR (300 MHz, CDCl₃) δ 7.74 – 7.65 (m, 2H), 7.49 – 7.34 (m, 2H), 5.17 (s, 2H), 2.43 (s, 3H) ppm. **¹³C NMR (75 MHz, CDCl₃)** δ 190.4, 139.2, 135.2, 133.9, 129.0, 128.5, 125.2, 121.8 (q, *J* = 256.5 Hz, ROCF₃), 68.4 (q, *J* = 2.9 Hz, RCH₂-OCF₃), 21.5 ppm. **¹⁹F NMR (188 MHz, CDCl₃)** δ -61.41 ppm. **HRMS (ASAP +)** Calcd for C₁₀H₁₀F₃O₂⁺ [M + H]⁺: 219.0627. Found: 219.0625.

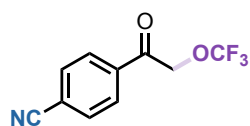
1-(*p*-tolyl)-2-(trifluoromethoxy)ethanone (54)



41% yield

¹H NMR (300 MHz, CDCl₃) δ 7.80 (d, *J* = 7.8 Hz, 2H), 7.30 (d, *J* = 7.8 Hz, 2H), 5.15 (s, 2H), 2.43 (s, 3H) ppm. **¹³C NMR (75 MHz, CDCl₃)** δ 189.9, 145.6, 131.4, 129.8, 128.2, 121.8 (q, *J* = 257 Hz, ROCF₃), 68.4 (q, *J* = 2.8 Hz, RCH₂-OCF₃), 21.9 ppm. **¹⁹F NMR (188 MHz, CDCl₃)** δ -61.46 ppm. **HRMS (ASAP +)** Calcd for C₁₀H₁₀F₃O₂⁺ [M + H]⁺: 219.0627. Found: 219.0627.

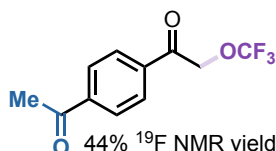
4-(2-(trifluoromethoxy)acetyl)benzonitrile (55)



27% yield

$^1\text{H NMR}$ (300 MHz, CDCl_3) δ 8.01 (d, $J = 7.8$ Hz, 2H), 7.82 (d, $J = 8.0$ Hz, 2H), 5.15 (s, 2H) ppm. $^{13}\text{C NMR}$ (75 MHz, CDCl_3) δ 189.6, 136.8, 133.0, 128.7, 121.7 (q, $J = 257.4$ Hz, ROCF_3), 117.8, 117.6, 68.5 (q, $J = 3.0$ Hz, $\text{RCH}_2\text{-OCF}_3$) ppm. $^{19}\text{F NMR}$ (188 MHz, CDCl_3) δ -61.63 ppm. HRMS (ASAP +) Calcd for $\text{C}_{10}\text{H}_7\text{F}_3\text{NO}_2^+$ [$\text{M} + \text{H}$] $^+$: 230.0423. Found: 230.0422.

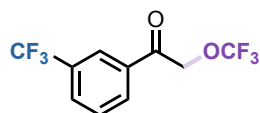
1-(4-acetylphenyl)-2-(trifluoromethoxy)ethan-1-one (56)



44% $^{19}\text{F NMR}$ yield

$^{19}\text{F NMR}$ (188 MHz, CDCl_3) δ -61.32 ppm.

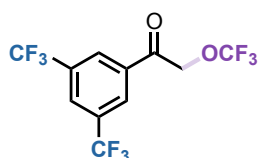
2-(trifluoromethoxy)-1-(3-(trifluoromethyl)phenyl)ethanone (57)



15% yield

$^1\text{H NMR}$ (300 MHz, CDCl_3) δ 8.16 (s, 1H), 8.10 (d, $J = 7.8$ Hz, 1H), 7.90 (d, $J = 7.7$ Hz, 1H), 7.68 (t, $J = 7.8$ Hz, 1H), 5.18 (s, 2H) ppm. $^{13}\text{C NMR}$ (75 MHz, CDCl_3) δ 189.4, 134.4, 131.9 (d, $J = 33$ Hz), 131.3, 130.8 (q, $J = 3.5$ Hz), 129.9, 125.1 (q, $J = 3.9$ Hz), 123.6 (d, $J = 272$ Hz) 121.7 (q, $J = 256$ Hz, ROCF_3), 68.4 (q, $J = 3.0$ Hz, $\text{RCH}_2\text{-OCF}_3$) ppm. $^{19}\text{F NMR}$ (188 MHz, CDCl_3) δ -61.59 (OCF_3), -63.44 (CF_3) ppm. HRMS (ASAP +) Calcd for $\text{C}_{10}\text{H}_7\text{F}_6\text{O}_2^+$ [$\text{M} + \text{H}$] $^+$: 273.0345. Found: 273.0341.

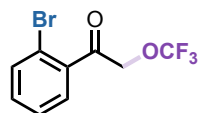
1-(3,5-bis(trifluoromethyl)phenyl)-2-(trifluoromethoxy)ethan-1-one (58)



13% $^{19}\text{F NMR}$ yield

$^{19}\text{F NMR}$ (188 MHz, CDCl_3) δ -61.23 (s, 3F), -63.36 (s, 6F) ppm.

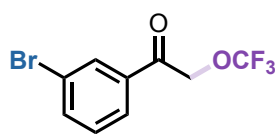
1-(2-bromophenyl)-2-(trifluoromethoxy)ethan-1-one (59)



18% yield

$^1\text{H NMR}$ (500 MHz, CDCl_3) δ 7.66 (d, $J = 7.8$ Hz, 1H), 7.51 – 7.33 (m, 3H), 5.05 (s, 2H) ppm. $^{13}\text{C NMR}$ (126 MHz, CDCl_3) δ 194.8, 137.8, 134.0, 133.1, 129.6, 127.8, 121.6 (q, $J = 256.8$ Hz, ROCF_3), 119.4, 69.8 (q, $J = 3.0$ Hz, $\text{RCH}_2\text{-OCF}_3$) ppm. $^{19}\text{F NMR}$ (188 MHz, CDCl_3) δ -61.53 ppm. HRMS (ASAP +) Calcd for $\text{C}_8\text{H}_5\text{BrF}_3\text{O}_2^+$ [$\text{M} + \text{H}$] $^+$: 282.9576. Found: 282.9580.

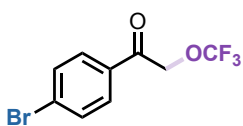
1-(3-bromophenyl)-2-(trifluoromethoxy)ethan-1-one (60)



27% yield

$^1\text{H NMR}$ (500 MHz, CDCl_3) δ 8.04 (t, $J = 1.8$ Hz, 1H), 7.83 (dt, $J = 7.8, 1.3$ Hz, 1H), 7.77 (ddd, $J = 8.0, 2.0, 1.0$ Hz, 1H), 7.40 (t, $J = 7.9$ Hz, 1H), 5.13 (s, 2H) ppm. $^{13}\text{C NMR}$ (126 MHz, CDCl_3) δ 189.2, 137.4, 135.6, 131.2, 130.7, 126.6, 123.6, 121.8 (q, $J = 256.8$ Hz, ROCF_3), 68.3 (q, $J = 3.0$ Hz, $\text{RCH}_2\text{-OCF}_3$) ppm. $^{19}\text{F NMR}$ (188 MHz, CDCl_3) δ -61.59 ppm. HRMS (ASAP +) Calcd for $\text{C}_8\text{H}_5\text{BrF}_3\text{O}_2^+$ [$\text{M} + \text{H}$] $^+$: 282.9576. Found: 282.9576.

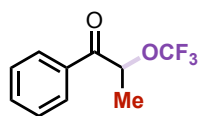
1-(4-bromophenyl)-2-(trifluoromethoxy)ethan-1-one (61)



34% yield

$^1\text{H NMR}$ (500 MHz, CDCl_3) δ 7.78 (d, $J = 8.6$ Hz, 2H), 7.66 (d, $J = 8.6$ Hz, 2H), 5.12 (s, 2H) ppm. $^{13}\text{C NMR}$ (126 MHz, CDCl_3) δ 189.6, 132.6, 132.6, 129.8, 129.6, δ 121.8 (q, $J = 256.8$ Hz, ROCF_3), 68.3 (q, $J = 3.0$ Hz, $\text{RCH}_2\text{-OCF}_3$) ppm. $^{19}\text{F NMR}$ (188 MHz, CDCl_3) δ -61.56 ppm. HRMS (ASAP +) Calcd for $\text{C}_8\text{H}_5\text{BrF}_3\text{O}_2^+$ [$\text{M} + \text{H}$] $^+$: 282.9576. Found: 282.9572.

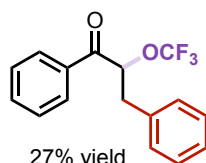
1-phenyl-2-(trifluoromethoxy)propan-1-one (62)



32% yield

$^1\text{H NMR}$ (500 MHz, CDCl_3) δ 7.97 (d, $J = 8.0$ Hz, 2H), 7.63 (t, $J = 7.4$ Hz, 1H), 7.51 (t, $J = 7.7$ Hz, 2H), 5.48 (q, $J = 6.9$ Hz, 1H), 1.66 (d, $J = 6.9$ Hz, 3H) ppm. $^{13}\text{C NMR}$ (126 MHz, CDCl_3) δ 195.1, 134.2, 133.7, 129.1, 128.9, 121.6 (q, $J = 256.2$ Hz, ROCF_3), δ 75.5 (q, $J = 2.5$ Hz, $\text{RCH}_2\text{-OCF}_3$), 18.8 ppm. $^{19}\text{F NMR}$ (188 MHz, CDCl_3) δ -59.29 ppm. HRMS (ASAP +) Calcd for $\text{C}_{10}\text{H}_{10}\text{F}_3\text{O}_2^+$ [$\text{M} + \text{H}$] $^+$: 219.0627. Found: 219.0629.

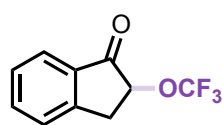
1,3-diphenyl-2-(trifluoromethoxy)propan-1-one (63)



27% yield

$^1\text{H NMR}$ (500 MHz, CDCl_3) δ 7.98 – 7.83 (m, 2H), 7.69 – 7.55 (m, 1H), 7.55 – 7.42 (m, 2H), 7.32 – 7.28 (m, 2H), 7.27 – 7.24 (m, 1H), 7.24 – 7.20 (m, 2H), 5.50 (dd, $J = 7.8, 5.3$ Hz, 1H), 3.31 – 3.14 (m, 2H) ppm. $^{13}\text{C NMR}$ (126 MHz, CDCl_3) δ 194.7, 135.0, 134.2, 134.2, 129.5, 129.1, 128.9, 127.6, 121.4 (q, $J = 256.8$ Hz, ROCF_3), 79.5 (q, $J = 2.0$ Hz, $\text{RCH}_2\text{-OCF}_3$), 39.0 ppm. $^{19}\text{F NMR}$ (188 MHz, CDCl_3) δ -59.46 ppm. HRMS (ASAP +) Calcd for $\text{C}_{10}\text{H}_{10}\text{F}_3\text{O}_2^+$ [$\text{M} + \text{H}$] $^+$: 295.0940. Found: 295.0941.

2-(trifluoromethoxy)-2,3-dihydro-1H-inden-1-one (64)

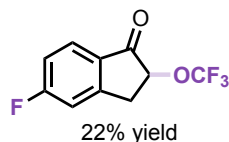


28% yield

$^1\text{H NMR}$ (300 MHz, CDCl_3) δ 7.82 (d, $J = 7.7$ Hz, 1H), 7.68 (t, $J = 7.1$ Hz, 1H), 7.50 – 7.40 (m, 2H), 4.98 – 4.89 (m, 1H), 3.68 (dd, $J = 17.1, 8.0$ Hz, 1H), 3.26 (dd, $J = 16.7, 4.2$ Hz, 1H) ppm. $^{13}\text{C NMR}$ (75 MHz, CDCl_3) δ 197.6, 149.7, 136.6, 133.8, 128.7, 126.8, 125.0, 122.1 (q, $J =$

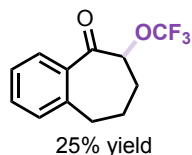
257 Hz, ROCF₃), 33.9 ppm. ¹⁹F NMR (188 MHz, CDCl₃) δ -59.73 ppm. HRMS (ASAP +) Calcd for C₂₀H₁₅F₆O₄⁺ [2M + H]⁺: 433.0869. Found: 433.0864.

5-fluoro-2-(trifluoromethoxy)-2,3-dihydro-1H-inden-1-one (65)



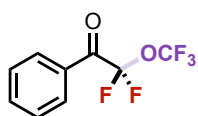
¹H NMR (300 MHz, CDCl₃) δ 7.88 – 7.80 (m, 1H), 7.20 – 7.09 (m, 2H), 4.98 – 4.89 (m, 1H), 3.67 (dd, *J* = 17.3, 7.9 Hz, 1H), 3.25 (dd, *J* = 17.1, 4.8 Hz, 1H) ppm. ¹³C NMR (75 MHz, CDCl₃) δ 195.6, 168.19 (d, *J* = 259 Hz, F-C_{Ar}), 152.66 (d, *J* = 10.5 Hz), 130.3, 127.61 (d, *J* = 10.6 Hz), 122.03 (q, *J* = 257 Hz, ROCF₃), 117.20 (d, *J* = 23.8 Hz), 113.62 (d, *J* = 22.8 Hz), 76.38 (q, *J* = 2.4 Hz, RCH₂-OCF₃), 33.8 ppm. ¹⁹F NMR (188 MHz, CDCl₃) δ -59.80 (s, CF₃), -99.41 (q, *J* = 7.7 Hz) ppm. HRMS (ASAP +) Calcd for C₁₀H₇F₄O₂⁺ [M + H]⁺: 235.0377. Found: 235.0380.

6-(trifluoromethoxy)-6,7,8,9-tetrahydro-5H-benzo[7]annulen-5-one (66)



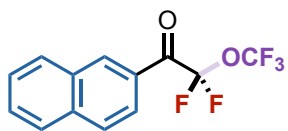
¹H NMR (300 MHz, CDCl₃) δ 7.71 (d, *J* = 7.6 Hz, 1H), 7.44 (t, *J* = 7.4 Hz, 1H), 7.33 (t, *J* = 7.6 Hz, 1H), 7.23 (s, 1H), 4.99 (t, *J* = 7.0 Hz, 1H), 3.14 – 2.91 (m, 2H), 2.40 – 2.24 (m, 1H), 2.22 – 2.0 (m, 2H), 1.99 – 1.81 (m, 1H) ppm. ¹³C NMR (75 MHz, CDCl₃) δ 198.9, 141.7, 136.5, 132.4, 130.2, 129.4, 127.0, 121.50 (q, *J* = 257 Hz, ROCF₃), 81.0 (q, *J* = 2.6 Hz, RCH₂-OCF₃), 34.2, 30.8, 23.2 ppm. ¹⁹F NMR (188 MHz, CDCl₃) δ -59.52 ppm. HRMS (ASAP +) Calcd for C₁₂H₁₂F₃O₂⁺ [M + H]⁺: 245.0784. Found: 245.0781.

2,2-difluoro-1-phenyl-2-(trifluoromethoxy)ethan-1-one (67)



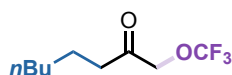
¹⁹F NMR yield of 20%. ¹⁹F NMR (188 MHz, CDCl₃) δ -54.91 (t, *J* = 8.7 Hz, 3F), -76.80 (q, *J* = 9.1 Hz, 2F) ppm.

2,2-difluoro-1-(naphthalen-2-yl)-2-(trifluoromethoxy)ethan-1-one (68)



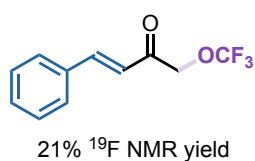
¹⁹F NMR yield of 19%. ¹⁹F NMR (188 MHz, CDCl₃) δ -54.92 (t, *J* = 8.7 Hz, 3F), -76.23 (q, *J* = 8.5 Hz, 2F) ppm.

1-(trifluoromethoxy)octan-2-one (69)



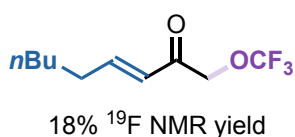
¹⁹F NMR yield of 16%. ¹⁹F NMR (188 MHz, CDCl₃) δ -61.30 ppm.

(E)-4-phenyl-1-(trifluoromethoxy)but-3-en-2-one (70)



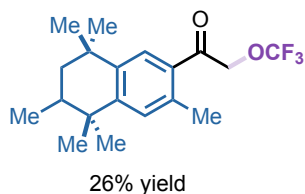
¹H NMR (300 MHz, CDCl₃) δ 7.76 (d, *J* = 16.1 Hz, 1H), 7.65 – 7.56 (m, 2H), 7.48 – 7.36 (m, 3H), 6.97 (d, *J* = 16.1 Hz, 1H), 4.69 (s, 2H) ppm. ¹³C NMR (75 MHz, CDCl₃) δ 191.4, 145.7, 134.0, 131.5, 129.2, 128.9, 128.6, 121.7 (q, *J* = 256 Hz, ROCF₃), 69.9 (q, *J* = 2.5 Hz, RCH₂-OCF₃) ppm. ¹⁹F NMR (188 MHz, CDCl₃) δ -61.63 ppm. HRMS (ASAP +) Calcd for C₁₁H₁₀F₃O₂⁺ [M + H]⁺: 231.0627. Found: 231.0634.

(E)-1-(trifluoromethoxy)non-3-en-2-one (71)



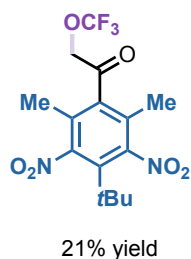
¹⁹F NMR (188 MHz, CDCl₃) δ -61.67 ppm. HRMS (ASAP +) Calcd for C₁₀H₁₆F₃O₂⁺ [M + H]⁺: 225.1097. Found: 225.1093.

1-(3,5,5,6,8,8-hexamethyl-5,6,7,8-tetrahydronaphthalen-2-yl)-2-(trifluoromethoxy)ethan-1-one (72)



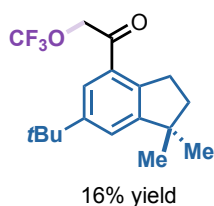
¹H NMR (500 MHz, CDCl₃) δ 7.48 (s, 1H), 7.26 (s, 1H), 5.02 (s, 2H), 2.50 (s, 3H), 1.88 (dq, *J* = 13.5, 6.8, 2.6 Hz, 1H), 1.64 (t, *J* = 13.3 Hz, 1H), 1.41 (dd, *J* = 13.6, 2.6 Hz, 1H), 1.33 (s, 3H), 1.32 (s, 3H), 1.27 (s, 3H), 1.08 (s, 3H), 1.00 (d, *J* = 6.8 Hz, 3H) ppm. ¹³C NMR (126 MHz, CDCl₃) δ 193.0, 151.7, 142.7, 136.5, 131.3 (x2), 127.2, 121.8, (q, *J* = 256.2 Hz, ROCF₃), 69.3 (q, *J* = 2.9 Hz, RCH₂-OCF₃), 43.4, 38.2, 34.5, 34.2, 32.6, 32.0, 28.4, 24.8, 21.3, 16.9 ppm. ¹⁹F NMR (188 MHz, CDCl₃) δ -61.29 ppm. HRMS (ESI+) Calcd. for C₁₉H₂₆F₃O₂⁺ [M + H]⁺: 343.1879. Found: 343.1870.

1-(4-(tert-butyl)-2,6-dimethyl-3,5-dinitrophenyl)-2-(trifluoromethoxy)ethanone (73)



¹H NMR (300 MHz, CDCl₃) δ 4.74 (s, 2H), 2.12 (s, 6H), 1.45 (s, 9H) ppm. ¹³C NMR (75 MHz, CDCl₃) δ 197.6, 150.7, 138.5, 133.8, 128.5, 121.4 (q, *J* = 258 Hz, ROCF₃), 70.7 (q, *J* = 2.9 Hz, RCH₂-OCF₃), 37.8, 30.4, 15.2 ppm. ¹⁹F NMR (188 MHz, CDCl₃) δ -61.74 ppm. HRMS (ASAP +) Calcd for C₁₅H₁₈F₃N₂O₆⁺ [M + H]⁺: 379.1111. Found: 379.1126.

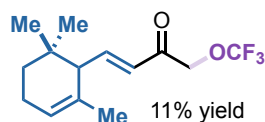
1-(6-(tert-butyl)-1,1-dimethyl-2,3-dihydro-1H-inden-4-yl)-2-(trifluoromethoxy)ethanone (74)



¹H NMR (300 MHz, CDCl₃) δ 7.52 (s, 1H), 7.40 (s, 1H), 5.12 (s, 2H), 3.17 (t, *J* = 7.3 Hz, 2H), 1.96 (t, *J* = 7.3 Hz, 2H), 1.36 (s, 9H), 1.27 (s, 6H) ppm. ¹³C NMR (75 MHz, CDCl₃) δ 191.8, 155.2, 150.5, 142.2, 130.2, 124.7, 123.2, 117.5 (q, *J* = 336.7 Hz, ROCF₃), 69.2 (q, *J* = 2.6 Hz, RCH₂-

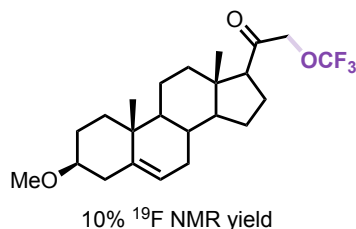
OCF₃). 43.7, 41.5, 34.9, 31.6, 30.9, 28.9 ppm. ¹⁹F NMR (188 MHz, CDCl₃) δ -61.24 ppm. HRMS (ASAP +) Calcd for C₁₈H₂₄F₃O₂⁺ [M + H]⁺: 329.1723. Found: 329.1679.

(E)-1-(trifluoromethoxy)-4-(2,6,6-trimethylcyclohex-2-en-1-yl)but-3-en-2-one (75)



¹H NMR (200 MHz, CDCl₃) δ 6.87 (dd, *J* = 15.7, 9.8 Hz, 1H), 6.28 (d, *J* = 15.6 Hz, 1H), 5.53 (bs, 1H), 4.61 (s, 2H), 2.32 (d, *J* = 9.6 Hz, 1H), 1.66 (s, 1H), 2.14 – 1.98 (m, 3H), 1.52 (s, 3H), 0.93 (s, 3H), 0.85 (s, 3H) ppm. ¹³C NMR (151 MHz, CDCl₃) δ 191.04, 151.82, 131.35, 125.79, 123.39, 69.54 (q, *J* = 2.9 Hz, CH₂OCF₃), 54.77, 28.00, 27.81, 26.89, 23.14, 22.87 ppm. ¹⁹F NMR (188 MHz, CDCl₃) δ -61.62 ppm. HRMS (ASAP +) Calcd for C₁₄H₂₀F₃O₂⁺ [M + H]⁺: 277.1410. Found: 277.1407.

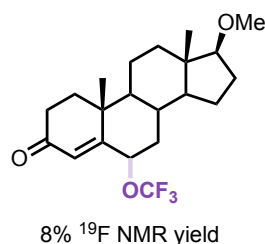
1-(3-methoxy-10,13-dimethyl-tetradecahydro-1H-cyclopenta[a]phenanthren-17-yl)-2-(trifluoromethoxy)ethan-1-one (76)



¹⁹F NMR (188 MHz, CDCl₃) δ -61.10 ppm.

10% ¹⁹F NMR yield

(8R,9S,10R,13S,14S,17S)-17-methoxy-10,13-dimethyl-6-(trifluoromethoxy)-dodecahydro-1H-cyclopenta[a]phenanthren-3(2H)-one (77)



8% ¹⁹F NMR yield

The compound was isolated as an inseparable 1:1 mixture of diastereoisomers.

In ¹H NMR, only characteristic peaks are listed.

¹H NMR (600 MHz, CDCl₃) δ 5.82 (d, *J* = 1.0 Hz, 1H, C=CHC=O), 5.77 (d, *J* = 1.4 Hz, 1H, C=CHC=O), 4.72 (dd, *J* = 14.0, 5.3 Hz, 1H, CHOCF₃), 4.57 (dd, *J* = 9.2, 4.5 Hz, 1H, CHOCF₃), 3.35 (s, 3H x2, OCH₃), 3.25 – 3.20 (m, 2H x2, CHOCH₃), 2.54 – 2.45 (m, 1H, CH₂C=O), 2.34 (dt, *J* = 4.9, 2.3 Hz, 1H, CH₂C=O), 2.29 (dd, *J* = 4.2, 2.6 Hz, 1H, CH₂C=O), 2.27 (dt, *J* = 5.2, 2.7 Hz, 1H, CH₂C=O), 1.32 (s, 3H, C-19 CH₃), 1.27 (s, 3H, C-19 CH₃), 0.80 (s, 3H, C-18 CH₃), 0.80 (s, 3H, C-18 CH₃). ¹³C NMR (151 MHz, CDCl₃) δ 191.5, 191.1, 173.6, 171.3, 123.5 (d, *J* = 239.1 Hz, ROCF₃), 121.8, 120.8, 117.1, 90.8, 90.5, 75.2 – 75.1 (m, CHOCF₃), 74.5 – 74.4 (m, CHOCF₃), 58.0 (x2), 54.4, 54.2, 52.7, 51.0, 50.7 (x2), 43.2, 43.0, 42.9, 42.7, 40.9, 40.4, 39.6, 38.0, 37.8, 37.7, 37.6, 35.7, 35.5, 35.0, 33.7, 33.6, 33.1, 32.7, 32.5, 32.1, 31.6, 29.8, 27.8, 27.7, 27.6, 23.4 (x3), 21.9, 21.8, 21.2, 20.8, 18.3, 17.6, 11.8, 11.7 (x2). ¹⁹F NMR (188 MHz, CDCl₃) δ -59.05 (s, CF₃), -59.11 (s, CF₃) ppm. HRMS (ASAP +) Calcd for C₂₁H₃₀F₃O₃⁺ [M + H]⁺: 387.2142. Found: 387.2152.

Quantum yield measurements

A ferrioxalate actinometry solution was prepared by following the Hammond variation of the Hatchard and Parker procedure outlined in Handbook of Photochemistry.^[17] Ferrioxalate actinometer solution measures the decomposition of ferric ions to ferrous ions, which are complexed by 1,10-phenanthroline and monitored by UV/Vis absorbance at 510 nm. The moles of iron-phenanthroline complex formed are related to moles of photons absorbed.

The solutions were prepared and stored in the dark:

1. Potassium ferrioxalate solution: 589.5 mg of potassium ferrioxalate (commercially available from Sigma Aldrich) and 278 μL of sulfuric acid (96%) were added to a 100 mL volumetric flask and filled to the mark with water (MilliQ grade).

2. Phenanthroline solution: 0.2% by weight of 1,10-phenanthroline in water (200 mg in 100 mL volumetric flask).

3. Buffer solution: to a 100 mL volumetric flask 4.94 g of NaOAc and 1 mL of sulfuric acid (96%) were added and filled to the mark with water (MilliQ grade).

The actinometry measurements were done as follows:

1a. 456 nm LED: 1 mL of the actinometer solution was added to a quartz cuvette (l = 10 mm). The actinometry solutions (placed 1 cm away from a 456 nm LED) were irradiated for specified time intervals (0, 15, 30, 45, 60) seconds.

1b. 400 nm LED: 1 mL of the actinometer solution was added to a quartz cuvette (l = 10 mm). The actinometry solutions (placed 2 cm away from a 3W 400 nm LED) were irradiated for specified time intervals (0, 15, 20, 30, 40) seconds.

2. After irradiation all the actinometer solution was removed and placed in a 10 mL volumetric flask. 0.5 mL of 1,10-phenanthroline solution and 2 mL of buffer solution was added to this flask and filled to the mark with water (MilliQ grade).

3. The UV-Vis spectra of actinometry samples were recorded for each time interval. The absorbance of the actinometry solution was monitored at 510 nm.

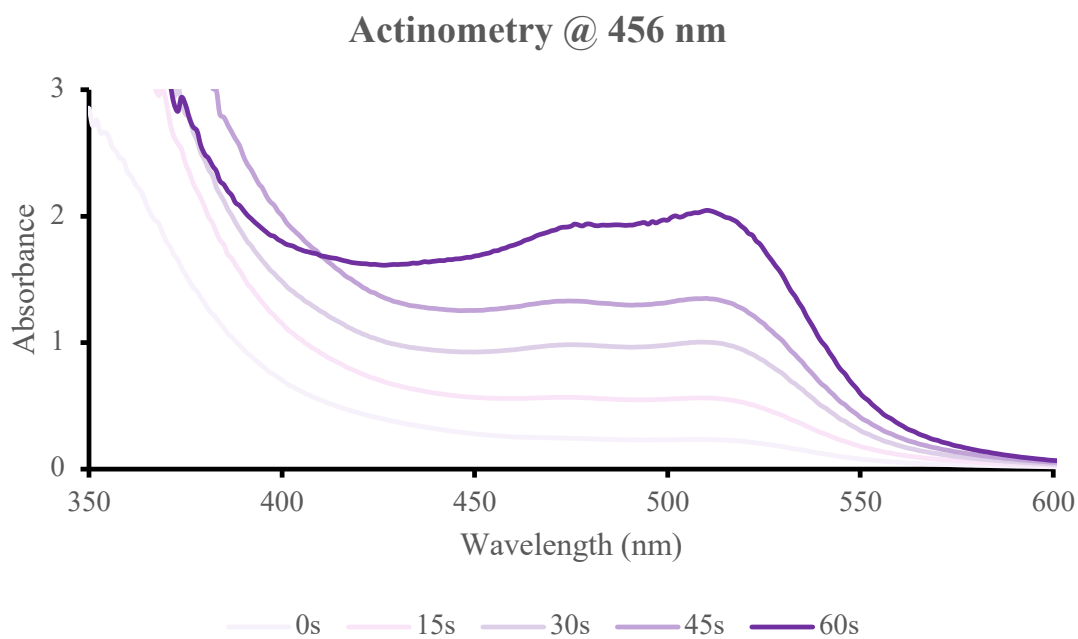


Figure 4.61. - UV-Vis spectra of actinometry samples irradiated with 456 nm light for the indicated time intervals.

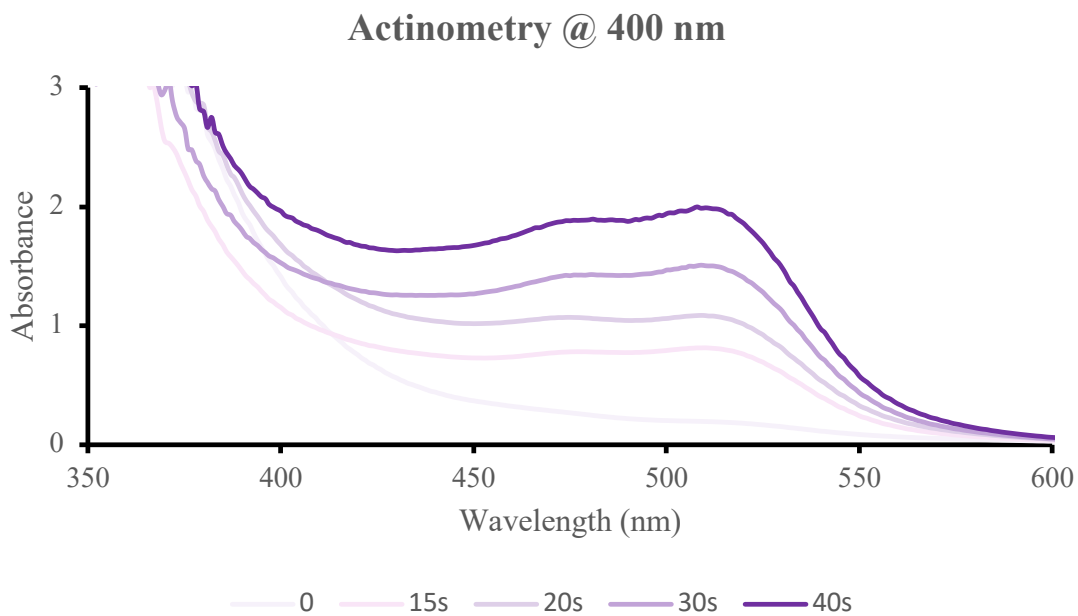


Figure 4.62. - UV-Vis spectra of actinometry samples irradiated with 400 nm light for the indicated time intervals.

4. The moles of Fe^{2+} formed for each sample are determined using Beers' Law:

$$\text{Moles } \text{Fe}^{2+} = \frac{V_1 V_3 \Delta A_{(510 \text{ nm})}}{10^3 V_2 l \varepsilon_{(510 \text{ nm})}}$$

where V_1 is the irradiated volume (1 mL), V_2 is the aliquot of the irradiated solution taken for the determination of the ferrous ions (1 mL), V_3 is the final volume after complexation with phenanthroline (10 mL), l is the optical path-length of the irradiation cell (1 cm), $\Delta A_{(510 \text{ nm})}$ the optical difference in absorbance between the irradiated solution and that taken in the dark, $\varepsilon_{(510 \text{ nm})}$ is the molar extinction coefficient of the complex $\text{Fe}(\text{phen})_3^{2+}$ ($11100 \text{ L mol}^{-1} \text{ cm}^{-1}$).

5. The moles of Fe^{2+} formed (N) are plotted as a function of time (t) (Figure 4.63 and Figure 4.64). The slope is a product of the photon flux (F) and the quantum yield for Fe^{2+} ($\phi(\text{Fe}^{2+}) = 1.13$), since $F = N/\phi(\text{Fe}^{2+}) \cdot t$.

456 nm: The $F_{456 \text{ nm}}$ was determined to be $2.20 \cdot 10^{-8} \text{ einstein s}^{-1}$.

400 nm: The $F_{400 \text{ nm}}$ was determined to be $3.52 \cdot 10^{-8} \text{ einstein s}^{-1}$.

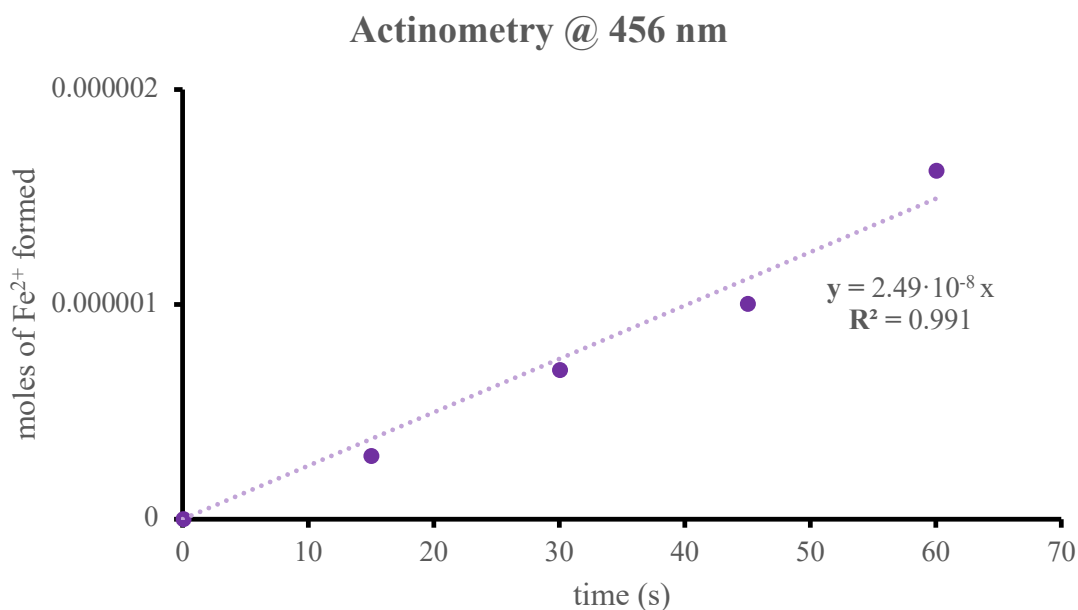


Figure 4.63. - Moles of Fe^{2+} formed after irradiation with the 456 nm light as function of time.

Actinometry @ 400 nm

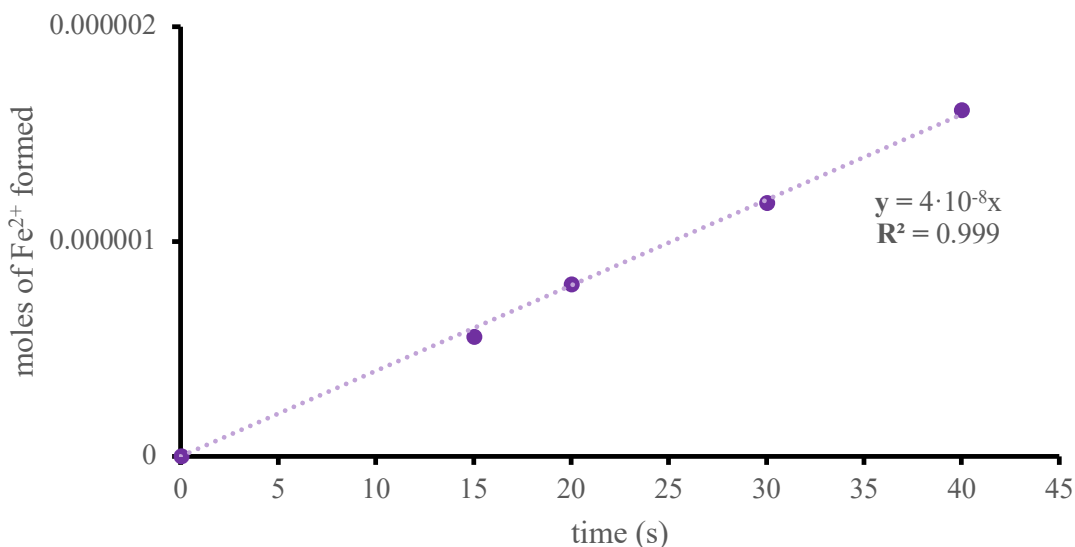


Figure 4.64. - Moles of Fe²⁺ formed after irradiation with the 400 nm light as function of time.

Since the ferrioxalate actinometer absorbance at 456 nm is 0.12 and at 400 nm is 0.47 and inferior to 2 in both cases (if is major than 2 at the wavelength used, it can be assumed that the entire incident light is absorbed), a correction factor (C) based on the fraction of light absorbed by the actinometer has to be considered to calculate the photon flux and the final quantum yield of the reaction (*note that this is also needed if the absorbance of the reaction under study at the optimized concentration is inferior to 2 at the wavelength used*).

Thus, according to the definition of quantum yield:^[18]

$$\Phi_{Fe2+} = \frac{\left(\frac{\partial \text{moles } Fe2+}{\partial \text{time}}\right)}{F C_{Fe2+}} \rightarrow F = \frac{\left(\frac{\partial \text{moles } Fe2+}{\partial \text{time}}\right)}{\Phi_{Fe2+} C_{Fe2+}} \quad C = 1 - 10^{-A(\lambda)}$$

The photon flux (F) previously found must be divided by the appropriate correction factor C.

456 nm: $C = 0.24$, calculated with $A_{456 \text{ nm}} = 0.12$.

Corrected photon flux: $5.33 \cdot 10^{-9}$ einstein s^{-1}

400 nm: $C = 0.66$, calculated with $A_{400 \text{ nm}} = 0.47$.

Corrected photon flux: $2.33 \cdot 10^{-8}$ einstein s^{-1}

6. 1 mL of the model reaction solutions were irradiated using the same systems and the moles of product formed for the reaction of interest are described below. The moles of product formed were determined by ^{19}F NMR measurements using the peak of triflimide as the internal standard. The number of moles of product per unit of time is related to the number of photons absorbed.



General Conclusions and Future Perspectives

This doctoral thesis provides with new tools to expand the synthetic potential of light-excited aryl ketones. The manuscript has been divided in four chapters:

- **Chapter I:** This chapter displays a general summary and the future perspectives of aryl ketone photochemistry as well as the key enabling potential of flow setups in the development of novel light-triggered transformations.
- **Chapter II:** This chapter establishes a Paternò-Büchi dearomatization reaction engaging indoles and aryl ketones. The results depicted in this part of the thesis show the ability of benzophenone- and benzil-derivates to form oxeto-indolinic polycycles with indoles and oxindole-derived silyl enol ethers in high yields and regio- and diastereo-selectivities. Moreover, the determination of the reaction mechanism highlighted the importance of the light source wavelength on the diastereoselectivity of the reaction (known as light stereodifferentiation process).
- **Chapter III:** This part of the thesis deals with the superior performances of microfluidic photoreactors with 2-alkylbenzophenones in terms of productivity and selectivity. Indeed, superior space-time yields were obtained when analyzing previously reported reactions, outcompeting batch reactors in up to 15-times. Additionally, a novel transformation, precluded in traditional conditions due to overirradiation problems, between 2-methylbenzophenone derivatives and coumarins has been reported. The derivatization of the obtained products yielded the naphthochromenone scaffold in high yields and reduced times.
- **Chapter IV:** In the last chapter of this dissertation, diverse concepts of organic photoredox catalysis have been discussed. Initially, structure-property and structure-activity relationships of naphthochromenone photocatalysts were assessed. Then, the implications of such sensitizers in both oxidative and reductive quenching processes were explored and, in some cases, outcompeting previously described protocols. Finally, the utilization of organic photocatalysts was studied to achieve α -functionalized ketones exploiting the reactivity of the OCF_3 radical. In this case, I report novel mild conditions in batch and in flow to access trifluoromethoxylated molecules.

In conclusion, during my PhD studies, I expanded the horizons of the photochemistry of organic compounds. For this reason, I envisage that the rationale behind the discussions of each chapter will be useful for the development of novel photochemical reactions in the future.

